frontiers | Research Topics

Immune regulation in sepsis

Edited by
Yufeng Zhou, Duanwu Zhang, Peisong Gao and Zuliang Jie

Published in
Frontiers in Immunology

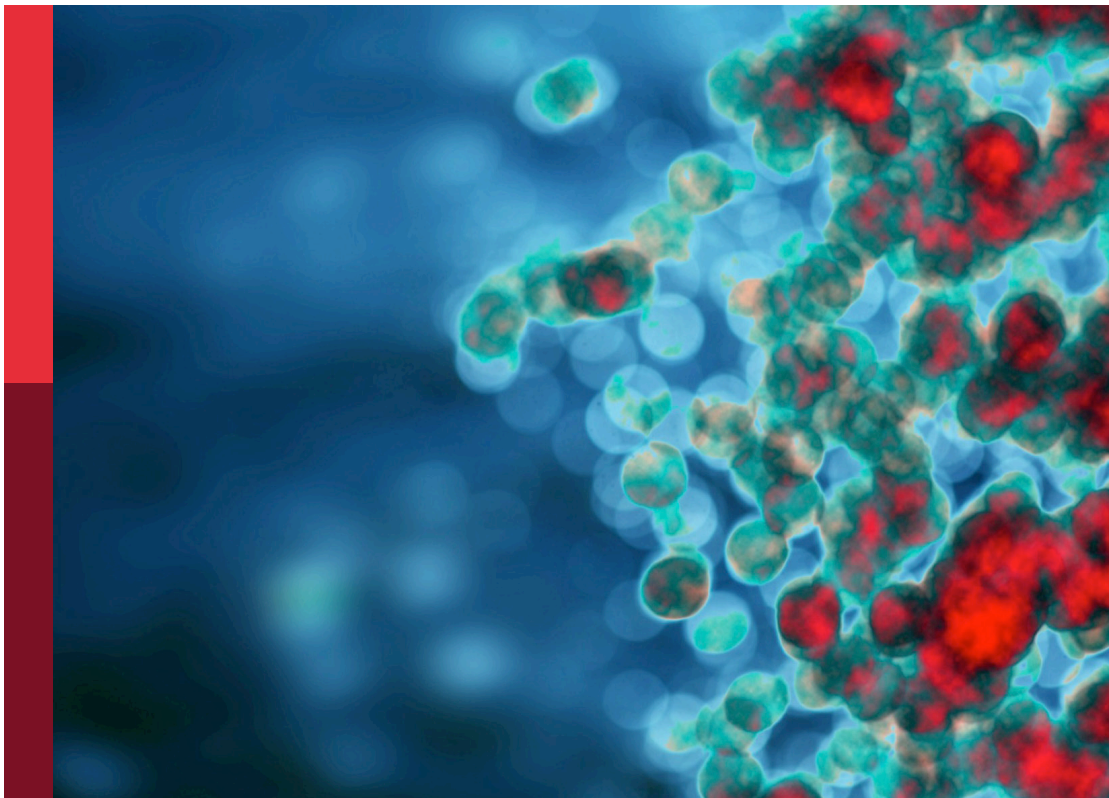

ISSN 1664-8714
ISBN 978-2-8325-3750-3
DOI 10.3389/978-2-8325-3750-3

About Frontiers

Frontiers is more than just an open access publisher of scholarly articles: it is a pioneering approach to the world of academia, radically improving the way scholarly research is managed. The grand vision of Frontiers is a world where all people have an equal opportunity to seek, share and generate knowledge. Frontiers provides immediate and permanent online open access to all its publications, but this alone is not enough to realize our grand goals.

Frontiers journal series

The Frontiers journal series is a multi-tier and interdisciplinary set of open-access, online journals, promising a paradigm shift from the current review, selection and dissemination processes in academic publishing. All Frontiers journals are driven by researchers for researchers; therefore, they constitute a service to the scholarly community. At the same time, the *Frontiers journal series* operates on a revolutionary invention, the tiered publishing system, initially addressing specific communities of scholars, and gradually climbing up to broader public understanding, thus serving the interests of the lay society, too.

Dedication to quality

Each Frontiers article is a landmark of the highest quality, thanks to genuinely collaborative interactions between authors and review editors, who include some of the world's best academicians. Research must be certified by peers before entering a stream of knowledge that may eventually reach the public - and shape society; therefore, Frontiers only applies the most rigorous and unbiased reviews. Frontiers revolutionizes research publishing by freely delivering the most outstanding research, evaluated with no bias from both the academic and social point of view. By applying the most advanced information technologies, Frontiers is catapulting scholarly publishing into a new generation.

What are Frontiers Research Topics?

Frontiers Research Topics are very popular trademarks of the *Frontiers journals series*: they are collections of at least ten articles, all centered on a particular subject. With their unique mix of varied contributions from Original Research to Review Articles, Frontiers Research Topics unify the most influential researchers, the latest key findings and historical advances in a hot research area.

Find out more on how to host your own Frontiers Research Topic or contribute to one as an author by contacting the Frontiers editorial office: frontiersin.org/about/contact

Immune regulation in sepsis

Topic editors

Yufeng Zhou — Fudan University, China
Duanwu Zhang — Fudan University, China
Peisong Gao — Johns Hopkins University, United States
Zuliang Jie — Xiamen University, China

Citation

Zhou, Y., Zhang, D., Gao, P., Jie, Z., eds. (2023). *Immune regulation in sepsis*. Lausanne: Frontiers Media SA. doi: 10.3389/978-2-8325-3750-3

Table of contents

frontiers | Frontiers in Immunology

TYPE Editorial
PUBLISHED 06 October 2023
DOI 10.3389/fimmu.2023.1298777

OPEN ACCESS

EDITED AND REVIEWED BY
Pietro Ghezzi,
University of Urbino Carlo Bo, Italy

*CORRESPONDENCE
Duanwu Zhang
duanwu@fudan.edu.cn

RECEIVED 22 September 2023
ACCEPTED 27 September 2023
PUBLISHED 06 October 2023

CITATION
Zhang H, Jie Z, Gao P, Zhou Y and Zhang D (2023) Editorial: Immune regulation in sepsis.
Front. Immunol. 14:1298777.
doi: 10.3389/fimmu.2023.1298777

Editorial: Immune regulation in sepsis

Huiling Zhang[1], Zuliang Jie[2], Peisong Gao[3], Yufeng Zhou[1] and Duanwu Zhang[1]*

[1]Children's Hospital of Fudan University, National Children's Medical Center, and Shanghai Key Laboratory of Medical Epigenetics, International Co-laboratory of Medical Epigenetics and Metabolism, Ministry of Science and Technology, Institutes of Biomedical Sciences, Fudan University, Shanghai, China, [2]State Key Laboratory of Cellular Stress Biology, School of Life Sciences, Faculty of Medicine and Life Sciences, Xiamen University, Xiamen, China, [3]Division of Allergy and Clinical Immunology, Johns Hopkins University School of Medicine, Baltimore, MD, United States

KEYWORDS

immune regulation, sepsis, inflammation, immunosuppression, macrophage, neutrophil

Editorial on the Research Topic
Immune regulation in sepsis

Sepsis leads to high morbidity and mortality worldwide without effective treatments. Patients with severe sepsis often develop symptoms of persistent inflammation, immunosuppression, and catabolic syndrome involving multiple cell types, organ systems, and pathophysiological mechanisms. Mechanistically, the immune response initiated by an invading pathogen fails to return to normal homeostasis, leading to sustained excessive inflammation and immune suppression in sepsis (1). Sepsis-associated excessive inflammation is prominently featured in leukocytes (i.e., neutrophils, macrophages, natural killer cells), endothelial cells, cytokines, complement products, and the coagulation system, while immunosuppression is related to impaired functions of immune cells (e.g., exhaustion of T cells, apoptosis of T cells, B cells and dendritic cells, reduced human leukocyte antigen-DR isotype (HLA-DR) expression by antigen-presenting cells), diminished production of proinflammatory cytokines through epigenetic modification and increased release of anti-inflammatory cytokines (2).

The goal of this Research Topic is to provide a forum to advance research on the contribution of immune system to the development and progression of sepsis. We seek to study the molecular mechanisms of cytokine release syndrome and immunosuppression, develop biomarkers for early diagnosis and prognosis, and explore innovative immunopharmacological interventions to treat sepsis.

We have received several original articles that report new targets for curing sepsis. Two of them concerned neutrophil infiltration and function. Ni et al. identified Fpr2 as a negative regulator of Streptococcus suis-induced streptococcal toxic shock-like syndrome (STSLS). They found that *Fpr2*-knockout mice were less susceptible to STSLS with increased neutrophil recruitment but without an impact on neutrophil extracellular trap (NET) construction. Koutsogiannaki et al. defined αDβ2 as a novel potential target of sepsis. They reported that αDβ2 deficiency attenuated lung injury and improved survival in experimental polymicrobial abdominal sepsis. Further

analyses showed that αDβ2 could increase phagocytosis and reduce apoptosis of neutrophils.

Two groups focused on the regulation of macrophage inflammation in sepsis. Wang et al. explored the effect of S1PR3 on NLRP3 inflammasome activation and sepsis mortality. They observed that one of the five S1PRs, S1PR3, was upregulated in macrophages in the inflammatory state. Inhibition of S1PR3 significantly suppressed ATP-induced NLRP3 inflammasome activation in macrophages. Mechanistically, inhibition of S1PR3 suppressed the LPS priming signal and reduced TWIK2 membrane trafficking-mediated potassium efflux. However, the S1PR3 antagonist increased mouse mortality in polymicrobial sepsis, suggesting the complexity between NLRP3 inflammasome activation and sepsis burden. Circular RNAs (circRNAs) have been linked to the regulation of macrophage polarization and subsequent inflammation in sepsis. Yang et al. built a sepsis circRNA expression pool and verified circ_0075723 as one of the markedly downregulated circRNAs, which might be related to pyroptosis. They detected the pyroptosis-associated signature in sepsis patients and linked pyroptosis with sepsis. circ_0075723 could inhibit pyroptosis by functioning as a sponge for miR-155-5p and regulating SHIP1 expression in macrophages. This work proposed that circ_0075723 could be a novel target for treating pneumonia-induced sepsis.

Vascular endothelial cells are the first cells to sense the damage induced by sepsis. Liu et al. identified an important role of Notch1 in maintaining vascular permeability during sepsis. Sepsis mediators downregulated the intracellular domain of Notch1 (NICD) and downstream signaling, further impairing endothelial barrier function. NICD overexpression and agonist stimulation alleviated endothelial dysfunction under inflammatory conditions *in vitro* and elevated the survival rate of septic mice *in vivo*. This study proposed the Notch1-Akt axis as a potential therapeutic target for sepsis. In line with this work, Ying et al. showed that circulating SDC1 levels were persistently upregulated in children with septic shock and that SDC1 shedding caused endothelial permeability under septic conditions. They found that the drug sulodexide could reduce endothelial permeability by preventing SDC1 shedding. Sulodexide administration alleviated lung injury and restored endothelial glycocalyx damage.

Cytokine signaling participates in the defense against pathogens. Wang et al. reported that γδT cell-intrinsic IL-1R signaling promoted survival during *Staphylococcus aureus* bacteremia. Using several systematic and conditional knockout mice, the authors found that IL-1R signaling in γδT cells (but not in other immune cells) was involved in the defense against bacterial infection by promoting monocyte recruitment.

Acute liver injury (ALI) is common in sepsis patients and is significantly associated with poor prognosis. Cai et al. investigated the roles and mechanisms of mesenchymal stem cells (MSCs) in treating ALI in sepsis. They found that either MSCs or exosome extracted from MSCs could attenuate ALI and subsequent death in sepsis. Further research showed that miR-26a-5p in MSC-derived exosome protected against hepatocyte death and liver injury caused by sepsis by targeting MALAT1. Therefore, they proposed miR-26a-5p/MALAT1 as novel targets for drug development in treating ALI in sepsis.

Two research articles focused on finding new prognostic markers for sepsis. Two markers were incidentally related to neutrophil infiltration. Liang et al. developed a new sepsis prognostic risk system. They first identified pyroptosis-related DEGs between sepsis patients and healthy cohorts, then narrowed down the field through functional analysis and immune infiltration analysis and constructed the prognostic risk system based on six pyroptosis-related genes (*GZMB*, *CHMP7*, *NLRP1*, *MYD88*, *ELANE*, and *AIM2*), which were all associated with neutrophils. Four of the six genes (*GZMB*, *CHMP7*, *NLRP1*, and *AIM2*) had potential diagnostic value in sepsis diagnosis. Preechanukul et al. utilized a reductionist approach leveraging publicly available transcriptomic data to explore effective risk and outcome predictors in sepsis. They searched for upregulated genes by *in vitro* exposure of neutrophils from healthy subjects with the serum of septic patients and identified *ACVR1B* as a candidate. *ACVR1B* expression was shown to be upregulated in septic melioidosis and could be a prognostic marker of sepsis.

The imbalance of pro-inflammation and anti-inflammation can lead to sepsis. FES tyrosine kinase is highly expressed in innate immune cells and plays a role in limiting the overactivation of the immune system. Laight et al. studied whether enhancing the expression of FES in early sepsis and inhibiting its effects in late sepsis could improve outcomes. They employed *in vivo*, *in vitro*, and clinical research methodologies to elucidate the role of FES in sepsis. Cell types, different sepsis models, agonists and antagonists, and timing of FES regulation were included in their research scope to accurately evaluate the role of FES in sepsis.

Gut motility dysfunction is the most common complication of post-septic organ dysfunction, which involves immune and neuronal cells. Yao et al. observed that muscular neutrophil infiltration leading to neuron loss in the intestinal muscle caused intestinal motility dysfunction after pneumonia sepsis. However, neutrophil blockade was ineffective in relieving sepsis. The authors found that $MHCII^{hi}$ $CX3CR1^{hi}$ macrophages could recover intestinal motility in pneumonia sepsis depending on prostaglandin E2 (PGE2). This work provides more insights into intestinal dysmotility after sepsis.

Immunoparalysis, an immunosuppressed state, is associated with worsened outcomes, including multiple organ dysfunction syndrome, secondary infections, and increased mortality. Joshi et al. reviewed that low human leukocyte antigen-DR isotype (HLA-DR) expression on peripheral blood monocytes was correlated with increased risks for infection and death. In particular, they emphasized that sargramostim, a recombinant human granulocyte-macrophage colony-stimulating factor (rhu GM-CSF), could stimulate and restore immune functions in sepsis immunoparalysis.

In summary, articles in this Research Topic highlight the critical roles of immune regulation in sepsis and are depicted in Figure 1. However, these insights into sepsis have yet

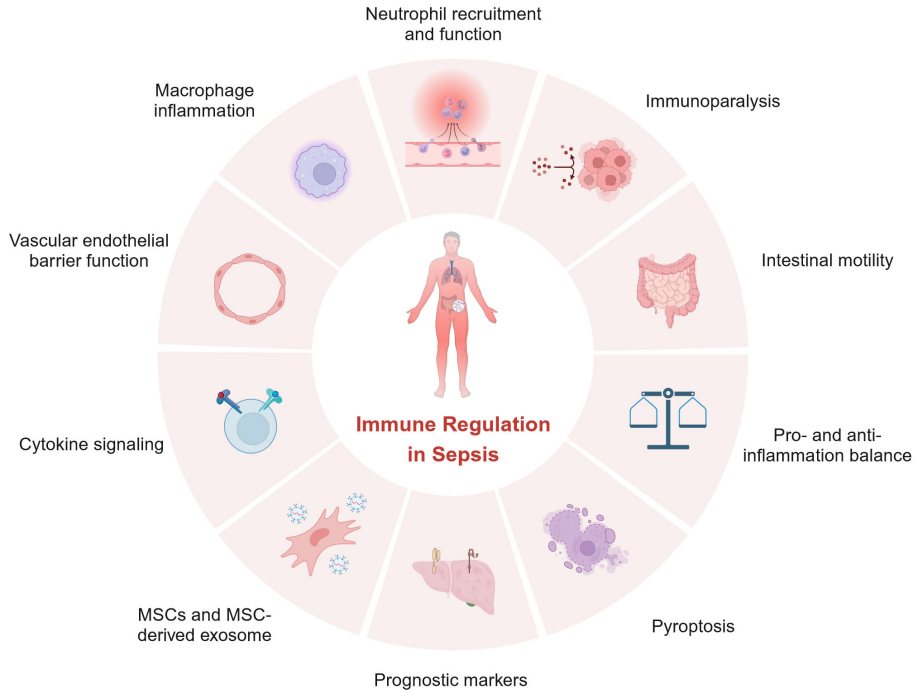

FIGURE 1
Perspectives of the Research Topic: Immune Regulation in Sepsis.

to be translated into effective treatments for sepsis. Further investigations are urgently needed to better understand the immunopathogenesis of sepsis so that better prognostic markers and effective treatments can be developed.

Author contributions

HZ: Writing – original draft. ZJ: Writing – review & editing. PG: Writing – review & editing. YZ: Writing – review & editing. DZ: Funding acquisition, Writing – original draft, Writing – review & editing.

Funding

The author(s) declare financial support was received for the research, authorship, and/or publication of this article. This work was supported by the National Key Research and Development Program of China (2021YFC2701800, 2021YFC2701802), National Natural Science Foundation of China (82071780, 32370926), Science and Technology Commission of Shanghai Municipality (21JC1400900).

Conflict of interest

The authors declare that the research was conducted in the absence of any commercial or financial relationships that could be construed as a potential conflict of interest.

Publisher's note

References

1. van der Poll T, van de Veerdonk FL, Scicluna BP, Netea MG. The immunopathology of sepsis and potential therapeutic targets. *Nat Rev Immunol* (2017) 17:407–20. doi: 10.1038/nri.2017.36

2. van der Poll T, Shankar-Hari M, Wiersinga WJ. The immunology of sepsis. *Immunity* (2021) 54:2450–64. doi: 10.1016/j.immuni.2021.10.012

frontiers | Frontiers in Immunology

TYPE Brief Research Report
PUBLISHED 18 November 2022
DOI 10.3389/fimmu.2022.1059996

OPEN ACCESS

EDITED BY
Zuliang Jie,
Xiamen University, China

REVIEWED BY
Mehmet Sen,
University of Houston, United States
Yuejin Liang,
University of Texas Medical Branch at Galveston, United States

*CORRESPONDENCE
Koichi Yuki
koichi.yuki@childrens.harvard.edu

SPECIALTY SECTION
This article was submitted to Inflammation, a section of the journal Frontiers in Immunology

RECEIVED 02 October 2022
ACCEPTED 17 October 2022
PUBLISHED 18 November 2022

CITATION
Koutsogiannaki S, Hou L, Okuno T, Shibamura-Fujiogi M, Luo HR and Yuki K (2022) αDβ2 as a novel target of experimental polymicrobial sepsis. *Front. Immunol.* 13:1059996. doi: 10.3389/fimmu.2022.1059996

αDβ2 as a novel target of experimental polymicrobial sepsis

Sophia Koutsogiannaki[1,2,3], Lifei Hou[1,2,3], Toshiaki Okuno[4], Miho Shibamura-Fujiogi[1,2,3], Hongbo R. Luo[5] and Koichi Yuki[1,2,3]*

[1]Department of Anesthesiology, Critical Care and Pain Medicine, Cardiac Anesthesia Division, Boston Children's Hospital, Boston, MA, United States, [2]Department of Anaesthesia, Harvard Medical School, Boston, MA, United States, [3]Department of Immunology, Harvard Medical School, Boston, MA, United States, [4]Department of Biochemistry, Juntendo University Faculty of Medicine, Tokyo, Japan, [5]Department of Pathology, Boston Children's Hospital, Boston, MA, United States

Since sepsis was defined three decades ago, it has been a target of intensive study. However, there is no specific sepsis treatment available, with its high mortality and morbidity. αDβ2 (CD11d/CD18) is one of the four β2 integrin members. Its role in sepsis has been limitedly studied. Using an experimental polymicrobial sepsis model, we found that the deficiency of αDβ2 was associated with less lung injury and better outcome, which was in sharp contrast to other β2 integrin member αLβ2 (CD11a/CD18), and αMβ2 (CD11b/CD18). This phenotype was supported by a reduction of bacterial loads in αDβ2 knockout mice. Further analysis showed that the deficiency of αDβ2 led to a reduction of neutrophil cell death as well as an increase in neutrophil phagocytosis in both murine and human systems. Our data showed a unique role of αDβ2 among the β2 integrin members, which would serve as a potential target to improve the outcome of sepsis.

KEYWORDS

integrin, aDb2, sepsis, cell death, phagocytosis

Introduction

Sepsis remains to be a huge health care burden. Sepsis is the leading cause of death in the non-cardiac intensive care units (ICUs), accounting for more than 750,000 deaths annually in the U.S. Lack of specific treatment against sepsis is largely responsible for its high morbidity and mortality. Sepsis is treated conservatively with antibiotic administration, fluid resuscitation, and respiratory support. Thus, the development of a therapeutic to attenuate sepsis is urgently needed.

β2 integrins are a leukocyte-specific glycoprotein adhesion molecule family consisting of α- and β-subunits responsible for a number of leukocyte functions during infection. The critical role of β2 integrins in infection is well illustrated by a rare genetic disease called leukocyte adhesion deficiency type I (LAD I), which is caused by a functional or expressional defect of β2 integrins, and characterized by recurrent infection, sepsis, and death (1). β2 integrins consist of the four members; αLβ2 (CD11a/CD18, leukocyte function-associated antigen-1), αMβ2 (CD11b/CD18, macrophage 1-antigen), αXβ2 (CD11c/CD18), and αDβ2 (CD11d/CD18). Among them, αLβ2 and αMβ2 have been extensively studied. αLβ2 is ubiquitously expressed on leukocytes, and involved in a number of important leukocyte functions including trafficking and immunological synapse formation (2). αMβ2 is expressed mainly on innate immune cells, and plays a major role in their recruitment and phagocytosis (3, 4). Both αLβ2 and αMβ2 deficiency significantly worsened infection and sepsis outcome (5–7). αXβ2 (CD11c) is widely known as a dendritic cell marker, and its deficiency also worsened the sepsis outcome (8). αDβ2 was cloned last among the β2 integrins, and the investigation on the role of αDβ2 in sepsis has been limited.

The inhibition of β2 integrins as a whole may not be desirable based on LAD I phenotype. However, the blockade of β2 integrins mitigated lung injury in sepsis (9, 10), suggesting that a subset of the β2 integrins serves as a potential target for sepsis treatment. Here we hypothesized that the inhibition of a subset of β2 integrin members would serve to protect from lung injury and lead to the improvement of sepsis outcome. Accordingly, the aim of this study was to determine the role of each β2 integrin member in the development of sepsis-associated lung injury. We found that αDβ2 played a unique role in sepsis among the β2 integrin members so that its inhibition led to the improvement of sepsis outcome with less lung injury.

Materials and methods

Mice

Wild type (11), CD11a (αL) knockout (KO) mice (12), CD11b (αM) KO mice (13), CD11d (αD) KO mice (14) were obtained from Jackson Laboratory (Bar Harbor, Maine, USA). CD11c (αX) KO mice were kindly given by Dr. Christie Ballantyne (Baylor University). CD18 KO (β2) KO mice were kindly given by Dr. Dennis Wagner (Boston Children's Hospital). They were housed under specific pathogen-free condition, with 12-hour light and dark cycles. All animal protocols were approved by the Institutional Animal Care and Use Committee (IACUC) at Boston Children's Hospital.

CLP surgery

All the experimental procedures complied with institutional and federal guidelines regarding the use of animals in research. Polymicrobial abdominal sepsis was induced by cecal ligation and puncture surgery, as we previously performed (7). In brief, mice were anesthetized with an intraperitoneal injection of ketamine 60 mg/kg and xylazine 5 mg/kg. Following its exteriorization, the cecum was ligated at a 1.0 cm from its tip and subjected to a single, through- and -through puncture using a 20-gauge needle. A small amount of fecal material was expelled with a gentle pressure to maintain the patency of puncture sites. The cecum was reinserted into the abdominal cavity. 0.1 mL/g of warmed saline was administered subcutaneously. Buprenorphine was given subcutaneously to alleviate postoperative surgical pain. For outcome study, mice were observed up to 7 days.

Lung injury analysis

For histological analysis, lung was fixed with 4% paraformaldehyde for histological analysis. Lung histology was subjected to Hematoxylin and Eosin (H&E) staining. In some cases, we also examined bronchial lavage fluid (BAL) for protein concentrations, and performed wet to dry ratio.

Quantitative organ culture

To determine the bacterial loads in the organs and blood, tissue homogenates or blood were loaded on 5% blood agar plates (Teknova; Hollister, California, USA) after surgical dilutions and incubated for 18 hours as previously described (15). Colonies of all morphologies on plates were counted. For neutrophil depletion experiment, 250 μg of rat anti-Ly6G antibody (clone 1A8, Bio X Cell, Lebanon, NH) was injected intraperitoneally one day before CLP procedure as previously described (16). As a control, normal rat IgG2a isotype control was used.

Escherichia coli intraabdominal infection model

Escherichia coli (*E. coli*)-GFP (ATCC25922-GFP) was overnight cultured in Luria-Bertani (17) ampicillin (100 μg/mL) medium at 37°C and washed twice with sterile PBS buffer. Mice were subjected to an intraperitoneal injection of *E. coli*-GFP (10^8 CFU). At 6 hours after the injection, peritoneal fluid was collected by lavage using 5 mL of cold PBS buffer. Serial dilutions of the final bacterial inocula were plated on LB-

ampicillin (100 μg/mL) agar plates and incubated overnight at 37°C to verify the number of live bacteria injected as above.

Cell death assay

Cell death was examined using Annexin V apoptosis detection kit (BD Biosciences, San Jose, CA, USA). Briefly cells were stained with Annexin V-FITC. Then, cells were subjected to flow cytometry analysis using BD Accuri C6 (BD Biosciences).

Chimeric mouse experiments

To generate mixed bone marrow chimeras, recipient mice on the C57BL/6 background were irradiated with two doses of 550 rad with 4-hour intervals. Wild-type (WT; CD45.1) and CD11dKO (CD45.2) derived bone marrow cells (total of 5×10^6 cells) were mixed at the ratio of 1:1 and injected into the tail vein of lethally irradiated recipients. Mice were evaluated for the reconstitution of the immune compartment at various time points after bone marrow transplantation. To prevent bacterial infection, the mice were provided with autoclaved drinking water containing sulfatrim for 1 week prior to and for 4 weeks after irradiation.

Phagocytosis

The neutrophil phagocytosis was done using Phagotest Kit (Glycotope Biotechnology; Heidelberg, Germany). Mouse neutrophils were incubated in complete RPMI 1640 on ice for 10 min, followed by the addition of FITC-*E. Coli*. Then the neutrophil suspension was kept on ice as cold control or was put into 37°C water bath for 10 min. At the end of incubation, cells were transferred back on ice, quenched, and washed. Cells were suspended in PBS/1% PFA and measured by BD Accuri C6 (BD Biosciences).

Reactive oxygen species

Mouse neutrophils (2×10^5 in 200 μl) were cultured in complete RPMI 1640 at 37°C for 30 min. Dihydrorhodamine-123 (1 μM; Sigma-Aldrich) was added for 5 min at 37°C. Neutrophils were washed once. PMA (100 nM) was added, and the cells were incubated for additional 15 min at 37°C. After one wash, the cells were resuspended in cold PBS with 1% FCS for detection of ROS-induced rhodamine-123 on BD Accuri C6 (BD Biosciences).

Chemotaxis

Bone marrow neutrophils were subjected to horizontal chemotaxis assay using the EZ-TAXIScan apparatus (Effector Cell Institute; Tokyo, Japan) as previously performed. Neutrophils suspended in RPMI1640 containing 10 mM HEPES, 0.1% BSA and 10 mM EDTA were aligned on one edge of the chemotaxis channel. At the other end, 1 μM N-formylmethionine-leucyl-phenylalanine (fMLP) was injected, creating a gradient along the channel. Pictures were taken every 30 seconds for 20min, and recorded movies were analyzed using FIJI software (National Institute of Health; Bethesda, MD).

Eicosanoid lipidomics

Reverse-phase mass spectrometry (MS)-based quantitation technique for eicosanoids was previously described (18). The lipids were extracted with methanol and diluted with water containing 0.1% formic acid to yield a final methanol concentration of 20%. After addition of deuterium-labeled internal standards, the samples were loaded on Oasis HLB cartridge (Waters, Milford, MA). The column was washed with 1 mL of water, 1 mL of 15% methanol, and 1 mL of petroleum ether and then eluted with 0.2 mL of methanol containing 0.1% formic acid. Eicosanoids were quantified by reverse-phase-HPLC-electrospray ionization-tandem MS method.

RNA sequencing

Blood or lung cells were stained with anti-Ly6G, CD11b, and CD45.2 antibodies. Neutrophils were sorted as $Ly6G^+/CD11b^+/CD45.2^+$ population. They were subjected to RNA purification using Qiagen RNeasy Plus Mini Kit. RNA samples were quantified using Qubit 2 Fluorometer (Life Technology; Carlsbad, CA) and RNA integrity was checked with Agilent TapeStation (Agilent Technologies; Palo Alto, CA). SMART-Seq v4 Ultra Low Input kit for Sequencing was used for full-length cDNA synthesis and amplification (Clonetech; Mountain View, CA), and Illumina Nextera XT library was used for sequencing library preparation. Briefly, cDNA was fragmented, and adaptor was added using transposase, followed by limited-cycle PCR to enrich and add index to the cDNA fragments. The final library was assessed with Qubit 2.0 Fluorometer and Agilent TapeStation. The sequencing libraries were multiplexed and clustered on one lane of a flowcell. After clustering, the flowcell was loaded on the Illumina HiSeq instrument according to the manufacturer's instructions. The samples were sequenced using a 2x150 paired end configuration. After

investigating the quality of the raw data, sequencing reads were trimmed to remove possible adapter sequences and nucleotides with poor quality using Trimmomatic v.0.36. The trimmed reads were mapped to the mouse reference genome using STAR aligner v.2.5.2b. Only unique reads that fell within exon regions were counted. After extraction of gene hit counts, the gene hit counts table was used. Using DESeq2, a comparison between the groups of samples was performed. The Wald test was used to generate p-value and Log_2 fold changes. Genes with adjusted p-values < 0.05 and absolute log_2 fold change > 1 were called differentially expressed genes. Data are available at GSE215749 (GEO).

CRISPR/Cas9 deletion of Itgad gene in HL-60 cells

CRISPR/Cas9 editing to delete αD (gene: Itgad) expression was done in HL-60 cells as follows. HL-60 cells were cultured at 37°C in RPMI1640 supplemented with 10% FBS, 1% penicillin/streptomycin. Confluency was maintained between 3 x10^5-1.5x 10^6/ml. Electroporation was performed one day after passaging when cells were in log phase of growth using the Lonza 4D Nucleofector with 20 µl Nucleocuvette strips as described (19, 20). Briefly, ribonucleoprotein (RNP) complex was made by combining 100 pmol Cas9 (IDT; Newark, NJ) and 100pmol modified sgRNA (Synthego; Redwood City, CA) targeting ITGAD using either sg1 (UUCUUAUCAUGGAUUCAACC) or sg2 (AUGAUAAGAAGCCAGGACUG) and incubating at room temperature for 15 minutes.

2 x10^5- 4 x 10^5 HL-60 cells were resuspended in 20 µl SF cell line solution (Lonza; Basel, Switzerland) and were mixed with RNP and underwent nucleofection with program EN-138 as per manufacturer recommendations. Cells were returned to RPMI1640 media and editing efficiency was measured 48 hours after electroporation by polymerase chain reaction (PCR). First, genomic DNA was extracted using the DNeasy kit (Qiagen; Hildgen, Germany) according to the manufacturer's instructions. Genomic PCR was performed using Platinum II Hotstart Mastermix (Thermo Fischer Scientific), and edited allele frequency was detected by Sanger sequencing and analyzed by ICE (21). The following primer pairs were used: ITGAD (forward: ATGATAAGAAGCCAGGACTG; reverse: CAGTCCTGGCTTCTTATCAT).

Statistical analysis

Data were analyzed as indicated in the figure legends. Statistical analysis methods were included under each figure legend. Statistical significance was defined as P<0.05. All the statistical calculations were performed using PRISM9 software (GraphPad Software, La Jolla, CA).

Results

αDβ2 deficiency attenuated lung injury and improved survival in experimental polymicrobial abdominal sepsis

Polymicrobial abdominal sepsis induced by CLP surgery is the most frequently used preclinical sepsis model that best recapitulates human sepsis (22, 23). We previously reported that sepsis outcomes of αL KO, αM KO and αX KO mice were worse than that of wild-type (11) mice in this model (5–7). Because blocking β2 integrin as a whole attenuated lung injury (9, 10), we examined the degree of lung injury in mice deficient of each of the β2 integrin members. In line, β2 KO mice had less lung injury following CLP (Figure 1A). Histological analysis demonstrated that lung injury was highly induced following sepsis in WT, αL KO, and αM KO mice (Figure 1A). In contrast, αD KO mice manifested less histological lung injury (Figure 1B). Wet-to-dry and BAL fluid analyses also supported the finding (Figure 1B). αD KO mice also showed better survival compared to WT mice (Figure 1C), suggesting that αDβ2 may be a good target to attenuate sepsis. We further examined bacterial loads at various organs. Bacterial loads at the lungs, spleen, kidney, and blood were significantly less in αD KO mice (Figure 1D), consistent with the survival data. However, bacterial loads at the peritoneal cavity did not show any difference between the two strains (Figure 1D). Neutrophils are the first-line defense immune cells critical for bacterial eradication (24). The relationship between neutrophil numbers in the blood, the peritoneal cavity, and the lungs between the two strains correlated with the data of bacterial loads above (Figure 1E), suggesting that the difference in neutrophil numbers at various sites was in part responsible for the degree of bacterial clearance. CLP sepsis is a sepsis with mixed bacterial flora. Considering the possibility that the flora between the two strains would not likely be the same., we also examined bacterial clearance in *E. coli* intraperitoneal injection model. Bacterial loads were significantly less in αD KO mice at 6 hours after an intraperitoneal injection (Figure 1D), indicating that integrin αD deficiency might enhance bacterial eradication.

αDβ2 KO neutrophils helped to eradicate bacterial loads in the lungs preferentially

The correlation of the degree of splenic apoptosis with sepsis outcome has been previously described (25–27). Splenic neutrophil and monocyte cell death was significantly less in αD KO mice (Figure 2A), consistent with the sepsis outcome data above. However, the degree of cell death was comparable in T and B cells between WT and αD KO mice (Figure 2A). The expression of αDβ2 was previously reported on neutrophils and

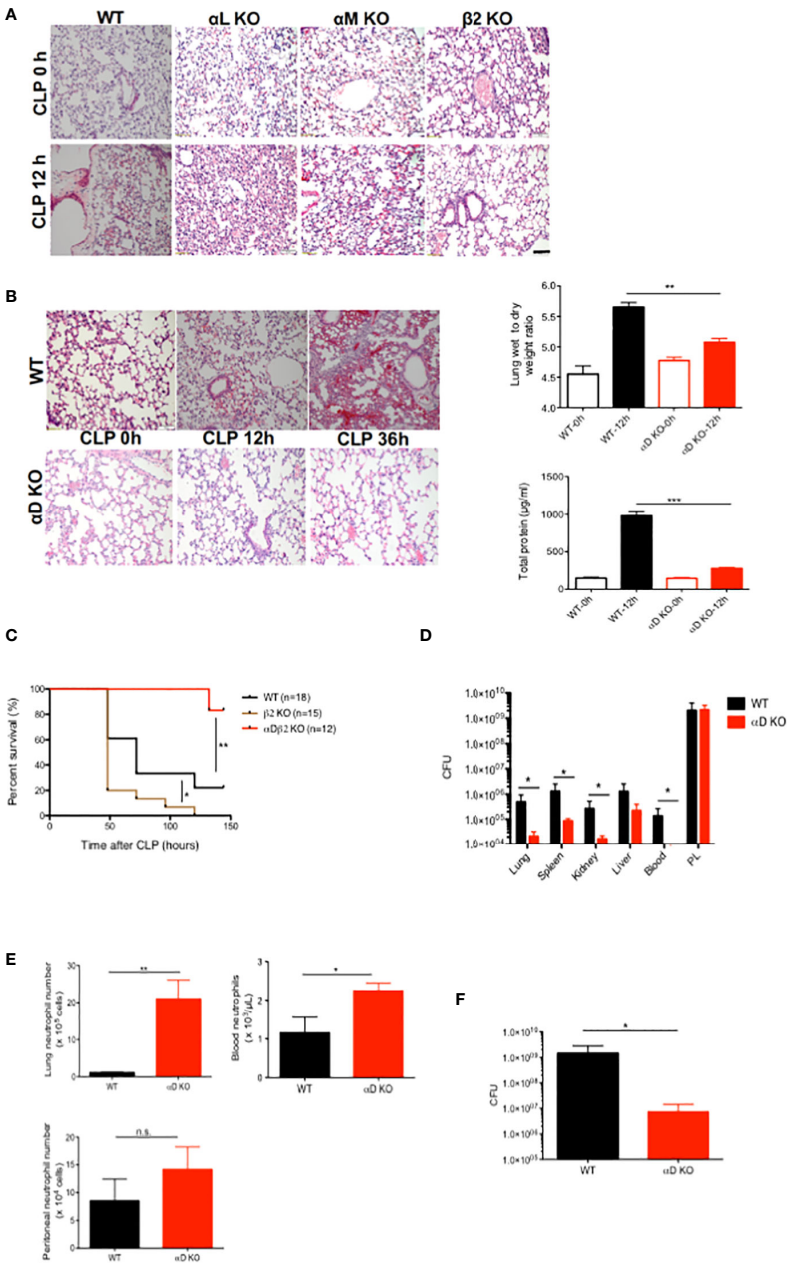

FIGURE 1
The role of αDβ2 in sepsis. **(A)** Representative lung histology of WT, αL KO, α KO, and β2 KO mice at the baseline and at 12 hours after CLP. Black bar indicates 50 μm. **(B)** Representative lung histology of WT and αD KO at the baseline, at 12 and 36 hours after CLP. Wet to lung analysis and BAL total protein analysis at the baseline and at 12 hours after CLP. Data were shown as mean +/- S.D. of 6 mice per group. One-way ANOVA with Bonferroni *post hoc* analysis was performed. **p < 0.01, ***p < 0.001. **(C)** Survival after CLP in WT (n=18), αD KO (n=12) and β2 KO (n=15) mice. Cox regression analysis was performed. *p <0.05, **p <0.01. **(D)** Bacterial loads in WT and αD KO mice at 12 hours after CLP. Data were shown as mean +/- S.D. of 8 mice per group. Two-way ANOVA analysis was performed. *p < 0.05. **(E)** Neutrophil counts at the lungs, the blood, and the peritoneal cavity in WT and αD KO mice at 12 hours after CLP. Data were shown as mean +/- S.D. of 6 mice. Student t test was performed. *P < 0.05, p < 0.01. **(F)** Bacterial loads at the peritoneal cavity at 6 hours after *E coli* intraperitoneal injection. Data were shown as mean +/- S.D. of 6 mice. Student t test was performed. *p < 0.05.

10.3389/fimmu.2022.1059996

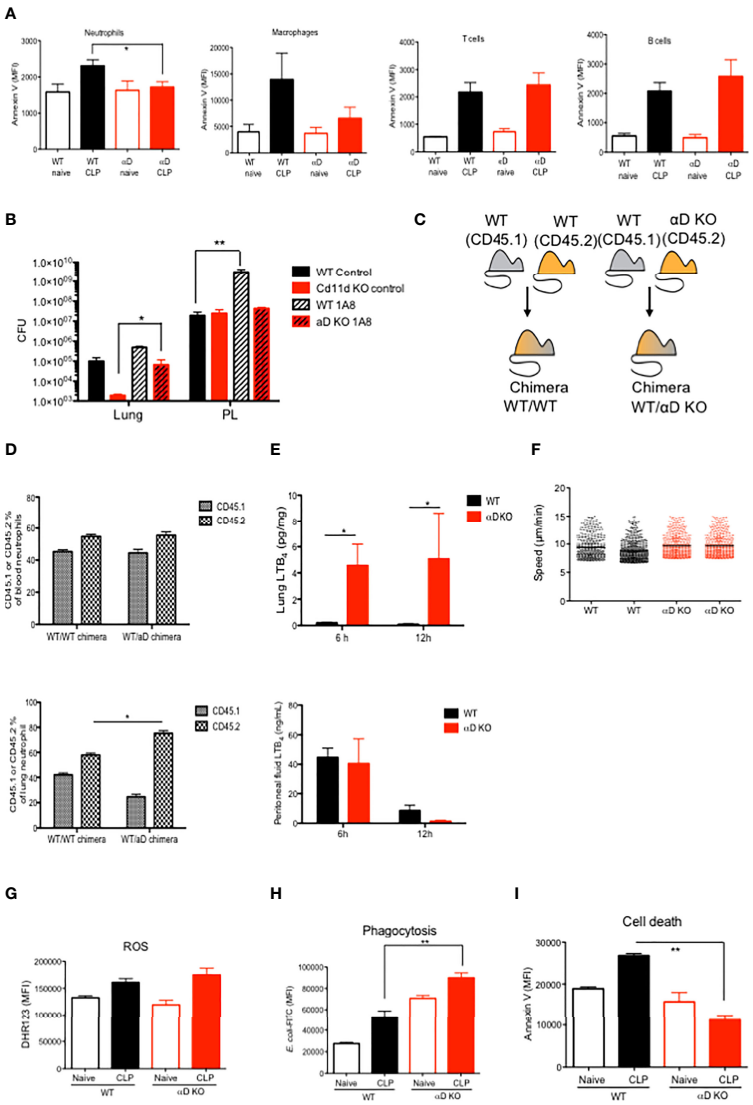

FIGURE 2
The functional of αDβ2 in neutrophils. **(A)** WT and αD KO lung leukocyte Annexin V expression at the baseline and at 12 hours after CLP. Data were shown as mean +/- S.D. of 4 mice. MFI; mean fluorescence intensity. One-way ANOVA with Bonferroni *post hoc* analysis was performed. *p < 0.05. **(B)** Bacterial loads at the lungs and the peritoneal lavage in WT and αD KO mice with or without neutrophil depletion. Mice were subjected to CLP sepsis and the samples were obtained at 12 hours after CLP. Data were shown as mean +/- S.D. of 6 mice. One-way ANOVA with Bonferroni *post hoc* analysis was performed. *p < 0.05, **p < 0.01. **(C)** Chimera scheme. **(D)** Blood and lung neutrophil analysis of chimeric mice at 12 hours after CLP. Data were shown as mean +/- S.D. of 4 mice. One-way ANOVA with Bonferroni *post hoc* analysis was performed. *p < 0.05. **(E)** Lung and peritoneal cavity LTB_4 levels at 6 and 12 hours after CLP. Data were shown as mean +/- S.D. of 4 mice. One-way ANOVA with Bonferroni *post hoc* analysis was performed. *p < 0.05. **(F)** LTB_4 mediated bone marrow neutrophil chemotaxis assay. Each dot represents one neutrophil. One-way ANOVA with Bonferroni *post hoc* analysis was performed. No significance was observed. **(G)** Lung neutrophil ROS activity from naïve and post CLP mice. For CLP mice, lungs were obtained at 12 hours after CLP. Data were shown as mean +/- S.D. of 6 mice. One-way ANOVA with Bonferroni *post hoc* analysis was performed. No significance was observed. **(H)** Lung neutrophil phagocytosis activity from naïve and post CLP mice. For CLP mice, lungs were obtained at 12 hours after CLP. Data were shown as mean +/- S.D. of 6 mice. One-way ANOVA with Bonferroni *post hoc* analysis was performed. **p < 0.01. **(I)** Lung neutrophil Annexin V expression from naïve and post CLP mice. For CLP mice, lungs were obtained at 12 hours after CLP. Data were shown as mean +/- S.D. of 6 mice. One-way ANOVA with Bonferroni *post hoc* analysis was performed. **p < 0.01.

monocytes/macrophages (28). We examined the contribution of neutrophils to CLP sepsis in both WT and αD KO mice by depleting neutrophils using 1A8 antibody. Neutrophil depletion worsened both lung and peritoneal bacterial loads in WT mice, but it significantly worsened only lung bacterial loads in αD KO mice (Figure 2B), which would likely be due to the difference in lung bacterial loads after CLP between the two strains. While lung bacterial loads were significantly lower in αD KO mice receiving isotype control compared to WT mice receiving isotype control, they were comparable between WT and αD KO mice subjected to neutrophil depletion.

αD KO neutrophil demonstrated higher phagocytic ability, less apoptosis and more tissue recruitment

Although we observed the difference in neutrophil numbers in the lungs between WT and αD KO mice, it is yet to be determined if the result was intrinsically derived from integrin αD. To validate if the result of higher αD KO neutrophil numbers in the lungs is intrinsic, we generated mixed bone marrow chimera to harbor both WT and αD KO mice-derived hematopoietic systems, which were distinguished by congenic markers CD45.1 and CD45.2, respectively. Control mixed chimeras were made by the reconstitution of CD45.1 and CD45.2 WT bone marrow cells (Figure 2C). At 12 weeks after bone marrow transplantation, we examined peripheral blood and confirmed the peripheral blood leukocytes were constituted equally by CD45.1 and CD45.2 cells (data not shown). We found that more αD KO derived neutrophils existed in the lungs compared to WT (CD45.1) neutrophils, supporting that the phenotype was intrinsic to αD KO neutrophils (Figure 2D). LTB_4 is a major neutrophil chemoattractant. At 6 and 12 hours after CLP in WT and αD KO mice, we observed LTB_4 level was significantly higher in the lungs of αD KO mice (Figure 2E). In contrast, peritoneal LTB_4 level was not statistically significant between the strains. We did not see any difference in neutrophil recruitment to neutrophil chemoattractant LTB_4 *in vitro* (Figure 2F), indicating that the difference of numbers between WT and αD KO neutrophils in chimera' lungs was not driven by chemotaxis. Here we examined the role of αDβ2 in neutrophils using WT and αD KO neutrophils. The level of reactive oxygen species (ROS) production was comparable between WT and αD KO mice (Figure 2G), while there was an increased phagocytosis by lung αD KO neutrophils (Figure 2H), supporting the result of the *E. coli* injection model (Figure 1F). To examine if higher αD KO neutrophil counts in the lung is explained by neutrophil survival, we also examined the cell death of lung neutrophils. Consistent with the result of splenic neutrophil apoptosis, the cell death of αD KO lung neutrophils was less compared to WT neutrophils (Figure 2I), which at least in part explains these results. Taken together, αD KO mice demonstrated a difference in neutrophil phenotypes characterized as less cell death and more efficient phagocytosis in the lungs. Higher lung αD KO neutrophil counts will be likely in part responsible for less neutrophil cell death.

αD KO neutrophil transcriptomic analysis demonstrated the association between αD and proliferation, and phagocytosis

To further characterize αD KO neutrophils, we performed transcriptomic analysis of blood and lung neutrophils. We found only 5 DEGs in blood and 7 DEGs in lung between WT and αD KO mice at the baseline. One DEG was overlapped between blood and lung. This result suggested that the transcriptomic signature of WT and αD KO neutrophils in the blood and lung at the baseline was quite similar (Figure 3A). The DEG analysis of αD KO neutrophils at 12 hours post CLP vs at the baseline (time 0h) in blood and lung showed that there was no DEG in lung, suggesting that there was no DEGs in the lung between baseline and 12 hours post-CLP (Figure 3B). When we compared lung neutrophils between WT and αD KO mice, we identified 55 upregulated DEGs and 90 upregulated DEGs in αD KO lung neutrophils (Figure 3C). Upregulated genes include phagocytosis related genes (Figure 3D), and downregulated genes include cell arrest and proliferation genes (Figure 3E).

Human validation

Human neutrophils were previously reported to express αDβ2 (29). To determine the role of αDβ2 in human neutrophils, we performed CRISPR/Cas9 deletion of αD in HL-60 cells. Expression of αD was confirmed by flow cytometry (Figure 4A).

Phagocytosis, ROS, and apoptosis were examined. We found that phagocytosis was significantly enhanced in αD KO HL-60 cells compared to the control (Figure 4B). No difference in ROS was observed (Figure 4C). Cell death was attenuated in αD KO HL-60 cells (Figure 4D). This is consistent with the findings in murine experiment, indicating the relevance of our findings in human.

Discussion

Integrin αDβ2 was the last β2 integrin member cloned (30). β2 integrins work by binding to their ligands. Ligands for αLβ2 include intercellular adhesion molecule (ICAM)-1, -2, and -3,

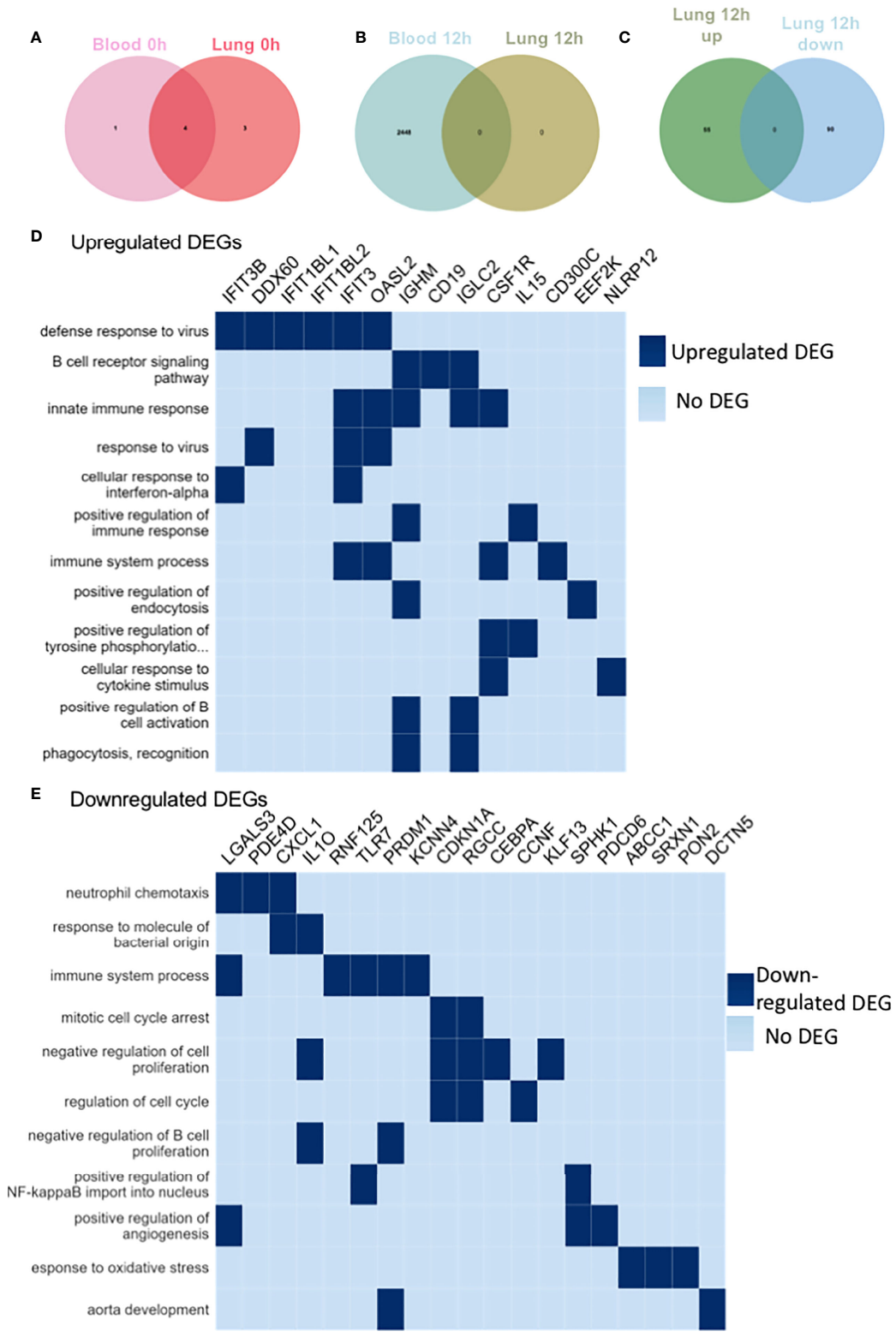

FIGURE 3 (Continued)

FIGURE 3 (Continued)
RNA sequencing of blood and lung neutrophils following CLP sepsis. RNA seq of triplicates for blood and lung neutrophils at baseline and 12 hours after CLP. Neutrophils were sorted by $CD45^+Ly6G^+CD11b^+$ population. **(A)** Venn diagram showing significant DEGs in the blood and lung of αD KO mice at 0h post-CLP compared to WT mice at 0h post-CLP. The light pink circle represents DEGs in the blood of αD KO mice at 0h post-CLP compared to the blood of WT mice at 0h post-CLP. The deep pink circle represents DEGs in the lung of αD KO mice at 0h post-CLP compared to the lung of WT mice at 0h post-CLP. The intersection of the two circles represents overlapping DEGs in the blood and lung of αD KO mice at 0h post-CLP compared to WT mice at 0h post-CLP. Overall, only 5 genes were differentially expressed in the blood of αD KO and 7 genes in the lungs of αD KO compared to the WT mice at the baseline (0h post-CLP) and 4 of these DEGs were common in the blood and lung, suggesting no significant differences in the transcriptomic profile of WT and αD KO mice at the baseline. **(B)** Venn diagram showing significant DEGs in the blood and lung of αD KO mice at 12h post-CLP compared to αD KO mice at 0h post-CLP. The light blue circle represents DEGs in the blood of αD KO mice at 12h post-CLP compared to the blood of αD KO mice at 0h post-CLP. The green circle represents DEGs in the lung of αD KO mice at 12h post-CLP compared to the lung of αD KO mice at 0h post-CLP. The intersection of the two circles represents overlapping DEGs in the blood and lung of αD KO mice at 12h post-CLP compared to αD KO mice at 0h post-CLP. Overall, 2448 genes were differentially expressed in the blood of αD KO at 12h post-CLP compared to 0h post-CLP and none was observed in the lungs, suggesting no differences in the transcriptomic profile of the lungs of αD KO mice between 0h and 12h post-CLP. **(C)** Venn diagram showing significant DEGs in the lung of αD KO mice at 12h post-CLP compared to WT mice at 12h post-CLP. The green circle represents DEGs upregulated in the lung of αD KO mice at 12h post-CLP compared to the lung of WT mice at 12h post-CLP. The blue circle represents DEGs downregulated in the lung of αD KO mice at 12h post-CLP compared to the lung of WT mice at 12h post-CLP. The intersection of the two circles represents overlapping DEGs in lung of αD KO mice at 12h post-CLP compared to WT mice at 12h post-CLP. Overall, 55 genes were significantly upregulated and 90 were significantly downregulated in the lung of αD KO at 12h post-CLP compared to WT mice at 12h post-CLP and these DEGs were used for pathway enrichment analysis **(D, E)**. **(D)** Pathway Enrichment Analysis (GO) of upregulated DEGs in the lung of αD KO mice at 12h post-CLP compared to WT mice at 12h post-CLP. Genes with adjusted p-values < 0.05 and absolute log2 fold change > 1 were considered differentially expressed genes. Heat map was created by plotting the enriched pathways and the genes that have contributed to the enrichment signal (indicated in deep blue). **(E)** Analysis of downregulated DEG pathway in lung of αD KO mice at 12h post-CLP compared to WT mice at 12h post-CLP. Genes with adjusted p-values < 0.05 and absolute log2 fold change > 1 were called differentially expressed genes.

while αMβ2 and αXβ2 bind to iC3b, ICAM-1, and fibrinogen. So far αDβ2 reportedly binds to ICAM-3, VCAM-1, and 2-(ω-carboxyethyl)pyrrole (CEP) (31). Those ligands have been reported from *in vitro* experiments, but how these ligand-αDβ2 interactions play a role *in vivo* has not been largely studied. αDβ2 expression on macrophages (30) and neutrophils (29, 32) has been reported. Foam cells are a type of macrophages that localize to fatty deposits on blood vessels. αDβ2 deficiency was associated with less lipid deposition in the atherosclerosis model (28). The involvement of αDβ2 in spinal cord injury was also described in the context of neutrophil invasion. The administration of anti-αD antibody attenuated spinal cord injury in rats (32, 33). In the context of infection, de Azevedo-Quintanilha et al. reported that αD KO mice demonstrated less lung injury in Malaria infection model (34). Here we reported a novel role of αDβ2 in sepsis model. The deficiency of αDβ2 attenuated lung injury and sepsis outcome, which is significantly important given that a specific treatment is urgently needed for sepsis.

For the first time, we showed that the deficiency of αDβ2 led to 1) the enhancement of phagocytosis and 2) the attenuation of cell death in neutrophils. This finding is interesting in contrast to αMβ2. αMβ2 is also called complement receptor 3 (CR3), and serves as one of the major phagocytosis receptors by binding to iC3b. αMβ2 also affects apoptosis. The deficiency of αMβ2 leads to the defect in apoptosis in the setting of infection (13). The mechanism of apoptosis induction *via* αMβ2 is not completely delineated yet, but it is proposed that phagocytosis of iC3b coated microbes induces ROS production, which leads to apoptosis (35). The major phagocytosis receptors include Fcγ receptor and αMβ2. At this point, it is unclear how the deficiency of αDβ2 leads to an enhancement of phagocytosis. Given that αMβ2 and αDβ2 have high sequence homology, αDβ2 could compete iC3b coated microbes against αMβ2. However, iC3b has not been reported as a ligand for αDβ2. In addition, the attenuation of apoptosis by αDβ2 is also confusing. If αDβ2 deficiency increases phagocytosis, ROS may increase, leading to more apoptosis based on the theory of αMβ2-mediated apoptosis.

The HL-60 cell experiment showed that the effect of αDβ2 on cell death is cell intrinsic. Thus, it is interesting how αDβ2 plays a functional role within neutrophils. Although αLβ2 and αMβ2 bind to ligands outside their cells for their activity, we previously reported that αXβ2 has its own ligand within neutrophils. It may be possible that αDβ2 has its intrinsic ligand within the cell, or surrounding HL-60 cells. For example, ICAM-3 is expressed on neutrophils, serving as a ligand for αDβ2. ICAM-3 binding to neutrophils induces apoptosis (36), so the deficiency of αDβ2 may lessen this interaction, leading to less apoptosis.

From sepsis standpoint, lung injury is one of the most serious organ injuries that patients succumbed to. The mortality of patients with lung injury in sepsis is quite high. Thus, our finding will offer a very interesting target for sepsis therapeutic. So far there is no αDβ2 antagonist reported. We primarily focused on the role of αDβ2 in sepsis in this study. It is also interesting to examine the role of this molecule in other disease states such as cancers. Among β2 integrin

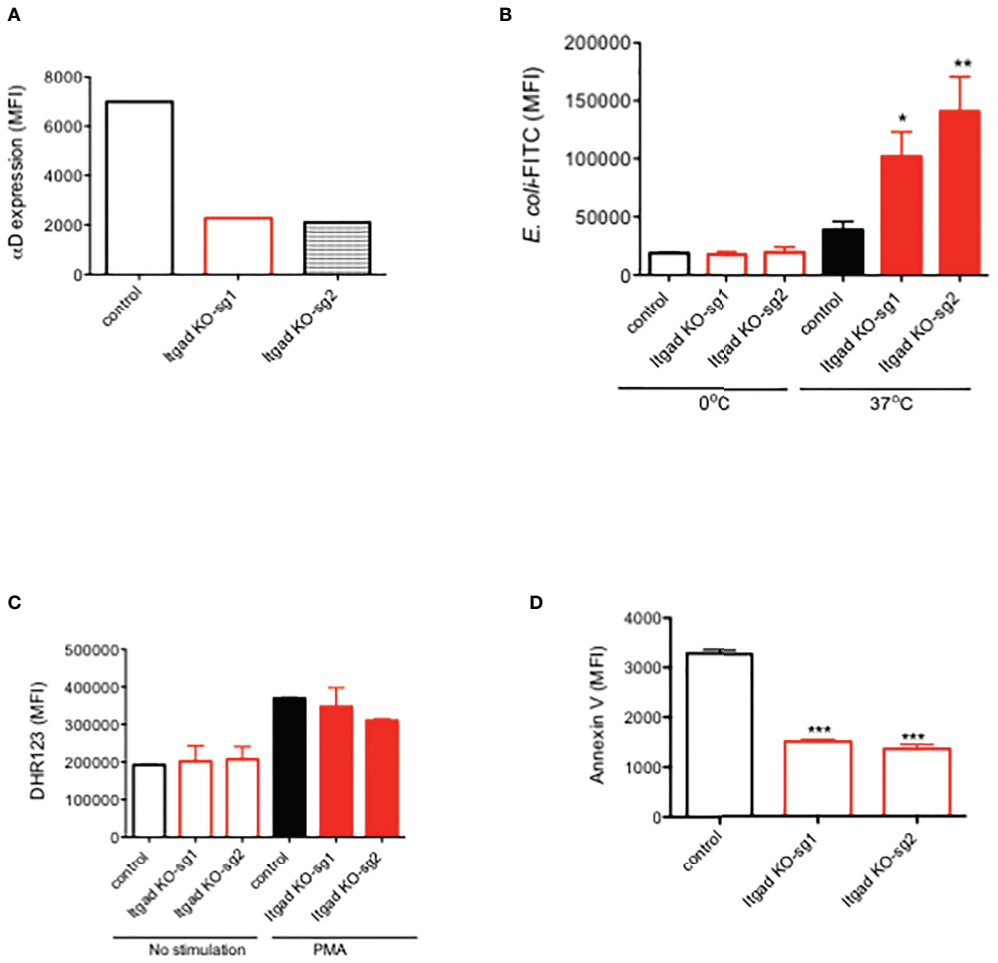

FIGURE 4
The role of αDβ2 in human HL60 cells. **(A)** αD expression of HL60 cells with or without αD CRISPR/Cas9 deletion. Representative data was shown. **(B)** Phagocytosis, **(C)** ROS, and **(D)** Annexin V expression of HL60 cells with or without αD CRISPR/Cas9 deletion. Data were shown as mean +/- S.D. of triplicates. Sg1 and sg2 denote two different guide RNA. One-way ANOVA with Bonferroni *post hoc* analysis was performed. *P < 0.05, **p < 0.01, ***p < 0.001.

members, αMβ2 has been most extensively studied in the context of cancer. Its inhibition enhanced tumor response to radiation (37). Its deficiency suppressed intestinal tumor growth (38). However, its agonist LA1 was reported to attenuate tumor growth (39). Thus, the role of αMβ2 in cancer may not be straightforward. So far there is a limited data available on the role of αDβ2 in cancer, which needs future study.

In conclusion, we found a novel role of αDβ2 in neutrophils and sepsis. Delineating the underlying mechanism of αDβ2-mediated modulation of neutrophil functions will help us to understand how αDβ2 contributes to sepsis pathophysiology for considering as a future therapeutic target.

Data availability statement

The data presented in the study are deposited in the Gene Expression Omnibus (GEO) repository accession number GSE215749.

Ethics statement

The animal study was reviewed and approved by Boston Children's Hospital IACUC.

Author contributions

SK - Designed experiment, performed experiment and wrote manuscript. LH - Designed experiment and performed experiment. TO - Designed experiment and performed experiment MS-F - Designed experiment and performed experiment. HL - Designed experiment KY - Designed experiment, performed experiment and wrote manuscript. All authors contributed to the article and approved the submitted version.

Funding

This study was in part supported by R21HD099194 (KY, SK).

Conflict of interest

The authors declare that the research was conducted in the absence of any commercial or financial relationships that could be construed as a potential conflict of interest.

Publisher's note

References

1. Kishimoto TK, Springer TA. Human leukocyte adhesion deficiency: Molecular basis for a defective immune response to infections of the skin. *Curr Probl Dermatol* (1989) 18:106–15. doi: 10.1159/000416845

2. Evans R, Patzak I, Svensson L, De Filippo K, Jones K, McDowall A, et al. Integrins in immunity. *J Cell Sci* (2009) 122:215–25. doi: 10.1242/jcs.019117

3. Dunne JL, Ballantyne CM, Beaudet AL, Ley K. Control of leukocyte rolling velocity in TNF-alpha-induced inflammation by LFA-1 and mac-1. *Blood* (2002) 99:336–41. doi: 10.1182/blood.V99.1.336

4. Harris ES, McIntyre TM, Prescott SM, Zimmerman GA. The leukocyte integrins. *J Biol Chem* (2000) 275:23409–12. doi: 10.1074/jbc.R000004200

5. Liu JR, Han X, Soriano SG, Yuki K. The role of macrophage 1 antigen in polymicrobial sepsis. *Shock* (2014) 42:532–9. doi: 10.1097/SHK.0000000000000250

6. Liu JR, Han X, Soriano SG, Yuki K. Leukocyte function-associated antigen-1 deficiency impairs responses to polymicrobial sepsis. *World J Clin cases* (2015) 3:793–806. doi: 10.12998/wjcc.v3.i9.793

7. Koutsogiannaki S, Schaefers MM, Okuno T, Ohba M, Yokomizo T, Priebe GP, et al. From the cover: Prolonged exposure to volatile anesthetic isoflurane worsens the outcome of polymicrobial abdominal sepsis. *Toxicol Sci* (2017) 156:402–11. doi: 10.1093/toxsci/kfw261

8. Hou L, Voit RA, Sankaran VG, Springer TA, Yuki K. CD11c regulates hematopoietic stem and progenitor cells under stress. *Blood Adv* (2020) 4:6086–97. doi: 10.1182/bloodadvances.2020002504

9. Guo RF, Riedemann NC, Laudes IJ, Sarma VJ, Kunkel RG, Dilley KA, et al. Altered neutrophil trafficking during sepsis. *J Immunol* (2002) 169:307–14. doi: 10.4049/jimmunol.169.1.307

10. Seekamp A, Mulligan MS, Till GO, Smith CW, Miyasaka M, Tamatani T, et al. Role of beta 2 integrins and ICAM-1 in lung injury following ischemia-reperfusion of rat hind limbs. *Am J Pathol* (1993) 143:464–72.

11. Weiss SL, Peters MJ, Alhazzani W, Agus MSD, Flori HR, Inwald DP, et al. Surviving sepsis campaign international guidelines for the management of septic shock and sepsis-associated organ dysfunction in children. *Pediatr Crit Care Med* (2020) 21:e52–106. doi: 10.1097/PCC.0000000000002198

12. Ding ZM, Babensee JE, Simon SI, Lu H, Perrard JL, Bullard DC, et al. Relative contribution of LFA-1 and mac-1 to neutrophil adhesion and migration. *J Immunol* (1999) 163:5029–38.

13. Coxon A, Rieu P, Barkalow FJ, Askari S, Sharpe AH, von Andrian UH, et al. A novel role for the beta 2 integrin CD11b/CD18 in neutrophil apoptosis: a homeostatic mechanism in inflammation. *Immunity* (1996) 5:653–66. doi: 10.1016/S1074-7613(00)80278-2

14. Wu H, Rodgers JR, Perrard XY, Perrard JL, Prince JE, Abe Y, et al. Deficiency of CD11b or CD11d results in reduced staphylococcal enterotoxin-induced T cell response and T cell phenotypic changes. *J Immunol* (2004) 173:297–306. doi: 10.4049/jimmunol.173.1.297

15. Koutsogiannaki S, Bernier R, Tazawa K, Yuki K. Volatile anesthetic attenuates phagocyte function and worsens bacterial loads in wounds. *J Surg Res* (2019) 233:323–30. doi: 10.1016/j.jss.2018.07.075

16. Osaka M, Ito S, Honda M, Inomata Y, Egashira K, Yoshida M. Critical role of the C5a-activated neutrophils in high-fat diet-induced vascular inflammation. *Sci Rep* (2016) 6:21391. doi: 10.1038/srep21391

17. Erickson SE, Martin GS, Davis JL, Matthay MA, Eisner MD, Network NNA. Recent trends in acute lung injury mortality: 1996-2005. *Crit Care Med* (2009) 37:1574–9. doi: 10.1097/CCM.0b013e31819fefdf

18. Okuno T, Koutsogiannaki S, Hou L, Bu W, Ohto U, Eckenhoff RG, et al. Volatile anesthetics isoflurane and sevoflurane directly target and attenuate toll-like receptor 4 system. *FASEB J* (2019) 33:14528–41. doi: 10.1096/fj.201901570R

19. Bak RO, Dever DP, Porteus MH. CRISPR/Cas9 genome editing in human hematopoietic stem cells. *Nat Protoc* (2018) 13:358–76. doi: 10.1038/nprot.2017.143

20. Bao EL, Nandakumar SK, Liao X, Bick AG, Karjalainen J, Tabaka M, et al. Inherited myeloproliferative neoplasm risk affects haematopoietic stem cells. *Nature* (2020) 586:769–75. doi: 10.1038/s41586-020-2786-7

21. Vaidyanathan S, Salahudeen AA, Sellers ZM, Bravo DT, Choi SS, Batish A, et al. High-efficiency, selection-free gene repair in airway stem cells from cystic fibrosis patients rescues CFTR function in differentiated epithelia. *Cell Stem Cell* (2020) 26:161–71.e164. doi: 10.1016/j.stem.2019.11.002

22. Buras JA, Holzmann B, Sitkovsky M. Animal models of sepsis: setting the stage. *Nat Rev Drug Discov* (2005) 4:854–65. doi: 10.1038/nrd1854

23. Rittirsch D, Huber-Lang MS, Flierl MA, Ward PA. Immunodesign of experimental sepsis by cecal ligation and puncture. *Nat Protoc* (2009) 4:31–6. doi: 10.1038/nprot.2008.214

24. Thompson BT, Chambers RC, Liu KD. Acute respiratory distress syndrome. *N Engl J Med* (2017) 377:1904–5. doi: 10.1056/NEJMra1608077

25. Hotchkiss RS, Chang KC, Swanson PE, Tinsley KW, Hui JJ, Klender P, et al. Caspase inhibitors improve survival in sepsis: a critical role of the lymphocyte. *Nat Immunol* (2000) 1:496–501. doi: 10.1038/82741

26. Hotchkiss RS, Nicholson DW. Apoptosis and caspases regulate death and inflammation in sepsis. *Nat Rev Immunol* (2006) 6:813–22. doi: 10.1038/nri1943

27. Koutsogiannaki S, Hou L, Babazada H, Okuno T, Blazon-Brown N, Soriano SG, et al. The volatile anesthetic sevoflurane reduces neutrophil apoptosis *via* fas death domain-fas-associated death domain interaction. *FASEB J* (2019) 33:12668–79. doi: 10.1096/fj.201901360R

28. Aziz MH, Cui K, Das M, Brown KE, Ardell CL, Febbraio M, et al. The upregulation of integrin alphaDbeta2 (CD11d/CD18) on inflammatory macrophages promotes macrophage retention in vascular lesions and development of atherosclerosis. *J Immunol* (2017) 198:4855–67. doi: 10.4049/jimmunol.1602175

29. Miyazaki Y, Vieira-de-Abreu A, Harris ES, Shah AM, Weyrich AS, Castro-Faria-Neto HC, et al. Integrin alphaDbeta2 (CD11d/CD18) is expressed by human circulating and tissue myeloid leukocytes and mediates inflammatory signaling. *PloS One* (2014) 9:e112770. doi: 10.1371/journal.pone.0112770

30. Van der Vieren M, Le Trong H, Wood CL, Moore PF, St John T, Staunton DE, et al. A novel leukointegrin, alpha d beta 2, binds preferentially to ICAM-3. *Immunity* (1995) 3:683–90. doi: 10.1016/1074-7613(95)90058-6

31. Yakubenko VP, Cui K, Ardell CL, Brown KE, West XZ, Gao D, et al. Oxidative modifications of extracellular matrix promote the second wave of inflammation *via* beta2 integrins. *Blood* (2018) 132:78–88. doi: 10.1182/blood-2017-10-810176

32. Geremia NM, Hryciw T, Bao F, Streijger F, Okon E, Lee JHT, et al. The effectiveness of the anti-CD11d treatment is reduced in rat models of spinal cord injury that produce significant levels of intraspinal hemorrhage. *Exp Neurol* (2017) 295:125–34. doi: 10.1016/j.expneurol.2017.06.002

33. Saville LR, Pospisil CH, Mawhinney LA, Bao F, Simedrea FC, Peters AA, et al. A monoclonal antibody to CD11d reduces the inflammatory infiltrate into the injured spinal cord: a potential neuroprotective treatment. *J Neuroimmunol* (2004) 156:42–57. doi: 10.1016/j.jneuroim.2004.07.002

34. de Azevedo-Quintanilha IG, Vieira-de-Abreu A, Ferreira AC, Nascimento DO, Siqueira AM, Campbell RA, et al. Integrin alphaDbeta2 (CD11d/CD18) mediates experimental malaria-associated acute respiratory distress syndrome (MA-ARDS). *Malar J* (2016) 15:393. doi: 10.1186/s12936-016-1447-7

35. Mayadas TN, Cullere X. Neutrophil beta2 integrins: moderators of life or death decisions. *Trends Immunol* (2005) 26:388–95. doi: 10.1016/j.it.2005.05.002

36. Kessel JM, Sedgwick JB, Busse WW. Ligation of intercellular adhesion molecule 3 induces apoptosis of human blood eosinophils and neutrophils. *J Allergy Clin Immunol* (2006) 118:831–6. doi: 10.1016/j.jaci.2006.05.026

37. Ahn GO, Tseng D, Liao CH, Dorie MJ, Czechowicz A, Brown JM. Inhibition of mac-1 (CD11b/CD18) enhances tumor response to radiation by reducing myeloid cell recruitment. *Proc Natl Acad Sci USA* (2010) 107:8363–8. doi: 10.1073/pnas.0911378107

38. Zhang QQ, Hu XW, Liu YL, Ye ZJ, Gui YH, Zhou DL, et al. CD11b deficiency suppresses intestinal tumor growth by reducing myeloid cell recruitment. *Sci Rep* (2015) 5:15948. doi: 10.1038/srep15948

39. Schmid MC, Khan SQ, Kaneda MM, Pathria P, Shepard R, Louis TL, et al. Integrin CD11b activation drives anti-tumor innate immunity. *Nat Commun* (2018) 9:5379. doi: 10.1038/s41467-018-07387-4

frontiers | Frontiers in Immunology

TYPE Original Research
PUBLISHED 21 December 2022
DOI 10.3389/fimmu.2022.1110602

OPEN ACCESS

EDITED BY
Peisong Gao,
Johns Hopkins University,
United States

REVIEWED BY
Bin Yi,
Army Medical University, China
Jie Sun,
Southeast University, China

*CORRESPONDENCE
Wangyuan Zou
wangyuanzou@csu.edu.cn

SPECIALTY SECTION
This article was submitted to Inflammation, a section of the journal Frontiers in Immunology

RECEIVED 29 November 2022
ACCEPTED 12 December 2022
PUBLISHED 21 December 2022

CITATION
Liang S, Xing M, Chen X, Peng J, Song Z and Zou W (2022) Predicting the prognosis in patients with sepsis by a pyroptosis-related gene signature.
Front. Immunol. 13:1110602.
doi: 10.3389/fimmu.2022.1110602

Predicting the prognosis in patients with sepsis by a pyroptosis-related gene signature

Shuang Liang[1], Manyu Xing[1], Xiang Chen[1], Jingyi Peng[1], Zongbin Song[1] and Wangyuan Zou[1,2]*

[1]Department of Anesthesiology, Xiangya Hospital, Central South University, Changsha, Hunan, China, [2]National Clinical Research Center for Geriatric Disorders, Xiangya Hospital, Central South University, Changsha, Hunan, China

Background: Sepsis remains a life-threatening disease with a high mortality rate that causes millions of deaths worldwide every year. Many studies have suggested that pyroptosis plays an important role in the development and progression of sepsis. However, the potential prognostic and diagnostic value of pyroptosis-related genes in sepsis remains unknown.

Methods: The GSE65682 and GSE95233 datasets were obtained from Gene Expression Omnibus (GEO) database and pyroptosis-related genes were obtained from previous literature and Molecular Signature Database. Univariate cox analysis and least absolute shrinkage and selection operator (LASSO) cox regression analysis were used to select prognostic differentially expressed pyroptosis-related genes and constructed a prognostic risk score. Functional analysis and immune infiltration analysis were used to investigate the biological characteristics and immune cell enrichment in sepsis patients who were classified as low- or high-risk based on their risk score. Then the correlation between pyroptosis-related genes and immune cells was analyzed and the diagnostic value of the selected genes was assessed using the receiver operating characteristic curve.

Results: A total of 16 pyroptosis-related differentially expressed genes were identified between sepsis patients and healthy individuals. A six-gene-based (*GZMB, CHMP7, NLRP1, MYD88, ELANE*, and *AIM2*) prognostic risk score was developed. Based on the risk score, sepsis patients were divided into low- and high-risk groups, and patients in the low-risk group had a better prognosis. Functional enrichment analysis found that NOD-like receptor signaling pathway, hematopoietic cell lineage, and other immune-related pathways were enriched. Immune infiltration analysis showed that some innate and adaptive immune cells were significantly different between low- and high-

risk groups, and correlation analysis revealed that all six genes were significantly correlated with neutrophils. Four out of six genes (*GZMB, CHMP7, NLRP1*, and *AIM2)* also have potential diagnostic value in sepsis diagnosis.

Conclusion: We developed and validated a novel prognostic predictive risk score for sepsis based on six pyroptosis-related genes. Four out of the six genes also have potential diagnostic value in sepsis diagnosis.

KEYWORDS

sepsis, pyroptosis, gene, prediction, prognosis, diagnosis

Introduction

Sepsis is a dysregulation of the host's response to infection, which is frequently accompanied by life-threatening organ dysfunction (1, 2). Despite advances in our understanding of sepsis, supportive therapies including early fluid resuscitation, the use of antibiotics, and the provision of supportive care for organ function have remained the standard of care, and the mortality rate of sepsis is still high, reaching about 26% (3, 4). Early diagnosis and intervention those sepsis patients who are associated with increased mortality risk are critical for a better prognosis (5). Therefore, it is important to explore diagnostic and prognostic signatures in sepsis patients.

Pyroptosis is a novel form of proinflammatory and programmed cell death, which also participates in the response of the innate immune system (6). With the clarification of the mechanism of pyroptosis, it is now considered that pyroptosis is mediated by the activation of the gasdermin-D (GSDMD) protein *via* the active caspase-1 (canonical pathway) or the active caspase-4/5/11 (non-canonical pathway), which causes cell swelling, rupture, and the release of inflammatory cytokines such as Interleukin 18 (IL-18) and Interleukin 1 β (IL-1β) (7–9). Previous studies demonstrated that pyroptosis may play an important role in the development of sepsis and sepsis-related organ dysfunction including acute kidney injury (10), acute lung injury (11), cardiac dysfunction (12), and disseminated intravascular coagulation (13). Therefore, pyroptosis-related genes were recognized as promising therapeutic targets of sepsis (14), and treatment by using non-specific or specific caspase inhibitors has shown therapeutic effects in experimental studies (15, 16). However, few studies focused on the value of the pyroptosis-related gene in predicting the prognosis and diagnosis of sepsis, and the prognostic and diagnostic value of pyroptosis-related genes have not been fully investigated.

In this study, we identified molecular subtypes of sepsis based on pyroptosis-related genes, developed and validated a novel pyroptosis-related prognostic risk score for sepsis patients, and investigated the correlation between pyroptosis-related genes and the immune cells. Based on the prognostic risk score and clinical characteristics of sepsis patients, a nomogram was created, and the diagnostic value of pyroptosis-related genes was also assessed. Our findings may provide new insight into the role of pyroptosis in the prognosis and diagnosis of sepsis.

Materials and methods

Microarray data and data process

Two peripheral-blood gene expression datasets (GSE65682 and GSE95233) and their corresponding clinical data were obtained from Gene Expression Omnibus (GEO) database (https://www.ncbi.nlm.nih.gov/gds/). The GSE65682 dataset and GSE95233 dataset were based on GPL13667 and GPL570 platforms, respectively. The GSE65682 dataset comprised 479 sepsis patients with complete data for survival status within 28 days and 42 healthy controls. Sepsis patients in GSE65682 were separated into the discovery cohort (n = 263) and validation cohort (n = 216) for its original investigation and we used these two cohorts for survival analysis in our study. The GSE95233 dataset comprised 51 sepsis patients and 22 healthy controls. Only the gene expression data of the blood sample collected at admission to the intensive care unit was used for analysis in the present study.

The gene probe was transformed into gene symbol by using the corresponding annotation profile in each dataset. We used 'limma' package in R software to quartile normalized for all gene expression values and generate normally distributed expression

values. For multiple same probes, the finial gene expression value was determined by calculating the average expression value.

Screening pyroptosis-related differentially expressed genes and consensus clustering analysis

A total of 60 pyroptosis-related genes were identified from gene set enrichment analysis (GSEA) website (http://www.gsea-msigdb.org/gsea/index.jsp) and previous literature (17–21) (Supplementary Table 1). Differentially expressed genes (DEGs) between sepsis and healthy samples in GSE65682 were screened using the 'limma' package, with $\log_2|\text{fold change}| > 0.5$ and adjust P value< 0.05 set as cut-off criteria to screen DEGs (22, 23). Pyroptosis-related DEGs were identified by intersecting the DEGs with the pyroptosis-related genes. A protein-protein interaction (PPI) network analysis was conducted by using the STRING website (https://cn.string-db.org/) to further explore the interaction between these pyroptosis-related genes. Based on the expression value of pyroptosis-related DEGs, we used "ConsensusClusterPlus" package to identify the molecular subtype of sepsis. The pam algorithm with euclidean distance was used, and the samples were iterated 1000 times. The k value was increased from 2 to 6 to identify the optimal clusters.

Identification of survival-related pyroptosis-related genes and construction of a prediction model for prognosis

Univariate Cox regression analysis was performed in the discovery cohort to evaluate the prognostic value of each pyroptosis-related DEGs. To avoid omissions, we set a P-value lower than 0.2 as a significant cut-off value (24). Pyroptosis-related DEGs with a significant correlation to survival status were selected as candidate genes for further investigation. Then, we used LASSO-Cox regression *via* 'glmnet' packages to screen the candidate genes and construct the prediction model. The penalty coefficient λ was determined by using the minimal criteria and candidate genes with a regression coefficient unequal to zero were included in the final model. The risk score of each case was calculated according to the following formula: $\text{Risk score} = \sum_i^k \text{Coefficient i} \times \text{Gene Expression value of i}$. After that, sepsis patients were divided into low- and high-risk groups based on the median risk score, and the survival time between the two risk groups was compared using Kaplan-Meier analysis. Time-dependent receiver operating characteristic (ROC) curve analysis was also performed by using 'survival', 'surviminer', 'timeROC' packages to assess the discrimination ability of the risk score. The risk score was further validated in the validation cohort and the whole sepsis patients in GSE65682 (test cohort). Furthermore, we compared the 28-day mortality rate of sepsis patients from the GSE95233 dataset who were classified as low- or high-risk based on risk score (GSE95233 cohort). We were unable to perform the Kaplan-Meier analysis because the GSE95233 dataset lacked "time to event" data. A ROC curve was depicted *via* 'pROC' package.

Independent prognostic evaluation of the risk score and construction of nomogram

Clinical information (age and sex) was extracted from patients in the GSE65682 dataset. These variables and risk score were analyzed together in univariate and multivariate Cox regression analyses. The 'rms' package was used to create a nomogram based on independent variables for visualization and potential clinical use in predicting the prognosis of sepsis patients. The ROC curve and calibration curve were used to assess the nomogram's performance.

Functional enrichment analysis and immune infiltration analysis

We used 'limma' package again and based on the same criteria ($\log_2|\text{fold change}| > 0.5$ and adjust P value< 0.05) to screen DEGs between low- and high-risk groups in the sepsis patients from GSE65682. To explore the DEGs-related signal pathways and biological function, "clusterprofiler" package (25) was applied to perform the Kyoto Encyclopedia of Genes and Genomes (KEGG) and Gene Ontology (GO) enrichment analysis. To quantify the relative proportion of immune cell infiltration, we used the CIBERSORT algorithm (26) with 1000 permutations to calculate 22 types of immune cell composition for each sample. The composition of these immune cells between low- and high-risk groups was compared *via* wilcoxson test. In addition, we performed a correlation analysis between the differentially immune cells and the pyroptosis-related genes.

Evaluation of the diagnostic value of the selected genes

We further investigated whether the selected prognostic pyroptosis-related genes also have potential value in the diagnosis of sepsis. The performance of these genes was

evaluated using the ROC curves in the GSE65682 dataset and GSE95233 dataset.

Statistical analysis

All statistical analyses were performed using R software (version 4.1.0) and R studio (Version 1.2.5042). The wilcoxon test was used to compare the gene expression level between sepsis patients and healthy individuals, and the composition of immune cells between low- and high-risk groups. Pearson chi-square test was applied to compare categorical variables. LASSO-Cox regression was used for candidate genes selection. The Kaplan-Meier method and log-rank test were used to compare the survival rate between the low- and high-risk groups. Univariate and multivariate cox regression analyses were used to assess the independent prognostic variables. A two-tailed *P* value<0.05 was considered statistically significant except for a certain *P* value was set.

Results

Identification of pyroptosis-related DEGs between sepsis patients and healthy individuals

A total of 3469 DEGs were identified from the GSE65682 dataset between sepsis and healthy samples, including 1571 upregulated genes and 1898 downregulated genes (Figure 1A; Supplementary Table 2). After intersecting with the pyroptosis-related genes, 16 pyroptosis-related DEGs were obtained (Figure 1B). Among them, the expression level of 7 genes (*MYD88, NLRP3, TLR2, CASP5, NLRC4, ELANE, AIM2*) were upregulated, while the expression level of 9 genes (*GZMB, CHMP7, NLRP1, IRF1, PLCG1, SCAF11, AKT1, GSDMB, IRF2*) were downregulated (Figure 1C). The result of the PPI analysis was presented in Figure 1D. There were 40 interaction relationships between these pyroptosis-related DEGs.

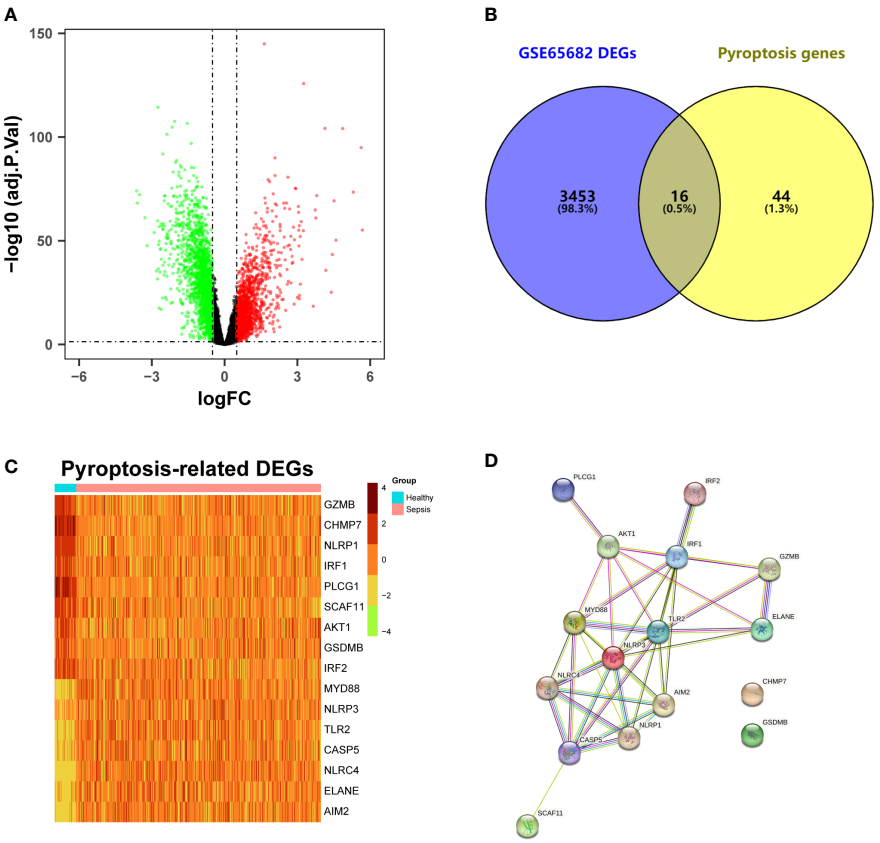

FIGURE 1
Identification of differentially expressed pyroptosis-related genes and interaction. **(A)** Volcano plot of DEGs in the GSE65682 dataset between sepsis patients and healthy individuals. **(B)** Venn plot of the DEGs and pyroptosis genes. **(C)** Heatmap of pyroptosis-related DEGs. **(D)** Protein-protein interaction (PPI) network analysis of proteins encoded by the pyroptosis-related DEGs.

Consensus clustering analysis based on the pyroptosis-related DEGs

According to the empirical CDF value, k = 2 was found to be the most acceptable point for the consensus cluster with the most distinct differences between clusters (Figure 2A; Supplementary Figure 1). Some of the expression levels of the pyroptosis-related DEGs were different between the two clusters (Figures 2B, D), and sepsis patients in cluster 1 had a worse prognosis than patients in cluster 2 (P = 0.0099) (Figure 2C).

Development of a prognostic risk score based on pyroptosis-related DEGs

Based on the univariate cox regression analysis, 10 out of 16 genes (*GZMB, CHMP7, NLRP1, IRF1, SCAF11, IRF2, MYD88, CASP5, ELANE, AIM2*) met P< 0.2 and were selected as prognostic candidate genes (Figure 3A). Of the 10 prognostic candidate genes, 1 gene (*ELANE*) was associated with increased risk with (HR > 1), while the remaining 9 genes (*GZMB, CHMP7, NLRP1, IRF1, SCAF11, IRF2, MYD88, CASP5*) were

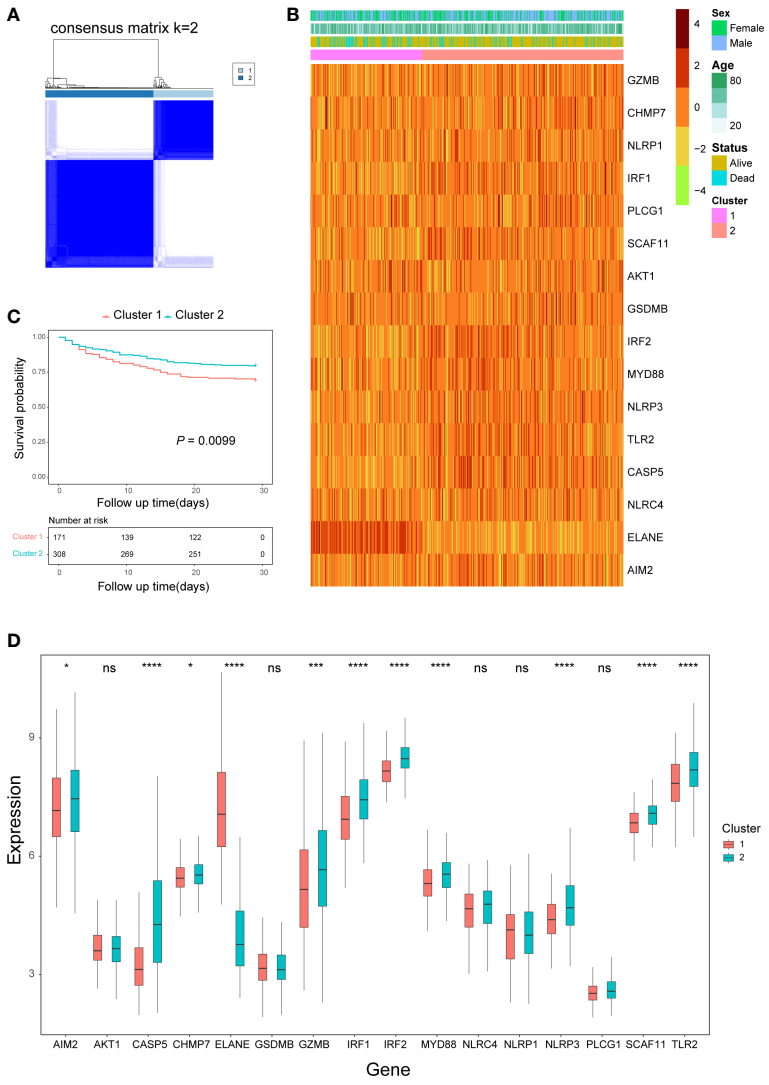

FIGURE 2
Consensus clustering analysis based on pyroptosis-related DEGs. **(A)** Consensus matrix when k=2. **(B)** Heatmap of pyroptosis-related DEGs expression and clinical characteristics in the two clusters. **(C)** Kaplan-Meier curves analysis for the survival of patients between the two clusters. **(D)** Box plots of pyroptosis-related DEGs expression level in the two clusters. ns, not significant; *P< 0.05,***P< 0.001, ****P< 0.0001.

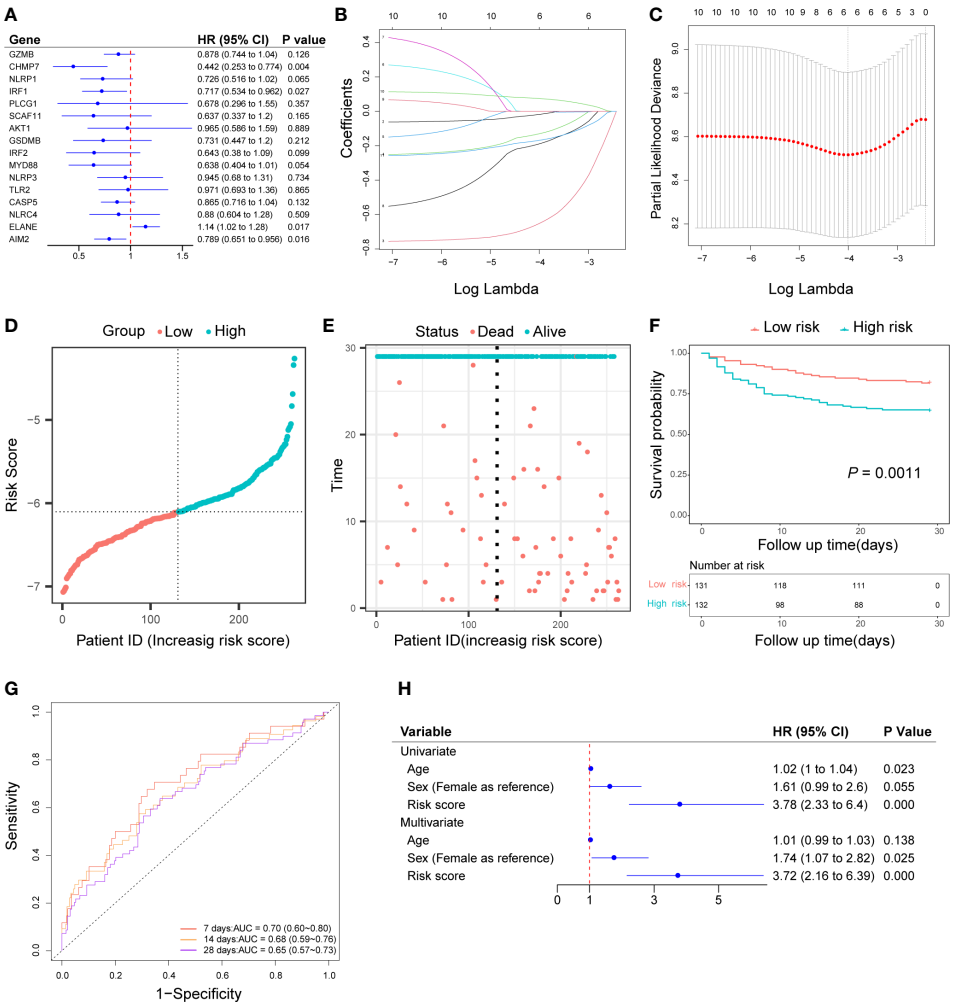

FIGURE 3
Construction of pyroptosis-related prognostic risk score and prediction of the prognosis in the discovery cohort. **(A)** Univariate cox regression analysis of survival for 16 pyroptosis-related DEGs, and 10 genes with a *P*< 0.2. **(B)** LASSO-Cox regression of the 10 candidate genes. **(C)** Cross-validation for tuning predictor selection. **(D)** Distribution of patients based on the risk score. **(E)** Survival time and status of patients. **(F)** Kaplan-Meier curves analysis for the survival of patients in low- and high-risk groups. **(G)** Time-dependent receiver operating characteristic curve for 7-, 14-, and 28-day survival of sepsis patients. **(H)** Univariate and multivariate cox regression.

associated with lower risk (HR< 1). By performing LASSO-Cox regression analysis with the above candidate genes, a subset of six genes (*GZMB, CHMP7, NLPR1, MYD88, ELANE, AIM2*) were determined to develop a prognostic risk score based on the minimal criteria of λ (Figures 3B, C). The calculation of the risk score for each sample was according to the formula as follows: Risk score = [(-0.01470407 x *GZMB* expression value) + (-0.63970285 x *CHMP7* expression value) + (-0.12447921 x *NLRP1* expression value) + (-0.18172740 x *MYD88* expression value) + (0.07255413 x *ELANE* expression value) + (-0.16451424 x *AIM2* expression value)]. After calculating the median risk score, 263 patients were stratified into two risk groups (131 in the low-risk group and 132 in the high-risk group) (Figure 3D). Patients in the high-risk group had more death (Figure 3E) and the Kaplan-Meier curve showed that patients in the low-risk group had a higher survival rate than those in the high-risk group (*P* = 0.0011, Figure 3F). Time-dependent ROC analysis of the risk score revealed that the area under the curve (AUC) was 0.70 (95% CI: 0.60 to 0.80), 0.68 (95% CI: 0.59 to 0.76), and 0.65 (95% CI: 0.57 to 0.73) for 7-, 14-, and 28-day survival, respectively (Figure 3G). Both univariate and multivariate cox regression analysis indicated that the risk score was an independent predictor for prognosis in sepsis patients (Univariate: HR = 3.78, 95% CI: 2.33 to 6.4, *P*< 0.001;

Multivariate: HR = 3.72, 95% CI: 2.16 to 6.39, $P< 0.001$; Figure 3H).

Validation of the prognostic risk score

Patients in the validation cohort and the test cohort were divided into two groups based on the median risk score, respectively (Figures 4A, E). Patients in the high-risk groups also occurred more death events (Figures 4B, F) and Kaplan-Meier curve showed that patients in the low-risk group had significantly higher survival rates than those in the high-risk group (In the validation cohort: $P = 0.013$, Figure 4C; In the test cohort: $P< 0.0001$, Figure 4G). AUC of the time-dependent ROC curve was 0.66 (95% CI: 0.53 to 0.79), 0.63 (95% CI: 0.52 to 0.73), and 0.64 (95% CI: 0.55 to 0.72) for 7-, 14-, and 28-day survival in the validation cohort (Figure 4D) and 0.69 (95% CI: 0.61 to 0.77), 0.65 (95% CI: 0.59 to 0.72), and 0.64 (95% CI: 0.59 to 0.70) for 7-, 14-, and 28-day survival in the test cohort (Figure 4H). According to the result of univariate and multivariate cox regression, the risk score also could be an independent prognostic factor in sepsis patients in these two cohorts (Supplementary Figure 2). In addition, patients in the low-risk group also had a higher survival rate than those in the high-risk group in the GSE95233 cohort ($P = 0.047$, Figure 4I). The AUC under the ROC curve was 0.687 (95% CI: 0.531 to 0.842) (Figure 4J).

Construction of a nomogram based on the risk score and independent clinical data

In order to potentially clinically used the risk score and predicted more precisely the prognosis of sepsis patients. We created a nomogram using the patient's age ($P = 0.029$, Supplementary Figure 2B) and risk score. (Figure 5A). The AUC of the nomogram for predicting 7-, 14-, and 28-day of survival were 0.69 (95% CI: 0.61 to 0.77), 0.69 (95% CI: 0.62 to 0.75), and 0.67 (95% CI: 0.61 to 0.72) (Figure 5B). The calibration curve indicated a good calibration between predicting probability and actual probability (Figures 5C–E).

Functional enrichment analysis between different risk groups

A total of 485 DEGs were identified between the low- and high-risk groups. Among them, 164 genes were downregulated and 321 genes were upregulated (Supplementary Table 3). On the basis of these DEGs, KEGG and GO analyses were performed. The results showed that the DEGs were mainly correlated with NOD-like receptor signaling pathway, hematopoietic cell lineage, and response to the virus (Figures 6A, B).

Comparison of immune infiltration between different risk groups

Based on the results of the functional analysis. We further compared immune infiltration between low- and high-risk groups by using the CIBERSORT algorithm. In the low-risk group, neutrophils, B cells memory, and mast cells activated were significantly higher than that in the high-risk group, while T cells CD4 naive, macrophages M0, mast cells resting, eosinophils, macrophages M2, plasma cells, and T cells CD4 memory resting were significantly lower (Figure 7A). The correlation analysis revealed that pyroptosis-related genes were significantly associated with many immune cells. All six genes were correlated with neutrophils, with *AIM2* (r = 0.34), *MYD88* (r = 0.4), and *NLRP1* (r = 0.47) showing a positive correlation, and *CHMP7* (r = -0.2), *ELANE* (r = -0.22), and *GZMB* (r = -0.17) showing a negative correlation (Figure 7B).

Performance of the selected pyroptosis-related genes in the diagnosis of sepsis

According to the ROC curves, four out of six genes (*GZMB, CHMP7, NLRP1*, and *AIM2*) had good diagnostic value in the diagnosis of sepsis, with AUC > 0.9 in both the GSE65682 and GSE95233 datasets (Figures 8A, B). In both datasets, the expression level of *AIM2*, *ELANE*, and *MYD88* were significantly higher in sepsis patients compared to healthy individuals, while the expression level of *CHMP7*, *GZMB*, and *NLRP1* were significantly lower. (Figures 8C, D).

Discussion

Over the past two decades, many biomarkers have been identified for sepsis including inflammatory factors, cell proteins, and miRNA (27). However, early diagnosis and prediction of the prognosis of sepsis are still difficult due to the complicated etiology, ambiguous pathogenic microorganisms, and early non-specific clinical signs of sepsis patients. Hence, it is still important to explore new biomarkers and provide new insight. In this study, we first identified 16 pyroptosis-related DEGs between sepsis patients and healthy individuals. Two pyroptosis-related sepsis clusters were identified and patients in cluster 1 had a poor prognosis than patients in cluster 2. To further explore the prognostic value of these genes, we constructed a prognostic risk score based on six genes' signatures *via* univariate cox regression analysis and LASSO-Cox regression analysis and validated its performance

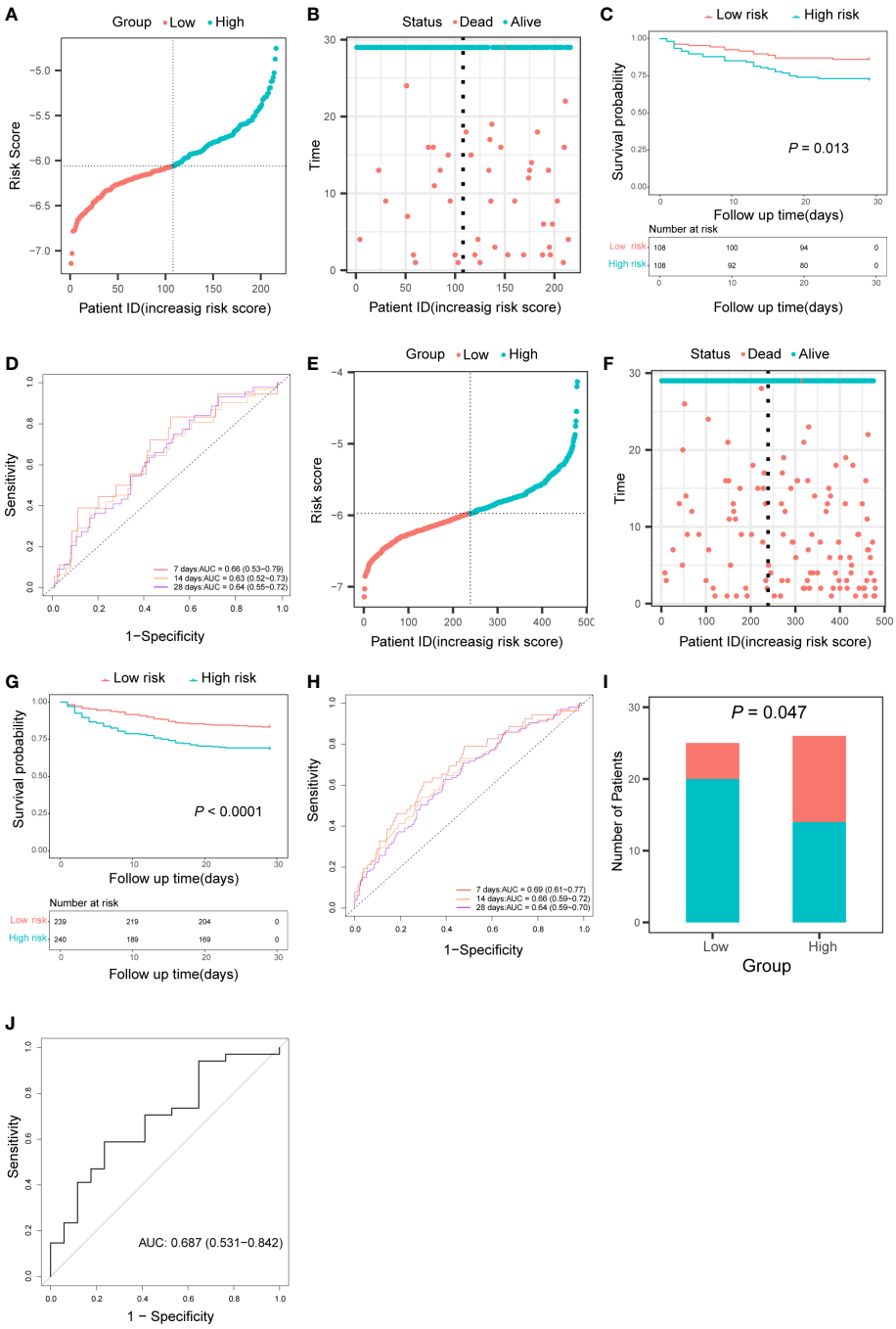

FIGURE 4
Validation of the pyroptosis-related prognostic risk score in the validation cohort, the test cohort, and the GSE95233 cohort. **(A, E)** Distribution of patients based on the risk score in the validation cohort **(A)** and the test cohort **(E)**. **(B, F)** Survival time and status of patients in the validation cohort **(B)** and the test cohort **(F)**. **(C, G)** Kaplan-Meier curves analysis for the survival of patients in low- and high-risk groups in the validation cohort **(C)** and the test cohort **(G)**. **(D, H)** Time-dependent receiver operating characteristic curve for 7-, 14-, and 28-day survival of patients in the validation cohort **(D)** and the test cohort **(H)**. **(I)** The survival of patients in low- and high-risk groups in the GSE95233 cohort. **(J)** Receiver operating characteristic curve for 28 days survival of patients in the GSE95233 dataset.

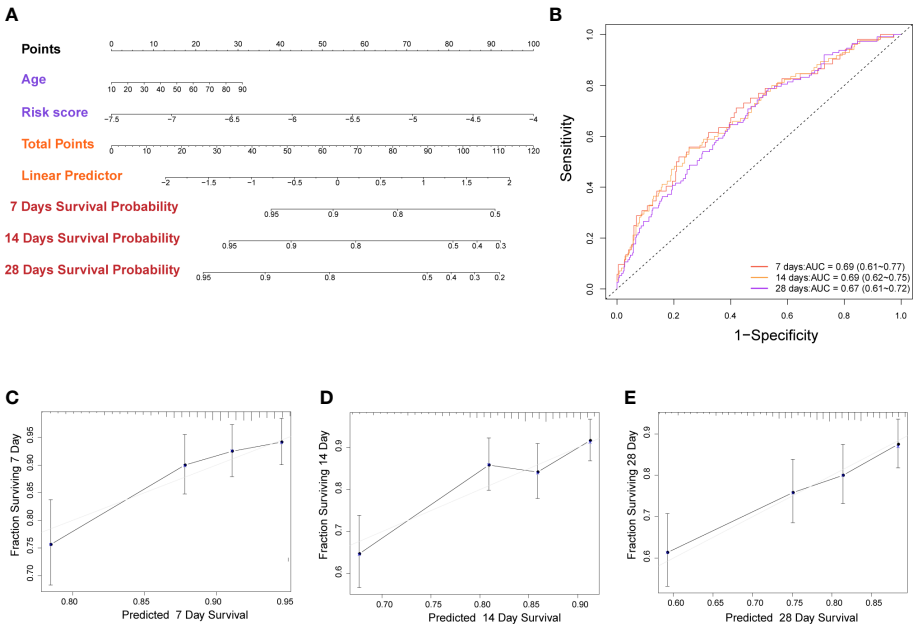

FIGURE 5
Construction of nomogram based on the pyroptosis-related prognostic risk score and clinical characteristic. **(A)** Nomogram for predicting 7-, 14-, and 28-day survival for sepsis patients. **(B)** Time-dependent receiver operating characteristic curves for 7-, 14-, and 28-day survival of patients. **(C-E)** Calibration curve of the nomogram for predicting 7-, 14-, and 28-day survival of patients.

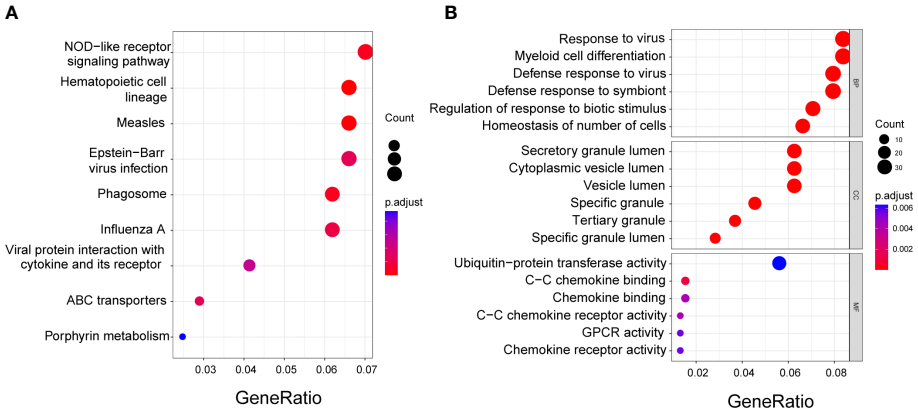

FIGURE 6
Functional enrichment analysis of the DEGs between low- and high-risk groups. **(A)** Kyoto Encyclopedia of Genes and Genomes (KEGG) analysis. **(B)** Gene Ontology (GO) enrichment analysis. BP, Biological process; CC, Cellular component; MF, Molecular function.

in external cohorts. After that, a nomogram was constructed based on the risk score and clinical information for clinical use. Functional enrichment analysis revealed that the DEGs between the low- and high-risk groups were related to immune-related pathways, and immune infiltration analysis revealed a significant difference in immune status between the two groups. Finally, we found that four out of the six genes also have diagnostic value for sepsis.

Pyroptosis plays a dual role in anti-infection and pro-inflammatory in sepsis. On the one hand, pyroptosis damaged the intracellular pathogen's living environment, reducing pathogen reproduction, and allowing intracellular pathogens to

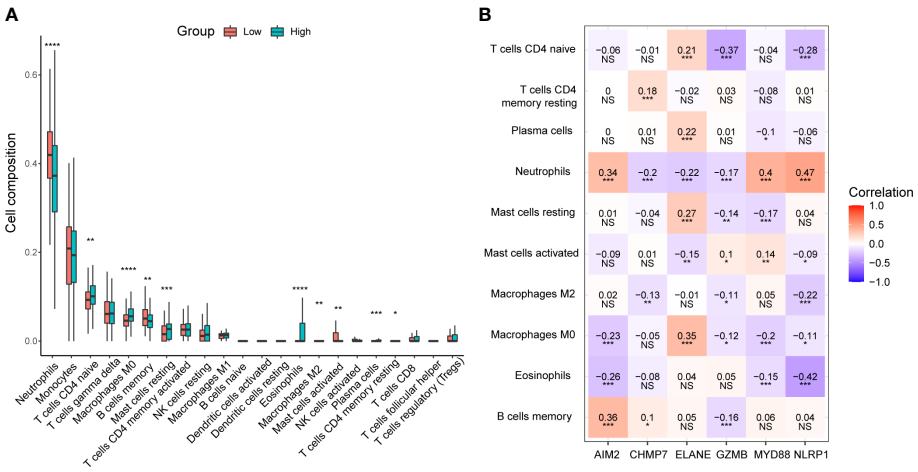

FIGURE 7
Immune infiltration analysis between low- and high-risk groups in the GSE65682 dataset. **(A)** Box plots of 22 types of immune cell composition between low- and high-risk groups. *P< 0.05; **P< 0.01; ***P< 0.001; ****P< 0.0001. **(B)** The correlation between the selected six pyroptosis-related genes and the immune cells. NS, Not significant, *P< 0.05; **P< 0.01; ***P< 0.001.

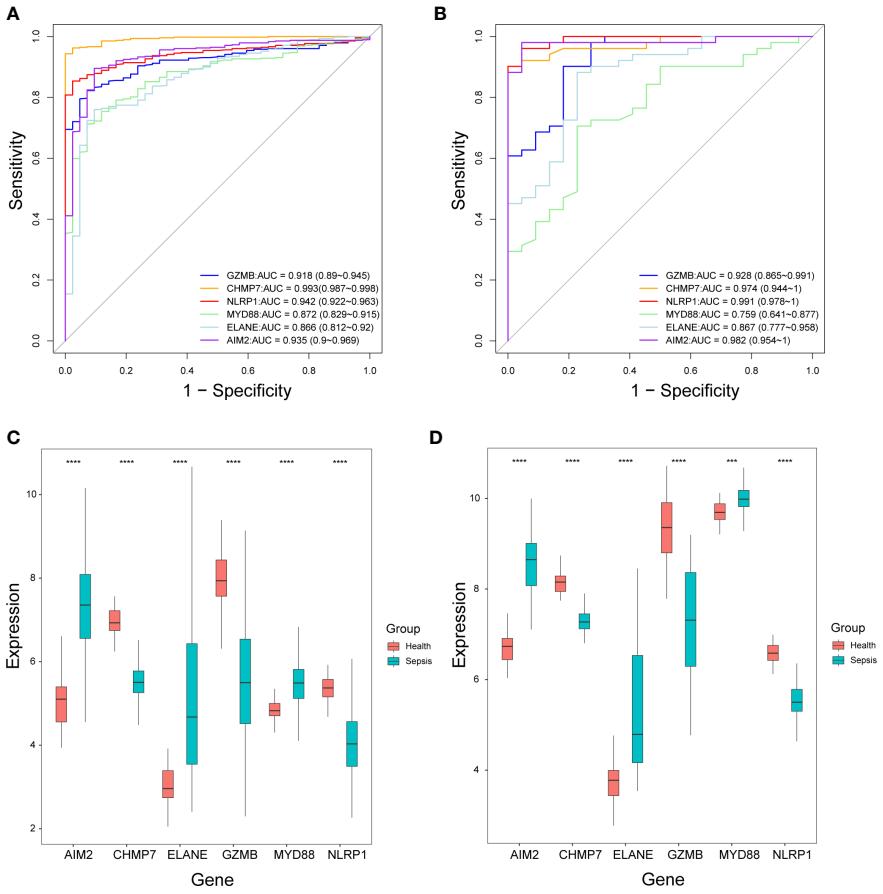

FIGURE 8
The performance of the selected six pyroptosis-related genes in the diagnosis of sepsis. **(A, B)** Receiver operating characteristic curves in the GSE65682 dataset **(A)** and GSE95233 dataset **(B)**. AUC, Area under the curve. **(C, D)** Box plots of the expression levels of the six genes between sepsis patients and healthy individuals in the GSE65682 dataset **(C)** and GSE95233 dataset **(D)**. ***P< 0.001, ****P< 0.0001.

be removed and cleared by immune cells (14). On the other hand, the inflammatory factors such as IL-18 and IL-1β released by pyroptosis and the damaged tissue may contribute to cytokine storm cascade. Moderate pyroptosis may play a protective role against pathogens, while excessive pyroptosis may cause uncontrolled cytokine storms (20). Therefore, pyroptosis may be significantly associated with the prognosis of sepsis. As a result of the present study, we found that pyroptosis-related genes could be used to cluster patients with sepsis, and patients in the different clusters had different prognoses, suggesting that pyroptosis in patients with sepsis may be different, which may lead to a different prognosis. Then, we developed a prognostic risk score with six pyroptosis-related genes, including *GZMB, CHMP7, NLRP1, MYD88, ELANE*, and *AIM2*, and found that it could predict the prognosis of sepsis patients.

Granzymes B (*GZMB*) is a member of grazymes family that was considered to exert cytotoxic effects against pathogen invasion (28). Recent studies reported that *GZMB* is involved in the coagulation cascade, regulating the function of platelets and endothelial barrier permeability in sepsis (29). The expression level of GZMB in sepsis may be associated with the underlying pathogen. An upregulation of *GZMB* was found in patients with gram-negative bacterial infection (30), while a downregulation of *GZMB* was found in sepsis patients caused by burns and trauma (31). Charged multivesicular body protein 7 (*CHMP7*) is a part of the endosomal sorting complex required for transport III (ESCRT-III), which take part in the process of nuclear envelope formation, endosomal sorting, neurodevelopment, and attention deficit hyperactivity disorder (ADHD) (32). Our results revealed that the expression of *CHMP7* was significantly lower in sepsis patients and a higher expression of *CHMP7* was associated with a better prognosis. Due to the limited number of studies, the role of *CHMP7* in sepsis remained unclear and our study may provide some insights for future study. The NLR family pyrin domain containing 1(*NLRP1*) and absent in melanoma 2 (*AIM2*) are pathogen pattern recognition (PRR) in the intracellular that respond to the pathogen-associated molecular patterns (PAMPs) or danger-associated molecular patterns (DAMPs), and activation caspase-1 mediated canonical pyroptosis pathway. Previous publications have found a significantly lower expression of *NLRP1* and a significantly higher expression of *AIM2* among sepsis patients (33, 34), besides, an even lower expression of *NLRP1* was found in the non-survivor (33). Our results were consistent with these findings and we also showed that a higher expression of *AIM2* is associated with a better prognosis. Further studies are still needed to clarify why the expression patterns of those genes are different even though they trigger the same canonical pathway of pyroptosis. Another PRR that is located in the cellular membrane called Toll-like receptor (TLR) is also involved in the recognition of PAMPs. Except for TLRP3, most TLR started its inflammatory response *via* a common signaling pathway by recruitment signaling adaptor protein including myeloid differentiation primary response protein (*MYD88*) (35). An overexpression of *MYD88* was associated with a poor prognosis of neonatal sepsis (36); However, our study found that a higher expression of *MYD88* was associated with a better prognosis. This discrepancy may be attributed to the difference in the immune system between adults and neonatal. *ELANE* encodes neutrophil elastase that is secreted by neutrophil. Neutrophil elastase could cleave GSDMD and cause neutrophil death, and the level of *ELANE* was reported to be associated with the severity of sepsis (37, 38). The expression level of *ELANE* was significantly higher in sepsis patients and associated with poor prognosis in our study.

Sepsis-induced both innate and adaptive immune dysfunction. The immune status of sepsis patients may be a crucial factor affecting the prognosis of sepsis (39, 40). The functional enrichment and immune infiltration analyses revealed differences in immune-related pathways and immune cell composition between the patients in the low-and high-risk groups, which may explain why the two risk groups have different prognoses. Besides, these findings also suggested that pyroptosis plays a role in immune dysfunction. The immune cell could also occur pyroptosis, which has been considered to play an essential role in the progression of sepsis. The regulation of immune cell pyroptosis has been shown to improve the prognosis of sepsis, with many studies focused on the regulation of macrophage pyroptosis (41). For example, Luo et al. found that inhibiting macrophage pyroptosis by Platelet endothelial cell adhesion molecule-1 (PECAM-1) could improve the prognosis in a septic murine model (42) and Song et al. reported Sphingosine-1-phosphate receptor 2 (S1PR2) knockout could reduce macrophage pyroptosis and improve sepsis outcome in mice (43). Notably, the correlation analysis showed that all six pyroptosis-related genes were correlated with neutrophils, implying that pyroptosis and neutrophils are closely related. Neutrophils constitute the majority of immune cells in human peripheral blood and play an important role in pathogen recognition and clearance. The role of neutrophil pyroptosis in sepsis remains unclear, and regulation of neutrophil pyroptosis has recently been assumed to have potential therapeutic value in sepsis (44, 45). Therefore, we believe that neutrophil pyroptosis in sepsis could be considered for further investigation in future studies.

There are several limitations that should be acknowledged in our study. First, although the prognostic risk score showed good performance, it still needs to be validated in large prospective cohort studies. Second, the prognostic factors from the GEO database were insufficient since other prognostic factors such as comorbidity diseases and infectious organisms were not included. Third, the molecular mechanism of the pyroptosis-related genes interacting with the immune cells needs to be further explored in the experimental study.

In summary, we developed and validated a novel prognostic predictive risk score for sepsis based on six pyroptosis-related genes. The risk score was an independent prognostic factor of

sepsis prognosis. Four out of the six genes also have potential diagnostic value in sepsis diagnosis. Our findings may provide new insight into the role of pyroptosis in sepsis and serve as a foundation for future research.

Data availability statement

The datasets presented in this study can be found in online repositories. The names of the repository/repositories and accession number(s) can be found in the article/Supplementary Material.

Author contributions

SL and WZ designed the study. SL, MX, XC, JP and ZS collected, analyzed, and interpreted the data. SL wrote the manuscript, WZ reviewed and revised the manuscript. All authors contributed to this study and approved the submitted version of the manuscript.

Funding

This work was supported by grants from the National Natural Science Foundation of China (82171236 and 81974172 to WZ) and the Key Research and Development Program of Hunan Province (2021SK2018 to WZ).

Conflict of interest

The authors declare that the research was conducted in the absence of any commercial or financial relationships that could be construed as a potential conflict of interest.

Publisher's note

Supplementary material

The Supplementary Material for this article can be found online at: https://www.frontiersin.org/articles/10.3389/fimmu.2022.1110602/full#supplementary-material

SUPPLEMENTARY FIGURE 1
Consensus clustering analysis based on pyroptosis-related DEGs. **(A)** Consensus empirical CDF. **(B)** Delta area.

SUPPLEMENTARY FIGURE 2
Univariate and multivariate cox regression of the prognostic predictors. **(A)** In the validation cohort. **(B)** In the test cohort.

References

1. Singer M, Deutschman CS, Seymour CW, Shankar-Hari M, Annane D, Bauer M, et al. The third international consensus definitions for sepsis and septic shock (Sepsis-3). *JAMA* (2016) 315(8):801–10. doi: 10.1001/jama.2016.0287

2. Liang X, Huang J, Xing M, He L, Zhu X, Weng Y, et al. Risk factors and outcomes of urosepsis in patients with calculous pyonephrosis receiving surgical intervention: A single-center retrospective study. *BMC anesthesiol* (2019) 19(1):61. doi: 10.1186/s12871-019-0729-3

3. Fleischmann-Struzek C, Mellhammar L, Rose N, Cassini A, Rudd KE, Schlattmann P, et al. Incidence and mortality of hospital- and icu-treated sepsis: Results from an updated and expanded systematic review and meta-analysis. *Intensive Care Med* (2020) 46(8):1552–62. doi: 10.1007/s00134-020-06151-x

4. Evans L, Rhodes A, Alhazzani W, Antonelli M, Coopersmith CM, French C, et al. Surviving sepsis campaign: International guidelines for management of sepsis and septic shock 2021. *Intensive Care Med* (2021) 47(11):1181–247. doi: 10.1007/s00134-021-06506-y

5. Hou N, Li M, He L, Xie B, Wang L, Zhang R, et al. Predicting 30-days mortality for mimic-iii patients with sepsis-3: A machine learning approach using xgboost. *J Transl Med* (2020) 18(1):462. doi: 10.1186/s12967-020-02620-5

6. Miao EA, Leaf IA, Treuting PM, Mao DP, Dors M, Sarkar A, et al. Caspase-1-Induced pyroptosis is an innate immune effector mechanism against intracellular bacteria. *Nat Immunol* (2010) 11(12):1136–42. doi: 10.1038/ni.1960

7. Shi J, Zhao Y, Wang K, Shi X, Wang Y, Huang H, et al. Cleavage of gsdmd by inflammatory caspases determines pyroptotic cell death. *Nature* (2015) 526 (7575):660–5. doi: 10.1038/nature15514

8. Aachoui Y, Leaf IA, Hagar JA, Fontana MF, Campos CG, Zak DE, et al. Caspase-11 protects against bacteria that escape the vacuole. *Science* (2013) 339 (6122):975–8. doi: 10.1126/science.1230751

9. Aglietti RA, Dueber EC. Recent insights into the molecular mechanisms underlying pyroptosis and gasdermin family functions. *Trends Immunol* (2017) 38 (4):261–71. doi: 10.1016/j.it.2017.01.003

10. Sun J, Ge X, Wang Y, Niu L, Tang L, Pan S. Usf2 knockdown downregulates Thbs1 to inhibit the tgf-beta signaling pathway and reduce pyroptosis in sepsis-induced acute kidney injury. *Pharmacol Res* (2022) 176:105962. doi: 10.1016/j.phrs.2021.105962

11. Jiao Y, Zhang T, Zhang C, Ji H, Tong X, Xia R, et al. Exosomal mir-30d-5p of neutrophils induces M1 macrophage polarization and primes macrophage pyroptosis in sepsis-related acute lung injury. *Crit Care* (2021) 25(1):356. doi: 10.1186/s13054-021-03775-3

12. Li N, Zhou H, Wu H, Wu Q, Duan M, Deng W, et al. Sting-Irf3 contributes to lipopolysaccharide-induced cardiac dysfunction, inflammation, apoptosis and pyroptosis by activating Nlrp3. *Redox Biol* (2019) 24:101215. doi: 10.1016/j.redox.2019.101215

13. Yang X, Cheng X, Tang Y, Qiu X, Wang Y, Kang H, et al. Bacterial endotoxin activates the coagulation cascade through gasdermin d-dependent phosphatidylserine exposure. *Immunity* (2019) 51(6):983–96.e6. doi: 10.1016/j.immuni.2019.11.005

14. Zheng X, Chen W, Gong F, Chen Y, Chen E. The role and mechanism of pyroptosis and potential therapeutic targets in sepsis: A review. *Front Immunol* (2021) 12:711939. doi: 10.3389/fimmu.2021.711939

15. Xu XE, Liu L, Wang YC, Wang CT, Zheng Q, Liu QX, et al. Caspase-1 inhibitor exerts brain-protective effects against sepsis-associated encephalopathy and cognitive impairments in a mouse model of sepsis. *Brain behavior Immun* (2019) 80:859–70. doi: 10.1016/j.bbi.2019.05.038

16. Weber P, Wang P, Maddens S, Wang P, Wu R, Miksa M, et al. Vx-166: A novel potent small molecule caspase inhibitor as a potential therapy for sepsis. *Crit Care* (2009) 13(5):R146. doi: 10.1186/cc8041

17. Karki R, Kanneganti TD. Diverging inflammasome signals in tumorigenesis and potential targeting. *Nat Rev Cancer* (2019) 19(4):197–214. doi: 10.1038/s41568-019-0123-y

18. Man SM, Kanneganti TD. Regulation of inflammasome activation. *Immunol Rev* (2015) 265(1):6–21. doi: 10.1111/imr.12296

19. Xia X, Wang X, Cheng Z, Qin W, Lei L, Jiang J, et al. The role of pyroptosis in cancer: Pro-cancer or pro-"Host"? *Cell Death Dis* (2019) 10(9):650. doi: 10.1038/s41419-019-1883-8

20. Xia D, Wang S, Yao R, Han Y, Zheng L, He P, et al. Pyroptosis in sepsis: Comprehensive analysis of research hotspots and core genes in 2022. *Front Mol Biosci* (2022) 9:955991. doi: 10.3389/fmolb.2022.955991

21. Wang B, Yin Q. Aim2 inflammasome activation and regulation: A structural perspective. *J Struct Biol* (2017) 200(3):279–82. doi: 10.1016/j.jsb.2017.08.001

22. Lai Y, Lin C, Lin X, Wu L, Zhao Y, Shao T, et al. Comprehensive analysis of molecular subtypes and hub genes of sepsis by gene expression profiles. *Front Genet* (2022) 13:884762. doi: 10.3389/fgene.2022.884762

23. Zhu S, Huang Y, Ye C. Identification of a ferroptosis-related prognostic signature in sepsis *Via* bioinformatics analyses and experiment validation. *BioMed Res Int* (2022) 2022:8178782. doi: 10.1155/2022/8178782

24. Ye Y, Dai Q, Qi H. A novel defined pyroptosis-related gene signature for predicting the prognosis of ovarian cancer. *Cell Death Discovery* (2021) 7(1):71. doi: 10.1038/s41420-021-00451-x

25. Yu G, Wang LG, Han Y, He QY. Clusterprofiler: An r package for comparing biological themes among gene clusters. *Omics J Integr Biol* (2012) 16 (5):284–7. doi: 10.1089/omi.2011.0118

26. Newman AM, Liu CL, Green MR, Gentles AJ, Feng W, Xu Y, et al. Robust enumeration of cell subsets from tissue expression profiles. *Nat Methods* (2015) 12 (5):453–7. doi: 10.1038/nmeth.3337

27. Barichello T, Generoso JS, Singer M, Dal-Pizzol F. Biomarkers for sepsis: More than just fever and leukocytosis-a narrative review. *Crit Care* (2022) 26(1):14. doi: 10.1186/s13054-021-03862-5

28. Kurschus FC, Jenne DE. Delivery and therapeutic potential of human granzyme b. *Immunol Rev* (2010) 235(1):159–71. doi: 10.1111/j.0105-2896.2010.00894.x

29. Garzon-Tituana M, Arias MA, Sierra-Monzon JL, Morte-Romea E, Santiago L, Ramirez-Labrada A, et al. The multifaceted function of granzymes in sepsis: Some facts and a lot to discover. *Front Immunol* (2020) 11:1054. doi: 10.3389/fimmu.2020.01054

30. Lauw FN, Simpson AJ, Hack CE, Prins JM, Wolbink AM, van Deventer SJ, et al. Soluble granzymes are released during human endotoxemia and in patients with severe infection due to gram-negative bacteria. *J Infect Dis* (2000) 182(1):206–13. doi: 10.1086/315642

31. Tang Y, Yang X, Shu H, Yu Y, Pan S, Xu J, et al. Bioinformatic analysis identifies potential biomarkers and therapeutic targets of septic-Shock-Associated acute kidney injury. *Hereditas* (2021) 158(1):13. doi: 10.1186/s41065-021-00176-y

32. Dark C, Williams C, Bellgrove MA, Hawi Z, Bryson-Richardson RJ. Functional validation of Chmp7 as an adhd risk gene. *Transl Psychiatry* (2020) 10(1):385. doi: 10.1038/s41398-020-01077-w

33. Esquerdo KF, Sharma NK, Brunialti MKC, Baggio-Zappia GL, Assuncao M, Azevedo LCP, et al. Inflammasome gene profile is modulated in septic patients, with a greater magnitude in non-survivors. *Clin Exp Immunol* (2017) 189(2):232–40. doi: 10.1111/cei.12971

34. Nasiri E, Kariminik A. Up-regulation of Aim2 and Tlr4 and down-regulation of Nlrc4 are associated with septicemia. *Indian J Med Microbiol* (2021) 39(3):334–8. doi: 10.1016/j.ijmmb.2021.05.002

35. Saikh KU. Myd88 and beyond: A perspective on Myd88-targeted therapeutic approach for modulation of host immunity. *Immunol Res* (2021) 69 (2):117–28. doi: 10.1007/s12026-021-09188-2

36. AbdAllah NB, Toraih EA, Al Ageeli E, Elhagrasy H, Gouda NS, Fawzy MS, et al. Myd88, Nfkb1, and Il6 transcripts overexpression are associated with poor outcomes and short survival in neonatal sepsis. *Sci Rep* (2021) 11(1):13374. doi: 10.1038/s41598-021-92912-7

37. Kumar S, Gupta E, Kaushik S, Srivastava VK, Saxena J, Mehta S, et al. Quantification of nets formation in neutrophil and its correlation with the severity of sepsis and organ dysfunction. *Clinica chimica acta; Int J Clin Chem* (2019) 495:606–10. doi: 10.1016/j.cca.2019.06.008

38. Burdette BE, Esparza AN, Zhu H, Wang S. Gasdermin d in pyroptosis. *Acta Pharm Sin B* (2021) 11(9):2768–82. doi: 10.1016/j.apsb.2021.02.006

39. Delano MJ, Ward PA. Sepsis-induced immune dysfunction: Can immune therapies reduce mortality? *J Clin Invest* (2016) 126(1):23–31. doi: 10.1172/jci82224

40. van der Poll T, Shankar-Hari M, Wiersinga WJ. The immunology of sepsis. *Immunity* (2021) 54(11):2450–64. doi: 10.1016/j.immuni.2021.10.012

41. Wen X, Xie B, Yuan S, Zhang J. The "Self-sacrifice" of immunecells in sepsis. *Front Immunol* (2022) 13:833479. doi: 10.3389/fimmu.2022.833479

42. Luo L, Xu M, Liao D, Deng J, Mei H, Hu Y. Pecam-1 protects against dic by dampening inflammatory responses *Via* inhibiting macrophage pyroptosis and restoring vascular barrier integrity. *Trans Res* (2020) 222:1–16. doi: 10.1016/j.trsl.2020.04.005

43. Song F, Hou J, Chen Z, Cheng B, Lei R, Cui P, et al. Sphingosine-1-Phosphate receptor 2 signaling promotes caspase-11-Dependent macrophage pyroptosis and worsens escherichia coli sepsis outcome. *Anesthesiology* (2018) 129(2):311–20. doi: 10.1097/aln.0000000000002196

44. Liu L, Sun B. Neutrophil pyroptosis: New perspectives on sepsis. *Cell Mol Life Sci* (2019) 76(11):2031–42. doi: 10.1007/s00018-019-03060-1

45. Zhang H, Chen Z, Zhou J, Gu J, Wu H, Jiang Y, et al. Nat10 regulates neutrophil pyroptosis in sepsis *Via* acetylating Ulk1 rna and activating sting pathway. *Commun Biol* (2022) 5(1):916. doi: 10.1038/s42003-022-03868-x

frontiers | Frontiers in Immunology

TYPE Original Research
PUBLISHED 27 January 2023
DOI 10.3389/fimmu.2023.1094331

OPEN ACCESS

EDITED BY
Peisong Gao,
Johns Hopkins University, United States

REVIEWED BY
Kingsley Yin,
Rowan University School of Osteopathic Medicine, United States
Guillaume Tabouret,
Institut National de recherche pour l'agriculture, l'alimentation et l'environnement (INRAE), France

*CORRESPONDENCE
Zhiqiang Mi
zhiqiangmi_ime@163.com
Decong Kong
kongdecong-118@163.com
Yongqiang Jiang
jiangyq@bmi.ac.cn

†These authors have contributed equally to this work and share first authorship

SPECIALTY SECTION
This article was submitted to Inflammation, a section of the journal Frontiers in Immunology

RECEIVED 10 November 2022
ACCEPTED 16 January 2023
PUBLISHED 27 January 2023

CITATION
Ni C, Gao S, Li X, Zheng Y, Jiang H, Liu P, Lv Q, Huang W, Li Q, Ren Y, Mi Z, Kong D and Jiang Y (2023) Fpr2 exacerbates *Streptococcus suis*-induced streptococcal toxic shock-like syndrome *via* attenuation of neutrophil recruitment. *Front. Immunol.* 14:1094331. doi: 10.3389/fimmu.2023.1094331

Fpr2 exacerbates *Streptococcus suis*-induced streptococcal toxic shock-like syndrome *via* attenuation of neutrophil recruitment

Chengpei Ni[1,2,3†], Song Gao[3†], Xudong Li[1,2†], Yuling Zheng[2], Hua Jiang[1,2], Peng Liu[2], Qingyu Lv[2], Wenhua Huang[2], Qian Li[2], Yuhao Ren[2], Zhiqiang Mi[1,2*], Decong Kong[2*] and Yongqiang Jiang[1,2*]

[1]School of Basic Medical Sciences, Anhui Medical University, Hefei, China, [2]State Key Laboratory of Pathogen and Biosecurity, Institute of Microbiology and Epidemiology, Academy of Military Medical Sciences, Beijing, China, [3]The Affiliated Wuxi Center for Disease Control and Prevention of Nanjing Medical University, Wuxi Center for Disease Control and Prevention, Wuxi, China

The life-threatening disease streptococcal toxic shock-like syndrome (STSLS), caused by the bacterial pathogen *Streptococcus suis* (*S. suis*). Proinflammatory markers, bacterial load, granulocyte recruitment, and neutrophil extracellular traps (NETs) levels were monitored in wild-type (WT) and Fpr2$^{-/-}$ mice suffering from STSLS. LXA4 and AnxA1, anti-inflammatory mediators related to Fpr2, were used to identity a potential role of the Fpr2 in STSLS development. We also elucidated the function of Fpr2 at different infection sites by comparing the STSLS model with the *S. suis*-meningitis model. Compared with the WT mice, Fpr2$^{-/-}$ mice exhibited a reduced inflammatory response and bacterial load, and increased neutrophil recruitment. Pretreatment with AnxA1 or LXA4 impaired leukocyte recruitment and increased both bacterial load and inflammatory reactions in WT but not Fpr2$^{-/-}$ mice experiencing STSLS. These results indicated that Fpr2 impairs neutrophil recruitment during STSLS, and this impairment is enhanced by AnxA1 or LXA4. By comparing the functions of Fpr2 in different *S. suis* infection models, inflammation and NETs was found to hinder bacterial clearance in *S. suis* meningitis, and conversely accelerate bacterial clearance in STSLS. Therefore, interference with neutrophil recruitment could potentially be harnessed to develop new treatments for this infectious disease.

KEYWORDS

***Streptococcus suis*, leukocyte recruitment, NETs, formyl peptide receptor 2, STSLS**

Introduction

Infection by the major pathogenic gram-positive bacterium *Streptococcus suis* can cause life-threatening meningitis and sepsis in humans and in swine, which can lead to significant economic losses by the pig breeding industry. The severe lethality of two recent outbreaks in humans was attributed to invasive multiple organ failure resulting from streptococcal toxic-shock-like syndrome (STSLS) (1, 2). Previous studies have indicated that Suilysin, a pore-forming cholesterol-dependent cytolysin of *S. suis*, could activate the inflammasome and cause STSLS (3–5). Although STSLS was long time considered to result from excessive activation of the inflammatory response, the inefficacy of anti-cytokine therapy in several clinical trials determined that the pathogenesis of sepsis was complex. Current research suggests that a proinflammatory response and an anti-inflammatory response occur concurrently in septic patients (6). Because of the ineffectiveness of current treatments, research focusing on the development of therapeutics for STSLS is urgent.

Fpr2 is an intriguing G-protein-coupled chemoattractant receptor (GPCR) known for its dual role in immunoregulation (7). It exerts pro-resolution properties by binding anti-inflammatory mediators such as annexin A1(AnxA1) and lipoxin A4 (LXA4), which has been confirmed in both *in vitro* and *in vivo* experiments (8). However, Fpr2 also possesses the ability to sense formyl peptides or serum amyloid A (SAA) to induce pro-inflammatory responses (9). Due to the diversity of Fpr2 ligands, the role of Fpr2 in host immune response depends on the stages of infection and associated ligand profile. The dual roles of Fpr2 make its function in pathogenesis difficult to determine. Although Fpr2 is widely distributed across multiple cells and tissues, it is mainly expressed in myeloid cells. The mouse Fpr2 is most similar to human Fpr2 structurally and functionally, as confirmed by *in vivo* and *in vitro* research (10).

As the most abundant granulocytes, neutrophils serve as the first line of defense against invading pathogens *via* their functions in phagocytosis, and reactive oxygen species (ROS) and protease production. Additionally, neutrophil extracellular traps (NETs), formulated by active neutrophils under certain conditions, have recently been identified as a novel bactericidal mechanism. NETs contain a web of extracellular DNA, histones, myeloperoxidase, and elastases, which strengthen their antimicrobial effect (11). NETs are highly effective at killing bacteria and hindering their spread. Although excessive activation of NETs in sepsis is associated with multiple organ failure, NETs undoubtedly play protective roles in the initial stages of infection. The role of Fpr2 in regulating NETs formation in active neutrophils when stimulated with methicillin-resistant *Staphylococcus aureus* (MRSA) is thought to be associated with an endogenous anti-inflammatory ligand of Fpr2 in the lipoxin pathway (12). The impact of neutrophil recruitment on disease development is dependent on disease pathology, genetics, and environmental stimuli.

Fpr2 impairs the neutrophil recruitment during infection, and AnxA1 has a protective effect in downregulating inflammation through Fpr2 (13). As the immunological responses to bacterial meningitis and STSLS may be quite different, we aimed to investigate the role of Fpr2 in *S. suis*-induced systemic infection, concentrating on the effects of the pro-resolution agents AnxA1 and LXA1 on STSLS progression. By comparing the *S. suis*-meningitis model to the STSLS models, we were able to identify differences in the immune regulation mechanism of Fpr2 in these different *S. suis* infection models. We demonstrated a regulatory role of Fpr2 in controlling neutrophil recruitment, which contributes to the pathogenesis of STSLS pathogenesis by decreasing neutrophil recruitment and NETs formation during the early stages of infection. We also found that inhibition of neutrophil recruitment and NETs formation produced opposing effects on disease progression between bacterial meningitis and systemic infection. This study provides valuable fundamental information for further research into treatment of *S. suis* infection and potentially other infectious diseases.

Materials and methods

Bacteria and animals

The wild-type strain *S. suis* 05ZYH33 is a clinical isolate that caused an STSLS outbreak in Sichuan Province of China. *S. suis* was grown in Todd–Hewitt Broth (THB) medium at 37°C and were harvested for experimentation at the mid-log growth phase bacteria. 6 to 8 weeks old C57BL/6J female mice were purchased from SPF (Beijing, China) Biotechnology Co., Ltd. C57BL/6J Fpr2 $^{-/-}$ mice was generated as indicated in previous studies (13). In brief, Fpr2-deficient mice were generated using the Cre/LoxP system. Mice harboring a floxed allele of Fpr2 ($Fpr2^{loxP}/^{+}$) were obtained from Cyagen Biosciences (Guangzhou, China); these mice were interbred to generate $Fpr2^{loxP/loxP}$ mice. $Fpr2^{loxP/loxP}$ mice were then mated with EIIa-cre transgenic mice to generate a null allele of Fpr2 ($Fpr2^{+/-}$). $Fpr2^{+/-}$ mice were identified by PCR genotyping using multiple primers (mFpr2_F1 [CTCATACGCATTTGCTGTCTTCACAC], mFpr2_R1 [TCCAATTATATCCCTTTCATGGCAAAC], and mFpr2_F3 [ACAAGGGCCTGCATGTGCCCTCTG]). Finally, $Fpr2^{+/-}$ mice were interbred to generate $Fpr2^{-/-}$ mice.

Infection

For the STSLS model, a standard bacterial dose (2×10^7 CFU) of bacterial suspensions or a vehicle solution (THB) were infused intraperitoneally in WT or $Fpr2^{-/-}$ mice. In survival experiments, high dose (5×10^7 CFU) of *S. suis* were used. Peritoneal lavage fluid (PLF), blood, and tissues were obtained for analysis at the indicated time point during infection. Bacterial viability was monitored by plating serial dilutions of blood or PLF. Cytokine and chemokine levels and hematoxylin and eosin (H&E) stain were also performed at 12 h post-infection. All the mice were monitored up to 5 d and clinical score were assigned according to the scoring criteria developed in a previous study (14): 4 = dead; 3 = non-responsive or walking in circles; 2 = responds only to repeated stimuli; 1 = ruffled coat and slow response to stimuli, and 0 = normal response to stimuli. For the meningitis model, mice were inoculated with 10 ul of bacterial suspension (1.25×10^5 CFU) suspension intracisternally after

general anesthesia (pentobarbital sodium, 50 mg/kg). Mice were monitored up to 72 h to record deaths. Bacterial load in the brain and blood were evaluated at 14 h, when most animals developed clinical symptoms.

Antagonist

For the interference test, Fpr2/ALX antagonist, WRW4 (Sangon, China) and BOC-2 (N-t-Boc-Phe-Leu-Phe-Leu-Phe; Sangon, China,10 μg/kg; i.p.) were administered after 1 h of infection. In the remaining experiments, animals were treated with AnxA1 (Biobry, UK, 50 μg/kg; i.p.) or LXA4 (Cayman Chemical Company, USA; 2.5 μg/kg; i.p.) 1 h after infection (15).

Neutrophil-depleting

26 mg/kg of anti-mouse Ly6G (BioXcell, USA, clone:1A8), InVivoMAb, or IgG2a isotype control (BioXcell, USA, clone:2A3) were injected into mice intraperitoneally (i.p.) before infection (16).

FACS analysis

To determine the activity of neutrophils or macrophage recruitment, the PLF of mice was collected and analysis by FACS. At each indicated time point, animals were euthanized by carbon dioxide asphyxiation, and the abdomen gently massaged. 10 ml sterile harvest solution (PBS+EDTA) was injected intraperitoneally, then the peritoneal fluid was withdrawn and centrifuged (10 min, 200 × g) to collect recruited leukocytes. After quantifying the absolute number, cells were treated with an FcR-blocking reagent (CD16/CD32, BD Pharmingen) for 15 min, then cells incubated with mixed antibodies: FITC-conjugated anti-mouse CD45 (N418, Biolegend, USA); PerCP-Cy5.5-conjugated anti-mouse CD11b (M1/70 Biolegend, USA) APC-conjμgated anti-mouse F4/80 (BM8, Biolegend, USA), PE-conjugated anti-mouse Ly6G (RB6-8C5 Biolegend, USA), PE-Cy7-conjμgated anti-mouse Ly6C (HK1.4 Biolegend, USA), and APC-Cy7-conjμgated fixable viability dye eFluor780 (Invitrogen). After washing, cells were suspended in sorting buffer for FACS analysis. Data analysis was performed using BD Verse software.

Multiplexed cytokines measurement

The ProcartaPlex™ Multiplex Immunoassay (EPXR360-26092-901, Invitrogen) was used for measuring cytokine and chemokine levels in the mouse serum after infection. The test was performed according to the manufacturer's instructions

Histopathology

Livers and spleen from infected mice were removed and fixed in formalin overnight before embedding in paraffin. Slides were stained with hematoxylin and eosin, and the histopathology of tissues was analyzed using microscope.

Confocal microscopy

The cells in PLF of infected mice were collected and pipetted into the wells of Lab-Tek Chamber Slides (ThermoFisher Scientific). After a 5 min incubation, detached cells were removed from each well. The cells were incubated with 4% paraformaldehyde for 10 min at room temperature, then permeabilized (0.25% Triton X-100) and blocked (1% BSA, 1 h, RT). Cells were stained with anti-mouse elastase (Bioss, dilution 1:200) and detected with Alexafluor 488-labeled secondary goat-anti-rabbit Fab antibody fragments (Life Technologies, dilution 1:1000). The slides were counterstained with DAPI by Prolong Diamond mounting medium (Invitrogen). Analysis was performed by confocal microscopy (Nikon Eclipse Ti).

Isolation of neutrophils from peritoneal fluids

Cell isolation and identification were conducted based on previous research (17). In brief, mice were injected with 1.0 ml casein solution into the peritoneal cavity, and a second injection was performed after one night. The peritoneal fluid was collected 3 h after the second injection. Peritoneal exudate cells were mixed with 9 ml of Percoll gradient solution in a 10-ml ultracentrifuge tube. After ultracentrifuging (20 min at 60,650 × g 4°C), neutrophils in the second opaque layer were collected. Cell purity and viability were determined by FACS.

Bactericidal activity of neutrophils

Neutrophils (2×10^6 cells) were incubated with *S. suis* (MOI=5) for 1 or 3 h at 37°C. A portion of the supernatants were taken and cultured overnight on THB plates at certain points to quantify non-engulfed extracellular bacteria. Part of the mixture was washed to remove the extracellular non-engulfed *S. suis*, then cells were laid onto 3 microscopic slides. Liu's Stain was used to visualize cell morphology and 200 neutrophils per slide were counted for bacterial clearance rate. Bactericidal activity of neutrophils was determined by counting the number of live extracellular bacterial colonies, and the bacterial clearance rate was determined using Romanowsky Stain. Three replicate experiments were done for each experiment.

Statistical analysis

The data in this study were statistically analyzed by GraphPad Prism 8 software and all data were present as the mean ± standard deviation (mean ± SD) unless otherwise noted. A two-way analysis of variance was used for the clinical scoring of mice. For the survival experiment, data was analyzed using the Kaplan-Meier method and Log-Rank test. For bacterial load, cytokine expression, and immune

cells detection, data were analyzed with the Mann-Whitney U test; $P < 0.05$, was considered significant.

Results

Fpr2 contribute to the pathogenesis of STSLS

To analyze the role of Fpr2 in the pathogenesis of STSLS, the expression of Fpr2 was detected in mice inoculated with *S. suis* intraperitoneally. Survival was monitored in WRW4 and BOC-2 (Fpr2 antagonist) intervention experiments. The increased expression of Fpr2 gene in the spleen implied a participatory role of Fpr2 during infection (Figure 1A). In the intervention trial, inhibiting Fpr2 with an antagonist significantly reduced the bacterial load and mortality of mice with STSLS (Figures 1B, C). $Fpr2^{-/-}$ mice were used for a more detailed study of *S. suis* infection. After monitoring the bacterial load and mortality in WT and $Fpr2^{-/-}$ STSLS mice, lower mortality rates and bacterial load were observed in the $Fpr2^{-/-}$ mice (Figures 1D-F). A significant difference in bacterial load was observed in 6 h and 12 h post-infection both in blood and PLF (Figures 1E, F). These results indicate that Fpr2 exacerbates the acute symptoms of STSLS.Cytokine production, pathological changes, body temperature changes, and clinical evaluation were also monitored in infected mice. Mice deficient in Fpr2 had a lower inflammatory response supported by decreased soluble mediators and alleviated tissue injury at 12 h post-infection (Figures 2A, B). The soluble mediators of PLF in infected mice at 3 and 6 h were also detected, the deceased cytokines were significantly observed at 6 h in $Fpr2^{-/-}$ mice, especially in CXCL1, CXCL2 and IL-6 (Figure S1). Hepatocyte apoptosis and splenocyte necrosis were only observed in WT mice (Figure 2B). Moreover, in contrast with $Fpr2^{-/-}$ mice, induction of STSLS yielded worse clinical scores and prolonged hypothermia for WT mice. (Figures 2C, D). Collectively, these data indicate a potential contributing role of Fpr2 in STSLS pathogenesis.

Fpr2 deficiency enhances neutrophil recruitment during the early stages of STSLS

We focused on leukocyte activity during infection to understand the role of Fpr2 in the STSLS-induced inflammatory response. WT and $Fpr2^{-/-}$ mice were inoculated with standard dose of *S. suis* (2×10^7 CFU) intraperitoneally. Counts of leukocyte in the PLF were determined during infection. Macrophages/monocytes and neutrophils are the two main immune cells in the PLF after infection (Figure 3A). Flow cytometry analysis revealed striking neutrophilia in $Fpr2^{-/-}$ mice at 3 and 6 h (Figure 3B). No significant difference was observed in macrophage counts between the two mice genotypes (Figure 3C). Higher level of NETs was also found in the plasma and PLF of $Fpr2^{-/-}$ mice at 6 h post-infection (Figures 3D, E), which was further confirmed by immunofluorescence results. The filamentous chromatin fibers, areas of decondensed extracellular thread-like DNA colocalizing with neutrophil elastase, as visualized by confocal microscopy depict the NETs. More NETs construction was observed in the PLF of $Fpr2^{-/-}$ mice (Figure 3F). Together, these

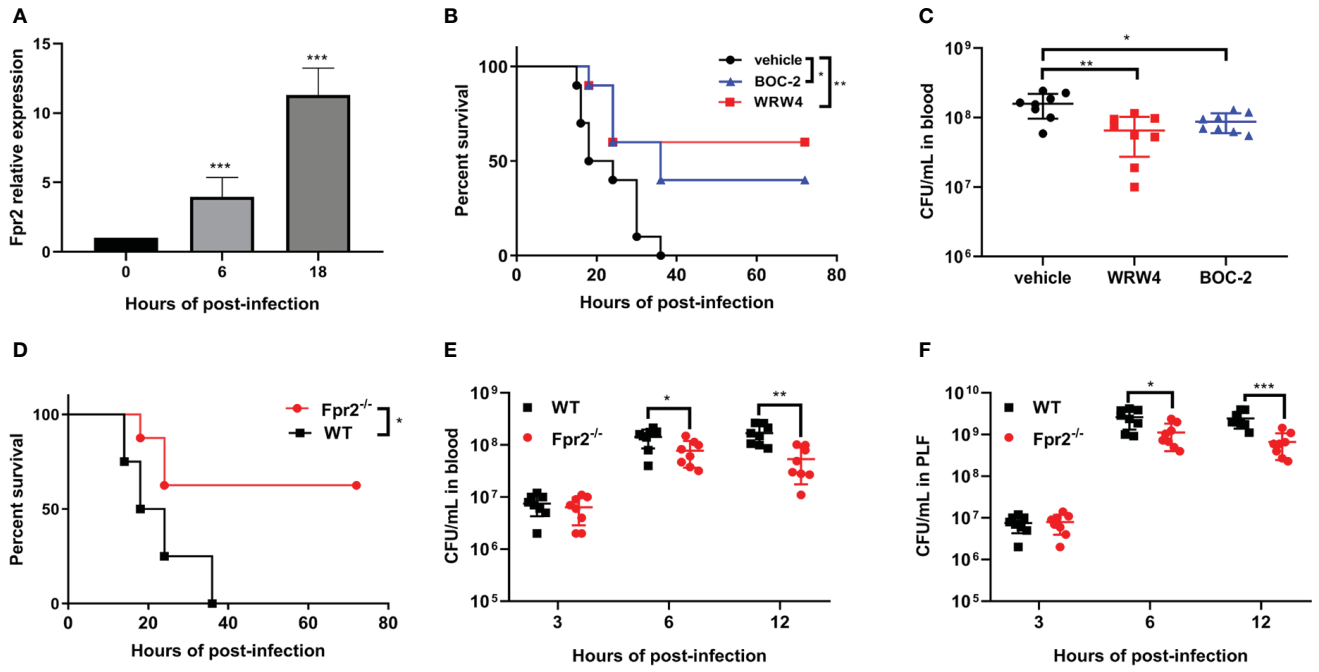

FIGURE 1
Fpr2 makes mice more susceptible to STSLS. **(A)** Wild-type mice were inoculated with standard *S. suis* dose intraperitoneally and Fpr2 mRNA levels in the spleen were evaluated. **(B)** Kaplan–Meier curves (N=10) of mice treated with BOC-2 (600 ng/kg), WRW4 (1 mg/kg), or a vehicle solution (THB) at 1 h after infection with a high dose of *S. suis*. **(C)** Blood bacteria in mice inoculated with standard dose of *S. suis*. **(D)** In WT and $Fpr2^{-/-}$ mice infected with high dose of *S. suis*, Kaplan–Meier curves (N=8) were monitored for 72 h. **(E)** Bacterial loads in blood and **(F)** peritoneal lavage fluid was monitored at the indicated time points in mice infected with a standard dose of *S. suis*. *, $P < 0.05$; **, $P < 0.01$; ***, $P < 0.001$.

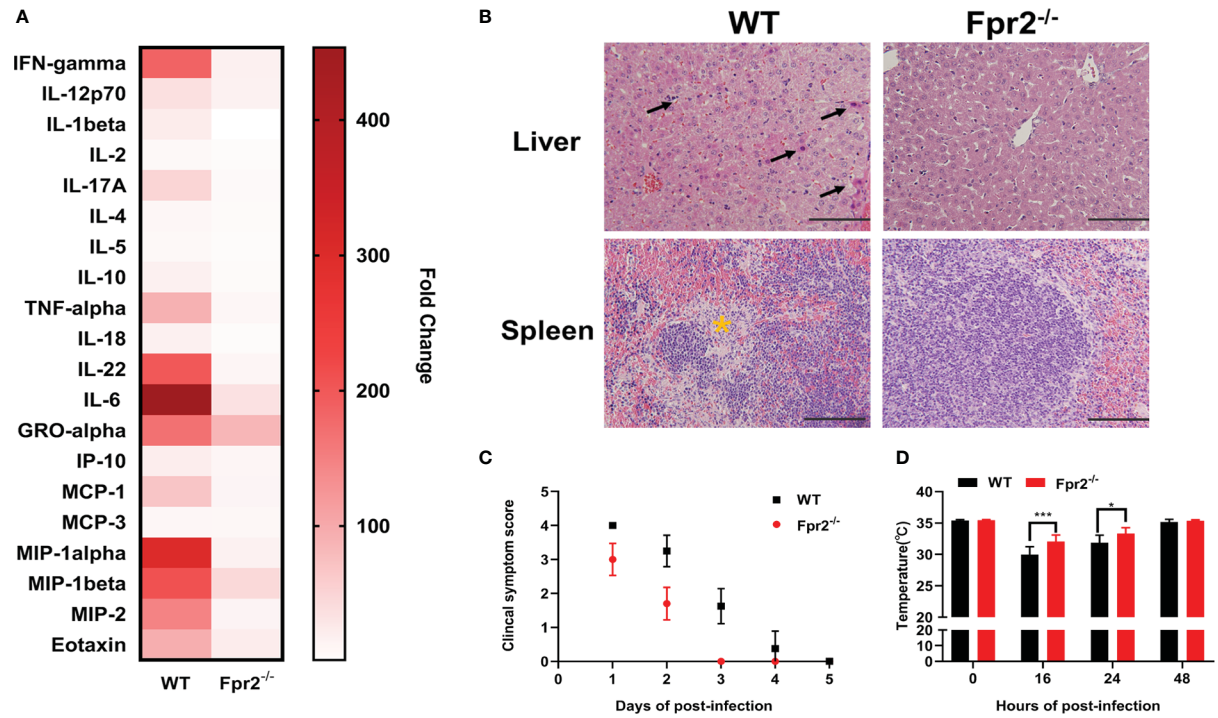

FIGURE 2
Fpr2 contributes to the induction of inflammation in STSLS. Wild-type and Fpr2$^{-/-}$ mice were inoculated with a standard bacterial dose of *S. suis* intraperitoneally. **(A)** Serum was collected to detect inflammatory mediators by Luminex Assay at 12 h (N=4). **(B)** Mouse tissues were extracted for histological analysis. Arrows indicate apoptosis of hepatocytes. The yellow star indicates necrosis of Splenocyte. Size bars represent 100 μm. In clinical the observation experiment, **(C)** clinical scores and **(D)** anal rectal temperature were performed according to the criteria (N=10). *, $P < 0.05$; ***, $P < 0.001$.

data suggest that Fpr2 impaired the recruitment of neutrophils and production of NETs during STSLS.

Fpr2 has no direct impact on NETs construction

Having established active neutrophil recruitment and higher levels of NETs structure in Fpr2$^{-/-}$ mice suffering from STSLS, we further explored how Fpr2 affects the morphology or function of neutrophils. The bactericidal ability and oxidative stress properties of WT and Fpr2$^{-/-}$ neutrophils were evaluated after cells were treated by *S. suis* (MOI=5) *in vitro*. To determine bactericidal ability, the bacterial clearance rate was evaluated at 1 and 3 h (Figure 4A). The extracellular bacterial load, which reflects the bactericidal capacity of WT and Fpr2$^{-/-}$ neutrophils, was also evaluated (Figure 4B). Bacterial clearance rate calculation of stimulated neutrophils revealed that Fpr2$^{-/-}$ cells exhibited lower bacterial clearance rate than WT mice at 1 h post treatment. However, this had no influence on the bactericidal ability of neutrophils, as the phagocytic bacteria and extracellular bacteria between the cells of the two genotypes showed no significant differences at 3 h. Regarding oxidative stress properties, ROS production was monitored when WT and Fpr2$^{-/-}$ cells were treated with *S. suis* at different MOIs. Although there was higher light intensity in the WT group before 25 min, as the infection progressed no differences were observed between the cells of the two genotypes at 40 min (Figure 4C). No significant difference was observed in the NETs production experiment when the two genotype neutrophils were treated with *S. suis* for 3 h *in vitro*. (Figure 4D). These results indicate that Fpr2 did not directly affect ROS and NETs production of neutrophils *in vitro*, and that the improved leukocyte infiltration of Fpr2 deficient mice may account for the higher levels of NETs observed *in vivo*.

LXA4 and AnxA1 promote bacterial proliferation through Fpr2

Administration of LXA4 or AnxA1 efficiently alleviates neutrophil accumulation, reduces inflammation, and attenuates many diseases. Our previous study elucidated the potential therapeutic effect of AnxA1 in *S. suis* meningitis. In this study, LXA4 and AnxA1 were used as an intervention in STSLS infection to explore the potential effects of LXA4 and AnxA1 in STSLS treatment. Analysis of cytometer results showed the potential anti-recruitment function of LXA4 and AnxA1 in WT mice at 3 and 6 h post-infection, although no effect was observed in Fpr2$^{-/-}$ mice. (Figures 5A-C). The bacterial load in the blood and PLF at 6 h was monitored. High bacterial loads were observed in LXA4 or AnxA1 treated WT mice, but this effect was not observed in Fpr2$^{-/-}$ mice (Figures 5D, E). In order to confirm that Fpr2 primarily affects the activity of neutrophils in STSLS, we used anti-Ly6G antibody to block the neutrophils. Treatment with anti-Ly6G eliminated observed differences between the WT and Fpr2$^{-/-}$ mice (Figure 5F). Compared to the isotype group, pretreatment with anti-Ly6G increased mortality and accelerated death from STSLS. Neutrophil

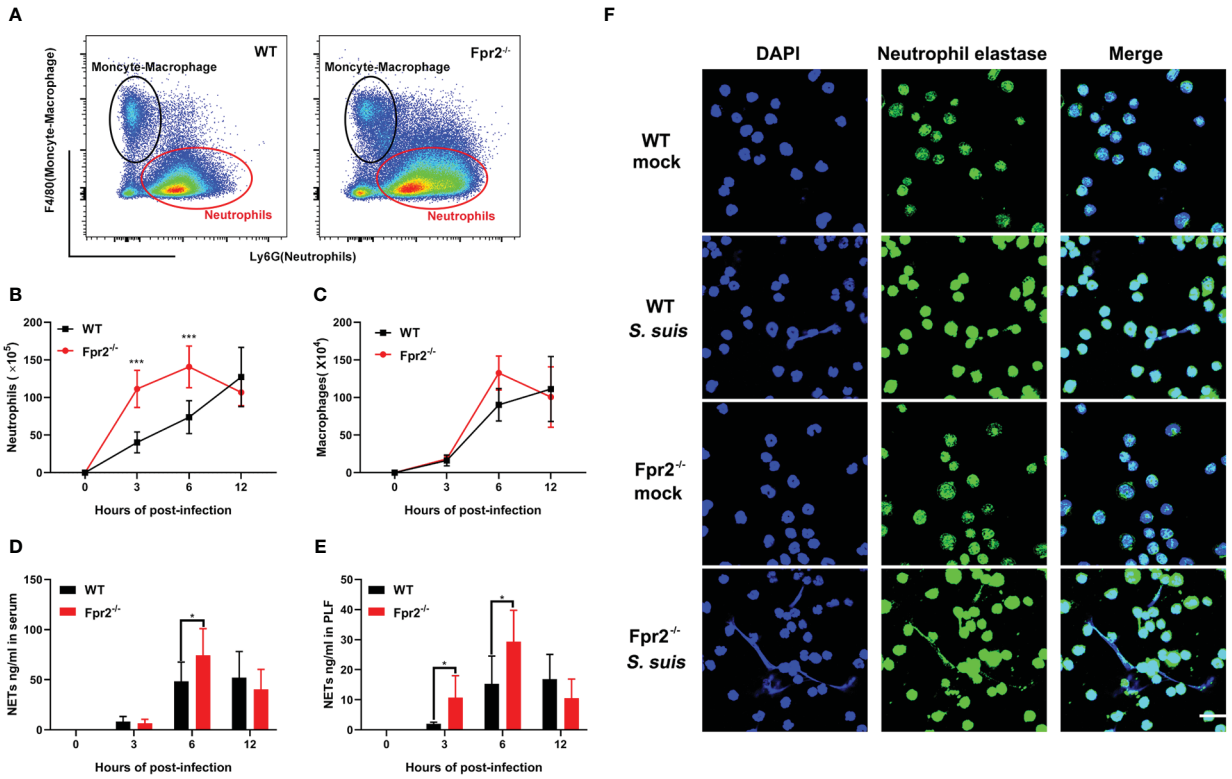

FIGURE 3
Fpr2 is involved in neutrophil migration. Wild-type and Fpr2$^{-/-}$ mice were inoculated with a standard bacterial dose of *S. suis* intraperitoneally. **(A)** Scattergrams of neutrophils (identified as Ly6G^{+} F4/80^{-}) and monocyte–macrophage (identified as Ly6G^{-}F4/80^{+}) positive events in peritoneal lavage fluids (PLF) from infected mice by flow cytometry analysis. **(B)** Absolute number of neutrophils or **(C)** macrophages/monocytes in PLF after infection at the indicated timepoint (N≥3). **(D)** NETs-detection in the serum or **(E)** PLF at the indicated timepoint (N≥3). **(F)** PLF of mice at 6 h post-infection visualized by immunofluorescence against neutrophil elastase (green) and DNA (blue). Size bars represent 10 μm. *, $P < 0.05$; ***, $P < 0.001$.

recruitment during the early stages of STSLS plays an indispensable role in bacterial clearance, which is a key step regulated by Fpr2 during the inflammation response.

Clinical symptoms score, lethality test and histopathology changes in STSLS, were also assessed when LXA4 and AnxA1 were used. Treatment with LXA4 or AnxA1 in WT mice increased the clinical symptom score and lethality in these mice, indicating a detrimental role of anti-recruitment drugs in STSLS (Figures 6A-C). Exaggerated tissue damage was also observed in WT but not Fpr2$^{-/-}$ mice (Figure 6D). Those data further demonstrate that neutrophil recruitment during the early stages of infection plays a crucial role in controlling bacterial proliferation and dissemination. The anti-recruitment mediators LXA4 and AnxA1 aggravated tissue damage and increased the inflammatory response in STSLS *via* Fpr2.

Bidirectional effects of NETs on *Streptococcus suis* proliferation and host protection

Previous studies from our laboratory have reported the beneficial role of Fpr2 in bacterial clearance and inflammation resolution during *S. suis* meningitis. Fpr2$^{-/-}$ mice were highly susceptible to *S. suis* meningitis, and displayed increased bacterial dissemination and neutrophil migration. AnxA1 attenuated inflammatory responses and neutrophil invasion through Fpr2 during *S. suis* meningitis. When compared with the current study on the STSLS model, both studies revealed an anti-recruitment function of Fpr2 during infection, but opposite effects on disease development in the different infection models. We speculated that neutrophil recruitment may play a different role in bacterial dissemination and disease treatment between meningitis and STSLS. Dexamethasone (dex) is a powerful anti-inflammatory compound inhibiting inflammatory cell recruitment and production of proinflammatory cytokines. Thus, dexamethasone was used to pretreat mice suffering from *S. suis* induced STSLS or meningitis to investigate the potential role of early inflammation at different infection sites. Injection of dexamethasone decreased the mortality of Fpr2$^{-/-}$ mice in the meningitis model, but accelerated the death in Fpr2$^{-/-}$ mice with STSLS (Figures 7A, B). Similar results were also obtained in WT mice (Figure S2). These results indicate that inflammation during the early stages of disease development is detrimental to host survival in the meningitis model, but beneficial to survival in the STSLS model. This finding was aligned with the results from a DNA intervention experiment which clarified the dual role of NETs during STSLS and meningitis. DNase I (DNase), which effectively degrades NET-associated DNA, was infused at the time of infection to prevent the accumulation of NETs in both the meningitis and STSLS models. Survival and bacterial load of infected mice in both infected models were evaluated. DNase significantly increased the mortality of the STSLS mice, but reduced the mortality of the meningitis mice (Figures 7C, D). Additionally, DNase treatment significantly

10.3389/fimmu.2023.1094331

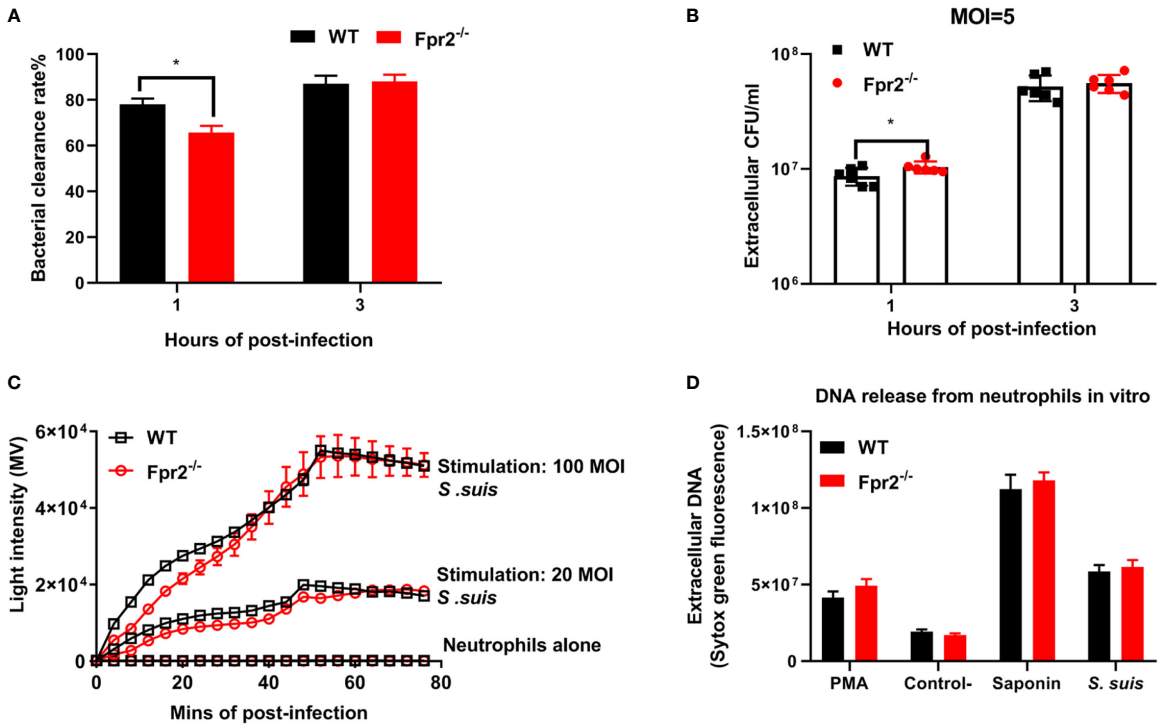

FIGURE 4
Fpr2 has no direct impact on NETs construction *in vitro*. WT and Fpr2 neutrophils stimulated with *S. suis* (MOI = 5) *in vitro*. **(A)** Bacterial clearance rate and **(B)** extracellular bacteria were monitored at 1 and 3 h. **(C)** In the ROS production experiment, the level of light intensity was measured when neutrophils were stimulated with different MOIs of *S. suis*. **(D)** The level of NETs produced by WT and Fpr2$^{-/-}$ neutrophils (MOI =100) was evaluated at 3 h post-infection. PMA was used as a positive control. Saponin was used to calibrate the number of cells. *, $P < 0.05$.

aggrandized the bacterial load in the STSLS mice, but had an opposite effect on the meningitis group (Figures 7E, F). This suggests that NETs play protective roles in bacterial cleaning and host individual survival in the initial stages of STSLS, whereas it interferes with bacterial clearance in the CNS and aggravates the severity of meningitis. These results highlight a dual role of neutrophils and NETs on *S. suis* proliferation and host protection in meningitis and STSLS models.

Discussion

The present study aimed to investigate the role of Fpr2 in the pathogenesis of the disease Streptococcal toxic shock-like syndrome (STSLS) and to explore the potential effects of the pro-resolution agents LXA4 or AnxA1 in disease treatment. The results demonstrated a detrimental impact of Fpr2 on STSLS pathogenesis by restricting the recruitment of neutrophils to the infection site, especially in the early stages of infection. Interference with Fpr2 or neutrophil recruitment activity may be a new therapeutic strategy to treat STSLS. Interestingly, a completely opposite effect of early neutrophil activity was observed in the *S. suis* meningitis models. Their powerful bactericidal and oxidative stress functions make neutrophils the most essential immune cells in the host defense system during infectious disease progression. However, neutrophils may exert opposite effects on disease progression in systemic or local infections in the early or late stages. The dual role of NETs may hinder bacterial clearance in the CNS, but accelerate bacterial clearance in the STSLS model. These findings indicate that regulating neutrophil recruitment is a potential treatment strategy to control infectious disease.

The therapeutic and anti-inflammatory effects of LXA4 have been demonstrated in many studies. During inflammatory brain injury after intracerebral hemorrhage, LxA4 reduced brain-infiltration by neutrophils and ameliorated the inflammatory brain injury (18). The administration of LXA4 has also been reported to suppress inflammation by and infiltration of neutrophils in experimental subarachnoid hemorrhage rat models (19). Interestingly, LXA4 exhibits a dual role in *Klebsiella pneumoniae* induced sepsis. Treatment with LXA4 worsened the infection and decreased cell migration in early sepsis but improved the survival rate by reducing the excessive inflammatory response in late sepsis (15). These findings are highly consistent with our results. Fpr2$^{-/-}$ mice have been used in many studies focused on infection or inflammation. Previous studies have confirmed that the antimigratory compounds lipoxin A and annexin A1 were reduced notably in Fpr2$^{-/-}$ mice (20). In the *Streptococcus pneumoniae* (*S. pneumoniae*) infected mouse model, increased infiltration made Fpr2$^{-/-}$ mice highly susceptible to *S. pneumoniae* meningitis (21). A study of ageing Fpr2$^{-/-}$ mice showed an integrative role of Fpr2 in cardiac inflammation-resolution processes and obesogenic aging. Fpr2 dysfunction magnified obesogenic cardiomyopathy and neutrophil recruitment in aging mice (22). These studies highlight the essential regulatory roles of Fpr2 in different inflammatory responses.

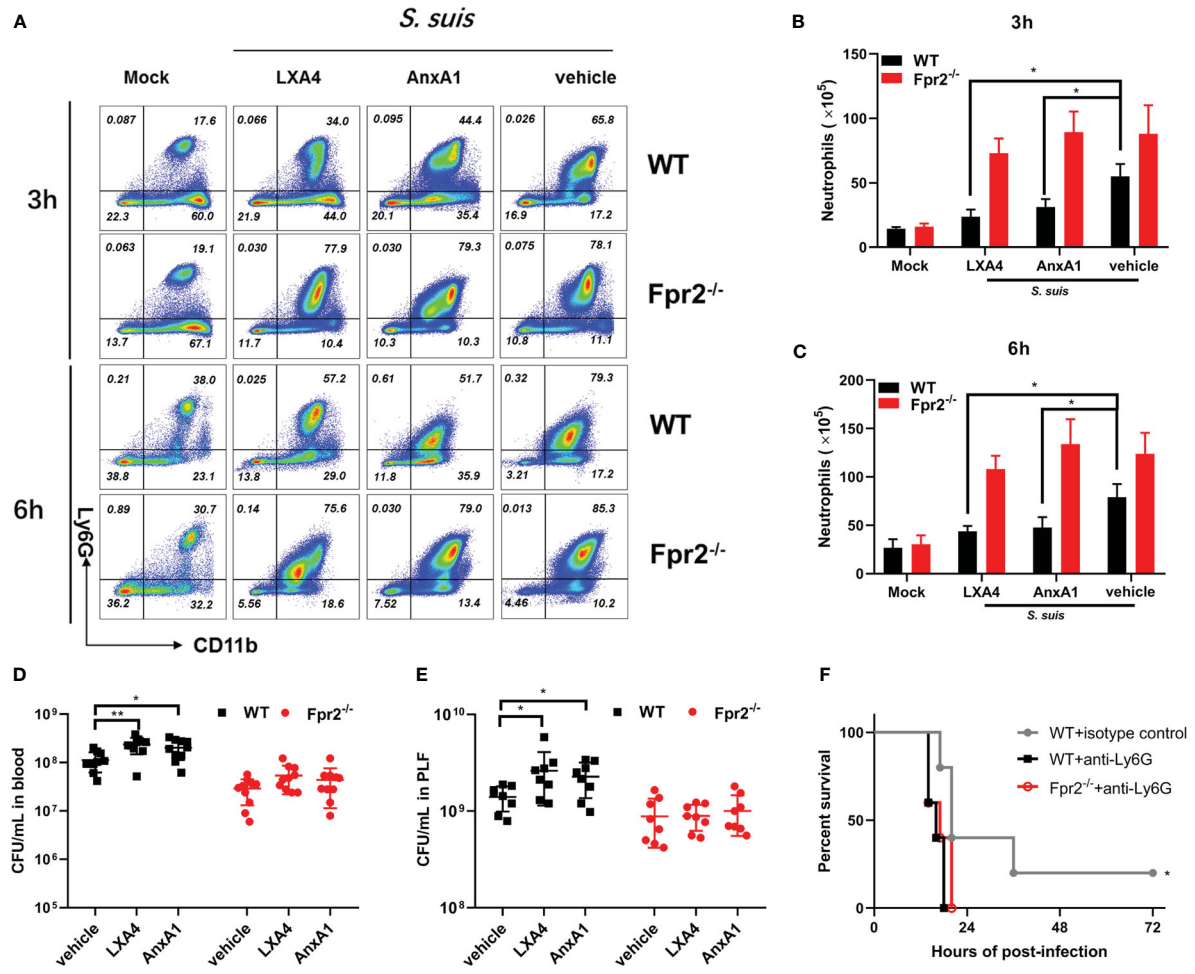

FIGURE 5
Fpr2 involvement in LXA4 or AnxA1-mediated anti-recruitment function. LXA4 or AnxA1 were used to intervene in STSLS in WT and Fpr2$^{-/-}$ mice. **(A)** Scattergrams of neutrophils (identified as Ly6G^{+} CD11b^{+}) positive events in PLF from WT and Fpr2$^{-/-}$ mice by flow cytometry analysis. Count of neutrophils in the PLF of WT and Fpr2$^{-/-}$ mice at **(B)** 3 h or **(C)** 6 h was evaluated (N≥3). Bacterial load in **(D)** blood or **(E)** PLF at 6 h was monitored (N≥8). **(F)** Survival of mice pretreated with anti-Ly6G antibody or isotype before infection (N=5). *, $P < 0.05$; **, $P < 0.01$.

Fpr2 performs both pro-inflammatory and pro-resolution immune functions depending on the presence of diverse ligands. Mice deficient in Fpr2 experienced more severity *Listeria* or *S. aureus* infection due to decreased leukocyte recruitment (23). This may be due to in the differing effects of Fpr2 on localized and systemic infections. Another potential explanation is the variable by-products generated during infection by different pathogens, as one virulence-associated factor of *S. suis*, Suilysin was associated with bacterial aggressiveness during infection by increasing cell-damaging effects. Formyl peptides of mitochondria, when released in response to cell damage, can be directly recognized by Fpr2 receptors and trigger an intense inflammatory response (24, 25).

The CNS has a poorly developed lymphatic drainage system and unique composition of the capillaries compared to most other organs (26). Since *Foldi* first proposed a role for the lymphatic system in the CNS and *Louveau* made the official discovery of it *in vivo* (27)much more about these processes are understood, but there are still plenty of mysteries surrounding the lymphatic network of the CNS. The unique composition of the capillaries in the brain, such as the end feet of astrocytes and pericytes, also results in different functions and behaviors. Strong neutrophil recruitment could potentially destroy normal tissue, interfere with cerebrospinal fluid circulation, and hinder bacterial clearance.

The protective function of NETs-including how they contribute to bacterial removal and inflammation resolution-in the initial stages of sepsis have been described for many infectious diseases, including those resulting from *S. suis*, *S. pneumoniae*, and *S. aureus* infections (28–30). A study on protein arginine deiminase 4 knockout mice demonstrated that killing of *Shigella flexneri* is mediated by NETs (31). However, detrimental effects of NETs in sepsis have also been described, as excessive NETs formation was associated with multiple organ injuries, a hyperinflammatory response, and thrombosis (32). Aberrant amounts of NETs could occlude capillaries, impair microcirculation, and injure normal tissues (33). Many pathogens have distinct DNases to degrade the DNA of NETs. Both endonuclease A (designated EndAsuis) and secreted *S. suis* nuclease A are capable of degrading NETs *in vitro* (34). Nuclease expression by *S. aureus* was associated with delayed bacterial clearance and facilitated bacterial escape from NETs (35). Hosts have also evolved unique tools, such as the antimicrobial peptide LL37, to protect against degradation by bacterial nucleases (36). A previous study revealed that Fpr2$^{-/-}$ mice had excessive NETs formation after

10.3389/fimmu.2023.1094331

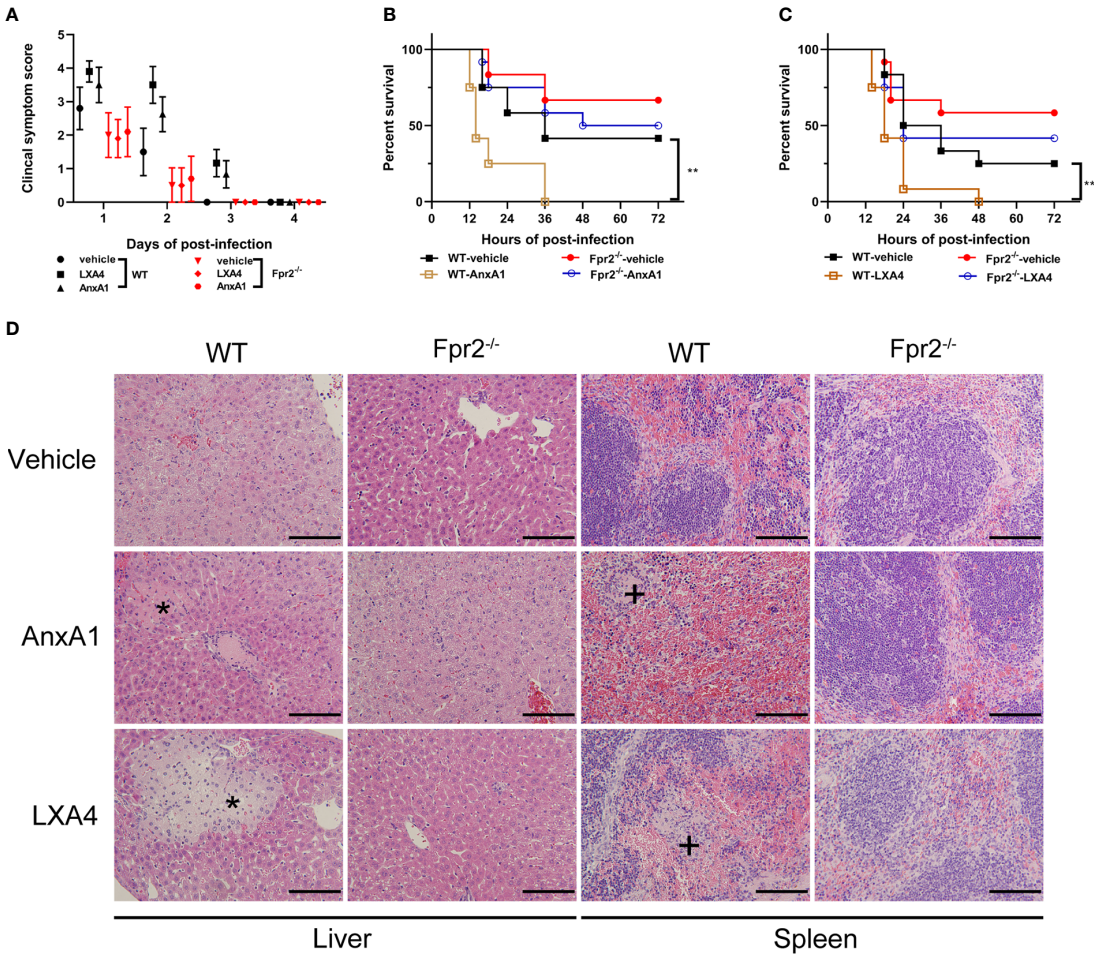

FIGURE 6
Down-regulation of recruitment by Fpr2 aggravate STSLS. LXA4 or AnxA1 were used to intervene in *S. suis* infection ($3x10^7$ CFU) of WT and $Fpr2^{-/-}$ mice. **(A)** Clinical symptom scores were evaluated (N=10). In survival experiments, **(B)** AnxA1, **(C)** LXA4, or a vehicle solution (THB) were used as pre-treatment in mice, then the mortality was recorded within 72 h (N=12). **(D)** Histopathological analysis was also performed (N=3). The asterisk (*) and plus (+) indicates histopathological lesion in the liver or spleen, respectively. Size bars represent 500 μm. **, $P < 0.01$.

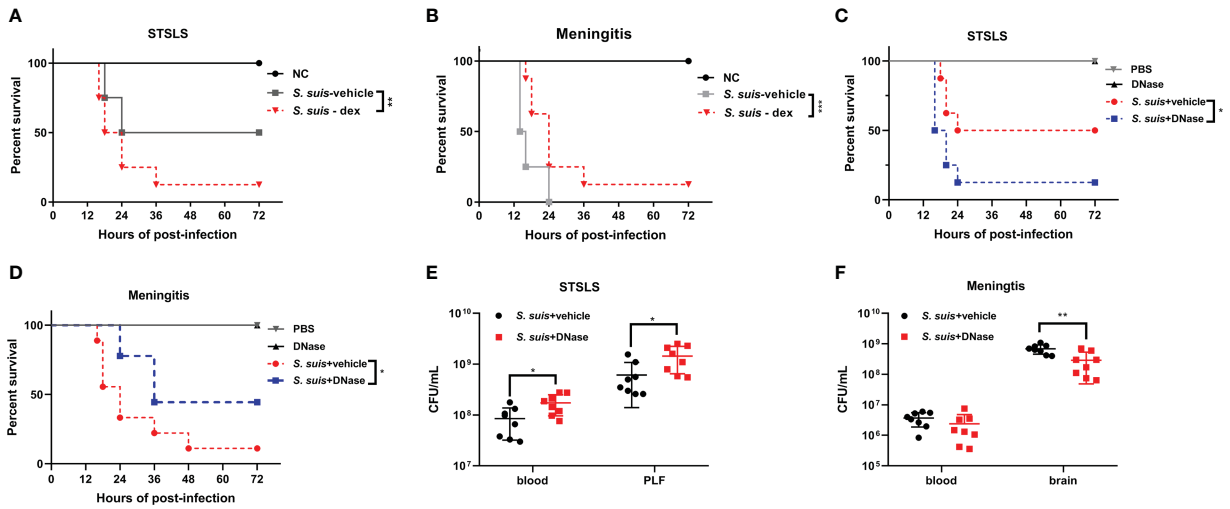

FIGURE 7
Bidirectional effects of recruitment in different *S. suis* infection pathway models. Kaplan–Meier curves of $Fpr2^{-/-}$ mice intervened with Dexamethasone in **(A)** STSLS or **(B)** *S. suis* meningitis (N=8). Kaplan–Meier curves of WT mice intervened with DNase in **(C)** STSLS or **(D)** meningitis model (N=8). Bacterial load of WT mice intervened with DNase in **(E)** STSLS or **(F)** meningitis model (N=8). *, $P < 0.05$; **, $P < 0.01$.

bacterial infection and that the lipoxin pathway could be a potent modulator (37). The involvement of Fpr2 in NETosis-related pathways may result from modifying calcium flux, which effectively promotes neutrophil apoptosis (33).

Fpr2 primarily causes increased neutrophil recruitment in *S. suis* infection, which exerts different effects on disease progression and host protection. Therapies that inhibit the synthesis or action of LXA4 and/or AnxA1, or that stimulate neutrophil activation could be useful for STSLS treatment. We also emphasize the delicate balance of inflammation response, which should be regulated under precise control with relation to different infection stages and sites. Therapy targeting Fpr2 or recruitment could potentially be developed as an additional treatment to antibiotics for infectious diseases.

Data availability statement

The original contributions presented in the study are included in the article/Supplementary Material. Further inquiries can be directed to the corresponding authors.

Ethics statement

The animal study was reviewed and approved by Animal Center of the Academy of Military Medical Sciences.

Author contributions

CN, SG and XL performed the whole experiment and formal analysis. CN and XL wrote the original draft preparation. YJ, ZM and DK designed the study and revised the manuscript. All authors contributed to the article and approved the submitted version.

Funding

This work was supported by the National Natural Science Foundation of China 82002116.

Conflict of interest

The authors declare that the research was conducted in the absence of any commercial or financial relationships that could be construed as a potential conflict of interest.

Publisher's note

All claims expressed in this article are solely those of the authors and do not necessarily represent those of their affiliated organizations, or those of the publisher, the editors and the reviewers. Any product that may be evaluated in this article, or claim that may be made by its manufacturer, is not guaranteed or endorsed by the publisher.

Supplementary material

The Supplementary Material for this article can be found online at: https://www.frontiersin.org/articles/10.3389/fimmu.2023.1094331/full#supplementary-material

SUPPLEMENTARY FIGURE 1
Wild-type and Fpr2$^{-/-}$ mice were inoculated with a standard bacterial dose of *S. suis* intraperitoneally. PLF was collected to detect inflammatory mediators **(A)** CXCL1, **(B)** CXCL2 and **(C)** IL-6 by ELISA at 3 and 6 h (N=4). ***, $P < 0.001$.

SUPPLEMENTARY FIGURE 2
Kaplan–Meier curves of Wild-type mice intervened with Dexamethasone in **(A)** STSLS or **(B)** *S. suis* meningitis (N=5). *, $P < 0.05$.

References

1. Hu B, Wang JP, Xu YC, Liu J, Li T, Jia J, et al. [Genomic investigation of human streptococcus suis infection in Shandong province]. *Zhonghua Yu Fang Yi Xue Za Zhi* (2021) 55(10):1232–9. doi: 10.3760/cma.j.cn112150-20210127-00084

2. Segura M. Streptococcus suis research: Progress and challenges. *Pathogens* (2020) 9 (9):707. doi: 10.3390/pathogens9090707

3. Lin L, Xu L, Lv W, Han L, Xiang Y, Fu L, et al. An Nlrp3 inflammasome-triggered cytokine storm contributes to streptococcal toxic shock-like syndrome (Stsls). *PloS Pathog* (2019) 15(6):e1007795. doi: 10.1371/journal.ppat.1007795

4. Song L, Li X, Xiao Y, Huang Y, Jiang Y, Meng G, et al. Contribution of Nlrp3 inflammasome activation mediated by suilysin to streptococcal toxic shock-like syndrome. *Front Microbiol* (2020) 11:1788. doi: 10.3389/fmicb.2020.01788

5. Xu L, Lin L, Lu X, Xiao P, Liu R, Wu M, et al. Acquiring high expression of suilysin enable non-epidemic streptococccus suis to cause streptococcal toxic shock-like syndrome (Stsls) through Nlrp3 inflammasome hyperactivation. *Emerg Microbes Infect* (2021) 10 (1):1309–19. doi: 10.1080/22221751.2021.1908098

6. Hotchkiss RS, Monneret G, Payen D. Immunosuppression in sepsis: A novel understanding of the disorder and a new therapeutic approach. *Lancet Infect Dis* (2013) 13(3):260–8. doi: 10.1016/S1473-3099(13)70001-X

7. Bozinovski S, Anthony D, Anderson GP, Irving LB, Levy BD, Vlahos R. Treating neutrophilic inflammation in copd by targeting Alx/Fpr2 resolution pathways. *Pharmacol Ther* (2013) 140(3):280–9. doi: 10.1016/j.pharmthera.2013.07.007

8. Bena S, Brancaleone V, Wang JM, Perretti M, Flower RJ. Annexin A1 interaction with the Fpr2/Alx receptor: Identification of distinct domains and downstream associated signaling. *J Biol Chem* (2012) 287(29):24690–7. doi: 10.1074/jbc.M112.377101

9. Abouelasrar Salama S, Gouwy M, Van Damme J, Struyf S. The turning away of serum amyloid a biological activities and receptor usage. *Immunology* (2021) 163(2):115–27. doi: 10.1111/imm.13295

10. Weiss E, Hanzelmann D, Fehlhaber B, Klos A, von Loewenich FD, Liese J, et al. Staphylococcus aureusformyl-peptide receptor 2 governs leukocyte influx in local infections. *FASEB J* (2018) 32(1):26–36. doi: 10.1096/fj.201700441r

11. Bleuze M, Gottschalk M, Segura M. Neutrophils in streptococcus suis infection: From host defense to pathology. *Microorganisms* (2021) 9(11):2392. doi: 10.3390/microorganisms9112392

12. Bjornsdottir H, Dahlstrand Rudin A, Klose FP, Elmwall J, Welin A, Stylianou M, et al. Phenol-soluble modulin alpha peptide toxins from aggressive staphylococcus aureus induce rapid formation of neutrophil extracellular traps through a reactive oxygen species-independent pathway. *Front Immunol* (2017) 8:257. doi: 10.3389/fimmu.2017.00257

13. Ni C, Gao S, Zheng Y, Liu P, Zhai Y, Huang W, et al. Annexin A1 attenuates neutrophil migration and il-6 expression through Fpr2 in a mouse model of streptococcus suis-induced meningitis. *Infect Immun* (2021) 89(3):e00680–20. doi: 10.1128/IAI.00680-20

14. Dominguez-Punaro MC, Segura M, Plante MM, Lacouture S, Rivest S, Gottschalk M. Streptococcus suis serotype 2, an important swine and human pathogen, induces strong systemic and cerebral inflammatory responses in a mouse model of infection. *J Immunol* (2007) 179(3):1842–54. doi: 10.4049/jimmunol.179.3.1842

15. Sordi R, Menezes-de-Lima OJr., Horewicz V, Scheschowitsch K, Santos LF, Assreuy J. Dual role of lipoxin A4 in pneumosepsis pathogenesis. *Int Immunopharmacol* (2013) 17(2):283–92. doi: 10.1016/j.intimp.2013.06.010

16. Pollenus E, Malengier-Devlies B, Vandermosten L, Pham TT, Mitera T, Possemiers H, et al. Limitations of neutrophil depletion by anti-Ly6g antibodies in two heterogenic immunological models. *Immunol Lett* (2019) 212:30–6. doi: 10.1016/j.imlet.2019.06.006

17. Swamydas M, Luo Y, Dorf ME, Lionakis MS. Isolation of mouse neutrophils. *Curr Protoc Immunol* (2015) 110:3 20 1–3 15. doi: 10.1002/0471142735.im0320s110

18. Zhang J, Hao N, Li W, Chen Q, Chen Z, Feng H, et al. Simvastatin upregulates lipoxin A4 and accelerates neuroinflammation resolution after intracerebral hemorrhage. *Curr neurovascular Res* (2022) 19(3):321–32. doi: 10.2174/1567202619666220913124627

19. Liu L, Zhang P, Zhang Z, Hu Q, He J, Liu H, et al. Lxa4 ameliorates cerebrovascular endothelial dysfunction by reducing acute inflammation after subarachnoid hemorrhage in rats. *Neuroscience* (2019) 408:105–14. doi: 10.1016/j.neuroscience.2019.03.038

20. Dufton N, Hannon R, Brancaleone V, Dalli J, Patel HB, Gray M, et al. Anti-inflammatory role of the murine formyl-peptide receptor 2: Ligand-specific effects on leukocyte responses and experimental inflammation. *J Immunol (Baltimore Md 1950)* (2010) 184(5):2611–9. doi: 10.4049/jimmunol.0903526

21. Oldekamp S, Pscheidl S, Kress E, Soehnlein O, Jansen S, Pufe T, et al. Lack of formyl peptide receptor 1 and 2 leads to more severe inflammation and higher mortality in mice with of pneumococcal meningitis. *Immunology* (2014) 143(3):447–61. doi: 10.1111/imm.12324

22. Tourki B, Kain V, Pullen AB, Norris PC, Patel N, Arora P, et al. Lack of resolution sensor drives age-related cardiometabolic and cardiorenal defects and impedes inflammation-resolution in heart failure. *Mol Metab* (2020) 31:138–49. doi: 10.1016/j.molmet.2019.10.008

23. Liu M, Chen K, Yoshimura T, Liu Y, Gong W, Wang A, et al. Formylpeptide receptors are critical for rapid neutrophil mobilization in host defense against listeria monocytogenes. *Sci Rep* (2012) 2:786. doi: 10.1038/srep00786

24. Banoth B, Cassel SL. Mitochondria in innate immune signaling. *Transl Res* (2018) 202:52–68. doi: 10.1016/j.trsl.2018.07.014

25. Votsch D, Willenborg M, Oelemann WMR, Brogden G, Valentin-Weigand P. Membrane binding, cellular cholesterol content and resealing capacity contribute to epithelial cell damage induced by suilysin of streptococcus suis. *Pathogens* (2019) 9(1):33. doi: 10.3390/pathogens9010033

26. Iliff JJ, Nedergaard M. Is there a cerebral lymphatic system? *Stroke* (2013) 44(6 Suppl 1):S93–5. doi: 10.1161/STROKEAHA.112.678698

27. Louveau A, Smirnov I, Keyes TJ, Eccles JD, Rouhani SJ, Peske JD, et al. Structural and functional features of central nervous system lymphatic vessels. *Nature* (2015) 523 (7560):337–41. doi: 10.1038/nature14432

28. Zhao J, Lin L, Fu L, Han L, Zhang A. Neutrophil extracellular taps play an important role in clearance of streptococcus suis *in vivo*. *Microbiol Immunol* (2016) 60 (4):228–33. doi: 10.1111/1348-0421.12367

29. Monteith AJ, Miller JM, Maxwell CN, Chazin WJ, Skaar EP. Neutrophil extracellular traps enhance macrophage killing of bacterial pathogens. *Sci Adv* (2021) 7 (37):eabj2101. doi: 10.1126/sciadv.abj2101

30. Herzog S, Dach F, de Buhr N, Niemann S, Schlagowski J, Chaves-Moreno D, et al. High nuclease activity of long persisting staphylococcus aureus isolates within the airways of cystic fibrosis patients protects against net-mediated killing. *Front Immunol* (2019) 10:2552. doi: 10.3389/fimmu.2019.02552

31. Li P, Li M, Lindberg MR, Kennett MJ, Xiong N, Wang Y. Pad4 is essential for antibacterial innate immunity mediated by neutrophil extracellular traps. *J Exp Med* (2010) 207(9):1853–62. doi: 10.1084/jem.20100239

32. Li RHL, Tablin F. A comparative review of neutrophil extracellular traps in sepsis. *Front Vet Sci* (2018) 5:291. doi: 10.3389/fvets.2018.00291

33. Tan C, Aziz M, Wang P. The vitals of nets. *J Leukoc Biol* (2021) 110(4):797–808. doi: 10.1002/JLB.3RU0620-375R

34. de Buhr N, Stehr M, Neumann A, Naim HY, Valentin-Weigand P, von Köckritz-Blickwede M, et al. Identification of a novel dnase of streptococcus suis (Endasuis) important for neutrophil extracellular trap degradation during exponential growth. *Microbiol (Reading)* (2015) 161(4):838–50. doi: 10.1099/mic.0.000040

35. Berends ET, Horswill AR, Haste NM, Monestier M, Nizet V, von Kockritz-Blickwede M. Nuclease expression by staphylococcus aureus facilitates escape from neutrophil extracellular traps. *J Innate Immun* (2010) 2(6):576–86. doi: 10.1159/000319909

36. Neumann A, Vollger L, Berends ET, Molhoek EM, Stapels DA, Midon M, et al. Novel role of the antimicrobial peptide ll-37 in the protection of neutrophil extracellular traps against degradation by bacterial nucleases. *J Innate Immun* (2014) 6(6):860–8. doi: 10.1159/000363699

37. Lefrancais E, Mallavia B, Zhuo H, Calfee CS, Looney MR. Maladaptive role of neutrophil extracellular traps in pathogen-induced lung injury. *JCI Insight* (2018) 3(3): e98178. doi: 10.1172/jci.insight.98178

frontiers | Frontiers in Immunology

TYPE Original Research
PUBLISHED 31 January 2023
DOI 10.3389/fimmu.2023.1090202

OPEN ACCESS

EDITED BY
Zuliang Jie,
Xiamen University, China

REVIEWED BY
Zhenguo Zeng,
The First Affiliated Hospital of Nanchang University, China
Yuan Xinxu,
Virginia Commonwealth University, United States

*CORRESPONDENCE
Ming Zhong
zhong_ming@fudan.edu.cn
Jing Cang
cang.jing@zs-hospital.sh.cn

SPECIALTY SECTION
This article was submitted to Inflammation, a section of the journal Frontiers in Immunology

RECEIVED 05 November 2022
ACCEPTED 16 January 2023
PUBLISHED 31 January 2023

CITATION
Wang Y, Wang C, He Q, Chen G, Yu J, Cang J and Zhong M (2023) Inhibition of sphingosine-1-phosphate receptor 3 suppresses ATP-induced NLRP3 inflammasome activation in macrophages *via* TWIK2-mediated potassium efflux. *Front. Immunol.* 14:1090202. doi: 10.3389/fimmu.2023.1090202

Inhibition of sphingosine-1-phosphate receptor 3 suppresses ATP-induced NLRP3 inflammasome activation in macrophages *via* TWIK2-mediated potassium efflux

Yingqin Wang[1], Chen Wang[2], Qiaolan He[2], Guannan Chen[2], Jie Yu[2], Jing Cang[1]* and Ming Zhong[2,3,4]*

[1]Department of Anesthesiology, Zhongshan Hospital, Fudan University, Shanghai, China, [2]Department of Critical Care Medicine, Zhongshan Hospital, Fudan University, Shanghai, China, [3]Shanghai Key Laboratory of Lung Inflammation and Injury, Shanghai, China, [4]Shanghai Institute of Infectious Disease and Biosecurity, School of Public Health, Fudan University, Shanghai, China

Background: Inhibition of sphingosine kinase 1 (SphK1), which catalyzes bioactive lipid sphingosine-1–phosphate (S1P), attenuates NLRP3 inflammasome activation. S1P exerts most of its function by binding to S1P receptors (S1PR1-5). The roles of S1P receptors in NLRP3 inflammasome activation remain unclear.

Materials and methods: The mRNA expressions of S1PRs in bone marrow-derived macrophages (BMDMs) were measured by real-time quantitative polymerase chain reaction (qPCR) assays. BMDMs were primed with LPS and stimulated with NLRP3 activators, including ATP, nigericin, and imiquimod. Interleukin-1β (IL-1β) in the cell culture supernatant was detected by enzyme-linked immunosorbent assay (ELISA). Intracellular potassium was labeled with a potassium indicator and was measured by confocal microscopy. Protein expression in whole-cell or plasma membrane fraction was measured by Western blot. Cecal ligation and puncture (CLP) was induced in C57BL/6J mice. Mortality, lung wet/dry ratio, NLRP3 activation, and bacterial loads were measured.

Results: Macrophages expressed all five S1PRs in the resting state. The mRNA expression of S1PR3 was upregulated after lipopolysaccharide (LPS) stimulation. Inhibition of S1PR3 suppressed NLRP3 and pro-IL-1β in macrophages primed with LPS. Inhibition of S1PR3 attenuated ATP-induced NLRP3 inflammasome activation, enhanced nigericin-induced NLRP3 activation, and did not affect imiquimod-induced NLRP3 inflammasome activation. In addition, inhibition of S1PR3 suppressed ATP-induced intracellular potassium efflux. Inhibition of S1PR3 did not affect the mRNA or protein expression of TWIK2 in LPS-primed BMDMs. ATP stimulation induced TWIK2 expression in the plasma membrane of LPS-primed BMDMs, and inhibition of S1PR3 impeded the membrane expression of TWIK2 induced by ATP. Compared with CLP mice treated with vehicle, CLP mice treated with the S1PR3 antagonist, TY52156, had aggravated pulmonary edema, increased

bacterial loads in the lung, liver, spleen, and blood, and a higher seven-day mortality rate.

Conclusions: Inhibition of S1PR3 suppresses the expression of NLRP3 and pro-IL-1β during LPS priming, and attenuates ATP-induced NLRP3 inflammasome activation by impeding membrane trafficking of TWIK2 and potassium efflux. Although inhibition of S1PR3 decreases IL-1β maturation in the lungs, it leads to higher bacterial loads and mortality in CLP mice.

KEYWORDS

sepsis, NLRP3 inflammasome, sphingosine-1-phosphate receptor, TWIK2, macrophage

Introduction

Sepsis is a critical clinical condition caused by infection. Globally, more than 19 million people are diagnosed with sepsis each year (1). Despite advances in supportive care for patients with sepsis, mortality remains over 25% (1). Currently, no specific treatment is available for sepsis. Sepsis is defined as a dysregulated host response to infection, and thus modulation of immune response is considered a reasonable approach to the treatment of sepsis.

Nucleotide-binding oligomerization domain-like receptor containing pyrin domain 3 (NLRP3) inflammasome is a multiprotein complex that triggers inflammatory responses in immune cells including macrophages (2). *Nlrp3* deficiency has been reported to protect mice from excessive pro-inflammatory cytokine storm and organ damage in inflammatory conditions including sepsis (3, 4). The activation of NLRP3 requires at least two signals (5). In the initial stage, the priming signals such as lipopolysaccharide (LPS) or tumor necrosis factor α (TNF-α) upregulate the transcription of NLRP3, interleukin-1β (IL-1β), and interleukin-18 (IL-18) in a nuclear factor κB (NF-κB)-dependent way (5). In addition, the priming signal licenses NLRP3 to rapidly respond to activating stimuli by post-translational modifications (6). Next, pathogen-associated molecular patterns (PAMPs) or danger-associated molecular patterns (DAMPs) such as adenosine triphosphate (ATP) act as the activation signal, which leads to the recruitment of the adaptor protein apoptosis-associated speck-like protein containing a caspase recruitment domain (ASC), never in mitosis A-related kinase 7 (NEK7) and pro-caspase-1 to NLRP3 (5). Then pro-caspase-1 is cleaved into bioactive caspase-1, which activates pro-IL-1β and pro-IL-18 into IL-1β and IL-18, respectively. Although reactive oxygen species production, metabolism disorder, mitochondrial dysfunction, lysosomal damage, and iron flux contribute contributes to NLRP3 activation, studies have shown that the decrease in intracellular potassium is an essential upstream event in NLRP3 activation induced by ATP and other DAMPs (7, 8). However, the mechanism of potassium efflux triggered by DAMPs remains poorly understood.

Sphingosine-1-phosphate (S1P) is a bioactive lipid that is generated from sphingosine by two key isoforms of sphingosine kinases, SphK1 and SphK2. S1P regulates diverse biologic processes by binding to five transmembrane sphingosine-1-phosphate receptors (S1PRs), S1PR1-S1PR5 (9). SphK1/S1P/S1PRs axis plays a key role in the pro-inflammatory response of macrophages and orchestrates the pathogenesis of inflammatory-related diseases such as inflammatory bowel disease, atherosclerosis, and infection (10). S1P is shown to stimulate NLRP3 inflammasome activation by acting as both priming and activation signals (11, 12). We have reported that inhibition of SphK1 improved the survival and lung vascular leakage in mice with cecal ligation and puncture (CLP)-induced sepsis by impeding NLRP3 inflammasome activation and subsequent IL-1β release from macrophages (11). However, the roles of S1PRs in NLRP3 inflammasome activation remain unclear. In this study, we explored whether the S1P receptors have a regulatory role in NLRP3 inflammasome activation and sepsis.

Materials and methods

Animals

Male C57BL/6 mice (10-to 12-week-old, 23-25g) were used in the experiments. All mice were housed in a specific pathogen-free facility with a 12:12 light: dark cycle and were free to food and water. Animal experimental protocols were approved by the Animal Care and Use Committee of the Zhongshan Hospital, Fudan University.

Polymicrobial sepsis model and drug treatment

Polymicrobial sepsis was induced by cecal ligation and puncture (CLP). Mice were intraperitoneally anesthetized with pentobarbital (80 mg/kg). Under the aseptic condition, laparotomy was performed with a 1 cm cut in the lower abdomen. The cecum was ligated at the point of 1 cm from the distal end of the cecum followed by a puncture with a 16-gauge needle. A small amount of feces was exteriorized from the cecum and the cecum was returned to the peritoneal cavity. The sham surgery was performed as surgical control, where the same operations were conducted except for cecal ligation, puncture, and exteriorization of feces. TY52156 was resolved in dimethyl sulfoxide (DMSO) at a concentration of 20mg/ml. Twenty minutes before surgery, TY52156 (10 mg/kg) or DMSO was injected intraperitoneally. No antibiotics

were given. An overdose of pentobarbital was used for the euthanasia of mice.

Measurement of bacterial burden

Blood and tissues were aseptically harvested from mice at 24 h after CLP. Tissues were homogenized in sterile PBS at 4°C, and the homogenates were diluted 10-fold with sterile PBS. Then blood and tissue homogenates were plated on LB agar plates, which were incubated at 37°C for 16 to 24 h under aerobic conditions. Colony-forming units (CFUs) were calculated and log-transformed for statistical analysis.

Measurement of wet/dry ratio

Left lung tissues harvested 24 h after CLP were weighed as the wet weight. Then, the lung tissues were dried in an oven at 60 °C for 48 h, the tissues were weighed again as the dry weight. The ratio of lung wet/dry weight was calculated.

Cell culture and stimulation

Bone marrow cells were prepared from C57BL/6J mice, as previously described. In brief, bone marrow cells were differentiated into bone marrow-derived macrophages (BMDMs) for 6-7 days with DMEM/F12 medium (Hyclone, USA) supplemented with 20% L929 conditioned media and 10% heat-inactivate fetal bovine serum (FBS) (Biological Industries, Israel). The medium was replaced every 2-3 days. BMDMs were primed with 1 μg/ml LPS for 3 h in FBS free medium, with S1PR1 antagonist (W146, 3602, Tocris Bioscience, USA), S1PR2 antagonist (JTE-013, 10009458, Cayman, USA), S1PR3 antagonist (TY52156, 19119, Cayman, USA), S1PR4 antagonist (CYM 50358, 4679, Tocris Bioscience, UK), S1PR5 agonist (A971432, SML1744, Sigma-Aldrich, USA) or vehicle. After priming, BMDMs were stimulated with 3 mM ATP (A2383-5G, Sigma-Aldrich, USA), 10μM Nigericin (tlrl-nig, *In vivo*gen, USA), 25μg/mL imiquimod (tlrl-imq, *In vivo*gen, USA) for 30 min; 2μg/mL flagellin (tlrl-stfla, *In vivo*gen, USA) with 2.5 μl/ml of Lipofectamine 2000, 5μg/mL dsDNA μg (tlrl-patn, *In vivo*gen, USA) with 2.5 μl/ml of Lipofectamine 2000 for 6h. Cells were lysed for Western blot, and the supernatant was collected after stimulation.

Real-time quantitative polymerase chain reaction assays

The total ribonucleic acid (RNA) was extracted from BMDMs using TRIzol reagent (Invitrogen, USA), and was converted to complementary deoxyribonucleic acid with the Reverse Transcription Master Mix (EZBioscience, USA). Quantitative real-time polymerase chain reaction (qPCR) was performed using SYBR Green qPCR Master Mix (EZBioscience, USA) according to the manufacturer's protocols. Primers are listed in Supplementary Table 1

Enzyme-linked immunosorbent assay

IL-1β in the supernatant was measured by Mouse IL-1 beta/IL-1F2 DuoSet enzyme-linked immunosorbent assay kit (R&D, DY401-05, USA) according to the manufacturer's instructions.

Western blot

Cells were lysed in Nonidet P-40 lysis buffer with phenylmethanesulfonyl fluoride and protease inhibitor. Boiled samples of cell lysate with loading buffer were electrophoresed and transferred onto a 0.2μm polyvinylidene fluoride membrane (Millipore, USA). Membranes were blocked with 5% nonfat dry milk for 1 h at room temperature followed by incubation with primary antibodies overnight at 4°C. Then the membranes were incubated with secondary antibodies for 1 h at room temperature and were detected with an enhanced chemical luminescence kit (Beyotime technology, China). Antibodies are shown in Supplementary Table 2.

Measurement of intracellular potassium

Cells were loaded with a potassium indicator, ION Potassium Green-2 AM (ab142806, Abcam, UK) at 5μM for 30 min at room temperature, according to the manufacturer's instructions. After two washes in warmed PBS, cells were imaged using an Olympus FV3000 inverted confocal microscope. The fluorescence signal between 530nm and 560 nm was recorded.

Plasma membrane protein separation

The plasma membrane was isolated using Plasma Membrane Protein Extraction Kit (ab65400, Abcam, UK) according to the manufacturer's instructions. One 10-cm plate of cells for each condition was scraped in phosphate-buffered saline (PBS). The cells were centrifugated at 3000 rpm for 5 minutes and washed once with ice-cold PBS. Then the cells were re-suspended in the Homogenize Buffer Mix in an ice-cold Dounce homogenizer and were homogenized 50 times. The homogenates were transferred to 1.5 ml microcentrifuge tubes and centrifuged at 700 g for 10 minutes at 4°C. The supernatants were transferred to new vials and centrifuged at 10,000 g for 30 min at 4°C to pellet total cellular membrane protein. Plasma membrane proteins were purified from the total cellular membrane protein with phase separation solutions and were pelleted and dissolved in 0.5% Triton X-100, followed by Western blot.

Statistical analysis

A two-tailed unpaired Student's t-test or Mann–Whitney U test was used to compare the two groups. Three or more groups were tested with the one-way analysis of variance (ANOVA) followed by Tukey's *post hoc* test. The Kaplan–Meier plot with log-rank (Mantel-Cox) test was adopted to assess survival differences between groups. Grayscale or

fluorescence intensity in image data was quantified with ImageJ (National Institutes of Health, USA). Statistical analyzes were performed in GraphPad Prism 9 (GraphPad Software Inc., USA). The RNA sequencing (RNAseq) data of healthy controls and septic patients on the Gene Expression Omnibus (GEO) database (GSE46955) was analyzed with an online GEO2R tool. The R scripts were got from GEO2R with some modifications to download and save the data. A two-tailed hypothesis test was used, and a p value less than 0.05 was considered statistically significant.

Results

Expression of S1PRs in macrophages in resting and inflammatory state

We first checked the relative mRNA expression of S1PR1-5 in BMDMs, and we found that BMDMs mainly expressed S1PR1, S1PR2, and S1PR4 in the resting state (Figure 1A). Only the expression of S1PR3 was upregulated in BMDMs after LPS stimulation (Figures 1B-F). Next, we analyzed the expressions of S1PR3 in monocytes of healthy volunteers and septic patients with the online RNAseq data. Five S1PRs were detected in human monocytes (Supplementary Figure 1). Human monocytes mainly expressed S1PR1 and S1PR4. The analysis showed that only the mRNA expression of S1PR3 was upregulated in human monocytes after LPS stimulation (Supplementary Figure 1). In addition, compared with healthy controls, septic patients had higher mRNA levels of S1PR3 in monocytes (Figure 1G).

Inhibition of S1PR3 suppresses ATP-induced NLRP3 inflammasome activation in macrophages

To determine the effects of S1PRs on NLRP3 activation, S1PR1-S1PR4 were inhibited with their respective antagonists during LPS priming followed by ATP stimulation in BMDMs, and S1PR5 was activated with its agonist during LPS priming because no commercial antagonist of S1PR5 was available (Figure 2; Supplementary Figure 2). Inhibition of S1PR3 significantly reduced both caspase-1 cleavage and IL-1β maturation in LPS-primed BMDMs after ATP stimulation (Figure 2A). Consistently, the level of IL-1β in the supernatant of BMDMs treated with LPS and the S1PR3 antagonist was lower than that of BMDMs treated with LPS (Figure 2B). Inhibition of S1PR2 also partially suppressed NLRP3 activation induced by ATP (Supplementary Figure 2B). Responses of BMDMs to ATP remained intact when treated with the S1PR1 antagonist or the S1PR4 antagonist (Supplementary Figures 2A, C). Activation of S1PR5 did not further potentiate IL-1β or caspase-1 activation in BMDMs after ATP stimulation (Supplementary Figure 2D). These results suggest that NLRP3 inflammasome activation induced by ATP is mainly limited by the suppression of S1PR3 signaling in BMDMs.

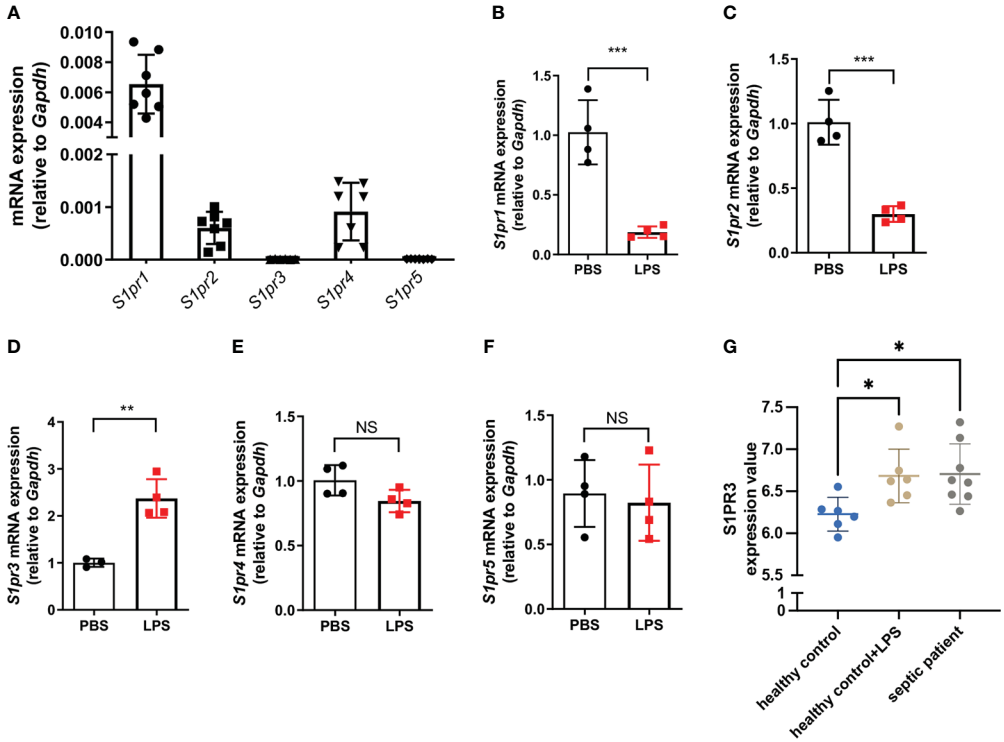

FIGURE 1
The expression of sphingosine-1-phosphate receptors in BMDMs. **(A)** Relative mRNA expression of S1PRs to GAPDH in BMDMs (n=7). **(B-F)** BMDMs were treated with LPS (1μg/mL) or PBS for 4h. The mRNA expressions of S1PRs in BMDMs were measured by RT-qPCR (n=4). **(G)** The mRNA expression values of S1PR3 in monocytes from healthy controls stimulated with or without LPS, and from septic patients were analyzed with data from the GEO database. Data are presented as mean ± SD. *p<0.05, **p < 0.01, ***p < 0.001, two-tailed t-test. NS, non-sense.

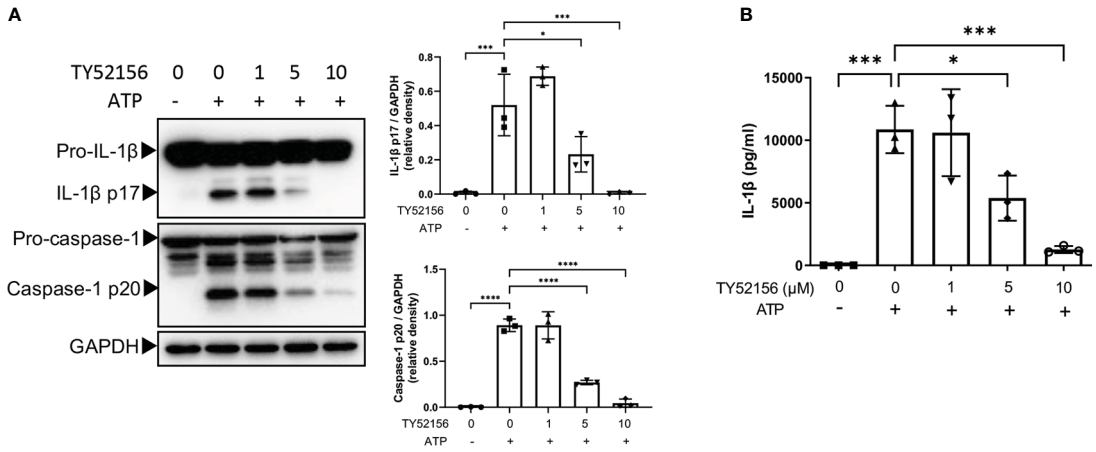

FIGURE 2
Inhibition of S1PR3 suppresses NLRP3 inflammasome activation induced by ATP. **(A, B)** BMDMs were primed with LPS (1μg/mL) and treated with TY52156 (0, 1, 5, 10μM) for 3.5h, followed by ATP (3mM) stimulation for 30 min. Pro-IL-1β, IL-1β p17, pro-caspase-1, and caspase-1 p20 in BMDMs were measured by Western blot (n= 3) **(A)**. IL-1β in the supernatant was measured by ELISA (n= 3) **(B)**. Values are presented as mean ± SD. *p < 0.05, ***p < 0.001, ****p < 0.0001, one-way ANOVA.

Inhibition of S1PR3 suppresses the LPS priming signal in BMDMs

To understand the mechanism by which inhibition of S1PR3 suppressed NLRP3 inflammasome activation, we first examined the roles of S1PR3 in LPS priming. The results show that inhibition of S1PR3 during LPS priming downregulated mRNA expression of IL-1β, IL-18, NLRP3 (Figure 3A), and protein levels of pro-IL-1β and NLRP3 in BMDMs (Figure 3B). Inhibition of S1PR3 did not affect the mRNA and protein expression of pro-caspase-1(Supplementary Figure 3). These data suggest that inhibition of S1PR3 suppresses the expression of IL-1β and NLRP3 in macrophages during LPS priming.

Inhibition of S1PR3 suppresses ATP-induced NLRP3 inflammasome activation *via* potassium efflux

Next, we explored the roles of S1PR3 in NLRP3 activation in LPS-primed BMDMs. Given that potassium efflux is a common upstream of NLRP3 inflammasome induced by DAMPs including ATP (8), we

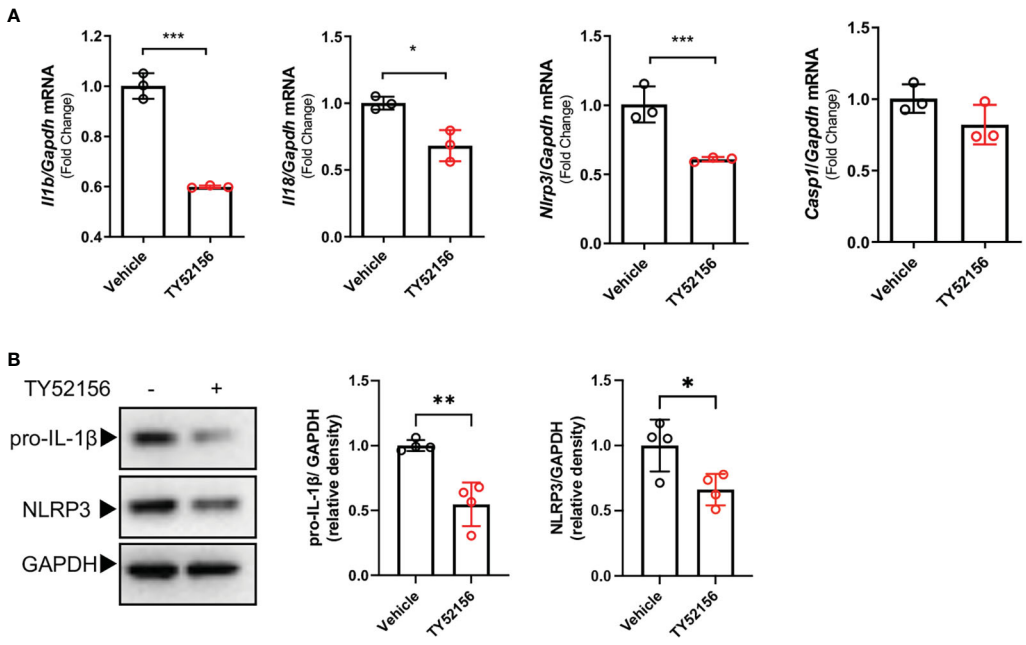

FIGURE 3
Inhibition of S1PR3 suppresses the LPS priming signal in BMDMs. **(A-B)** BMDMs treated with LPS (1μg/mL) for 4h with or without TY52156 (10 μM). The mRNA expressions of IL-1β, IL-18, NLRP3, and caspase-1 were measured by RT-qPCR **(A)**. The protein expression of pro-IL-1β and NLRP3 **(B)** were measured by Western blot (n=3). Values are presented as mean ± SD. *p < 0.05, **p < 0.01, ***p < 0.001, two-tailed t-test.

10.3389/fimmu.2023.1090202

tested whether S1PR3 can regulate potassium efflux induced by ATP. We found that inhibition of S1PR3 significantly reduced potassium efflux after ATP stimulation (Figure 4A). We further investigated the effects of inhibition of S1PR3 in NLRP3 inflammasome activation by nigericin, a bacterial potassium pore-forming toxin, which induces NLRP3 activation *via* directly mediating potassium efflux, and imiquimod, which activates NLRP3 inflammasome independent of potassium efflux (13). We found that inhibition of S1PR3 potentiated NLRP3 inflammasome activation induced by nigericin, but did not affect on that induced by imiquimod (Figures 4B-E). Furthermore, we

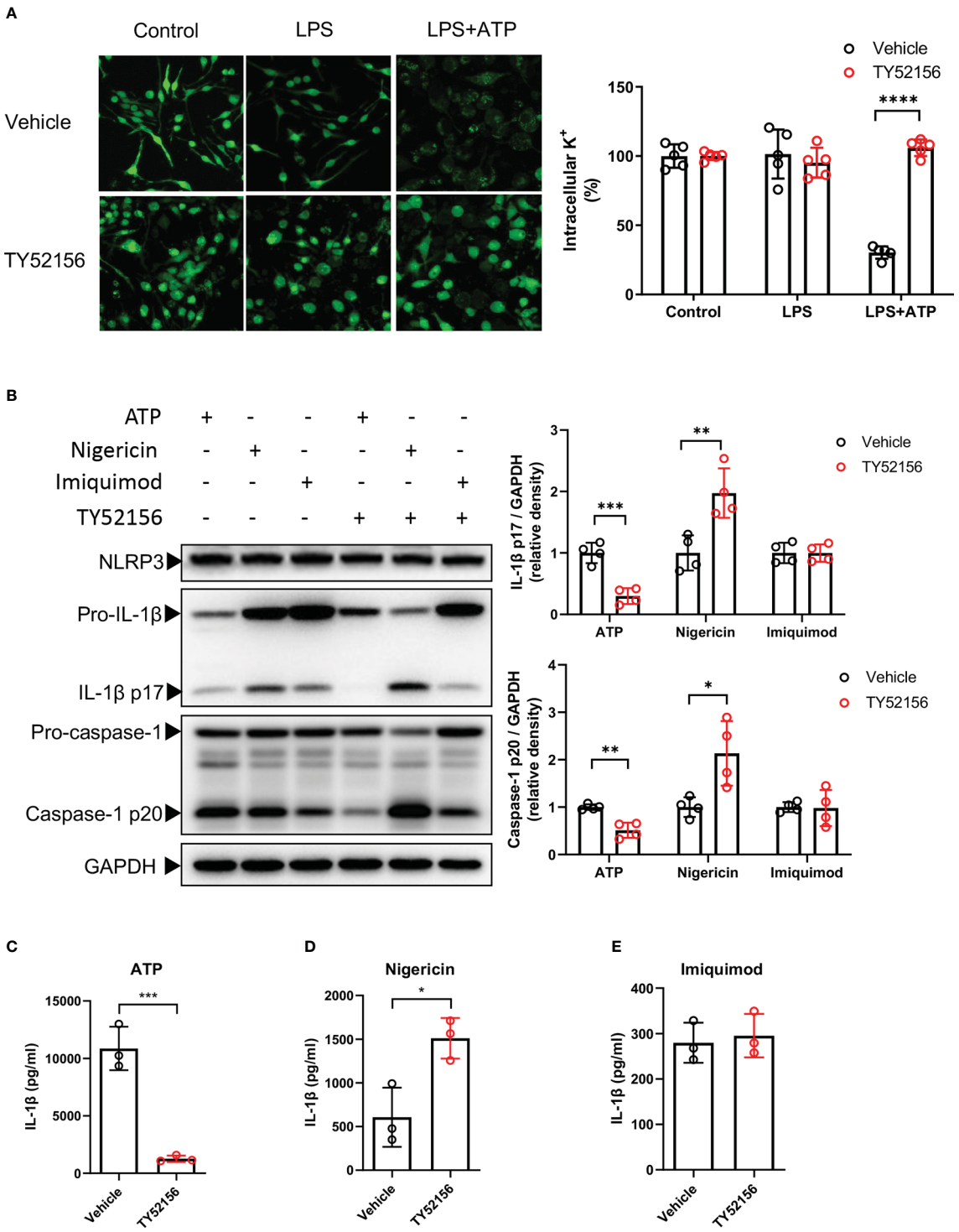

FIGURE 4
Inhibition of S1PR3 suppresses ATP-induced NLRP3 inflammasome activation *via* potassium efflux. **(A)** BMDMs were primed with LPS (1μg/mL) and treated with TY52156 (10μM) or vehicle for 3.5h, followed by ATP (3mM) stimulation for 30 min. Representative intracellular potassium fluorescence image of 5 fields from 3 independent experiments. Values are presented as mean ± SD. ****p < 0.0001, two-tailed t-test. **(B-E)** BMDMs were primed with LPS (1μg/mL) and treated with TY52156 (10μM) or vehicle for 3.5h, followed by ATP (3mM), nigericin (10μM), or imiquimod (25μg/mL) stimulation for 30 min. Pro-IL-1β, IL-1β p17, pro-caspase-1, and caspase-1 p20 in BMDMs were measured by Western blot (n= 4) **(B)**. IL-1β in the supernatant was measured by ELISA (n= 3) **(C-E)**. Values are presented as mean ± SD. *p < 0.05, **p < 0.01, ***p < 0.001, two-tailed t-test.

found that inhibition of S1PR3 enhanced dsDNA-induced AIM2 inflammasome and salmonella infection-induced NLRC4 inflammasome activation, as indicated by enhanced caspase-1 cleavage (Supplementary Figures 4A, B). These results thus demonstrate a specific role of S1PR3 signaling in ATP-induced NLRP3 inflammasome activation by suppressing potassium efflux.

Inhibition of S1PR3 suppresses ATP-induced potassium efflux through TWIK2 membrane trafficking

The evidence has shown that TWIK2-mediated potassium efflux is required for ATP-induced NLRP3 inflammasome activation (13). In macrophages, ATP binds to P2X7 receptors to activate NLRP3 inflammasome. Thus, we investigated the effect of S1PR3 on the expression of TWIK2 and P2X7 receptors in macrophages. Inhibition of S1PR3 did not affect the mRNA or protein expression of TWIK2 in BMDMs primed with LPS (Figures 5A, B). The mRNA levels of P2X7 receptors in macrophages were slightly increased after LPS stimulation, but the protein expression of P2X7 receptors was unchanged (Supplementary Figures 5A, B). Recent evidence has indicated that both TWIK2 and P2X7 receptors dynamically move between the plasma membrane and cytosol (14–17). We found that the expression of TWIK2 on the plasma membrane was induced by ATP stimulation in LPS-primed BMDMs (Figure 5C). Meanwhile, compared with the control BMDMs, less TWIK2 was expressed on the plasma membrane of S1PR3–inhibited BMDMs (Figure 5C). The

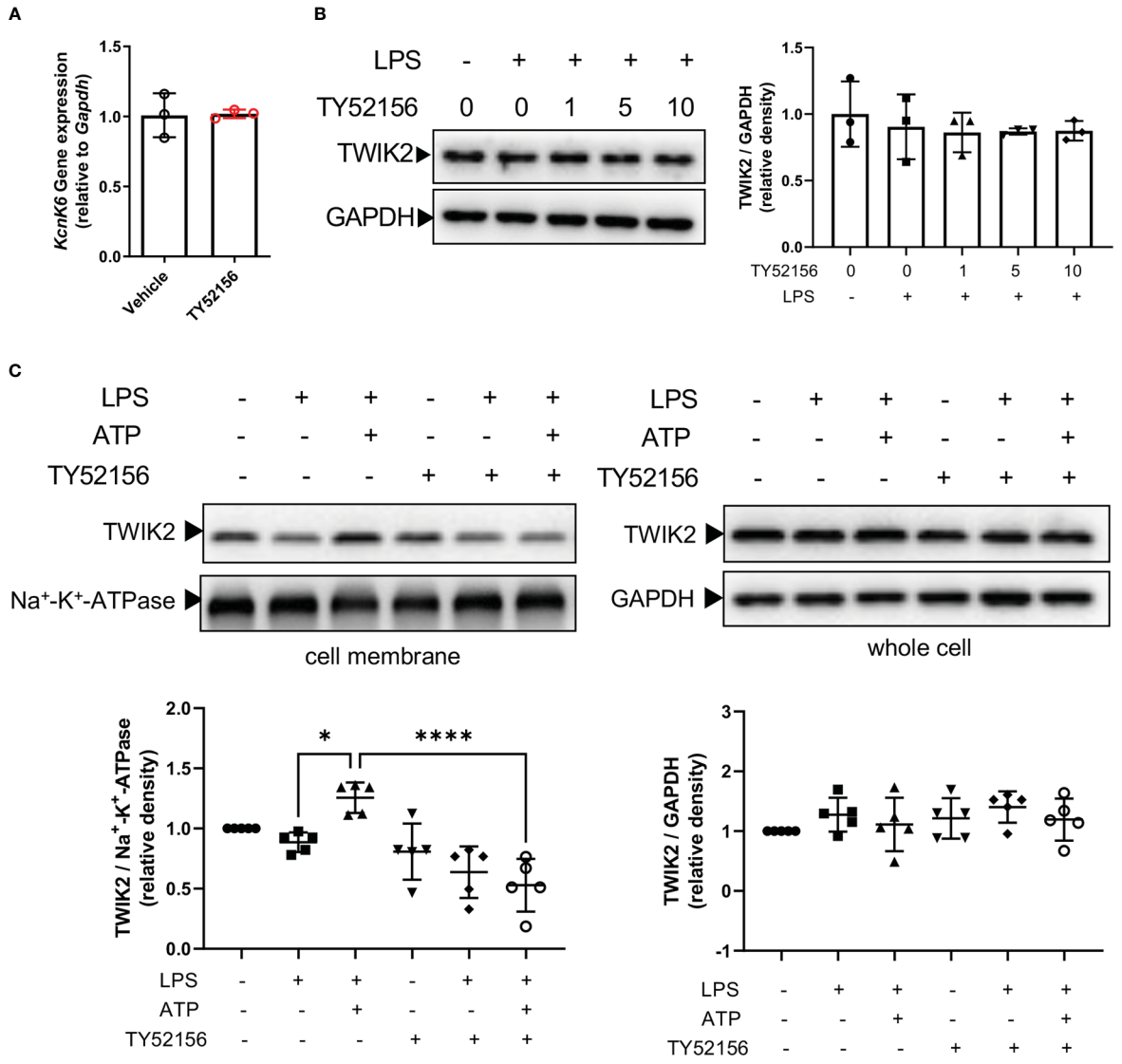

FIGURE 5
Inhibition of S1PR3 suppresses ATP-induced potassium efflux through TWIK2 membrane trafficking. **(A)** BMDMs were primed with LPS (1μg/mL) and treated with TY52156 (10μM) or vehicle for 4h. The mRNA expression of KcnK6, which codes TWIK2, was measured by RT-qPCR (n=3). Values are presented as mean ± SD. Data were analyzed with a two-tailed t-test. **(B)** BMDMs were primed with LPS (1μg/mL) and treated with TY52156 (0, 1, 5, 10μM) for 4h. The TWIK2 in BMDMs was measured by Western blot (n= 3). Values are presented as mean ± SD. Data were analyzed with one-way ANOVA. **(C)** BMDMs were primed with LPS (1μg/mL) and treated with TY52156 (10μM) or vehicle, followed by ATP (3mM) stimulation for 30 min. The TWIK2 in the plasma membrane and whole-cell were measured by Western bot (n= 5). Values are presented as mean ± SD. *p < 0.05, ****p < 0.0001, one-way ANOVA.

protein expression of P2X7 receptors on the plasma membrane was unaffected by LPS, LPS plus ATP stimulation, or S1PR3 inhibition (Supplementary Figure 5C). These results suggest that inhibition of S1PR3 could suppress ATP-induced NLRP3 inflammasome activation by limiting TWIK2 membrane trafficking.

Inhibition of S1PR3 increases mice mortality in polymicrobial sepsis

Next, we examined the role of S1PR3 in sepsis with the S1PR3 antagonist, TY52156. Twenty-four hours after CLP, mice in the S1PR3 inhibition group had lower levels of cleaved IL-1β in the lungs, compared with mice in the vehicle control group (Figure 6A). However, mice in the S1PR3 inhibition group had higher wet/dry ratios and heavier bacterial burdens in the lungs, livers, spleens, and blood than those in the vehicle control group (Figures 6B-F). The survival rate of CLP mice was 11.11% and 44.44% in the S1PR3 inhibition group and the vehicle control group ($p < 0.001$) (Figure 6G), respectively.

Discussion

Activation of the inflammatory NLRP3 inflammasome is an important mechanism by which macrophages combat invading pathogens in the early stages of sepsis. Our data suggested that inhibition of S1PR3 suppressed the expression of NLRP3 and IL-1β during LPS priming and attenuated ATP-induced NLRP3 inflammasome activation by limiting TWIK2 membrane trafficking and subsequent potassium efflux (Supplementary Figure 6).

ATP is a common NLRP3 stimulus that was released in large quantities during sepsis, contributing to systemic inflammation and secondary organ damage (18, 19). Thus, we first tested the effects of S1PRs on NLRP3 inflammasome activation with ATP. Upon ATP stimulation, inhibition of S1PR3 significantly attenuated NLRP3 activation in LPS-primed macrophages. Notably, our results showed that inhibition of S1PR2 also partially hampered NLRP3 inflammasome activation in macrophages. A possibility is that the S1PR family members are functionally redundant. Indeed, it is reported that both S1PR2 and S1PR3 can activate the receptor-bound G-proteins $G_{\alpha i}$, $G_{\alpha q}$, and $G_{\alpha 12/13}$ (20, 21). Evidence for the functional redundancy of S1PR2 and S1PR3 has also been described in modulating macrophage behaviors, such as motility in cholestatic liver injury (22), phenotype reprograming in mycobacteria infection (23), and phagocytosis in lung infection (24). Our results show that LPS stimulation only induced the expression of S1PR3 in both BMDMs and human monocytes, and that inhibition of S1PR3 attenuates NLRP3 inflammasome activation more efficiently than inhibition of S1PR2 in BMDMs. Therefore, we speculate that S1PR3 plays a major role in ATP-induced NLRP3 activation in macrophages under inflammatory conditions.

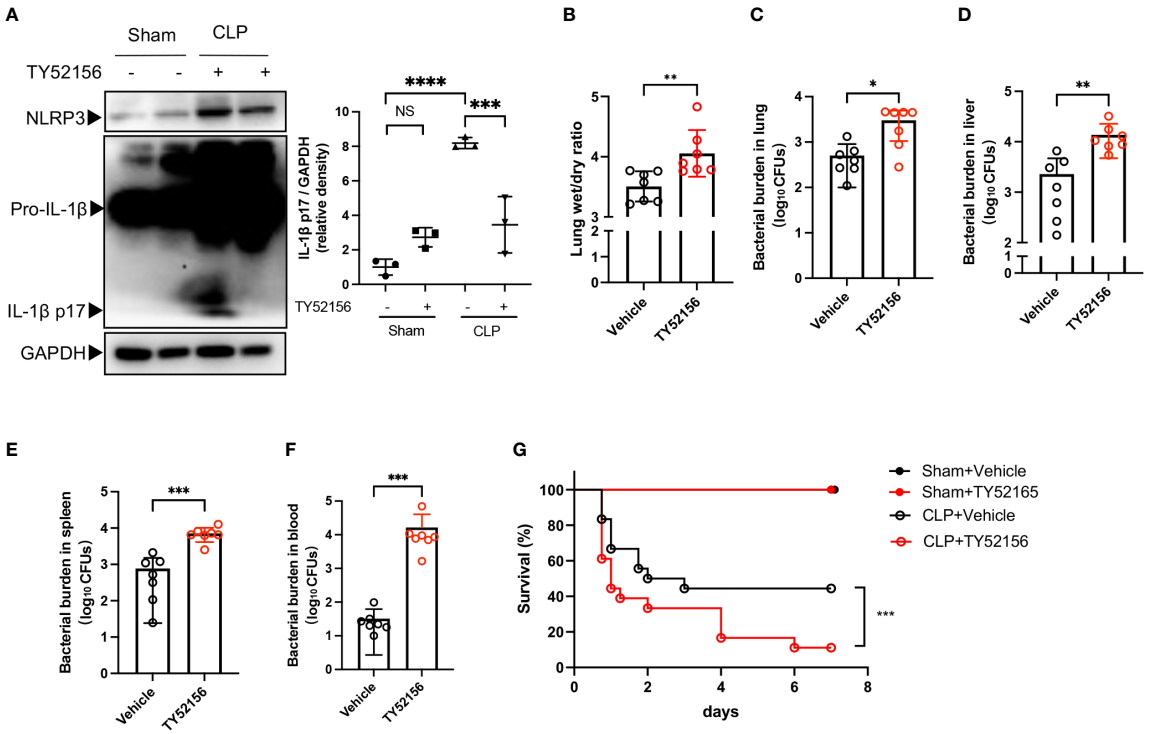

FIGURE 6
Inhibition of S1PR3 increases mortality and bacterial burden in sepsis. **(A)** Western blots of lung tissues from CLP mice treated with TY52156 or vehicle, and sham surgery control treated with TY52156 or vehicle (n=3 in each group) Values are presented as mean ± SD. ***$p < 0.001$, ****$p < 0.0001$, one-way ANOVA. **(B)** Lung wet/dry ratio of mice undergone CLP and then treated with TY52156 (10mg/kg) or vehicle (n=7 in each group). Values are presented as mean ± SD. **$p < 0.01$, two-tailed t-test. **(C-F)** Bacterial burden in the lung **(C)**, liver **(D)**, spleen **(E)**, and blood **(F)** of mice undergone CLP and then treated with TY52156 (10mg/kg) or vehicle (n=7 in each group). Values are presented as the mean of log10 CFU ± SD **(C-F)**. *$p < 0.05$, **$p < 0.01$, ***$p < 0.001$, Mann-Whitney test. **(G)** Kaplan Meier survival curves of mice undergone CLP or Sham surgery and then treated with TY52156 (10mg/kg) or vehicle (n=6 in Sham groups, n=18 in CLP groups). ***$p < 0.001$, log-rank test. NS, non-sense.

Potassium efflux is a main upstream event in NLRP3 inflammasome activation induced by various stimuli including ATP (13, 25). Our results indicate that inhibition of S1PR3 suppresses potassium efflux induced by ATP. Notably, inhibition of S1PR3 enhanced NLRP3 activation induced by nigericin, a potassium ionophore directly leading to potassium efflux (26, 27), and inhibition of S1PR3 had no effects on NLRP3 activation induced by imiquimod, which is independent of potassium efflux (28). Besides, inhibition of S1PR3 also enhanced AIM2 or NLRC4 inflammasome activation. These results suggest that the effects of S1PR3 on canonical inflammasome depend on the given stimulus and that inhibition of S1PR3 has an exclusive role in ATP-induced NLRP3 inflammasome activation *via* potassium efflux. Since ATP plays an essential role as an extracellular signaling molecule in the development of sepsis and septic organ failure (6), we focused on the mechanism of S1PR3 in ATP-induced NLRP3 inflammasome activation in our research. The mechanisms underlying the effects of S1PR3 on NLRP3 inflammasome activation induced by other stimuli need further investigation.

A recent study has identified TWIK2 as the potassium efflux channel required for ATP-induced NLRP3 inflammasome activation downstream of the ATP ligand, P2X7 receptors (13). However, the mechanism by which ATP enhanced potassium efflux *via* TWIK2 remains elusive. Our work here adds to the knowledge that ATP can stimulate potassium efflux by increasing the plasma membrane trafficking of TWIK2 without affecting the expression of P2X7 receptors. We also find that inhibition of S1PR3 limited the expression of TWIK2 on the cell membrane induced by ATP. Experimental data from Madin-Darby canine kidney (MDCK) cells show that exogenous expressed TWIK2 preferentially expresses in the Lamp1-positive lysosomal compartment, and functional relocates at the plasma membrane when its lysosomal targeting C terminal trafficking motifs are inactivated (17). Whether S1PR3 signaling engages with ATP-induced TWIK2 membrane trafficking by modulating this trafficking motif remains to be determined.

NLRP3 inflammasome activation is a double-edged sword in bacterial infection. On the one hand, a large number of inflammatory factors released after inflammasome activation can cause tissue damage; on the other hand, inflammasome activation and cell pyroptosis help to confine bacteria within macrophages, and the release of IL-1β facilitates the recruitment of neutrophils to clear bacteria (29). Previous studies have consistently demonstrated that *Nlrp3* deficiency protects mice from lethal sepsis, which is associated with lower levels of IL-1β (3, 4). In contrast, the benefit of *Nlrp3* deficiency in bacteria clearance in the septic mice remains controversial, which was possibly due to variations in experimental protocols (3, 4, 30, 31). Recent data has indicated that maintaining a certain amount of IL-1β prevented mice from death after sepsis in the long term (32). Clinical data shows that septic patients present an early impairment of the NLRP3 inflammasome is associated with a higher late-death rate (33). In our study, the antagonist of S1PR3 was used to investigate the effects of S1PR3 inhibition on CLP-induced septic mice. The dose of TY52156 we used, 10mg/kg, is also widely used in previously published studies (34, 35). In our results, this dose of TY52156 did not lead to the death of mice in the sham surgery group, which demonstrates that no significant toxicity of TY52156 is shown with this dose. Though inhibition of S1PR3 suppressed IL-1β activation in the lungs of septic mice, it also led to higher mortality and bacterial burdens, which were consistence with the results reported by Hou et al. in *S1pr3*$^{-/-}$ mice. Hou et al. have also reported that S1PR3 had a critical role in the bactericidal activity of macrophages (36). Compared with the healthy controls, the S1PR3 mRNA levels were higher in ICU controls and septic patients than that in healthy controls (36). However, the S1PR3 mRNA levels were negatively associated with the Sequential Organ Failure Assessment scores of the septic patients, and it was lower in septic non-survivors than that in septic survivors (36). Concerning the role of S1PR3 in promoting the bactericidal activity of macrophages, inhibition of S1PR3 can hamper both inflammation response and bacteria clearance, leading to poor outcomes.

Conclusions

In conclusion, we report that suppression of S1PR3 has a specific inhibitory role in ATP-induced NLRP3 inflammasome activation in macrophages. Mechanically, inhibition of S1PR3 suppresses the expression of IL-1β and NLRP3 during LPS priming and attenuates NLRP3 inflammasome activation induced by ATP *via* downregulating membrane expression of TWIK2 and potassium efflux. Although inhibition of S1PR3 decreases IL-1β maturation in the lungs, it increases bacterial load and mortality of CLP mice.

Data availability statement

Publicly available datasets were analyzed in this study. This data can be found here: https://www.ncbi.nlm.nih.gov/geo/query/acc.cgi?acc=GSE46955. Gene Expression Omnibus database (GSE46955).

Ethics statement

The animal study was reviewed and approved by Zhongshan Hospital, Fudan University.

Author contributions

Study conception and design: MZ, JC. *In vivo* experiment: YW, CW. *In vitro* experiment: YW. Collection and assembly of data, YW, CW, GC, JY. Data analysis and interpretation: YW, CW. Manuscript writing: YW. All authors contributed to the article and approved the submitted version.

Funding

This work was supported by the National Natural Science Foundation of China (grant number 81971807), the Science and Technology Commission of Shanghai Municipality (grant number 20XD1420800), and the Science and Technology Commission of Shanghai Municipality (grant number 20DZ2261200).

Conflict of interest

The authors declare that the research was conducted in the absence of any commercial or financial relationships that could be construed as a potential conflict of interest.

Publisher's note

All claims expressed in this article are solely those of the authors and do not necessarily represent those of their affiliated organizations, or those of the publisher, the editors and the reviewers. Any product that may be evaluated in this article, or claim that may be made by its manufacturer, is not guaranteed or endorsed by the publisher.

Supplementary material

The Supplementary Material for this article can be found online at: https://www.frontiersin.org/articles/10.3389/fimmu.2023.1090202/full#supplementary-material

References

1. James SL, Abate D, Abate KH, Abay SM, Abbafati C, Abbasi N, et al. Global, regional, and national incidence, prevalence, and years lived with disability for 354 diseases and injuries for 195 countries and territories, 1990-2017: A systematic analysis for the global burden of disease study 2017. *Lancet* (2018) 392(10159):1789–858. doi: 10.1016/s0140-6736(18)32279-7

2. van der Poll T, van de Veerdonk FL, Scicluna BP, Netea MG. The immunopathology of sepsis and potential therapeutic targets. *Nat Rev Immunol* (2017) 17(7):407–20. doi: 10.1038/nri.2017.36

3. Jin L, Batra S, Jeyaseelan S. Deletion of Nlrp3 augments survival during polymicrobial sepsis by decreasing autophagy and enhancing phagocytosis. *J Immunol (Baltimore Md 1950)* (2017) 198(3):1253–62. doi: 10.4049/jimmunol.1601745

4. Lee S, Nakahira K, Dalli J, Siempos II, Norris PC, Colas RA, et al. Nlrp3 inflammasome deficiency protects against microbial sepsis *Via* increased lipoxin B4 synthesis. *Am J Respir Crit Care Med* (2017) 196(6):713–26. doi: 10.1164/rccm.201604-0892OC

5. Swanson KV, Deng M, Ting JP. The Nlrp3 inflammasome: Molecular activation and regulation to therapeutics. *Nat Rev Immunol* (2019) 19(8):477–89. doi: 10.1038/s41577-019-0165-0

6. Ledderose C, Bao Y, Kondo Y, Fakhari M, Slubowski C, Zhang J, et al. Purinergic signaling and the immune response in sepsis: A review. *Clin Ther* (2016) 38(5):1054–65. doi: 10.1016/j.clinthera.2016.04.002

7. Petrilli V, Papin S, Dostert C, Mayor A, Martinon F, Tschopp J. Activation of the Nalp3 inflammasome is triggered by low intracellular potassium concentration. *Cell Death Differ* (2007) 14(9):1583–9. doi: 10.1038/sj.cdd.4402195

8. Munoz-Planillo R, Kuffa P, Martinez-Colon G, Smith BL, Rajendiran TM, Nunez G. K(+) efflux is the common trigger of Nlrp3 inflammasome activation by bacterial toxins and particulate matter. *Immunity* (2013) 38(6):1142–53. doi: 10.1016/j.immuni.2013.05.016

9. Maceyka M, Spiegel S. Sphingolipid metabolites in inflammatory disease. *Nature* (2014) 510(7503):58–67. doi: 10.1038/nature13475

10. Weigert A, Olesch C, Brune B. Sphingosine-1-Phosphate and macrophage biology-how the sphinx tames the big eater. *Front Immunol* (2019) 10:1706. doi: 10.3389/fimmu.2019.01706

11. Zhong M, Wu W, Wang Y, Mao H, Song J, Chen S, et al. Inhibition of sphingosine kinase 1 attenuates sepsis-induced microvascular leakage *Via* inhibiting macrophage Nlrp3 inflammasome activation in mice. *Anesthesiology* (2020) 132(6):1503–15. doi: 10.1097/ALN.0000000000003192

12. Lee CH, Choi JW. S1P/S1P2 signaling axis regulates both Nlrp3 upregulation and Nlrp3 inflammasome activation in macrophages primed with lipopolysaccharide. *Antioxid (Basel)* (2021) 10(11):1706. doi: 10.3390/antiox10111706

13. Di A, Xiong S, Ye Z, Malireddi RKS, Kometani S, Zhong M, et al. The Twik2 potassium efflux channel in macrophages mediates Nlrp3 inflammasome-induced inflammation. *Immunity* (2018) 49(1):56–65.e4. doi: 10.1016/j.immuni.2018.04.032

14. Wiley JS, Dao-Ung LP, Li C, Shemon AN, Gu BJ, Smart ML, et al. An ile-568 to asn polymorphism prevents normal trafficking and function of the human P2x7 receptor. *J Biol Chem* (2003) 278(19):17108–13. doi: 10.1074/jbc.M212759200

15. Denlinger LC, Sommer JA, Parker K, Gudipaty L, Fisette PL, Watters JW, et al. Mutation of a dibasic amino acid motif within the c terminus of the P2x7 nucleotide receptor results in trafficking defects and impaired function. *J Immunol (Baltimore Md 1950)* (2003) 171(3):1304–11. doi: 10.4049/jimmunol.171.3.1304

16. Feliciangeli S, Tardy MP, Sandoz G, Chatelain FC, Warth R, Barhanin J, et al. Potassium channel silencing by constitutive endocytosis and intracellular sequestration. *J Biol Chem* (2010) 285(7):4798–805. doi: 10.1074/jbc.M109.078535

17. Bobak N, Feliciangeli S, Chen CC, Ben Soussia I, Bittner S, Pagnotta S, et al. Recombinant tandem of pore-domains in a weakly inward rectifying k(+) channel 2 (Twik2) forms active lysosomal channels. *Sci Rep* (2017) 7(1):649. doi: 10.1038/s41598-017-00640-8

18. Martin C, Leone M, Viviand X, Ayem ML, Guieu R. High adenosine plasma concentration as a prognostic index for outcome in patients with septic shock. *Crit Care Med* (2000) 28(9):3198–202. doi: 10.1097/00003246-200009000-00014

19. Sumi Y, Woehrle T, Chen Y, Bao Y, Li X, Yao Y, et al. Plasma atp is required for neutrophil activation in a mouse sepsis model. *Shock* (2014) 42(2):142–7. doi: 10.1097/shk.0000000000000180

20. Cartier A, Leigh T, Liu CH, Hla T. Endothelial sphingosine 1-phosphate receptors promote vascular normalization and antitumor therapy. *Proc Natl Acad Sci United States America* (2020) 117(6):3157–66. doi: 10.1073/pnas.1906246117

21. Kono M, Mi Y, Liu Y, Sasaki T, Allende ML, Wu YP, et al. The sphingosine-1-Phosphate receptors S1p1, S1p2, and S1p3 function coordinately during embryonic angiogenesis. *J Biol Chem* (2004) 279(28):29367–73. doi: 10.1074/jbc.M403937200

22. Yang L, Han Z, Tian L, Mai P, Zhang Y, Wang L, et al. Sphingosine 1-phosphate receptor 2 and 3 mediate bone marrow-derived Monocyte/Macrophage motility in cholestatic liver injury in mice. *Sci Rep* (2015) 5:13423. doi: 10.1038/srep13423

23. Arish M, Naz F. Sphingosine-1-Phosphate receptors 2 and 3 reprogram resting human macrophages into M1 phenotype following mycobacteria infection. *Curr Res Immunol* (2022) 3:110–7. doi: 10.1016/j.crimmu.2022.05.004

24. Arish M, Husein A, Ali R, Tabrez S, Naz F, Ahmad MZ, et al. Sphingosine-1-Phosphate signaling in leishmania donovani infection in macrophages. *PloS Negl Trop Dis* (2018) 12(8):e0006647. doi: 10.1371/journal.pntd.0006647

25. Ousingsawat J, Wanitchakool P, Kmit A, Romao AM, Jantarajit W, Schreiber R, et al. Anoctamin 6 mediates effects essential for innate immunity downstream of P2x7 receptors in macrophages. *Nat Commun* (2015) 6:6245. doi: 10.1038/ncomms7245

26. Perregaux D, Barberia J, Lanzetti AJ, Geoghegan KF, Carty TJ, Gabel CA. Il-1 beta maturation: Evidence that mature cytokine formation can be induced specifically by nigericin. *J Immunol (Baltimore Md 1950)* (1992) 149(4):1294–303. doi: 10.4049/jimmunol.149.4.1294

27. Mariathasan S, Weiss DS, Newton K, McBride J, O'Rourke K, Roose-Girma M, et al. Cryopyrin activates the inflammasome in response to toxins and atp. *Nature* (2006) 440(7081):228–32. doi: 10.1038/nature04515

28. Gross CJ, Mishra R, Schneider KS, Medard G, Wettmarshausen J, Dittlein DC, et al. K(+) efflux-independent Nlrp3 inflammasome activation by small molecules targeting mitochondria. *Immunity* (2016) 45(4):761–73. doi: 10.1016/j.immuni.2016.08.010

29. Miao EA, Leaf IA, Treuting PM, Mao DP, Dors M, Sarkar A, et al. Caspase-1-Induced pyroptosis is an innate immune effector mechanism against intracellular bacteria. *Nat Immunol* (2010) 11(12):1136–42. doi: 10.1038/ni.1960

30. Dikshit N, Kale SD, Khameneh HJ, Balamuralidhar V, Tang CY, Kumar P, et al. Nlrp3 inflammasome pathway has a critical role in the host immunity against clinically relevant acinetobacter baumannii pulmonary infection. *Mucosal Immunol* (2018) 11(1):257–72. doi: 10.1038/mi.2017.50

31. Zhong Y, Lu Y, Yang X, Tang Y, Zhao K, Yuan C, et al. The roles of Nlrp3 inflammasome in bacterial infection. *Mol Immunol* (2020) 122:80–8. doi: 10.1016/j.molimm.2020.03.020

32. Guo HL, Shi FD, Zhou Q, Liu QY, Wang YX, Song Y, et al. Interleukin-1beta protection against experimental sepsis in mice. *Inflammation* (2021) 44(1):358–70. doi: 10.1007/s10753-020-01341-7

33. Martínez-García JJ, Martínez-Banaclocha H, Angosto-Bazarra D, de Torre-Minguela C, Baroja-Mazo A, Alarcón-Vila C, et al. P2x7 receptor induces mitochondrial failure in monocytes and compromises Nlrp3 inflammasome activation during sepsis. *Nat Commun* (2019) 10(1):2711. doi: 10.1038/s41467-019-10626-x

34. Zhao J, Liu J, Lee JF, Zhang W, Kandouz M, VanHecke GC, et al. Tgf-B/Smad3 pathway stimulates sphingosine-1 phosphate receptor 3 expression: Implication of sphingosine-1 phosphate receptor 3 in lung adenocarcinoma progression. *J Biol Chem* (2016) 291(53):27343–53. doi: 10.1074/jbc.M116.740084

35. Gril B, Paranjape AN, Woditschka S, Hua E, Dolan EL, Hanson J, et al. Reactive astrocytic S1p3 signaling modulates the blood-tumor barrier in brain metastases. *Nat Commun* (2018) 9(1):2705. doi: 10.1038/s41467-018-05030-w

36. Hou J, Chen Q, Wu X, Zhao D, Reuveni H, Licht T, et al. S1pr3 signaling drives bacterial killing and is required for survival in bacterial sepsis. *Am J Respir Crit Care Med* (2017) 196(12):1559–70. doi: 10.1164/rccm.201701-0241OC

frontiers | Frontiers in Immunology

TYPE Review
PUBLISHED 07 February 2023
DOI 10.3389/fimmu.2023.1130214

OPEN ACCESS

EDITED BY
Yufeng Zhou,
Fudan University, China

REVIEWED BY
Nevena Arsenovic-Ranin,
University of Belgrade, Serbia
Vladimir M. Pisarev,
Federal Research and Clinical Center of Intensive Care Medicine and Rehabilitation, Russia

*CORRESPONDENCE
Ila Joshi
ila.joshi@partnertx.com

†These authors have contributed equally to this work

SPECIALTY SECTION
This article was submitted to Inflammation, a section of the journal Frontiers in Immunology

RECEIVED 23 December 2022
ACCEPTED 16 January 2023
PUBLISHED 07 February 2023

CITATION
Joshi I, Carney WP and Rock EP (2023) Utility of monocyte HLA-DR and rationale for therapeutic GM-CSF in sepsis immunoparalysis.
Front. Immunol. 14:1130214.
doi: 10.3389/fimmu.2023.1130214

Utility of monocyte HLA-DR and rationale for therapeutic GM-CSF in sepsis immunoparalysis

Ila Joshi[1*†], Walter P. Carney[2†] and Edwin P. Rock[1†]

[1]Development and Regulatory Department, Partner Therapeutics, Inc., Lexington, MA, United States, [2]Walt Carney Biomarkers Consulting, LLC., North Andover, MA, United States

Sepsis, a heterogeneous clinical syndrome, features a systemic inflammatory response to tissue injury or infection, followed by a state of reduced immune responsiveness. Measurable alterations occur in both the innate and adaptive immune systems. Immunoparalysis, an immunosuppressed state, associates with worsened outcomes, including multiple organ dysfunction syndrome, secondary infections, and increased mortality. Multiple immune markers to identify sepsis immunoparalysis have been proposed, and some might offer clinical utility. Sepsis immunoparalysis is characterized by reduced lymphocyte numbers and downregulation of class II human leukocyte antigens (HLA) on innate immune monocytes. Class II HLA proteins present peptide antigens for recognition by and activation of antigen-specific T lymphocytes. One monocyte class II protein, mHLA-DR, can be measured by flow cytometry. Downregulated mHLA-DR indicates reduced monocyte responsiveness, as measured by *ex-vivo* cytokine production in response to endotoxin stimulation. Our literature survey reveals low mHLA-DR expression on peripheral blood monocytes correlates with increased risks for infection and death. For mHLA-DR, 15,000 antibodies/cell appears clinically acceptable as the lower limit of immunocompetence. Values less than 15,000 antibodies/cell are correlated with sepsis severity; and values at or less than 8000 antibodies/cell are identified as severe immunoparalysis. Several experimental immunotherapies have been evaluated for reversal of sepsis immunoparalysis. In particular, sargramostim, a recombinant human granulocyte-macrophage colony-stimulating factor (rhu GM-CSF), has demonstrated clinical benefit by reducing hospitalization duration and lowering secondary infection risk. Lowered infection risk correlates with increased mHLA-DR expression on peripheral blood monocytes in these patients. Although mHLA-DR has shown promising utility for identifying sepsis immunoparalysis, absence of a standardized, analytically validated method has thus far prevented widespread adoption. A clinically useful approach for patient inclusion and identification of clinically correlated output parameters could address the persistent high unmet medical need for effective targeted therapies in sepsis.

KEYWORDS

sepsis, immunoparalysis, immunosuppression, granulocyte-macrophage colony-stimulating factor, human leukocyte antigen-DR, monocytes, compensatory anti-inflammatory response syndrome, sargramostim

Introduction

Sepsis, a heterogeneous clinical syndrome, reflects a pathophysiologic state of robust systemic inflammatory response, typically to infection (1–4). This inflammatory response leads to biochemical and physiologic abnormalities that in some patients progress to multiple organ dysfunction syndrome (MODS) and death. Sepsis outcomes have improved over time with advances in antibiotic therapy, fluid/pressor therapy, and dysfunctional organ support. Although most patients recover, sepsis remains a primary cause of intensive care unit (ICU) deaths with mortality at about 26% (1, 5, 6). In the United States (US), an estimated 1.7 million adult sepsis cases are diagnosed annually, leading to more than 350,000 deaths each year (7). Globally, 49 million sepsis cases in 2017 led to 11 million deaths (8). Incidence is highest in the elderly and very young. With high morbidity, mortality, and associated costs, sepsis remains a serious, life-threatening disease with persistent high unmet medical need (9).

Clinical sepsis typically presents with fever, low blood pressure, elevated heart rate, and elevated white cell count (3, 10, 11). While these signs are non-specific, they result from systemic innate immune cell activation due to infectious agents (bacterial, viral, or fungal) or noninfectious etiologies, such as: trauma; burns; surgery; pancreatitis; and cardiac, kidney, or liver injury (1, 4). Regardless of underlying cause, sepsis progression can lead to shock, organ dysfunction, and death (3, 12, 13). In this setting, a constellation of findings support diagnosis, including: clinical, lab, radiologic, physiologic, and microbiologic data (10, 11). Nonetheless, knowledge around sepsis and septic shock continues to advance as we learn more about immunological interactions of innate and adaptive immune responses to infection (10, 11, 14–17).

Over recent decades, molecular and cellular studies have sought to categorize sepsis into endotypes that stratify patient risk and identify therapeutic options (18). While antimicrobial therapy is recommended for all patients with sepsis, level of supportive care varies for those with mild *vs* severe sepsis (19–21). For patients with mild sepsis, fluid therapy, metabolic support, and corticosteroids may be sufficient. In severe sepsis, organ dysfunction necessitates additional supportive care, such as ventilation, vasopressors, and blood product transfusions. Identification of patient subsets might enable effective targeting of new therapies, either to inhibit a disease driver or to correct a deficiency (22). Similarly, selection of patients with elevated risk based on host characteristics or responses might enable targeting study therapies to those in greatest need (23). Despite progress in identifying sepsis endotypes, challenges persist in their clinical validation, as well as their implementation to improve outcomes (24, 25).

Sepsis immunoparalysis

One prominent model of sepsis pathophysiology describes 2 opposing states of immune dysregulation (26). In this model, a systemic inflammatory response syndrome (SIRS) induces a subsequent compensatory anti-inflammatory response syndrome (CARS). CARS is associated with an increased risk for secondary infections, shock, and organ dysfunction and increased mortality (1, 3, 27). While CARS is clinically occult, hyporesponsive innate and adaptive immune cells have been identified (3, 4, 28).

Severe CARS is also known as immunoparalysis (IP) (3, 26). Sepsis IP has been described to feature dysfunctional monocytes, immune cell depletion, and emergence of regulatory T cells (1, 29, 30). Also, sepsis IP associates with MODS, nosocomial infections, longer ICU hospitalization, and increased mortality (3, 4, 26, 29, 31–33). Notably, MODS comprises impaired function in multiple visceral organs and is associated with high mortality (34).

Despite potential validity and utility of markers for sepsis IP, such as human leukocyte antigen-DR (HLA-DR), tumor necrosis factor (TNF)-α, or absolute lymphocyte counts (ALC), the CARS paradigm faces 2 fundamental challenges (3, 4, 28, 35). First, compensatory molecular or cellular anti-inflammatory mechanisms by which immune cells become hyporesponsive in CARS remain undefined. Second, no diagnostic criteria exist to identify CARS. Rather, tests for immunosuppression/IP focus on immune cell dysfunction alone, independently of causation (35).

We propose here a biologic model of sepsis IP. This model combines recent observations in myeloid cell biology with key features of sepsis immunology (3, 26, 31). In addition, it provides rationale for therapeutic use of sargramostim (Leukine®), a yeast-derived, glycosylated recombinant human (rhu) granulocyte-macrophage colony-stimulating factor (GM-CSF).

Proposed mechanism of sepsis IP

Mononuclear phagocytes (MNPs) include circulating blood monocytes, dispersed tissue-bound macrophages, and dendritic cells (DCs) that may be either circulating or tissue-bound (36). While macrophages may live for years, blood monocytes have a circulating half-life of only 2 to 3 days (36, 37). Also, while circulating monocytes can replace tissue-resident macrophages, turnover rate varies by organ system. Turnover is higher in barrier organs—for example, gut and dermis—than in other organs, such as heart, pancreas, liver, and central nervous system. Replacement may be hastened in any organ by a local inflammatory process that leads to monocyte influx.

Innate immune responses act rapidly as a first line of defense against invasive, infectious pathogens (1). Initially, neutrophils and monocytes recognize pathogen-associated molecular patterns (PAMPs) and damage-associated molecular patterns (DAMPs). These interactions induce MNPs to release multiple cytokines, such as TNF-α, interleukin (IL)-1, and IL-6, that attract and activate other immune cells (1, 4). While neutrophils primarily kill microbes, MNPs kill microbes and, in addition, present their unique antigenic content to the adaptive immune system (4, 38).

MNPs link innate and adaptive immune systems by their ability to adopt either pro- or anti-inflammatory functions (4, 39). Pro-inflammatory functions eliminate infectious or injurious stimuli and activate antigen-specific helper T lymphocytes, whereas anti-inflammatory functions maintain homeostasis, conduct efferocytosis, and thereby control autoimmunity. Critically, MNPs express class II major histocompatibility complex (MHC) proteins that activate antigen-specific helper T lymphocytes and secrete cytokines to nourish and/or activate diverse cell types (Figure 1). More numerous neutrophils by contrast are primarily pro-inflammatory,

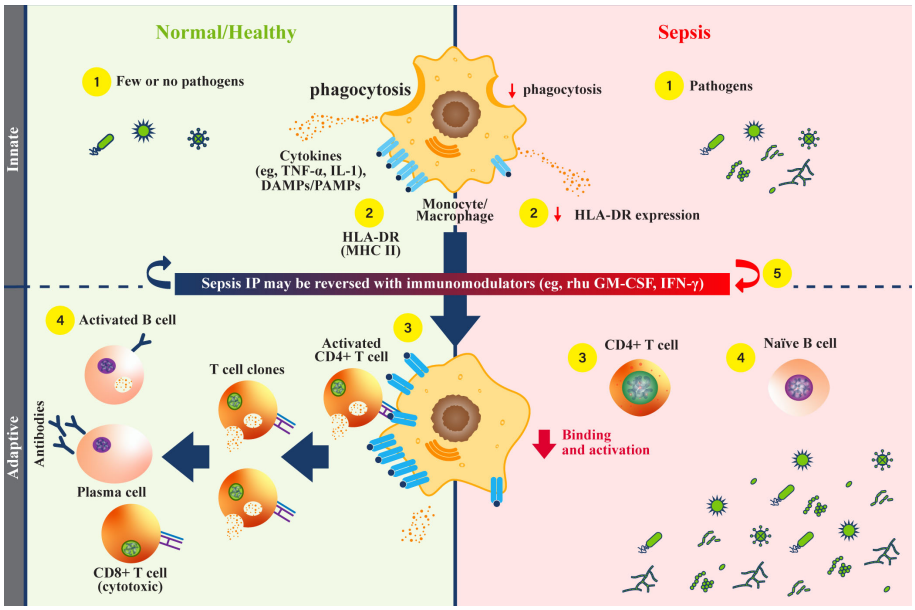

FIGURE 1
Monocytes and HLA-DR function during sepsis. **(Normal/Healthy; left)** (1) Innate immune cells respond to infectious pathogens by phagocytosis, cytokine secretion, and antigen presentation (1, 4). (2) Phagocytosed pathogens are broken down, then combined as peptides with class II major histocompatibility complex (MHC) (e.g., human leukocyte antigen-DR isotype [HLA-DR], and localized to the cell surface) (4, 40). (3) Peptide-MHC complexes on antigen presenting cells engage with CD4+ helper T cells to activate an adaptive immune response, triggering cytokine release (4, 40). (4) Activated CD4+ T helper cells undergo clonal expansion, activate CD8+ T cells, and mediate B cell activation (1, 26, 41). Activated B cells then differentiate into plasma cells that secrete antibodies, comprising a humoral response. **(Sepsis IP; right)** (1) Dysfunctional monocytes/macrophages demonstrate reduced pathogen phagocytosis, reduced antigen presentation, and variable cytokine profiles (4). (2) Dysfunctional monocytes/macrophages express less antigen-bound HLA-DR proteins, leading to reduced engagement with the adaptive immune system (4). (3) Without effective antigen presentation by monocytes/macrophages, CD4+ T cells are not activated, and adaptive immune responses are rendered ineffective in clearing pathogens (1). (4) Naïve B cells are not activated by CD4+ T cells, and antibody producing plasma cells are not generated. With an inadequate humoral immune response, pathogens survive and replicate (1, 42). (5) Recombinant human (rhu) granulocyte-macrophage colony-stimulating factor (GM-CSF) may restore monocyte/macrophage function (4). DAMP, damage-associated molecular patterns; GM-CSF, granulocyte-macrophage colony-stimulating factor; HLA-DR, human leukocyte antigen-DR isotype; IFN, interferon; IL, interleukin; IP, immunoparalysis; PAMP, pathogen-associated molecular patterns; MHC II, class II major histocompatibility complex; rhu, recombinant human; TNF, tumor necrosis factor.

live only for days after a 6- to 12-hour circulating half-life, and do not characteristically present foreign antigens to adaptive immune lymphocytes (43).

The adaptive immune system comprises antigen-specific T lymphocytes that are cytotoxic, or are responsible for self-tolerance (T regulatory cells) as well as antibody-producing plasma cells that result from B cell differentiation (1, 3). Although initially slower to respond than the innate immune system, the adaptive immune system drives antigen-specific recognition and generates immunologic memory. Immunologic memory generates faster, stronger repeat immune responses against previously encountered antigens.

In sepsis, both innate and adaptive arms of the human immune system are altered (1). In addition, multiple cytokine levels are elevated, including GM-CSF. These cytokines drive proliferation of circulating innate immune cells, including neutrophils, monocytes, and eosinophils, by signaling through specific cell surface receptors (44, 45). For example, high affinity GM-CSF receptors are found principally on myeloid cells, including neutrophils, MNPs, and eosinophils.

Numerous cytokines, including GM-CSF, have pleiotropic effects that vary depending on local cytokine concentrations in the vicinity of specific cell surface receptors (44, 46–48). GM-CSF pleiotropism relies on higher order extracellular assembly of heterodimeric receptor chains, as well as 4 distinct intracellular signaling pathways, including: mitogen activated protein kinase (MAPK); nuclear factor kappa-B cells (NFκB); phosphoinositide 3-kinase (PI3K); and signal transducer and activator of transcription 5 (STAT5). Such diversity explains GM-CSF's capacity to generate survival, differentiation, activation, and/or proliferation signals, depending on cytokine concentration at the receptor level, as well as other local stimuli. At low GM-CSF concentrations, PI3K signaling leads to survival, whereas at high concentrations, PI3K, MAPK, and STAT5 signaling lead to survival and cell proliferation (47, 48). Correspondingly, both ligand and dose-specific effects on NFκB signaling have been described in primary macrophages (49, 50), and such effects have been observed to influence epigenomic programming (51).

Recently, GM-CSF effects on MNP metabolism were revealed in mouse models with disrupted GM-CSF signaling (52). These models demonstrated a critical role of GM-CSF in maintaining mitochondrial structure and function, as well as fatty acid beta oxidation, tricarboxylic acid cycle activity, oxidative phosphorylation, and adenosine triphosphate (ATP) generation. These effects of GM-CSF on metabolic capacity enable MNPs to fulfill energy-intensive innate immune functions, including: respiratory burst generation, phagocytosis, antigen presentation, cytokine secretion, and

efferocytosis (52–54). All these functions rely on metabolic energy and fail in its absence. By extension, metabolic capacity in tissue-bound macrophages throughout the body may be maintained by ongoing low-level and/or pulsatile GM-CSF expression. This activity aligns with known ongoing low-level yet plastic GM-CSF expression by diverse cell types, including endothelial, epithelial, and immune cells, as well as fibroblasts (2, 55).

We hypothesize that myeloid proliferation driven by high cytokine levels in sepsis leads to cell division that outpaces time and/or GM-CSF stimulation needed for maturation of cellular metabolic capacity. Thus, sustained high inflammatory cytokine secretion may counterintuitively result in degradation of metabolic capacity of newly formed MNPs to fulfill immune functions. Consequently, immature MNPs with insufficient metabolic capacity to support normal innate immune functions appear "immunosuppressive." In support of this model, GM-CSF reverses monocyte hyporesponsiveness in multiple *in-vitro* systems (56–60). Multiple reports support that GM-CSF increases blood monocyte levels, upregulates monocyte responsiveness, and increases HLA-DR expression, which is known to enhance antigen presentation and adaptive immune responses (48, 54, 61, 62).

Immune biomarkers in sepsis IP

Numerous immune biomarkers have been assessed to seek prognostic and/or predictive markers for patient stratification and therapy in sepsis (12). Methods studied include: neutrophil respiratory burst in response to pathogen exposure; lymphocyte and monocyte counts; neutrophil-to-lymphocyte and monocyte-to-lymphocyte ratios; monocyte programmed death-ligand 1 (PD-L1) expression; IL-10; and transcriptomics, among others (26, 63–67). Most such methods have not been widely adopted due to challenges in analytic validity, clinical validity, and/or clinical utility. Methods with evidence of clinical validity include HLA-DR quantitation of blood monocytes, TNF-α release from peripheral blood cells after *ex-vivo* lipopolysaccharide (LPS) stimulation, and ALC (29, 30). Biological rationale, validation challenges, and clinical data for each of these 3 markers are summarized below.

Blood monocyte HLA-DR expression

The polymorphic MHC gene family in humans is on chromosome 6 and encodes multiple class II MHC proteins, including HLA-DP, HLA-DQ, and HLA-DR (68). Historically, these proteins were recognized as transplantation antigens, serving as targets for immune rejection of transplanted tissue. During infection, MNPs phagocytose pathogens that are then digested to yield foreign peptides that combine intracellularly with class II MHC proteins, such as HLA-DR (4, 69). Normally, monocytes and macrophages express HLA-DR levels ranging from 15,000 antibodies bound per cell (Ab/c) to as high as 60,000 Ab/c (70, 71); and a commonly used lower limit of HLA-DR in healthy subjects is 15,000 Ab/c (33, 72, 73). The large spread in the reported HLA-DR levels is most likely explained by biologic variability, as well as differences in assay reagents and flow cytometry methods used over years to quantitate HLA-DR expression levels (74–77). Peptide-MHC complexes are transported to the cell surface where they mediate antigen-specific recognition by CD4+ helper T lymphocytes. Once activated by peptide-MHC recognition, CD4+ T lymphocytes boost adaptive immune responses by activating other T and B lymphocytes that can recognize and target the invading pathogen (3, 4, 26). Because HLA-DR functions as the bridge between innate MNPs and antigen-specific T lymphocytes, low HLA-DR levels lead to diminished antigen presentation and reduced adaptive immune activation (4, 78). When HLA-DR is low, CD4+ T lymphocytes are not activated, hence cannot augment either B-cell stimulation to produce specific antibodies or CD8+ cytotoxic T lymphocyte generation to target infected cells directly (3, 4).

Despite HLA protein diversity, common determinants recognized by monoclonal antibodies enable flow cytometric quantitation of surface class II MHC expression level on blood cells (4, 40, 76). Although flow cytometry enables monocyte HLA-DR (mHLA-DR) quantitation, other cells expressing HLA-DR are also detected, including DCs, macrophages, B cells, and T cells (4, 30, 76, 79–82). Thus, to generate mHLA-DR specificity, cells are also stained for CD14 (also known as the LPS receptor), of which, expression is restricted to monocytes. Combined CD14 and HLA-DR staining enables quantitation of CD14+ classical and intermediate monocytes, the most abundant and rapidly replenished populations in blood. Results are typically reported either as percent of CD14+ monocytes expressing HLA-DR or as mean fluorescence intensity (MFI) of antibody against HLA-DR on CD14+ monocytes (77, 83).

HLA-DR downregulation and reduced monocyte responsiveness are described features of sepsis IP (4, 26). As detailed in Table 1, low HLA-DR correlates with adverse clinical outcomes, including increased risk for nosocomial infections, end-organ failure, longer ICU hospitalizations, and mortality (30, 33, 75, 84–89, 91–93).

Inter-laboratory variability initially posed a challenge to analytic validity of HLA-DR testing to identify sepsis IP (4). Now, a system offering standardized quantitative measurement of cell surface HLA-DR proteins (Quantibrite™; Becton, Dickinson and Company [BD]) is available. Developed in 2001, Quantibrite™ beads allow estimation of Ab/c, enabling monocyte cell surface HLA-DR protein quantitation to stratify patients based on mHLA-DR levels (79, 94–96). This assay uses phycoerythrin (PE)-labeled anti-HLA-DR monoclonal antibodies for estimating Ab/c (97). Geometric MFI values can be analyzed further to calculate numbers of Ab/c, which represents numbers of HLA-DR proteins on the monocyte surface (96, 97). Using standard instrument settings, flow cytometry data are converted into number of PE molecules per cell. Based on a known ratio of PE to antibodies against HLA-DR, Ab/c can be calculated, hence quantitating HLA-DR protein on CD14+ monocytes. With Quantibrite™, moderate immunosuppression is defined as about 10,000–15,000 Ab/c (74, 79). In several studies, a cut-off value of 8000 Ab/c was used to indicate IP. HLA-DR levels below 8000 Ab/c indicate more severe sepsis IP (4, 79). In some studies, 30% CD14+/HLA-DR+ cells corresponded to 5000 Ab/c for severe IP, whereas 45% CD14+/HLA-DR+ cells corresponded to about 8000 Ab/c for moderate IP (4, 79). Numerous studies have employed Quantibrite™ to measure HLA-DR-defined IP (26, 33, 70, 73–75, 77, 88, 90, 98–101).

Multiple literature analyses support mHLA-DR expression by flow cytometry as a sepsis IP biomarker and mortality predictor (80).

10.3389/fimmu.2023.1130214

TABLE 1 Studies connecting monocyte HLA-DR to clinical outcomes.

Study	Condition	Monocyte Function (Test)	mHLA-DR Monitoring	Results	Clinical Implications
Prospective, single center, observational study (n=1053) (84)	Sepsis	mHLA-DR Ab/c (FC)	Sample 1 collected and analyzed within 3 days of ICU admission; sample 2 collected and analyzed within first week	• Low mHLA-DR expression at presentation associated with initial disease severity assessment (R2 = 0.28; p<0.01) • Persistence of a low mHLA-DR (< 8000 Ab/c), measured between Day 5 and Day 7, was associated with a later occurrence of IAIs (p=0.01)	Higher IAI risk associated with persistent low mHLA-DR measure
Prospective, single center, observational study (n=51) (85)	Cardiac arrest	mHLA-DR MFI (FC)	Samples collected at 12, 24, and 48 hours after cardiac arrest	• In patients following cardiac arrest and cardiopulmonary resuscitation, downregulation of HLA-DR expression was observed mainly in classical monocytes and correlated with norepinephrine dose	No correlation between mHLA-DR expression and 30-day mortality
Prospective, single center, observational study (n=36) (86)	Trauma	mHLA-DR Ab/c (FC)	Periodic monitoring; samples collected and analyzed at Days 1, 3, and 8 after injury	• 22% of patients had secondary infections, all of which had HLA-DR < 15,000 Ab/c at Days 3–4 • Not powered to establish an association between HLA-DR and secondary infections (p=0.22)	Trend for secondary infections with low mHLA-DR levels at Day 3
***Post-hoc* analysis of ETASS Study (n=273)** (87)	Sepsis	%mHLA-DR+ (FC)	Single measurement; early immune status evaluated by the %mHLA-DR in total monocytes within 48 hours after onset of sepsis	• Patient classified as IP when mHLA-DR ≤ 30% and non-IP when > 30% mHLA-DR • Higher mortality rate for elderly with IP *vs* elderly without IP (53.4% *vs* 32.5%; p=0.009) • For non-elderly patients, no difference in mortality rates for IP *vs* non-IP (33.5% *vs* 26.0%; p=0.541)	Higher hospital and ICU mortality risk associated with low mHLA-DR measure for elderly
Prospective, observational study (n=24) (88)	Critically ill, COVID-19	mHLA-DR Ab/c (FC)	Periodic monitoring	• Lower mHLA-DR expression for COVID-19 *vs* healthy subjects (11,860 Ab/c *vs* 15,000–45,000 Ab/c; p-value not reported) • Higher mHLA-DR expression for COVID-19 *vs* sepsis (bacterial infections were the drivers of sepsis (75); 11,860 Ab/c *vs* 5211 Ab/c; p<0.0001)	mHLA-DR expression kinetics revealed no change over time. No secondary infections were observed during the follow-up period for patients with COVID-19
Prospective, observational study (n=241) (75)	Sepsis	mHLA-DR Ab/c (FC)	Periodic monitoring; samples collected and analyzed at 3 time points (Day 1 or 2; Day 3 or 4; Day 6, 7, or 8)	• No difference in mHLA-DR expression between pathogen categories (e.g., Gram-positive, Gram-negative) and sites of infection (e.g., abdominal, respiratory tract, urinary tract) • Greater increase in mHLA-DR expression for survivors *vs* non-survivors (AUROC, 0.65; p=0.01)	Increased risk of secondary infections and 28-day mortality associated with declining mHLA-DR expression
Retrospective, observational study (n=297) (89)	Sepsis	%mHLA-DR+ (FC)	Periodic monitoring; samples collected at Days 1, 3, and 7 after hospital admission	• Lower %mHLA-DR+ expression on Day 3 for patients with secondary infections *vs* those without secondary infections (28.6% *vs* 41.1%; p=0.048) • Higher in-hospital (45.7% *vs* 25.4%; OR, 2.472; p=0.001), 30-day (34.8% *vs* 23.4%; OR, 1.744; p=0.041), and 90-day mortality rates (42.4% *vs* 25.4%; OR, 2.165; p=0.003) for patients with secondary infections *vs* those without secondary infections	Increased risk of secondary infections associated with lower mHLA-DR expression
Prospective, single center, observational study (n=56) (90)	Sepsis	mHLA-DR Ab/c (FC)	Periodic monitoring; samples collected and analyzed at Days 1, 3, and 7 after injury	• Lower levels of mHLA-DR (5913–7927 Ab/c *vs* 25,477–34,295 Ab/c; p<0.001) and lower CD4+ T cells (332–1186 cells/μL *vs* 895–2187 cells/μL; p<0.01) for patients with septic shock *vs* healthy controls • Lower levels of mHLA-DR for those with secondary infection *vs* those without secondary infection (Days 1–2 mHLA-DR, 4146 Ab/c *vs* 8704 Ab/c; p=0.28; Days 3–5, 4398 Ab/c *vs* 8474 Ab/c; p=0.022) (91)	Increased secondary infections associated with lower mHLA-DR expression
Prospective, controlled study (n=74) (92)	Critically ill (including sepsis; n=12)	%mHLA-DR+ and mHLA-DR MFI (FC)	Daily monitoring; samples collected and analyzed Days 1–4 of PICU stay	• Lower mHLA-DR expression (67% *vs* 95%; p<0.001) and lower HLA-DR MFI within monocyte subsets (3219 *vs* 6545; p<0.001) for critically ill children *vs* controls	Increased nosocomial infection risk with lower mHLA-DR expression on classical monocytes

(Continued)

TABLE 1 Continued

Study	Condition	Monocyte Function (Test)	mHLA-DR Monitoring	Results	Clinical Implications
Prospective, single center, *ex-vivo* study (n=19) (30)	Sepsis	mHLA-DR MFI (FC) and HLA-DR mRNA (PCR)	Single measurement; samples collected and analyzed on Day 1 of inclusion	• Higher monocyte numbers in peripheral blood ($p<0.001$) but lower HLA-DR MFI ($p<0.001$) and mRNA HLA-DR levels ($p<0.001$) for patients with sepsis *vs* controls	Higher 28-day mortality rate associated with low HLA-DR
Prospective, observational study (n=100) (33)	Trauma	ΔmHLA-DR (FC)	Periodic monitoring; samples collected every 2 days; subsequent samples after Day 5 were not presented (occurred after sepsis development)	• mHLA-DR has predictive potential for development of sepsis after major trauma: • Slope of mHLA-DR expression between Days 3–4 and Days 1–2 (OR, 9.0; $p=0.0009$)	Higher risk for sepsis development with greater reduction of mHLA-DR levels between Days 1–2 and Days 3–4
Prospective, observational study (n=79) (93)	Sepsis	ΔmHLA-DR (FC)	Periodic monitoring; samples collected and analyzed between Days 0, 3, and 7 after injury	• Greater ΔmHLA-DR from Day 0 to Day 7 for survivors *vs* non-survivors (16.9 *vs* 4.55; $p=0.038$) • Smaller ΔmHLA-DR from Day 0 were associated with higher 28-day mortality (ΔmHLA-DR, Days 0–3 ≤ 4.8%; OR, 94.71; $p<0.001$; ΔmHLA-DR, Days 0–7 ≤ 9%; OR, 51.04; $p<0.001$)	Higher 28-day mortality associated with smaller ΔmHLA-DR over 7 days

ΔmHLA-DR, change in monocyte human leukocyte antigen-DR; %mHLA-DR+, percent of monocytes positive for human leukocyte antigen-DR; Ab/c, antibodies bound per cell; AUROC, area under receiver operating curve; COVID-19, coronavirus disease of 2019; ETASS, Efficacy of Thymosin Alpha 1 for Severe Sepsis; FC, flow cytometry; IAI, intensive care unit-associated infections; ICU, intensive care unit; IP, immunoparalysis; MFI, mean fluorescence intensity; mHLA-DR, monocyte human leukocyte antigen-DR; mRNA, messenger ribonucleic acid; OR, odds ratio; PCR, polymerase chain reaction; PICU, pediatric intensive care unit.

One such review evaluated mHLA-DR in patients with complicated intra-abdominal infections and sepsis from 12 studies (n=761) (102). Results from 10 of these studies showed strong associations between low mHLA-DR expression and mortality. By contrast, 2 studies showed no prognostic value of mHLA-DR expression level. Proposed factors contributing to nonsignificant results in these 2 studies include: homogeneity of enrolled patients, young age, small sample sizes, and heterogeneity among experimental protocols (77, 87, 100, 103). Another review assessed mHLA-DR in critically ill patients with coronavirus disease of 2019 (COVID-19), sepsis, or bacterial infections from 15 studies (n=1160) (104). Of these studies, 4 monitored mHLA-DR expression with flow cytometry by a standardized protocol that reported results as Ab/c. Initial mHLA-DR expression was lower for COVID-19 patients than for controls (10,000 Ab/c *vs* 15,000 Ab/c) yet higher for COVID-19 patients than for septic shock patients (10,000 Ab/c *vs* 5000 Ab/c). Lower mHLA-DR expression was associated with higher ICU mortality and greater disease severity at hospital admission. A meta-analysis evaluated 8 prospective cohort studies to evaluate HLA-DR as a biomarker for sepsis in patients after trauma (n=639) (105). Results from 7 studies showed that HLA-DR by flow cytometry for detecting sepsis IP had a pooled sensitivity of 81% and a pooled specificity of 67%.

While various thresholds for detecting IP have been proposed, a minimum threshold for raising secondary infection and mortality risks has to date been neither standardized nor adopted (3, 4, 77, 84, 106). Hence, HLA-DR testing by flow cytometry can now be implemented with analytic validity, and multiple studies support its clinical validity. Yet, both a definitive threshold for sepsis IP and clinical utility for therapeutic response prediction remain, for now, unconfirmed.

Notably, 3 additional approaches to mHLA-DR measurement have been investigated. First, measurement of HLA-DR expression levels by polymerase chain reaction (PCR) was explored in several clinical studies (4, 70, 80). In 1 such study, quantitative real-time PCR (qRT-PCR) and mHLA-DR flow cytometry were used to assess HLA-DR and class II transactivator (CIITA) in patients with bacteremic sepsis (n=60) (70). TaqMan gene qRT-PCR expression assays were used to measure HLA-DR-α subunit (HLA-DRA) and CIITA, whereas Quantibrite™ was used to measure mHLA-DR by flow cytometry. Similar patterns for initial reductions in HLA-DRA, mHLA-DR, and CIITA were all followed by subsequent increases over time ($p<0.001$). Hence, qRT-PCR yields results somewhat similar to flow cytometry with low variability and reproducibility. While qRT-PCR may be robust for detecting HLA-DR expression in patients with sepsis, qRT-PCR results are non-specific for monocytes since circulating DCs, B cells, and activated T cells also express HLA-DR (70, 80). As such, it may not reliably reflect mHLA-DR expression in monocytes that drives sepsis IP (4, 80, 107).

Second, myeloid-derived suppressor cells (MDSCs) have been described in patients with sepsis (4, 108–110). Although not standardized, all MDSC descriptions include "low HLA-DR expression." Hence, MDSCs are invariably monocytes with low HLA-DR. In sepsis, MDSCs associate with: prolonged immunosuppression, diminished T cell functions, development of nosocomial infections, higher reinfection rates, and hospital readmissions (4, 109, 111, 112).

Finally, several studies support that dynamic changes by serial mHLA-DR monitoring might predict mortality better than static mHLA-DR monitoring (80, 113, 114). Correspondingly, persistence of low mHLA-DR levels suggests slow or no recovery from sepsis IP (4, 12, 13, 113, 115, 116). Given inter-individual variability of mHLA-DR in sepsis, dynamic change or HLA-DR slope might increase prognostic significance of low mHLA-DR expression for mortality prediction (4, 13, 93, 98, 117). Thus far, no standardized approaches to serial mHLA-DR monitoring have been either developed or

tested prospectively.

Pediatric *vs* adult mHLA-DR

As in adults, low mHLA-DR in children associates with nosocomial infections and mortality (92, 118–121). Nonetheless, patient age affects monocyte subtypes and function, so direct comparison of adults *vs* children may be confounding (121). While adult monocytes are predominantly classical (CD14+/CD16-), neonatal monocytes are mostly intermediate (CD14+/CD16+) or nonclassical (CD14-lo/CD16+) subtypes that express lower levels of HLA-DR (121–123). These differences result in reduced T cell activation in neonates compared with adults (121). Also, neonates have proportionally more regulatory T cells than adults, and that difference may also limit immune responses in children with sepsis (124, 125).

One study compared mHLA-DR expression among critically ill children with sepsis, trauma-related hospital acquired infection, or recent surgery (n=37; median age, 9 years) *vs* healthy control children (n=37; median age, 3 years) (92). Results showed lower mHLA-DR expression (67% *vs* 95%; p<0.001) and lower mHLA-DR MFI (3219 *vs* 6545; p<0.001) for critically ill children *vs* healthy controls at all examined time points, in particular on classical monocytes and in children admitted for sepsis. Another study evaluated blood samples in hospitalized children with sepsis (n=30) *vs* healthy controls (n=21) for mHLA-DR expression using Quantibrite™ technology (98). As with adults, mHLA-DR expression in pediatric patients with sepsis was lower than that in controls (p=0.0001). Finally, a prospective, single-center, observational study evaluated mHLA-DR levels using Quantibrite™ in children with septic shock admitted to a pediatric ICU (n=26; median age, 2 years) with healthy controls (n=30) (90). As seen elsewhere, mHLA-DR levels were lower for patients with septic shock than for healthy controls (p<0.001).

Ex-vivo blood cell TNF-α secretion

While HLA-DR is well-documented for sepsis IP detection, other potential biomarkers are also being explored. LPS-induced TNF-α production from peripheral blood cells reflects innate immune system function *via* myeloid cell capacity to respond to an inflammatory stimulus (3, 30, 126). Although both *ex-vivo* TNF-α secretion and HLA-DR expression assess monocyte dysfunction *via* metabolic capacity to fulfill basic immune functions, *ex-vivo* TNF-α secretion is less specific for monocytes as responding myeloid cells include both neutrophils and monocytes. Independent of sepsis IP, TNF-α levels may also be influenced by a variety of other factors, such as: type of LPS used, blood volume, incubation conditions, and LPS concentration (3).

In contrast to substantial literature examining mHLA-DR prognostic significance in adult sepsis, there are fewer reports on TNF-α, and most are in small groups of children (3, 74, 91, 127, 128). Overall, these studies support clinical validity of measuring TNF-α by *ex-vivo* LPS stimulation. Although a few studies describe standardized protocols for measuring LPS-induced TNF-α production for sepsis, scalable analytic validity may remain challenging (29, 129). As seen for HLA-DR quantitation, no receiver operating characteristic (ROC) curve analysis has been performed to define a TNF-α threshold for sepsis IP.

Absolute lymphocyte count

ALC is another laboratory parameter that reflects immune system function (29, 130). The reference range for ALC varies with age. Normal for adults varies between 1000 and 4800 cells/μL, and for children, between 3000 and 9500 cells/μL (131, 132). Lymphopenia occurs when a patient's ALC is below normal and can increase risk for infection (133).

In sepsis IP, circulating lymphocyte populations (e.g., CD4+ T cells, CD8+ T cells, B cells) are characteristically reduced due to tissue sequestration and apoptosis (26). Reductions at sepsis onset typically persist for up to 28 days. Increased apoptosis of both innate immune cells and adaptive immune cells in sepsis results in leukopenia, which associates with higher risks of secondary infections and death (134–136).

A retrospective, single-center cohort study monitored blood parameters in patients with bacteremia and sepsis (n=335) for secondary infection risk and mortality (130). Results showed higher ALC at Day 4 for survivors *vs* non-survivors (1100 cells/μL *vs* 700 cells/μL; p<0.0001). Also, 28-day and 1-year mortality were higher in severe (40% *vs* 10% and 58% *vs* 29%; p<0.001) and moderate (25% *vs* 10%; p=0.003, and 40% *vs* 29%; p=0.025) lymphopenia *vs* those without persistent lymphopenia. Multivariable analysis showed that Day 4 ALC was associated with both 28-day (odds ratio [OR], 0.68; p=0.009) and 1-year mortality (OR, 0.74; p=0.008). Severe persistent lymphopenia (< 0.6 x 10^3 cells/μL) was also associated with development of secondary infections (OR, 2.11; 95% confidence interval [CI], 1.02–4.39; p=0.04) (26, 130). Thus, persistent lymphopenia on the fourth day after a sepsis diagnosis predicted mortality and may be a valid marker of sepsis-induced immunosuppression.

In another single-center study, cross-sectional analysis was performed of ALC as an outcome predictor in patients with sepsis presenting to an emergency department (n=124) (137). Results showed a higher need for ICU admission (51.9% *vs* 14%; p<0.001) and higher rates of 28-day mortality (88.1% *vs* 11.9%; p<0.001) for patients with lymphopenia *vs* those without lymphopenia. In addition, age and sequential organ failure assessment (SOFA) scores were higher for patients with lymphopenia *vs* without.

Lower monocyte counts are also seen in sepsis and can impact health outcomes (64). A retrospective, single-center database analysis of patients with sepsis (n=2012) showed higher 28-day mortality rates, higher bacteremia rates, and higher incidence of organ dysfunction for patients with initial monocyte counts < 250 cells/μL.

Comparison of HLA-DR, TNF-α secretion, and ALC

Pros and cons of mHLA-DR expression, TNF-α secretion, and ALC as prognostic indicators in sepsis IP are summarized in Table 2 (4, 26, 27, 30, 35, 130, 138, 139). mHLA-DR expression and TNF-α responsiveness seek to measure similar biology of innate immune MNP dysfunction (26, 27, 130). Correspondingly, in an *ex-vivo* study using blood samples from patients with sepsis or septic shock (n=20), mHLA-DR expression correlated with TNF-α response (30). By contrast, ALC reflects distinct, complementary biology of deficient adaptive immune responsiveness (66).

TABLE 2 Pros and cons of immune biomarkers for sepsis IP (4, 26, 27, 30, 35, 74, 130, 138, 139).

Biomarker	Analysis Method	Pros	Cons
mHLA-DR	Flow cytometry	• Reflects monocyte state • Specific to classical monocytes • High analytic validity with BD Quantibrite™ technology	• Requires flow cytometry at or near point of sample collection or expedited shipping to a flow cytometry laboratory • Time sensitive analysis post-sample collection • Sample stability
TNF-α	ELISA	• Reflects monocyte state	• Neutrophils also responsive, thus the level of TNF-α is not specific for monocytes • Includes multiple steps • Cell culture, incubation, and centrifugation to isolate supernatants at or near point of sample collection • Analytic validity could be confounded by variation in LPS source
Lymphocyte	ALC	• Routinely available	• No differentiation among types of lymphocytes • Thresholds undefined

ALC, absolute lymphocyte count; BD, Becton, Dickinson and Company; ELISA, enzyme-linked immunosorbent assay; LPS, lipopolysaccharide; mHLA-DR, monocyte human leukocyte antigen-DR; TNF, tumor necrosis factor.

HLA-DR expression offers acceptable analytic validity based on well characterized monoclonal antibodies and Quantibrite™ technology (74). Nonetheless, testing for this biomarker requires flow cytometry of fresh or stabilized cells, necessitating either shipping to a central facility or timely local analysis (74, 140). By contrast, TNF-α secretion requires local site addition of LPS to blood samples and incubation followed by analysis of frozen cell supernatants by enzyme-linked immunosorbent assay (ELISA) (138). This procedure generates need for trained site staff to perform *ex-vivo* LPS stimulation reliably. Notable analytic validity hurdles for TNF-α secretion include variability in LPS source and *ex-vivo* stimulation protocols, as well as non-specificity for monocyte *vs* neutrophil secretion. Neutrophils may be a significant source of TNF-α due to their higher abundance in whole blood relative to monocytes (138, 139, 141). While ALC measurement is logistically simple, inexpensive, and reflects adaptive immune function directly, ALC alone does not directly reflect innate immune function (142). Also, a threshold to define sepsis IP based on ALC remains, to date, undefined (130).

Immunostimulatory agents in sepsis

Consequences of sepsis IP are severe and contribute to sepsis mortality (26, 29). However, sepsis IP may be reversible since about one third of severe sepsis survivors regain immune function (29). As such, many drug trials have focused on targeting the clinically overt state of SIRS with pharmacologic agents that have anti-inflammatory effects. Though, most such agents have failed to improve outcome, and none has yet been shown to improve survival. Nonetheless, investigation continues of immunostimulatory agents that aim to reverse CARS effects (1, 3).

Experimental immunotherapies for sepsis IP have been shown to decrease ICU stay duration and secondary infection risk (3, 62). Notably, immunostimulating agents have shown promise for reversing IP, including: recombinant IL-7, programmed death 1 (PD-1)/PD-L1-specific antibodies, recombinant interferon (IFN)-γ, and recombinant GM-CSF (3, 12, 29, 62).

IL-7 is a potent anti-apoptotic cytokine required for lymphocyte survival and expansion that has shown potential benefits in patients with sepsis (143). The phase 2 IRIS-7 study evaluated IL-7 at varying frequencies *vs* placebo in patients with septic shock and severe lymphopenia (n=27). At Day 29, results showed higher ALC for IL-7 relative to placebo study therapy (+0.99–1.30 x 10^3 lymphocytes/μL *vs* 0.99 x 10^3 lymphocytes/μL; p=0.004). Elevated ALC persisted for 2–4 weeks after discontinuing IL-7.

PD-1 and PD-L1 are upregulated in sepsis and other inflammatory states (including cancer) (144). Clinical responses seen with PD-1/PD-L1 inhibitors in tumors suggested potential benefits for sepsis IP (27, 29), and a phase 1 trial of nivolumab in patients with sepsis (n=31) demonstrated safety. Larger clinical studies, however, were stopped by the sponsor (29, 145).

Pro-inflammatory cytokine IFN-γ plays a role in both innate and adaptive immune responses (146). One trial showed that IFN-γ study treatment restored mHLA-DR expression in patients with sepsis IP (4, 147). A separate, small, randomized, double-blind study (n=18) evaluated recombinant IFN-γ *vs* recombinant GM-CSF *vs* placebo in healthy volunteers given *E. coli* endotoxin. IFN-γ increased mHLA-DR expression and TNF-α levels but did not significantly improve symptom scores (148). In contrast, treatment with GM-CSF showed results trending in the same direction as IFN-γ, but were not statistically significant compared with placebo. Finally, a prospective case series described patients with invasive fungal infections treated with recombinant IFN-γ (n=8) (149). Notably, 5 of these 8 patients were considered to have IP, defined as < 50% HLA-DR+ monocytes. Treatment with recombinant IFN-γ restored immune function as indicated by increased HLA-DR expression in those with IP, increased *ex-vivo* cytokine production (e.g., TNF-α, IL-17, IL-22), and increased total leukocyte counts.

Therapeutic GM-CSF is available as a rhu protein (sargramostim) that was approved by the US Food and Drug Administration (FDA) in 1991 for myeloid cell reconstitution after cytotoxic chemotherapy (150, 151). Notably, rhu GM-CSF (including sargramostim) augments monocyte metabolic capacity, function, and proliferation (Figure 2) (3, 29, 77, 150, 152). In addition, sargramostim has been administered to acutely and critically ill patients, including children across multiple trials (Table 3) (31, 99, 126, 148, 153–155). No serious adverse events have been ascribed to sargramostim in these studies, and it did not increase systemic inflammation as measured by pro-inflammatory cytokines (e.g., IL-6 or IL-8). Doses studied were at or

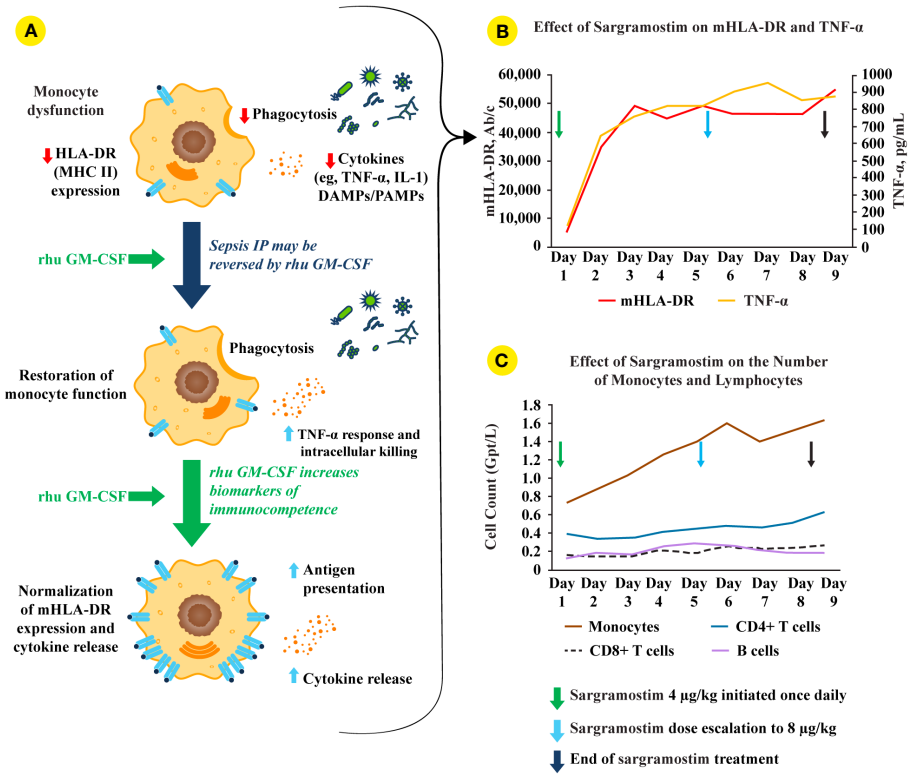

FIGURE 2
rhu GM-CSF (including sargramostim) stimulates and restores immune function in sepsis IP. **(A; top monocyte)** Impaired monocyte function leads to reduced pro-inflammatory mediator responses, decreased pathogen phagocytosis, and lower human leukocyte antigen-DR isotype (HLA-DR) expression (4). **(A; middle and bottom monocytes)** Treatment with recombinant human (rhu) granulocyte-macrophage colony-stimulating factor (GM-CSF) leads to increased intracellular killing, cytokine secretion, phagocytosis, monocyte (m)HLA-DR expression, and antigen presentation (2, 4). **(B)** In a biomarker-guided study of patients with sepsis IP (n=38), sargramostim was given daily for up to 8 days to patients with sepsis and mHLA-DR lower than 8000 Ab/c (31). Sargramostim treatment led to improved mHLA-DR expression and tumor necrosis factor (TNF)-α responses. **(C)** Sargramostim increased absolute numbers of monocytes and lymphocyte subsets (e.g., CD4+ T cells, CD8+ T cells, B cells) (31). Ab/c, antibody numbers bound per cell; DAMP, damage-associated molecular patterns; GM-CSF, granulocyte-macrophage colony-stimulating factor; HLA-DR, human leukocyte antigen-DR isotype; IL, interleukin; IP, immunoparalysis; MHC II, class II major histocompatibility complex; mHLA-DR, monocyte human leukocyte antigen-DR; PAMP, pathogen-associated molecular patterns; rhu, recombinant human; TNF, tumor necrosis factor.

TABLE 3 Use of sargramostim in sepsis to improve clinical outcome and restore normal monocyte function.

Study Design, Patient Population	Results	Clinical Outcomes	Monocyte Function
Randomized, unblinded, prospective study of sargramostim *vs* placebo: 40 patients with sepsis and a documented infection (153)	• Sargramostim *vs* placebo: • More patients experienced cure/improvement of infection (14/18 *vs* 5/15; p=0.01) • More patients survived at 14 days (14/18 *vs* 10/15; p=0.10), 28 days (14/18 *vs* 9/15; p=0.53), and were discharged (12/18 *vs* 8/15; p=0.18) • Sargramostim increased mHLA-DR expression to a level that was not different from that of healthy controls (p=0.27) • Positive correlation between the amount of increase in HLA-DR expression and the clearance of infection (r=0.41; p=0.02)	• Sargramostim increased the proportion of patients whose infections were either cured or improved • Improvement in 28-day survival and hospital discharge in patients who received sargramostim (p=NS)	• Sargramostim normalized mHLA-DR expression • Increased mHLA-DR expression correlated with infection clearance
Prospective, single-arm study of sargramostim: 4 children[a] with recurrent infections (154)	• Sargramostim treatment *vs* baseline:	• Sargramostim treatment reduced the number and severity of infections	• Sargramostim treatment increased absolute monocyte counts at Week 12

(Continued)

10.3389/fimmu.2023.1130214

TABLE 3 Continued

Study Design, Patient Population	Results	Clinical Outcomes	Monocyte Function
	• Decreased number of repeated viral infection complaints (patients 1-3) • Increased diameter of induration for antigens tested *via* DHT (all patients) • Higher absolute monocyte counts at Week 12 (0.4–0.7 x 10^3 *vs* 0.2–0.4 x 10^3; p=NR)	• Sargramostim improved immune function as reflected in positive DHT response	
Randomized, double-blind, phase 2 study of sargramostim *vs* placebo: 38 patients with severe sepsis or septic shock and sepsis IP (31)	• Sargramostim *vs* placebo: • Shorter ICU LOS (40.9 days *vs* 52.1 days; p=NS) • Shorter intrahospital LOS (58.8 days *vs* 68.9 days; p=NS) • Shorter time on ventilator (147.9 days *vs* 207.2 days; p=0.037) • Similar 28-day mortality (16% *vs* 21%; p=NS) • Higher Day 9 mHLA-DR (50,907 Ab/c *vs* 10,426 Ab/c; p<0.0001) • Higher proportion of patients with normalized mHLA-DR levels (100% *vs* 16%) • Higher TLR4-induced cytokine release at Day 9 (IL-6, p<0.05; IL-8, p<0.01)	• Time of mechanical ventilation, ICU LOS, and intrahospital LOS shorter in patients who received sargramostim • No significant change for 28-day mortality between the groups	• Sargramostim normalized mHLA-DR levels • Sargramostim treatment restored cytokine production
Randomized placebo-controlled study of sargramostim *vs* placebo: 36 patients with severe sepsis and sepsis IP (155)	• Sargramostim *vs* placebo: • Lower Day 9 kynurenine levels (p=0.009) • Similar 28-day mortality (17% *vs* 22%; p=0.9) • Lower Day 9 IDO activity (p=0.03) • Correlation with procalcitonin and IDO activity (r=0.56; p<0.0001) • Inverse correlation of mHLA-DR and IDO activity (r=-0.28; p=0.005)	• Sargramostim improved antibacterial defense as indicated by decreased IDO activity and reduction in kynurenine pathway catabolites	• Sargramostim treatment induced normalization of monocytic function that is accompanied with decreased levels of IDO activity and metabolites downstream of IDO
Randomized, open label, phase 2 study of sargramostim *vs* SoC: 14 children with MODS and IP (defined by whole-blood *ex-vivo* LPS-stimulated TNF-α response) (126)	• Sargramostim *vs* SoC: • No nosocomial infections in sargramostim-treated group (p<0.05) • For children who received SoC, IP reversal required > 7 days in the PICU • For children who received sargramostim: • IP reversal occurred in < 7 days • Rapid recovery of *ex-vivo* LPS-induced TNF-α production (200 pg/mL) compared with children who received SoC (p=0.001)	• Sargramostim reduced nosocomial infections without increasing systemic inflammation • Sargramostim-treated patients required fewer days in the PICU	• Sargramostim treatment restored monocyte responsiveness
Randomized, double-blind, placebo-controlled study of sargramostim *vs* IFN-γ and placebo: 18 healthy volunteers, experimental endotoxemia leading to IP induced with *E. coli* endotoxin (148)	• During the second LPS challenge: • Lower reduction in symptom scores with sargramostim (50%; p=0.03) *vs* placebo (72%; p=0.03) • Decrease in TNF-α release (from Visit 1 to Visit 2) with sargramostim (38% [-2 to 63, p=0.16]) and placebo (60% [48–71%; p= 0.03]) • During the treatment period, sargramostim *vs* placebo:	• Sargramostim treatment diminished a reduction in symptom score response to a second LPS exposure in experimental endotoxemia IP model	• Sargramostim treatment stabilized mHLA-DR and prevented a reduction in monocyte responsiveness after second LPS exposure

(Continued)

TABLE 3 Continued

Study Design, Patient Population	Results	Clinical Outcomes	Monocyte Function
	• Stable mHLA-DR (85% to 94%; p=0.40 *vs* 80% to 76%; p=0.30) • Higher leukocyte counts (+21% *vs* -24%; p=0.009)		
Randomized, single-blinded, phase 2a study of sargramostim *vs* placebo: 38 patients with sepsis and impaired neutrophil function (99)	• Sargramostim *vs* placebo: • Higher neutrophil function (phagocytosis ≥ 50%) at Day 6/7 (100% *vs* 44%; p=0.004) • Lower all-cause 30-day mortality (23.5% *vs* 28.6%; for those who received ≥ 2 doses of trial drug, 7.7% *vs* 30%) • Higher mHLA-DR at Day 2 (p<0.01)	• Sargramostim improved neutrophil function • Sargramostim improved all-cause 30-day mortality	• Sargramostim treatment was associated with a significant rise in mHLA-DR at Day 2 (p<0.01)

[a]Three children with severe and recurrent viral respiratory tract infections; 1 child with recurrent bacterial sepsis.
Ab/c, antibodies bound per cell; AUC, area under the curve; DHT, delayed hypersensitivity skin test; HLA-DR, human leukocyte antigen-DR isotype; ICU, intensive care unit; IDO, indoleamine 2,3-dioxygenase; IFN, interferon; IL, interleukin; IP, immunoparalysis; LOS, length of stay; LPS, lipopolysaccharide; mHLA-DR, monocyte human leukocyte antigen-DR; MODS, multiple organ dysfunction syndrome; NR, not reached; NS, not significant; PICU, pediatric intensive care unit; SoC, standard of care; TLR4, toll-like receptor 4; TNF, tumor necrosis factor.

below the labeled dose for myeloid reconstitution (250 μg/m^2/day). In some studies, immune recovery was prompt, within 3 days of sargramostim administration, with trends toward improved infection recovery, reduced hospital stays, and fewer days of mechanical ventilation. Nonetheless, all these studies were underpowered to confirm effects on outcomes. Results of 2 multicenter randomized trials of sargramostim in sepsis IP are also awaited. The ongoing GRACE-2 study (NCT05266001) will evaluate sargramostim *vs* placebo in 400 children with sepsis-induced MODS and IP. Furthermore, mHLA-DR expression will be assessed in this study to establish its clinical utility. In addition, the United Kingdom (UK)-based National Institute for Health and Care Research (NIHR) will sponsor the SepTIC trial that includes investigation of sargramostim for improving outcomes in a high-risk subset of patients admitted to the ICU with sepsis, which is anticipated to begin in mid-2023 (156). Of 3758 adult patients to be enrolled, 1300 with ALC below 1200 cells/μL will be randomized to sargramostim *vs* placebo. The primary endpoint will be 90-day all-cause mortality.

Discussion

While mHLA-DR, TNF-α secretion, and ALC each show promise as potentially useful biomarkers for sepsis IP, analytic validity of HLA-DR expression and its direct biologic linkage with MNP functional state make it attractive as a potential future gold standard for identification of sepsis IP (157, 158). Numerous publications, dating back 20 years, support use of either HLA-DR+ CD14+ cells or the actual number of HLA-DR proteins on CD14+ monocytes as clinically useful biomarkers for identifying patients with sepsis. Furthermore, sepsis IP severity might be detected by either low HLA-DR levels or diminishing HLA-DR levels during hospitalization. Nonetheless, while sepsis IP can be detected by diminished mHLA-DR expression, absence of either validated testing or an approved therapy to correct sepsis IP have thus far prevented widespread adoption of this biomarker.

Based on data presented here, we conclude therapeutic GM-CSF restores mHLA-DR levels and may improve clinical outcomes in patients with sepsis IP. Multiple trials of critically ill adults and children indicate that study treatment with sargramostim restored HLA-DR expression and immunocompetence. Furthermore, sargramostim led to trends toward improved clinical outcomes *via* reduced days of ICU stay and 28-day mortality. The GRACE-2 and SepTIC trials will further inform benefit from therapeutic GM-CSF (sargramostim) in sepsis IP.

Author contributions

IJ, WPC, and EPR contributed equally to this work. All authors contributed to conceptualization and writing (drafting, reviewing, editing) of this manuscript. All authors contributed to the article and approved the submitted version.

Funding

This publication has been funded by Partner Therapeutics, Inc. This project has been funded in part with federal funds from the Department of Health and Human Services; Office of the Assistant Secretary of Preparedness and Response; Biomedical Advanced Research and Development Authority under contract No. 75A50121C00080. The funders had no role in study design, data collection and analysis, decision to publish, or preparation of the manuscript.

Acknowledgments

The authors thank the Biomedical Advanced Research and Development Authority and their colleagues, Debasish Roychowdhury, MD, John McManus, and Anthony Fusco from

Partner Therapeutics, Inc., who provided insight and expertise. The authors also acknowledge Tim Yeung, PharmD and Caytlinn Batal at Wiesen Medical Writing for providing literature support, medical writing support, and editorial assistance.

Conflict of interest

IJ is an employee of and has stock options for Partner Therapeutics, Inc. WPC is the owner of Walt Carney Biomarkers Consulting and a paid consultant for Partner Therapeutics, Inc. At the time of the drafting of this manuscript, EPR was an employee of Partner Therapeutics, Inc. and has stock options.

Publisher's note

References

1. Brady J, Horie S, Laffey JG. Role of the adaptive immune response in sepsis. *Intensive Care Med Exp* (2020) 8(Suppl 1):20. doi: 10.1186/s40635-020-00309-z

2. Chousterman BG, Arnaud M. Is there a role for hematopoietic growth factors during sepsis? *Front Immunol* (2018) 9:1015. doi: 10.3389/fimmu.2018.01015

3. Hall MW. Immune modulation in pediatric sepsis. *J Pediatr Intensive Care* (2019) 8 (1):42–50. doi: 10.1055/s-0038-1676607

4. Pfortmueller CA, Meisel C, Fux M, Schefold JC. Assessment of immune organ dysfunction in critical illness: Utility of innate immune response markers. *Intensive Care Med Exp* (2017) 5(1):49. doi: 10.1186/s40635-017-0163-0

5. Sakr Y, Jaschinski U, Wittebole X, Szakmany T, Lipman J, Ñamendys-Silva SA, et al. Sepsis in intensive care unit patients: Worldwide data from the intensive care over nations audit. *Open Forum Infect Dis* (2018) 5(12):ofy313. doi: 10.1093/ofid/ofy313

6. Prescott HC, Angus DC. Enhancing recovery from sepsis: A review. *JAMA* (2018) 319(1):62–75. doi: 10.1001/jama.2017.17687

7. Centers for Disease Control and Prevention (CDC). *What is sepsis?* (2022). Available at: https://www.cdc.gov/sepsis/what-is-sepsis.html.

8. Rudd KE, Johnson SC, Agesa KM, Shackelford KA, Tsoi D, Kievlan DR, et al. Global, regional, and national sepsis incidence and mortality, 1990-2017: Analysis for the global burden of disease study. *Lancet* (2020) 395(10219):200–11. doi: 10.1016/s0140-6736(19)32989-7

9. World Health Organization (WHO). *Global report on the epidemiology and burden of sepsis: Current evidence, identifying gaps and future directions* (2020). Available at: https://apps.who.int/iris/bitstream/handle/10665/334216/9789240010789-eng.pdf.

10. Singer M, Deutschman CS, Seymour CW, Shankar-Hari M, Annane D, Bauer M, et al. The third international consensus definitions for sepsis and septic shock (Sepsis-3). *JAMA* (2016) 315(8):801–10. doi: 10.1001/jama.2016.0287

11. Neviere R. *Sepsis syndromes in adults: Epidemiology, definitions, clinical presentation, diagnosis, and prognosis* (2022). Available at: https://www.uptodate.com/contents/sepsis-syndromes-in-adults-epidemiology-definitions-clinical-presentation-diagnosis-and-prognosis?search=sepsis&source=search_result&selectedTitle=1~150&usage_type=default&display_rank=1#H1227723412.

12. Hotchkiss RS, Monneret G, Payen D. Sepsis-induced immunosuppression: From cellular dysfunctions to immunotherapy. *Nat Rev Immunol* (2013) 13(12):862–74. doi: 10.1038/nri3552

13. Monneret G, Lepape A, Voirin N, Bohé J, Venet F, Debard AL, et al. Persisting low monocyte human leukocyte antigen-DR expression predicts mortality in septic shock. *Intensive Care Med* (2006) 32(8):1175–83. doi: 10.1007/s00134-006-0204-8

14. Annane D, Bellissant E, Cavaillon JM. Septic shock. *Lancet* (2005) 365(9453):63–78. doi: 10.1016/s0140-6736(04)17667-8

15. Levy MM, Fink MP, Marshall JC, Abraham E, Angus D, Cook D, et al. 2001 SCCM/ESICM/ACCP/ATS/SIS international sepsis definitions conference. *Crit Care Med* (2003) 31(4):1250–6. doi: 10.1097/01.Ccm.0000050454.01978.3b

16. Shankar-Hari M, Phillips GS, Levy ML, Seymour CW, Liu VX, Deutschman CS, et al. Developing a new definition and assessing new clinical criteria for septic shock: For the third international consensus definitions for sepsis and septic shock (Sepsis-3). *JAMA* (2016) 315(8):775–87. doi: 10.1001/jama.2016.0289

17. Bone RC, Balk RA, Cerra FB, Dellinger RP, Fein AM, Knaus WA, et al. Definitions for sepsis and organ failure and guidelines for the use of innovative therapies in sepsis. The ACCP/SCCM consensus conference committee. American College of Chest Physicians/Society of Critical Care Medicine. *Chest* (1992) 101(6):1644–55. doi: 10.1378/chest.101.6.1644

18. Leligdowicz A, Matthay MA. Heterogeneity in sepsis: New biological evidence with clinical applications. *Crit Care* (2019) 23(1):80. doi: 10.1186/s13054-019-2372-2

19. Polat G, Ugan RA, Cadirci E, Halici Z. Sepsis and septic shock: Current treatment strategies and new approaches. *Eurasian J Med* (2017) 49(1):53–8. doi: 10.5152/eurasianjmed.2017.17062

20. Evans L, Rhodes A, Alhazzani W, Antonelli M, Coopersmith CM, French C, et al. Surviving sepsis campaign: International guidelines for management of sepsis and septic shock 2021. *Crit Care Med* (2021) 49(11):e1063–e143. doi: 10.1097/ccm.0000000000005337

21. Lamontagne F, Rochwerg B, Lytvyn L, Guyatt GH, Møller MH, Annane D, et al. Corticosteroid therapy for sepsis: A clinical practice guideline. *BMJ* (2018) 362:k3284. doi: 10.1136/bmj.k3284

22. Vignon P, Laterre PF, Daix T, François B. New agents in development for sepsis: Any reason for hope? *Drugs* (2020) 80(17):1751–61. doi: 10.1007/s40265-020-01402-z

23. Stanski NL, Wong HR. Prognostic and predictive enrichment in sepsis. *Nat Rev Nephrol* (2020) 16(1):20–31. doi: 10.1038/s41581-019-0199-3

24. Varon J, Baron RM. Sepsis endotypes: The early bird still gets the worm. *EBioMedicine* (2022) 76:103832. doi: 10.1016/j.ebiom.2022.103832

25. Baghela A, Pena OM, Lee AH, Baquir B, Falsafi R, An A, et al. Predicting sepsis severity at first clinical presentation: The role of endotypes and mechanistic signatures. *EBioMedicine* (2022) 75:103776. doi: 10.1016/j.ebiom.2021.103776

26. Davies R, O'Dea K, Gordon A. Immune therapy in sepsis: Are we ready to try again? *J Intensive Care Soc* (2018) 19(4):326–44. doi: 10.1177/1751143718765407

27. Delano MJ, Ward PA. The immune system's role in sepsis progression, resolution, and long-term outcome. *Immunol Rev* (2016) 274(1):330–53. doi: 10.1111/imr.12499

28. Bline KE, Hall MW. Immune function in critically ill septic children. *Pathogens* (2021) 10(10):1239. doi: 10.3390/pathogens10101239

29. Peters van Ton AM, Kox M, Abdo WF, Pickkers P. Precision immunotherapy for sepsis. *Front Immunol* (2018) 9:1926. doi: 10.3389/fimmu.2018.01926

30. Winkler MS, Rissiek A, Priefler M, Schwedhelm E, Robbe L, Bauer A, et al. Human leucocyte antigen (HLA-DR) gene expression is reduced in sepsis and correlates with impaired TNFα response: A diagnostic tool for immunosuppression? *PloS One* (2017) 12 (8):e0182427. doi: 10.1371/journal.pone.0182427

31. Meisel C, Schefold JC, Pschowski R, Baumann T, Hetzger K, Gregor J, et al. Granulocyte-macrophage colony-stimulating factor to reverse sepsis-associated immunosuppression: A double-blind, randomized, placebo-controlled multicenter trial. *Am J Respir Crit Care Med* (2009) 180(7):640–8. doi: 10.1164/rccm.200903-0363OC

32. Papadopoulos P, Pistiki A, Theodorakopoulou M, Christodoulopoulou T, Damoraki G, Goukos D, et al. Immunoparalysis: Clinical and immunological associations in SIRS and severe sepsis patients. *Cytokine* (2017) 92:83–92. doi: 10.1016/j.cyto.2017.01.012

33. Gouel-Chéron A, Allaouchiche B, Guignant C, Davin F, Floccard B, Monneret G. Early interleukin-6 and slope of monocyte human leukocyte antigen-DR: A powerful association to predict the development of sepsis after major trauma. *PloS One* (2012) 7(3): e33095. doi: 10.1371/journal.pone.0033095

34. Spapen H, Jacobs R, Honore P. Sepsis-induced multi-organ dysfunction syndrome–a mechanistic approach. *J Emerg Crit Care Med* (2021) 5:13. doi: 10.21037/jeccm.2017

35. Albert-Vega C, Tawfik DM, Trouillet-Assant S, Vachot L, Mallet F, Textoris J. Immune functional assays, from custom to standardized tests for precision medicine. *Front Immunol* (2018) 9:2367. doi: 10.3389/fimmu.2018.02367

36. Ginhoux F, Guilliams M. Tissue-resident macrophage ontogeny and homeostasis. *Immunity* (2016) 44(3):439–49. doi: 10.1016/j.immuni.2016.02.024

37. Gonzalez-Mejia ME, Doseff AI. Regulation of monocytes and macrophages cell fate. *Front Biosci (Landmark Ed)* (2009) 14(7):2413–31. doi: 10.2741/3387

38. Cassatella MA. Human mature neutrophils as atypical APC. *Blood* (2017) 129 (14):1895–6. doi: 10.1182/blood-2017-02-767574

39. Korns D, Frasch SC, Fernandez-Boyanapalli R, Henson PM, Bratton DL. Modulation of macrophage efferocytosis in inflammation. *Front Immunol* (2011) 2:57. doi: 10.3389/fimmu.2011.00057

40. van Lith M, McEwen-Smith RM, Benham AM. HLA-DP, HLA-DQ, and HLA-DR have different requirements for invariant chain and HLA-DM. *J Biol Chem* (2010) 285 (52):40800–8. doi: 10.1074/jbc.M110.148155

41. Kumamoto Y, Mattei LM, Sellers S, Payne GW, Iwasaki A. CD4+ T cells support cytotoxic T lymphocyte priming by controlling lymph node input. *Proc Natl Acad Sci U.S.A.* (2011) 108(21):8749–54. doi: 10.1073/pnas.1100567108

42. Xu W, Banchereau J. The antigen presenting cells instruct plasma cell differentiation. *Front Immunol* (2014) 4:504. doi: 10.3389/fimmu.2013.00504

43. Rosales C. Neutrophil: A cell with many roles in inflammation or several cell types? *Front Physiol* (2018) 9:113. doi: 10.3389/fphys.2018.00113

44. Bhattacharya P, Thiruppathi M, Elshabrawy HA, Alharshawi K, Kumar P, Prabhakar BS. GM-CSF: An immune modulatory cytokine that can suppress autoimmunity. *Cytokine* (2015) 75(2):261–71. doi: 10.1016/j.cyto.2015.05.030

45. Gasson JC, Kaufman SE, Weisbart RH, Tomonaga M, Golde DW. High-affinity binding of granulocyte-macrophage colony-stimulating factor to normal and leukemic human myeloid cells. *Proc Natl Acad Sci U.S.A.* (1986) 83(3):669–73. doi: 10.1073/pnas.83.3.669

46. Hansen G, Hercus TR, McClure BJ, Stomski FC, Dottore M, Powell J, et al. The structure of the GM-CSF receptor complex reveals a distinct mode of cytokine receptor activation. *Cell* (2008) 134(3):496–507. doi: 10.1016/j.cell.2008.05.053

47. Hercus TR, Thomas D, Guthridge MA, Ekert PG, King-Scott J, Parker MW, et al. The granulocyte-macrophage colony-stimulating factor receptor: Linking its structure to cell signaling and its role in disease. *Blood* (2009) 114(7):1289–98. doi: 10.1182/blood-2008-12-164004

48. Zhan Y, Lew AM, Chopin M. The pleiotropic effects of the GM-CSF rheostat on myeloid cell differentiation and function: More than a numbers game. *Front Immunol* (2019) 10:2679. doi: 10.3389/fimmu.2019.02679

49. Adelaja A, Taylor B, Sheu KM, Liu Y, Luecke S, Hoffmann A. Six distinct NFkB signaling codons convey discrete information to distinguish stimuli and enable appropriate macrophage responses. *Immunity* (2021) 54(5):916–30.e7. doi: 10.1016/j.immuni.2021.04.011

50. Tang Y, Adelaja A, Ye FX, Deeds E, Wollman R, Hoffmann A. Quantifying information accumulation encoded in the dynamics of biochemical signaling. *Nat Commun* (2021) 12(1):1272. doi: 10.1038/s41467-021-21562-0

51. Cheng QJ, Ohta S, Sheu KM, Spreafico R, Adelaja A, Taylor B, et al. NFkB dynamics determine the stimulus specificity of epigenomic reprogramming in macrophages. *Science* (2021) 372(6548):1349–53. doi: 10.1126/science.abc0269

52. Wessendarp M, Watanabe-Chailland M, Liu S, Stankiewicz T, Ma Y, Kasam RK, et al. Role of GM-CSF in regulating metabolism and mitochondrial functions critical to macrophage proliferation. *Mitochondrion* (2022) 62:85–101. doi: 10.1016/j.mito.2021.10.009

53. Zhang S, Weinberg S, DeBerge M, Gainullina A, Schipma M, Kinchen JM, et al. Efferocytosis fuels requirements of fatty acid oxidation and the electron transport chain to polarize macrophages for tissue repair. *Cell Metab* (2019) 29(2):443–56.e5. doi: 10.1016/j.cmet.2018.12.004

54. Perry SE, Mostafa SM, Wenstone R, Shenkin A, McLaughlin PJ. HLA-DR regulation and the influence of GM-CSF on transcription, surface expression and shedding. *Int J Med Sci* (2004) 1(3):126–36. doi: 10.7150/ijms.1.126

55. Wculek SK, Dunphy G, Heras-Murillo I, Mastrangelo A, Sancho D. Metabolism of tissue macrophages in homeostasis and pathology. *Cell Mol Immunol* (2022) 19(3):384–408. doi: 10.1038/s41423-021-00791-9

56. Börgermann J, Friedrich I, Scheubel R, Kuss O, Lendemans S, Silber RE, et al. Granulocyte-macrophage colony-stimulating factor (GM-CSF) restores decreased monocyte HLA-DR expression after cardiopulmonary bypass. *Thorac Cardiovasc Surg* (2007) 55(1):24–31. doi: 10.1055/s-2006-924621

57. Bundschuh DS, Barsig J, Hartung T, Randow F, Döcke WD, Volk HD, et al. Granulocyte-macrophage colony-stimulating factor and IFN-γ restore the systemic TNF-α response to endotoxin in lipopolysaccharide-desensitized mice. *J Immunol* (1997) 158 (6):2862–71. doi: 10.4049/jimmunol.158.6.2862

58. Flohé S, Lendemans S, Selbach C, Waydhas C, Ackermann M, Schade FU, et al. Effect of granulocyte-macrophage colony-stimulating factor on the immune response of circulating monocytes after severe trauma. *Crit Care Med* (2003) 31(10):2462–9. doi: 10.1097/01.Ccm.0000089640.17523.57

59. Lendemans S, Kreuzfelder E, Waydhas C, Schade FU, Flohé S. Differential immunostimulating effect of granulocyte-macrophage colony-stimulating factor (GM-CSF), granulocyte colony-stimulating factor (G-CSF) and interferon gamma (IFNγ) after severe trauma. *Inflammation Res* (2007) 56(1):38–44. doi: 10.1007/s00011-007-6069-7

60. Randow F, Döcke WD, Bundschuh DS, Hartung T, Wendel A, Volk HD. *In vitro* prevention and reversal of lipopolysaccharide desensitization by IFN-γ, IL-12, and granulocyte-macrophage colony-stimulating factor. *J Immunol* (1997) 158(6):2911–8. doi: 10.4049/jimmunol.158.6.2911

61. Hornell TM, Beresford GW, Bushey A, Boss JM, Mellins ED. Regulation of the class II MHC pathway in primary human monocytes by granulocyte-macrophage colony-stimulating factor. *J Immunol* (2003) 171(5):2374–83. doi: 10.4049/jimmunol.171.5.2374

62. Mathias B, Szpila BE, Moore FA, Efron PA, Moldawer LL. A review of GM-CSF therapy in sepsis. *Med (Baltimore)* (2015) 94(50):e2044. doi: 10.1097/md.0000000000002044

63. Bruns T, Peter J, Hagel S, Herrmann A, Stallmach A. The augmented neutrophil respiratory burst in response to Escherichia coli is reduced in liver cirrhosis during infection. *Clin Exp Immunol* (2011) 164(3):346–56. doi: 10.1111/j.1365-2249.2011.04373.x

64. Chung H, Lee JH, Jo YH, Hwang JE, Kim J. Circulating monocyte counts and its impact on outcomes in patients with severe sepsis including septic shock. *Shock* (2019) 51 (4):423–9. doi: 10.1097/shk.0000000000001193

65. Reinhart K, Bauer M, Riedemann NC, Hartog CS. New approaches to sepsis: Molecular diagnostics and biomarkers. *Clin Microbiol Rev* (2012) 25(4):609–34. doi: 10.1128/cmr.00016-12

66. Agnello L, Giglio RV, Bivona G, Scazzone C, Gambino CM, Iacona A, et al. The value of a complete blood count (CBC) for sepsis diagnosis and prognosis. *Diagnostics (Basel)* (2021) 11(10):1881. doi: 10.3390/diagnostics11101881

67. Buonacera A, Stancanelli B, Colaci M, Malatino L. Neutrophil to lymphocyte ratio: An emerging marker of the relationships between the immune system and diseases. *Int J Mol Sci* (2022) 23(7):3636. doi: 10.3390/ijms23073636

68. Alelign T, Ahmed MM, Bobosha K, Tadesse Y, Howe R, Petros B. Kidney transplantation: The challenge of human leukocyte antigen and its therapeutic strategies. *J Immunol Res* (2018) 2018:5986740. doi: 10.1155/2018/5986740

69. Roche PA, Furuta K. The ins and outs of MHC class II-mediated antigen processing and presentation. *Nat Rev Immunol* (2015) 15(4):203–16. doi: 10.1038/nri3818

70. Cajander S, Tina E, Bäckman A, Magnuson A, Strålin K, Söderquist B, et al. Quantitative real-time polymerase chain reaction measurement of HLA-DRA gene expression in whole blood is highly reproducible and shows changes that reflect dynamic shifts in monocyte surface HLA-DR expression during the course of sepsis. *PloS One* (2016) 11(5):e0154690. doi: 10.1371/journal.pone.0154690

71. Hagedoorn NN, Kolukirik P, Nagtzaam NMA, Nieboer D, Verbruggen S, Joosten KF, et al. Association of monocyte HLA-DR expression over time with secondary infection in critically ill children: A prospective observational study. *Eur J Pediatr* (2022) 181(3):1133–42. doi: 10.1007/s00431-021-04313-7

72. Turrel-Davin F, Guignant C, Lepape A, Mougin B, Monneret G, Venet F. Upregulation of the pro-apoptotic genes BID and FAS in septic shock patients. *Crit Care* (2010) 14(4):R133. doi: 10.1186/cc9181

73. Zorio V, Venet F, Delwarde B, Floccard B, Marcotte G, Textoris J, et al. Assessment of sepsis-induced immunosuppression at ICU discharge and 6 months after ICU discharge. *Ann Intensive Care* (2017) 7(1):80. doi: 10.1186/s13613-017-0304-3

74. Quadrini KJ, Patti-Diaz L, Maghsoudlou J, Cuomo J, Hedrick MN, McCloskey TW. A flow cytometric assay for HLA-DR expression on monocytes validated as a biomarker for enrollment in sepsis clinical trials. *Cytometry B Clin Cytom* (2021) 100 (1):103–14. doi: 10.1002/cyto.b.21987

75. Leijte GP, Rimmelé T, Kox M, Bruse N, Monard C, Gossez M, et al. Monocytic HLA-DR expression kinetics in septic shock patients with different pathogens, sites of infection and adverse outcomes. *Crit Care* (2020) 24(1):110. doi: 10.1186/s13054-020-2830-x

76. Mizrahi O, Ish Shalom E, Baniyash M, Klieger Y. Quantitative flow cytometry: Concerns and recommendations in clinic and research. *Cytometry B Clin Cytom* (2018) 94 (2):211–8. doi: 10.1002/cyto.b.21515

77. Tamulyte S, Kopplin J, Brenner T, Weigand MA, Uhle F. Monocyte HLA-DR assessment by a novel point-of-care device is feasible for early identification of ICU patients with complicated courses-a proof-of-principle study. *Front Immunol* (2019) 10:432. doi: 10.3389/fimmu.2019.00432

78. Marionneaux S. Nonmalignant leukocyte disorders. In: Keohane EM, Otto CN, Walenga JM Eds. *Rodak's Hematology 6th ed.* Elsevier (2020), 445–65. Accessed January 19, 2023. doi: 10.1016/B978-0-323-53045-3.00035-0

79. Döcke WD, Höflich C, Davis KA, Röttgers K, Meisel C, Kiefer P, et al. Monitoring temporary immunodepression by flow cytometric measurement of monocytic HLA-DR expression: A multicenter standardized study. *Clin Chem* (2005) 51(12):2341–7. doi: 10.1373/clinchem.2005.052639

80. Zhuang Y, Peng H, Chen Y, Zhou S, Chen Y. Dynamic monitoring of monocyte HLA-DR expression for the diagnosis, prognosis, and prediction of sepsis. *Front Biosci (Landmark Ed)* (2017) 22(8):1344–54. doi: 10.2741/4547

81. Hiki N, Berger D, Prigl C, Boelke E, Wiedeck H, Seidelmann M, et al. Endotoxin binding and elimination by monocytes: Secretion of soluble CD14 represents an inducible mechanism counteracting reduced expression of membrane CD14 in patients with sepsis and in a patient with paroxysmal nocturnal hemoglobinuria. *Infect Immun* (1998) 66 (3):1135–41. doi: 10.1128/iai.66.3.1135-1141.1998

82. Patel AA, Zhang Y, Fullerton JN, Boelen L, Rongvaux A, Maini AA, et al. The fate and lifespan of human monocyte subsets in steady state and systemic inflammation. *J Exp Med* (2017) 214(7):1913–23. doi: 10.1084/jem.20170355

83. Kanakoudi-Tsakalidou F, Debonera F, Drossou-Agakidou V, Sarafidis K, Tzimouli V, Taparkou A, et al. Flow cytometric measurement of HLA-DR expression on circulating monocytes in healthy and sick neonates using monocyte negative selection. *Clin Exp Immunol* (2001) 123(3):402–7. doi: 10.1046/j.1365-2249.2001.01471.x

84. de Roquetaillade C, Dupuis C, Faivre V, Lukaszewicz AC, Brumpt C, Payen D. Monitoring of circulating monocyte HLA-DR expression in a large cohort of intensive care patients: Relation with secondary infections. *Ann Intensive Care* (2022) 12(1):39. doi: 10.1186/s13613-022-01010-y

85. Asmussen A, Busch HJ, Helbing T, Bemtgen X, Smolka C, Bode C, et al. Monocyte subset distribution and surface expression of HLA-DR and CD14 in patients after cardiopulmonary resuscitation. *Sci Rep* (2021) 11(1):12403. doi: 10.1038/s41598-021-91948-z

86. Cour-Andlauer F, Morrow BM, McCulloch M, Javouhey E, Lecour S, van As S, et al. Decreased human leukocyte antigen DR on circulating monocytes expression after severe pediatric trauma: An exploratory report. *Pediatr Crit Care Med* (2021) 22(5):e314–e23. doi: 10.1097/pcc.0000000000002604

87. Pei F, Zhang GR, Zhou LX, Liu JY, Ma G, Kou QY, et al. Early immunoparalysis was associated with poor prognosis in elderly patients with sepsis: Secondary analysis of the ETASS study. *Infect Drug Resist* (2020) 13:2053–61. doi: 10.2147/idr.S246513

88. Kox M, Frenzel T, Schouten J, van de Veerdonk FL, Koenen H, Pickkers P. COVID-19 patients exhibit less pronounced immune suppression compared with bacterial septic shock patients. *Crit Care* (2020) 24(1):263. doi: 10.1186/s13054-020-02896-5

89. Chen Y, Hu Y, Zhang J, Shen Y, Huang J, Yin J, et al. Clinical characteristics, risk factors, immune status and prognosis of secondary infection of sepsis: A retrospective observational study. *BMC Anesthesiol* (2019) 19(1):185. doi: 10.1186/s12871-019-0849-9

90. Remy S, Kolev-Descamps K, Gossez M, Venet F, Demaret J, Javouhey E, et al. Occurrence of marked sepsis-induced immunosuppression in pediatric septic shock: A pilot study. *Ann Intensive Care* (2018) 8(1):36. doi: 10.1186/s13613-018-0382-x

91. Remy S, Kolev-Descamps K, Gossez M, Venet F, Demaret J, Javouhey E, et al. Occurrence of marked sepsis-induced immunosuppression in pediatric septic shock: A pilot study. *Ann Intensive Care* (2018) 8(suppl_1):1–5. doi: 10.1186/s13613-018-0382-x

92. Boeddha NP, Kerklaan D, Dunbar A, van Puffelen E, Nagtzaam NMA, Vanhorebeek I, et al. HLA-DR expression on monocyte subsets in critically ill children. *Pediatr Infect Dis J* (2018) 37(10):1034–40. doi: 10.1097/inf.0000000000001990

93. Wu JF, Ma J, Chen J, Ou-Yang B, Chen MY, Li LF, et al. Changes of monocyte human leukocyte antigen-DR expression as a reliable predictor of mortality in severe sepsis. *Crit Care* (2011) 15(5):R220. doi: 10.1186/cc10457

94. Demaret J, Walencik A, Jacob MC, Timsit JF, Venet F, Lepape A, et al. Inter-laboratory assessment of flow cytometric monocyte HLA-DR expression in clinical samples. *Cytometry B Clin Cytom* (2013) 84(1):59–62. doi: 10.1002/cyto.b.21043

95. Drewry AM, Ablordeppey EA, Murray ET, Beiter ER, Walton AH, Hall MW, et al. Comparison of monocyte human leukocyte antigen-DR expression and stimulated tumor necrosis factor alpha production as outcome predictors in severe sepsis: A prospective observational study. *Crit Care* (2016) 20(1):334. doi: 10.1186/s13054-016-1505-0

96. Raghavan M, Yarzabek B, Zaitouna AJ, Krishnakumar S, Ramon DS. Strategies for the measurements of expression levels and half-lives of HLA class I allotypes. *Hum Immunol* (2019) 80(4):221–7. doi: 10.1016/j.humimm.2019.02.001

97. Pannu KK, Joe ET, Iyer SB. Performance evaluation of Quantibrite phycoerythrin beads. *Cytometry* (2001) 45(4):250–8. doi: 10.1002/1097-0320(20011201)45:4<250::aid-cyto10021>3.0.co;2-t

98. Manzoli TF, Troster EJ, Ferranti JF, Sales MM. Prolonged suppression of monocytic human leukocyte antigen-DR expression correlates with mortality in pediatric septic patients in a pediatric tertiary intensive care unit. *J Crit Care* (2016) 33:84–9. doi: 10.1016/j.jcrc.2016.01.027

99. Pinder EM, Rostron AJ, Hellyer TP, Ruchaud-Sparagano MH, Scott J, Macfarlane JG, et al. Randomised controlled trial of GM-CSF in critically ill patients with impaired neutrophil phagocytosis. *Thorax* (2018) 73(10):918–25. doi: 10.1136/thoraxjnl-2017-211323

100. Skirecki T, Mikaszewska-Sokolewicz M, Hoser G, Zielińska-Borkowska U. The early expression of HLA-DR and CD64 myeloid markers is specifically compartmentalized in the blood and lungs of patients with septic shock. *Mediators Inflammation* (2016) 2016:3074902. doi: 10.1155/2016/3074902

101. Strohmeyer JC, Blume C, Meisel C, Doecke WD, Hummel M, Hoeflich C, et al. Standardized immune monitoring for the prediction of infections after cardiopulmonary bypass surgery in risk patients. *Cytometry B Clin Cytom* (2003) 53(1):54–62. doi: 10.1002/cyto.b.10031

102. Dimitrov E, Enchev E, Minkov G, Halacheva K, Yovtchev Y. Poor outcome could be predicted by lower monocyte human leukocyte antigen-DR expression in patients with complicated intra-abdominal infections: A review. *Surg Infect (Larchmt)* (2020) 21(2):77–80. doi: 10.1089/sur.2019.050

103. Perry SE, Mostafa SM, Wenstone R, Shenkin A, McLaughlin PJ. Is low monocyte HLA-DR expression helpful to predict outcome in severe sepsis? *Intensive Care Med* (2003) 29(8):1245–52. doi: 10.1007/s00134-003-1686-2

104. Benlyamani I, Venet F, Coudereau R, Gossez M, Monneret G. Monocyte HLA-DR measurement by flow cytometry in COVID-19 patients: An interim review. *Cytometry A* (2020) 97(12):1217–21. doi: 10.1002/cyto.a.24249

105. Chen G, Wen D, Qiu J, Wang Q, Peng G, Du J, et al. *The role of mHLA-DR in the early diagnosis of sepsis patients with severe trauma: A meta-analysis* (2021). Available at: https://assets.researchsquare.com/files/rs-770184/v1/97eee162-f6ef-4d98-9309-0934a71253e8.pdf?c=1631887620.

106. Remy S, Gossez M, Belot A, Hayman J, Portefaix A, Venet F, et al. Massive increase in monocyte HLA-DR expression can be used to discriminate between septic shock and hemophagocytic lymphohistiocytosis-induced shock. *Crit Care* (2018) 22(1):213. doi: 10.1186/s13054-018-2146-2

107. Cazalis MA, Friggeri A, Cavé L, Demaret J, Barbalat V, Cerrato E, et al. Decreased HLA-DR antigen-associated invariant chain (CD74) mRNA expression predicts mortality after septic shock. *Crit Care* (2013) 17(6):R287. doi: 10.1186/cc13150

108. Darcy CJ, Minigo G, Piera KA, Davis JS, McNeil YR, Chen Y, et al. Neutrophils with myeloid derived suppressor function deplete arginine and constrain T cell function in septic shock patients. *Crit Care* (2014) 18(4):R163. doi: 10.1186/cc14003

109. Fenner BP, Darden DB, Kelly LS, Rincon J, Brakenridge SC, Larson SD, et al. Immunological endotyping of chronic critical illness after severe sepsis. *Front Med (Lausanne)* (2020) 7:616694. doi: 10.3389/fmed.2020.616694

110. Janols H, Bergenfelz C, Allaoui R, Larsson AM, Rydén L, Björnsson S, et al. A high frequency of MDSCs in sepsis patients, with the granulocytic subtype dominating in gram-positive cases. *J Leukoc Biol* (2014) 96(5):685–93. doi: 10.1189/jlb.5HI0214-074R

111. Mathias B, Delmas AL, Ozrazgat-Baslanti T, Vanzant EL, Szpila BE, Mohr AM, et al. Human myeloid-derived suppressor cells are associated with chronic immune suppression after severe sepsis/septic shock. *Ann Surg* (2017) 265(4):827–34. doi: 10.1097/sla.0000000000001783

112. Uhel F, Azzaoui I, Grégoire M, Pangault C, Dulong J, Tadié JM, et al. Early expansion of circulating granulocytic myeloid-derived suppressor cells predicts development of nosocomial infections in patients with sepsis. *Am J Respir Crit Care Med* (2017) 196(3):315–27. doi: 10.1164/rccm.201606-1143OC

113. Udovicic I, Stanojevic I, Djordjevic D, Zeba S, Rondovic G, Abazovic T, et al. Immunomonitoring of monocyte and neutrophil function in critically ill patients: From sepsis and/or trauma to COVID-19. *J Clin Med* (2021) 10(24):5815. doi: 10.3390/jcm10245815

114. Haveman JW, Muller Kobold AC, Tervaert JW, van den Berg AP, Tulleken JE, Kallenberg CG, et al. The central role of monocytes in the pathogenesis of sepsis: Consequences for immunomonitoring and treatment. *Neth J Med* (1999) 55(3):132–41. doi: 10.1016/s0300-2977(98)00156-9

115. Monneret G, Venet F, Pachot A, Lepape A. Monitoring immune dysfunctions in the septic patient: A new skin for the old ceremony. *Mol Med* (2008) 14(1-2):64–78. doi: 10.2119/2007-00102.Monneret

116. Schefold JC. Measurement of monocytic HLA-DR (mHLA-DR) expression in patients with severe sepsis and septic shock: Assessment of immune organ failure. *Intensive Care Med* (2010) 36(11):1810–2. doi: 10.1007/s00134-010-1965-7

117. Landelle C, Lepape A, Voirin N, Tognet E, Venet F, Bohé J, et al. Low monocyte human leukocyte antigen-DR is independently associated with nosocomial infections after septic shock. *Intensive Care Med* (2010) 36(11):1859–66. doi: 10.1007/s00134-010-1962-x

118. Carson WF, Cavassani KA, Dou Y, Kunkel SL. Epigenetic regulation of immune cell functions during post-septic immunosuppression. *Epigenetics* (2011) 6(3):273–83. doi: 10.4161/epi.6.3.14017

119. Gentile LF, Cuenca AG, Efron PA, Ang D, Bihorac A, McKinley BA, et al. Persistent inflammation and immunosuppression: A common syndrome and new horizon for surgical intensive care. *J Trauma Acute Care Surg* (2012) 72(6):1491–501. doi: 10.1097/TA.0b013e318256e000

120. Winters BD, Eberlein M, Leung J, Needham DM, Pronovost PJ, Sevransky JE. Long-term mortality and quality of life in sepsis: A systematic review. *Crit Care Med* (2010) 38(5):1276–83. doi: 10.1097/CCM.0b013e3181d8cc1d

121. Doughty C, Oppermann L, Hartmann N, Dreschers S, Gille C, Orlikowsky T. Monocytes in neonatal bacterial sepsis: Think tank or workhorse? *BioChem* (2022) 2(1):27–42. doi: 10.3390/biochem2010003

122. Damasceno D, Teodosio C, van den Bossche WBL, Perez-Andres M, Arriba-Méndez S, Muñoz-Bellvis L, et al. Distribution of subsets of blood monocytic cells throughout life. *J Allergy Clin Immunol* (2019) 144(1):320–3.e6. doi: 10.1016/j.jaci.2019.02.030

123. Kapellos TS, Bonaguro L, Gemünd I, Reusch N, Saglam A, Hinkley ER, et al. Human monocyte subsets and phenotypes in major chronic inflammatory diseases. *Front Immunol* (2019) 10:2035. doi: 10.3389/fimmu.2019.02035

124. Hibbert JE, Currie A, Strunk T. Sepsis-induced immunosuppression in neonates. *Front Pediatr* (2018) 6:357. doi: 10.3389/fped.2018.00357

125. Semmes EC, Chen JL, Goswami R, Burt TD, Permar SR, Fouda GG. Understanding early-life adaptive immunity to guide interventions for pediatric health. *Front Immunol* (2020) 11:595297. doi: 10.3389/fimmu.2020.595297

126. Hall MW, Knatz NL, Vetterly C, Tomarello S, Wewers MD, Volk HD, et al. Immunoparalysis and nosocomial infection in children with multiple organ dysfunction syndrome. *Intensive Care Med* (2011) 37(3):525–32. doi: 10.1007/s00134-010-2088-x

127. Levin G, Boyd JG, Day A, Hunt M, Maslove DM, Norman P, et al. The relationship between immune status as measured by stimulated ex-vivo tumour necrosis factor alpha levels and the acquisition of nosocomial infections in critically ill mechanically ventilated patients. *Intensive Care Med Exp* (2020) 8(1):55. doi: 10.1186/s40635-020-00344-w

128. Snyder A, Jedreski K, Fitch J, Wijeratne S, Wetzel A, Hensley J, et al. Transcriptomic profiles in children with septic shock with or without immunoparalysis. *Front Immunol* (2021) 12:733834. doi: 10.3389/fimmu.2021.733834

129. Frazier WJ, Hall MW. Immunoparalysis and adverse outcomes from critical illness. *Pediatr Clin North Am* (2008) 55(3):647–68. doi: 10.1016/j.pcl.2008.02.009

130. Drewry AM, Samra N, Skrupky LP, Fuller BM, Compton SM, Hotchkiss RS. Persistent lymphopenia after diagnosis of sepsis predicts mortality. *Shock* (2014) 42(5):383–91. doi: 10.1097/shk.0000000000000234

131. National Institutes of Health (NIH). *Lymphopenia: Diagnosis* (2022). Available at: https://www.nhlbi.nih.gov/health/lymphopenia/diagnosis.

132. Karamikhah R, Karimzadeh I. Acute lymphoblastic leukemia in children: A short review. *Trends Pharm Sci* (2020) 6(4):283–96. doi: 10.30476/tips.2021.88938.1073

133. National Institutes of Health (NIH). *Lymphopenia: What is lymphopenia?* (2022). Available at: https://www.nhlbi.nih.gov/health/lymphopenia.

134. Belok SH, Bosch NA, Klings ES, Walkey AJ. Evaluation of leukopenia during sepsis as a marker of sepsis-defining organ dysfunction. *PloS One* (2021) 16(6):e0252206. doi: 10.1371/journal.pone.0252206

135. Cao C, Yu M, Chai Y. Pathological alteration and therapeutic implications of sepsis-induced immune cell apoptosis. *Cell Death Dis* (2019) 10(10):782. doi: 10.1038/s41419-019-2015-1

136. Nedeva C, Menassa J, Puthalakath H. Sepsis: Inflammation is a necessary evil. *Front Cell Dev Biol* (2019) 7:108. doi: 10.3389/fcell.2019.00108

137. Vahedi H, Bagheri A, Jahanshir A, Seyedhosseini J, Vahidi E. Association of lymphopenia with short term outcomes of sepsis patients; a brief report. *Arch Acad Emerg Med* (2019) 7(1):e14. doi: 10.22037/aaem.v7i1.117

138. Bidar F, Bodinier M, Venet F, Lukaszewicz AC, Brengel-Pesce K, Conti F, et al. Concomitant assessment of monocyte HLA-DR expression and ex vivo TNF-α release as markers of adverse outcome after various injuries-insights from the realism study. *J Clin Med* (2021) 11(1):96. doi: 10.3390/jcm11010096

139. Grivennikov SI, Tumanov AV, Liepinsh DJ, Kruglov AA, Marakusha BI, Shakhov AN, et al. Distinct and nonredundant in vivo functions of TNF produced by T cells and macrophages/neutrophils: Protective and deleterious effects. *Immunity* (2005) 22(1):93–104. doi: 10.1016/j.immuni.2004.11.016

140. Monneret G, Venet F, Meisel C, Schefold JC. Assessment of monocytic HLA-DR expression in ICU patients: Analytical issues for multicentric flow cytometry studies. *Crit Care* (2010) 14(4):432. doi: 10.1186/cc9184

141. Prame Kumar K, Nicholls AJ, Wong CHY. Partners in crime: neutrophils and monocytes/macrophages in inflammation and disease. *Cell Tissue Res* (2018) 371(3):551–65. doi: 10.1007/s00441-017-2753-2

142. Tang G, Yuan X, Luo Y, Lin Q, Chen Z, Xing X, et al. Establishing immune scoring model based on combination of the number, function, and phenotype of lymphocytes. *Aging (Albany NY)* (2020) 12(10):9328–43. doi: 10.18632/aging.103208

143. Francois B, Jeannet R, Daix T, Walton AH, Shotwell MS, Unsinger J, et al. Interleukin-7 restores lymphocytes in septic shock: The IRIS-7 randomized clinical trial. *JCI Insight* (2018) 3(5):e98960. doi: 10.1172/jci.insight.98960

144. Qin W, Hu L, Zhang X, Jiang S, Li J, Zhang Z, et al. The diverse function of PD-1/PD-L pathway beyond cancer. *Front Immunol* (2019) 10:2298. doi: 10.3389/fimmu.2019.02298

145. Hotchkiss RS, Colston E, Yende S, Crouser ED, Martin GS, Albertson T, et al. Immune checkpoint inhibition in sepsis: A phase 1b randomized study to evaluate the safety, tolerability, pharmacokinetics, and pharmacodynamics of nivolumab. *Intensive Care Med* (2019) 45(10):1360–71. doi: 10.1007/s00134-019-05704-z

146. Ambruso DR, Briones NJ, Baroffio AF, Murphy JR, Tran AD, Gowan K, et al. *In vivo* interferon-gamma induced changes in gene expression dramatically alter neutrophil phenotype. *PloS One* (2022) 17(2):e0263370. doi: 10.1371/journal.pone.0263370

147. Döcke WD, Randow F, Syrbe U, Krausch D, Asadullah K, Reinke P, et al. Monocyte deactivation in septic patients: Restoration by IFN-γ treatment. *Nat Med* (1997) 3(6):678–81. doi: 10.1038/nm0697-678

148. Leentjens J, Kox M, Koch RM, Preijers F, Joosten LA, van der Hoeven JG, et al. Reversal of immunoparalysis in humans in vivo: A double-blind, placebo-controlled, randomized pilot study. *Am J Respir Crit Care Med* (2012) 186(9):838–45. doi: 10.1164/rccm.201204-0645OC

149. Delsing CE, Gresnigt MS, Leentjens J, Preijers F, Frager FA, Kox M, et al. Interferon-gamma as adjunctive immunotherapy for invasive fungal infections: A case series. *BMC Infect Dis* (2014) 14:166. doi: 10.1186/1471-2334-14-166

150. Lazarus HM, Ragsdale CE, Gale RP, Lyman GH. Sargramostim (rhu GM-CSF) as cancer therapy (systematic review) and an immunomodulator. A drug before its time? *Front Immunol* (2021) 12:706186. doi: 10.3389/fimmu.2021.706186

151. *Leukine (Sargramostim)*. Lexington, MA: Partner Therapeutics, Inc. (2022).

152. Na YR, Gu GJ, Jung D, Kim YW, Na J, Woo JS, et al. GM-CSF induces inflammatory macrophages by regulating glycolysis and lipid metabolism. *J Immunol* (2016) 197(10):4101–9. doi: 10.4049/jimmunol.1600745

153. Rosenbloom AJ, Linden PK, Dorrance A, Penkosky N, Cohen-Melamed MH, Pinsky MR. Effect of granulocyte-monocyte colony-stimulating factor therapy on leukocyte function and clearance of serious infection in nonneutropenic patients. *Chest* (2005) 127(6):2139–50. doi: 10.1378/chest.127.6.2139

154. Nelson LA. Use of granulocyte-macrophage colony-stimulating factor to reverse anergy in otherwise immunologically healthy children. *Ann Allergy Asthma Immunol* (2007) 98(4):373–82. doi: 10.1016/s1081-1206(10)60885-x

155. Schefold JC, Zeden JP, Pschowski R, Hammoud B, Fotopoulou C, Hasper D, et al. Treatment with granulocyte-macrophage colony-stimulating factor is associated with reduced indoleamine 2,3-dioxygenase activity and kynurenine pathway catabolites in patients with severe sepsis and septic shock. *Scand J Infect Dis* (2010) 42(3):164–71. doi: 10.3109/00365540903405768

156. National Institute for Health and Care Research (NIHR). *Funding and awards: Sepsis trials in critical care (SepTIC)* (2022). Available at: https://fundingawards.nihr.ac.uk/award/17/136/02.

157. Monneret G, Gossez M, Aghaeepour N, Gaudilliere B, Venet F. How clinical flow cytometry rebooted sepsis immunology. *Cytometry A* (2019) 95(4):431–41. doi: 10.1002/cyto.a.23749

158. Ruiz-Rodriguez J, Plata-Menchaca E, Chiscano-Camón L, Ruiz-Sanmartin A, Pérez-Carrasco M, Palmada C, et al. Precision medicine in sepsis and septic shock: From omics to clinical tools. *World J Crit Care Med* (2022) 11(1):1–21. doi: 10.5492/wjccm.v11.i1.1

frontiers | Frontiers in Immunology

TYPE Original Research
PUBLISHED 27 February 2023
DOI 10.3389/fimmu.2023.1095457

OPEN ACCESS

EDITED BY
Zuliang Jie,
Xiamen University, China

REVIEWED BY
Gan Zhao,
University of Pennsylvania, United States
Lihua Duan,
Jiangxi Provincial People's Hospital, China

*CORRESPONDENCE
Lunxian Tang
456tlx@163.com

†These authors have contributed equally to this work and share first authorship

SPECIALTY SECTION
This article was submitted to Inflammation, a section of the journal Frontiers in Immunology

RECEIVED 11 November 2022
ACCEPTED 16 February 2023
PUBLISHED 27 February 2023

CITATION
Yang D, Zhao D, Ji J, Wang C, Liu N, Bao X, Liu X, Jiang S, Zhang Q and Tang L (2023) *CircRNA_0075723* protects against pneumonia-induced sepsis through inhibiting macrophage pyroptosis by sponging miR-155-5p and regulating SHIP1 expression. *Front. Immunol.* 14:1095457. doi: 10.3389/fimmu.2023.1095457

CircRNA_0075723 protects against pneumonia-induced sepsis through inhibiting macrophage pyroptosis by sponging miR-155-5p and regulating SHIP1 expression

Dianyin Yang[1,2†], Dongyang Zhao[1,2†], Jinlu Ji[2†], Chunxue Wang[1,2], Na Liu[3], Xiaowei Bao[1,2], Xiandong Liu[1], Sen Jiang[1], Qianqian Zhang[2] and Lunxian Tang[1*]

[1]Department of Internal Emergency Medicine, Shanghai East Hospital, Tongji University School of Medicine, Shanghai, China, [2]Medical School, Tongji University, Shanghai, China, [3]Department of Nephrology, Shanghai East Hospital, Tongji University School of Medicine, Shanghai, China

Introduction: Circular RNAs (circRNAs) have been linked to regulate macrophage polarization and subsequent inflammation in sepsis. However, the underlying mechanism and the function of circRNAs in macrophage pyroptosis in pneumonia-induced sepsis are still unknown.

Methods: In this study, we screened the differentially expressed circRNAs among the healthy individuals, pneumonia patients without sepsis and pneumonia-induced sepsis patients in the plasma by RNA sequencing (RNA-seq). Then we evaluated macrophage pyroptosis in sepsis patients and in vitro LPS/nigericin activated THP-1 cells. The lentiviral recombinant vector for circ_0075723 overexpression (OE-circ_0075723) and circ_0075723 silence (sh-circ_0075723) were constructed and transfected into THP-1 cells to explore the potential mechanism of circ_0075723 involved in LPS/nigericin induced macrophage pyroptosis.

Results: We found circ_0075723, a novel circRNA that was significantly downregulated in pneumonia-induced sepsis patients compared to pneumonia patients without sepsis and healthy individuals. Meanwhile, pneumonia-induced sepsis patients exhibited activation of NLRP3 inflammasome and production of the pyroptosis-associated pro-inflammatory cytokines IL-1β and IL-18. circ_0075723 inhibited macrophage pyroptosis via sponging miR-155-5p which promoted SHIP1 expression directly. Besides, we found that circ_0075723 in macrophages promoted VE-cadherin expression in endothelial cells through inhibiting the release of NLRP3 inflammasome-related cytokines, IL-1β and IL-18, and protects endothelial cell integrity.

10.3389/fimmu.2023.1095457

Discussion: Our findings propose a unique approach wherein circ_0075723 suppresses macrophage pyroptosis and inflammation in pneumonia-induced sepsis via sponging with miR-155-5p and promoting SHIP1 expression. These findings indicate that circRNAs could be used as possible potential diagnostic and therapeutic targets for pneumonia-induced sepsis.

KEYWORDS

CircRNA_0075723, miR-155-5p, SHIP1, pyroptosis, pneumonia-induced sepsis, THP-1

Introduction

Sepsis is defined as a life-threatening organ dysfunction caused by a dysregulated host response to infection (1). Despite significant advances of sepsis therapy in the past decade, sepsis remains the primary reason for death in the intensive care unit (ICU) (2). Infection in the respiratory system is the most common of sepsis, which accounts for about 50%. Meanwhile pulmonary infections lead to nearly 30% mortality of patients with sepsis, much higher than infections from other sources (3, 4). However, the mechanisms driving pneumonia-induced sepsis remain poorly understood. Macrophage death is critical to the pathophysiology of pneumonia and related sepsis (5, 6). Of note, pyroptosis, a sort of programmed cell death driven by NLRP3 inflammasome activation, is a major contributor to sepsis. It is characterized by formation of cell membrane pores and the production of inflammatory factors IL-1β and IL-18 (7). In reaction to pathogen-associated molecular patterns (PAMPs) and damage-associated molecular patterns (DAMPs), NLRP3 is activated and oligomerized through NACHT domain, which then recruits apoptosis-associated speck-like protein containing a CARD (ASC) and pro-caspase 1 to form NLRP3 inflammasome. This results in the transformation of pro-caspase1 into active caspase1. The active caspase1 then converts pro-IL-1β and pro-IL-18 to their active forms. With its pore-forming activity, Caspase1 also cleaves gasdermin D (GSDMD) into N-terminal form (N-GSDMD). Inflammatory factors (IL-1β and IL-18) are ultimately released from pores formed by N-GSDMD. Increasing evidence have indicated that NLRP3 inflammasome and pyroptosis in macrophages are essential for the occurrence and development of sepsis (8, 9). However, whether macrophage pyroptosis is involved in pneumonia-induced sepsis and the precise regulatory mechanisms of macrophage pyroptosis remain not clear.

Circular RNAs (circRNAs) are covalently closed single-strand RNAs generated by mRNA back-splicing, which comprise a widespread subtype of non-coding RNAs (10). The main function of circRNAs is regulation of transcription and translation of mRNA by sponging miRNAs (11). Till now, circRNAs have been implicated in numerous areas of biological processes, including cell differentiation, apoptosis, autophagy, and proliferation, which are all closely related to septic pathogenesis (12). We previously reported global changes of circRNAs and the circRNA-miRNA-mRNA networks in pulmonary macrophages activation from cecal ligation and puncture (CLP)-induced acute respiratory distress syndrome (ARDS) mice model by microarray analysis, suggesting that circRNAs are required for macrophages function and the development of ARDS (13). Further, we have revealed that *circN4bp1* facilitated sepsis-induced ARDS through promoting macrophage polarization by means of miR-138-5p/EZH2 axis *in vivo* and ex vivo (14). Recent reports have implicated circular RNAs in the regulation of macrophage pyroptosis. *CircACTR2* is identified to promote macrophage pyroptosis and the subsequent fibrosis (15). Inhibition of *circ_0029589* by IFN regulatory Factor-1 (IRF-1) may also promote macrophage pyroptosis and inflammation in patients with acute coronary syndrome (ACS) (16). However, it remains unknown whether circRNAs regulate macrophage pyroptosis in sepsis, especially pneumonia-induced sepsis. In this investigation, we screened for differential expression circRNAs in plasma of healthy individuals, pneumonia patients without sepsis, and pneumonia-induced sepsis patients using RNA-seq and recognized the significantly downregulated circRNA, *circ_0075723*, which is generated from the exons of gene *NUP153*. We also showed that *circ_0075723* acted as a negative regulator of macrophage pyroptosis and inflammatory damage in pneumonia-induced sepsis, in addition to the pathways associated with miR-155-5p and SHIP1. Our findings present new insights of circRNAs into the regulation of macrophage pyroptosis and provide possible treatment targets for pneumonia-induced sepsis.

Materials and methods

Clinical samples collection

This study was authorized by the Research Ethics Board of East Hospital, Tongji University (Shanghai, China). All recruited patients or their authorized family members were provided with a consent form. Peripheral blood (4ml) was taken from 7 eligible patients with pneumonia-induced sepsis, 7 pneumonia patients without sepsis and 7 healthy donors. The participants' clinical parameters are shown in Supplementary Table 1. The pneumonia

patients were classified as sepsis according to the Surviving Sepsis Campaign definitions (17) from the emergency and/or general intensive care unit (ICU) of East Hospital. The pneumonia patients without sepsis who came from emergency internal medicine ward of East Hospital and healthy volunteers came to East hospital for routine physical examination. Pneumonia was defined by a new pulmonary infiltrate on chest radiograph accompanied with at least one of the following signs (18): (a) the presence of cough, sputum production, and dyspnea; (b) core body temperature > 38.0°C; (c) peripheral white blood cell counts > 10×10^9/L or < 4×10^9/L. Among the 21 samples, 3 sepsis samples, 3 pneumonia samples and 3 healthy people samples were used for RNA sequencing analysis, and the remaining samples were used for subsequent tests.

Cell extraction

Peripheral blood mononuclear cells (PBMCs) were isolated from peripheral blood according to the protocol as previously reported (19) and $CD14^+$ monocytes were sorted from PBMCs with a magnetic cell sorting system (Miltenyi Biotec, Germany). PBMCs were added with CD14 Microbeads(20μl/10^7cells), and then the $CD14^+$ monocytes were magnetically labeled with CD14 Microbeads. When PBMCs passed through a MACS column, the magnetically labeled $CD14^+$ monocytes were retained within the column, and then CD14+monocytes were extracted as positively selected cell fraction.

RNA sequencing analysis

Plasma from patients with pneumonia-induced sepsis, pneumonia patients without sepsis, and healthy individuals was isolated using TRIzol reagent (Invitrogen, USA) per the manufacturer's instructions. NanoDrop ND-1000 was utilized to measure the RNA's purity and concentration (NanoDrop Thermo). Through denaturing agarose gel electrophoresis, the RNA integrity of the samples was evaluated. The rRNA was removed using the Ribo-Zero rRNA Removal Kit (Illumina, San Diego, CA, USA). Cloud-Seq Biotech (Shanghai, China) performed the high-throughput whole transcriptome sequencing and subsequent bioinformatics analysis as previously reported (20). The sequencer Illumina HiSeq 6000 was used to obtain paired-end readings. The circular RNA was detected and identified using DCC software (v0.4.4) and the identified circular RNA was annotated using the circBase database and Circ2Tuits. Edger software (v3.16.5) was utilized to identify circRNAs with differential expression.

RNA extraction and quantitative Real-Time PCR (qRT-PCR)

Total RNA (2μg) was extracted using TRIzol (Invitrogen, USA) followed by reverse transcription of mRNAs and circRNAs using PrimeScript II 1st Strand cDNA Synthesis Kit (Takara, Japan) per the standard manufacturer's instructions. qRT-PCR assay was performed to measure mRNAs and circRNAs expression with SYBR® Premix Ex Taq™ II (Takara, Japan) using the Roche 480 Real Time PCR System. GAPDH (encoding glyceraldehyde-3-phosphate dehydrogenase) was used as an internal control for circRNAs and mRNAs, and U6 was employed as an endogenous control for the miRNAs. Relative quantification ($2^{-\Delta\Delta CT}$) was used for result analysis. All the primers used were included in Supplementary Table 2.

Cell culture and transfection

The human monocytic leukemia cell line THP-1 was purchased from Chinese Academy of Sciences (Shanghai, China) and was grown in RPMI-1640 medium supplemented with 10% fetal bovine serum and 1% penicillin and streptomycin. THP-1 cells were differentiated into macrophages for 3 hr in the presence of 100 nM phorbol myristate (PMA) and replated. For stimulation, cells were primed with different or indicated concentrations (0.1, 0.5 and 1 μg/ml) LPS for 4 hrs in Opti-MEM, then stimulated with 10 μM nigericin for 2 hrs. GenePharma designed and produced the *Circ_0075723* overexpression vector, miR-155-5p mimic, SHIP1 overexpression vector and *circ_0075723* silence vector (sh-*circ_0075723*) (Shanghai, China). THP-1 cells were transfected with overexpression vector (2 μg), miRNA mimic (25 nM) or shRNA (25 nM) using Lipofectamine 3000 (Invitrogen) per the manufacturer's instructions 24h before LPS/nigericin stimulation. After different stimulations, the supernatants of THP-1 cells were collected for IL-1β and IL-18 analyses or applied to culture human lung microvascular endothelial cells (HLMVEC) (Chinese Academy of Sciences, China) for 24 hours.

Fluorescence *in situ* hybridization (FISH) assay

The location of *circ_0075723* in THP-1 cells is determined by FISH. THP-1 cells are fixed with 4% paraformaldehyde and gradient dehydrated with ethanol. Fluorescent-labeled probe (1 μM) for *circ_0075723* is applied during hybridization. We use DAPI (Beyotime, Shanghai, China) to stain the nucleus of macrophages.

Luciferase reporter assay

The wild-type (WT) sequence and mutant-type (MUT) sequences (binding site mutation with miR-155-5p) of *circ_0075723* and SHIP1 were amplified and cloned into PmirGLO reporter plasmid, respectively. The fusion plasmid was cotransfected with either miR-155-5p or miR-NC into HEK293T cells. 48 hours after transfection, the luciferase activity was measured using Picagene Dual SeaPansy luminescence kit (Toyo

Inc., Japan) according to the manufacturer's instructions as reported (21).

RNase R digestion RNA stability

4 μg total RNA from THP-1 cells was either untreated (control) or treated with 20 units of RNase R (Epicenter; USA, RNR07250) in the presence of 1× reaction buffer and incubated for 30 min at 37°C. RNA was extracted using acid phenol-chloroform after digestion (5: 1). Then, reverse transcription and qRT-PCR were performed, as described in the RNA extraction and qRT-PCR section. THP-1 cells (1×10^5) were placed in 24-well plates and treated with 250 ng/ml actinomycin D (Act D, Sigma) added to the cell culture medium. The levels of *circ_0075723* and *NUP153* were measured at 0, 8, 12, and 24 hrs.

RNA pull-down assay

Biotin-labeled *circ_0075723* probe and oligo probe were obtained from Ribobio. THP-1 cells transfected with *circ_0075723* probe or oligo probe were lysed and used for pull-down assay using the Pierce Magnetic RNA ProteinPull-down Kit (Thermo Fisher Scientific) in accordance with the instructions. qRT-PCR was used to detect the expression of specified miRNAs.

ELISA analysis

ELISAs were performed to measure the concentrations of IL-18 and IL-1β protein from supernatants according to the manufacturer's instructions (R&D Systems).

Immunoblotting analysis

Immunoblotting analysis was performed as described previously (19, 22). Densitometry analysis of immunoblot results was conducted by using ImageJ software. The results of three replicated experiments are expressed as mean ± standard deviation (SD) (primary antibodies are listed in Supplementary Table 3).

Statistical analysis

All experiments were done in triplicates and replicated at least three times and all experimental data are presented as the means ± SD. The two-tailed Student t-tests were used for comparisons between two groups, and one-way or two-way analysis of variance (ANOVA) were used for multifactorial comparisons. Statistical analyses were performed with SPSS 20.0 software (SPSS Inc., Chicago, IL, USA) or GraphPad Prism 8.0 (GraphPad Software, La Jolla, CA, United States). A value of $P < 0.05$ was considered to indicate a statistically significant difference.

Results

Specifical expression profiles of circRNAs in pneumonia-induced sepsis

To determine circRNAs expression profiles and to identify those that are differentially expressed in pneumonia-induced sepsis, we selected healthy people and pneumonia patients without sepsis as controls and performed RNA-seq analysis of circRNA in the plasma of these three groups. In total, 32,229 circRNAs were expressed in the plasma samples among the healthy people, pneumonia patients without sepsis and pneumonia-induced sepsis patients (Supplementary Table 4). Using the cutoff values of fold change > 2.0 and $P < 0.05$, 382 circRNAs showed significantly differential expression between the pneumonia-induced sepsis patients and healthy people, including 233 circRNAs that were upregulated and 149 circRNAs that were downregulated (Supplementary Tables 5, 6) (Figures 1A, B, Supplementary Figure 1). Meanwhile, 172 differentially expressed circRNAs were detected between the pneumonia-induced sepsis patients and pneumonia patients without sepsis, in which 98 of them were upregulated and 74 were downregulated (Supplementary Tables 7, 8) (Figures 1A, B). Gene ontology (GO) and Kyoto Encyclopedia of Genes and Genomes (KEGG) analysis of differentially expressed circRNAs were showed in Supplementary Figure 2. GO enrichment analysis showed that the differentially expressed circRNAs were involved in the biological processes, such as cell energy metabolism and histone modification. On the other hand, KEGG analysis revealed that RNA transport and MAPK signaling pathway, which is associated with inflammatory activation of macrophages, was related to the differential expression of circRNAs. Of all the differential circRNAs, we chose markedly downregulated *circ_0075723* for next investigations because one of its most likely targeted gene, SHIP1(Src homology 2 domain–containing inositol-5-phosphatase 1), had been previously documented to be one of the negative regulators of TLR4 signaling which was involved in regulating NLRP3 inflammasome activation and pyroptosis (23, 24). Furthermore, we validated the expression of *circ_0075723* in $CD14^+$ monocytes by qRT-PCR among the three groups and found that *circ_0075723* was significantly downregulated in pneumonia-induced sepsis patients comparing to the other two groups (Figure 1C). Taken together, we screened multiple differently expressed circRNAs in pneumonia-induced sepsis compared to healthy people and pneumonia without sepsis by RNA-seq and validated the significant downregulation of *circ_0075723* in pneumonia-induced sepsis, the differential expression of circRNAs from sepsis suggest possible functions of circRNAs in pathogenesis of sepsis.

The characterization of the *circ_0075723*

Circ_0075723, located at chr6:17648038-17649531, which is derived from the human *NUP153* gene and generated by back-splicing mechanism (Figure 2A). The sequence was located at the back-splice junction location of *circ_0075723* according to Sanger sequencing (Figure 2B). Further, we treated THP-1 cells with RNase

10.3389/fimmu.2023.1095457

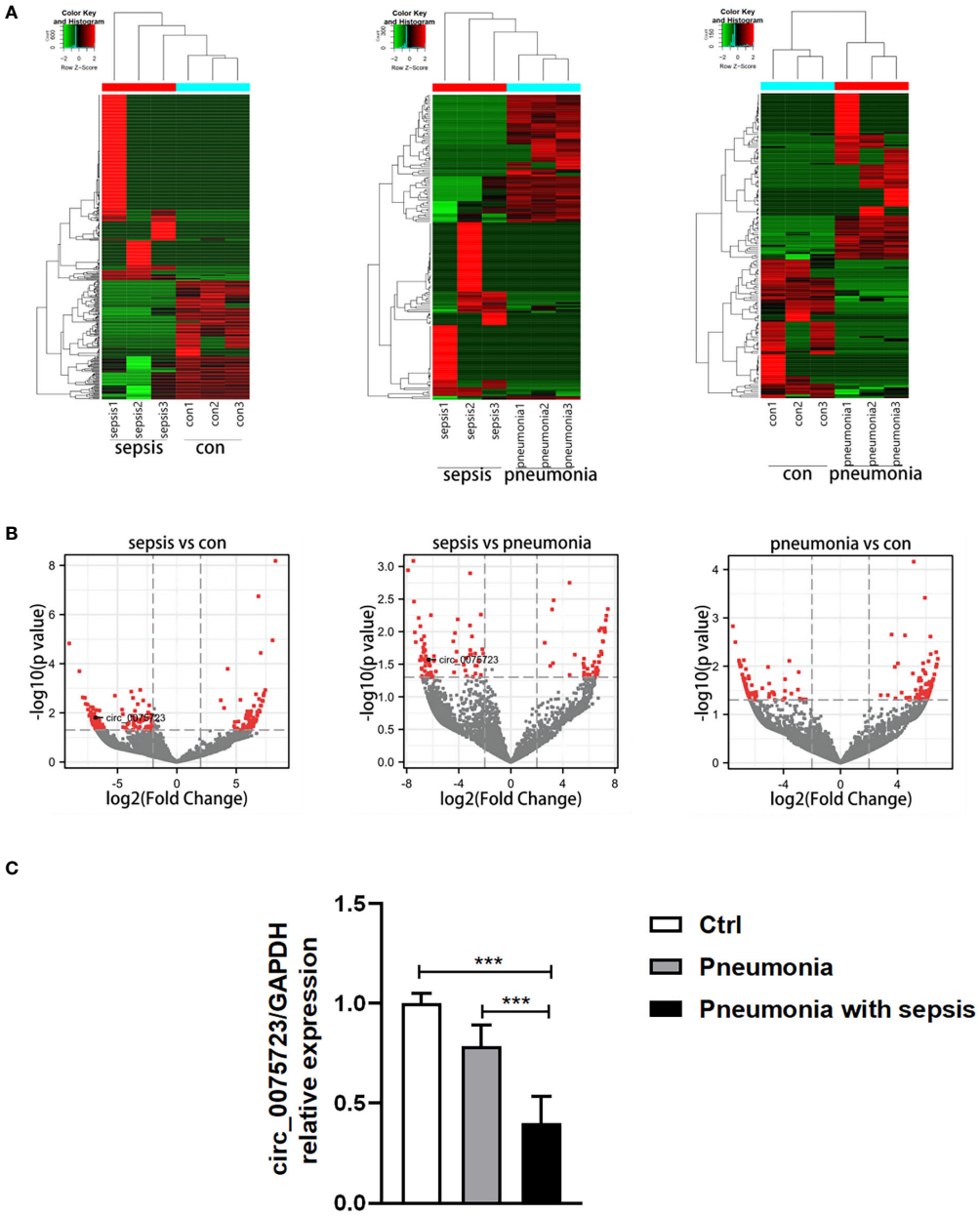

FIGURE 1
Specifical expression profiles of circRNAs in pneumonia-induced sepsis. **(A)** Hierarchical cluster analysis of differentially expressed circRNAs between the two compared groups of plasma. **(B)** Volcano plots showing the differentially expressed circRNAs among the three groups [Plot of circRNA expression log2-transformed fold-changes (x-axis) vs -log10 P-value (y-axis)]. The red dots represent the circRNAs having fold change > 2.0 and P < 0.05 between the two compared groups of plasma. **(C)** qRT-PCR analysis of circ_0075723 expression in CD14+ monocytes among the pneumonia-induced sepsis, pneumonia without sepsis and healthy control group. Each group has 4 samples. Data are presented as means ± SD; significant difference was identified with one-way ANOVA. ***p < 0.001 vs. Control or Pneumonia.

R exonuclease or actinomycin D to confirm *circ_0075723* authenticity and found that the expression of *circ_0075723* exhibited RNase R (Figure 2C) and actinomycin D resistance (Figure 2D), while that of *NUP153* mRNA was significantly decreased. This indicated *circ_0075723* was stable in THP-1 cells. We then investigated the sub-cellular location of *circ_0075723*. By RNA fluorescence *in situ* hybridization (FISH) assays, we found *circ_0075723* was mainly localized in the cytoplasm (Figure 2E). These studies indicated that *circ_0075723* as a circRNA, its biological stability may be advantageous to its function.

Pyroptosis is activated following pneumonia-induced sepsis and *Circ_0075723* inhibits pyroptosis of THP-1 *in vitro*

We then analyzed *circ_0075723* function in pneumonia-induced sepsis. Given that pyroptosis, a typical inflammatory cell death, is a major features/characteristics of sepsis (7, 9), we wondered whether *circ_0075723* was involved in the regulation of

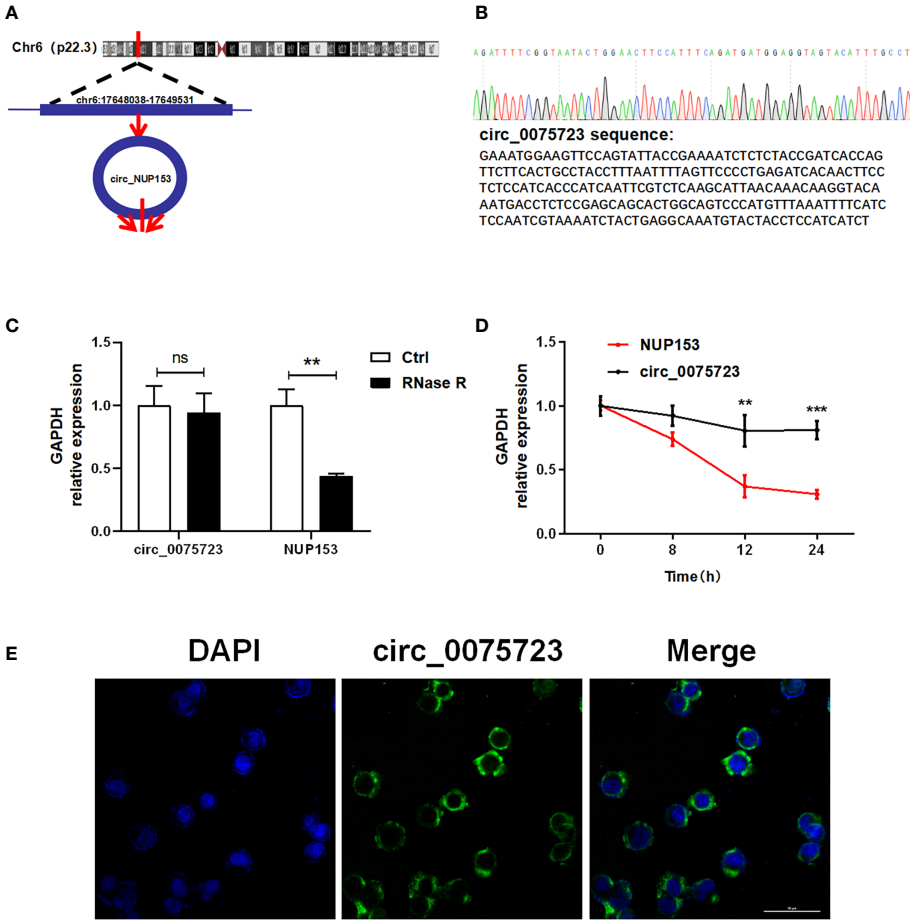

FIGURE 2
The characterization of the circ_0075723. **(A)** The location of circ_0075723 in genome. **(B)** Sanger sequencing showing the "head-to-tail" splicing of circ_0075723 in THP-1 cell. **(C)** qRT-PCR analysis of the expression of circ_0075723 and NUP153 in THP-1 cells after treatment with RNase R. Data are presented as means ± SD; significant difference was identified with two-way ANOVA. **p < 0.01; ns: no significant. **(D)** qRT-PCR analysis of the expression of circ_0075723 and NUP153 in THP-1 cells after treatment with actinomycin **(D)** Data are presented as means ± SD; significant difference was identified with Student *t*-tests. **p < 0.01, ***p < 0.001 **(E)** RNA FISH for circ_0075723. Nuclei were stained with DAPI.

macrophage pyroptosis. Firstly, we found that CD14+ monocytes from pneumonia-induced sepsis patients had considerably greater levels of the proteins TLR4, NLRP3, ASC1, cleaved caspase-1, IL-1, and GSDMD in contrast to pneumonia patients without sepsis and healthy people (Figure 3A, Supplementary Figure 3A). In addition, pneumonia-induced sepsis patients showed a markedly enhanced expression of IL-1β and IL-18 from plasma in comparison to pneumonia patients without sepsis and healthy people (Figure 3B). These results indicated that pyroptosis is activated in pneumonia-induced sepsis. Due to the markedly downregulated expression of *circ_0075723* in $CD14^+$ monocytes from pneumonia-induced sepsis patients, we next examined the specific role of *circ_0075723* in pyroptosis of pneumonia-induced sepsis. By usage of different doses of LPS together with nigericin to induce pyroptosis of THP1 *in vitro*, we found that LPS/nigericin treatment increased the production of proteins and cytokines associated with pyroptosis, including TLR4, NLRP3, ASC1, cleaved caspase-1, IL-1β and GSDMD, whereas downregulated the expression of *circ_0075723* in a manner dependent on dose (Figures 3C, D). To further examine the direct impacts of *circ_0075723* in macrophage pyroptosis, we transfected the *circ_0075723*-overexpressing vector (OE-*circ_0075723*) or *circ_0075723* silence vector (sh-*circ_0075723*) to overexpress or knockdown *circ_0075723* expression in LPS/nigericin-treated THP-1 cells (Figure 3E). Subsequently, we choose sh2-*circ_0075723* for further experiments due to the relatively lower expression of *circ_0075723* in transfected THP-1 cells than sh1-*circ_0075723* and sh3-*circ_0075723* (Supplementary Figure 3B). Overexpression of *circ_0075723* in THP-1 cells showed a strong inhibition of pyroptosis-related proteins and cytokines expression, while silencing of circ_0075723 exhibited the opposite effect (Figures 3F, G, Supplementary Figure 3C). In general, these studies indicate that macrophages pyroptosis is activated in pneumonia-induced sepsis patients and *circ_0075723* essentially prohibits macrophages pyroptosis *in vitro*.

Circ_0075723 functions as a sponge for miR-155-5p in THP-1

Based on bioinformatic predictions from the miRanda and TargetScan databases, miR-155-5p was predicted to bind with

10.3389/fimmu.2023.1095457

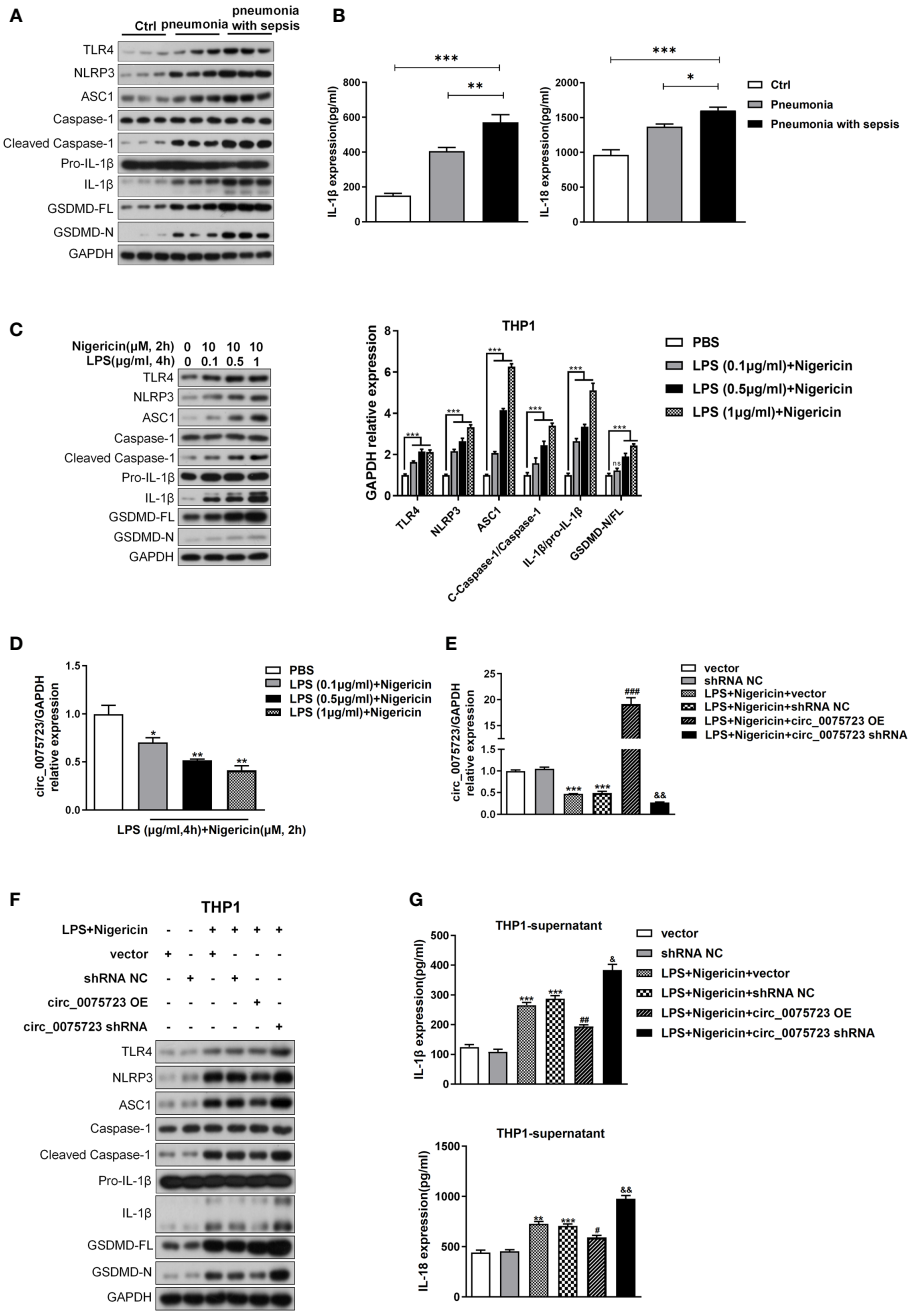

FIGURE 3
Pyroptosis is activated following pneumonia-induced sepsis and Circ_0075723 inhibits pyroptosis of THP-1 *in vitro*. **(A)** Western blot analysis of TLR4, NLRP3, ASC1, caspase1, cleaved caspase-1, Pro-IL1β, IL-1β, GSDMD and GAPDH in CD14+ monocytes from pneumonia-induced sepsis, pneumonia without sepsis and healthy people. **(B)** ELISA of IL-18 and IL-1β in the plasma from pneumonia-induced sepsis, pneumonia without sepsis and healthy people. Each group has 4 samples. Data are presented as means ± SD; significant difference was identified with one-way ANOVA. *p < 0.05 vs. Pneumonia; **p < 0.01 vs. Pneumonia; ***p < 0.001 vs. Control. **(C)** Western blot analysis of TLR4, NLRP3, ASC1, caspase1, cleaved caspase-1, Pro-IL1β, IL-1β, GSDMD and GAPDH in THP-1 cells primed with different doses of LPS (0.1, 0.5 and 1 μg/ml) for 4 h and stimulated with nigericin (10 μM) for 2h. Data are presented as means ± SD; significant difference was identified with two-way ANOVA. ***p < 0.001 vs. PBS; ns: no significant. **(D)** qRT-PCR analysis of the expression of circ_0075723 primed with different doses of LPS (0.1, 0.5 and 1 μg/ml) for 4 h and stimulated with nigericin (10 μM) for 2h in THP-1 cells. Data are presented as means ± SD; significant difference was identified with Student *t*-tests. *p < 0.05 vs. PBS; **p < 0.01 vs. PBS. THP-1 cells were transfected with vector or shRNA scrambled control (shRNA NC) or were transfected with circ_0075723-overexpressing lentivirus plasmids (OE-circ_0075723), sh-circ_0075723-expressing lentivirus plasmids (sh-circ_0075723), vector or shRNA scrambled control (shRNA NC) and then were primed with LPS (1 μg/ml) for 4 h and stimulated with nigericin (10 μM) for 2h. **(E)** qRT-PCR analysis of the expression of circ_0075723 in THP-1 cells. Data are presented as means ± SD; significant difference was identified with Student *t*-tests. ***p < 0.001 vs. vector or shRNA NC; ###p < 0.001 vs. LPS/nigericin + Vector; &&p < 0.01 vs. LPS/nigericin + shRNA NC. **(F)** Western blot analysis of TLR4, NLRP3, ASC1, caspase1, cleaved caspase-1, Pro-IL1β, IL-1β, GSDMD and GAPDH in THP-1 cells. **(G)** ELISA of IL-18 and IL-1β in THP-1 supernatant. Data are presented as means ± SD; significant difference was identified with Student *t*-tests. **p < 0.01 vs. vector; ***p < 0.001 vs. vector or shRNA NC; #p < 0.05 vs. LPS/nigericin + Vector; ##p < 0.01 vs. LPS/nigericin + Vector; &p < 0.05 vs. LPS/nigericin + shRNA NC; &&p < 0.01 vs. LPS/nigericin + shRNA NC.

10.3389/fimmu.2023.1095457

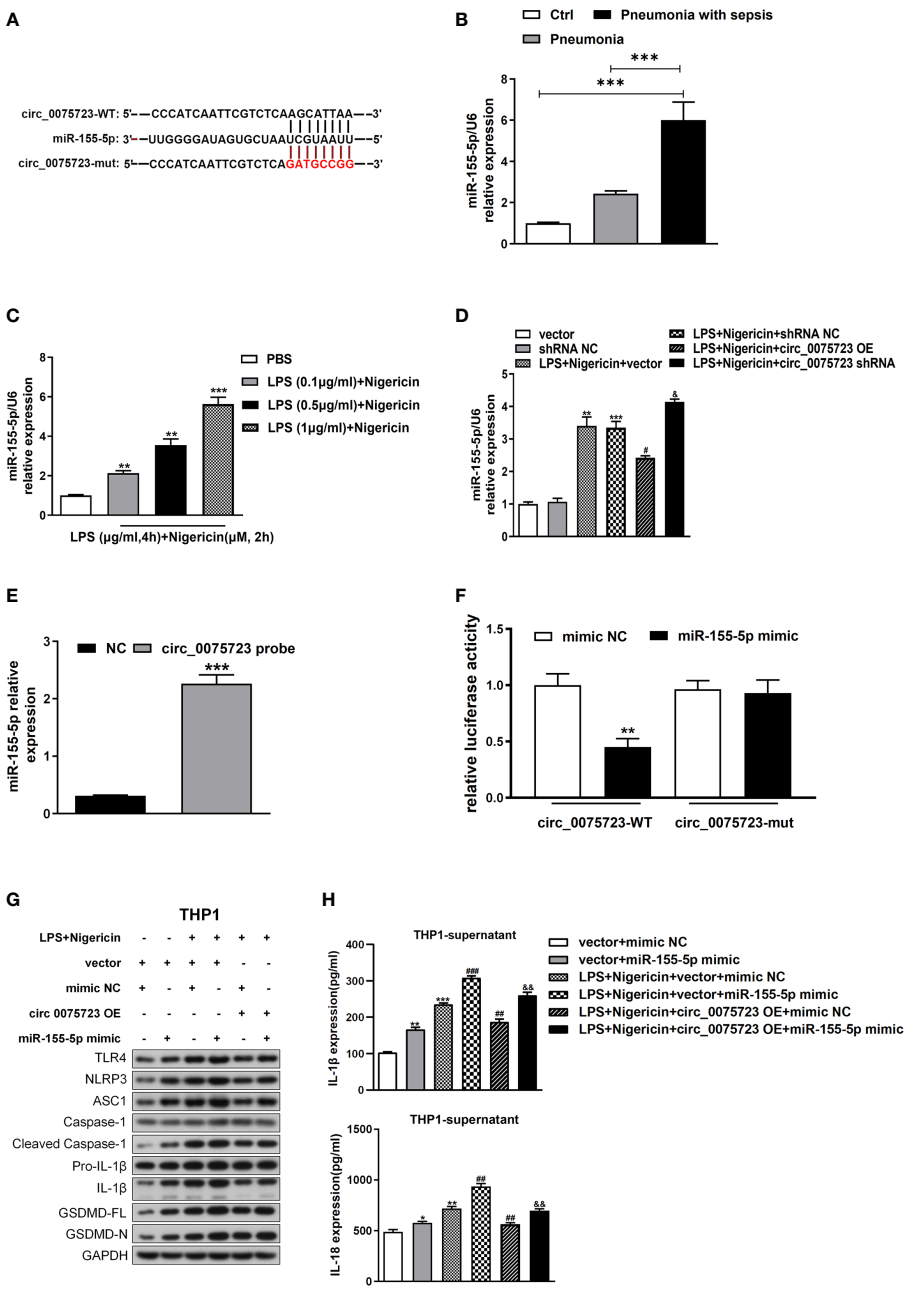

FIGURE 4
Circ_0075723 functions as a sponge for miR-155-5p in THP-1. **(A)** Schematic showing the predicted miR-155-5p sites in circ_0075723. **(B)** qRT-PCR analysis of the expression of miR-155-5p in CD14+ monocytes among the pneumonia-induced sepsis, pneumonia without sepsis and healthy control group. Each group has 4 samples. Data are presented as means ± SD; significant difference was identified with one-way ANOVA; ***P < 0.001 vs. Control or Pneumonia. **(C)** qRT-PCR analysis of the expression of miR-155-5p in THP-1 cells primed with different doses of LPS (0.1, 0.5 and 1 μg/ml) for 4 h and stimulated with nigericin (10 μM) for 2h. Data are presented as means ± SD; significant difference was identified with Student *t*-tests. **p < 0.01 vs. PBS; ***p < 0.001 vs. PBS. **(D)** THP-1 cells were transfected with vector or shRNA scrambled control (shRNA NC) or were transfected with circ_0075723-overexpressing lentivirus plasmids (OE-circ_0075723), sh-circ_0075723-expressing lentivirus plasmids (sh-circ_0075723), vector or shRNA scrambled control (shRNA NC) and then were primed with LPS (1 μg/ml) for 4 h and stimulated with nigericin (10 μM) for 2h. qRT-PCR analysis of the expression of miR-155-5p in THP-1 cells. Data are presented as means ± SD; significant difference was identified with Student *t*-tests. **p < 0.01 vs. vector; ***p < 0.001 vs. shRNA NC; #p < 0.05 vs. LPS/nigericin + Vector; &p < 0.05 vs. LPS/nigericin + shRNA NC. **(E)** RNA pull-down analysis of the interaction between miR-155-5p and circ_0075723. Data are presented as means ± SD; significant difference was identified with Student *t*-tests. ***p < 0.001 vs. NC group. **(F)** Dual-luciferase reporter assay was performed to validate the association between miR-155-5p and circ_0075723. Data are presented as means ± SD; significant difference was identified with one-way ANOVA. **p < 0.01 vs. mimic NC group. THP-1 cells were transfected with vector + mimic scrambled control (mimic NC) or vector + miR-155-5p mimic or were transfected with vector + mimic NC, vector + miR-155-5p mimic, mimic NC + circ_0075723 lentivirus plasmids (circ_0075723 OE), or miR-155-5p mimic + circ_0075723 OE and then were primed with LPS (1 μg/ml) for 4 h and stimulated with nigericin (10 μM) for 2h. **(G)** Western blot analysis of TLR4, NLRP3, ASC1, caspase1, cleaved caspase-1, Pro-IL1β, IL-1β, GSDMD and GAPDH in THP-1 cells. **(H)** ELISA of IL-18 and IL-1β in THP-1 supernatant. Data are presented as means ± SD; significant difference was identified with Student *t*-tests. *p < 0.05 vs. vector + mimic NC; **p < 0.01 vs. vector + mimic NC; ***p < 0.001 vs. vector + mimic NC; ##p < 0.01 vs. LPS/nigericin + vector + mimic NC; ###p < 0.001 vs. LPS/nigericin + vector + mimic NC; &&p < 0.01 vs. LPS/nigericin + circ_0075723-OE + mimic NC.

circ_0075723, and *circ_0075723*–miR-155-5p network was depicted in Figure 4A. Additionally, we found the miR-155-5p level were considerably higher in CD14+ monocytes of pneumonia-induced sepsis patients than that of pneumonia patients without sepsis and healthy people (Figure 4B). Intriguingly, miR-155-5p expression was dramatically increased in LPS/nigericin-treated THP-1 cells in dose-dependent manner (Figure 4C). Further, miR-155-5p expression was modulated *via circ_0075723* as miR-155-5p was downregulated by OE-*circ_0075723* and upregulated by *sh-circ_0075723* (Figure 4D). According to these results, we hypothesized that *circ_0075723* may modulate macrophages pyroptosis by sponging miR-155-5p. Therefore, we performed RNA pull-down assay to verify the specific connection between *circ_0075723* with miR-155-5p and found that miR-155-5p could directly interact with *circ_0075723* (Figure 4E). Besides, dual-luciferase reporter assay revealed that miR-155-5p mimics dramatically decreased the activity of the *circ_0075723* wild-type luciferase reporter but had no effect on the Mut luciferase reporter (Figure 4F). As we had observed that *circ_0075723* could inhibit macrophages pyroptosis, we further adopted the rescue trials to find that miR-155-5p mimics could partly reduce protective effect of *circ_0075723* on macrophages pyroptosis (Figures 4G, H, Supplementary Figure 4). Collectively, our findings indicated that *circ_0075723* acts as a "molecular sponge" for miR-155-5p.

Circ_0075723-miR-155-5p ceRNA modulates macrophage pyroptosis by directly regulating SHIP1

To further study the downstream mRNA targets of *circ_0075723*-miR-155-5p ceRNA network, bioinformatic analysis

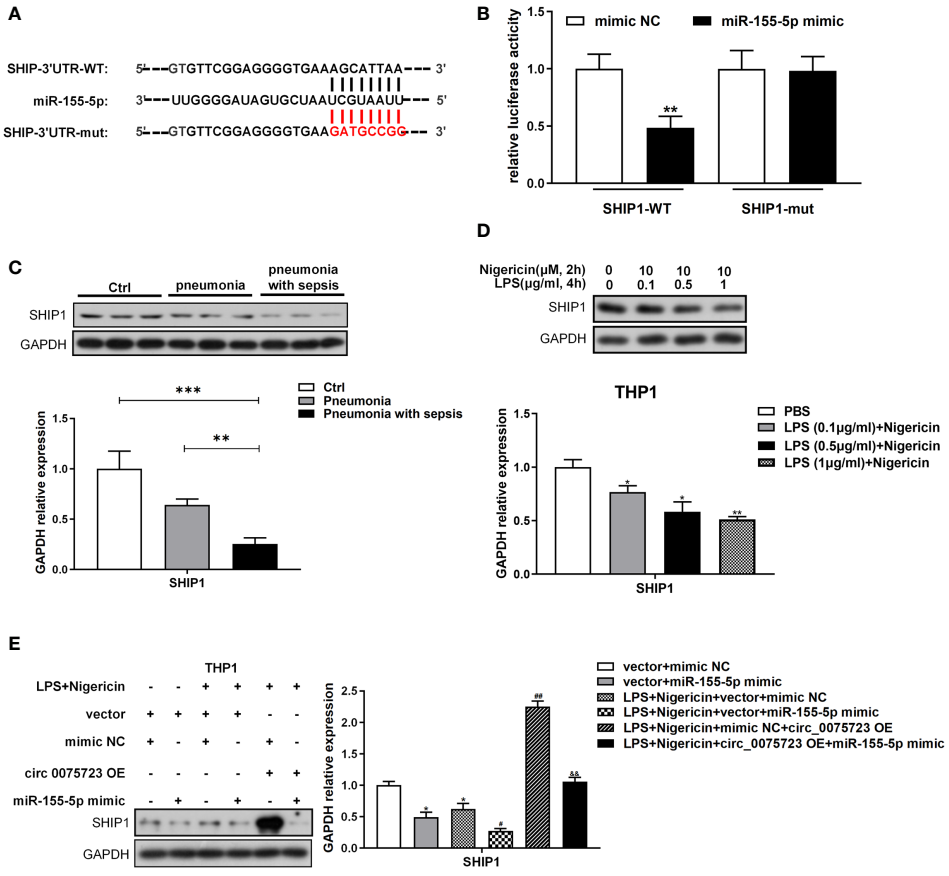

FIGURE 5
Circ_0075723-miR-155-5p ceRNA modulates macrophage pyroptosis by directly regulating SHIP1. **(A)** Schematic showing the predicted miR-155-5p sites in SHIP1. **(B)** Dual-luciferase reporter assay was performed to validate the association between miR-155-5p and SHIP1. Data are presented as means ± SD; significant difference was identified with one-way ANOVA. **p < 0.01 vs. mimic NC group. **(C)** Western blot analysis of SHIP1 and GAPDH in CD14+ monocytes from pneumonia-induced sepsis, pneumonia without sepsis and healthy control group. Each group has 4 samples. Data are presented as means ± SD; significant difference was identified with one-way ANOVA. **P < 0.01 vs. Pneumonia; ***P < 0.001 vs. Control. **(D)** Western blot analysis of SHIP1 and GAPDH in THP-1 cells primed with different doses of LPS (0.1, 0.5 and 1 μg/ml) for 4 h and stimulated with nigericin (10 μM) for 2h. Data are presented as means ± SD; significant difference was identified with Student *t*-tests. *p < 0.05 vs. PBS; **p < 0.01 vs. PBS. **(E)** THP-1 cells were transfected with vector + mimic scrambled control (mimic NC) or vector + miR-155-5p mimic or were transfected with vector + mimic NC, vector + miR-155-5p mimic, mimic NC + circ_0075723 lentivirus plasmids (circ_0075723 OE) or miR-155-5p mimic + circ_0075723 OE and then were primed with LPS (1 μg/ml) for 4 h and stimulated with nigericin (10 μM) for 2h. Western blot analysis of SHIP1 and GAPDH in THP-1 cells. Data are presented as means ± SD; significant difference was identified with Student *t*-tests. *p < 0.01 vs. vector + mimic NC; #p < 0.05 vs. LPS/nigericin + vector + mimic; ##p < 0.01 vs. LPS/nigericin + vector + mimic; &&p < 0.01 vs. LPS/nigericin + circ_0075723-OE + mimic NC.

of the TargetScan database revealed that miR-155-5p could target the 3′-untranslated region (UTR) of SHIP1 (Figure 5A). By dual-luciferase reporter assay, we showed that miR-155-5p mimics significantly inhibited the wild-type luciferase reporter activity of SHIP1 and validated the connection relationship between SHIP1 and miR-155-5p (Figure 5B). Therefore, SHIP1 might be the gene of interest for miR-155-5p. Additionally, SHIP1 expression was markedly diminished in $CD14^+$ monocytes of pneumonia-induced sepsis patients compared with that of pneumonia patients without sepsis and healthy people (Figure 5C). Corroborating with the clinical findings, vitro tests also confirmed that LPS/nigericin treatment suppressed SHIP1 expression in a dose-dependent way (Figure 5D). As it had reported that SHIP1 was involved in the interplay of miR-155 and TLR4 activation by acting as a key negative regulator of TLR4 signaling (23, 25, 26), while TLR4 signaling might activate NLRP3 inflammasome and promote alveolar macrophage pyroptosis (24). We hypothesized that *circ_0075723* might inhibit macrophages pyroptosis through promoting SHIP1 expression by sponging miR-155-5p. To investigate this assertion, we overexpressed miR-155-5p mimics in the LPS/nigericin activated THP-1 cells and found that SHIP1 expression was increased in the company of the *circ_0075723* overexpression, meanwhile miR-155-5p mimics could markedly decrease SHIP1 upregulation induced by the *circ_0075723* overexpression (Figure 5E). Besides, we further transfected SHIP1-overexpression lentivirus vector (OE-SHIP1) and (or) miR-155-5p mimics into the LPS/nigericin activated THP-1 cells, and found that the production of pyroptosis-related proteins and cytokines, such as TLR4, NLRP3, ASC1, cleaved caspase-1, GSDMD, IL-1β and IL-18, were decreased in OE-SHIP1 group, meanwhile miR-155-5p mimics could significantly reverse these effects of SHIP1-overexpression (Supplementary Figures 5A, B).

Overexpression of *Circ_0075723* in macrophages downregulates IL-1β and IL-18 expression and protects endothelial cell integrity

The pathological process of sepsis is complex, and the permeability change caused by vascular endothelial cell damage has a significant role in the pathophysiology of sepsis (27). We have shown that *circ_0075723* in macrophages could inhibit pyroptosis-related pro-inflammatory cytokines IL-1β and IL-18 expression by *circ_0075723*/miR-155-5p/SHIP1 axis, and previous studies had documented that NLRP3 inflammasome associated cytokines IL-1β and IL-18 could increase endothelial cells permeability through inhibiting VE-cadherin expression in endothelial cells (28, 29). We further evaluated whether *circ_0075723* in macrophages could modulate VE-cadherin expression in endothelial cells through inhibiting NLRP3 inflammasome associated cytokines IL-1β and IL-18 by *circ_0075723*/miR-155-5p/SHIP1 axis. To examine the proposition, we collected supernatant from aforementioned-LPS/nigericin activated THP-1 cells bearing altered expression of *circ_0075723*, miR-155-5p and SHIP1, and then used them to culture human lung microvascular endothelial cells (HLMVEC) *in vitro*. Firstly, Western blotting outcomes demonstrated that VE-cadherin expression in HLMVEC cells was downregulated culturing in supernatant harvested from LPS/nigericin-treated THP-1 cells in contrast to control and further dramatically downregulated in supernatant from sh-*circ_0075723*-transfected THP-1 cells, whereas transfected OE-*circ_0075723* THP-1 cells supernatant exhibit the opposite (Figure 6A). Besides, the expression trend of VE-cadherin in HLMVEC cells was contrary to the expression of IL-1β and IL-18 in above supernatant (Figure 3G). Furthermore, rescue tests showed that the effect of *circ_0075723* and SHIP1 on VE-cadherin expression in HLMVEC cells and IL-1β and IL-18 expression in the supernatant could be inhibited by miR-155-5p mimics (Figures 4H, 6B, C, Supplementary Figure 5B). Collectively, these results may indicate that Overexpression *circ_0075723* downregulates IL-1β and IL-18 expression, promotes VE-cadherin expression in endothelial cells and further protects endothelial cell integrity.

Discussion

Sepsis, especially caused by pneumonia, affects a great many patients all over the world, with high morbidity, mortality and economic expenses (30). Although comprehension of the pathogenesis has grown, and modern therapeutic technologies, such as the use of proper antibiotics, vigorous resuscitation and organ support have also made great progress, the high mortality rate caused by sepsis remains a significant issue (17, 31). Therefore, it is necessary to clarify the potential mechanism to find effective targets for the treatment of pneumonia-induced sepsis. In this investigation, RNA-seq was used to determine the expression profile of circRNAs in the plasma of pneumonia-induced sepsis patients. Through screening the differentially expressed cicRNAs, we identified that *circ_0075723* as a significantly downregulated circRNA in the serum and monocytes of pneumonia-induced sepsis patients as compared to healthy people and pneumonia patients without sepsis. Moreover, we found that *circ_0075723* protected against macrophage pyroptosis through targeting *circ_0075723*-miR-155-5p-SHIP1 axis. In addition, we found that *circ_0075723* suppressed macrophage pyroptosis-induced endothelial permeability by up-regulating VE-cadherin expression. In sum, we firstly determined the influence of *circ_0075723*/miR-155-5p/SHIP1 axis on macrophage pyroptosis, which represents a new mechanism for pneumonia associated sepsis progression. The newly identified *circ_0075723* may be a possible therapeutic target for pneumonia-induced sepsis.

It is generally recognized that sepsis pathophysiology is extremely complex, hence understanding the underlying molecular mechanisms in the occurrence and development of the disease is still a prerequisite to find effective biomarkers and specific treatments to improve survival rate (32). Through regulating the patients' immune system against different pathogens, circRNAs were revealed to be essential for the pathogenesis of sepsis and sepsis-induced organ dysfunction (33). However, to date, very little clinical research documented specifically expressed circRNAs in the peripheral blood of sepsis patients. Recent research showed the

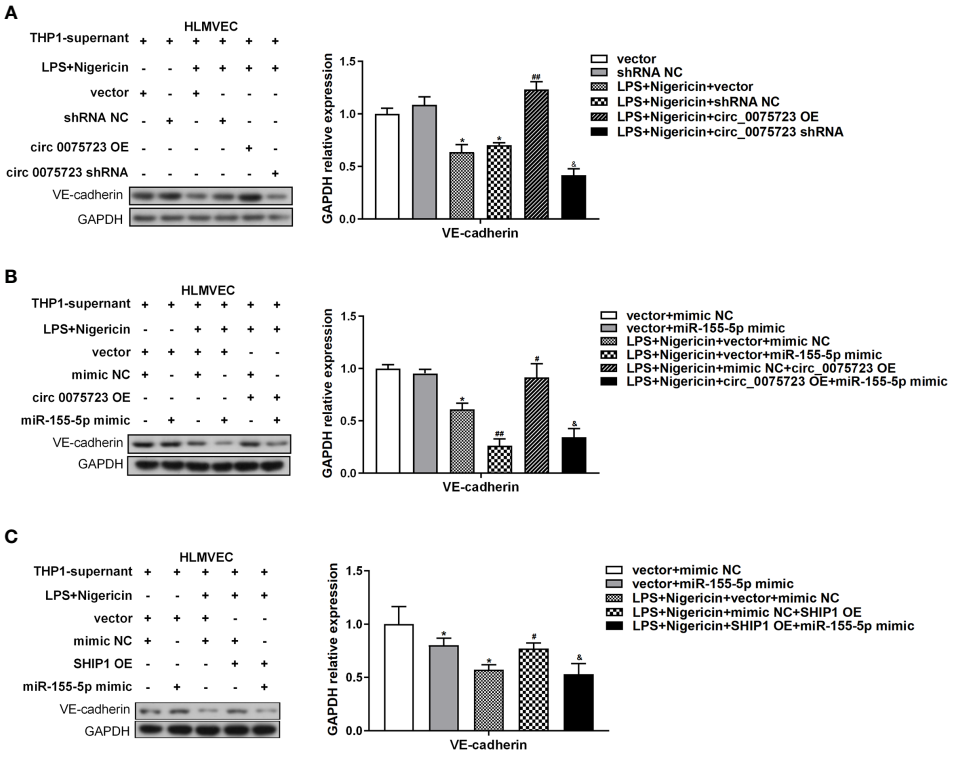

FIGURE 6
Circ_0075723 in macrophages regulate endothelial permeability through the inhibition expression of IL-1β and IL-18 by circ_0075723/miR-155-5p/SHIP1 axis. **(A)** Western blot analysis of VE-cadherin in HLMVEC cultured with the supernatant for 24 h. The supernatant was collected from aforementioned-LPS-primed THP-1 stimulated with nigericin bearing altered expression of circ_0075723. Data are presented as means ± SD; significant difference was identified with Student *t*-tests. *p < 0.05 vs. Vector or shRNA NC; ##p < 0.01 vs. LPS/nigericin + Vector; &p < 0.05 vs. LPS/nigericin + shRNA NC. **(B)** Western blot analysis of VE-cadherin in HLMVEC cultured with the supernatant for 24 h. The supernatant was collected from aforementioned-LPS-primed THP-1 stimulated with nigericin bearing altered expression of circ_007572 and miR-155-5p. Data are presented as means ± SD; significant difference was identified with Student *t*-tests. *p < 0.05 vs. vector + mimic NC; #p < 0.05 vs. LPS/nigericin + vector + mimic NC; ##p < 0.01 vs. LPS/nigericin + vector + mimic NC; &p < 0.05 vs. LPS/nigericin + mimic NC + circ_0075723-OE. **(C)** Western blot analysis of VE-cadherin in HLMVEC cultured with the supernatant for 24 h. The supernatant was collected from aforementioned-LPS-primed THP-1 stimulated with nigericin bearing altered expression of miR-155-5 and SHIP1. Data are presented as means ± SD; significant difference was identified with Student *t*-tests. *p < 0.05 vs. vector + mimic NC; #p < 0.05 vs. LPS/nigericin + vector + mimic NC; &p < 0.05 vs. LPS/nigericin +mimic NC + SHIP1-OE.

differential expression of circRNAs in lung tissues of patients with sepsis-induced ARDS (34). We also reported the expression of *circN4bp1* in the PBMCs being a diagnostic and predictive marker in ARDS post sepsis (14). In the clinical setting, pneumonia-induced sepsis is one of the most prevalent causes of sepsis and is associated with the greatest fatality rate (3, 4). Therefore, we set out to establish the expression profile of circRNAs using RNA-seq in the plasma of sepsis originated from pneumonia. We discovered that there were variations in plasma circRNA expressions from pneumonia-induced sepsis patients relative to pneumonia patients without sepsis and healthy people, which could contribute to the development and course of the disease. Furthermore, we identified that *circ_0075723* was significantly decreased in the plasma and $CD14^+$ monocytes of sepsis patients secondary to pneumonia.

Uncontrolled or excessive inflammation is a hallmark of sepsis. A increasing body of research has shown that pyroptosis, a distinct instance of proinflammatory programmed death, contributes to the excessive inflammatory responses of sepsis and sepsis-related organ damage (35). Therefore, targeting NLRP3 inflammasome activation and the subsequent pyroptosis would be a critical for the therapy of sepsis. Macrophages, as one of the most important cells of the innate immune system, play an important role in inflammatory and immune processes (6). $CD14^+$ monocytes are the major subpopulation of monocytes (36), and several clinical studies have shown that changes in the number and function of circulating CD14+ monocytes in patients with sepsis (37–39). However, there have been no reports of CD14+ monocytes pyroptosis in clinical patients with sepsis. Recently, LPS-triggered TLR4 signaling is involved in promoting pulmonary macrophage pyroptosis with activation of NLRP3 inflammasome and elevated expression of the pyroptosis-related proinflammatory cytokines IL-1β and IL-18 (24). Platelet endothelial cell adhesion molecule-1 has been shown to safeguard from sepsis-associated diffuse intravascular coagulation (DIC) through inhibiting macrophage pyroptosis (40). In additional, caspase-11-mediated inflammasome activation and macrophage pyroptosis were controlled by the cAMP metabolism, which attenuated excessive inflammatory responses in sepsis (41). Consistently, we did reveal the upregulation of TLR4,

activation of NLRP3 inflammasome, enhanced cleavage of GSDMD, IL-1β and IL-18, and increased release of IL-1β and IL-18 in serum and CD14+ monocytes of pneumonia-induced sepsis patients comparing to pneumonia individuals without sepsis and healthy controls, shedding light on the importance of macrophage pyroptosis in the clinical pathogenesis of sepsis.

Previous studies indicated that circRNAs potentially regulated the macrophage pyroptosis in other clinical conditions, such as ACS (16) and renal fibrosis (15). In our study, we also showed this function in pneumonia-induced sepsis. Since a main way by which circular RNAs exert their effects is by sponging miRNAs *via* ceRNA crosstalk (11), we identified possible miRNAs that interact with *circ_0075723* using bioinformatics. Our study discovered potential regulatory connections between miR-155-5p and SHIP1, as well as between *circ_0075723* and miR-155-5p. The dysregulation of all three genes in pneumonia-induced sepsis patients was confirmed in monocyte/macrophage THP-1 cells. It has been reported that serum exosome-derived miR-155 promoted macrophage proliferation and inflammation involved in sepsis-related acute lung injury (42) and SHIP1 regulated Phagocytosis and M2 Polarization in Pseudomonas aeruginosa Infection as a negative regulator of inflammatory responses (43). Previous studies also documented that SHIP1 is the major target of miR-155 in a wide range of inflammatory diseases (25, 26) and negatively regulates LPS-triggered TLR signaling (22). We discovered that miR-155-5p may bind to the 3′UTR of SHIP1 and suppress its expression, further upregulating the levels of TLR4, thereby activating macrophage pyroptosis as evidenced by the enhanced expression of NLRP3, caspase-1, ASC1, GSDMD and related cytokines as IL-1β and IL-18. In addition, we found that *circ_0075723* could increase SHIP1 expression in macrophage *in vitro*, whereas miR-155-5p mimics could partially counteract this impact. We also confirmed that *circ_0075723* could attenuate the macrophage inflammation and pyroptosis involved in blocking the formation and activation of NLRP3 inflammasome *in vitro*. Therefore, we have revealed a new mechanism of the NLRP3 inflammasome activation through the *circ_0075723*/miR-155-5/SHIP1 axis, which has vital clinical transformation prospects.

One hallmark of acute sepsis is microvessel dysfunction, in which increased endothelial permeability especially lung vascular permeability plays pivotal roles in pneumonia origin sepsis (27, 44). Endothelial permeability is controlled by VE-cadherin, a central component of endothelial adherens junctions (AJs) that modulate the integrity of endothelial junctions and lung fluid balance (45, 46). Previous research demonstrated that pyroptotic immune cells, such as macrophages, release IL-1β and IL-18, which alter vascular integrity and cause organ damage (24, 28). For example, over-released IL-18 caused diabetic retinopathy by increasing retinal vascular permeability (28), and IL-1β could destroy vascular integrity during sepsis-induced lung injury through suppressing VE-cadherin expression in lung endothelial cell (24). Consistent with these findings, we further discovered that *circ_0075723*-miR-155-5p-SHIP1 signaling suppressed IL-1β and IL-18, release from macrophages, which maintained endothelial barrier stability of vascular endothelial cells by repressing the VE-cadherin expression. Future investigations are required to delineate the consequences and the underlying mechanisms of macrophage pyroptosis in mediating endothelial cells permeability of sepsis *in vivo* and further experiments are needed to verify that *circ_0075723* suppressed macrophage pyroptosis in the sepsis mouse model. In summary, our research uncovers a new mechanism by which *circ_0075723* inhibits macrophage pyroptosis and inflammation *via* sponging miR-155-5p, thus enhancing SHIP1 expression. These findings imply that *circ_0075723* may represent a novel therapeutic target for treating pneumonia-induced sepsis.

Data availability statement

The data presented in the study are deposited in the GEO repository, accession number GSE218494.

Ethics statement

The studies involving human participants were reviewed and approved by the Research Ethics Board of East Hospital, Tongji University (Shanghai, China). The patients/participants provided their written informed consent to participate in this study.

Author contributions

DY, DZ, JJ, CW, NL, XB, XL, SJ, and QZ designed, carried out experiments, and performed the genetic analyses. DY, DZ, and JJ wrote the manuscript. LT guided and coordinated the work. All authors contributed to the article and approved the submitted version.

Funding

This work was supported by grants from the National Natural Science Foundation of China (81970072 to LT), the leading medical talent project of Shanghai Pudong heath bureau (PWRI2019-05 to LT), the action plan for scientific and technological innovation of Shanghai Scientific Committee of China (20Y11901200 to LT), the municipal Natural Science Foundation of Shanghai Scientific Committee of China (22ZR1451000 to LT), the clinical peak discipline of Shanghai Pudong heath bureau (PWYgf2021-03).

Acknowledgments

We are grateful to Prof. Kun Chen in the School of Life Sciences and Technology, Tongji University, Shanghai, China for revising the manuscript.

Conflict of interest

The authors declare that the research was conducted in the absence of any commercial or financial relationships that could be construed as a potential conflict of interest.

Publisher's note

All claims expressed in this article are solely those of the authors and do not necessarily represent those of their affiliated organizations, or those of the publisher, the editors and the reviewers. Any product that may be evaluated in this article, or claim that may be made by its manufacturer, is not guaranteed or endorsed by the publisher.

Supplementary material

The Supplementary Material for this article can be found online at: https://www.frontiersin.org/articles/10.3389/fimmu.2023.1095457/full#supplementary-material

References

1. Seymour CW, Liu VX, Iwashyna TJ, Brunkhorst FM, Rea TD, Scherag A, et al. Assessment of clinical criteria for sepsis: For the third international consensus definitions for sepsis and septic shock (Sepsis-3). *JAMA* (2016) 315(8):762–74. doi: 10.1001/jama.2016.0288

2. Chousterman BG, Swirski FK, Weber GF. Cytokine storm and sepsis disease pathogenesis. *Semin Immunopathol* (2017) 39(5):517–28. doi: 10.1007/s00281-017-0639-8

3. Abe T, Ogura H, Kushimoto S, Shiraishi A, Sugiyama T, Deshpande GA, et al. Variations in infection sites and mortality rates among patients in intensive care units with severe sepsis and septic shock in Japan. *J Intensive Care* (2019) 7:28. doi: 10.1186/s40560-019-0383-3

4. Jeganathan N, Yau S, Ahuja N, Otu D, Stein B, Fogg L, et al. The characteristics and impact of source of infection on sepsis-related icu outcomes. *J Crit Care* (2017) 41:170–6. doi: 10.1016/j.jcrc.2017.05.019

5. Fan EKY, Fan J. Regulation of alveolar macrophage death in acute lung inflammation. *Respir Res* (2018) 19(1):50. doi: 10.1186/s12931-018-0756-5

6. Qiu P, Liu Y, Zhang J. Review: The role and mechanisms of macrophage autophagy in sepsis. *Inflammation* (2019) 42(1):6–19. doi: 10.1007/s10753-018-0890-8

7. Shi J, Gao W, Shao F. Pyroptosis: Gasdermin-mediated programmed necrotic cell death. *Trends Biochem Sci* (2017) 42(4):245–54. doi: 10.1016/j.tibs.2016.10.004

8. Kim MJ, Bae SH, Ryu JC, Kwon Y, Oh JH, Kwon J, et al. Sesn2/Sestrin2 suppresses sepsis by inducing mitophagy and inhibiting Nlrp3 activation in macrophages. *Autophagy* (2016) 12(8):1272–91. doi: 10.1080/15548627.2016.1183081

9. Guo H, Callaway JB, Ting JP. Inflammasomes: Mechanism of action, role in disease, and therapeutics. *Nat Med* (2015) 21(7):677–87. doi: 10.1038/nm.3893

10. Kristensen LS, Andersen MS, Stagsted LVW, Ebbesen KK, Hansen TB, Kjems J. The biogenesis, biology and characterization of circular rnas. *Nat Rev Genet* (2019) 20 (11):675–91. doi: 10.1038/s41576-019-0158-7

11. Holdt LM, Kohlmaier A, Teupser D. Circular rnas as therapeutic agents and targets. *Front Physiol* (2018) 9:1262. doi: 10.3389/fphys.2018.01262

12. Zhang TN, Li D, Xia J, Wu QJ, Wen R, Yang N, et al. Non-coding rna: A potential biomarker and therapeutic target for sepsis. *Oncotarget* (2017) 8(53):91765–78. doi: 10.18632/oncotarget.21766

13. Bao X, Zhang Q, Liu N, Zhuang S, Li Z, Meng Q, et al. Characteristics of circular rna expression of pulmonary macrophages in mice with sepsis-induced acute lung injury. *J Cell Mol Med* (2019) 23(10):7111–5. doi: 10.1111/jcmm.14577

14. . Circn4bp1 facilitates sepsis-induced acute respiratory distress syndrome through mediating macrophage polarization *Via* the mir-138-5p/Ezh2 axis. *Mediat Inflammation* (2021) 2021:7858746. doi: 10.1155/2021/7858746

15. Fu H, Gu YH, Tan J, Yang YN, Wang GH. Circactr2 in macrophages promotes renal fibrosis by activating macrophage inflammation and epithelial-mesenchymal transition of renal tubular epithelial cells. *Cell Mol Life Sci* (2022) 79(5):253. doi: 10.1007/s00018-022-04247-9

16. Guo M, Yan R, Ji QW, Yao HM, Sun M, Duan LQ, et al. Ifn regulatory factor-1 induced macrophage pyroptosis by modulating M6a modification of Circ_0029589 in patients with acute coronary syndrome. *Int Immunopharmacol* (2020) 86:106800. doi: 10.1016/j.intimp.2020.106800

17. Rhodes A, Evans LE, Alhazzani W, Levy MM, Antonelli M, Ferrer R, et al. Surviving sepsis campaign: International guidelines for management of sepsis and septic shock: 2016. *Intens Care Med* (2017) 43(3):304–77. doi: 10.1007/s00134-017-4683-6

18. Niederman MS, Mandell LA, Anzueto A, Bass JB, Broughton WA, Campbell GD, et al. Guidelines for the management of adults with community-acquired pneumonia - diagnosis, assessment of severity, antimicrobial therapy, and prevention. *Am J Resp Crit Care* (2001) 163(7):1730–54. doi: 10.1164/ajrccm.163.7.at1010

19. Zhang Q, Sun H, Zhuang S, Liu N, Bao X, Liu X, et al. Novel pharmacological inhibition of Ezh2 attenuates septic shock by altering innate inflammatory responses to sepsis. *Int Immunopharmacol* (2019) 76:105899. doi: 10.1016/j.intimp.2019.105899

20. Xu H, Wang C, Song H, Xu Y, Ji G. Rna-seq profiling of circular rnas in human colorectal cancer liver metastasis and the potential biomarkers. *Mol Cancer* (2019) 18 (1):8. doi: 10.1186/s12943-018-0932-8

21. Yang JH, Cheng M, Gu BJ, Wang JH, Yan SS, Xu DH. Circrna_09505 aggravates inflammation and joint damage in collagen-induced arthritis mice *Via* mir-6089/Akt1/Nf-Kappa b axis. *Cell Death Dis* (2020) 11(10):833. doi: 10.1038/s41419-020-03038-z

22. Bao X, Liu X, Liu N, Zhuang S, Yang Q, Ren H, et al. Inhibition of Ezh2 prevents acute respiratory distress syndrome (Ards)-associated pulmonary fibrosis by regulating the macrophage polarization phenotype. *Respir Res* (2021) 22(1):194. doi: 10.1186/s12931-021-01785-x

23. Guo J, Liao MF, Wang J. Tlr4 signaling in the development of colitis-associated cancer and its possible interplay with microrna-155. *Cell Commun Signal* (2021) 19 (1):90. doi: 10.1186/s12964-021-00771-6

24. He X, Qian Y, Li Z, Fan EK, Li Y, Wu L, et al. Tlr4-upregulated il-1beta and il-1ri promote alveolar macrophage pyroptosis and lung inflammation through an autocrine mechanism. *Sci Rep* (2016) 6:31663. doi: 10.1038/srep31663

25. Li BS, Guo LY, He Y, Tu XR, Zhong JL, Guan HB, et al. Microrna-155 expression is associated with pulpitis progression by targeting Ship1. *Mol Biol Rep* (2022) 49 (9):8575–86. doi: 10.1007/s11033-022-07690-w

26. Xue H, Hua LM, Guo M, Luo JM. Ship1 is targeted by mir-155 in acute myeloid leukemia. *Oncol Rep* (2014) 32(5):2253–9. doi: 10.3892/or.2014.3435

27. Li Z, Yin M, Zhang H, Ni W, Pierce RW, Zhou HJ, et al. Bmx represses thrombin-Par1-Mediated endothelial permeability and vascular leakage during early sepsis. *Circ Res* (2020) 126(4):471–85. doi: 10.1161/CIRCRESAHA.119.315769

28. Chen W, Zhao M, Zhao S, Lu Q, Ni L, Zou C, et al. Activation of the Txnip/Nlrp3 inflammasome pathway contributes to inflammation in diabetic retinopathy: A novel inhibitory effect of minocycline. *Inflammation Res* (2017) 66(2):157–66. doi: 10.1007/s00011-016-1002-6

29. Xiong S, Hong Z, Huang LS, Tsukasaki Y, Nepal S, Di A, et al. Il-1beta suppression of ve-cadherin transcription underlies sepsis-induced inflammatory lung injury. *J Clin Invest* (2020) 130(7):3684–98. doi: 10.1172/JCI136908

30. Reinhart K, Daniels R, Kissoon N, Machado FR, Schachter RD, Finfer S. Recognizing sepsis as a global health priority - a who resolution. *New Engl J Med* (2017) 377(5):414–7. doi: 10.1056/NEJMp1707170

31. Seymour CW, Gesten F, Prescott HC, Friedrich ME, Iwashyna TJ, Phillips GS, et al. Time to treatment and mortality during mandated emergency care for sepsis. *New Engl J Med* (2017) 376(23):2235–44. doi: 10.1056/NEJMoa1703058

32. Huang M, Cai S, Su J. The pathogenesis of sepsis and potential therapeutic targets. *Int J Mol Sci* (2019) 20(21):5376. doi: 10.3390/ijms20215376

33. Ghafouri-Fard S, Khoshbakht T, Hussen BM, Taheri M, Arefian N. Regulatory role of non-coding rnas on immune responses during sepsis. *Front Immunol* (2021) 12:798713. doi: 10.3389/fimmu.2021.798713

34. Guo W, Wang Z, Wang S, Liao X, Qin T. Transcriptome sequencing reveals differential expression of circrnas in sepsis induced acute respiratory distress syndrome. *Life Sci* (2021) 278:119566. doi: 10.1016/j.lfs.2021.119566

35. Zheng X, Chen W, Gong F, Chen Y, Chen E. The role and mechanism of pyroptosis and potential therapeutic targets in sepsis: A review. *Front Immunol* (2021) 12:711939. doi: 10.3389/fimmu.2021.711939

36. Liepelt A, Hohlstein P, Gussen H, Xue J, Aschenbrenner AC, Ulas T, et al. Differential gene expression in circulating Cd14(+) monocytes indicates the prognosis of critically ill patients with sepsis. *J Clin Med* (2020) 9(1):127. doi: 10.3390/jcm9010127

37. Flores-Mejia LA, Cabrera-Rivera GL, Ferat-Osorio E, Mancilla-Herrera I, Torres-Rosas R, Bosco-Garate IB, et al. Function is dissociated from activation-related immunophenotype on phagocytes from patients with Sirs/Sepsis syndrome. *Shock* (2019) 52(5):e68–75. doi: 10.1097/SHK.0000000000001314

38. Daix T, Guerin E, Tavernier E, Mercier E, Gissot V, Herault O, et al. Multicentric standardized flow cytometry routine assessment of patients with sepsis to predict clinical worsening. *Chest* (2018) 154(3):617–27. doi: 10.1016/j.chest.2018.03.058

39. Winkler MS, Rissiek A, Priefler M, Schwedhelm E, Robbe L, Bauer A, et al. Human leucocyte antigen (Hla-Dr) gene expression is reduced in sepsis and correlates with impaired tnf alpha response: A diagnostic tool for immunosuppression? *PLos One* (2017) 12(8):e0182427. doi: 10.1371/journal.pone.0182427

40. Luo L, Xu M, Liao D, Deng J, Mei H, Hu Y. Pecam-1 protects against dic by dampening inflammatory responses *Via* inhibiting macrophage pyroptosis and restoring vascular barrier integrity. *Transl Res* (2020) 222:1–16. doi: 10.1016/j.trsl.2020.04.005

41. Chen R, Zeng L, Zhu S, Liu J, Zeh HJ, Kroemer G, et al. Camp metabolism controls caspase-11 inflammasome activation and pyroptosis in sepsis. *Sci Adv* (2019) 5 (5):eaav5562. doi: 10.1126/sciadv.aav5562

42. Jiang KF, Yang J, Guo S, Zhao G, Wu HC, Deng GZ. Peripheral circulating exosome-mediated delivery of mir-155 as a novel mechanism for acute lung inflammation. *Mol Ther* (2019) 27(10):1758–71. doi: 10.1016/j.ymthe.2019.07.003

43. Qin SG, Li JX, Zhou CM, Privratsky B, Schettler J, Deng X, et al. Ship-1 regulates phagocytosis and M2 polarization through the Pi3k/Akt-Stat5-Trib1 circuit in pseudomonas aeruginosa infection. *Front Immunol* (2020) 11:307. doi: 10.3389/fimmu.2020.00307

44. Schouten M, Wiersinga WJ, Levi M, van der Poll T. Inflammation, endothelium, and coagulation in sepsis. *J Leukoc Biol* (2008) 83(3):536–45. doi: 10.1189/jlb.0607373

45. Komarova YA, Kruse K, Mehta D, Malik AB. Protein interactions at endothelial junctions and signaling mechanisms regulating endothelial permeability. *Circ Res* (2017) 120(1):179–206. doi: 10.1161/Circresaha.116.306534

46. Wettschureck N, Strilic B, Offermanns S. Passing the vascular barrier: Endothelial signaling processes controlling extravasation. *Physiol Rev* (2019) 99 (3):1467–525. doi: 10.1152/physrev.00037.2018

frontiers | Frontiers in Immunology

TYPE Perspective
PUBLISHED 20 March 2023
DOI 10.3389/fimmu.2023.1072732

OPEN ACCESS

EDITED BY
Yufeng Zhou,
Fudan University, China

REVIEWED BY
Yaprak Ozakman,
Memorial Sloan Kettering Cancer Center, United States
Jing Xing,
Lingang Laboratory, China

*CORRESPONDENCE
Mathieu Garand
mathieu.garand@gmail.com
Narisara Chantratita
narisara@tropmedres.ac

SPECIALTY SECTION
This article was submitted to Inflammation, a section of the journal Frontiers in Immunology

RECEIVED 17 October 2022
ACCEPTED 01 March 2023
PUBLISHED 20 March 2023

CITATION
Preechanukul A, Yimthin T, Tandhavanant S, Brummaier T, Chomkatekaew C, Das S, Syed Ahamed Kabeer B, Toufiq M, Rinchai D, West TE, Chaussabel D, Chantratita N and Garand M (2023) Abundance of *ACVR1B* transcript is elevated during septic conditions: Perspectives obtained from a hands-on reductionist investigation. *Front. Immunol.* 14:1072732. doi: 10.3389/fimmu.2023.1072732

Abundance of *ACVR1B* transcript is elevated during septic conditions: Perspectives obtained from a hands-on reductionist investigation

Anucha Preechanukul[1], Thatcha Yimthin[1], Sarunporn Tandhavanant[1], Tobias Brummaier[2,3], Chalita Chomkatekaew[4], Sukanta Das[4,5], Basirudeen Syed Ahamed Kabeer[6], Mohammed Toufiq[6], Darawan Rinchai[6], T. Eoin West[1,7,8], Damien Chaussabel[6], Narisara Chantratita[1,4]* and Mathieu Garand[6,9]*

[1]Department of Microbiology and Immunology, Faculty of Tropical Medicine, Mahidol University, Bangkok, Thailand, [2]Swiss Tropical and Public Health Institute, Basel, Switzerland, [3]University of Basel, Basel, Switzerland, [4]Mahidol-Oxford Tropical Medicine Research Unit (MORU), Faculty of Tropical Medicine, Mahidol University, Bangkok, Thailand, [5]Department of Molecular Tropical Medicine and Genetics, Faculty of Tropical Medicine, Mahidol University, Bangkok, Thailand, [6]Systems Biology and Immunology Department, Sidra Medicine, Doha, Qatar, [7]Division of Pulmonary, Critical Care and Sleep Medicine, Department of Medicine, University of Washington, Seattle, WA, United States, [8]Department of Global Health, University of Washington, Seattle, WA, United States, [9]Division of Pediatric Cardiothoracic Surgery, Department of Surgery, Washington University School of Medicine, St. Louis, MI, United States

Sepsis is a complex heterogeneous condition, and the current lack of effective risk and outcome predictors hinders the improvement of its management. Using a reductionist approach leveraging publicly available transcriptomic data, we describe a knowledge gap for the role of ACVR1B (activin A receptor type 1B) in sepsis. ACVR1B, a member of the transforming growth factor-beta (TGF-beta) superfamily, was selected based on the following: 1) induction upon *in vitro* exposure of neutrophils from healthy subjects with the serum of septic patients (GSE49755), and 2) absence or minimal overlap between ACVR1B, sepsis, inflammation, or neutrophil in published literature. Moreover, *ACVR1B* expression is upregulated in septic melioidosis, a widespread cause of fatal sepsis in the tropics. Key biological concepts extracted from a series of PubMed queries established indirect links between ACVR1B and "cancer", "TGF-beta superfamily", "cell proliferation", "inhibitors of activin", and "apoptosis". We confirmed our observations by measuring ACVR1B transcript abundance in buffy coat samples obtained from healthy individuals (n=3) exposed to septic plasma (n = 26 melioidosis sepsis cases) *ex vivo*. Based on our re-investigation of publicly available transcriptomic data and newly generated *ex vivo* data, we provide perspective on the role of ACVR1B during sepsis. Additional experiments for addressing this knowledge gap are discussed.

KEYWORDS

activin A, sepsis, melioidosis, innate immunity, blood transcriptomics

Introduction

Sepsis is a heterogeneous syndrome that arises from a dysregulated host inflammatory response to an infection (1–3). The response is accompanied by activation of vascular endothelial cells, neutrophils and platelets which together can contribute to collateral tissue damage in the vasculature. Inflammation worsen with the influx of neutrophils to the site of infection. Subsequent clearance of infected neutrophils are part of the way to the resolution of inflammation (4, 5). Clinical biomarkers of sepsis have been assessed (reviewed in (6)). Some, like C-reactive protein and procalcitonin, are routinely used in clinical practice but have significant limitations. The lack of clinical biomarkers for risk and outcome prediction hinders the improvement of sepsis management. As early detection and treatment of sepsis are key to favorable outcomes, predictive markers (e.g., gene expression signatures) are needed (7).

In tropical countries, melioidosis is a common cause of community-acquired infection and associated with high mortality. Melioidosis is caused by the environmental bacterium, *Burkholderia pseudomallei* via ingestion, inhalation or inoculation. The global incidence of melioidosis is estimated to be 165,000 cases with a mortality rate of approximately 89,000 cases per year (8). To improve the outcome of melioidosis patients, there is a need to understand the immunopathogenesis of severe sepsis from melioidosis.

The ACVR1B gene (*ACVR1B*) encodes the activin A receptor type 1B. Activins are a pluripotent growth and differentiation factors, believed to be involved in numerous processes such as male germ cell development (9), follicle development (10), stem cell differentiation (11) as well as immune response (12). Activin isoforms are dimeric protein complexes and belong to the transforming growth factor-beta (TGF-beta) superfamily (13). Activin A is released rapidly into the circulation during inflammation and has been shown to modulate the inflammatory response by alteration of cytokine secretion, induction of nitric oxide production, and regulation of immune cell activity (14). Activin signaling pathways involve activins binding to a heteromeric complex of receptors that consist of at least two type I and two type II receptors. Both types of receptors possess serine-threonine kinase activity and regulation of gene expression is signaled via SMAD proteins. The ACVR1B gene encodes a type I receptor which is essential for activin signaling. Mutations in this gene are associated with cancer (15), cell proliferation (16).

High-throughput profiling technologies have revolutionized biomedical research by enabling assessment of physiological as well as pathological states of biological systems at an unprecedented depth. Moreover, an increasing amount of research data is available in public repositories (e.g., NCBI Gene Expression Omnibus [GEO]). These vast data collections have been postulated to serve as valuable training materials for the next generation of biomedical data scientists (17). Here, we report the upregulation of the ACVR1B gene during sepsis in human melioidosis and discuss additional possible avenues to investigate its putative role in the pathogenesis of sepsis. We acknowledge that the definition of sepsis may vary in each study and that it is challenging to properly summarize all interpretations. Also, the pathophysiology of sepsis is known to differ between age groups, e.g., neonates vs. adults. In this study, we were interested in the host response to severe infection across lifespan, experimental settings, and cell types, therefore, we use the word sepsis or septic as a broad term to encompass this syndrome which is often appreciated as a continuum of clinical presentation.

Materials and methods

In silico reductionist approach

Public repositories of articles and data, such as PubMed and GEO, constitute a vast resource but they can be difficult to explore. Here we present a logical reductionist approach to investigate putative novel biomarkers for sepsis.

The steps consist of 1) identifying a gene of interest based on its differential expression in the pathological/physiological context of interest, 2) confirming the reproducibility of the initial observation, 3) determining the current body of literature linking the gene and topic, 4) extracting the known biological concepts concerning the gene, and 5) inferring putative novel roles for the gene with literature support.

All datasets were obtained from GEO and used to confirm the initial findings in relevant clinical settings/samples. Datasets were selected without prior knowledge of ACVR1B expression levels and consisted only of human studies in which transcriptome profiles were generated in septic patients and compared to uninfected controls (Table 1). The task of identifying datasets was facilitated by using an interactive database recently created by our group and called SysInflam HuDB (sepsis.gxbsidra.org/dm3/geneBrowser/filteredSampleSets) (18). Other relevant information was retrieved from each GEO entry, such as: the geographic localization of the patient population, and the type of biological samples.

Ethical approval

The work involving human subjects was approved by the ethical committee of Faculty of Tropical Medicine, Mahidol University (approval no. MUTM 2015-002-04, MUTM 2018-046-01 and MUTM 2018-039-02), Udon Thani Hospital (approval no.6/2561), Nakhon Phanom Hospital (approval no. IEC-NKP1-No.15/2558), Roi Et Hospital (approval no. 166/2559), Buriram Hospital (approval no. BR 0032, 102.3/57), and Surin Hospital (approval no. 21/2560). This study was conducted in accordance with the principles of the Declaration of Helsinki (2008) and the International Council for Harmonization and Good Clinical Practice guidelines. Written informed consent/assent form was obtained from all participants or their legal guardians.

10.3389/fimmu.2023.1072732

TABLE 1 Demographic characteristics of 26 patients with melioidosis.

Patient characteristics	
Median age in years (IQR)	58 (39-80)
Male (%)	20 (76.9)
Comorbidity (may be represented multiple times)	
Diabetes (%)	13 (50.0)
Hypertension (%)	12 (46.2)
None (%)	12 (46.2)
Clinical conditions	
Bacteremia (%) Pneumonia (%)	20 (76.9) 6 (23.1)
Fever	
< 15 days (%) ≥ 15 days (%) None (%	16 (61.5) 2 (7.7) 8 (30.8)
Clinical outcome	
Died within 28 days	13 (50.0)

Sample collection

Plasma was collected from 26 patients diagnosed with melioidosis and 9 healthy subjects. Participants were recruited at five hospitals in northeastern of Thailand (endemic region for melioidosis): Udon Thani Hospital, Nakhon Phanom Hospital, Roi Et Hospital, Buriram Hospital, and Surin Hospial. This study was part of a multi-center study of patients aged ≥15 years who were culture positive for *B. pseudomallei* from any clinical samples and admitted to the hospitals between January 2015 and December 2019. The inclusion and exclusion criteria were described previously by Kaewarpai et al. (19). Plasma was collected at the time of enrolment (within 24 hours of reporting of the culture results). Patients' characteristics and clinical information was obtained from the medical records. Ten milliliters blood were collected from 3 healthy donors aged more than 18 years old at the Faculty of Tropical Medicine, Mahidol University, Bangkok and immediately used for cell stimulation.

Buffy coat isolation and plasma stimulation

Buffy coat from EDTA whole blood of three healthy individuals was isolated by centrifugation at 1500 x g for 15 min. Fresh buffy coat was diluted three-fold with RPMI 1640 medium (Gibco, Invitrogen, CA, USA) supplemented with 10% fetal bovine serum (FBS, Himedia, Mumbai, India), 100 U/ml penicillin (Gibco), 100 µg/ml streptomycin (Gibco), and 2 mM GLutaMAX (Gibco) and added to 96-well plates (Costar Corporation, Cambridge, MA, USA) in duplicate wells at $2x10^5$ cells in 150 µl per well. The cells were stimulated with 50 µl of plasma from melioidosis patients (n = 26), healthy donors from an endemic area (n = 9) and autologous donors (n = 3 replicates). Stimulated buffy coat was incubated at 37°C in a 5% CO_2 atmosphere incubator for 4 h.

RNA extraction

Total RNA was extracted from buffy coat of healthy donors following stimulation using the TRIzol® reagent (Thermo Fisher Scientific, Darmstadt, Germany) according to manufacturer's instruction. The RNA was re-purified using the RNeasy Mini Kit and treated with DNase according to the manufacturer's instruction (Qiagen, Valencia, USA). RNA quantity was measured using a nanodrop spectrophotometer (Thermo Fisher Scientific).

Quantitative reverse-transcriptase PCR

cDNA was generated by the iScript cDNA Synthesis Kit (Bio-Rad Laboratories, Hercules, USA). Transcription level of *ACVR1B* was analyzed using real-time PCR with iTaq Universal SYBR Green (Bio-Rad). The primers for *ACVR1B* were: *ACVR1B*, forward 5′ CAGCAGAACCTTGGCGGTTTA 3′, reverse 5′ GTTGGCAG ATCCCAGAGGCTAC 3′ (15) and for a housekeeping gene *HuP0* were forward 5′ GCTTCCTGGAGGGTGTCC 3′, reverse 5′ GGACTCGTTTGTACCCGTTG 3 ′ (20). The PCR reaction was conducted in the CFX96™ Real-Time system (Bio-Rad) as follows: 1 cycle of 95°C for 30s followed by 50 cycles of 95°C for 10s and 60°C for 30s. After amplification, melting curve analysis was carried out from 65°C to 95°C. The fold change of *ACVR1B* expression was calculated by $2^{(-\Delta\Delta Ct)}$, normalized with ΔCt = mean Ct of *ACVR1B* – mean Ct of *HuP0* derived from the same cDNA sample.

Statistical analysis

The average *ACVR1B* expression was calculated from source data for case (i.e., sepsis) and control groups in each dataset. To compare case to control groups, linear fold-changes (FC) were calculated for each dataset by dividing the average expression of the cases by the average expression of the control groups. An F-test of equality of variances was used to determine whether a homoscedastic or heteroscedastic t-test was adequate to compare population means. To assess statistically significant difference in gene expression, a t-test was applied to compute a p-value. The Mann-Whitney and Kruskal-Wallis tests were used to compare differences between *ACVR1B* expression of 3 healthy donors-derived buffy coat, which was exposed to septic plasma. A of $P < 0.05$ was considered statistically significant.

Results

In silico reductionist approach identified *ACVR1B* as differentially expressed during sepsis

The *ACVR1B* gene was identified from data we previously generated (GSE49755) (21). An increase in ACRV1B transcript abundance was observed upon the exposure of neutrophils from healthy donors to plasma of septic patients. Briefly in this study, polymorphonuclear neutrophils (PMNs) were obtained from two healthy donors, isolated, and incubated for 6 hours with the plasma from 12 patients with confirmed melioid sepsis and 12 uninfected controls, respectively. PMN transcriptional profiles were generated using Illumina Bead arrays. As shown in Figure 1A, *ACVR1B* gene expression levels and variance between exposure to plasma from the control and septic groups were significantly different (Figure 1B; Additional File 1).

The current body of literature on the overlap of ACVR1B on one hand and sepsis, inflammation, or neutrophil on the other hand was assessed. Literature was retrieved using a PubMed query which comprised the official gene symbol, name and known aliases for ACVR1B, with the search restricted to the title and abstract: ACVR1B[tw] OR ACTRIB[tw] OR ALK4[tw] OR SKR2[tw] OR Actr-IB[tw] OR ALK-4[tw]. As of August of 2022, this query returned 510 results. In a Boolean search, no overlap was found between the ACVR1B literature and the search term "sepsis". Extending the search to the literature on inflammation and neutrophil returned 13 and 2 articles, respectively. Supplementary Figure 1 summarizes the number of articles returned in the respective searches.

The increase in *ACVR1B* transcript abundance in the context of sepsis was validated in independent datasets

Datasets relevant to septic conditions (clinically or experimentally) were retrieved from GEO, made available on Gene Expression Browser (GXB) GXB, and used for independent validation of our initial finding. The characteristic of the datasets retrieved are shown in Figure 2 and Supplementary Table 1. These datasets encompassed gene expression profiling of *in-vivo, ex-vivo* and *in-vitro* experiments, and were all derived from human samples. Various inflammatory conditions, including cell exposure to bacterial products, were evaluated in case-control designs. Strong evidence ($p < 0.05$) for an increased *ACVR1B* expression in sepsis was found in 6 out of 11 datasets. The other five datasets had a p-value between 0.1 and 0.05. Four of those datasets were from experiments performed *in-vitro*. These four *in vitro* experiments all have smaller sample size (ranging from 3 to 17) when compared to the *in-vivo* experiments (ranging from 13 to 127). Te magnitude of *ACVR1B* expression was associated with the experimental conditions, such as the cell types used and whether plasma of septic patients or synthetic bacterial components (e.g., bacterial lipopolysaccharide) was used.

Regulation of cell survival and proliferation indirectly links ACVR1B with sepsis

As a first step to bridging the gap between the postulated upregulation of ACVR1B in sepsis and the rational for this observation, another systematic literature search was conducted in PubMed. The following query, restricted to title-words and excluding

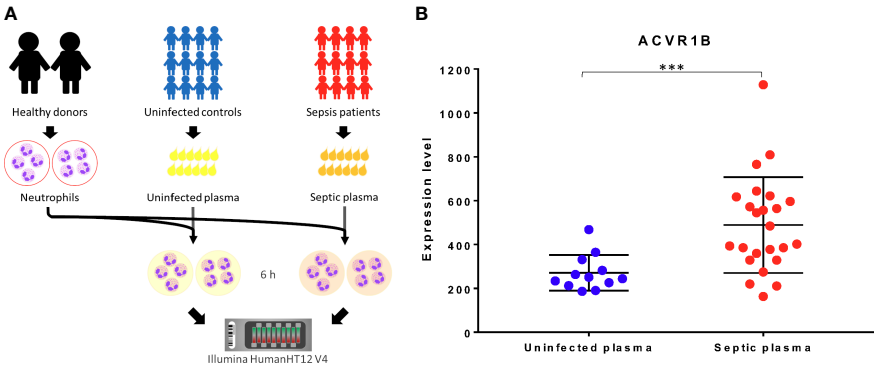

FIGURE 1
Primary observation: upregulation of ACVR1B in neutrophils in response to septic plasma. **(A)** The study design of dataset. The study was conducted in adult patients with sepsis in Khon Kaen province, northeast of Thailand. Polymorphonuclear cells (PMN) were isolated from two healthy donors. Each isolation of PMN was exposed to 20% of heparinized plasma samples which were collected from uninfected patients (n = 12) and patients with culture-confirmed sepsis (n = 12) for 6 h. The cultures in the presence of medium alone or lipopolysaccharide were used as controls (not shown). The RNA expression profile was determined using Illumina HumanHT12 V4.0 BeadChips. The dataset was deposited in the NCBI GEO public repository (GSE49755) **(B)** *ACVR1B* expression in neutrophils after exposure to uninfected plasma and septic plasma for 6 h was shown in the graph. The y-axis denotes the quantile normalized intensity values of the probes. The error bar demonstrated the mean ± standard deviation. Significant differences were determined by using the following statistical tests: T-test and F-test which results in $p<0.005$ (***) and $p<0.001$, respectively.

the term "homeobox" to avoid irrelevant gene target (ALK4 can also referred to Aristaless-like homeobox 4), was executed: ACVR1B[ti] OR ACTRIB[ti] OR ALK4[ti] OR ALK-4[ti] NOT ("genes, homeobox"[MeSH Terms] OR ("genes"[All Fields] AND "homeobox"[All Fields]) OR "homeobox genes"[All Fields] OR "homeobox"[All Fields]) AND "humans"[MeSH Terms].

We obtained 33 articles and scanned the titles to extract key biological processes/terms and fit them into 5 biologically relevant categories: biological process, biomolecules, pathway, disease, and cell type. A word-cloud summary of the words contained in the titles is shown Supplementary Figure 1B. Next, literature searches were performed on the intersection between ACVR1B and each of these key biological processes/terms. To maximize the output, the search queries regarding ACVR1B, and its synonyms were extended to text words ([tw]) as follows: ACVR1B[tw] OR ACTRIB[tw] OR ALK4[tw] OR SKR2[tw] OR Actr-IB[tw] OR ALK-4[tw]. A summary of the categories and concepts is shown in Supplementary Figure 1C.

Ex vivo validation of *ACVR1B* gene expression in buffy coat exposed to septic plasma

To test the findings of our in silico exploration, we measured *ACVR1B* transcript abundance in the buffy coat from healthy individuals that has been incubated with septic plasma. Septic plasma obtained from melioidosis patients were used for *ex vivo* validation. The clinical characteristics of melioidosis patients are shown in Table 1. Buffy coats were isolated from three healthy donors and stimulated for 4 hours with plasma from melioidosis patients (n=26) and healthy controls from endemic areas (n=9), and autologous plasma (n=3). *ACVR1B* expression was measured by RT-qPCR. Abundance of *ACVR1B* transcripts was significantly higher in cells from two healthy donors (HC-01 and HC-02) stimulated with plasma of melioidosis patients compared with plasma of healthy donors ($p < 0.01$) (Figure 3).

ACVR1B gene expression in buffy coat exposed to plasma and characteristics of melioidosis patients

As melioidosis is associated with many underlying diseases, the patients' preexisting conditions/status and potential consequences (i.e., bacteremia, pneumonia) of an infection with *B. pseudomallei* were examined as factors of *ACVR1B* gene expression in buffy coat after exposure to plasma of melioidosis patients. Blood cells of 3 healthy donors were incubated with plasma from patients with melioidosis. *ACVR1B* expression was significantly different between survivors and non-survivors (p<0.05), but no differences were found between male and female, diabetes and non-diabetes, bacteraemia

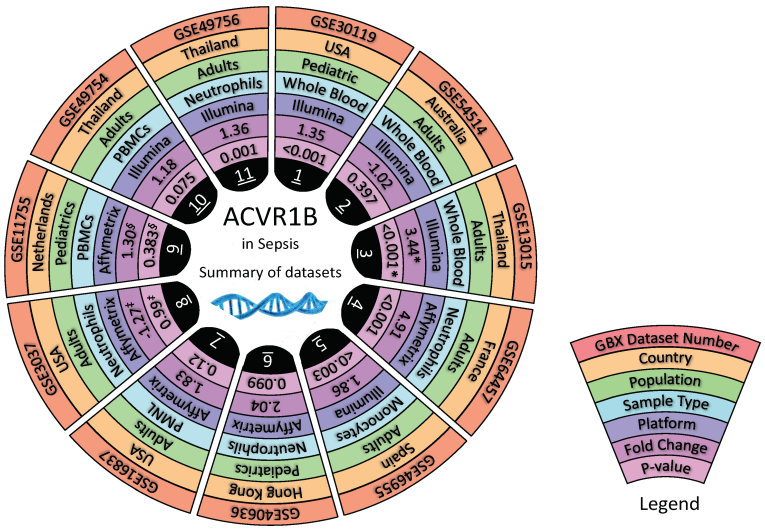

FIGURE 2
In silico validation of *ACVR1B* gene expression in sepsis. Characteristics of 11 datasets are shown in a concentric circle chart with each segment representing one dataset. From the outside to the inside, the following information is depicted: Gene Expression Omnibus (GEO) identification number, country in which samples were acquired, study population, sample type, and analysis platform. The inner 2 circles represent the fold-change (FC) and the p-value for comparing samples from septic patients to healthy controls. Average *ACVR1B* expression was calculated from source data for sepsis and control groups in each dataset and used to calculate FC. * Dataset contains gene expression data of healthy individuals as well as patients with sepsis caused by (*B*) *pseudomallei* and sepsis caused by other pathogens. Two comparisons were performed for this dataset. However, FC and p-value are only shown for patients with sepsis caused by (*B*) *pseudomallei* and compared to healthy controls. ‡ In this study, gene expression from neutrophils harvested from patients with sepsis-induced acute lung injury and stimulated with *High Mobility Group Box Protein 1* (HMGB1) as well as lipopolysaccharides were compared to neutrophils from healthy controls stimulated in the same manner. Fc and p-value are only shown for neutrophil stimulation with lipopolysaccharides at 1 hour after incubation. § In this dataset gene expression of monocytes and lymphocytes were compared between healthy controls and patients with meningococcal meningitis 24 hours after admission to the pediatric intensive care unit. Fc and p-value are only shown for *AVCR1B* expression in monocytes.

10.3389/fimmu.2023.1072732

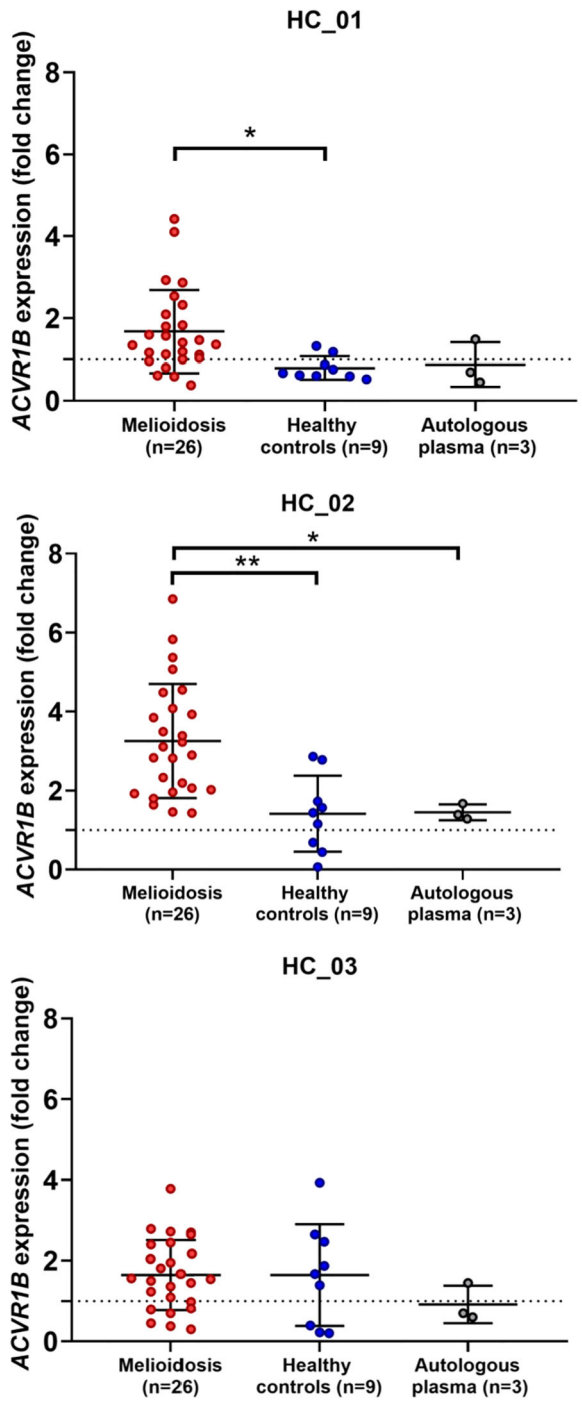

FIGURE 3
Ex vivo validation of *ACVR1B* upregulation in buffy coat in response to plasma from septic melioidosis patients. Buffy coat was isolated from heparinized whole blood of three healthy individuals (HC_01, HC_02 and HC_03). Each isolation of buffy coat was exposed to 25% plasma obtained from melioidosis patients (n = 26), healthy control in endemic area (n = 9) and autologous plasma (n = 3, i.e., replicates). *ACVR1B* gene expression of stimulated buffy coat were determined by RT-qPCR. Fold change in ACVR1B gene expression represent the response to exposure to melioidosis, healthy control, and autologous plasma. Scatter plots of *ACVR1B* expression show fold changes of buffy coat exposed to different plasma samples. Shown are the medians with interquartile ranges and each dot represents data obtained from one individual sample. A Kruskal-Wallis test was performed for comparison and two-tailed *P* values were calculated. Comparision with statistically significant differences are indicated (*p <0.05; **p <0.01).

and non-bacteremia, hypertension and non-hypertension, pneumonia, and non-pneumonia (Supplementary Figure 2).

Discussion

High-throughput profiling technologies have changed our understanding of biological systems. More and more data are shared in public repositories, paving new avenues for exploration of these datasets from various angles. Following this approach, we described how we identified and validated the changes in *ACVR1B* gene expression in septic melioidosis *in silico* and *ex vivo*.

We provided evidence that the ACVR1B gene is upregulated during sepsis, a finding that is substantiated by its known physiological role (e.g., in cell proliferation and apoptosis). To our knowledge there is no previous assessment of ACVR1B in melioidosis. Although induction of *ACVR1B* transcription was observed in several cohort studies assessing adult and pediatric sepsis, additional experimental data are necessary to confirm the role of ACVR1B in sepsis. Validation of our preliminary findings could be achieved by an *in vitro* culture system by exposing neutrophils to septic plasma from patients as it was done in the initial study described in Figure 1. Furthermore, changes in *ACVR1B* gene expression can be confirmed through qPCR in healthy whole blood, leukocytes and neutrophils (negative selection purification) upon exposure to septic plasma. Knowing that not all mRNA transcripts are translated and resulting in protein formation, a next step would be to verify whether an increase in abundance observed at the transcript level translates in increase in protein abundance.

We observed variable responses from HC-03 to septic plasma which suggest other physiological factors influenced the host production of *ACVR1B*. Our healthy donors satisfied the inclusion/exclusion criteria (Supplementary Table 2) and had similar age. There is no evidence that would lead us to think that sex and blood type can affect *ACVR1B* expression in response to septic plasma. Of note, however, single nucleotide polymorphisms (SNP) in the ACVR1B gene have been associated with increased risk of lung cancer from tobacco smoke exposure (22). Another more recent study found possible implication for ACVR1B gene SNPs in chronic obstructive pulmonary disease (23). Based on these observations linking ACVR1B and inflammatory conditions, we speculate that *ACVR1B* polymorphisms may be one of the factors influencing gene expression in the HC-03 individual. While we didn't look at gene polymorphisms of the healthy donors in this study, the subject will remain a point of interest for future work.

Additional inferences can be made by exploring the literature on ACVR1B. For example, during the latency period in human cytomegalovirus infections, miR-UL148D is one of the most expressed micro-RNAs (miRNA) in myeloid cells and directly targets ACVR1B (16). This result could suggest that ACVR1B is the target of an immune evasion strategy employed by the virus. It could be of interest to measure the co-expression of miRNAs during sepsis and assess if, in particular, miR-UL148D correlates with *ACVR1B* gene expression and the severity of symptoms. Interestingly, another miRNA, miR-199a-5p, has been shown to inhibit monocyte/macrophage differentiation by targeting ACVR1B (24); additional

downstream experiments could aim to associate miR-199-5p expression with the immune responses from monocyte/macrophages. Finally, other mechanisms for the increased expression of *ACVR1B* may involve the regulation of apoptosis in leukocytes. Apoptosis in immune cells, such as neutrophils, can help eliminate infected cells, thus reducing the pathogen burden.

Data availability statement

The raw data supporting the conclusions of this article will be made available by the authors, without undue reservation.

Ethics statement

The studies involving human participants were reviewed and approved by Faculty of Tropical Medicine, Mahidol University, Udon Thani Hospital, Nakhon Phanom Hospital, Roi Et Hospital, Buriram Hospital, and Surin Hospital. The patients/participants provided their written informed consent to participate in this study.

Author contributions

Conceptualization: MG, NC, DR, DC. Data curation and validation: MG, AP, TY, NC, TB, CC, ST, SD. Visualization: MG, TB, CC, ST, SD, NC, TEW Analysis and interpretation: MG, AP, TY, TB, CC, ST, SD, NC. Writing of the first draft: MG, AP, TY, TB, CC, ST, SD. Funding acquisition: DC, TEW, and NC. Methodology development: MG, DC, DR, AP, TY, NC. Project administration: MG, NC and DC. Software development: MT. Writing – review & editing MG, NC, TEW, AP, TY, TB, CC, ST, SD, DR, BS, MT, DC. The contributor's roles listed above follow the Contributor Roles Taxonomy (CRediT) managed by The Consortia Advancing Standards in Research Administration Information (CASRAI) (https://casrai.org/credit/). All authors contributed to the article and approved the submitted version.

Funding

This research project was supported by Mahidol University (Basic Research Fund: fiscal year 2021), Grant No. BRF2-NDFR06/2564 and supported in part via a grant from the Qatar National Research Fund: QNRF NPRP10-0205-170348. NC and TEW were supported by the National Institute of Allergy and Infectious Diseases (NIH/NIAID) (https://www.niaid.nih.gov) under award number U01AI115520. AP was supported by the Royal Golden Jubilee PhD scholarship (PHD/0069/2561) from the Thailand Research Fund (TRF), and the National Research Council of Thailand (NRCT). This research was funded in part, by the Wellcome Trust [220211]. For the purpose of Open Access, the author has applied a CC BY public copyright licence to any Author Accepted Manuscript version arising from this submission.

Acknowledgments

MG expresses special thanks to Dr. Susie S.Y. Huang (Sidra Medicine) for reviewing and editing of the manuscript. Sidra Medicine is a member of the Qatar Foundation for Education, Science and Community Development. We thank staff from Faculty of Tropical Medicine, Mahidol University, Udon Thani Hospital, Nakhon Phanom Hospital, Roi Et Hospital, Buriram Hospital, Surin Hospital.

Conflict of interest

The authors declare that the research was conducted in the absence of any commercial or financial relationships that could be construed as a potential conflict of interest.

Publisher's note

Supplementary material

The Supplementary Material for this article can be found online at: https://www.frontiersin.org/articles/10.3389/fimmu.2023.1072732/full#supplementary-material

References

1. van der Poll T, van de Veerdonk FL, Scicluna BP, Netea MG. The immunopathology of sepsis and potential therapeutic targets. *Nat Rev Immunol* (2017) 17(7):407–20. doi: 10.1038/nri.2017.36

2. Rubio I, Osuchowski MF, Shankar-Hari M, Skirecki T, Winkler MS, Lachmann G, et al. Current gaps in sepsis immunology: New opportunities for translational research. *Lancet Infect Dis* (2019) 19(12):e422–36. doi: 10.1016/S1473-3099(19)30567-5

3. Oikonomakou M Z, Gkentzi D, Gogos C, Akinosoglou K. Biomarkers in pediatric sepsis: A review of recent literature. *biomark Med* (2020) 14(10):895–917. doi: 10.2217/bmm-2020-0016

4. Greenlee-Wacker MC. Clearance of apoptotic neutrophils and resolution of inflammation. *Immunol Rev* (2016) 273(1):357–70. doi: 10.1111/imr.12453

5. Rosales C. Neutrophil: A cell with many roles in inflammation or several cell types? *Front Physiol* (2018) 9:113. doi: 10.3389/fphys.2018.00113

6. Pierrakos C, Vincent JL. Sepsis biomarkers: A review. *Crit Care* (2010) 14(1):R15. doi: 10.1186/cc8872

7. Lukaszewski RA, Yates AM, Jackson MC, Swingler K, Scherer JM, Simpson AJ, et al. Presymptomatic prediction of sepsis in intensive care unit patients. *Clin Vaccine Immunol* (2008) 15(7):1089–94. doi: 10.1128/CVI.00486-07

8. Limmathurotsakul D, Golding N, Dance DAB, Messina JP, Pigott DM, Moyes CL, et al. Predicted global distribution of burkholderia pseudomallei and burden of melioidosis. *Nat Microbiol* (2016) 1:15008. doi: 10.1038/nmicrobiol.2015.8

9. Miles DC, Wakeling SI, Stringer JM, van den Bergen JA, Wilhelm D, Sinclair AH, et al. Signaling through the TGF beta-activin receptors ALK4/5/7 regulates testis formation and male germ cell development. *PloS One* (2013) 8(1):e54606. doi: 10.1371/journal.pone.0054606

10. Li R, Phillips DM, Mather JP. Activin promotes ovarian follicle development *in vitro*. *Endocrinology* (1995) 136(3):849–56. doi: 10.1210/endo.136.3.7867593

11. Sulzbacher S, Schroeder IS, Truong TT, Wobus AM. Activin a-induced differentiation of embryonic stem cells into endoderm and pancreatic progenitors-the influence of differentiation factors and culture conditions. *Stem Cell Rev* (2009) 5 (2):159–73. doi: 10.1007/s12015-009-9061-5

12. Qi Y, Ge J, Ma C, Wu N, Cui X, Liu Z. Activin a regulates activation of mouse neutrophils by Smad3 signalling. *Open Biol* (2017) 7(5):1–10. doi: 10.1098/rsob.160342

13. Xia Y, Schneyer AL. The biology of activin: Recent advances in structure, regulation and function. *J Endocrinol* (2009) 202(1):1–12. doi: 10.1677/JOE-08-0549

14. Phillips DJ, de Kretser DM, Hedger MP. Activin and related proteins in inflammation: not just interested bystanders. *Cytokine Growth Factor Rev* (2009) 20 (2):153–64. doi: 10.1016/j.cytogfr.2009.02.007

15. Togashi Y, Sakamoto H, Hayashi H, Terashima M, de Velasco MA, Fujita Y, et al. Homozygous deletion of the activin a receptor, type IB gene is associated with an aggressive cancer phenotype in pancreatic cancer. *Mol Cancer* (2014) 13:126. doi: 10.1186/1476-4598-13-126

16. Lau B, Poole E, Krishna B, Sellart I, Wills MR, Murphy E, et al. The expression of human cytomegalovirus MicroRNA MiR-UL148D during latent infection in primary myeloid cells inhibits activin a-triggered secretion of IL-6. *Sci Rep* (2016) 05:6:31205. doi: 10.1038/srep31205

17. Chaussabel D, Rinchai D. Using "collective omics data" for biomedical research training. *Immunology.* (2018) 155(1):18–23. doi: 10.1111/imm.12944

18. Toufiq M, Huang SSY, Boughorbel S, Alfaki M, Rinchai D, Saraiva LR, et al. SysInflam HuDB, a Web Resource for Mining Human Blood Cells Transcriptomic Data Associated with Systemic Inflammatory Responses to Sepsis. *J Immunol.* (2021) 207(9):2195–202.

19. Kaewarpai T, Ekchariyawat P, Phunpang R, Wright SW, Dulsuk A, Moonmueangsan B, et al. Longitudinal profiling of plasma cytokines in melioidosis and their association with mortality: A prospective cohort study. *Clin Microbiol Infect* (2020) 26(6):783.e1–8. doi: 10.1016/j.cmi.2019.10.032

20. Cliff JM, Cho JE, Lee JS, Ronacher K, King EC, van Helden P, et al. Excessive cytolytic responses predict tuberculosis relapse after apparently successful treatment. *J Infect Dis* (2016) 213(3):485–95. doi: 10.1093/infdis/jiv447

21. Khaenam P, Rinchai D, Altman MC, Chiche L, Buddhisa S, Kewcharoenwong C, et al. A transcriptomic reporter assay employing neutrophils to measure immunogenic activity of septic patients' plasma. *J Transl Med* (2014) 12:65. doi: 10.1186/1479-5876-12-65

22. Spitz MR, Gorlov IP, Amos CI, Dong Q, Chen W, Etzel CJ, et al. Variants in inflammation genes are implicated in risk of lung cancer in never smokers exposed to second-hand smoke. *Cancer Discovery* (2011) 1(5):420–9. doi: 10.1158/2159-8290.CD-11-0080

23. Morrow JD, Cho MH, Platig J, Zhou X, DeMeo DL, Qiu W, et al. Ensemble genomic analysis in human lung tissue identifies novel genes for chronic obstructive pulmonary disease. *Hum Genomics* (2018) 12(1):1. doi: 10.1186/s40246-018-0132-z

24. Lin HS, Gong JN, Su R, Chen MT, Song L, Shen C, et al. miR-199a-5p inhibits monocyte/macrophage differentiation by targeting the activin a type 1B receptor gene and finally reducing C/EBPα expression. *J Leukoc Biol* (2014) 96(6):1023–35. doi: 10.1189/jlb.1A0514-240R

frontiers | Frontiers in Immunology

TYPE Original Research
PUBLISHED 29 March 2023
DOI 10.3389/fimmu.2023.1147674

OPEN ACCESS

EDITED BY
Duanwu Zhang,
Fudan University, China

REVIEWED BY
Alberto N. Peón,
Sociedad Española de Beneficencia, Mexico
Catarina Teixeira,
Butantan Institute, Brazil

*CORRESPONDENCE
Yan Kang
kangyan@scu.edu.cn
Qin Wu
Qinwu0221@gmail.com

SPECIALTY SECTION
This article was submitted to Inflammation, a section of the journal Frontiers in Immunology

RECEIVED 19 January 2023
ACCEPTED 16 March 2023
PUBLISHED 29 March 2023

CITATION
Yao H, Fu X, Xu Q, Li T, Li Y, Kang Y and Wu Q (2023) The macrophages regulate intestinal motility dysfunction through the PGE2 Ptger3 axis during Klebsiella pneumonia sepsis.
Front. Immunol. 14:1147674.
doi: 10.3389/fimmu.2023.1147674

The macrophages regulate intestinal motility dysfunction through the PGE2 Ptger3 axis during Klebsiella pneumonia sepsis

Hua Yao, Xin Fu, Qian Xu, Tingting Li, Yao Li, Yan Kang* and Qin Wu*

Department of Critical Care Medicine, West China Hospital, Sichuan University, Chengdu, China

Introduction: Gut motility dysfunction, the most common complication of post-septic organ dysfunction, depends on immune and neuronal cells. This study aimed to investigate the mechanisms that activate these cells and the contribution of macrophages to the recovery of intestinal motility dysfunction after sepsis.

Materials and methods: Postoperative gut motility dysfunction was induced by establishing Klebsiella pneumonia sepsis in mice with selective deletion of neutrophils and macrophages in the gut. The distribution of orally administered fluorescein isothiocyanate-dextran and carmine excretion time was used to determine the severity of small bowel disease. The effect of macrophages on intestinal motility was evaluated after prostaglandin E2 therapy.

Results: We found that muscular neutrophil infiltration leading to neuronal loss in the intestine muscle triggered intestinal motility dysfunction after pneumonia sepsis; however, reduced neutrophil infiltration did not improve intestinal motility dysfunction. Moreover, macrophage depletion aggravated gut motility dysfunction. The addition of macrophages directly to a smooth muscle was responsible for the recovery of intestinal motility.

Conclusion: Our results suggest that a direct interaction between macrophages and smooth muscle is neurologically independent of the restoration of intestinal dysmotility.

KEYWORDS

macrophages regulate intestinal motility dysfunction sepsis, immunity, neutrophils, muscular neurons, intestinal muscular macrophages

Abbreviations: KP, Klebsiella pneumonia; MMϕs, muscularis macrophages; TRP, transient receptor potential; RNA, ribonucleic acid; BSA, bovine serum albumin; SMC, smooth muscle cells; PGE2, prostaglandin E2; NO, nitric oxide; CLP, cecal ligation and puncture; ICCs, interstitial cells of Cajal.

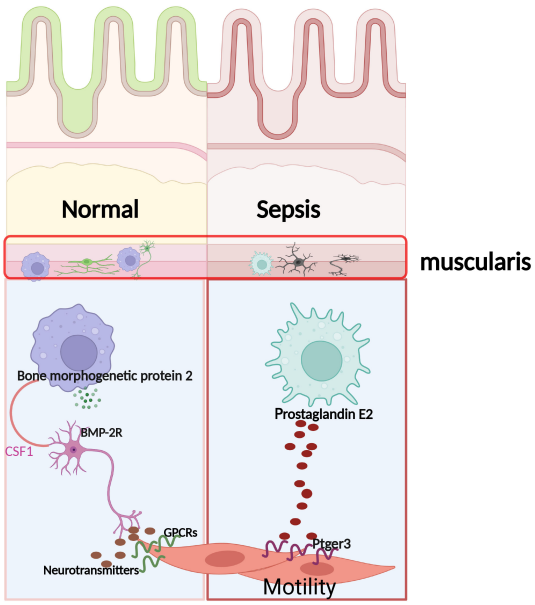

GRAPHICAL ABSTRACT
Illustration of normal intestine motility and sepsis intestine motility. CSF1: Colony stimulating factor 1, GPCRs: G-protein-coupled receptors. Ptger3: Prostaglandin E Receptor 3. Created with BioRender.com.

1 Introduction

Klebsiella pneumonia (KP) is a common leading cause of sepsis in humans and is characterized by high morbidity and mortality (1). Notably, Klebsiella bacteria causes pneumonia, urinary tract infections, and bloodstream infections, among other diseases (2). The mouse model of pneumonia replicating manifestations of KP in humans is being used to explore related diseasemechanisms, including massive inflammation, edema, and an influx of polymorphonuclear neutrophils (3).

Intestinal dysfunction contributes significantly to the development of potentially fatal infections and multiorgan dysfunction (4). Therefore, the development of intestinal dysmotility in sepsis is recognized as a major complication. Although several intestinal dysfunction pathogenic mechanisms caused by sepsis have been proposed, the mechanisms underlying this process are poorly understood.

Smooth muscle contraction or relaxation is widely known to play a crucial role in gastrointestinal motility (5). However, the immune and nervous systems of the gut have been reported to detect and integrate intraluminal signals to regulate physiological processes, including gastrointestinal motility.

Furthermore, neutrophils are the most abundant subset of leukocytes in the bloodstream. They are the first line of defense of the host during tissue injury or infection (6). The induction of a pro-inflammatory environment within the injured tissue results in an influx of neutrophils and monocytes (7). For example, in mice with experimental colitis. Neutrophils impair intestinal permeability, causing bacterial translocation to generate inflammation, In addition, they induce epithelial cell apoptosis and disrupt the integrity of tight junctions and adherent junctions, resulting in colon motility dysfunction (8). However, macrophages have many properties and play vital roles in tissue homeostasis throughout the body (9). It has been reported that muscularis macrophages (MMϕs) are a particular subpopulation of intestinal macrophages, anatomically and physically associated with the myenteric plexus (10). In postoperative ileus, IL-10 produced by intestinal MMϕs affects the migration of neutrophils to the intestinal muscularis by regulating the expression of neutrophil chemokines, contributing to the healing process of postoperative ileus and solving the occurrence (11).

The transient receptor potential (TRP) family in the gastrointestinal tract is highly expressed and can regulate physiological functions, such as gastrointestinal motility, visceral secretion, and visceral hypersensitivity (12). TRP channels are a superfamily of transmembrane cation channels; TRPC (Canonical), TRPV (Vanilloid), TRPA (Ankyrin), TRPM (Melastatin), TRPML (Mucolipin), and TRPP (Polycystin) are the six subfamilies of this superfamily, the majority of which are related to Ca2+ influx (13). They are triggered by endogenous, chemical, mechanical, thermal, osmotic, and other signals and may be crucial regulators of various gastrointestinal tract functions (14). Notably, TRPV1 is reportedly activated by submucosal plexus-expressed capsaicin and associated with stress-induced visceral hypersensitivity (15). Inspired by the co-stimulatory properties of these natural products, investigating whether sepsis stimulates gastrointestinal motility *via* a similar mechanism would be worthwhile.

2 Materials and methods

2.1 Animals

The Dashuo Laboratory (Chengdu, China) provided C57BL/6 specific pathogen-free WT female mice bred at the West China Hospital Frontiers Science Center for Disease-related Molecular Network following HuaXi guidelines. In addition, all animal experiments were approved by the Institutional Animal Care and Use Committee, West China Hospital (study number:20220211010). Neutrophils were exhausted using the anti- Ly6g mAb RB6-8C5 (BioXCell, New Hampshire, USA). Furthermore, mice were intravenously administered mouse anti-Ly6gmAb RB6-8C5 (0.1 mg/day) a day before KP infection to deplete neutrophils. Meanwhile, 200 μL of clodronate-containing liposomes were injected intravenously to deplete MMϕs (YEASEN, Shanghai, China) 24 h before KP infection. Finally, flow cytometry was used to confirm the effectiveness of neutrophil and macrophage depletion in the KP-infected mice.

2.2 Pneumonia lung infection

KP strain was cultivated in tryptic soy broth at 37°C for 16 h. Subsequently, 750 μL of the tryptic soy broth culture was added to 30 mL of fresh broth, and the organism was grown for an additional 2 h to achieve log phage. The bacteria were pelleted for 10 min by centrifugation at 4,500 rpm, washed in cold sterile normal saline, and resuspended at the desired concentration. Subsequently, the absorbance at 600 nm was used to calculate KP concentration. Finally, the mice were briefly sedated with isoflurane pre-inoculation. The bacterial inoculum (30 μL) was applied using a pipette tip to the trachea of a mouse and was involuntarily inhaled.

2.3 RNA isolation and blood enzyme-linked immunosorbent assay

Total RNA samples were isolated from intestine muscularis using TRIzol reagent (Invitrogen, Thermo Fisher Scientific). Briefly, separating intestine muscularis and using liquid nitrogen quick freezing, then extracted with ethanol, isopropanol, and chloroform. A Thermo Fisher Scientific Superscript III Reverse Transcriptase kit was used to create cDNA, and RT-PCR was performed using a Bio-Rad machine. The data were subjected to relative quantification using 18S ribosomal RNA (2–ΔΔCt) as a control. Each sample was analyzed thrice. A list of RT-qPCR primers used is provided in Table 1. At 12 hours and 1 day after the control or KP sepsis operation (n = 6 per group), mice were euthanasia and rapidly harvested blood samples. Blood samples clot for 30 min at room temperature and then centrifugation for 15 min at 1000 g. Subsequently the supernatants were saved at −80 °C for detection. Blood supernatant protein concentration was measured by enzyme-linked immunosorbent assay kits for IL-1β (R0201-1, Nuohe Bio, Chengdu, China), IL-6 (R0201-6, Nuohe Bio, Chengdu, China), lactic acid (R0201-19, Nuohe Bio, Chengdu, China), TNFα (R0201-8, Nuohe Bio, Chengdu, China), and CCL5 (R0201-12, Nuohe Bio, Chengdu, China) to detect expression levels. These assays were carried out according to the instructions provided by the manufacturer. Each sample was detected twice at least.

2.4 Measurement of small intestinal transit

Each mouse received an oral dose of carmine (50 μL; 3 mg of carmine in 0.5% methylcellulose). Subsequently, the mice were put back in separate cages and placed on a blank piece of paper, the duration for the first red feces to be excreted was noted. Furthermore, five to ten animals of each genotype were used to measure the gut transit time.

2.5 Flow-cytometry

The muscularis layers of 9 or 12 mice per group were harvested for further analyses to collect enough intestinal muscularis propria neutrophils and macrophage cells. A single-cell suspension was prepared as described previously (16). Briefly, the intestinal muscularis layer tissue was cut into 1-2 mm, and added to 8 mL HBSS (Gibco, America) of digestion solution containing 10 mg/L II collagenase (9001-12-1, Sigma, Germany), 2.4mg/mL II dispase (D6430, Solarbio, Beijing, China), 0.1mg/mL DNase I (D8071, Solarbio, Beijing, China), 1 mg/mL bovine serum albumin (V900933, Sigma, Germany), and 0.7 mg/L soybean trypsin inhibitor (T8031, Solarbio, Beijing, China). Furthermore, the resulting solution was put in a constant temperature water bath at 37°C for 15 min to see the intestinal segment become transparent, and add 10 mL of HBSS (Gibco, America) containing 5% BSA was added to stop digestion. Next, it was passed through a 70-mesh sieve and centrifuged at 400 g/4°C for 7 min, then use 10 mL of DPBS washing buffer containing 0.04% BSA was used twice. Approximately, 10 mL of DMEM (Gibco, America) culture solution was used to resuspend the cells. Finally, the cells were stained for 30 min at 4°C with the relevant antibodies after incubation with FcR-block (anti-CD16/32, BioLegend). The antibodies used in this study are listed in Table 2. Different cell

TABLE 1 Primer sequences of mouse Ccl5 and Actg1.

	CCL5	Ptger3
Forward Primer	GCTGCTTTGCCTACCTCTCC	CCGGAGCACTCTGCTGAAG
Reverse Primer	TCGAGTGACAAACACGACTGC	CCCCACTAAGTCGGTGAGC

TABLE 2 Sources of commercial antibodies used in flow-cytometry experiments.

Specificity	Fluorochrome	Cat#	Supplier
CD45	APC	103112	BioLegend
CD11b	PE-Cy7	101216	BioLegend
LY6G	PerCP/Cy5.5	127672	BioLegend
LY6C	PE	128008	BioLegend
MHCII	FITC	107606	BioLegend
DAPI	BV421	C1002	Beyotime

populations were captured in PBS with 10% FCS after cell sorting was completed on the FACSAria III (BD Bioscience) platform.

2.6 Immunofluorescence staining and transmission electron microscopic

We gently separated the smooth muscle from the mucosal layer using microscopic forceps. One part of muscularis propria was fixed in 0.1 M phosphate buffered saline containing 4% paraformaldehyde for 4 h at 4°C. After washing in PBS containing 5% BSA thrice, the muscular tissue of each group was blocked in blocking solution (PBS containing 0.3% Triton X-100 (Beyotime), 5% normal donkey serum (Beyotime), and 5% BSA (Sigma)) for 1 h at room temperature and then incubated at 4°C for 72 h with primary antibody. Table 3 shows the primary antibodies and secondary antibody staining. Secondary antibody staining was performed for 2 h. Subsequently, after washing three times with PBS containing 5% BSA, the nuclei were labeled with Beyotime's DAPI for 5 min. For each sample, at least five fields were blindly evaluated. Another part of muscularis propria was fixed at 4°C in 0.1 M phosphate buffered 3% glutaraldehyde and postfixed in 1% osmium tetroxide in the same buffer. After fully rinsed in distilled water, the samples were dehydrated in graded acetone series and embedded in SPI-Pon812. Ultrathin sections were cut with a Leica EM UC7 ultramicrotome, and attached to copper grids with Formvar film, then stained with 2% uranyl acetate and Reynolds lead citrate and examined under a Hitachi HT7800 electron microscope at 80 kV.

TABLE 3 Sources of commercial antibodies used in immunofluorescence experiments.

Specificity	Cat#	Supplier
HUC/D	A-21271	thermofisher
GFAP	A14673	Abclonal
CD117/ckit	A0357	Abclonal
Ptger3	ab21227	abcam
Caspase3	ab104787	abcam
DAPI	C1002	Beyotime
Tunnel	C1086	Beyotime
Goat Anti-Rabbit IgG H&L	ab150077	abcam
Goat Anti-Mouse IgG H&L	ab150118	abcam
Goat Anti-Rabbit IgG H&L	Ab150083	abcam

2.7 Small intestine organ bath experiment

Mice were sacrificed *via* cervical dislocation, and the small intestine was excised completely and immediately transferred to a cold Krebs solution (Solarbio, China). The contents of the intestinal lumen were removed by gently flushing the lumen with Krebs solution using a syringe. Subsequently, the same small intestinal site (2–3 cm) from different groups were carefully mounted longitudinally and gently suspended using cotton thread from force transducers before being submerged in 10 mL organ bath chambers filled with warmed 37°C Krebs solution and gassed with 95% O_2 and 5% CO_2. A dedicated data collection system was used to record changes in the tension of the sensor after amplification and processing.

2.8 Isolation of primary intestinal SMCs and measurement of the cellular contractile response

The small intestinal muscularis layer of the sepsis mouse model was peeled off and placed in an ice-cold modified Krebs solution (G0430, Solarbio, Beijing, China). The tissue was cut into 1-2 mm small pieces and digested in 6 mL Ca2+ free DPBS solution containing 100 mg/mL collagenase II (001-12-1, Sigma, Germany), 100 mg/mL collagenase IV (C8160, Solarbio, Beijing, China), 1 mg/mL soybean trypsin inhibitor (T8031, Solarbio, Beijing, China), and 1 mg/mL bovine serum albumin (V900933, Sigma, Germany). The resulting solution was shaken at 37°C for 30 min. After digestion, DPBS buffer containing 5% fetal bovine serum was double diluted to stop the digestion and gently blown repeatedly with a dropper. The solution was then centrifuged at 1 000 r/min for 3 min. Next, 10 mL of DMEM/F12 culture solution containing 10% fetal bovine serum was used to resuspend the cells. Furthermore, the sample was passed through a 100-mesh sieve, and centrifuged at 1000 rpm/4°C for 7 min. The cell filtrate was taken and stained with trypan blue to check the cell viability and confirm that the viable cells were above 90%. Moreover, after 24 h of DMEM/F12 culture, the medium was changed, and the non-adherent cells were discared. DMEM/F12 culture medium was added to continue culturing until used for experiments. Each group of cells (Sep7d, Sep7d + PGE2, Sep 7d +PGE2 +EP3 antagonist) was loaded with the Fluo-4 (IF1500, Solarbio, Beijing, China) for 30 min in an incubator under 37°C and 5% CO2 and subsequently washed gently using iced DPBS. Finally, using an experimental device (Leica Stellaris Microsystems, Germany) that combines immunofluorescence and live cell imaging to capture images, the contraction response of smooth muscle cells was expressed by the change of intracellular fluorescence intensity (FI) after using PGE2 and EP3 antagonist to represent the relative concentration change of intracellular free calcium, and analyzed by ImageJ (NIH, Bethesda).

2.9 Statistical analyses

All statistical analyses were performed using GraphPad Prism version 8.0(GraphPad Software, Inc., San Diego, CA). We compared the results of the sepsis and control groups using a T-test and one-ANOVA to assess the differences between multiple groups. Differences between groups were significant at a P value of <0.05. * Represents p <0.001, ** represents p <0.01, and *** represents p <0.001. All results are shown as mean ± standard deviation.

3 Results

3.1 Alterations of intestinal motor dysfunction of KP-infected mice

The development of KP sepsis-induced intestinal dysmotility dysfunction involves multiple pathogenic mechanisms. Therefore, expanding and deepening our understanding of host defenses and developing new therapeutic strategies is imperative. First, compared with uninfected mice, IL-6, IL-1β, TNF-α, and lactic acid levels in KP-infected mice increased significantly starting at 12 h (Figure 1A), and the lung wet-to-dry weight ratio after 1 day. In addition, the pathological sections changed significantly, and the infiltration of neutrophils and monocytes increased (Figures S1A–C). Moreover, the clinical score in the sepsis group increased; however, the body weight decreased significantly, with approximately 10% weight loss compared with that of the control group (Figures S1D–F).

Gastrointestinal transit was significantly delayed in sepsis mice compared with that in the control group. The total small intestine transit time in the control group was similar to that in the sepsis group pre-operation; however, carmine red and fluorescence *in vivo* imaging showed that the total transit time increased after sepsis (Figures 1B, C). The gastrointestinal wall musculature comprises an inner circular and an outer longitudinal smooth muscle layer, both essential for the gastrointestinal tract's contractile functionality (17). Our result showed that the thickening of the muscular layer of the intestine differs between the control and sepsis groups (con vs. sep1d: 17.42 ± 2.348 vs. 65.28 ± 21.45 μm, P <0.001; con vs. sep3d: 17.42 ± 2.348 vs. 101.5 ± 13.89 μm, P <0.001; con vs. sep7d: 17.42 ± 2.348 vs.

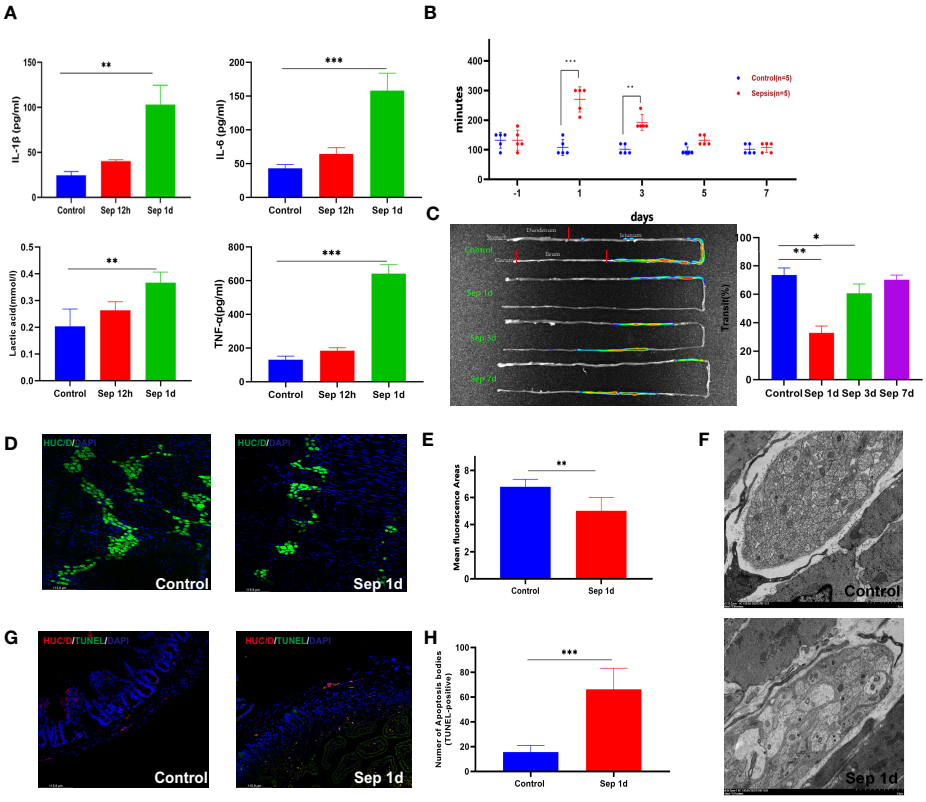

FIGURE 1
Changes after manipulation of Klebsiella pneumonia (KP)-sepsis mice. **(A)** Changes in plasma IL-6, IL-1β, TNF-α, and lactate levels at 12 and 24 h after KP sepsis. **(B)** The carmine red experiment detected changes in intestinal transit time between the control and KP sepsis groups. **(C)** *In vivo* fluorescence imaging of fluorescein 5-isothiocyanate (FITC)-dextran visually displays intestinal motility changes and histograms of statistical results. **(D, E)** Control and sepsis 1 day after intestinal whole-mount HUC/D fluorescent staining and statistical histogram of neuron fluorescence area changes. **(F)** Transmission electron micrographs of mouse intestinal muscular layer neurons 1 day after control and KP sepsis. **(G, H)** Control and sepsis 1 day of intestine transverse HUC/D and terminal deoxynucleotidyl transferase dUTP nick end labeling (TUNEL) double fluorescent staining and statistical histogram of neuronal apoptosis. Differences between groups were significant at a P value of <0.05. * Represents p <0.05, ** represents p <0.01, and *** represents p<0.001.

88.28 ± 17.31 μm, P <0.001) (Figures S1G, H). In addition to smooth muscle contractile activity, the generation of intestinal contractile forces is further controlled by the enteric nervous system, which comprises of interstitial cells of Cajal (ICCs) and the myenteric plexus (18). We stained adult murine myenteric neurons with a HUC/D antibody, which has been previously shown to mark intestinal neurons (19). We observed a significant loss of HUC/D+ neurons areas by day 1 (mean ± SE of percent HUC/D+ neurons areas 5.52 ± 1.58 vs. 6.73 ± 1.36 at sepsis 1 day vs. control 1 day, from 5 adult mice) (Figures 1D , E). c-Kit immunofluorescence staining of intestinal cells of ICCs and Glial fibrillary acidic protein immunofluorescence staining of intestinal glial cells showed no significant differences between the two groups (Figures S1I, J). Transmission electron microscopic images of septic enteric neurons showed swelling, rupture, and vacuolation (Figure 1F). To determine the impact of lung infections on enteric neuron loss, we quantified enteric neuron loss with HUC/D and tunnel double staining according to the manufacturer's protocol (Beyotime). Consequently, we found that the number of apoptotic bodies (TUNEL-positive) increased in the sepsis group (con vs. sep1d: 15.64 ± 5.203 vs. 66.25 ± 17.01, P =0.002) (Figures 1G, H).

3.2 Upregulated expression of neutrophils contributes to myenteric neurons loss

Neutrophil activation is required for tissue infiltration, contributing to inflammatory responses (20), whereas exaggerated activation and uncontrolled infiltration of neutrophils may cause sepsis (21). Meanwhile, *Mashkaryan* and colleagues identified that macrophages in the brain cause a chronic inflammatory environment and exacerbate neuronal loss in Alzheimer's disease (22). Moreover, an enteric neuron programmed death has been demonstrated to be closely related to gastrointestinal motility disorder (23, 24). The early onset of neuronal loss led us to examine immune cells in the inflamed small intestine. By immunohistochemistry and immunofluorescence methods, we found that myeloperoxidase expression significantly increased in sepsis on day 1 (Figures 2A, B), higher levels of CCL5 occurred at the plasma level as early as 12 h post-sepsis, and CCL5 mRNA levels increased in parallel with those in the muscularis (Figures 2C, D). Since we detected a systemic increase in the amounts of myeloperoxidase and CCL5, which are known to be associated with neutrophils, we further detected changes in neutrophils in the intestinal muscularis using Ly6G-positive cells by flow cytometry; this showed a significant increase in the proportion of neutrophils at the time of the most severe intestinal motility dysfunction, which was the first day after KP infection (Figure 2E). We further assessed whether neutrophils induce apoptosis in neurons, using flow cytometry to sort out bone marrow neutrophils and resuspend them to a concentration of 10^6 neutrophils/mL. After 24 h of co-culture with the neuronal cell line PC12-GFP transgenic cells, cells were stained for immunofluorescence, and the percentages of caspase3-positive cells were determined. The results showed a marked increase in the caspase3 percent in sepsis 1-day (Figures 2F, G). These results show that enteric neuron loss is caused by the recruitment and activation of pro-inflammatory neutrophils. Subsequently, we sought to determine whether neutrophil blockade could help restore gut motility earlier. Figures 2H–J showed that neutrophil depletion *in vivo* reduces apoptosis of intestinal muscularis neurons; however, it had no significant effect on sepsis-induced intestinal motility and was insufficient to restore intestinal motility. In contrast, we observed that a population of $MHCII^{hi}$ -expressing cells emerged from sepsis after 3 days (Figure 2I). MMϕs is a newly discovered population of immune cells exclusively populated by $MHCII^{hi}$ $CX3CR1^{hi}$ that express low levels of CD11c (25). MMϕs have a different transcriptome compared with mucosal Mϕs, underlying a unique function. Muller et al. discovered that MMϕs modulate gastrointestinal motility through direct intercommunication with enteric neurons (26). Clodronate-containing liposomes-mediated depletion of macrophages significantly increased animal mortality and aggravated dysmotility (Figure 2J). These findings indicated that in KP sepsis, macrophages might be essential for efficient recovery of intestinal motility, with neutrophils playing an insignificant role.

3.3 Muscle contraction caused by macrophages specific TRPV4 expression stimulation requires PGE2

In addition to MMϕs interaction with neurons, one recent study has shown that MMϕs can directly interact with SMCs by releasing prostaglandin E2 (PGE2), affecting colonic motility(27). Previous studies have demonstrated that nitric oxide and PGE2, two crucial inflammatory mediators released by activated intestinal macrophages, regulate GI motility (28).

We determined whether macrophage- specific TRPV4 and PGE2 play a similar role in promoting GI movement in pneumonia sepsis. To determine whether TRPV4 signaling on MMϕs could cause macrophage cells to produce PGE2 directly, we used flow cytometry to separate $MHCII^{hi}$ cells from the muscularis externa, activated them for 24 h with GSK101 (TRPV4 agonist), and then collected the cell supernatant to evaluate PGE2 levels. PGE2 released from sepsis-related MMϕs was an approximately 1.5-fold increase in response to GSK101 stimulation 7 days mice versus sepsis at day 1 of therapy (Figure 3A). To explore whether activation of PGE2 secretion by MMs affects intestinal contractions under physiological conditions, we applied exogenous PGE2 to the small intestinal segments of mice isolated from each group using the small intestinal organ bath system. We measured changes in spontaneous contraction force and frequency using a dedicated instrument. Compared with the control group, sepsis 1-day small intestine showed a noticeable reduction in spontaneous contractions, as illustrated in Figures 3B, C. Likewise, adding exogenous PGE2 (100 μM) to the organ bath system of sepsis 1-day mice significantly increased the spontaneous contraction force. Another study showed that PGE2 differentially affects GI motility by binding to four membrane-bound G protein-coupled E-prostaglandin receptors (EP1–EP4), which can increase or decrease intestinal muscle contraction (29, 30). Our data

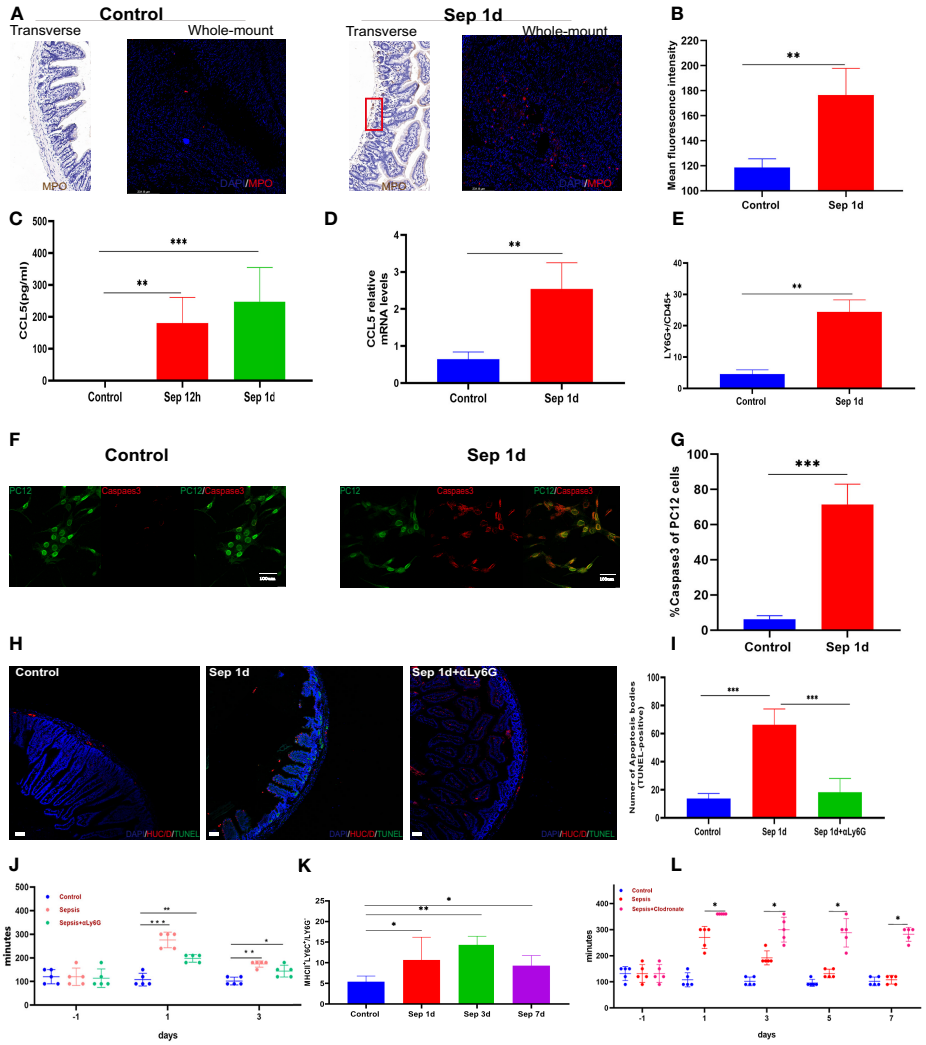

FIGURE 2
Up-regulates the expression of neutrophils. **(A, B)** Control and sepsis on day 1 of intestine transverse and intestine whole mount myeloperoxidase immunohistochemistry, immunofluorescence staining, and statistical histogram of myeloperoxidase fluorescence intensity changes. **(C)** Changes of plasma CCL5 levels 12 and 24 h after KP sepsis. **(D)** Changes in CCL5 mRNA levels in the intestinal muscularis **(E)**: $LY6G^{+}$ neutrophils in the intestinal muscularis 24 h after KP sepsis. **(F, G)** Immunofluorescence staining of PC12-GFP transgenic cells after co-culture with bone marrow neutrophils and percentages of Caspase3-positive cells. **(H, I)** Control, sepsis 1 day, and neutrophil depletion sepsis 1 day of intestine transverse HUC/D and terminal deoxynucleotidyl transferase dUTP nick end labeling (TUNEL) double fluorescent staining and statistical histogram of neuronal apoptosis. **(J)** The carmine red experiment detects changes in intestinal transit time between the control, KP sepsis, and neutrophil depletion sepsis groups. **(K)** The histogram of statistical changes in $MHCII^{hi}$ expressing cell populations shows the changes in MMϕs detected by flow cytometry experiments. **(L)** The carmine red experiment detects changes in intestinal transit time between the control group and KP sepsis and macrophage depletion sepsis groups. Differences between groups were significant at a P value of <0.05. * Represents p <0.05, ** represents p <0.01, and *** represents p<0.001.

indicated that the recovery of intestinal motor function significantly increased mRNA levels of Ptger3 in the muscularis externa (Figure 3D). Moreover, TRPV4 regulation of gut motility was shown to be dependent on EP3-mediated PGE2 signaling in our immunohistochemistry and western blot results (Figures 3E–G). Similarly, we extracted the primary intestinal smooth muscle of sepsis 7 days mice for *in vitro* experiments. Fluo4, a well-established membrane-permeable compound that indicates intracellular Ca2+, and the change of intracellular calcium ion concentration was used to replace the movement of the intestinal tract in animals (31, 32). The laser confocal and incucyte real-time observation results showed that when we used the EP3 antagonist to primary smooth muscle cells in advance, the ability of PGE2 to cause calcium ion release was weakened (Figures 3H, I, Figure S1K). These results indicated that the contraction of intestinal smooth muscle caused by PGE2 depends on the Ptger3 receptor. Collectively, these studies revealed that macrophage mediated small intestine contraction is PGE2-dependent.

4 Discussion

The major findings of our study are as follows: intestinal motor dysfunction owing to KP is associated with damage to the

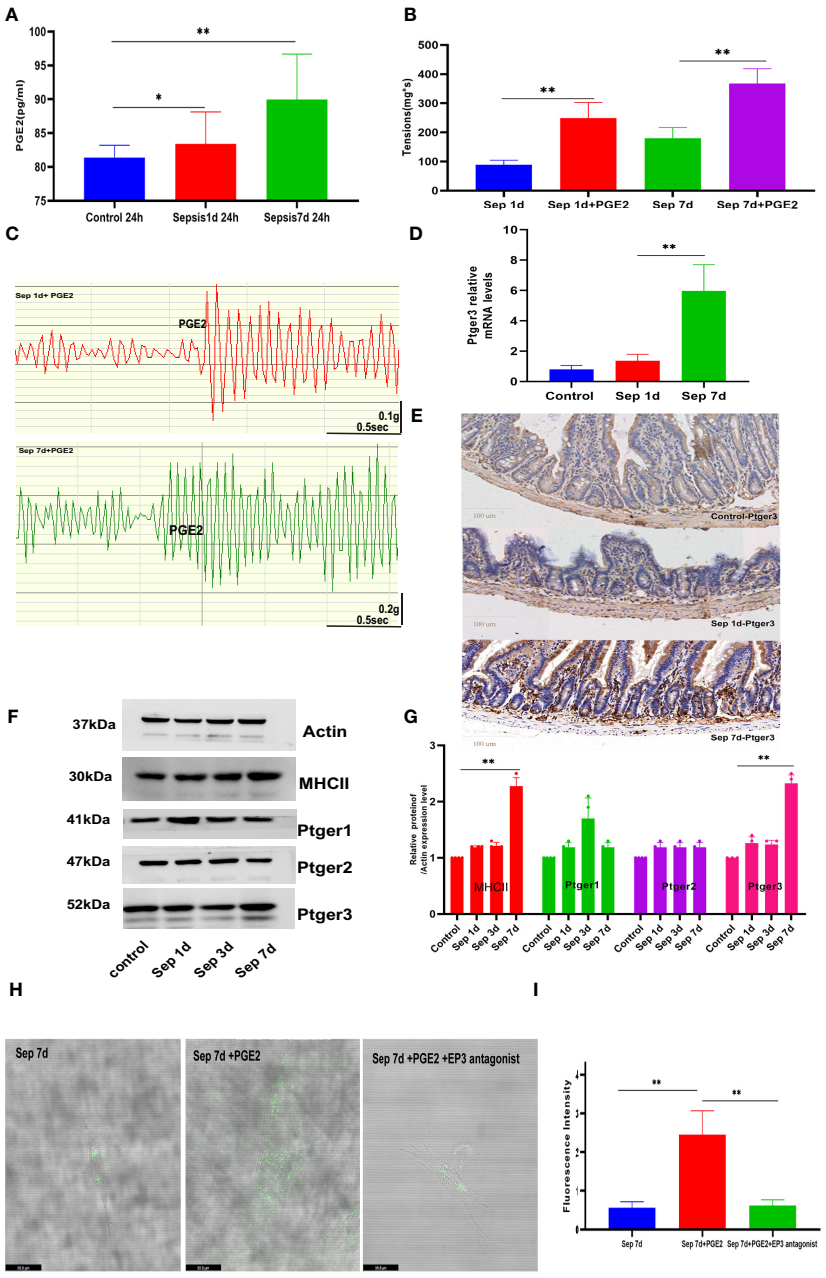

FIGURE 3
Macrophage-mediated small intestine contraction is prostaglandin E2 (PGE2)-dependent **(A)** Compared sepsis 7 days in mice to sepsis 1 day, PGE2 release from MMϕs increased in response to GSK101(TRPV4 agonist) stimulation. **(B, C)** Exogenous PGE2 increased the spontaneous contraction force and histogram of the statistical. **(D, E)** Changes in intestinal muscularis Ptger3 mRNA levels and intestinal transverse Ptger3 immunohistochemical staining after control, KP sepsis 1 day and KP 7 days. **(F, G)** E-prostaglandin receptor (EP1–EP3) protein expression was measured by western blotting and histogram of statistical analysis. **(H, I)** The effects of PGE2 and ptger3 antagonists on primary smooth muscle were determined by fluorescence analysis using the fluorescent probe Fluo-4 and histogram of fluorescence intensity statistical analysis. Differences between groups were significant at a P value of <0.05. * Represents p <0.05, ** represents p <0.01, and *** represents p<0.001.

intestinal muscularis neurons; neuronal injury is associated with the infiltration of muscle-infiltrating pro-inflammatory neutrophils; and smooth muscle contraction induced by MMϕs requires PGE2.

KP is a severe multidrug-resistant pathogen in ICU patients and is associated with high morbidity and mortality owing to limited treatment options (3). KP is characterized by an enhanced inflammatory response with hyper infiltration of neutrophils and macrophages, massive production of pro-inflammatory cytokines, and severe lung injury accompanied by damage to other organs (33). Following the development of pneumonia sepsis, we observed pulmonary and hepatic edema and marked intestinal motility dysfunction. It is generally accepted that GI movement is determined by the synchronized activity of motor

neurons in the intestinal SMC, ICC, and ENS. In a cecal ligation and puncture sepsis model, *Li* et al. found that septic small bowel motility dysfunction was associated with marked activation of the IL-17 signaling pathway in the muscularis propria (34). Miao et al. revealed that lipopolysaccharide induced septic mouse model dysmotility was associated with morphological changes in the interstitial cells of ICCs. Meanwhile, magnolol pretreatment significantly accelerated intestinal transit, increased muscle contraction, and prevented ICC morphological changes (35). However, in our study, intestinal motor dysfunction in mice post- KP sepsis was mainly related to the loss of intestinal muscularis neurons. The underlying mechanism involved in neuronal damage is infiltration with pro-inflammatory neutrophils.

Mikkelsen et al. were the first to identify "macrophage-like" cells in the muscularis propria of the small intestine using immunohistochemistry and electron microscopy (36). Muscularis MΦ plays a recognized role in regulating innate immunity; they can also communicate with cells required for motility in the gastrointestinal tract. For example, one study showed that muscularis MΦ increased the production of pro-inflammatory cytokines and was correlated with decreased ICCs in Hirschsprung disease (HSCR) associated with intestinal dysmotility (37). Moreover, EGC-muscularis MΦ crosstalk was observed in intestinal motility dysfunction caused by postoperative ileus, which was associated with muscularis MΦ elevated IL-1β levels (38). However, this study showed that TRPV4 muscularis MΦ promoted GI motility through PGE2, directly interacting with SMC.

However, our study had some limitations. First, the blocking agents we used, including neutrophils or macrophages, are for systemic blocking; knockout mice targeting the intestinal muscularis should be used to be more convincing. Second, our choice of bone marrow-derived neutrophils may be biased due to the low number of neutrophils in the muscle layer to verify cell experiments. We will improve our experimental technology in the future. Third, we did not obtain a perfect rescue result regarding whether exogenous administration of PGE2 after macrophage blockade changes intestinal motility.

In conclusion, this study showed that infiltrating neutrophils, leading to neuronal loss, were significantly associated with small bowel motility dysfunction in mice with KP sepsis. The direct effect of macrophage secreted PGE2 binding to the Ptger3 receptor on intestinal smooth muscle can help the motor function recovery of intestinal neuron damage, which indicates the changes in intestinal dysmotility function after the occurrence of sepsis. In addition, further research should focus on changes in the muscle, nerve cells, and immune cells.

Data availability statement

The original contributions presented in the study are included in the article/Supplementary Material. Further inquiries can be directed to the corresponding author.

Ethics statement

The animal study was reviewed and approved by the Institutional Animal Care and Use Committee, West China Hospital (study number:20220211010).

Author contributions

HY, QW and YK conceived and designed the experiments. HY, XF, TL and YL performed the experiments. HY, XF and QX contributed materials/analysis tools. HY, XF and QX analyzed the data. HY wrote the manuscript. HY, YK and WQ reviewed all data and finalized the manuscript. All authors contributed to the article and approved the submitted version.

Funding

This study was supported by the 1.3.5 project for disciplines of excellence, West China Hospital, Sichuan University (ZYJC18006), the China National Key R&D Program of China (No.2022YFC2504500), and the China National Key Research and Development Program (No. 2020AAA0105005).

Acknowledgments

Thanks for the help of transmission electron microscopic for *Xiang Zheng* from Laboratory of Electron Microscopy, West China School of Basic Medical Sciences, Sichuan University. Great thanks for the help of flow cytometry analysis for *Xiaojiao Wang* from Core Facilities of West China Hospital.

Conflict of interest

The authors declare that the research was conducted in the absence of any commercial or financial relationships that could be construed as a potential conflict of interest.

Publisher's note

Supplementary material

The Supplementary Material for this article can be found online at: https://www.frontiersin.org/articles/10.3389/fimmu.2023.1147674/full#supplementary-material

SUPPLEMENTARY FIGURE 1

Histopathological evaluation between control and Klebsiella pneumonia-septic mice. **(A, C)** Gross and hematoxylin and eosin (HE) staining changes in inflammatory cell infiltration in the whole lung of mice. **(D, F)** Control and sepsis mice clinical scores and score indicator related pictures, and weight loss percent. **(G, H)** HE stains changes in intestine transverse cut muscle thickness in control, sepsis 1, 3, and 7 days and statistical histogram results. **(I, J)** Intestine whole-mount immunofluorescence staining of ICCs and intestinal glial cells and a statistical histogram of mean immunofluorescence intensity and mean immunofluorescence areas. **(K)** Effects of PGE2 and ptger3 antagonists on primary smooth muscle using Incucyte live-view serial photography.

References

1. Wu T, Xu F, Su C, Li H, Lv N, Liu Y, et al. Alterations in the gut microbiome and cecal metabolome during klebsiella pneumoniae-induced pneumosepsis. *Front Immunol* (2020) 11:1331. doi: 10.3389/fimmu.2020.01331

2. Chang D, Sharma L, Dela CC, Zhang D. Clinical epidemiology, risk factors, and control strategies of klebsiella pneumoniae infection. *Front Microbiol* (2021) 12:750662. doi: 10.3389/fmicb.2021.750662

3. Bengoechea JA, Sa PJ. Klebsiella pneumoniae infection biology: living to counteract host defences. *FEMS Microbiol Rev* (2019) 43(2):123–44. doi: 10.1093/femsre/fuy043

4. Assimakopoulos SF, Triantos C, Thomopoulos K, Fligou F, Maroulis I, Marangos M, et al. Gut-origin sepsis in the critically ill patient: pathophysiology and treatment. *Infection* (2018) 46(6):751–60. doi: 10.1007/s15010-018-1178-5

5. Kwon TH, Jung H, Cho EJ, Jeong JH, Sohn UD. The signaling mechanism of contraction induced by ATP and UTP in feline esophageal smooth muscle cells. *Mol Cells* (2015) 38(7):616–23. doi: 10.14348/molcells.2015.2357

6. Wang X, Hossain M, Bogoslowski A, Kubes P, Irimia D. Chemotaxing neutrophils enter alternate branches at capillary bifurcations. *Nat Commun* (2020) 11(1):2385. doi: 10.1038/s41467-020-15476-6

7. Minutti CM, Knipper JA, allen JE, Zaiss DM. Tissue-specific contribution of macrophages to wound healing. *Semin Cell Dev Biol* (2017) 61:3–11. doi: 10.1016/j.semcdb.2016.08.006

8. Lin EY, Lai HJ, Cheng YK, Leong KQ, Cheng LC, Chou YC, et al. Neutrophil extracellular traps impair intestinal barrier function during experimental colitis. *Biomedicines* (2020) 8(8):275. doi: 10.3390/biomedicines8080275

9. Han X, Ding S, Jiang H, Liu G. Roles of macrophages in the development and treatment of gut inflammation. *Front Cell Dev Biol* (2021) 9:625423. doi: 10.3389/fcell.2021.625423

10. Margolis KG, Gershon MD, Bogunovic M. Cellular organization of neuroimmune interactions in the gastrointestinal tract. *Trends Immunol* (2016) 37(7):487–501. doi: 10.1016/j.it.2016.05.003

11. Stein K, Lysson M, Schumak B, Vilz T, Specht S, Heesemann J, et al. Leukocyte-derived interleukin-10 aggravates postoperative ileus. *Front Immunol* (2018) 9:2599. doi: 10.3389/fimmu.2018.02599

12. Niu L, Wang J, Shen F, Gao J, Jiang M, Bai G. Magnolol and honokiol target TRPC4 to regulate extracellular calcium influx and relax intestinal smooth muscle. *J Ethnopharmacol* (2022) 290:115105. doi: 10.1016/j.jep.2022.115105

13. Gees M, Colsoul B, Nilius B. The role of transient receptor potential cation channels in Ca2+ signaling. *Cold Spring Harb Perspect Biol* (2010) 2(10):a003962. doi: 10.1101/cshperspect.a003962

14. Koivisto AP, Belvisi MG, Gaudet R, Szallasi A. Advances in TRP channel drug discovery: from target validation to clinical studies. *Nat Rev Drug Discov* (2022) 21(1):41–59. doi: 10.1038/s41573-021-00268-4

15. Akbar A, Yiangou Y, Facer P, Walters JR, Anand P, Ghosh S. Increased capsaicin receptor TRPV1-expressing sensory fibres in irritable bowel syndrome and their correlation with abdominal pain. *Gut* (2008) 57(7):923–9. doi: 10.1136/gut.2007.138982

16. Ji S, Traini C, Mischopoulou M, Gibbons SJ, Ligresti G, Faussone-Pellegrini MS, et al. Muscularis macrophages establish cell-to-cell contacts with telocytes/PDGFRα-positive cells and smooth muscle cells in the human and mouse gastrointestinal tract. *Neurogastroenterol Motil* (2021) 33(3):e13993. doi: 10.1111/nmo.13993

17. Sanders KM, Koh SD, Ro S, Ward SM. Regulation of gastrointestinal motility–insights from smooth muscle biology. *Nat Rev Gastroenterol Hepatol* (2012) 9(11):633–45. doi: 10.1038/nrgastro.2012.168

18. Spencer NJ, Hu H. Enteric nervous system: sensory transduction, neural circuits and gastrointestinal motility. *Nat Rev Gastroenterol Hepatol* (2020) 17(6):338–51. doi: 10.1038/s41575-020-0271-2

19. Li Q, Michel K, Annahazi A, Demir IE, Ceyhan GO, Zeller F, et al. Anti-hu antibodies activate enteric and sensory neurons. *Sci Rep* (2016) 6:38216. doi: 10.1038/srep38216

20. Oliveira-costa KM, Menezes GB, Paula NH. Neutrophil accumulation within tissues: A damage x healing dichotomy. *BioMed Pharmacother* (2022) 145:112422. doi: 10.1016/j.biopha.2021.112422

21. Brown KA, Brain SD, Pearson JD, Edgeworth JD, Lewis SM, Treacher DF. Neutrophils in development of multiple organ failure in sepsis. *Lancet* (2006) 368(9530):157–69. doi: 10.1016/S0140-6736(06)69005-3

22. Mashkaryan V, Siddiqui T, Popova S, Cosacak MI, Bhattarai P, Brandt K, et al. Type 1 interleukin-4 signaling obliterates mouse astroglia *in vivo* but not *in vitro*. *Front Cell Dev Biol* (2020) 8:114. doi: 10.3389/fcell.2020.00114

23. Bassotti G, Villanacci V, Maurer CA, Fisogni S, Di Fabio F, Cadei M, et al. The role of glial cells and apoptosis of enteric neurones in the neuropathology of intractable slow transit constipation. *Gut* (2006) 55(1):41–6. doi: 10.1136/gut.2005.073197

24. Ye L, Li G, Goebel A, Raju AV, Kong F, Lv Y, et al. Caspase-11-mediated enteric neuronal pyroptosis underlies Western diet-induced colonic dysmotility. *J Clin Invest* (2020) 130(7):3621–36. doi: 10.1172/JCI130176

25. De Schepper S, Stakenborg N, Matteoli G, Verheijden S, Boeckxstaens GE. Muscularis macrophages: Key players in intestinal homeostasis and disease. *Cell Immunol* (2018) 330:142–50. doi: 10.1016/j.cellimm.2017.12.009

26. Muller PA, Koscso B, Rajani GM, Stevanovic K, Berres ML, Hashimoto D, et al. Crosstalk between muscularis macrophages and enteric neurons regulates gastrointestinal motility. *Cell* (2014) 158(2):300–13. doi: 10.1016/j.cell.2014.04.050

27. Luo J, Qian A, Oetjen LK, Yu W, Yang P, Feng J, et al. TRPV4 channel signaling in macrophages promotes gastrointestinal motility *via* direct effects on smooth muscle cells. *Immunity* (2018) 49(1):107–119.e4. doi: 10.1016/j.immuni.2018.04.021

28. Mori D, Watanabe N, Kaminuma O, Murata T, Hiroi T, Ozaki H, et al. IL-17A induces hypo-contraction of intestinal smooth muscle *via* induction of iNOS in muscularis macrophages. *J Pharmacol Sci* (2014) 125(4):394–405. doi: 10.1254/jphs.14060fp

29. Wang D, Mann JR, Dubois RN. The role of prostaglandins and other eicosanoids in the gastrointestinal tract. *Gastroenterology* (2005) 128(5):1445–61. doi: 10.1053/j.gastro.2004.09.080

30. Reader J, Holt D, Fulton A. Prostaglandin E2 EP receptors as therapeutic targets in breast cancer. *Cancer Metastasis Rev* (2011) 30(3-4):449–63. doi: 10.1007/s10555-011-9303-2

31. Berridge MJ. Smooth muscle cell calcium activation mechanisms. *J Physiol* (2008) 586(21):5047–61. doi: 10.1113/jphysiol.2008.160440

32. Zhou H, Kong DH, Pan QW, Wang HH. Sources of calcium in agonist-induced contraction of rat distal colon smooth muscle *in vitro*. *World J Gastroenterol* (2008) 14(7):1077–83. doi: 10.3748/wjg.14.1077

33. Vieira AT, Rocha VM, Tavares L, Garcia CC, Teixeira MM, Oliveira SC, et al. Control of klebsiella pneumoniae pulmonary infection and immunomodulation by oral treatment with the commensal probiotic bifidobacterium longum 5(1A). *Microbes Infect* (2016) 18(3):180–9. doi: 10.1016/j.micinf.2015.10.008

34. Li J, Kong P, Chen C, Tang J, Jin X, Yan J, et al. Targeting IL-17A improves the dysmotility of the small intestine and alleviates the injury of the interstitial cells of cajal during sepsis. *Oxid Med Cell Longev* (2019) 2019:1475729. doi: 10.1155/2019/1475729

35. Miao B, Zhang S, Wang H, Yang T, Zhou D, Wang BE. Magnolol pretreatment prevents sepsis-induced intestinal dysmotility by maintaining functional interstitial cells of cajal. *Inflammation* (2013) 36(4):897–906. doi: 10.1007/s10753-013-9617-z

36. Rumessen JJ, Thuneberg L. Plexus muscularis profundus and associated interstitial cells. i. light microscopical studies of mouse small intestine. *Anat Rec* (1982) 203(1):115–27. doi: 10.1002/ar.1092030111

37. Chen X, Meng X, Zhang H, Feng C, Wang B, Li N, et al. Intestinal proinflammatory macrophages induce a phenotypic switch in interstitial cells of cajal. *J Clin Invest* (2020) 130(12):6443–56. doi: 10.1172/JCI126584

38. Stoffels B, Hupa KJ, Snoek SA, van Bree S, Stein K, Schwandt T, et al. Postoperative ileus involves interleukin-1 receptor signaling in enteric glia. *Gastroenterology* (2014) 146(1):176–87.e1. doi: 10.1053/j.gastro.2013.09.030

frontiers | Frontiers in Immunology

TYPE Study Protocol
PUBLISHED 14 April 2023
DOI 10.3389/fimmu.2023.1145826

OPEN ACCESS

EDITED BY
Yufeng Zhou,
Fudan University, China

REVIEWED BY
Marisa Mariel Fernandez,
Institute of Studies on Humoral Immunity (IDEHU), Argentina
Antonio Ferrante,
South Australia Pathology, Australia

*CORRESPONDENCE
Peter A. Greer
greerp@queensu.ca

SPECIALTY SECTION
This article was submitted to Inflammation, a section of the journal Frontiers in Immunology

RECEIVED 16 January 2023
ACCEPTED 03 April 2023
PUBLISHED 14 April 2023

CITATION
Laight BJ, Jawa NA, Tyryshkin K, Maslove DM, Boyd JG and Greer PA (2023) Establishing the role of the FES tyrosine kinase in the pathogenesis, pathophysiology, and severity of sepsis and its outcomes.
Front. Immunol. 14:1145826.
doi: 10.3389/fimmu.2023.1145826

Establishing the role of the FES tyrosine kinase in the pathogenesis, pathophysiology, and severity of sepsis and its outcomes

Brian J. Laight[1,2,3], Natasha A. Jawa[2,4], Kathrin Tyryshkin[5], David M. Maslove[6,7], J. Gordon Boyd[4,6,7] and Peter A. Greer[1,3]*

[1]Department of Pathology and Molecular Medicine, Faculty of Health Sciences, Queen's University, Kingston, Ontario, ON, Canada, [2]School of Medicine, Faculty of Health Sciences, Queen's University, Kingston, Ontario, ON, Canada, [3]Queen's Cancer Research Institute, Queen's University, Kingston, Ontario, ON, Canada, [4]Centre for Neuroscience Studies, Faculty of Health Sciences, Queen's University, Kingston, Ontario, ON, Canada, [5]School of Computing, Queen's University, Kingston, Ontario, ON, Canada, [6]Division of Medicine and Critical Care Medicine, Department of Medicine, Faculty of Health Sciences, Queen's University, Kingston, Ontario, ON, Canada, [7]Departments of Medicine and Critical Care Medicine, Kingston General Hospital, Kingston, Ontario, ON, Canada

Introduction: Sepsis is a result of initial over-activation of the immune system in response to an infection or trauma that results in reduced blood flow and life-threatening end-organ damage, followed by suppression of the immune system that prevents proper clearance of the infection or trauma. Because of this, therapies that not only limit the activation of the immune system early on, but also improve blood flow to crucial organs and reactivate the immune system in late-stage sepsis, may be effective treatments. The tyrosine kinase FES may fulfill this role. FES is present in immune cells and serves to limit immune system activation. We hypothesize that by enhancing FES in early sepsis and inhibiting its effects in late sepsis, the severity and outcome of septic illness can be improved.

Methods and analysis: *In vitro* and *in vivo* modeling will be performed to determine the degree of inflammatory signaling, cytokine production, and neutrophil extracellular trap (NET) formation that occurs in wild-type (WT) and FES knockout ($FES^{-/-}$) mice. Clinically available treatments known to enhance or inhibit FES expression (lorlatinib and decitabine, respectively), will be used to explore the impact of early *vs.* late FES modulation on outcomes in WT mice. Bioinformatic analysis will be performed to examine *FES* expression levels in RNA transcriptomic data from sepsis patient cohorts, and correlate *FES* expression data with clinical outcomes (diagnosis of sepsis, illness severity, hospital length-of-stay).

Ethics and dissemination: Ethics approval pending from the Queen's University Health Sciences & Affiliated Teaching Hospitals Research Ethics Board. Results will be disseminated through scientific publications and through lay summaries to patients and families.

KEYWORDS

sepsis, innate immunity, dysregulated inflammation, coagulation, personalized medicine

Highlights

- This will be the first study to explore the utility of FES modulation in the treatment of sepsis.
- This study will illustrate the importance of differential regulation of sepsis at both early and late timepoints.
- This study will employ *in vivo, in vitro*, and clinical research methodologies to elucidate the role of FES in sepsis.
- There exists the potential for off-target effects of the drugs used in this study that may complicate the interpretation of results or outcomes, as they are not specific enhancers or inhibitors of FES.

Introduction

Sepsis is the leading cause of death among hospitalized patients in North America, and is present in over 50% of adult hospitalizations resulting in death or discharge to hospice care (1). Globally, sepsis accounts for 19.7% of all deaths (2), and is the most expensive healthcare problem requiring in-hospital treatment (3), costing the healthcare system approximately $1 billion per year in Ontario alone ($670 million for severe cases, $420 million for non-severe cases) (4). Importantly, the consequences of sepsis extend beyond the duration of the patient's hospitalization, with lasting impairments being increasingly recognized as comprising "post-sepsis syndrome" (5); resulting in additional costs to the healthcare system for auxiliary care after discharge. Targeted treatments for sepsis are therefore urgently needed to simultaneously improve patient outcomes and alleviate the burden of sepsis on global healthcare systems.

Sepsis is characterized by widespread inflammation and life-threatening organ dysfunction, resulting from dysregulation of the patient's response to infection and coagulation cascades (6, 7). Specifically, sepsis occurs upon disruption of the tightly regulated balance of pro- and anti-inflammatory mediators activated in response to pathogen- (e.g., virus, bacteria) or damage-associated molecular patterns (e.g., trauma; PAMPs and DAMPs, respectively) (8). Binding of PAMPs and DAMPs to toll-like receptors (TLRs) on the surface of antigen presenting cells (APCs) and monocytes causes nuclear translocation of nuclear factor kappa light chain enhancer of activated B cells (NF-κB), resulting in expression of genes encoding pro-inflammatory cytokines, tumor necrosis factor (TNF)-α, interferons, and components of complement and coagulation pathways (2). Clinically, activation of these pathways results in hypercoagulation, endothelial dysfunction, and ultimately to end organ damage (2).

While sepsis pathophysiology remains to be fully elucidated, we have previously shown that the FES kinase, which is highly expressed in APCs, plays a role in limiting over-stimulation of the innate immune system (9). *FES* knockout mice are hypersensitive to endotoxin lipopolysaccharide (LPS), a TLR-4 agonist, as a result of overactive TLR-4 signaling-induced innate immune responses (10) including increased transcription of genes encoding pro-inflammatory mediators, such as TNF-α (9). Our group and others have implicated FES as a regulator of TLR-4 signaling (9, 11). TLR-4 is also a critical inducer of both platelet-dependent and -independent NET formation, where neutrophils and platelets express both FES and TLR-4. Hyperactive TLR-4 signaling may therefore exacerbate the immune response and coagulation in severe sepsis (12, 13). Furthermore, *FES* knockout ($FES^{-/-}$) mice demonstrate dysregulation of signal transducer and activator of transcription 3 (STAT3) (13), which plays a vital role in the pathophysiology of sepsis by initiating endothelial dysfunction, vasoplegia, coagulopathy, and multi-organ failure (14, 15). FES may also contribute to thrombin formation (16), which is known to contribute to hypercoagulation during the early inflammatory stage of sepsis (17).

There are currently no approved targeted molecular therapies available for the treatment of sepsis (6). The mainstay of treatment for sepsis involves management of infection, optimizing the patient's fluid balance, improving hemodynamic stability, and sedative management; however, there is controversy over whether these interventions contribute to reduced mortality and morbidity in this cohort (3, 6, 18). Furthermore, early pre-clinical trials employing anti-TNF antibodies or corticosteroids to block proinflammatory cytokine cascades have since been shown to be ineffective in larger and later-stage clinical trials (3, 6). Identifying and targeting the key events and their regulators that precede these dysregulated immune responses characteristic of sepsis is therefore critical to optimize patients' responses to systemic infection (6).

Due to its expression in innate immune cells and its involvement in regulating TLR-4 signaling (9, 11), we expect that increased FES expression will limit hyper-inflammatory phenotypes of immune cells (9, 11), reduce platelet aggregation (19), and we hypothesize it will also reduce NET formation (12, 20, 21). Consequently, targeting FES may allow for specific inhibition of two key aspects underlying the pathophysiology of sepsis: the coagulation cascade and the innate immune system. This study aims to elucidate the role of FES in sepsis pathophysiology using both an established mouse model of sepsis and a repository of data from patients with sepsis, as a first step toward being able to develop targeted immune-based therapies to enhance patient care and improve outcomes.

Overarching hypothesis

We hypothesize that FES expression is related to outcomes in *in vivo* and *in vitro* models of sepsis, as well as in clinical populations of patients with sepsis. We further hypothesize that modulating FES can be used as a method of improving sepsis outcomes. Figure 1 illustrates the hypothesized role of FES in the pathophysiology of sepsis. Figure 2 illustrates how FES regulation could be used therapeutically to treat sepsis.

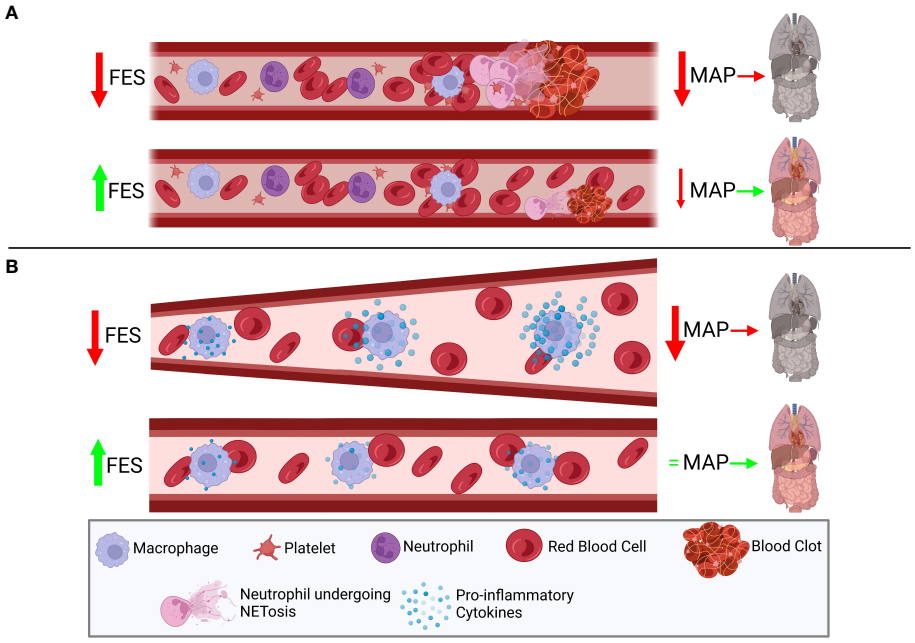

FIGURE 1
Decreased FES levels may correlate with worse septic outcomes by modulating host immune and coagulation pathways. **(A)** FES has been shown to play a role in limiting coagulation cascades through modulation of platelets and we hypothesize a role for FES in decreasing NETosis from neutrophils. Therefore, low FES expression is hypothesized to correlate with reduced lysis of blood clots, and an increase in NETosis in both a platelet-dependent and –independent manner, thus leading to reduced mean arterial pressure (MAP), leading to end organ damage. However, in patients with high FES expression, there is hypothesized to be reduced NETosis, and increased disaggregation of platelets, leading to a less dramatic impact on MAP, and improved perfusion of end organs. **(B)** FES has been shown to suppress the toll-like receptor (TLR) 4 signaling cascade, which leads to the production of pro-inflammatory cytokines regulated by NF-κB and IRF3. In patients with low FES expression, it is hypothesized that this signaling cascade will be poorly regulated, leading to the over-activation of the TLR4 cascade, stimulated by components of bacterial cell walls (lipopolysaccharide) or in response to tissue damage (high mobility group box 1), and ultimately leading to the over-production of inflammatory cytokines. This production of excess cytokines can lead to vasodilation, leading to reduced MAP, and reducing perfusion to end organs. However, with high FES expression, this cascade is tightly regulated, and the over-production of pro-inflammatory cytokines is limited, reducing changes in vasodilation, and preventing drastic changes in MAP, thus protecting end organs. Created with BioRender.com.

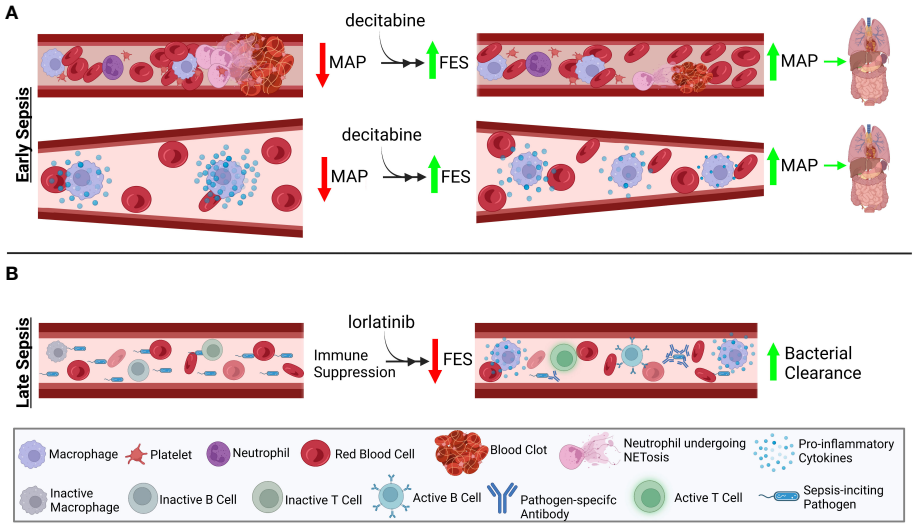

FIGURE 2
Therapeutic efficacy of FES expression level changes is stage-dependent. Sepsis can be separated into two stages: early stage, characterized by overactive immune responses leading to decreased end organ perfusion; and late stage, characterized by immune suppression, preventing the efficient clearance of the sepsis-inciting event. **(A)** Due to the over-stimulation of the immune system in early sepsis, treatment with decitabine, known to induce increased *FES* expression, will prevent overactivation of the immune system. **(B)** In contrast, overcoming the characteristic late-stage immunosuppression by treatment with lorlatinib, an inhibitor of FES activity, will promote greater pro-inflammatory cytokine production from immune cells. This increase in immune activation will aid in resolving the inciting event of sepsis. Created with BioRender.com.

Aims and specific hypotheses

Cell types responsible for sepsis severity and their effect on sepsis outcomes

This study aims to determine the cell types responsible for increased sepsis severity and their effects on outcomes in WT or *FES*$^{-/-}$ mice. We hypothesize that FES limits over-activation of innate immune cells and suppresses vascular hypercoagulation. We expect that *FES*$^{-/-}$ immune cells will take on a hyper-inflammatory phenotype when stimulated with infectious or damaging agents and will produce increased levels of pro-inflammatory cytokines (such as Interleukin (IL) -1, IL-6, Tumor Necrosis Factor (TNF)-α) and NETs relative to WT mice. *In vivo*, we expect to find an increase in both immune cell numbers and their degree of activation, as well as increased coagulation and end-organ damage in septic *FES*$^{-/-}$ mice compared to WT.

Timing of FES regulation on sepsis outcomes

This study will aim to evaluate whether FES regulation, and the timing of FES regulation, can affect sepsis outcomes. Early sepsis pathogenesis is characterized by hyperinflammation and coagulation, while late sepsis pathogenesis is characterized by immune suppression and organ dysfunction. It is hypothesized that the observed late-stage immunosuppression is as a commensal response to the initial overactive immune response. The early hyper-inflammatory stage of sepsis is characterized by increased immune cell activation and production proinflammatory cytokine secretion such as IL-1, IL-6, and TNF-α (22), a dangerous condition known as cytokine storm (23). This late stage is characterized by production of anti-inflammatory cytokines, such as IL-10 and Transforming Growth Factor-β (TGF-β), which serve to repress the overstimulated immune cells, reduced antigen presenting cells functions, lymphocyte anergy and apoptosis, and reduced responsiveness to activating stimuli, such as LPS (24). Simultaneous inflammation and immunosuppression is now being described in late-stage sepsis (22), suggesting that while there may be immunostimulatory molecules circulating, immune cells may be unable to appropriately respond to these stimuli. This provides additional rational for regulating FES, as it plays a role in limiting innate immune cell activation in response to stimulatory molecules such as LPS. We therefore hypothesize that artificially enhancing FES activation will improve early-stage sepsis, and that inhibiting FES will improve outcomes in late-stage sepsis. Figure 2 illustrates the timeline of sepsis and the expected impact of FES regulation at each stage of illness.

Association between FES expression and clinical sepsis presentation and outcomes

This study will seek to determine whether the RNA expression levels of FES are associated with the incidence, severity, and outcome of sepsis using bioinformatic analysis. We expect that FES will be upregulated in early-stage and downregulated in late-stage sepsis. Furthermore, we hypothesize that decreased *FES* RNA levels will be associated with receiving a clinical diagnosis of sepsis, increased illness severity, and poorer clinical outcomes including greater risk for ICU mortality and increased length of hospitalization.

Furthermore, we aim to determine whether clinical sepsis outcomes are correlated with single nucleotide polymorphisms (SNPs) associated with differential *FES* expression. Recently, two SNPs have been associated with reduced *FES* expression: rs17514846, located within in the 5' proximal region of the neighbouring gene *FURIN*, and rs1894401, located within the *FES* gene. The presence or absence of these two SNPs will be correlated with clinical outcomes in a cohort of sepsis patients (25).

Methods and analysis

Patient and public involvement

Patient partners who have recovered from sepsis will be recruited from the ICU Follow-Up Clinic at Kingston Health Sciences Centre (Kingston, Ontario). Patient partners will help to guide decision-making around the clinical outcomes that are most important to study, such that our analysis can be focused on patient-centred outcomes.

Study design and setting

To expand our understanding of FES involvement in mediating sepsis, we will perform *in vitro* and *in vivo* modeling to elucidate the degree of inflammatory signaling, cytokine production, and NET formation that occurs in wild-type (WT) and *FES* knockout (*FES*$^{-/-}$) mice. Using clinically available treatments that either enhance *FES* expression or inhibit FES activity, we will explore the utility of early *vs.* late FES modulation on outcomes in WT mice. Finally, we will explore the clinical relevance of FES in the pathogenesis of sepsis by using bioinformatic analyses to examine *FES* expression levels in RNA transcriptomic data from publicly available cohorts of patients with sepsis and healthy controls and correlating this with clinical outcomes. All analyses will take place in the Queen's Cancer Research Institute facility at Queen's University (for experimental laboratory-based aims), or the Centre for Advanced Computing (for the clinical bioinformatics aims).

In vitro methodology

Bone marrow derived macrophages (BMDMs) (26) or neutrophils (27) isolated from WT or *FES*$^{-/-}$ mice will be stimulated with infectious surrogates (LPS or PolyI:C), or a surrogate for tissue damage-mediated sepsis (High Mobility Group Box 1; HMGB1). The degree of inflammatory signaling (e.g., NF-κB and IRF-3 phosphorylation) will be assessed via immunoblot analysis. Supernatants will be analyzed by cytokine multiplex (28) methods to determine differential cytokine

production in WT or *FES*$^{-/-}$ immune cells, and the type of cytokines (e.g., proinflammatory, such as IL-1, IL-6, IL-12, TNF-α, and Interferon-α/β (23); or anti-inflammatory, such as, IL-10 and TGF-β (29)) (Figure 3A). Finally, WT and *FES*$^{-/-}$ neutrophils will be evaluated for their ability to produce NETs using flow cytometry (30) (Figure 3B).

BMDMs and neutrophils isolated from WT or *FES*$^{-/-}$ mice will be pre-treated with either a drug that inhibits FES activity (*lorlatinib* (31)), or one that increases *FES* transcription (*decitabine* (32)). These cells will then be stimulated with LPS, PolyI:C, or HMGB1 to simulate the immune cell activation associated with sepsis, and the same methodology as in Aim 1 will be used to assess increased (in the case of lorlatinib treatment) or decreased (in the case of decitabine treatment) hyper-inflammatory signaling, cytokine production, and NET production.

In vivo methodology

WT or *FES*$^{-/-}$ mice will be treated in one of two ways, either simulating different insults resulting in sepsis: 1) cecal ligation and puncture (CLP), the gold-standard sepsis model (33) or 2) a cecal slurry (CS) of 0.5mL of a solution at a fecal concentration of 45mg/mL (33–35). Following induction of sepsis, mice will be closely monitored and scored on the murine sepsis score (MSS), which assesses sepsis severity based on appearance, level of consciousness, activity, response to stimulus, eyes, respiration rate, and respiration quality (35). The MSS has been shown to have a specificity of 57%, and a sensitivity of 100% for predicting onset of severe sepsis and death following CS. Blood will be collected by cardiac puncture at the 24h time point and analyzed by cytokine multiplex to assess differential cytokine production, which will demonstrate differences in cytokine production from either WT or *FES*$^{-/-}$ genotypes and can also be correlated with sepsis severity (35). Additionally, the following biomarkers will be assayed from the blood, as these have been associated with sepsis in murine models: C-reactive protein (CRP), soluble triggering receptor expressed on myeloid cells-1 (sTERM-1), CD163, procalcitonin (PCT) and hypoxia-inducible factor (HIF-1α) by ELISA, where CD163 and procalcitonin can stratify mice further into a state of severe sepsis (36) (Figure 4). Spleens will be isolated, dissociated and analyzed by flow cytometry for the presence and activation of immune cells (i.e., macrophages, neutrophils, T cells, B cells), as well as NET formation (30). Finally, differences in clotting ability and end-organ damage

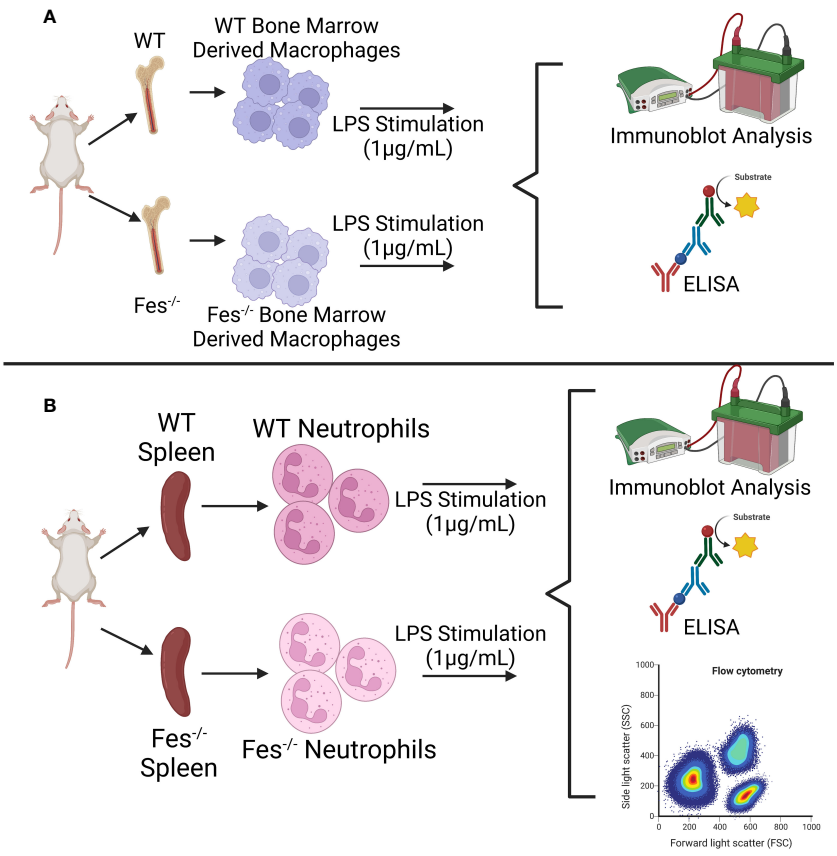

FIGURE 3
Graphical depiction of *in vitro* methodology. **(A)** Wildtype (WT) or FES$^{-/-}$ bone marrow derived macrophages will be stimulated with LPS or other stimulating agents and analyzed for differential signaling cascade activation (immunoblot analysis) and cytokine production (enzyme-linked immunosorbent assay (ELISA)). **(B)** WT or FES$^{-/-}$ neutrophils isolated from the spleen will be stimulated with LPS or other stimulating agents and analyzed for differential signaling cascade activation (immunoblot analysis), cytokine production (ELISA), and neutrophil extracellular trap formation (flow cytometry). The same methodology will be followed with the addition of decitabine and lorlatinib. Created with BioRender.com.

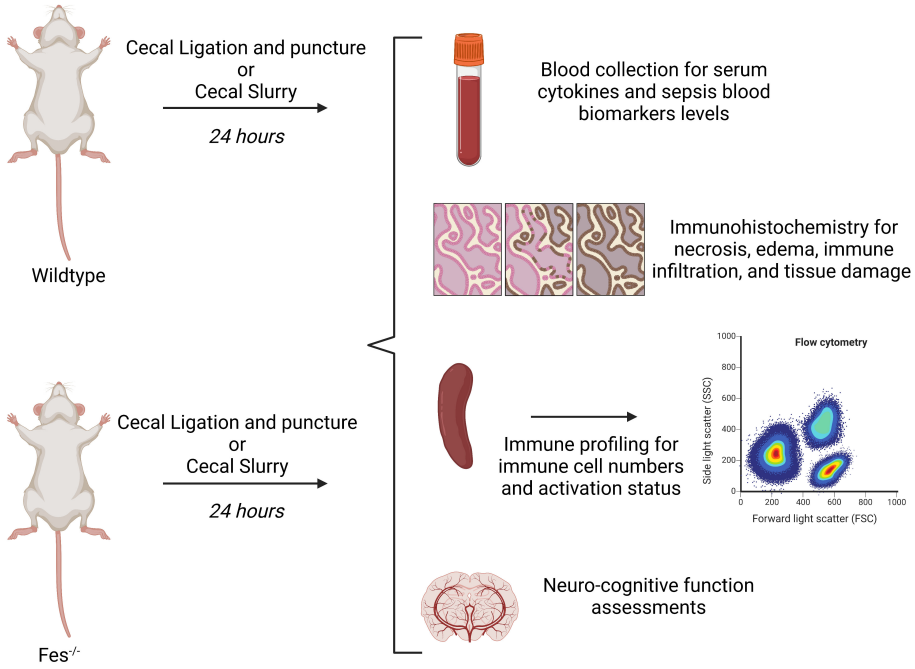

FIGURE 4
Graphical depiction of *in vivo* methodology. Wildtype (WT) or FES$^{-/-}$ mice will be undergo a cecal ligation and puncture (CLP) or receive a cecal slurry injected intraperitoneally. 24 hours later, mice will be assessed for the following: neurologic function assessment, serum cytokine and biomarker analysis, immunohistochemistry, and spleen immune profiling. The same methodology will be used with the addition of decitabine or lorlatinib. Created with BioRender.com.

between WT and *FES*$^{-/-}$ mice will be assessed by histopathological analysis of hematoxylin & eosin-stained necropsy tissues. Briefly, livers, kidneys, small intestines, lungs, and brains will be assessed for necrosis, edema, accumulation of immune cells within tissues (e.g. macrophages, neutrophils, T-cells) and signs of damage to the tissues (e.g., loss of goblet cells and villi in small intestines, debris, and loss of organization and structure of epithelium) (35). As CS with a fecal concentration of 45mg/mL is associated with a 40% survival in C57BL/6 wildtype mice, mice will be assessed for neurocognitive impairments: a significant sequalae of post-sepsis syndrome (37, 38) A recent systematic review listed several common forms of cognitive impairment found in pre-clinical models of sepsis (e.g., aversive memory, learning, locomotor and exploratory activities, short-term and long-term memories), which may mimic what happens in patient populations (37). Therefore, any surviving mice will be subjected to the Y-maze novel arm preference test (a measure of testing spatial memory and attention), buried food test (a measure of attention and organized thinking), attentional set-shifting task (a measure of attention and cognitive flexibility), and finally the open field test (a measure of motor performance) (39) (Figure 4). Following neurocognitive assessments, mice will be euthanized and assessed for hyper-inflammation, coagulation, and histopathology as described above.

To determine the effect of the timing of FES regulation on outcomes, WT or *FES*$^{-/-}$ mice will be subjected to either CLP or CS and treated with lorlatinib or decitabine at either 1h (mimicking regulation in early-stage sepsis) or 12h (mimicking regulation in late-stage sepsis). Hyper-inflammation, coagulation, histopathology, and neurocognition will be assessed at 24h, as previously mentioned. Finally, to determine differential susceptibility of WT mice to sepsis, we will perform an LD_{50} analysis of both early- and late-stage treatment regimens with either drug.

Clinical and bioinformatics methodology

We have previously extracted RNA from whole blood samples in critically ill patients at various time points during their admission, as well as from healthy controls, as part of the "Prevention of nosocomial infections in critically ill patients with lactoferrin (PREVAIL)" study (NCT01996579). Briefly, blood was collected into PAXgene tubes, frozen, RNA extracted, and gene expression was profiled using the Affymetrix PrimeView microarray (40). Data on 69 patients and 21 healthy controls from this analysis is publicly available (41) and will be analyzed for the current study. Machine-learning approaches will be used to identify key variables associated with FES RNA expression levels, including a) *clinical diagnosis of sepsis*; b) *illness severity*, as measured by Acute Physiology and Chronic Health Evaluation II (APACHE II) and Sequential Organ Failure Assessment (SOFA) scores; and c) clinical outcomes including *hospital length of stay and ICU mortality*.

A publicly available dataset comprised of clinical outcome data as well as SNP analysis from genome wide association studies (GWAS) will be sought through collaborations with local and international experts in the field of sepsis genetics. Multivariable analysis will be used to determine the association between the two

SNPs (rs17514846 and rs1894401) related to differential FES expression, and clinical, patient-centred outcomes. Additionally, we will apply for access to the United Kingdom BioBank (https://www.ukbiobank.ac.uk/), a large-scale database with in-depth genetic and clinical outcomes for a wide variety of diseases (including sepsis) in over half a million patients. This database currently has SNP and transcriptomic data available to be paired with clinical outcomes and will soon be releasing proteomic data which can be analyzed further to pair the two SNPs (rs17514846 and rs1894401) related to differential FES expression with protein expression, and clinical outcomes.

Expected impact

These results will determine if FES modulates sepsis severity by preventing hyper-inflammation and suppressing coagulation cascades, providing a rationale for using FES regulation as a therapeutic strategy to reduce sepsis severity. The results of these experiments will further improve our understanding of the process by which NETs are produced, which has implications not only for sepsis but also for many other diseases.

In lorlatinib treated WT immune cells, we expect to see a phenocopy of the *FES*$^{-/-}$ immune cells, and prevention of inflammatory signaling with decitabine. Irrespective of the timing of treatment, we do not expect either lorlatinib or decitabine to affect sepsis severity in *FES*$^{-/-}$ mice (as there is no FES present to be regulated by either of these drugs). By contrast, in WT mice we expect to see increased septic severity following early lorlatinib treatment, and decreased septic severity following early decitabine treatment. We further expect to see decreased septic severity following late lorlatinib treatment (protective effect) and increased septic severity with late decitabine treatment (detrimental effect). These findings would support the notion that FES is a critical regulator of sepsis; and would further demonstrate that sepsis severity can be attenuated using currently available treatments by differentially modulating FES depending on the stage of a patient's illness progression.

While it is our expectation that high FES expression levels in early sepsis and low FES expression levels in late sepsis will result in improved murine and patient outcomes, it is possible that this will not be the case. However, irrespective of the direction of the association, we will capitalize on the FES expression results found in order to improve *in vitro*, *in vivo* outcomes. For example, if we find that low FES expression is associated with improved outcomes in early sepsis (contrary to our hypothesis), we will expand upon this finding by seeking to reduce FES expression in our models of early sepsis. Similarly, if–contrary to our expectations–we find that high FES expression is associated with improved outcomes in late sepsis, we will aim to increase FES expression in our models of late sepsis and evaluate changes in outcomes seen as a result of this shift in expression. Additionally, if FES expression plays no role in sepsis severity, it will allow us to rule out a potential regulator heavily involved in many aspects of sepsis, which will help to narrow in on true regulators of sepsis severity and outcomes. We expect that *FES* expression levels on microarray analysis can be used alone or in combination with other genetic features as a biomarker to determine the presence, stage, severity, and outcome of sepsis. The heterogeneity of sepsis presentation and progression has long posed a problem for determining which patients will benefit from specific therapies, and the appropriate timing of these interventions. If we find that FES expression differs between time points in the progression of septic illness (i.e., between early- *vs*. late-stage sepsis), these results may then be used in future studies to help with targeting treatments toward specific subsets of patients who may differentially benefit from therapeutic interventions applied at different time points.

Finally, we expect that two SNPs associated with differential FES expression will be useful as prognostic biomarkers to stratify patients with sepsis based on risk for adverse outcomes that are relevant to patients, with the potential predictive value to inform FES-targeted treatments based on risk.

An important note about the involvement of FES in the pathophysiology is the association of SNP rs4957796, located within an intron of the FER gene (Fps/Fes related tyrosine kinase), with reduced mortality from sepsis (42), and reduced incidence of bloodstream infections, but increased mortality in those who do develop a bloodstream infection (43). FES and FER share similar biological functions such as platelet aggregation (19), mast cell activation (13, 44) and signaling of the immunosuppressive cytokine IL-10 (13), an important signalling pathway known to limit inflammation, whose function may have differing important roles during early- (important to limit the overactivation of the immune system) and late-stage (contribution to characteristic late-stage immunosuppression) sepsis. These observations may suggest a partial explanation to the improved outcomes in patients containing the SNP, rs4957796 (42) as well as the observations surrounding bloodstream infections (43). This hints that the impact of FER and potentially FES is double-edged sword where it is crucial to have the right amount of expression at the right time to have protective effects and not exacerbate the illness. If true, this would suggest a problem that the application of precision medicine might be able to overcome.

Sepsis is a disease that is constantly under investigation to find an effective treatment because of the major consequences on human life and healthcare burden. Unfortunately, there has not been much success towards this aim; over 100 randomized clinical trials which identify a target, and directly modulate that target, have failed (45), suggesting a need for novel approaches to treating sepsis. Not only do we believe we have identified a novel target capable of regulating multiple aspects of sepsis pathophysiology, but also the timing of intervention. This lends itself to identifying FES as a treatable trait (46), where, depending on the timing of intervention and the levels of FES expression or activity, may result in a different approach to treating a patient's sepsis (upregulating FES expression or inhibiting FES activity).

Significance

Sepsis is one of the greatest healthcare problems worldwide, causing significant mortality and costing the Canadian healthcare system billions of dollars annually (4). Even among those who survive, sepsis is associated with long-term morbidities and reduced

quality of life (4, 47). This project will provide crucial insight into the pathophysiology underlying sepsis, laying the foundation for future work to manage the dangerous side effects of immunotherapy-based treatments, and study the effect of systemic FES inhibition on this vulnerable cohort.

Author contributions

BL, DM, and PG designed the study. BL and NJ wrote the study protocol. BL, NJ, KT, DM, JB, and PG reviewed and revised the manuscript. All authors contributed to the article and approved the submitted version.

Funding

Physician' Services Incorporated Foundation: Research Trainee Award- (GRANT # 2022-2744) providing funding in support of the first author stipend and additional funding to be used on reagents and publication costs.

Conflict of interest

The authors declare that the research was conducted in the absence of any commercial or financial relationships that could be construed as a potential conflict of interest.

Publisher's note

References

1. Rhee C, Jones TM, Hamad Y, Pande A, Varon J, O'Brien C, et al. Prevalence, underlying causes, and preventability of sepsis-associated mortality in us acute care hospitals. *JAMA Network Open* (2019) 2(2):e187571. doi: 10.1001/jamanetworkopen.2018.7571

2. Jarczak D, Kluge S, Nierhaus A. Sepsis-pathophysiology and therapeutic concepts. *Front Med (Lausanne)* (2021) 8:628302. doi: 10.3389/fmed.2021.628302

3. Gyawali B, Ramakrishna K, Dhamoon AS. Sepsis: The evolution in definition, pathophysiology, and management. *SAGE Open Med* (2019) 7:1–13. doi: 10.1177/2050312119835043

4. Farrah K, McIntyre L, Doig CJ, Talarico R, Taljaard M, Krahn M, et al. Sepsis-associated mortality, resource use, and healthcare costs: A propensity-matched cohort study. *Crit Care Med* (2021) 49(2):215–27. doi: 10.1097/CCM.0000000000004777

5. Mostel Z, Perl A, Marck M, Mehdi SF, Lowell B, Bathija S, et al. Post-sepsis syndrome - an evolving entity that afflicts survivors of sepsis. *Mol Med* (2019) 26(1):6. doi: 10.1186/s10020-019-0132-z

6. Gotts JE, Matthay MA. Sepsis: Pathophysiology and clinical management. *BMJ* (2016) 353:i1585. doi: 10.1136/bmj.i1585

7. Singer M, Deutschman CS, Seymour CW, Shankar-Hari M, Annane D, Bauer M, et al. The third international consensus definitions for sepsis and septic shock (Sepsis-3). *JAMA* (2016) 315(8):801–10. doi: 10.1001/jama.2016.0287

8. Nedeva C, Menassa J, Puthalakath H. Sepsis: Inflammation is a necessary evil. *Front Cell Dev Biol* (2019) 7:108. doi: 10.3389/fcell.2019.00108

9. Parsons SA, Greer PA. The Fps/Fes kinase regulates the inflammatory response to endotoxin through down-regulation of Tlr4, nf-κb activation, and tnf-α secretion in macrophages. *J Leukocyte Biol* (2006) 80(6):1522–8. doi: 10.1189/jlb.0506350

10. Zirngibl RA, Senis Y, Greer PA. Enhanced endotoxin sensitivity in Fps/Fes-null mice with minimal defects in hematopoietic homeostasis. *Mol Cell Biol* (2002) 22 (8):2472–86. doi: 10.1128/mcb.22.8.2472-2486.2002

11. Xu S, Liu X, Bao Y, Zhu X, Han C, Zhang P, et al. Constitutive mhc class I molecules negatively regulate tlr-triggered inflammatory responses Via the fps-Shp-2 pathway. *Nat Immunol* (2012) 13(6):551–9. doi: 10.1038/ni.2283

12. Clark SR, Ma AC, Tavener SA, McDonald B, Goodarzi Z, Kelly MM, et al. Platelet Tlr4 activates neutrophil extracellular traps to ensnare bacteria in septic blood. *Nat Med* (2007) 13(4):463–9. doi: 10.1038/nm1565

13. Greer P. Closing in on the biological functions of Fps/Fes and fer. *Nat Rev Mol Cell Biol* (2002) 3(4):278–89. doi: 10.1038/nrm783

14. Lei W, Liu D, Sun M, Lu C, Yang W, Wang C, et al. Targeting Stat3: A crucial modulator of sepsis. *J Cell Physiol* (2021) 236(11):7814–31. doi: 10.1002/jcp.30394

15. Clere-Jehl R, Mariotte A, Meziani F, Bahram S, Georgel P, Helms J. Jak-stat targeting offers novel therapeutic opportunities in sepsis. *Trends Mol Med* (2020) 26 (11):987–1002. doi: 10.1016/j.molmed.2020.06.007

16. Sangrar W, Senis Y, Samis JA, Gao Y, Richardson M, Lee DH, et al. Hemostatic and hematological abnormalities in gain-of-Function Fps/Fes transgenic mice are associated with the angiogenic phenotype. *J Thromb Haemost* (2004) 2(11):2009–19. doi: 10.1111/j.1538-7836.2004.00956.x

17. Simmons J, Pittet JF. The coagulopathy of acute sepsis. *Curr Opin Anaesthesiol* (2015) 28(2):227–36. doi: 10.1097/ACO.0000000000000163

18. Gattinoni L, Brazzi L, Pelosi P, Latini R, Tognoni G, Pesenti A, et al. A trial of goal-oriented hemodynamic therapy in critically ill patients. Svo2 collaborative group. *N Engl J Med* (1995) 333(16):1025–32. doi: 10.1056/NEJM199510193331601

19. Senis YA, Sangrar W, Zirngibl RA, Craig AW, Lee DH, Greer PA. Fps/Fes and fer non-receptor protein-tyrosine kinases regulate collagen- and adp-induced platelet aggregation. *J Thromb Haemost* (2003) 1(5):1062–70. doi: 10.1046/j.1538-7836.2003.t01-1-00124.x

20. McDonald B, Davis RP, Kim SJ, Tse M, Esmon CT, Kolaczkowska E, et al. Platelets and neutrophil extracellular traps collaborate to promote intravascular coagulation during sepsis in mice. *Blood* (2017) 129(10):1357–67. doi: 10.1182/blood-2016-09-741298

21. Shinde-Jadhav S, Mansure JJ, Rayes RF, Marcq G, Ayoub M, Skowronski R, et al. Role of neutrophil extracellular traps in radiation resistance of invasive bladder cancer. *Nat Commun* (2021) 12(1):2776. doi: 10.1038/s41467-021-23086-z

22. Koutroulis I, Batabyal R, McNamara B, Ledda M, Hoptay C, Freishtat RJ. Sepsis immunometabolism: From defining sepsis to understanding how energy production affects immune response. *Crit Care Explor* (2019) 1(11):e0061. doi: 10.1097/cce.0000000000000061

23. Fajgenbaum DC, June CH. Cytokine storm. *New Engl J Med* (2020) 383 (23):2255–73. doi: 10.1056/nejmra2026131

24. Boomer JS, To K, Chang KC, Takasu O, Osborne DF, Walton AH, et al. Immunosuppression in patients who die of sepsis and multiple organ failure. *JAMA* (2011) 306(23):2594. doi: 10.1001/jama.2011.1829

25. Karamanavi E, McVey DG, Laan SW, Stanczyk PJ, Morris GE, Wang Y, et al. The fes gene at the 15q26 coronary-Artery-Disease locus inhibits atherosclerosis. *Circ Res* (2022) 131(12):1004–17. doi: 10.1161/CIRCRESAHA.122.321146

26. Zhang X, Goncalves R, Mosser DM. The isolation and characterization of murine macrophages. *Curr Protoc Immunol* (2008) 14:14.1.1–14.1.14. doi: 10.1002/0471142735.im1401s83

27. Swamydas M, Lionakis MS. Isolation, purification and labeling of mouse bone marrow neutrophils for functional studies and adoptive transfer experiments. *J Vis Exp* (2013) 77):e50586. doi: 10.3791/50586

28. Leng SX, McElhaney JE, Walston JD, Xie D, Fedarko NS, Kuchel GA. Elisa And multiplex technologies for cytokine measurement in inflammation and aging research. *Biol Sci Med Sci* (2008) 63(8):879–84. doi: 10.1093/gerona/63.8.879

29. Bergmann CB, Beckmann N, Salyer CE, Hanschen M, Crisologo PA, Caldwell CC. Potential targets to mitigate trauma- or sepsis-induced immune suppression. *Front Immunol* (2021) 12:622601. doi: 10.3389/fimmu.2021.622601

30. Masuda S, Shimizu S, Matsuo J, Nishibata Y, Kusunoki Y, Hattanda F, et al. Measurement of net formation *in vitro* and *in vivo* by flow cytometry. *Cytometry A* (2017) 91(8):822–9. doi: 10.1002/cyto.a.23169

31. Nielsen SR, Strobech JE, Horton ER, Jackstadt R, Laitala A, Bravo MC, et al. Suppression of tumor-associated neutrophils by lorlatinib attenuates pancreatic cancer growth and improves treatment with immune checkpoint blockade. *Nat Commun* (2021) 12(1):3414. doi: 10.1038/s41467-021-23731-7

32. Shaffer JM, Smithgall TE. Promoter methylation blocks fes protein-tyrosine kinase gene expression in colorectal cancer. *Genes Chromosomes Cancer* (2009) 48 (3):272–84. doi: 10.1002/gcc.20638

33. Stortz JA, Raymond SL, Mira JC, Moldawer LL, Mohr AM, Efron PA. Murine models of sepsis and trauma: Can we bridge the gap? *ILAR J* (2017) 58(1):90–105. doi: 10.1093/ilar/ilx007

34. Starr ME, Steele AM, Saito M, Hacker BJ, Evers BM, Saito H. A new cecal slurry preparation protocol with improved long-term reproducibility for animal models of sepsis. *PloS One* (2014) 9(12):e115705. doi: 10.1371/journal.pone.0115705

35. Shrum B, Anantha RV, Xu SX, Donnelly M, Haeryfar SM, McCormick JK, et al. A robust scoring system to evaluate sepsis severity in an animal model. *BMC Res Notes* (2014) 7(1):233. doi: 10.1186/1756-0500-7-233

36. Li J-L, Li G, Jing X-Z, Li Y-F, Ye Q-Y, Jia H-H, et al. Assessment of clinical sepsis-associated biomarkers in a septic mouse model. *J Int Med Res* (2018) 46(6):2410–22. doi: 10.1177/0300060518764717

37. Barichello T, Sayana P, Giridharan VV, Arumanayagam AS, Narendran B, Della Giustina A, et al. Long-term cognitive outcomes after sepsis: A translational systematic review. *Mol Neurobiol* (2019) 56(1):186–251. doi: 10.1007/s12035-018-1048-2

38. Mostel Z, Perl A, Marck M, Mehdi SF, Lowell B, Bathija S, et al. Post-sepsis syndrome – an evolving entity that afflicts survivors of sepsis. *Mol Med* (2020) 26(1):1–14. doi: 10.1186/s10020-019-0132-z

39. Illendula M, Osuru HP, Ferrarese B, Atluri N, Dulko E, Zuo Z, et al. Surgery, anesthesia and intensive care environment induce delirium-like behaviors and impairment of synaptic function-related gene expression in aged mice. *Front Aging Neurosci* (2020) 12:542421. doi: 10.3389/fnagi.2020.542421

40. Muscedere J, Maslove D, Boyd JG, O'Callaghan N, Lamontagne F, Reynolds S, et al. Prevention of nosocomial infections in critically ill patients with lactoferrin (Prevail study): Study protocol for a randomized controlled trial. *Trials* (2016) 17 (1):474. doi: 10.1186/s13063-016-1590-z

41. [Dataset]. Available at: https://www.ncbi.nlm.nih.gov/geo/geo2r/?acc=GSE118657.

42. Rautanen A, Mills TC, Gordon AC, Hutton P, Steffens M, Nuamah R, et al. Genome-wide association study of survival from sepsis due to pneumonia: An observational cohort study. *Lancet Respir Med* (2015) 3(1):53–60. doi: 10.1016/s2213-2600(14)70290-5

43. Rogne T, Damås JK, Flatby HM, Åsvold BO, DeWan AT, Solligård E. The role of fer Rs4957796 in the risk of developing and dying from a bloodstream infection: A 23-year follow-up of the population-based nord-trøndelag health study. *Clin Infect Dis* (2021) 73(2):e297–303. doi: 10.1093/cid/ciaa786

44. Udell CM, Samayawardhena LA, Kawakami Y, Kawakami T, Craig AWB. Fer and Fps/Fes participate in a Lyn-dependent pathway from fcεri to platelet-endothelial cell adhesion molecule 1 to limit mast cell activation. *J Biol Chem* (2006) 281 (30):20949–57. doi: 10.1074/jbc.m604252200

45. Marshall JC. Why have clinical trials in sepsis failed? *Trends Mol Med* (2014) 20 (4):195–203. doi: 10.1016/j.molmed.2014.01.007

46. Maslove DM, Tang B, Shankar-Hari M, Lawler PR, Angus DC, Baillie JK, et al. Redefining critical illness. *Nat Med* (2022) 28(6):1141–8. doi: 10.1038/s41591-022-01843-x

47. Su Y-X, Xu L, Gao X-J, Wang Z-Y, Lu X, Yin C-F. Long-term quality of life after sepsis and predictors of quality of life in survivors with sepsis. *Chin J Traumatol* (2018) 21(4):216–23. doi: 10.1016/j.cjtee.2018.05.001

frontiers | Frontiers in Immunology

TYPE Original Research
PUBLISHED 02 May 2023
DOI 10.3389/fimmu.2023.1134556

OPEN ACCESS

EDITED BY
Dennis Nurjadi,
University Medical Center Schleswig-Holstein, Germany

REVIEWED BY
Xuanyou Liu,
University of Missouri, United States
Bo-tao Ning,
Shanghai Children's Medical Center, China

*CORRESPONDENCE
Yufeng Zhou
yfzhou1@fudan.edu.cn
Guoping Lu
13788904150@163.com

†These authors have contributed equally to this work

RECEIVED 30 December 2022
ACCEPTED 21 April 2023
PUBLISHED 02 May 2023

CITATION
Liu T, Zhang C, Ying J, Wang Y, Yan G, Zhou Y and Lu G (2023) Inhibition of the intracellular domain of Notch1 results in vascular endothelial cell dysfunction in sepsis. *Front. Immunol.* 14:1134556. doi: 10.3389/fimmu.2023.1134556

Inhibition of the intracellular domain of Notch1 results in vascular endothelial cell dysfunction in sepsis

Tingyan Liu[1†], Caiyan Zhang[1†], Jiayun Ying[1], Yaodong Wang[1], Gangfeng Yan[1], Yufeng Zhou[2,3*] and Guoping Lu[1*]

[1]Department of Critical Care Medicine, Children's Hospital of Fudan University, Shanghai, China, [2]Institute of Pediatrics, Children's Hospital of Fudan University, National Children's Medical Center, and the Shanghai Key Laboratory of Medical Epigenetics, International Co-laboratory of Medical Epigenetics and Metabolism, Ministry of Science and Technology, Institutes of Biomedical Sciences, Fudan University, Shanghai, China, [3]National Health Commission (NHC) Key Laboratory of Neonatal Diseases, Fudan University, Shanghai, China

Background: Notch signaling is critical for regulating the function of vascular endothelial cells (ECs). However, the effect of the intracellular domain of Notch1 (NICD) on EC injury in sepsis remains unclear.

Methods: We established a cell model of vascular endothelial dysfunction and induced sepsis in a mouse model *via* lipopolysaccharide (LPS) injection and cecal ligation and puncture (CLP). Endothelial barrier function and expression of endothelial-related proteins were determined using CCK-8, permeability, flow cytometry, immunoblot, and immunoprecipitation assays. The effect of NICD inhibition or activation on endothelial barrier function was evaluated *in vitro*. Melatonin was used for NICD activation in sepsis mice. The survival rate, Evans blue dye of organs, vessel relaxation assay, immunohistochemistry, ELISA, immunoblot were used to explore the specific role of melatonin for sepsis induced vascular dysfunction *in vivo*.

Results: We found that LPS, interleukin 6, and serum collected from septic children could inhibit the expression of NICD and its downstream regulator Hes1, which impaired endothelial barrier function and led to EC apoptosis through the AKT pathway. Mechanistically, LPS decreased the stability of NICD by inhibiting the expression of a deubiquitylating enzyme, ubiquitin-specific proteases 8 (USP8). Melatonin, however, upregulated USP8 expression, thus maintaining the stability of NICD and Notch signaling, which ultimately reduced EC injury in our sepsis model and elevated the survival rate of septic mice.

Conclusions: We found a previously uncharacterized role of Notch1 in mediating vascular permeability during sepsis, and we showed that inhibition of NICD resulted in vascular EC dysfunction in sepsis, which was reversed by melatonin. Thus, the Notch1 signaling pathway is a potential target for the treatment of sepsis.

KEYWORDS

NICD, vascular endothelial dysfunction, melatonin, LPS (lipopolysaccharide), sepsis

1 Introduction

Sepsis is a life-threatening disease contributing to global health loss (1). Sepsis-induced vascular dysfunction is pivotal to the pathobiology of sepsis and leads to septic shock and even multiple organ failure (2). Children suffering from septic shock exhibit higher mortality (3). Therefore, exploring the underlying molecular mechanisms of sepsis-induced vascular dysfunction could help to improve clinical outcomes in patients with sepsis. Over the past few years, treatments for septic shock have focused on early fluid resuscitation, application of vasoconstrictive drugs, removal of the inflammatory factor waterfall released in large quantities, immune modulation with glucocorticoids, and antimicrobial and endotoxin neutralization (4). However, these treatments often fail to reverse disease progression.

Vascular endothelial cells (ECs) are the primary cells that regulate vascular function (5, 6). As an important part of the blood vessel wall, ECs are the first cells to sense the damage induced by sepsis. For example, lipopolysaccharide (LPS) produced by pathogens and cytokines can directly cause EC injury and disrupt endothelial cytoskeletal proteins as well as intercellular junctions and adhesions, resulting in increased vascular EC permeability and the diversion of fluids into extravascular tissues, leading to edema. Upregulation of endothelial nitric oxide synthase in vascular ECs generates large amounts of nitric oxide, causing vasodilation and increased expression of inducible nitric oxide synthase. Sustained elevation of nitric oxide levels in the late phase of shock affects the function of vascular smooth muscle. Damaged vascular smooth muscle cells can further lead to impaired vascular responsiveness, which makes fluid resuscitation and vasopressor therapy ineffective (7). Therefore, strategies that ameliorate or even prevent endothelial dysfunction are essential for treating septic shock.

Notch1 signaling pathway is a conserved pathway that regulates vascular EC function (8). When the Notch1 receptor is bound by one of its ligands (such as DLL4, Jagged1), the Notch1 protein is sheared by specific enzymes into extracellular and intracellular segments. The intracellular segment region (Notch intracellular domain, NICD) is transported into the nucleus where it forms a complex with DNA-binding proteins, thereby derepressing target genes, especially Hes1, and allowing them to be transcriptionally activated to fulfil their biological roles. Given that the formation of NICD is the most critical event in the activation of the Notch1 signaling pathway, the cellular level of NICD reflects the activity of Notch1 signaling (9). Previous studies have revealed that activation of Notch1 directly regulates vascular barrier function in an engineered organotypic model (10). The reduction of endothelial Notch1 was identified as a predisposing factor for the onset of vascular inflammation and initiation of atherosclerosis (11). Furthermore, loss of Notch1 in adult endothelium increases hypercholesterolemia-induced atherosclerosis in the descending aorta (12). These findings indicate that Notch1 expression is downregulated in vascular cells in response to chronic inflammation during atherosclerosis. However, the significance of Notch1 signaling, especially NICD, in sepsis-induced vascular dysfunction is unknown.

Here, we report a previously uncharacterized role of Notch1 in mediating vascular permeability during sepsis. We found that levels of NICD and its downstream regulator Hes1 in ECs were reduced during sepsis, which further impaired vascular permeability *via* the Akt signaling pathway. We propose that LPS inhibits expression of a deubiquitylating enzyme USP8 to decrease the level of NICD. We also observed that melatonin mitigated sepsis-induced EC injury by upregulating USP8, thus stabilizing NICD, providing scientific support for the application of melatonin to treat sepsis. In summary, our study suggests that NICD in the Notch1 signaling pathway is a promising target for the treatment of sepsis.

Abbreviations: NICD, intracellular domain of Notch1; LPS, lipopolysaccharide; EC, endothelial cell;IL-6, interleukin 6; USP8, ubiquitin-specific proteases 8; TGN, tangeretin; PICU, pediatric intensive care unit; CLP, cecal ligation and puncture; DUBs, deubiquitinating enzymes.

2 Materials and methods

2.1 Ethical approval of participants

Blood samples were collected from six normal controls and children diagnosed with sepsis shock between January 2020 and December 2020 from the pediatric intensive care unit (PICU) of the Children's Hospital of Fudan University, China. Septic shock in children is defined as a severe infection that leads to cardiovascular dysfunction, including hypotension requiring treatment with vasoactive medication, or impaired perfusion (13). Blood collection was performed on the day of admission to the PICU, and samples were centrifuged at 400 g for 10 min to separate serum in the supernatant. Written informed consent was obtained from all participants. The study was approved by the Research Ethics Board in the Children's Hospital of Fudan University (IRB protocol number: 2020-424). General patient information and representative laboratory data are listed in Table 1.

2.2 Antibodies and reagents

The following primary antibodies were purchased from Cell Signaling Technology (Danvers, USA): anti-cleaved Notch1 (4147s; 1:1,000), anti-Hes1 (11988s; 1:1,000), p-eNOS (9570s, 1:1,000), eNOS (32027s, 1:1,000), iNOS (13120s,1:1,000), anti-AKT (4691s; 1:1,000), anti-phospho-AKT antibody (Ser473) (4060s; 1:1,000), anti-PTEN antibody (9559s; 1:1,000), anti-Actin antibody (4970s; 1:1,000), and anti-USP8 (11832s; 1:1,000). The following primary antibodies were obtained from Abcam (Waltham, USA): anti-USP11 (ab109232; 1:1,000), anti-VE-Cad antibody (ab33168; 1:1,000), and anti-Zo-1 antibody (ab216880; 1:1,000). LPS (L4516) and interleukin 6 (IL-6) were acquired from Sigma-Aldrich Merck KGaA (Germany). Melatonin and tangeretin (TGN) were purchased from Aladdin (purity >95%; Aladdin, China).

2.3 Cell culture

The human-derived vascular EC line (Ea.hy 926) was provided by the Cell Bank of the Chinese Academy of Sciences Shanghai Branch

TABLE 1 Characteristics of serum from septic shock children used for cell stimulation.

Patient No.	Age (months)	Gender	Pathogen	Infection source	IL-6 (pg/mL)	LPS (EU/mL)	PCIS score	Clinical outcome
1	19	Male	/	Central nervous system	0.0135	0.0254	84	Dead
2	33	Female	Acinetobacter baumannii	Abdominal	288.9	0.129	86	Alive
3	6	Male	/	Respiratory tract	131.5	<0.01	96	Alive
4	48	Female	Adenovirus	Respiratory tract	889.5	0.0309	90	Alive
5	23	Male	Methicillin resistant staphylococcus aureus	Skin	204.7	0.0135	90	Alive
6	108	Female	Acinetobacter baumannii	Respiratory tract	3164	0.0276	90	Dead
7	29	Female	/	Abdominal	34.76	0.0392	76	Alive

IL-6, interleukin-6; PCIS, Pediatrics Critical Illness Score.
/, culture-negative

(Shanghai, China). Cells were cultured in high glucose Dulbecco's modified Eagle's medium (DMEM) with 1% antibiotics (Hyclone, USA) and 10% fetal bovine serum (FBS) in an incubator at 37°C with 95%/5% air/CO_2. The authenticity of cell lines was confirmed by short tandem repeat (STR) profiling. All cell lines were passaged twice a week at a ratio of 1:4. For signaling studies, cells were cultured in serum-starved medium to avoid masking stimulation signals. All cell lines were regularly checked for morphological changes and the presence of mycoplasma. Only mycoplasma-negative cell lines were used in subsequent experiments.

2.4 Western blot analysis

For immunoblotting, total protein was extracted from cells using RIPA lysis buffer (Beyotime, China). The amount of protein was quantified using the BCA protein assay kit (Beyotime, China), and 20 μg of total protein was subjected to SDS–PAGE (10%, Bio-Rad) and then transferred to a PVDF membrane (Merck Millipore, Germany). The membrane was blocked with 5% skim milk for 1 h and subsequently incubated with the indicated primary antibodies overnight at 4°C. Horseradish peroxidase-conjugated anti-rabbit antibody (1:5,000) was utilized as the secondary antibody. Protein bands were visualized using a chemiluminescent HRP substrate (ThermoFisher, USA) and imaged with a Molecular Imager® ChemiDocTM XRS+ Imaging System (Bio-Rad).

2.5 Cell proliferation assay

Ea.hy 926 cells were seeded in 96-well culture plates at a density of 1×10^3/well and stimulated for 24 h according to the experimental requirements. The rate of cell proliferation was determined using the CCK8 assay (Dojindo, Japan). Cells were incubated for 1 h and tested every 24 h using a microplate reader at 450 nm.

2.6 Permeability assay

A classic Transwell chamber assay was conducted to evaluate EC permeability using fluorescence-labeled dextran (40 kDa, Sigma-Aldrich Merck KGaA, Germany) (14). The assay was performed in a 12-well plate using individual polycarbonate membrane inserts with a 0.4 μm pore (Corning, USA). Ea.hy 926 cells were seeded at a density of 1×10^5 cells/insert. The medium in both upper and bottom compartments was replaced with fresh medium 24 h after seeding, and cells were treated according to the indicated protocols. Inserts were transferred into a new plate containing 600 μL PBS, and 60 μg of fluorescence-labeled dextran (40 kDa) diluted in 300 μL PBS was then added to the upper compartment of the insert. Inserts were cultured for 1 h in the incubator, and then PBS from the lower chamber was transferred to a plate reader (BioTek, Synergy2) and measured (excitation: 480 nm; emission: 510 nm).

2.7 Wound healing assay

Ea.hy 926 cells seeded in 6-well cell culture plates were scraped by P10 tips and then incubated with serum-free medium. Images of wells under the same view were obtained using a Leica Microscope immediately and 24 h after scratch. The rate of cell migration, calculated as the average percent of wound closure, was determined using Image J.

2.8 Cell apoptosis assay

Cell apoptosis was determined using an AnnexinV-fluorescein isothiocyanate (FITC)/propidium iodide (PI) double-staining kit (BD Biosciences, USA), according to the manufacturer's instructions. Ea.hy 926 cells were cultured in 6-well plates (1×10^6 cells/well) for 24 h. After treatment with LPS and melatonin, the cells were digested with ethylenediaminetetraacetic acid (EDTA)-free trypsin, stained with AnnexinV-FITC and PI, and subjected to flow cytometry using FACSCanto™ II (BD Biosciences). FlowJo V10 software (Tree Star, USA) was used for data analysis. Cells that were negative for both Annexin V-FITC and PI were considered viable. Annexin V-FITC positive and PI negative cells were recognized as early apoptosis; Annexin V-FITC and PI positive cells were late apoptosis; and Annexin V-FITC negative and PI positive cells were necrotic cells.

Early and late apoptotic cells were used to calculate the percentage of apoptotic cells.

2.9 Plasmid and siRNA transfection

The expression plasmid containing NICD sequence (aa 1757-2555) was purchased from Genechem (China) and transfected into Ea.hy 926 cells using Lipofectamine 3000 reagents (Invitrogen, USA). Stable clones were selected using puromycin at a concentration of 2 μg/mL for two weeks. siRNA targeting USP8 and scramble control siRNA were purchased from RiboBio (China) and transfected using Lipofectamine 3000 reagent. The siRNA sequences were: si-USP8 1# (human) (5'-CTGGAACCTTTCGTTATTA-3'), si-USP8 2# (human) (5'- TCATCTCGATGACTTTAAA-3'), and si-USP8 3# (human) (5'-CTACGATGGCAGGTGGAAA-3'). The efficiency of si-USP8 transfection was evaluated using western blot analysis.

2.10 Ubiquitination and immunoprecipitation (IP) assay

Ea.hy 926 cells were lysed with 1% SDS in lysis buffer for the ubiquitination assay or RIPA lysis buffer for the IP assay. The cell lysates were diluted to 1 mg/mL and mixed with the indicated primary antibody and then incubated at 4°C overnight. Protein A/G magnetic beads were added to the lysate-antibody mixture and incubated for 2 h at room temperature. Western blot analysis was performed to detect ubiquitin modification or IP proteins as described above.

2.11 Quantitative real-time PCR

Total RNA from aortic tissue samples of mice was extracted using Trizol (Invitrogen, USA) following the manufacturer's protocol. A total of 1 μg RNA was reverse-transcribed into cDNA using the Primer Script RT reagent kit (Takara, Japan). *Gapdh* and *Actin* were used as endogenous standards. Triplicate PCR reactions were performed, and the relative expression levels were calculated using the $2^{-\triangle\triangle Ct}$ equation. The sequences of all primers are provided in Supplemental Table 1.

2.12 Assay for NICD stability

Ea.hy 926 cells were pretreated with 20 μM cycloheximide (CHX, Sigma-Aldrich Merck KGaA, Germany), an inhibitor of protein synthesis, and were collected at different time points (0, 2, 4, and 6 h) after indicated treatments. NICD expression was determined using Western blot analysis.

2.13 Animals

Male C57BL/6 mice aged 3-4 weeks were obtained from Shanghai Slake Laboratory Animal Company (China). All animals were housed at 25°C, with a 12-h light/12-h dark cycle under specific pathogen-free conditions and free to food and water. Experiments were conducted one week after the mice adapted to the new environment. The experimental protocols used in this study were approved by the Animal Studies Committee of the Children's Hospital of Fudan University (IRB protocol number: 2019-321).

2.14 Animal models and melatonin administration

For LPS-induced-sepsis models, mice were injected intraperitoneally with one dose of LPS at 10 mg/kg body weight, and saline was administered to the controls. For survival analysis, LPS at 15 mg/kg body weight was used for LPS-induced sepsis model. The mouse model of polymicrobial sepsis was induced by CLP as previously described (15). Mice were fasted for 12 h before surgery and were anesthetized with tribromoethanol. The midline laparotomy was performed after shaving the skin and disinfection, and 50% of the distal end of the cecum was ligated. A single through-and-through puncture was implemented using 22-gauge needles between the end of the cecum and the ligation site, and then a small amount of feces was squeezed out through the puncture. The cecum was returned to the abdominal cavity. Abdominal musculature and skin incision were closed with sutures. The animals undergoing laparotomy and cecum exposure without ligation and puncture were used as sham-operated controls. All mice were revived with 1 mL of saline.

Once the sepsis models were established, mice in the melatonin treatment group were injected intraperitoneally for LPS-induced sepsis mice and subcutaneously for CLP mice with melatonin dissolved in saline at a dose of 30 mg/kg, which was modified based on our pilot experiments and previous literature (16). Based on the half-time of melatonin *in vivo*, repeated administration of the drug was performed. All experiments were conducted three times.

2.15 Immunohistochemistry

Mice were sacrificed at 24 h post-surgery/LPS administration under anesthesia followed by blood and organ collection. Fresh aorta samples were first fixed in 4% paraformaldehyde and then embedded in paraffin. For immunohistochemistry assays, tissues were sectioned at 5 μm and then incubated in citrate antigen retrieval solution (pH = 6.8) for 15 min at 95°C. The sections were then stained with NICD antibody (Abcam) at 4°C overnight. Next, the sections were incubated with corresponding HRP-conjugated secondary antibodies (Absin, China) for 1 h at room temperature and were visualized using diaminobenzidine (Absin, China).

2.16 Enzyme-linked immunosorbent assay (ELISA)

Mouse serum was collected for cytokines detection using a mouse TNF-α ELISA kit (JL10484, Jianglai, Shanghai, China), a

mouse IL-6 ELISA kit (JL20268, Jianglai, Shanghai, China) and a mouse melatonin ELISA kit (JL10087, Jianglai, Shanghai, China) according to the manufacturer's instructions.

2.17 Measurement of lactate

Lactate levels in the serum of mice were determined using a lactate assay kit (Nanjing Jiancheng Bioengineering Institute, China) according to the manufacturer's instructions.

2.18 Endothelium-dependent relaxation function of vessels assay

The thoracic aorta was carefully dissected, cleaned of fat and adherent connective tissues, and then cut into 2–3 mm vessel rings and mounted on two stainless-steel stirrups in the 10 mL organ chamber of a Multi Myograph System (Danish Myo Technology (DMT), Aarhus, Denmark) containing 5 mL PSS (1000 mL contained 7.6 g NaCl; 0.35 g KCl; 0.29 g $MgSO_4$; 0.16 g KH_2PO_4; 1.25 g $NaHCO_3$; 1 g glucose; 0.01 g Na_2-EDTA; and 1.6 mL of 1 mol/L $CaCl_2$). The PSS was kept at 37°C and bubbled continuously with 95% O_2 and 5% CO_2. The vessel rings were stretched to a resting tension of 3.5 mN and equilibrated for 60 min with PSS buffer. After equilibration, the rings were stimulated twice with KPSS (1000 mL contained 4.37 g NaCl; 4.47 g KCl; 0.29 g $MgSO_4$; 0.16 g KH_2PO_4; 1 g $NaHCO_3$; 1 g glucose; 0.01 g Na_2-EDTA, and 1.6 mL of 1 mol/L $CaCl_2$) for 15 min. Vasodilatation was assessed by applying acetylcholine (Ach) (17). When a contractile plateau was reached after norepinephrine (10^{-9} to 10^{-5}M), concentration-response dilations to cumulative Ach (10^{-9} to 10^{-5}M) were performed. Doses were added every 3–5 min.

2.19 Evans blue assay for the permeability of vessels

0.5% Evans Blue dye (Solarbio, Beijing, China) was injected *via* a tail vein 30 min before the mice were killed. Subsequently, mice were perfused with PBS *via* the left ventricle to remove the intravascular dye. Lungs, livers, and hearts were removed and dried for 1 h. Evans blue dye was extracted in formamide by incubating tissues overnight at 55°C. Evans blue dye levels in tissue supernatant were measured by spectrophotometric analysis at 620 nm (18).

2.20 Statistical analysis

Statistical significance of the differences between groups was determined using the Student's t-test or one-way ANOVA plus Tukey's analysis using SPSS software (version 22.0) for comparisons of two groups or multiple groups, respectively. Kaplan-Meier survival analysis was utilized to compare survival rate between the sepsis group and treatment group. Data are presented as the mean ± standard error of the mean (SEM). $P < 0.05$ was considered statistically significant.

3 Results

3.1 NICD expression and activity are decreased *in vitro* models of sepsis

To investigate the effect of serum collected from children with sepsis on ECs, Ea.hy 926 cells were incubated with 10% septic serum in DMEM for 4 h. FBS and healthy serum at equal concentrations were used as controls (Figure 1A). Expression of NICD, the effector of Notch signaling, and its related proteins including Hes1, ADAM10, VE-Cad, iNOS, p-eNOS, and eNOS were detected using Western blot analysis. Compared to the control groups, cells cultured with septic serum displayed a notable decrease in the expression of NICD, Hes1, VE-Cad, and p-eNOS, whereas the expression of ADAM10 was not significantly altered. Furthermore, there was a substantial increase in the expression of iNOS in the cells treated with septic serum (Figures 1B, C). These results indicate that septic serum can downregulate the expression of NICD and its downstream molecules.

LPS and inflammatory cytokines, such as IL-6, in septic serum may play an essential role in inducing EC dysfunction. LPS and IL-6 have been utilized to induce *in vitro* models of sepsis in cultured ECs (19, 20). Therefore, we investigated whether LPS and IL-6 could alter the expression of NICD, Hes1, and VE-Cad. We found that NICD, Hes1, and VE-Cad expression in Ea.hy 926 cells were reduced by LPS (Figures 1D–G) or IL-6 (Figures 1H–K) in a concentration- and time-dependent manner. These results suggest that septic serum, LPS, and IL-6 can inhibit NICD and its downstream signaling molecules.

3.2 Inhibition of NICD impairs the endothelial barrier and leads to EC injury

To explore the role of NICD in endothelial barrier function, Ea.hy 926 cells were treated with TGN, a flavonoid that can inhibit the Notch signaling pathway (21). Consistent with a previous study (22), we found that TGN inhibited protein expression of NICD, Hes1, and VE-Cad in a concentration-dependent manner (Figures 2A, B), which was similar to the results of Ea.hy 926 cells treated with LPS or IL-6. Next, we analyzed the impact of LPS and TGN on endothelial barrier function and found that both TGN and LPS impaired cell proliferation (Figure 2C), promoted cell apoptosis (Figure 2D), increased cell permeability (Figure 2E) and inhibited cell migration (Figure 2F), increased the levels of cleaved PARP (an apoptosis indicator protein) and decreased Zo-1 expression (cell junction protein) in Ea.hy 926 cells (Figures 2G, H). These results demonstrate that NICD and Notch signaling are critical in regulating EC functions.

Since Akt signaling is known for maintaining endothelial barrier function (23), we further investigated if the Akt signaling pathway was involved in Notch signaling in our sepsis model. We

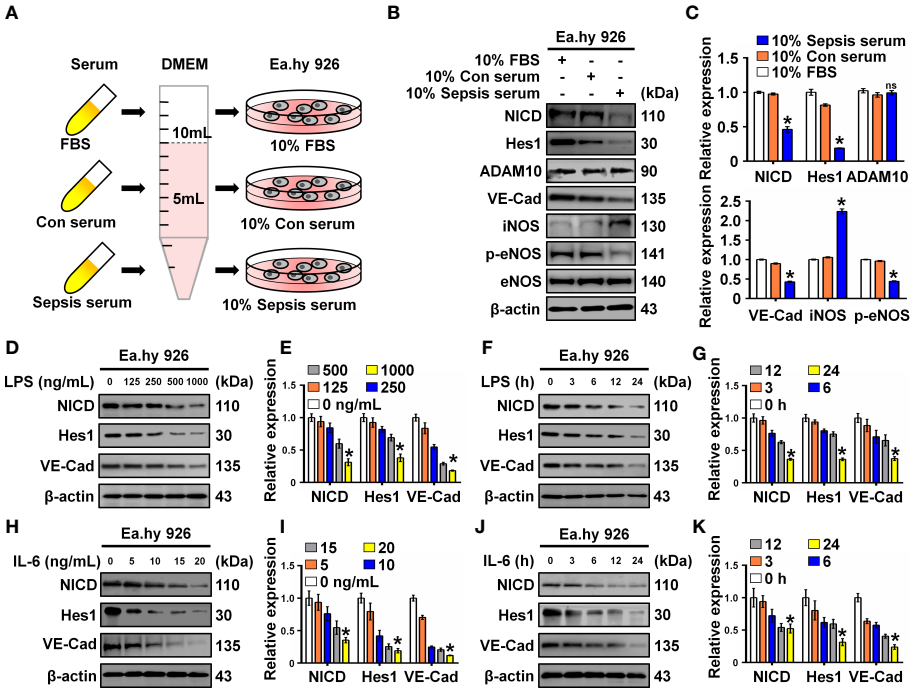

FIGURE 1
Serum from sepsis patients, LPS and IL-6 inhibit Notch signaling. **(A)** FBS, control, and sepsis serum were collected to treat Ea.hy 926 cells. **(B, C)** The expression of NICD, Hes1, ADAM10, VE-Cad, iNOS, p-eNOS, and eNOS in Ea.hy 926 cells were tested by Western blot after treating with the collected serum for 4 (h) Representative images **(B)** and three experiments replicates **(C)** were displayed. **(D, E)** The levels of NICD, Hes1 and VE-Cad were detected by Western blot in Ea.hy 926 cells stimulated with the indicating concentration of LPS for 24 (h) Representative images **(D)** and three experiments replicates **(E)** were displayed. **(F, G)** The expression of NICD, Hes1 and VE-Cad were detected by Western blot in Ea.hy 926 cells stimulated with 1000 ng/mL LPS for indicating time. Representative images **(F)** and three experiments replicates **(G)** were displayed. **(H, I)** The expression of NICD, Hes1 and VE-Cad were quantified by Western blot in Ea.hy 926 cells stimulated with the indicating concentration of IL-6 for 24 (h) Representative images **(H)** and three experiments replicates **(I)** were displayed. **(J, K)** The levels of NICD, Hes1 and VE-Cad were quantified by Western blot in Ea.hy 926 cells stimulated with 20 ng/ml IL-6 for indicating time. Representative images **(J)** and three experiments replicates **(K)** were displayed. Data are shown as the mean ± SEM. ns, no significance; $*p < 0.05$.

found that p-AKT was decreased while PTEN, a negative regulator of p-AKT, was increased in cells treated with TGN, LPS or IL-6 (Figures 2I, J; Supplementary Figures 1 A, B), suggesting that the damage to EC function resulting from sepsis was likely mediated by the AKT pathway.

3.3 Overexpression of NICD alleviates LPS-induced endothelial dysfunction

To determine whether NICD overexpression could reverse or alleviate LPS-induced endothelial dysfunction, we overexpressed NICD in the Ea.hy 926 cells and confirmed the overexpression using Western blot analysis (Figures 3A, B). We found that NICD overexpression reversed the reduced cell viability and elevated cell apoptosis induced by LPS treatment (Figures 3C, D). Furthermore, the increased intercellular permeability and impaired cell migration caused by LPS were alleviated following NICD overexpression (Figures 3E, F). Subsequently, expression of NICD downstream genes including Hes1, VE-Cad, and Zo-1, and Akt signaling pathway molecules, such as p-AKT and PTEN, were restored following NICD overexpression (Figures 3G, H). These data demonstrate that NICD overexpression can alleviate EC dysfunction induced by LPS.

3.4 Melatonin alleviates LPS-induced endothelial dysfunction by upregulating NICD and activating AKT signaling

It was reported that melatonin could improve the soluble Aβ1-42-induced impairment of spatial learning and memory *via* the Notch1/Hes1 signaling pathway (24). Therefore, we assayed expression of NICD in Ea.hy 926 cells treated with increasing concentrations of melatonin (0, 1, 10, 100 μM). We found that melatonin upregulated the expression of NICD and activated AKT signaling in the Ea.hy 926 cells (Figures 4A, B). To investigate the effect of melatonin on EC function, we first treated cells with LPS for 24 h and then with melatonin for 4 h. We found melatonin ameliorated the alterations in both cell proliferation (Figure 4C) and cell apoptosis (Figure 4D) of Ea.hy 926 cells stimulated with LPS. We also observed that melatonin significantly decreased intercellular permeability and promoted cell migration induced by LPS (Figures 4E, F). Moreover, melatonin reversed the effects of LPS on cleaved PARP, as well as the changes in Hes1, VE-Cad, Zo-1,

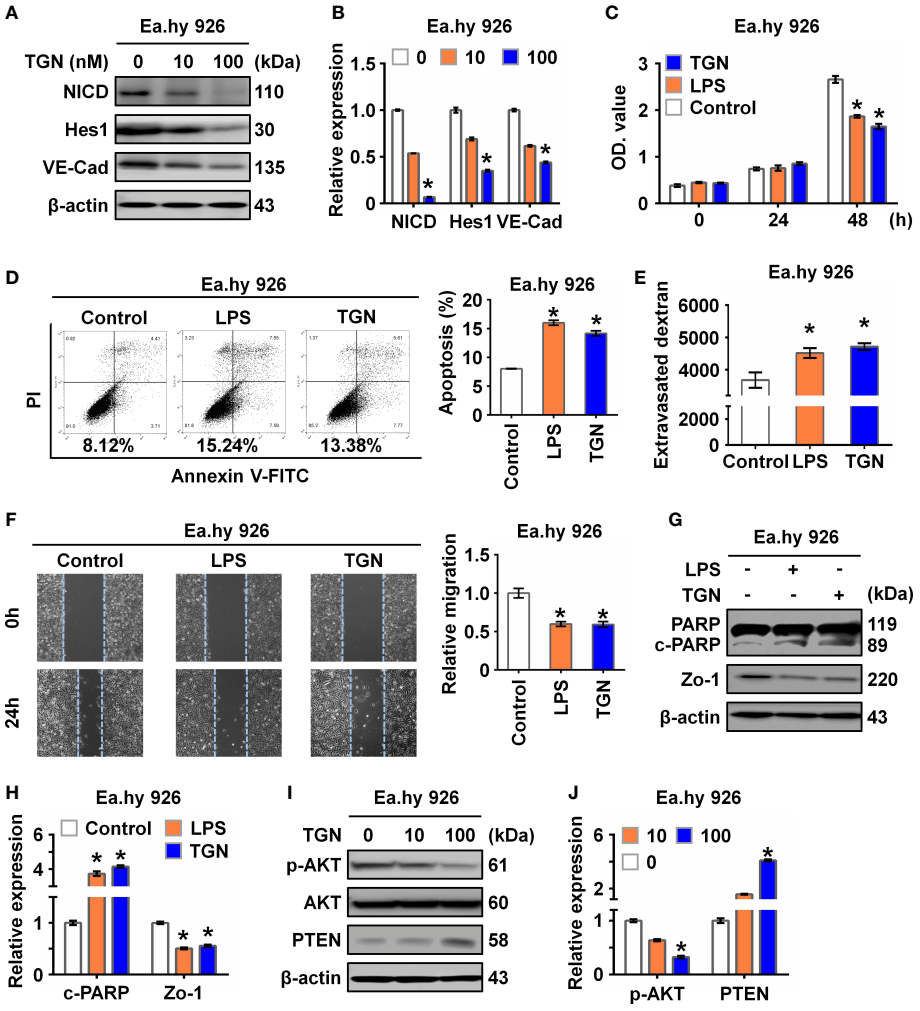

FIGURE 2
Inhibition of NICD impairs endothelial function. **(A, B)** The expression of NICD, Hes1, and VE-Cad in Ea.hy 926 cells were tested by Western blot after treating with different concentrations of TGN for 24 (h) Representative images **(A)** and three experiments replicates **(B)** were displayed. **(C)** CCK8 assay was used to evaluate the proliferation of Ea.hy 926 cells treated with LPS and TGN for 24 (h) **(D)** The apoptosis of Ea.hy 926 cells regulated by LPS or TGN was tested with Annexin V-FITC/PI staining by flow cytometry. **(E)** The endothelial permeability was determined by the transwell assay after being treated with LPS and TGN for 24 (h) Quantitative analysis was performed by measuring FD40 fluorescence intensity relative to the control. **(F)** The migration of Ea.hy 926 cells was tested by wounding healing assay after being treated with LPS and TGN for 24 (h) The percentage of wound closure was determined at 0 h and 24 (h) Representative microscopic cell images (F-left) immediately after wound creation and 24 h later and statistical analysis of migration **(F)**-right) were shown. **(G, H)** The expression of cleaved PARP and Zo-1 were tested by western blot in LPS-induced Ea.hy 926 cells with or without TGN. Representative images **(G)** and three experiments replicates **(H)** were displayed. **(I, J)** The protein levels of PTEN and p-AKT were tested in Ea.hy 926 cells treated with indicated concentration of TGN. The data were obtained from three independent experiments. Data are shown as the mean ± SEM. $*p < 0.05$.

PTEN, and p-AKT expression (Figures 4G, H). These results reveal that melatonin can alleviate LPS-induced endothelial dysfunction by increasing cellular levels of NICD and activating AKT signaling.

3.5 LPS decreases NICD stability through downregulating USPexpression

NICD is an intracellular domain protein generated by the cleavage activity of ADAM10 in the Notch pathway. We found that ADAM10 expression was not altered by LPS treatment (Figure 1B). Thus, we hypothesized that LPS likely promotes ubiquitination of NICD to affect its stability. As expected, we observed that LPS increased the ubiquitination of NICD, which was inhibited by melatonin (Figure 5A; Supplementary Figure 2A). Several studies have reported that NICD is highly ubiquitinated and regulated by deubiquitinating enzymes (DUBs) (25, 26). We investigated a series of deubiquitinating enzymes in Ea.hy 926 cells using RT-qPCR and observed that the mRNA levels of USP8 and USP11 decreased more than 2-fold in the LPS-treated cells compared with control cells (Figure 5B). Furthermore, Western blot data showed that USP8, but not USP11, was downregulated by LPS treatment (Figure 5C; Supplementary Figure 2B). We speculated that USP8 could interact with NICD to modulate NICD levels at the

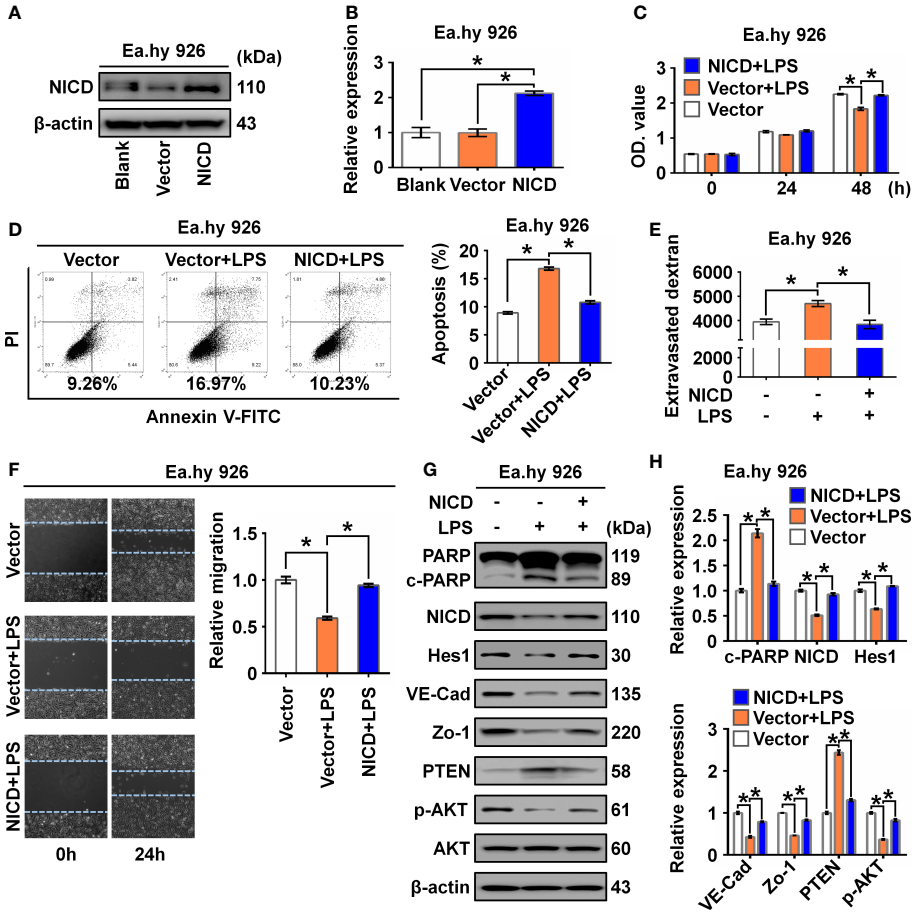

FIGURE 3
Overexpression of NICD reversed LPS-caused endothelial dysfunction. **(A, B)** The expression of NICD in Ea.hy 926 cells was tested by Western blot after transfected with blank plasmids, vector or NICD plasmids. Representative images **(A)** and three experiments replicates **(B)** were displayed. **(C)** CCK8 assay was used to evaluate the proliferation of Ea.hy 926 cells treated with the indicated conditions. **(D)** The apoptosis of Ea.hy 926 cells treated with indicated conditions was tested with Annexin V-FITC/PI staining by flow cytometry. Representative images **(D)**-left) and statistical analysis of apoptosis **(D)**-right) for Ea.hy 926 cells transfected by blank plasmids, vector or NICD plasmids after LPS treatment were shown. **(E)** The endothelial permeability was determined by the transwell assay after being treated with the indicated conditions. **(F)** The migration of Ea.hy 926 cells was tested by wounding healing assay. Representative images **(F)**-left) and statistical analysis of migration **(F)**-right) for Ea.hy 926 cells transfected by blank plasmids, vector or NICD plasmids after LPS treatment were shown. **(G, H)** The protein levels of cleaved PARP, NICD, Hes1, VE-Cad, Zo-1, PTEN, and p-AKT was tested in LPS-treated Ea.hy 926 cells with or without NICD-transfected. Representative images **(G)** and three experiments replicates **(H)** were displayed. The data were obtained from three independent experiments. Data are shown as the mean ± SEM. *$p < 0.05$.

post-translational stage. The interaction between endogenous NICD and USP8 was validated by IP assays (Figure 5D, Supplementary Figure 2C).

Next, we knocked down USP8 expression in Ea.hy 926 cells using siRNA, which resulted in decreased expression of NICD (Figure 5E; Supplementary Figure 2D). To further confirm the function of USP8 in terms of NICD stabilization, Ea.hy 926 cells transfected with negative control siRNA or si-USP8 were treated with CHX for the indicated times (Figure 5F; Supplementary Figure 2E). Compared with the presence of USP8, the half-life of endogenous NICD was significantly shortened in USP8 knockdown cells (Figure 5G). To verify whether si-USP8 inhibited the stability of NICD by increasing NICD ubiquitination, we measured the ubiquitination of NICD in Ea.hy 926 cells with or without si-USP8 transfection. NICD exhibited more pronounced ubiquitination in the USP8 knockdown cells, and the LPS-induced ubiquitination of NICD was rescued by melatonin, regardless of USP8 expression (Figures 5H, I; Supplementary Figures 2F, G). In summary, these data demonstrate that LPS decreases the stability of NICD through downregulating the expression of USP8.

3.6 Melatonin attenuates sepsis-induced endothelial dysfunction *in vivo*

To verify the functional effects of melatonin on vascular ECs in sepsis *in vivo*, we intraperitoneally injected LPS and used the CLP method to establish two sepsis models (27). In the LPS-induced sepsis model, the C57BL/6 mice were divided into three groups: Control, LPS with saline (M-), and LPS with melatonin (M+). Both saline and melatonin were injected every 2 h (Figure 6A), respectively. C57BL/6 mice in the CLP group were divided into four groups: Control, Sham, CLP with saline (M-), and CLP with melatonin (M+). Saline and melatonin were injected 0.5 h before

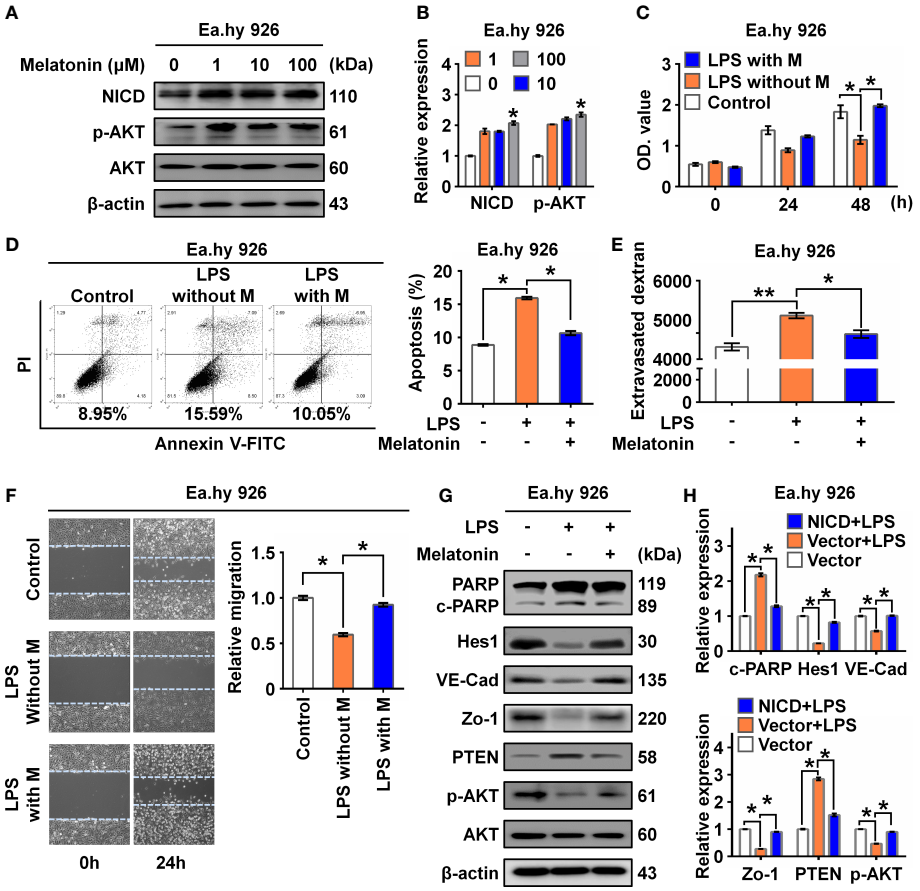

FIGURE 4
Melatonin alleviated LPS-induced endothelial dysfunction. **(A, B)** The level of NICD and p-AKT in Ea.hy 926 cells treated with indicated concentrations of melatonin were tested with Western blot. Representative images **(A)** and three experiments replicates **(B)** were displayed. **(C)** CCK8 assay was used to evaluate the proliferation of Ea.hy 926 cells treated with the control, LPS without melatonin or LPS with melatonin for indicated time. **(D)** The apoptosis of Ea.hy 926 cells treated with indicated conditions tested with Annexin V-FITC/PI staining by flow cytometry. Representative images **(D)**-left) and statistical analysis of apoptosis **(D)**-right) for Ea.hy 926 cells treated with the control, LPS without melatonin or LPS with melatonin were shown. **(E)** The endothelial permeability was determined by the transwell assay after being treated with the control, LPS without melatonin or LPS with melatonin. **(F)** The migration of Ea.hy 926 cells was tested by wounding healing assay after being treated with the control, LPS without melatonin or LPS with melatonin. Representative images **(F)**-left) and statistical analysis of migration **(F)**-right) of Ea.hy 926 regulated by indicated treatment were shown. **(G, H)** The protein levels of cleaved PARP, Hes1, VE-Cad, Zo-1, PTEN, and p-AKT were tested in LPS-treated Ea.hy 926 cells with or without melatonin. Representative images **(G)** and three experiments replicates **(H)** were displayed. The data were obtained from three independent experiments. Data are shown as the mean ± SEM. $*p < 0.05$. $**p < 0.01$.

CLP surgery, just after surgery, and 4 h and 8 h after surgery (Figure 6B). To examine changes in endothelium-dependent vasodilation in septic mice, the responses of arteries to acetylcholine (Ach) were measured. Compared with the control group, thoracic aorta vasodilation was significantly reduced in septic mice (Figures 6C, D), which were improved by melatonin treatment. To investigate whether melatonin contributes to vascular barrier function of septic mice, we examined EC permeability by measuring Evans Blue dye (EBD) penetration into tissues (liver, lung and heart). Our data showed that melatonin obviously reduced sepsis-induced vascular permeability as evidenced by the decreased penetration of EBD in liver and lung (Figures 6E, F), but not heart (Figure 6G). Of note, We observed that melatonin significantly rescued the death of septic mice, compared with vehicle-treated septic mice (Figures 6H, I). In addition, sepsis significantly increased serum levels of lactate, TNF-α and IL-6, which were effectively decreased by melatonin administration (Figures 6J, K, 7A–D). The aortic mRNA levels of TNF-α and IL-6 were also obviously upregulated in LPS injection (Supplementary Figures 3A, B) and CLP group (Supplementary Figures 3C, D). Next, aortas were isolated to detect the level of NICD using immunohistochemistry and protein levels of NICD, USP8, Hes1, VE-Cad, and p-AKT in indicated groups by immunoblotting. As shown in Figures 7E, F, sepsis decreased NICD in the aortas, which were rescued by melatonin treatment. Immunoblotting results showed that melatonin recovered the expression of NICD, USP8, Hes1, VE-Cad, and p-AKT in aorta tissues of septic mice (Figures 7G, H). Similarly, sepsis-induced downregulation of NICD and its downstream molecules were rescued by melatonin (Figures 7I, J). These data suggest that melatonin could be used to attenuate sepsis-induced endothelial dysfunction and promote the survival rate.

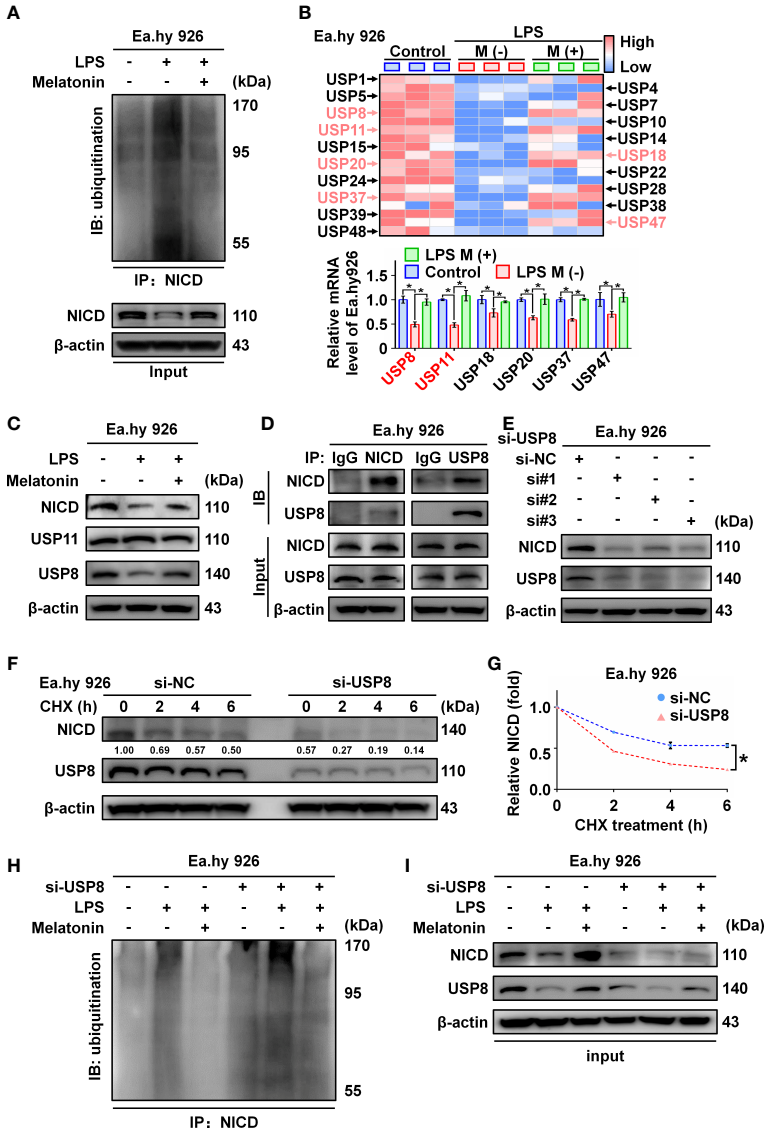

FIGURE 5
The ubiquitination of NICD was regulated by USP8. **(A)** Ubiquitinated NICD measured by immunoprecipitation with anti-NICD antibody and immunoblotting with anti-ubiquitin antibody in LPS treated Ea.hy 926 cells with or without melatonin. **(B)** The mRNA expression of a series of DUBs in Ea.hy 926 cells was tested by real-time qPCR. **(C)** The protein expression of USP8 and USP11 was detected by western blot in LPS-treated Ea.hy 926 cells with or without melatonin. **(D)** The interaction of NICD and USP8 in Ea.hy 926 cells was detected using Co-immunoprecipitation. **(E)** The expression of NICD and USP8 in Ea.hy 926 cells transfected with different USP8 siRNA. Scramble siRNA was used as negative control (si-NC). **(F, G)** The stability of NICD was tested in Ea.hy 926 cells transfected without or with si-USP8 at the indicated time after CHX (20 μM) treatment **(F)**. The quantitative analysis of **(G)** with Image J. **(H, I)** The ubiquitination of NICD in Ea.hy 926 cells with indicated treatment through NICD immunoprecipitation **(H)** and input **(I)**. Data are shown as the mean ± SEM. *$p < 0.05$. ns, no significance.

4 Discussion

In this study, we found that LPS, IL-6, or septic serum could inhibit NICD and its downstream signaling molecules, resulting in impaired endothelial barrier function and EC apoptosis. Mechanistically, LPS decreased the stability of NICD through downregulating the expression of USP8. Overexpression of NICD or the application of the NICD-activating drug melatonin alleviated LPS-induced endothelial dysfunction. The therapeutic effects of melatonin on endothelial dysfunction in sepsis were mediated by upregulating USP8 expression and inhibiting NICD degradation, maintaining the stability of Notch signaling. Therefore, melatonin could be used to treat sepsis-mediated endothelial dysfunction by targeting NICD.

Endothelial dysfunction is a critical event in the pathophysiology of sepsis, which can lead to organ failure by enhancing vascular permeability, fomenting coagulation cascade activation and tissue edema, and compromising organ perfusion. Notch receptors seemingly play opposite roles in the endothelium and a majority of research has focused on the expression of Notch but not NICD, which is the functional downstream molecule of Notch activation. Numerous studies have shown that Notch activity in ECs is necessary to maintain endothelial barrier function and smooth muscle contractile phenotype, mainly through synergistic

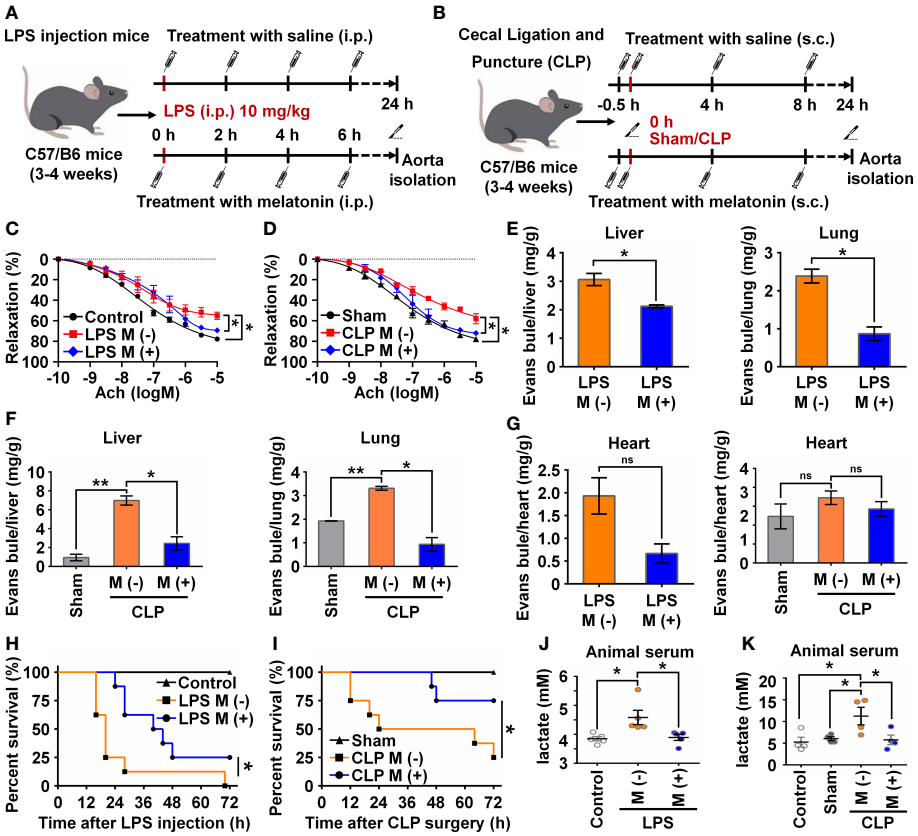

FIGURE 6
Melatonin attenuated sepsis-induced endothelial dysfunction. **(A, B)** Animal experiment flow chart in LPS group **(A)** and CLP group **(B)**. **(C, D)** The endothelium-dependent relaxation function of vessels was measured in LPS group treated without or with melatonin **(C)** and in CLP group treated without or with melatonin **(D)**. **(E)** Evans blue experiment in LPS group treated without or with melatonin was analyzed to test the vascular permeability function of liver (left) and lung (right). **(F)** Evans blue experiment in CLP group treated without or with melatonin was analyzed to test the vascular permeability function of liver (left) and lung (right). **(G)** Evans blue experiment in LPS group (left) and CLP group (right) treated without or with melatonin was analyzed to test the vascular permeability function of heart. **(H, I)** The survival rate of LPS group **(H)** and CLP group **(I)** treated with or without melatonin was analyzed (n=8 in each group). **(J, K)** The serum lactate level in LPS group **(J)** and CLP group **(K)** was tested by a lactic acid assay kit. Data are shown as the mean ± SEM. $*p < 0.05$. $**p < 0.01$. ns, no significance.

interactions with other pathways to coordinate vascular morphogenesis, differentiation, and function. *In vitro* experiments have shown that overexpression of the Notch ligand Jagged1 can promote EC proliferation (28), and activation of the Notch4 receptor can inhibit EC apoptosis (29). Notch signaling can also influence the kinetics of VE-Cad in retinal blood vessels (30).

To investigate the role of the Notch1 signaling pathway in sepsis-induced vascular injury, we used a Notch1 receptor-targeted drug, TGN, to inactivate the Notch1 signaling pathway. Previous studies have shown that TGN can inhibit the expression of Notch1, Hes1, and Hey1 in tumor cells but does not affect the expression levels of Notch2 and Notch3 (31). NICD and Hes1 expression were significantly decreased by TGN in this study. Furthermore, vascular EC injury caused by TGN was similar to that of LPS-induced vascular EC injury, indicating that downregulation of the Notch1 signaling pathway is involved in LPS-induced vascular EC injury. Patenaude et al. revealed that the inhibition of Notch signaling could lead to the loss of functional blood vessels, reducing endothelial carbon monoxide and nitrogen synthetase production and further inhibiting tumor growth and angiogenesis (32). Previous reports and our study consistently showed that inactivation of the Notch1 signaling pathway in vascular EC could lead to endothelial dysfunction, suggesting that LPS induces vascular endothelial injury through downregulating the Notch1 signaling pathway.

Yet the multi-function of Notch signaling in the same disease, even in the same cell is undeniable. For example, EC junctional integrity is impaired not only upon loss of Notch function but also due to sustained overactivation of endothelial Notch1. There are also conflicting data regarding the role of endothelial Notch and inflammation. On one hand, it has been reported that endothelial Notch activity reduces inflammation and is protective against atherosclerosis. In contrast, endothelial Notch signaling leads to higher expression of proinflammatory mediators, and inhibition of Notch reduces inflammation (33). In addition, Bai et al. found that the levels of Notch signaling molecules, including Notch1, Notch2, Hes1, and NICD, were increased in LPS-induced sepsis. Correcting the dysregulated Notch signaling pathway can rescue mice organ dysfunction and reduce inflammatory factor release (34). A likely explanation for the opposite expressions of NICD in macrophages and ECs during sepsis may be attributed to different Notch signaling downstream targets.

10.3389/fimmu.2023.1134556

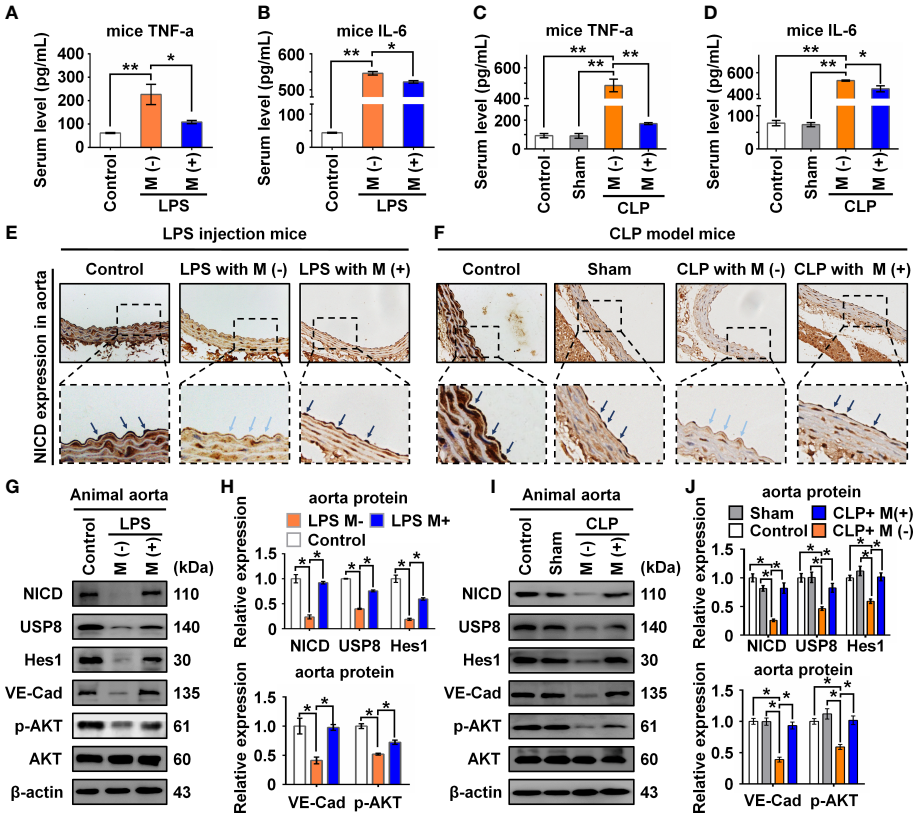

FIGURE 7
Melatonin attenuated sepsis-induced NICD downregulation in sepsis mice. **(A, B)** The serum levels of TNF-α **(A)** and IL-6 **(B)** in mice with the indicated treatment in LPS injection mice were detected by ELISA. **(C, D)** The serum levels of TNF-α **(C)** and IL-6 **(D)** in mice with the indicated treatment in CLP group were detected by ELISA. **(E, F)** Representative images of NICD expression in aorta tissues were detected by immunohistochemistry with indicated treatment in LPS group **(E)** and CLP group **(F)**. **(G, H)** The expression of NICD, USP8, Hes1, VE-Cad, and p-AKT in LPS group in aorta tissues were tested using Western blot analysis. Representative images **(G)** and three experiments replicates **(H)** were displayed. **(I, J)** The expression of NICD, USP8, Hes1, VE-Cad, and p-AKT in CLP group mice aorta tissues were tested using Western blot analysis. Representative images **(I)** and three experiments replicates **(J)** were displayed. Data are shown as the mean ± SEM. $*p < 0.05$. $**p < 0.01$.

Here, we showed that the Notch1 signaling pathway was activated by overexpressing NICD in vascular ECs. Overexpression of Notch4 in ECs has also been shown to upregulate anti-apoptotic proteins to inhibit apoptosis induced by LPS. However, the effect of LPS on Notch4 expression in ECs was not mentioned. A similar study suggested that NICD could resist LPS-induced apoptosis of ECs. Further, while some studies detected the expression of the Notch receptor in LPS-treated vascular ECs, activation of the entire Notch signaling pathway was not reported. The innovation of this current study was to determine the activated form of Notch1 and its downstream effector molecules.

The Akt pathway has been associated with several human diseases and is mainly responsible for the response to extracellular signals, cell metabolism, proliferation, survival, and angiogenesis (23). In this study, we found that the Notch1 signaling pathway regulated the phosphorylation of Akt, which is mainly controlled by PI3K, PDK1, and PDK2. In addition, as a negative regulator of the Akt signaling pathway, PTEN can dephosphorylate PIP3, which is produced by PI3K, and Akt cannot be translocated to the cell membrane, making it accessible to phosphorylation (35). In this study, we found that the Notch1 signaling pathway negatively regulated PTEN expression and affected the phosphorylation level of Akt.

Melatonin is an endogenous compound in the human body that shares an amino acid sequence homologous to melatonin in cyanobacteria. Melatonin can also be used as a dietary supplemented (36). As a soluble substance, melatonin readily crosses cell membranes, binds to melatonin receptors in cells, and exerts various biological functions (37). Melatonin is metabolized rapidly, so melatonin is very safe at high doses with no significant clinical side effects. Studies have shown that melatonin can improve organ function and survival rate in various models of sepsis (38). Melatonin has been shown to improve hemodynamics in rats with endotoxemia by scavenging TNF-α in the plasma, nitric oxide synthase in the liver, and oxygen free radicals in the aorta (39). In a mouse model of sepsis, melatonin can alleviate blood-brain barrier dysfunction and brain edema through the SIRT-1 pathway (40). In the past, many studies have focused on melatonin's anti-inflammatory and anti-oxidant effects on vascular ECs, but melatonin can also act as an inhibitor of the ubiquitin-proteasome system (41). We proposed that melatonin enhances the continuous expression of NICD and its downstream signaling

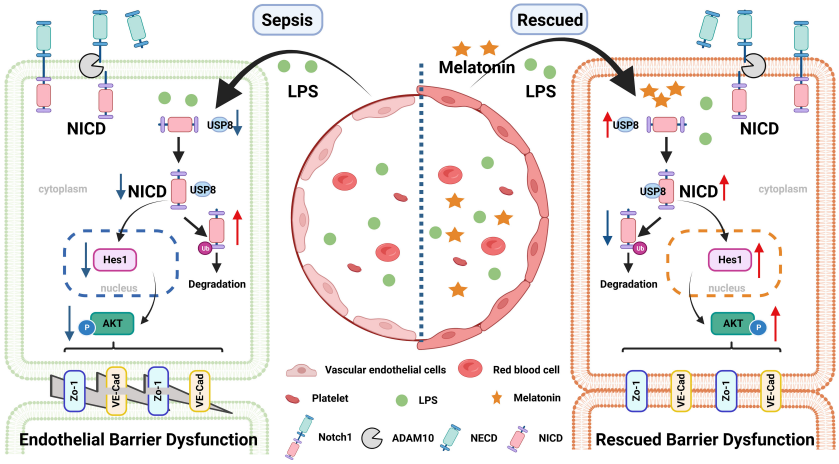

FIGURE 8
A pattern schematic created with BioRender. LPS promotes the ubiquitination of NICD by downregulating the level of USP8 to induce endothelial cell dysfunction in sepsis, which is rescued by melatonin.

molecules by inhibiting NICD ubiquitination. Consistent with our expectation, we observed that melatonin inhibited NICD ubiquitination and restored the decreased expression of USP8 induced by LPS, thus maintaining the stability of the Notch signaling pathway. USP8 has been suggested to exert protective effects against LPS-induced cognitive and motor deficits in mice by modulating microglial phenotypes *via* TLR4/MyD88/NF-κB signaling (42). However, the molecular mechanisms by which LPS regulates USP8 remain unknown. Considering that the mRNA levels of *Usp8* were downregulated in response to LPS, we hypothesized that post-transcriptional RNA modifications, such as m6A RNA methylation, could be involved in regulating *Usp8* levels. It has been demonstrated that methyltransferase-like 14-induced m6A modification participates in the regulation of USP48 in hepatocellular carcinoma by maintaining *Usp48* mRNA stability (43). Although emerging evidence has implicated a role for m6A modification in sepsis (44, 45), whether m6A modification directly associates with *Usp8* requires further exploration. In summary, our findings provide new insight into the molecular mechanisms by which melatonin improves sepsis-induced vascular injury, expanding our knowledge of melatonin in treating sepsis.

Since the Notch1 signaling pathway is essential to embryonic growth and development, complete or conditional knockout will cause high mortality in homozygous mice. As such, Notch1 knockout mice were not used in our study to verify the mechanism of Notch1 in vascular ECs *in vivo*. Notch1 knockdown has been limited to only *in vitro* experiments in previous studies, and Notch1 knockdown has not been reported in mice or animal models. In future studies, we plan to overexpress the NICD protein *via* an AAV approach that targets blood vessels to construct NICD conditional knockout mice to provide a more solid understanding of Notch1 *in vivo*.

In summary, our findings indicate that LPS-induced NICD downregulation and AKT inactivation may play important roles during endothelial dysfunction of sepsis. Our study also provides evidence that melatonin could be a potential therapeutic molecule in sepsis (Figure 8).

Data availability statement

The raw data supporting the conclusions of this article will be made available by the authors, without undue reservation.

Ethics statement

The studies involving human participants were reviewed and approved by the Research Ethics Board in the Children's Hospital of Fudan University (IRB protocol number: 2020-424). Written informed consent to participate in this study was provided by the participants' legal guardian/next of kin. The animal study was reviewed and approved by the Animal Studies Committee of the Children's Hospital of Fudan University (IRB protocol number: 2019-321). Written informed consent was obtained from the owners for the participation of their animals in this study.

Author contributions

TL, CZ, YW, and JY designed and carried out experiments and analyzed the data. TL, YZ, and GL wrote the manuscript. YZ and GL planned, designed, supervised, and coordinated the overall research efforts. All authors contributed to the article and approved the submitted version.

Funding

This work was supported by grants from the National Key R&D Program of China (2021YFC2701800, 2021YFC2701805 to GL; 2021YFC2701802 to YZ), National Natural Science Foundation of China (82241038, 81974248 to YZ, 82202374 to CZ), and Shanghai Committee of Science and Technology (23ZR1407600, 21140902400, 21ZR1410000, 19ZR1406400 to YZ, 22ZR1408500 to CZ, 22Y11900500 to YW).

Conflict of interest

The authors declare that the research was conducted in the absence of any commercial or financial relationships that could be construed as a potential conflict of interest.

Publisher's note

Supplementary material

The Supplementary Material for this article can be found online at: https://www.frontiersin.org/articles/10.3389/fimmu.2023.1134556/full#supplementary-material

References

1. Rudd KE, Johnson SC, Agesa KM, Shackelford KA, Tsoi D, Kievlan DR, et al. Global, regional, and national sepsis incidence and mortality, 1990-2017: analysis for the global burden of disease study. *Lancet* (2020) 395(10219):200–11.

2. Cecconi M, Evans L, Levy M, Rhodes A. Advances in sepsis diagnosis and management: a paradigm shift towards nanotechnology. sepsis and septic shock. *Lancet* (2018) 392(10141):75–87.

3. Lelubre C, Vincent JL. Mechanisms and treatment of organ failure in sepsis. *Nat Rev Nephrol* (2018) 14(7):417–27.

4. Weiss SL, Peters MJ, Alhazzani W, Agus MSD, Flori HR, Inwald DP, et al. Surviving sepsis campaign international guidelines for the management of septic shock and sepsis-associated organ dysfunction in children. *Pediatr Crit Care Med* (2020) 21 (2):e52–e106.

5. Ince C, Mayeux PR, Nguyen T, Gomez H, Kellum JA, Ospina-Tascon GA, et al. The endothelium in sepsis. *Shock* (2016) 45(3):259–70.

6. Spicer A, Calfee CS. Fixing the leak: targeting the vascular endothelium in sepsis. *Crit Care* (2012) 16(6):177.

7. Shapiro NI, Aird WC. Sepsis and the broken endothelium. *Crit Care* (2011) 15 (2):135.

8. Guruharsha KG, Kankel MW, Artavanis-Tsakonas S. The notch signalling system: recent insights into the complexity of a conserved pathway. *Nat Rev Genet* (2012) 13(9):654–66.

9. Gordon WR, Arnett KL, Blacklow SC. The molecular logic of notch signaling–a structural and biochemical perspective. *J Cell Sci* (2008) 121(Pt 19):3109–19.

10. Polacheck WJ, Kutys ML, Yang J, Eyckmans J, Wu Y, Vasavada H, et al. A non-canonical notch complex regulates adherens junctions and vascular barrier function. *Nature* (2017) 552(7684):258–62.

11. Briot A, Civelek M, Seki A, Hoi K, Mack JJ, Lee SD, et al. Endothelial NOTCH1 is suppressed by circulating lipids and antagonizes inflammation during atherosclerosis. *J Exp Med* (2015) 212(12):2147–63.

12. Mack JJ, Mosqueiro TS, Archer BJ, Jones WM, Sunshine H, Faas GC, et al. NOTCH1 is a mechanosensor in adult arteries. *Nat Commun* (2017) 8(1):1620.

13. Weiss SL, Peters MJ, Alhazzani W, Agus MSD, Flori HR, Inwald DP, et al. Surviving sepsis campaign international guidelines for the management of septic shock and sepsis-associated organ dysfunction in children. *Intensive Care Med* (2020) 46 (Suppl 1):10–67.

14. Martins-Green M, Petreaca M, Yao M. An assay system for *in vitro* detection of permeability in human "endothelium". *Methods Enzymol* (2008) 443:137–53.

15. Mishra SK, Choudhury S. Experimental protocol for cecal ligation and puncture model of polymicrobial sepsis and assessment of vascular functions in mice. *Methods Mol Biol* (2018) 1717:161–87.

16. Rahim I, Djerdjouri B, Sayed RK, Fernandez-Ortiz M, Fernandez-Gil B, Hidalgo-Gutierrez A, et al. Melatonin administration to wild-type mice and nontreated NLRP3 mutant mice share similar inhibition of the inflammatory response during sepsis. *J Pineal Res* (2017) 63(1).

17. Hu S, Pi Q, Xu X, Yan J, Guo Y, Tan W, et al. Disrupted eNOS activity and expression account for vasodilator dysfunction in different stage of sepsis. *Life Sci* (2021) 264:118606.

18. Wu J, Deng Z, Sun M, Zhang W, Yang Y, Zeng Z, et al. Polydatin protects against lipopolysaccharide-induced endothelial barrier disruption *via* SIRT3 activation. *Lab Invest* (2020) 100(4):643–56.

19. Chen H, Li Y, Wu J, Li G, Tao X, Lai K, et al. RIPK3 collaborates with GSDMD to drive tissue injury in lethal polymicrobial sepsis. *Cell Death Differ* (2020) 27(9):2568–85.

20. Kang S, Tanaka T, Inoue H, Ono C, Hashimoto S, Kioi Y, et al. IL-6 trans-signaling induces plasminogen activator inhibitor-1 from vascular endothelial cells in cytokine release syndrome. *Proc Natl Acad Sci USA* (2020) 117(36):22351–6.

21. Raza W, Luqman S, Meena A. Prospects of tangeretin as a modulator of cancer targets/pathways. *Pharmacol Res* (2020) 161:105202.

22. Xu S, Kong YG, Jiao WE, Yang R, Qiao YL, Xu Y, et al. Tangeretin promotes regulatory T cell differentiation by inhibiting Notch1/Jagged1 signaling in allergic rhinitis. *Int Immunopharmacol* (2019) 72:402–12.

23. Shiojima I, Walsh K. Role of akt signaling in vascular homeostasis and angiogenesis. *Circ Res* (2002) 90(12):1243–50.

24. Zhang S, Wang P, Ren L, Hu C, Bi J. Protective effect of melatonin on soluble Abeta1-42-induced memory impairment, astrogliosis, and synaptic dysfunction *via* the Musashi1/Notch1/Hes1 signaling pathway in the rat hippocampus. *Alzheimers Res Ther* (2016) 8(1):40.

25. Luo Z, Mu L, Zheng Y, Shen W, Li J, Xu L, et al. NUMB enhances notch signaling by repressing ubiquitination of NOTCH1 intracellular domain. *J Mol Cell Biol* (2020) 12(5):345–58.

26. Moretti J, Chastagner P, Gastaldello S, Heuss SF, Dirac AM, Bernards R, et al. The translation initiation factor 3f (eIF3f) exhibits a deubiquitinase activity regulating notch activation. *PloS Biol* (2010) 8(11):e1000545.

27. Rittirsch D, Huber-Lang MS, Flierl MA, Ward PA. Immunodesign of experimental sepsis by cecal ligation and puncture. *Nat Protoc* (2009) 4(1):31–6.

28. Nus M, Martinez-Poveda B, MacGrogan D, Chevre R, D'Amato G, Sbroggio M, et al. Endothelial Jag1-RBPJ signalling promotes inflammatory leucocyte recruitment and atherosclerosis. *Cardiovasc Res* (2016) 112(2):568–80.

29. MacKenzie F, Duriez P, Wong F, Noseda M, Karsan A. Notch4 inhibits endothelial apoptosis *via* RBP-jkappa-dependent and -independent pathways. *J Biol Chem* (2004) 279(12):11657–63.

30. Bentley K, Franco CA, Philippides A, Blanco R, Dierkes M, Gebala V, et al. The role of differential VE-cadherin dynamics in cell rearrangement during angiogenesis. *Nat Cell Biol* (2014) 16(4):309–21.

31. Zhang X, Zheng L, Sun Y, Wang T, Wang B. Tangeretin enhances radiosensitivity and inhibits the radiation-induced epithelial-mesenchymal transition of gastric cancer cells. *Oncol Rep* (2015) 34(1):302–10.

32. Patenaude A, Fuller M, Chang L, Wong F, Paliouras G, Shaw R, et al. Endothelial-specific notch blockade inhibits vascular function and tumor growth through an eNOS-dependent mechanism. *Cancer Res* (2014) 74(9):2402–11.

33. Hasan SS, Fischer A. Notch signaling in the vasculature: angiogenesis and angiocrine functions. *Cold Spring Harb Perspect Med* (2023) 13(2).

34. Bai X, He T, Liu Y, Zhang J, Li X, Shi J, et al. Acetylation-dependent regulation of notch signaling in macrophages by SIRT1 affects sepsis development. *Front Immunol* (2018) 9:762.

35. Li J, Qi X, Wang X, Li W, Li Y, Zhou Q. PTEN inhibition facilitates diabetic corneal epithelial regeneration by reactivating akt signaling pathway. *Transl Vis Sci Technol* (2020) 9(3):5.

36. Byeon Y, Lee K, Park YI, Park S, Back K. Molecular cloning and functional analysis of serotonin n-acetyltransferase from the cyanobacterium synechocystis sp. *PCC 6803. J Pineal Res* (2013) 55(4):371–6.

37. Leon J, Acuna-Castroviejo D, Escames G, Tan DX, Reiter RJ. Melatonin mitigates mitochondrial malfunction. *J Pineal Res* (2005) 38(1):1–9.

38. Ji MH, Xia DG, Zhu LY, Zhu X, Zhou XY, Xia JY, et al. Short- and long-term protective effects of melatonin in a mouse model of sepsis-associated encephalopathy. *Inflammation* (2018) 41(2):515–29.

39. Wu CC, Chiao CW, Hsiao G, Chen A, Yen MH. Melatonin prevents endotoxin-induced circulatory failure in rats. *J Pineal Res* (2001) 30(3):147–56.

40. Zhao L, An R, Yang Y, Yang X, Liu H, Yue L, et al. Melatonin alleviates brain injury in mice subjected to cecal ligation and puncture *via* attenuating inflammation, apoptosis, and oxidative stress: the role of SIRT1 signaling. *J Pineal Res* (2015) 59(2):230–9.

41. Vriend J, Reiter RJ. Melatonin and ubiquitin: what's the connection? *Cell Mol Life Sci* (2014) 71(18):3409–18.

42. Zhao J, Bi W, Zhang J, Xiao S, Zhou R, Tsang CK, et al. USP8 protects against lipopolysaccharide-induced cognitive and motor deficits by modulating microglia phenotypes through TLR4/MyD88/NF-kappaB signaling pathway in mice. *Brain Behav Immun* (2020) 88:582–96.

43. Du L, Li Y, Kang M, Feng M, Ren Y, Dai H, et al. USP48 is upregulated by Mettl14 to attenuate hepatocellular carcinoma *via* regulating SIRT6 stabilization. *Cancer Res* (2021) 81(14):3822–34.

44. Shen H, Xie K, Li M, Yang Q, Wang X. N(6)-methyladenosine (m(6)A) methyltransferase METTL3 regulates sepsis-induced myocardial injury through IGF2BP1/HDAC4 dependent manner. *Cell Death Discov* (2022) 8(1):322.

45. Zhang H, Liu J, Zhou Y, Qu M, Wang Y, Guo K, et al. Neutrophil extracellular traps mediate m(6)A modification and regulates sepsis-associated acute lung injury by activating ferroptosis in alveolar epithelial cells. *Int J Biol Sci* (2022) 18 (8):3337–57.

frontiers | Frontiers in Immunology

TYPE Original Research
PUBLISHED 15 June 2023
DOI 10.3389/fimmu.2023.1157793

OPEN ACCESS

EDITED BY
Zuliang Jie,
Xiamen University, China

REVIEWED BY
Lara Campana,
Resolution Therapeutics Ltd,
United Kingdom
Adil Bhat,
University of California, Los Angeles,
United States

*CORRESPONDENCE
Jian Shi
xyshijian@csu.edu.cn

†These authors have contributed equally to this work

RECEIVED 03 February 2023
ACCEPTED 18 May 2023
PUBLISHED 15 June 2023

CITATION
Cai J, Tang D, Hao X, Liu E, Li W and Shi J (2023) Mesenchymal stem cell-derived exosome alleviates sepsis-associated acute liver injury by suppressing MALAT1 through microRNA-26a-5p: an innovative immunopharmacological intervention and therapeutic approach for sepsis. *Front. Immunol.* 14:1157793. doi: 10.3389/fimmu.2023.1157793

Mesenchymal stem cell-derived exosome alleviates sepsis-associated acute liver injury by suppressing MALAT1 through microRNA-26a-5p: an innovative immunopharmacological intervention and therapeutic approach for sepsis

Jizhen Cai[1†], Da Tang[2†], Xiao Hao[3,4], Enyi Liu[3,4], Wenbo Li[5] and Jian Shi[1*]

[1]Department of Critical Care Medicine and Hematology, The Third Xiangya Hospital, Central South University, Changsha, China, [2]Department of General Surgery, The Third Xiangya Hospital, Central South University, Changsha, China, [3]Department of Hematology, Xiangya Hospital, Central South University, Changsha, China, [4]Key Laboratory of Sepsis Translational Medicine of Hunan, Central South University, Changsha, China, [5]Department of Plastic and Aesthetic (Burn) Surgery, The Second Xiangya Hospital of Central South University, Changsha, China

Background: Sepsis is a syndrome with the disturbed host response to severe infection and is a major health problem worldwide. As the front line of infection defense and drug metabolism, the liver is vulnerable to infection- or drug-induced injury. Acute liver injury (ALI) is thus common in patients with sepsis and is significantly associated with poor prognosis. However, there are still few targeted drugs for the treatment of this syndrome in clinics. Recent studies have reported that mesenchymal stem cells (MSCs) show potential for the treatment of various diseases, while the molecular mechanisms remain incompletely characterized.

Aims and methods: Herein, we used cecal ligation puncture (CLP) and lipopolysaccharide (LPS) plus D-galactosamine (D-gal) as sepsis-induced ALI models to investigate the roles and mechanisms of mesenchymal stem cells (MSCs) in the treatment of ALI in sepsis.

Results: We found that either MSCs or MSC-derived exosome significantly attenuated ALI and consequent death in sepsis. miR-26a-5p, a microRNA downregulated in septic mice, was replenished by MSC-derived exosome. Replenishment of miR-26a-5p protected against hepatocyte death and liver injury

Abbreviations: ALI, acute liver injury; MSC, mesenchymal stem cell; MALAT1, metastasis associated lung adenocarcinoma transcript 1; CLP, Cecum Ligation and Puncture; AST, aspartate aminotransferase; ALT, alanine aminotransferase; WT, wild type; LPS, Lipopolysaccharides; GSH, glutathione; MDA, Malondialdehyde.

caused by sepsis through targeting Metastasis Associated Lung Adenocarcinoma Transcript 1 (MALAT1), a long non-coding RNA highly presented in hepatocyte and liver under sepsis and inhibiting anti-oxidant system.

Conclusion: Taken together, the results of the current study revealed the beneficial effects of MSC, exosome or miR-26a-5p on ALI, and determined the potential mechanisms of ALI induced by sepsis. MALAT1 would be a novel target for drug development in the treatment of this syndrome.

KEYWORDS

sepsis, MALAT1, exosome, immunopharmacological interventions, immune regulation, mesenchymal stem cells, miR-26a-5p

1 Introduction

Sepsis is a life-threatening syndrome secondary to severe infection, accounting for a majority of death in critical-care patients (1, 2). With the development of multi-drug resistant bacteria and the boost of the aging population, the incidence of sepsis has been increasing in recent decades (3). Although the advance in antibiotics and life-supporting techniques allows a decreasing mortality rate, therapeutic strategies are still limited in clinics for the treatment of sepsis.

As the frontier of infection defense, the liver has a central role during sepsis and is essential for the regulation of immune defense and drug metabolism (4, 5). The liver could be activated by microbes or alarm signals, and thus releases pro-inflammatory cytokines and recruits immune cells, facilitating the clearance of microbes. In addition, the liver, with the interaction of parenchymal and non-parenchymal cells, modulates the inflammatory response to infection so as to maintain immunological homeostasis (4, 5). However, the liver is also a target for sepsis-related injury, where excessive microbes and cytokine storm induced by severe infection can over-activate inflammatory response and interrupt the homeostasis, thereby rendering hepatocytes to be hyperactive or fall into irreversible death (6, 7). Acute liver injury (ALI) has been reported to be a common complication of sepsis, occurring in approximately 50% of septic patients (8). Sepsis is the most common trigger for liver failure and results in increased mortality. Acute liver dysfunction substantially impairs the prognosis of sepsis and serves as a powerful independent predictor of mortality in the intensive care unit. Therefore, it is urging to explore novel methods or drugs for rescuing ALI in the treatment of sepsis.

Mesenchymal stem cell (MSC) is a type of pluripotent cell, characterized by excellent self-renewing and immunomodulatory properties. MSCs are widely applied in a series of preclinical studies for the treatment of tissue injury and inflammatory diseases, such as central nerve injury, graft-versus-host disease, lupus, and so on (8). MSCs have also been reported to show potential for the treatment of sepsis (9). However, potential tumorigenic properties, quality variation and undesirable side effects in hyperinflammatory circumstance limit the application of MSCs (10, 11). Alternatively, MSCs-derived exosome, a cell-free particle carrying majority of the modulatory function of MSCs, shows high potential efficacy in preclinical studies. It has been demonstrated that MSC-derived exosome protects against ischemia-reperfusion-induced liver injury by inhibiting the release of inflammatory cytokines or alarming stimuli, such as TNFα, IL-6 and high mobility group box 1 (HMGB1) (12). Above all, MSCs or MSC-derived exosome play vital roles and present promising diagnostic and therapeutic targets in organ injury.

Exosome exerts its function by transferring and releasing the contents, including proteins, microRNA, and so on (13). MicroRNAs (miRNAs), as small noncoding RNA molecules, regulate many biological processes, such as cell proliferation, differentiation, and apoptosis by being complementary to target mRNAs, resulting in gene silence (14–16). Literature suggests that the abnormal expression level of miRNAs is relevant to the pathogenesis of various diseases (17, 18). Plasma exosomal microRNAs (miRNAs) are considered as valid circulating biomarkers for disease diagnosis and prognosis. However, the function of miRNAs from MSC-derived exosome in ALI induced by sepsis remains unclear.

Metastasis Associated Lung Adenocarcinoma Transcript 1 (MALAT1) is an evolutionally conserved long non-coding RNA, implicated in various cancer and inflammatory diseases (19). Once stimulation or subjected to environmental stress, such as oxidized-LDL, lipopolysaccharides, hypoxia and high glucose, MALAT1 is commonly upregulated in different cells, thus inducing pro-inflammatory cytokine release, inflammatory cell infiltration and cell death, thereby facilitating inflammatory responses and tissue injury (20–22). Herein, we discovered that MSCs, MSCs-derived exosome, and miR-26a-5p have the capacity to protect against sepsis-associated ALI. Using genetically modified mice, we identified that this protection could be mainly attributed to the inhibition of MALAT1 *via* the exosome-delivered miR-26a-5p.

Thus, the findings of the present study suggest that MSCs, MSC-derived exosome and miR-26a-5p are potential therapeutics, and MALAT1 is a promising target for the treatment of ALI in sepsis, which provides a new avenue and new insights for rescuing the syndrome.

2 Materials and methods

2.1 Mice

Malat1$^{-/-}$ and WT mice on a C57BL/6J background were purchased from Gempharmatech Co., Ltd and Hunan SJA Laboratory Animal Company, respectively. Animals were maintained in a specific pathogen-free environment at the Department of Laboratory Animals of Central South University. Male mice with an age of 8 weeks and a body weight of 22-25g were used in the present study. Free access to water and standard chow was provided to all mice during the whole experiment process. The experiment was conducted in a standard condition with a room temperature of 22-25°C and 12/12h light-dark cycles after obtaining the approval of the research ethics committee of Central South University.

2.2 Cecum ligation and puncture

We followed the previously reported method to conduct CLP model for polymicrobial sepsis. In brief, mice were anesthetized and the lower abdomen was split for exposing the cecum which was subsequently ligated (75%) and punctured using an 18-gauge needle. Afterward, the cecum was reloaded and the wound was closed, followed by a resuscitation *via* injecting warm saline subcutaneously. The plasma and the liver were then harvested 12h after the operation for further experiments. Time of death was recorded within 7 days.

2.3 Hepatocyte purification and culture

A collagenase perfusion technique was used for the purification of primary mouse hepatocytes as shown previously (19). In brief, pre-wormed PBS was injected *via* the inferior vena cava, followed by perfusion using collagenase type IV. The liver was then dissociated for releasing hepatocytes. After removing debris by a passthrough *via* a 70 μm strainer (Falcon), hepatocytes were purified by a following centrifuge (50g) using 40% percoll (Sigma-Aldrich), and plated on collagen-coated plates in Williams E medium (Sigma) containing 5% fetal bovine serum (FBS). The primary mouse hepatocytes were treated with LPS (1ug/ml) plus D-gal (10mM) for 24h. Cell viability was assessed using CCK8 (Ck04, Dojindo). In some experiments, cell lysates and supernatants were collected at indicated time points for RNA, ELISA, Cytochrome P450 activity and albumin release assay.

2.4 Liver dysfunction and oxidative stress

Liver dysfunction was monitored by the augment of plasma levels of aspartate aminotransferase (AST) and alanine aminotransferase (ALT), which were determined by an automatic biochemical analyzer (Sysmex DRICHEM3500, Fuji, Japan) according to the manufacturer's instructions. For determining oxidative stress, liver homogenate in PBS was prepared and the levels of GSH and MDA were assessed using commercial kits (A006-2-1 and A003-1-2, Nanjing Jiancheng Bioengineering Institute). Albumin and Cytochrome P450 concentration in the supernatant of primary hepatocytes were analyzed using ELISA kits according to the manufacturer's instructions (AF2818-A and AF2766-A, Hunan Aifang Biological).

2.5 Real-time PCR

After extracted and purified by using Trizol (Life Technologies, Gaithersburg, MD), total RNA was reversely transcribed into cDNA by using Reverse Transcription Kit (Thermo Fisher Scientific). The expression levels of target genes were assessed by quantitative real-time polymerase chain reaction (qRT-PCR) using qPCR mix (Vazymebiotech, China) and designed primers, in which β-actin was used as the endogenous control. For determining the level of microRNA, qRT-PCR miRNA Detection kit (RiboBio, China) was applied and U6 snRNA was used as the endogenous control.

2.6 MSCs culture and exosome purification

Human umbilical cord derived mesenchymal stem cells were cultured in Dulbecco's modified Eagles medium containing 10% exosome-free fetal bovine serum and harvested when 90% confluence was achieved. The cells were washed and resuspended using PBS for intervention, whilst the supernatant medium was collected for exosome purification. After removing dead cells, cell debris, and large vesicles by sequential centrifugation at 200 ×g for 10 min, 2000 ×g for 20 min, and 15,000 ×g for 30 min respectively, the supernatants were centrifuged at 100,000 ×g for 80 min. Exosome was harvested by collecting the pellets after one time wash using PBS. The morphology and size distribution of exosome were examined by transmission electron microscopy and particle size analyzer, respectively. The purified exosome was finally identified by determining the expression of markers including CD9, CD63, and TSG101 *via* Western Blotting (Anti-CD9, anti-CD63 and anti-TSG101 antibodies were ab263019, ab134045 and ab125011 from Abcam, respectively, with a dilution of 1:1000).

2.7 Tissue histology

Mice were sacrificed after the sham-operation or the challenge of CLP at the target time point. The liver was dissociated and fixed in 4% paraformaldehyde overnight, followed by dehydration before being embedded in paraffin. Sections of the tissues were then obtained at a thickness of 4 μm and stuck onto glass slides. After dewaxed, the sections were handled using a standard hematoxylin & eosin (H&E) staining prior to imaging by using a microscope (Eclipse80i, Nikon). The liver damage was mainly determined by augment levels of plasma AST and ALT, with the assistance of the representative image of H&E stained histological section using

optical microscopy. All slides were blindly examined in more than 5 high-power fields to assess the damage in each section.

2.8 Luciferase reporter assay

To confirm the target of miR-26a-5p, luciferase reporter vectors containing WT (UUACUUGA) and mutant (AAUGAACU) binding sites of MALAT1 were constructed and transfected into 293T cells using Lipofectamine™ 3000 (L3000015, Invitrogen), followed by a transfection of miR-26a-5p and mimic controls (100 nM using riboFECT™ CP, C10511-05, Ribobio). The luciferase activity of cells was determined 48 h later by using Luciferase Assay system (Promega Corporation).

2.9 Statistical analyses

Statistical analyses were conducted by using GraphPad Prism 7.0. Student *t*-test was used for comparison between two groups, whilst One- or Two-way ANOVA with Bonferroni's *post hoc* test was used for comparisons among more than two groups. Association between groups was assessed using Spearman correlation. The survival rates of mice were analyzed using the log-rank test (n=10 per group). Data were expressed as mean ± standard error of the mean in six biological or three technical replications (23), and P value less than 0.05 was considered as a significant difference.

3 Results

3.1 Mesenchymal stem cells attenuate acute liver injury in sepsis model

To investigate the role of MSCs in the treatment of sepsis-associated ALI, we administrated MSCs to mice *via* caudal vein 1h prior to the challenge of CLP, a classical model of poly-bacterial sepsis (Figure 1A). We found that AST and ALT, two markers of ALI, were significantly increased after challenge with CLP, indicating that sepsis induces significant liver dysfunction. The intervention of MSCs

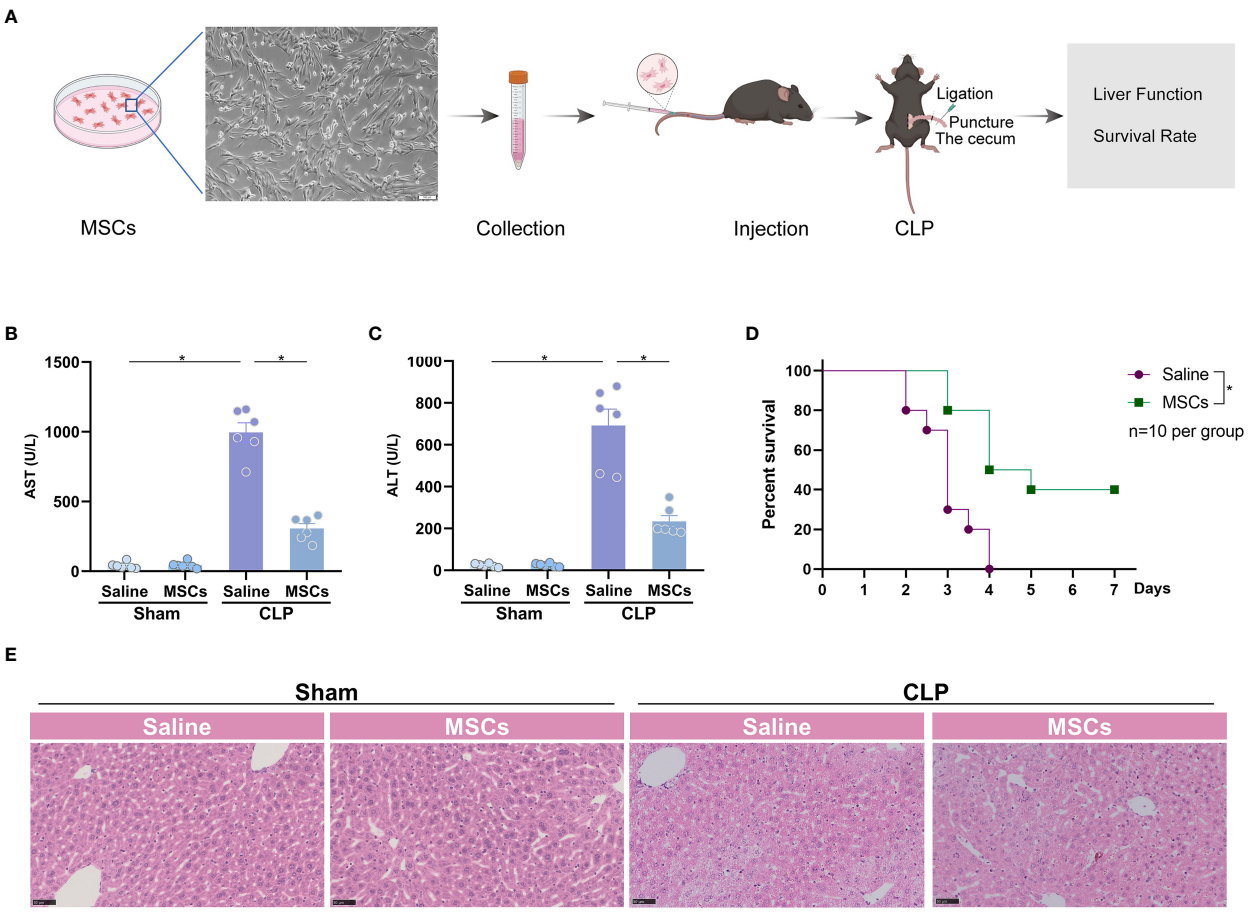

FIGURE 1
MSCs protect from sepsis-induced acute liver injury. **(A)** Schematic illustration indicating the strategy of MSCs in the treatment of CLP-induced acute liver injury. **(B, C)** Serum aspartate aminotransferase (AST) and alanine transaminase (ALT) level of mice challenged with CLP or treated with MSCs (10^6 cells per mouse, n=6 per group). **(D)** Survival analysis of mice challenged with CLP in the presence or absence of MSCs (n=10 per group). **(E)** Representative images of H&E staining of livers from mice treated with MSCs before CLP or not (n=3 per group). Data are expressed as mean ± SEM of independent experiments analyzed by one-way ANOVA **(B, C)**, and survival curve comparison [log-rank (Mantel-Cox) test]. * Means *P*<0.05.

robustly reduced the augmented levels of AST and ALT (Figures 1B, C). Similarly, H&E staining showed that the liver was pathologically injured after CLP model, which was alleviated by the administration MSCs (Figure 1E). As a consequence, MSCs significantly improved the survival rate of mice in a sepsis model (Figure 1D). Taken together, MSCs are capable of protecting ALI in sepsis.

3.2 Exosome of mesenchymal stem cell exerts protective effects against sepsis-associated liver injury

Exosome is a functional compartment of stem cells in various physiological circumstances (13). To investigate whether protective effects of MSCs are attributed to exosome, we collected and purified exosome from the medium of cultured MSCs (Figure 2A), and subjected mice to CLP model 1h after the treatment of the MSCs-derived exosome (exosome from 5×10^6 cells per mouse). Electron microscope showed regular spherical particles with a normal distributed size of around 100 nm for the purified exosome (Figures 2B, C). Three markers of exosome, such as CD9, CD63 and TSG101, were detectable as shown by western blotting (Figure 2D). The purified exosome was subsequently administrated to mice 1 h prior to a challenge of CLP. The results suggested that the exosome significantly reduced CLP-augmented AST and ALT (Figures 2E, F). H&E staining also pointed out a similar trend, in which the liver injury was significantly attenuated by administration of exosome (Figure 2G). As a result, the

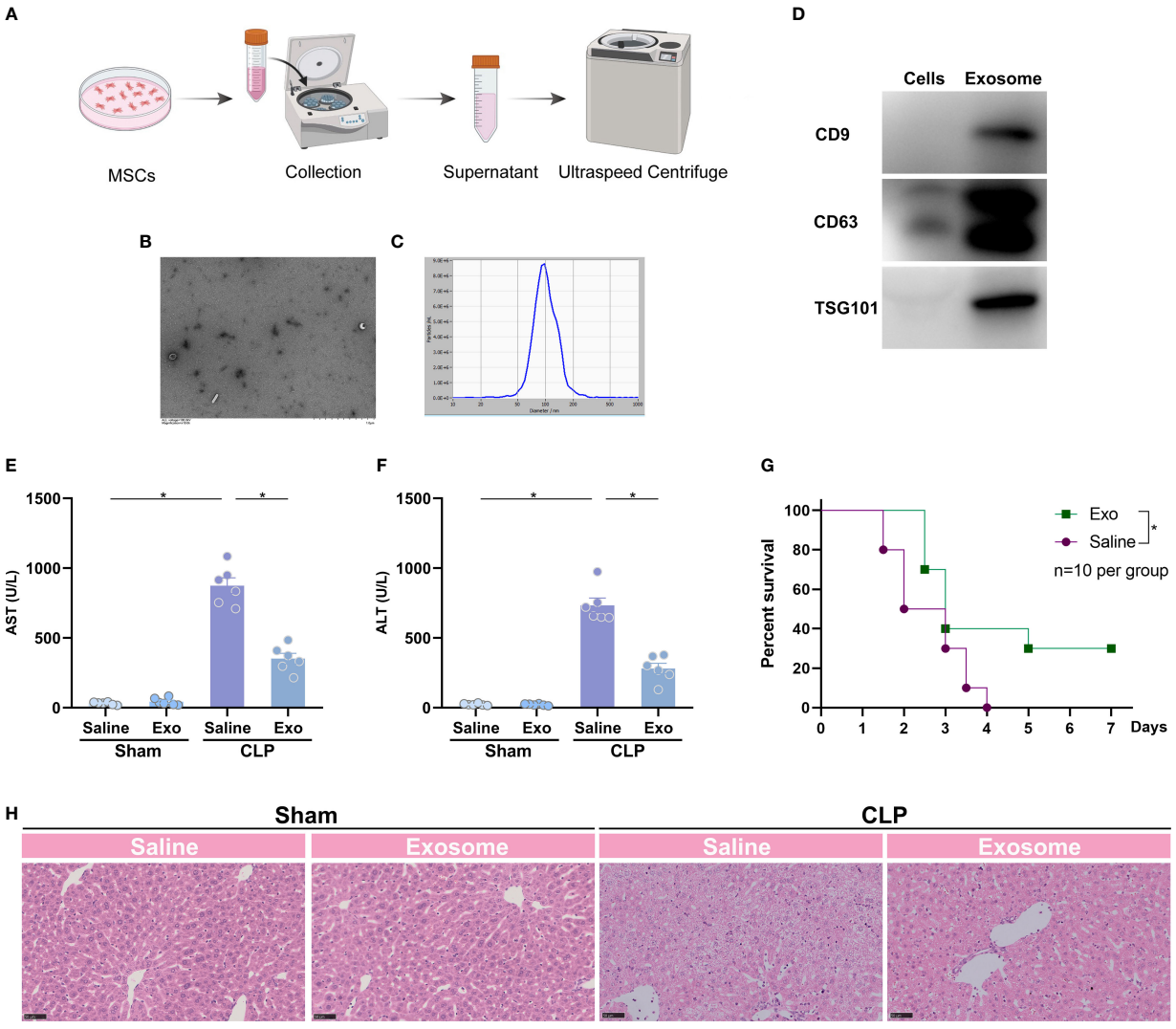

FIGURE 2
Exosome of MSCs attenuates sepsis-induced acute liver injury. **(A)** Schematic illustration indicating the purification of exosome from MSCs. **(B)** Quality of the purified exosome identified by electron microscope (white arrows). **(C)** size distribution of the purified exosome. **(D)** Expression of exosome markers, such as CD9, CD63 and TSG101, in purified exosome and MSCs. **(E, F)** Serum spartate aminotransferase (AST) and alanine transaminase (ALT) level of mice challenged with CLP or treated with the purified exosome (exosome from 5×10^6 cells per mouse, n=6 per group). **(G)** Representative images of H&E staining of the liver from mice challenged with CLP or treated with the purified exosome (n=3 per group). **(H)** Survival analysis of mice challenged with CLP in the presence or absence of the purified exosome (n=10 per group). Data are expressed as mean ± SEM of independent experiments analyzed by one-way ANOVA **(E, F)**, and survival curve comparison [log-rank (Mantel-Cox) test]. * Means $P<0.05$.

intervention of the exosome ameliorated CLP-induced death (Figure 2H). Thus, the exosome is the main executor of MSCs in the inhibition of sepsis-associated ALI.

3.3 Exosome of mesenchymal stem cell replenishes sepsis-downregulated miR-26a-5p in the liver

Exosome exerts its function by transferring and releasing the contents, including proteins, microRNA, and so on (13). MicroRNA is a type of RNA around 22nt mediating target mRNA degradation and thus silencing the expression of target genes. To investigate whether MSC-derived exosome inhibits sepsis-associated ALI by microRNA and, if so, which microRNA is involved, we determined the expression of sepsis-associated microRNA in the liver of CLP-challenged mice (24). It was found that miR-26a-5p, miR-126, miR-125b, miR-146a and miR-223 were significantly downregulated in the liver after the challenge of CLP (Figures 3A–E). Besides, the five microRNAs were significantly upregulated in the primary hepatocytes after treated with MSC-derived exosome, with the highest expression of miR-26a-5p (Figures 3F–J), indicating that microRNA can be transferred into primary hepatocytes *via* MSC-derived exosome. In line with the cellular observation, we found that the five microRNA were replenished in the liver after administrated with MSC-derived exosome in the CLP model (Figures 3K–O). These data demonstrate that MSC-derived exosome resumes miR-26a-5p that is reduced by sepsis in the liver.

3.4 MiR-26a-5p alleviates sepsis-associated acute liver injury

MiR-26a-5p is reported to function in a series of physiological processes (25). To confirm the role of miR-26a-5p in ALI, we transfected the microRNA into murine hepatocytes before a challenge of LPS plus D-gal. It was discovered that LPS/D-gal

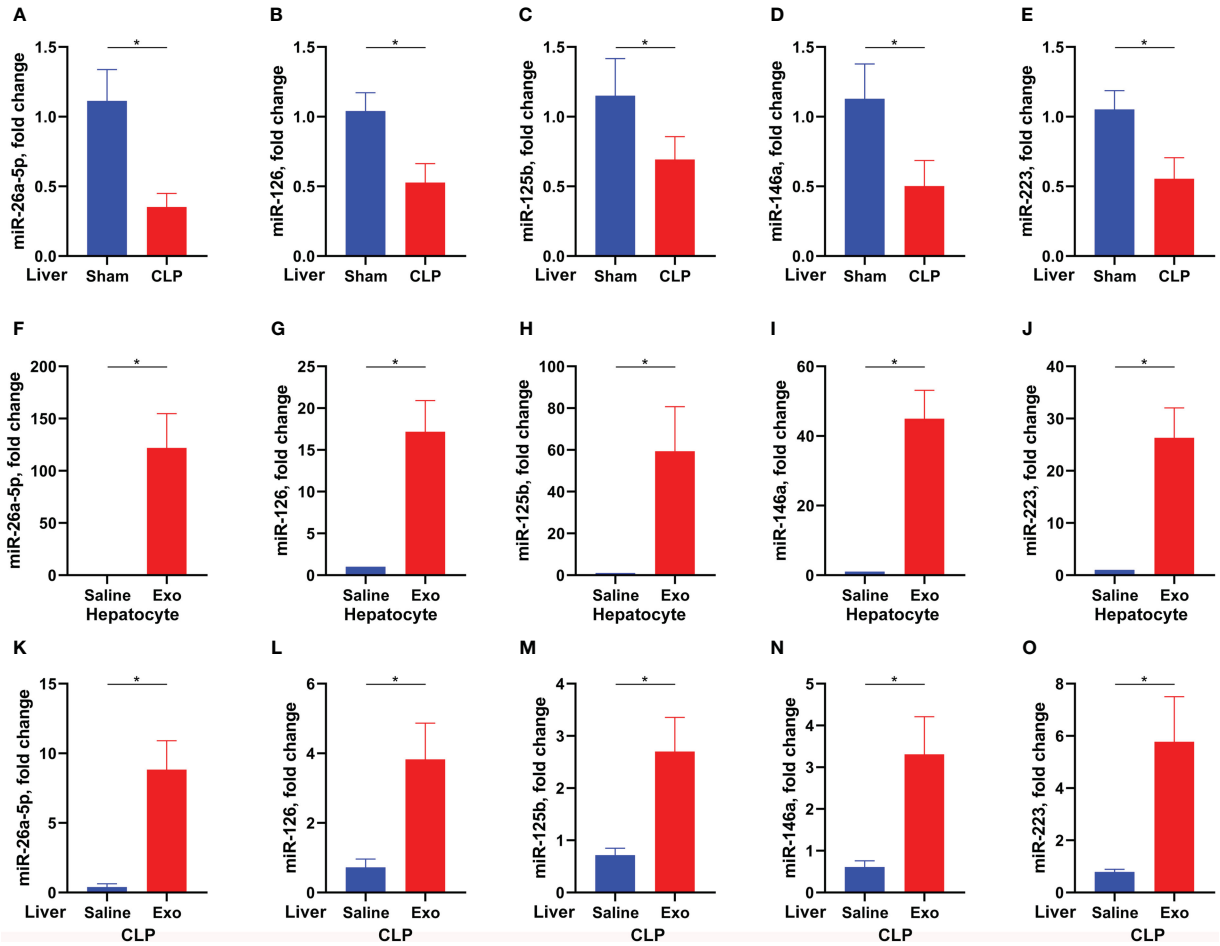

FIGURE 3
Exosome replenishes sepsis-downregulated microRNA. **(A–E)** Levels of miR-26a-5p **(A)**, miR-126 **(B)**, miR-125b **(C)**, miR-146 **(D)** and miR-223 **(E)** in the liver of mice challenged with CLP or not (n=6 per group). F-J. Levels of miR-26a-5p **(F)**, miR-126 **(G)**, miR-125b **(H)**, miR-146 **(I)** and miR-223 **(J)** in the hepatocytes treated with or without MSC-derived exosome (exosome from $1x10^5$ cells per ml, 3 technical repeats). **(K–O)** Levels of miR-26a-5p **(K)**, miR-126 **(L)**, miR-125b **(M)**, miR-146 **(N)** and miR-223 **(O)** in the liver of mice challenged with CLP and treated with or without MSC-derived exosome (exosome from $5x10^6$ cells per mouse, n=6 per group). Data are expressed as mean ± SEM of independent experiments analyzed by student *t* tests. * Means $P<0.05$.

dramatically induced hepatocyte death, which was significantly reversed by the addition of miR-26a-5p (Figure 4A). In addition, the reversion was in a dose-dependent manner (Figure 4B), indicating the essential role of miR-26a-5p in the protection against hepatocyte death caused by ALI. Consistent with the cell observations, administration of miR-26a-5p attenuated CLP-induced liver injury (Figures 4C–E), and rescued approximately 40% of the lethality (Figure 4F). In line with these observation, administration of exosome alone or combining miR-26a-5p with exosome rescued approximately 50% of the lethality, which was a little higher than miR-26a-5p alone, but none of statistical significance (Figure 4F). Thus, these findings support that the protective effect of MSC-derived exosome against ALI is primarily mediated by miR-26a-5p in sepsis.

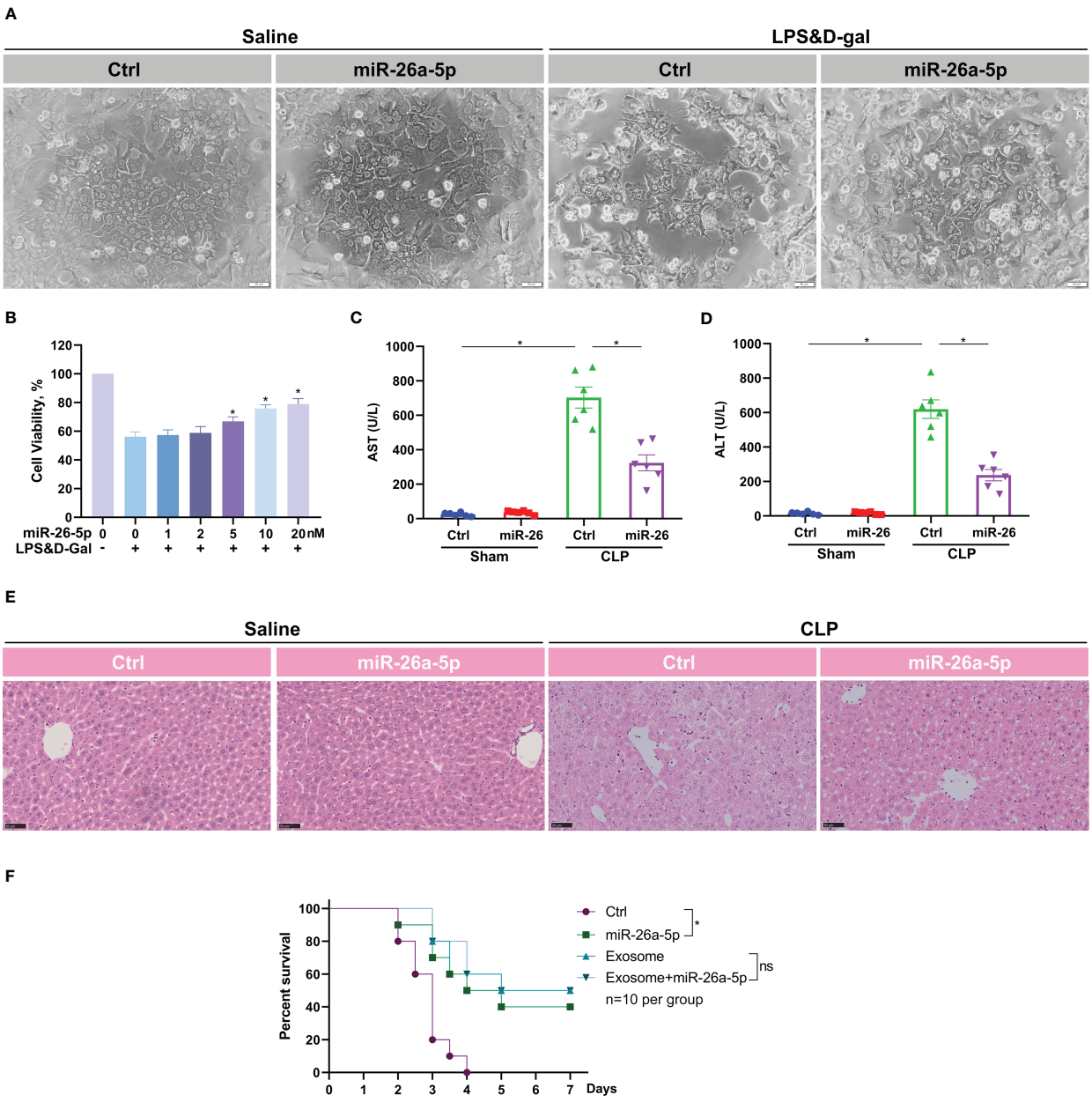

FIGURE 4
miR-26a-5p alleviates hepatocyte death and sepsis-induced acute liver injury. **(A)** Hepatocytes challenged with LPS plus D-gal or not in the presence and absence of miR-26a-5p (n=3 repeats). **(B)** Cell viability of hepatocytes challenged with LPS plus D-gal or not in the presence of various dose of miR-26a-5p (n=3 repeats). **(C, D)** Serum AST and ALT level of mice challenged with CLP or treated with the miR-26a-5p or corresponding mimic control RNA (10 nmol per mouse, n=6 per group). **(E)** Representative images of H&E staining of livers from mice treated with miR-26a-5p or corresponding mimic control RNA after CLP or not (n=3 per group). **(F)** Survival analysis of mice challenged with CLP and treated with the miR-26a-5p, corresponding mimic control RNA and/or MSC-derived exosome (n=10). Data are expressed as mean ± SEM of independent experiments analyzed by one-way ANOVA **(B, C)**, and survival curve comparison [log-rank (Mantel-Cox) test]. * Means $P<0.05$.

3.5 MALAT1 is the target of miR-26a-5p in acute liver injury

To reveal the target of miR-26a-5p, we used Encyclopedia of RNA Interactomes (ENCORI) to conduct a screening. We found that MALAT1, a well-known long non-coding RNA, showed a high binding score with miR-26a-5p (Figure 5A). LPS plus D-gal stimulate increased MALAT1 transcription in hepatocytes, which could be restored in a dose-dependent and time-dependent manner by transfection of miR-26a-5p (Figures 5B, C). Mutation of the putative target site of MALAT1 prevented the reduction of luciferase activity through the specific binding site of miR-26a-5p induced by LPS plus D-gal stimulation (Figure 5D). In line with these observations, further *in-vivo* study revealed that miR-26a-5p was significantly dampened when MALAT1 was robustly boosted in the liver of mice challenged with CLP (Figures 5E, F). In addition, the downregulation of miR-26a-5p was significantly associated with the upregulation of MALAT1 (Figure 5G). Thus, MALAT1 is the target of miR-26a-5p in the treatment of sepsis-associated ALI.

3.6 MiR-26a-5p suppresses acute liver injury in sepsis by silencing MALAT1

To identify the role of MALAT1 and miR-26a-5p in sepsis-associated ALI, we subjected WT or *Malat1*-deficient mice with CLP in the presence or absence of miR-26a-5p. We found that MALAT1 deficiency significantly reduced the CLP-augmented plasma levels of AST and ALT, indicating recovery of liver dysfunction (Figures 6A, B). Administration of miR-26a-5p did not additionally reduce the level of AST and ALT in *Malat1*-deficient mice (Figures 6A, B). A recent study reported that MALAT1 inhibits anti-oxidant system and thus promotes sepsis in CLP model (26). To investigate the mechanism of MALAT1 involving sepsis-associated ALI, we determined MDA and GSH levels in the liver of mice. The result demonstrated that CLP boosted the levels of MDA, and reduced the level of GSH in the liver, which was significantly attenuated by deleting *Malat1* without further reduction by administrating miR-26a-5p (Figures 6C, D). We also extracted primary hepatocytes from WT and Malat1-deficient mice to detect indicators of oxidative stress. The role of the radical scavenger enzymes catalase (Cat) and glutathione peroxidase (GPX), which remove oxygen radicals, has been assessed in this context. In our study, we provide evidence that Cat and GPX expression was diminished at the RNA level in primary hepatocytes after challenge with LPS plus D-gal, suggesting impaired detoxification of ROS, which were all attenuated by MALAT1 deficiency (Figures 6E, F). Albumin and Cytochrome P450 activity were analyzed to measure the link between hepatocytes function and oxidative stress. We found that the decreased albumin and impaired activity of Cytochrome P450 activity were significantly restored by deleting MALAT1 (Figures 6G, H), indicating that the oxidative stress contributes to the enhancement of liver damage by MALAT1. Moreover, Malat1 deficiency dramatically rescued CLP-induced mice death (Figure 6I) and liver injury (Figure 6J), and administration of miR-26a-5p did not provide further prevention on the basis of MALAT1 deficiency (Figure 6G).

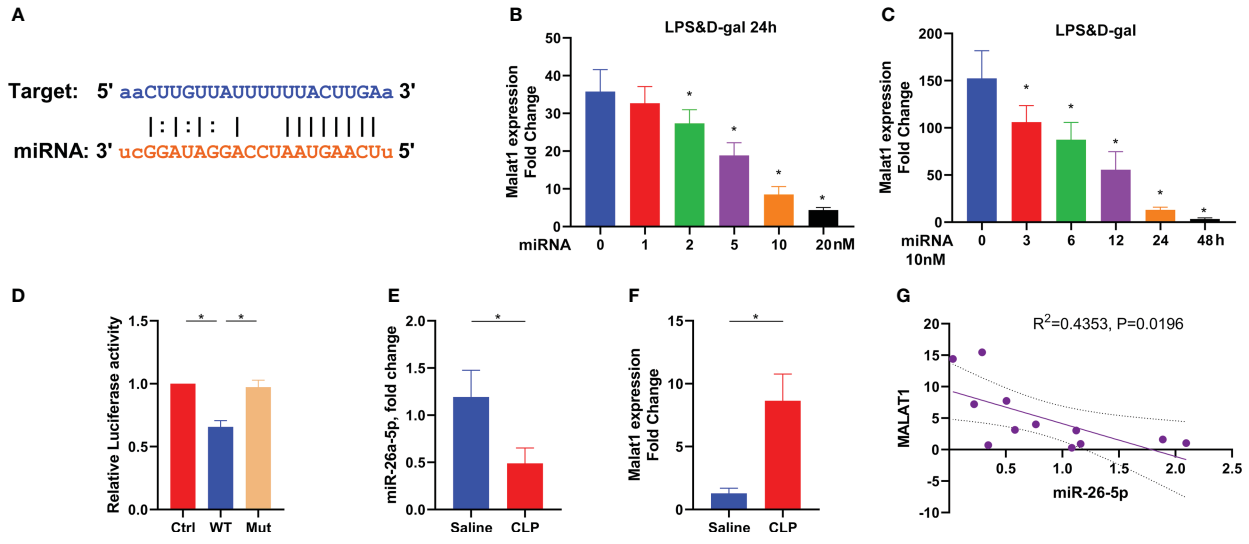

FIGURE 5
Target of miR-26a-5p in the treatment of sepsis-induced acute liver injury. **(A)** Sequence align between miR-26a-5p and MALAT1 by using ENCORI. **(B)** Levels of MALAT1 in the hepatocyte challenged with LPS&D-gal and treated with various doses of miR-26a-5p for 24 h (n=3). **(C)** Levels of MALAT1 in the hepatocyte challenged with LPS&D-gal and treated with miR-26a-5p (single dose, 10 nM) at various time points (n=3). **(D)** Luciferase activity in 293T cells transfected with miR-26a-5p and luciferase vectors containing WT and mutant target site of MALAT1 (n=3). **(E–G)** Levels of miR-26a-5p **(E)** and MALAT1 **(F)** in the liver of mice challenged with CLP or not, and the association between each other by using Spearman correlation **(G)** (n=6 per group). Data are expressed as mean ± SEM of independent experiments analyzed by one-way ANOVA **(B–F)**. * Means $P<0.05$.

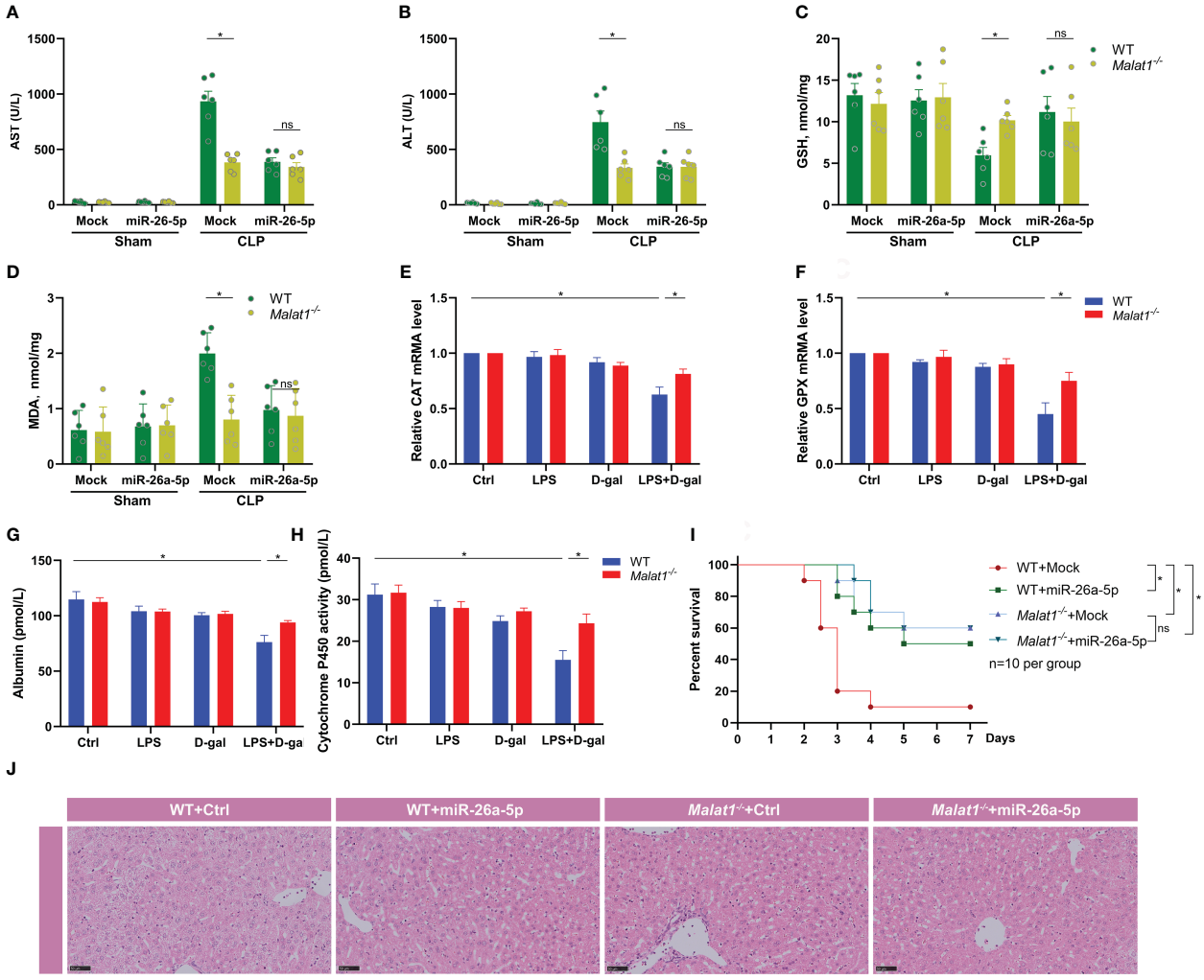

FIGURE 6
miR-26a-5p suppresses sepsis-induced acute liver injury by inhibiting MALAT-1-associated oxidative stress. **(A, B)** Serum aspartate aminotransferase (AST) and alanine transaminase (ALT) level of WT or *Malat1*$^{-/-}$ mice challenged with CLP or treated with the miR-26a-5p (n=6 per group). **(C, D)** GSH and MDA activity in the liver of WT or *Malat1*$^{-/-}$ mice challenged with CLP or treated with the miR-26a-5p (n=6 per group). **(E, F)** Quantitative real-time PCR (qRT–PCR) analysis of Catalase (Cat, **E**) and glutathione peroxidase (GPX, **F**) in primary hepatocytes (n=3 repeats). **(G, H)** Albumin **(G)** and Cytochrome P450 activity **(H)** in the supernatant of primary hepatocytes (n=3 repeats). **(I)** Survival analysis of WT or *Malat1*$^{-/-}$ mice challenged with CLP and treated with or without miR-26a-5p (n=10 per group). **(J)** Representative images of H&E staining of livers from WT or *Malat1*$^{-/-}$ mice challenged with CLP and treated with or without miR-26a-5p. Data are expressed as mean ± SEM of independent experiments analyzed by two-way ANOVA **(A–F)**, and survival curve comparison [log-rank (Mantel-Cox) test]. * Means $P<0.05$.

These data demonstrate that miR-26a-5p inhibits sepsis-induced ALI by targeting MALAT1, which inhibits anti-oxidant system.

4 Discussion

Liver injury is a common complication of sepsis, contributing to the pathogenesis of multiple organ dysfunction and predicting poor outcomes (27). However, the specific treatment targeting sepsis-associated ALI is scant in clinics. In the present study, we discovered a novel role of MSCs and MSC-derived exosome for treating ALI in sepsis, and revealed the underlying mechanism that exosome-delivered miR-26a-5p attenuate the syndrome by silencing MALAT1.

Based on the understanding of the mechanisms, a series of preclinical studies or clinical trials have investigated the effects of anti-inflammation and anti-death medicine in the treatment or prevention of liver failure in sepsis. It has been reported that pyroptosis commonly occurring in infection-induced liver injury, is a therapeutic target for the treatment of this syndrome. As important inhibitors of pyroptosis, AC-YVAD-CMK and/or Glyburide display a protective effect against liver injury in sepsis model (28).

MSCs are widely investigated in the treatment of tissue repair and various inflammatory diseases due to the excessive renewing and immunomodulatory properties (10). MSC-derived exosome suppresses pro-inflammatory cytokines and promotes anti-inflammatory cytokines and responses in a concanavalin-A-induced liver injury model (29). In addition, the particle also exerts anti-oxidant and anti-apoptotic properties, thereby attenuating liver failure and improving survival rate in mice

challenged by D-galactosamine plus TNFα (30). In another liver injury model induced by carbon tetrachloride (CCL4), MSC-derived exosome delivers glutathione peroxidase 1 (GPX1) to the liver, which consequently alleviates oxidative stress and hepatic injury (31). Nevertheless, it is still unknown whether MSC-derived exosome has a protective effect on sepsis-induced liver injury. In line with previous study, we herein found that the exosome dramatically prevented hepatocyte death, liver injury and so-caused mice mortality by inhibiting MALAT1 *via* delivery of miR-26a-5p.

MALAT1 is an evolutionally conserved long non-coding RNA, implicated in various cancer and inflammatory diseases (19). It has been reported that MALAT1 is highly expressed in septic patients or mice with sepsis model (26). Depletion of MALAT1 significantly inhibited sepsis-induced mice death by improving the anti-oxidant capacity of glutathione (26). Consistently, our study found that sepsis boosts oxidative stress in the liver, thereby facilitating hepatocyte death and liver injury. MALAT1 deficiency dramatically inhibits oxidative stress, and thus attenuates liver injury in sepsis. MSC-derived exosome delivered miR-26a-5p mediated MALAT1 breakdown and consequently protected sepsis-associated ALI. Thus, silencing MALAT1 by miR-26a-5p from MSC-derived exosome ameliorates liver injury in sepsis.

In conclusion, MSCs, MSCs-derived exosome and miR-26a-5p could effectively protect against sepsis-induced ALI by inhibiting MALAT1 and MALAT1-enhanced oxidative stress. Our findings provide a new insight for understanding the molecular mechanism of ALI, and provide a potential approach and drug target for the treatment of liver injury in sepsis. However, this was a preliminary study and the pathogenesis of ALI in sepsis is complex. Therefore, large-scale studies will be needed to confirm the detailed mechanisms of MALAT1, miR-26a-5p, MSCs-derived exosome, and MSCs pathway in ALI injury of sepsis through animal experiments and clinical tests in the future.

Data availability statement

The original contributions presented in the study are included in the article/supplementary material. Further inquiries can be directed to the corresponding author.

Ethics statement

The animal study was reviewed and approved by Central South University.

Author contributions

JC and DT conducted the experiments, analyzed the data and composited the figures. XH and EL assisted with experiment operation, data analysis and figure composition. EL monitored the study and wrote the first version of the manuscript. JS designed the study. JS and EL contributed to the conceptualization, data curation. JC, DT, WL and JS made the revision and the final version write-up. All authors contributed to the article and approved the submitted version.

Funding

This work was supported by Key Scientific Project of Hunan Province (2022SK2056), Natural Science Foundation of Hunan Province (2021JJ41006 &2022JJ30817), Postgraduate Research Innovation Project of Central South University (No.1053320191556) and Chen Xiao Ping Foundation of the Development of Science and Technology (CXPJJH12000009-102).

Conflict of interest

The authors declare that the research was conducted in the absence of any commercial or financial relationships that could be construed as a potential conflict of interest.

Publisher's note

References

1. Stevenson EK, Rubenstein AR, Radin GT, Wiener RS, Walkey AJ. Two decades of mortality trends among patients with severe sepsis: a comparative meta-analysis*. *Crit Care Med* (2014) 42(3):625–31. doi: 10.1097/CCM.0000000000000026

2. Gando S, Levi M, Toh CH. Disseminated intravascular coagulation. *Nat Rev Dis Primers* (2016) 2:16037. doi: 10.1038/nrdp.2016.37

3. Rudd KE, Johnson SC, Agesa KM, Shackelford KA, Tsoi D, Kievlan DR, et al. Global, regional, and national sepsis incidence and mortality, 1990-2017: analysis for the global burden of disease study. *Lancet* (2020) 395(10219):200–11. doi: 10.1016/S0140-6736(19)32989-7

4. Kubes P, Jenne C. Immune responses in the liver. *Annu Rev Immunol* (2018) 36:247–277.12. doi: 10.1146/annurev-immunol-051116-052415

5. Racanelli V, Rehermann B. The liver as an immunological organ. *Hepatology* (2006) 43(2 Suppl 1):S54–62. doi: 10.1002/hep.21060

6. Bauer M, Press AT, Trauner M. The liver in sepsis: patterns of response and injury. *Curr Opin Crit Care* (2013) 19(2):123–7. doi: 10.1097/MCC.0b013e32835eba6d

7. Bauer M, Coldewey SM, Leitner M, Löffler B, Weis S, Wetzker R, et al. Deterioration of organ function as a hallmark in sepsis: the cellular perspective. *Front Immunol* (2018) 9:1460. doi: 10.3389/fimmu.2018.01460

8. Nesseler N, Launey Y, Aninat C, Morel F, Mallédant Y, Seguin P, et al. Clinical review: the liver in sepsis. *Crit Care* (2012) 16(5):235. doi: 10.1186/cc11381

9. Galstian GM, Parovichnikova EN, Makarova PM, Kuzmina LA, Troitskaya VV, Gemdzhian E, et al. The results of the Russian clinical trial of mesenchymal stromal cells (MSCs) in severe neutropenic patients (pts) with septic shock (SS) (RUMCESS trial). *Blood* (2015) 126(23):2220. doi: 10.1182/blood.V126.23.2220.2220

10. Galipeau J, Sensébé L. Mesenchymal stromal cells: clinical challenges and therapeutic opportunities. *Cell Stem Cell* (2018) 22(6):824–33. doi: 10.1016/j.stem.2018.05.004

11. Røsland GV, Svendsen A, Torsvik A, Sobala E, McCormack E, Immervoll H, et al. Long-term cultures of bone marrow-derived human mesenchymal stem cells frequently undergo spontaneous malignant transformation. *Cancer Res* (2009) 69 (13):5331–9. doi: 10.1158/0008-5472.CAN-08-4630

12. Nong K, Wang W, Niu X, Hu B, Ma C, Bai Y, et al. Hepatoprotective effect of exosomes from human-induced pluripotent stem cell-derived mesenchymal stromal cells against hepatic ischemia-reperfusion injury in rats. *Cytotherapy* (2016) 18(12):1548–59. doi: 10.1016/j.jcyt.2016.08.002

13. Shi Y, Wang Y, Li Q, Liu K, Hou J, Shao C, et al. Immunoregulatory mechanisms of mesenchymal stem and stromal cells in inflammatory diseases. *Nat Rev Nephrol* (2018) 14(8):493–507. doi: 10.1038/s41581-018-0023-5

14. Fabris L, Ceder Y, Chinnaiyan AM, Jenster GW, Sorensen KD, Tomlins S, et al. The potential of MicroRNAs as prostate cancer biomarkers. *Eur Urol* (2016) 70:312–22. doi: 10.1016/j.eururo.2015.12.054

15. Gandellini P, Doldi V, Zaffaroni N. microRNAs as players and signals in the metastatic cascade: implications for the development of novel anti-metastatic therapies. *Semin Cancer Biol* (2017) 44:132–40. doi: 10.1016/j.semcancer.2017.03.005

16. Chhabra R, Dubey R, Saini N. Cooperative and individualistic functions of the microRNAs in the miR-23aB27aB24- 2 cluster and its implication in human diseases. *Mol Cancer* (2010) 9:232. doi: 10.1186/1476-4598-9-232

17. Pers YM, Jorgensen C. MicroRNA in 2012: biotherapeutic potential of microRNAs in rheumatic diseases. *Nat Rev Rheumatol* (2013) 9:76–8. doi: 10.1038/nrrheum.2012.236

18. Hayes J, Peruzzi PP, Lawler S. MicroRNAs in cancer: biomarkers, functions and therapy. *Trends Mol Med* (2014) 20:460–9. doi: 10.1016/j.molmed.2014.06.005

19. Page DT, Garvey JS. Isolation and characterization of hepatocytes and kupffer cells. *J Immunol Methods* (1979) 27(2):159–73. doi: 10.1016/0022-1759(79)90262-X

20. Huangfu N, Xu Z, Zheng W, Wang Y, Cheng J, Chen X. LncRNA MALAT1 regulates oxLDL-induced CD36 expression via activating beta-catenin. *Biochem Biophys Res Commun* (2018) 495(3):2111–7. doi: 10.1016/j.bbrc.2017.12.086

21. Song Y, Yang L, Guo R, Lu N, Shi Y, Wang X. Long noncoding RNA MALAT1 promotes high glucose-induced human endothelial cells pyroptosis by affecting NLRP3 expression through competitively binding miR-22. *Biochem Biophys Res Commun* (2019) 509(2):359–66. doi: 10.1016/j.bbrc.2018.12.139

22. Zhuang YT, Xu DY, Wang GY, Sun JL, Huang Y, Wang SZ, et al. IL-6 induced lncRNA MALAT1 enhances TNF-alpha expression in LPS-induced septic cardiomyocytes via activation of SAA3. *Eur Rev Med Pharmacol Sci* (2017) 21 (2):302–9.

23. Yuan FF, Cai J, Wu J, Tang Y, Zhao K, Liang F, et al. Z-DNA binding protein 1 promotes heatstroke-induced cell death. *Science* (2022) 376:609–15. doi: 10.1126/science.abg5251

24. Hashemian SM, Du J, Yu M, Suo L. Non-coding RNAs and exosomes: their role in the pathogenesis of sepsis. *Mol Ther-Nucl Acids* (2020) 21:51–74. doi: 10.1016/j.omtn.2020.05.012

25. Zhang D, Du J, Yu M, Suo L, et al. Urine-derived stem cells-extracellular vesicles ameliorate diabetic osteoporosis through HDAC4/HIF-1α/VEGFA axis by delivering microRNA-26a-5p. *Cell Biol Toxicol* (2022). doi: 10.1007/s10565-022-09713-5

26. Chen J, Tang S, Ke S, Cai JJ, Osorio D, Golovko A, et al. Ablation of long noncoding RNA MALAT1 activates antioxidant pathway and alleviates sepsis in mice. *Redox Biol* (2022) 54:102377. doi: 10.1016/j.redox.2022.102377

27. Kramer L, Jordan B, Druml W, Bauer P, Metnitz PG. Incidence and prognosis of early hepatic dysfunction in critically ill patients–a prospective multicenter study. *Crit Care Med* (2007) 35(4):1099–104. doi: 10.1097/01.CCM.0000259462.97164.A0

28. Chen YL, Xu G, Liang X, Wei J, Luo J, Chen GN, et al. Inhibition of hepatic cells pyroptosis attenuates CLP-induced acute liver injury. *Am J Transl Res* (2016) 8(12):5685–95.

29. Tamura R, Uemoto S, Tabata Y. Immunosuppressive effect of mesenchymal stem cell-derived exosomes on a concanavalin a-induced liver injury model. *Inflamm Regener* (2016) 36:26. doi: 10.1186/s41232-016-0030-5

30. Haga H, Yan IK, Takahashi K, Matsuda A, Patel T. Extracellular vesicles from bone marrow-derived mesenchymal stem cells improve survival from lethal hepatic failure in mice. *Stem Cells Transl Med* (2017) 6(4):1262–72. doi: 10.1002/sctm.16-0226

31. Yan Y, Jiang W, Tan Y, Zou S, Zhang H, Mao F, et al. hucMSC exosome-derived GPX1 is required for the recovery of hepatic oxidant injury. *Mol Ther* (2017) 25(2):465–79. doi: 10.1016/j.ymthe.2016.11.019

frontiers | Frontiers in Immunology

TYPE Brief Research Report
PUBLISHED 07 July 2023
DOI 10.3389/fimmu.2023.1171934

OPEN ACCESS

EDITED BY
Pietro Ghezzi,
University of Urbino Carlo Bo, Italy

REVIEWED BY
Xin Liu,
Third Military Medical University, China
Toby K. Eisenstein,
Temple University, United States

*CORRESPONDENCE
Nathan K. Archer
narcher2@jhmi.edu

RECEIVED 22 February 2023
ACCEPTED 16 June 2023
PUBLISHED 07 July 2023

CITATION
Wang Y, Ahmadi MZ, Dikeman DA, Youn C and Archer NK (2023) γδ T cell-intrinsic IL-1R promotes survival during *Staphylococcus aureus* bacteremia. *Front. Immunol.* 14:1171934. doi: 10.3389/fimmu.2023.1171934

γδ T cell-intrinsic IL-1R promotes survival during *Staphylococcus aureus* bacteremia

Yu Wang, Michael Z. Ahmadi, Dustin A. Dikeman, Christine Youn and Nathan K. Archer*

Department of Dermatology, Johns Hopkins University School of Medicine, Baltimore, MD, United States

Staphylococcus aureus is a leading cause of bacteremia, further complicated by the emergence of antibiotic-resistant strains such as methicillin-resistant *S. aureus* (MRSA). A better understanding of host defense mechanisms is needed for the development of host-directed therapies as an alternative approach to antibiotics. The levels of IL-1, IL-17, and TNF-α cytokines in circulation have been associated with predictive outcomes in patients with *S. aureus* bacteremia. However, their causative role in survival and the cell types involved in these responses during bacteremia is not entirely clear. Using a mouse model of *S. aureus* bacteremia, we demonstrated that IL-17A/F and TNF-α had no significant impact on survival, whereas IL-1R signaling was critical for survival during *S. aureus* bacteremia. Furthermore, we identified that T cells, but not neutrophils, monocytes/macrophages, or endothelial cells were the crucial cell type for IL-1R-mediated survival against *S. aureus* bacteremia. Finally, we determined that the expression of IL-1R on γδ T cell, but not $CD4^+$ or $CD8^+$ T cells was responsible for survival against the *S. aureus* bacteremia. Taken together, we uncovered a role for IL-1R, but not IL-17A/F and TNF-α in protection against *S. aureus* bacteremia. Importantly, γδ T cell-intrinsic expression of IL-1R was crucial for survival, but not on other immune cells or endothelial cells. These findings reveal potential cellular and immunological targets for host-directed therapies for improved outcomes against *S. aureus* bacteremia.

KEYWORDS

***Staphylococcus aureus*, IL-1R, bacteremia, T cells, host defense, cytokines**

1 Introduction

Staphylococcus aureus is a leading cause of bacteremia (1), with a mortality rate of ~25% due to the emergence of antibiotic-resistant strains such as methicillin-resistant *S. aureus* (MRSA) (2). Furthermore, all vaccines to date have failed in clinical trials against *S. aureus* invasive infections (3, 4). Thus, a better understanding of host defense mechanisms

is needed for the development of host-directed therapies as an alternative approach to antibiotics.

The IL-1, IL-17, and TNF-α cytokines have been implicated in host defense against *S. aureus* skin and orthopedic infections (5–8). Moreover, IL-1, IL-17, and TNF-α cytokine levels in circulation have been associated with predictive outcomes in patients with *S. aureus* bacteremia (4, 9–12). For instance, elevated IL-1β at the time of patient admission correlated with reduced duration of the *S. aureus* bacteremia (11). However, whether the IL-1, IL-17, and TNF-α cytokines have a causative role in host survival and the cell types involved in these responses during *S. aureus* bacteremia is not entirely clear.

In this study, we evaluated the contributions of IL-1α/β, IL-17A/F, and TNF-α to host survival during *S. aureus* bacteremia using a preclinical mouse model. Furthermore, we identified the specific cell types that promote host survival using mice with specific deletion of IL-1R on T cells, myeloid cells, neutrophils, and endothelial cells.

2 Materials and methods

2.1 Bacterial preparation

The community-acquired methicillin-resistant *S. aureus* (MRSA) USA300 SF8300 strain, a kind gift from Dr. Binh Diep (UCSF), was cultured in tryptic soy broth (TSB) as previously described (13, 14). Briefly, SF8300 was streaked onto a tryptic soy agar (TSA) plate (TSB plus 1.5% bacto agar (BD Biosciences)) and grown overnight at 37°C in a bacterial incubator. Two to three single colonies were picked and cultured in TSB at 37°C in a shaking incubator (240 rpm) overnight (18 h), followed by a 1:50 subculture at 37°C for 2 h to obtain mid-logarithmic phase bacteria. The bacteria were pelleted, washed 3 times with sterile PBS, resuspended in sterile freezing medium (10% glycerol in sterile PBS) at a concentration of 1×10^{10} CFU/ml and aliquots stored in cryovials at -80°C until needed. The number of CFUs was confirmed with overnight culture on TSA plates.

2.2 Mice

Age-matched 6-8-week-old female mice on C57BL/6 background were used for all experiments. The IL-1α$^{-/-}$, IL-1β$^{-/-}$, and IL-17A/F$^{-/-}$ mice were provided by Dr. Yoichiro Iwakura (University of Tokyo). The VE-Cad^{Cre}×IL-1R$^{fl/fl}$ (VE-Cad-IL-1R$^{-/-}$) mice, which lack IL-1R signaling in endothelial cells were provided by Dr. Michael O'Connell (NIH/NIAID). WT C57BL/6, TNF-α$^{-/-}$ (B6.129S-tnf^{tm1Gkl}/J), IL-1R$^{-/-}$ (B6.129S7-Il1r1^{tm1Imx}/J), Lck^{Cre} (B6.Cg-Tg(Lck-cre)548Jxm/J), LysM^{Cre} (B6.129P2-Lyz2$^{tm1(cre)Ifo}$/J), CD4^{Cre} (Tg(Cd4-cre)1Cwi/BfluJ), S100A8^{Cre} (B6.Cg-Tg(S100A8-cre,-EGFP)1Ilw/J), TCRδ^{CreER} (B6.129S-Tcrd$^{tm1.1(cre/ERT2)Zhu}$/J), and IL-1R$^{fl/fl}$ mice (B6.129(Cg)-Il1r1$^{tm1.1Rbl}$/J) were obtained from Jackson Laboratories (Bar Harbor, ME).

Lck^{Cre} mice were crossed with IL-1R$^{fl/fl}$ mice to obtain Lck^{Cre}×IL-1R$^{fl/fl}$ (Lck-IL-1R$^{-/-}$), which lack IL-1R signaling in pan-T cells. LysM^{Cre} were crossed with IL-1R$^{fl/fl}$ mice to obtain LysM^{Cre}×IL-1R$^{fl/fl}$ (LysM-IL-1R$^{-/-}$) mice, which lack IL-1R signaling in myeloid cells. S100A8^{Cre} were crossed with IL-1R$^{fl/fl}$ mice to obtain S100A8^{Cre}×IL1R$^{fl/fl}$ (S100A8-IL-1R$^{-/-}$) mice, which lack IL-1R signaling in neutrophils. CD4^{Cre} were crossed with IL-1R$^{fl/fl}$ mice to obtain CD4^{Cre}×IL1R$^{fl/fl}$ (CD4-IL-1R$^{-/-}$) mice, which lack IL-1R signaling in CD4-expressing cells, including both CD4^{+} and CD8^{+} T cells (due to dual expression of CD4 in both T cell types during thymic development). TCRδ^{CreER} mice were crossed with IL-1R$^{fl/fl}$ mice to obtain TCRδ^{CreER}×IL1R$^{fl/fl}$ (TCRδ-IL-1R$^{-/-}$) mice, which lack IL-1R signaling in γδ T cells upon tamoxifen-inducible deletion.

2.3 Study approval

All mouse strains were bred and maintained under the same specific pathogen-free conditions, with air-isolated cages at an American Association for the Accreditation of Laboratory Animal Care (AAALAC)-accredited animal facility at Johns Hopkins University and handled according to procedures described in the Guide for the Care and Use of Laboratory Animals as well as Johns Hopkins University's policies and procedures as outlined in the Johns Hopkins University Animal Care and Use Training Manual. This study was approved by the Johns Hopkins Animal Care and Use Committee (Protocol #: MO21M378).

2.4 Intravenous infection

The *S. aureus* bacteremia model was modified from previously described protocols (15, 16). Briefly, 6-to-8-week-old female C57BL/6 mice were anesthetized (inhalation of 2% isoflurane) and inoculated intravenously with $4.8\text{-}5.8\times10^{7}$ SF8300 in a 100-µL volume of PBS using a 29-gauge insulin syringe *via* the retro-orbital vein to achieve an LD90.

2.5 Tamoxifen-inducible deletion of IL-1R

The inducible deletion of IL-1R on γδ T cells was modified from a previously described protocol (17). The TCRδ-IL-1R$^{-/-}$ mice were treated daily with 100 µl of 1 mg/ml tamoxifen in sunflower oil injected intraperitoneally for 5 consecutive days. The bacteremia infections were performed 10 days after the last tamoxifen injection. Wild-type (WT) mice were subjected to the same tamoxifen regimen when paired with TCRδ-IL-1R$^{-/-}$ mice. Tamoxifen-inducible deletion of IL-1R was confirmed by flow cytometry, which was comparable to the ~60% deletion efficiency in γδ T cells in TCRδ^{creER} mice based on prior reports (18).

2.6 Flow cytometry

For flow cytometric analysis, 100 µl of peripheral blood and spleen was collected from tamoxifen-treated WT and TCRδ-IL-1R$^{-/-}$

mice 3h after intravenous infection. Red blood cells were lysed with ACK lysis buffer (ThermoFisher Scientific) and cells were resuspended in FACS buffer (PBS containing 1% BSA and 2mM EDTA). Spleen was manually pushed through a cell separation filter (40 μm) and resuspended in FACS buffer. Single cell suspensions were stained for viability (Viobility 405/520 viability kit, Miltenyi Biotec) and TruStain fcX (Biolegend) was used to block Fc receptor binding. Next, blood single cells were surface stained with the following mAbs: PE-Vio770-CD3 (REA641, Miltenyi Biotec), PE-CD8a (REA601, Miltenyi Biote), APC-Vio770-CD4 (REA604, Miltenyi Biote) VioBlue-TCRγδ (REA633, Miltenyi Biotec), and APC-CD121α (clone JAMA-147, BioLegend). The γδ T cells were identified as $CD3^+CD4^-CD8^-TCR\gamma\delta^+$ cells from the live cell population. Spleen single cells were surface stained with the following mAbs: PerCP-Vio700-CD45 (REA737, Miltenyi Biotec), APC-CD11b (REA592, Miltenyi Biotec), VioBlue-Ly6C (REA796, Miltenyi Biotec), APC-Vio770-Ly6G (REA526, Miltenyi Biotec), and PE-Vio770-F4/80 (REA126, Miltenyi Biotec). Cell acquisition was performed on a MACSQuant analyzer (Miltenyi Biotec) and data analyzed using MACSQuantify software (Miltenyi Biotec). See Supplementary Figure 1 for gating strategy.

2.7 Ex vivo CFU enumeration

At 3h post infection, mice were euthanized, and the spleen, liver, and kidneys were harvested and ex vivo CFU were isolated as previously described (5, 19). The tissue specimens were homogenized (PRO200 Series homogenizer; PRO Scientific) and then serially diluted and cultured overnight on TSA plates at 37°C. Ex vivo CFU from the homogenized tissue were then enumerated from the plates.

2.8 Statistical analyses

Survival rates were compared by log rank (Mantel-Cox) test and data from single comparisons analyzed by Student's t test (two-tailed), as indicated in the figure legends. All statistical analyses were calculated with Prism software (GraphPad 9.5 Software, La Jolla, California). CFU data are presented as geometric mean ± geometric standard deviation (SD). All other data are presented as mean ± standard error of the mean (SEM) and values of $P < 0.05$ were considered statistically significant.

3 Results

3.1 IL-1R signaling improves survival during *S. aureus* bacteremia

The levels of IL-1, IL-17, and TNF-α cytokines in circulation have been associated with predictive outcomes in patients with *S. aureus* bacteremia (4, 9–12). Therefore, we set out to determine the mechanistic effect of IL-1α/β, TNF-α, and IL-17A/F on survival during *S. aureus* bacteremia using a preclinical mouse model whereby 4.8-5.8 × 10^7 CFUs of *S. aureus* USA300 (SF8300) were injected i.v. and survival measured over time (15, 16). To determine the role of IL-1R signaling, we first performed our bacteremia model on wild-type (WT) C57BL/6 and IL-$1R^{-/-}$ mice and found that IL-$1R^{-/-}$ mice had a statistically significant decrease in survival compared to WT mice (Figure 1A). Since IL-1α and IL-1β signal through the IL-1R (20), we next tested IL-$1\alpha^{-/-}$ and IL-$1\beta^{-/-}$ mice and discovered that both IL-$1\alpha^{-/-}$ and IL-$1\beta^{-/-}$ mice had a markedly reduced survival compared to WT mice (Figure 1A). Next, we examined IL-17A/$F^{-/-}$ and TNF-$\alpha^{-/-}$ mice and found no statistically significant differences compared to WT mice (Figure 1B). Taken together, our data indicated that IL-1α and IL-1β signaling *via* IL-1R enhanced survival during *S. aureus* bacteremia infections.

3.2 γδ T cell-intrinsic IL-1R signaling promotes survival during *S. aureus* bacteremia

Since IL-1R signaling was important for survival during *S. aureus* bacteremia infections, we next elucidated the specific cell types involved in the IL-1R response. Various cell types use IL-1R signaling to drive host defense and inflammation (20), including myeloid cells, T cells, and non-immune cells (21). Thus, we developed mice with specific deletion of IL-1R in T cells (Lck-IL-$1R^{-/-}$), myeloid cells (LysM-IL-$1R^{-/-}$), and neutrophils (S100A8-IL-$1R^{-/-}$). We also used mice with specific deletion of IL-1R in endothelial cells (VE-Cad-IL-$1R^{-/-}$), since *S. aureus* interacts with endothelial cells upon bacteremia infections (22). We discovered that only the Lck-IL-$1R^{-/-}$ mice had a significant defect in survival compared to WT mice (Figure 2A), suggesting that IL-1R signaling on T cells, but not myeloid cells, neutrophils, or endothelial cells was important for host survival.

We next determined the specific T cell subset required for IL-1R signaling, since CD4+ and γδ T cells are reported to be involved in host defense against *S. aureus* infections (7, 23–25). To this end, we developed and tested mice with specific deletion of IL-1R in CD4+ T cells (CD4-IL-$1R^{-/-}$) and tamoxifen-inducible deletion of IL-1R in γδ T cells (TCRδ-IL-$1R^{-/-}$). We discovered that CD4-IL-$1R^{-/-}$ mice had no difference in survival compared to WT mice (Figure 2B). Interestingly, there was markedly decreased survival in TCRδ-IL-$1R^{-/-}$ mice compared to WT mice (Figure 2C). There was a trend towards increased circulating γδ T cells counts in TCRδ-IL-$1R^{-/-}$ mice compared to WT mice (Figure 3A). We confirmed tamoxifen-inducible deletion of IL-1R on γδ T cells in the TCRδ-IL-$1R^{-/-}$ mice by flow cytometry (Figure 3B). Collectively, IL-1R signaling on γδ T cells was important for survival during *S. aureus* bacteremia infections.

3.3 γδ T cell-intrinsic IL-1R signaling increases monocyte recruitment to the spleen during *S. aureus* bacteremia

We next elucidated whether γδ T cell-intrinsic IL-1R signaling affected immune cell levels and *S. aureus* burden during the

10.3389/fimmu.2023.1171934

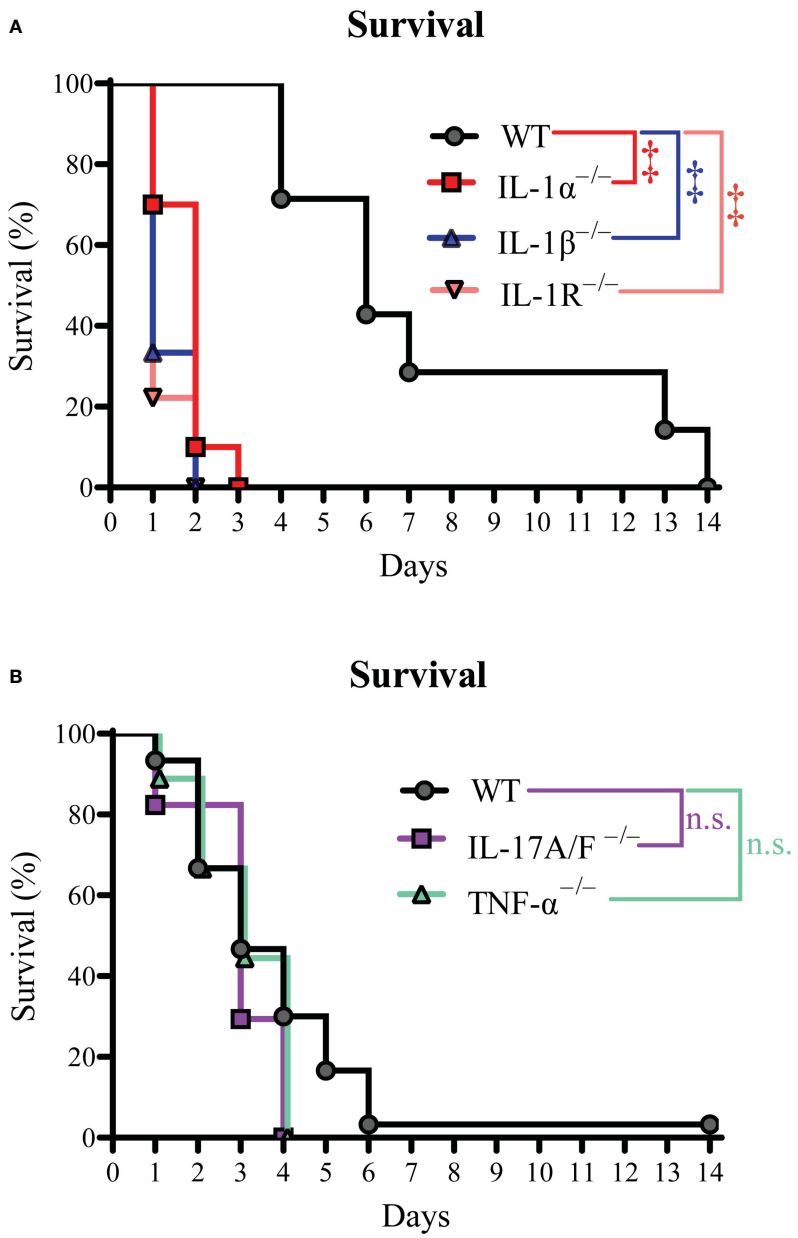

FIGURE 1
IL-1R signaling improves survival during *S. aureus* bacteremia. The *S. aureus* bacteremia infection was performed on WT, IL-1α$^{-/-}$, IL-1β$^{-/-}$, IL-1R$^{-/-}$, IL-17A/F$^{-/-}$, and TNF-α$^{-/-}$ mice. **(A)** Survival (%) of WT, IL-1α$^{-/-}$, IL-1β$^{-/-}$, and IL-1R$^{-/-}$ mice (n=7-10 per group, average inoculum = 4.8 × 10^7 CFUs). **(B)** Survival (%) of WT, IL-17A/F$^{-/-}$, and TNF-α$^{-/-}$ mice (n=9-30 per group, average inoculum = 5.4 × 10^7 CFUs). ‡$P < 0.001$ and n.s. = not significant; WT versus IL-1α$^{-/-}$, IL-1β$^{-/-}$, IL-1R$^{-/-}$, IL-17A/F$^{-/-}$, and TNF-α$^{-/-}$ as calculated by log rank (Mantel-Cox) test. Data were combined from at least 2 independent experiments.

bacteremia. To this end, we first measured neutrophil, monocyte, and macrophage population levels in the spleens of TCRδ-IL-1R$^{-/-}$ and WT mice 3 hours post-infection. We found that monocytes, but not neutrophils or macrophages, were significantly decreased in TCRδ-IL-1R$^{-/-}$ mice compared to WT mice (Figures 3C-E). Next, we measured *S. aureus* CFUs in the spleen, liver, and kidney, but found no difference in bacterial burden between TCRδ-IL-1R$^{-/-}$ and WT mice (Figures 3F-H). These data indicated that γδ T cell-intrinsic IL-1R signaling promoted monocyte recruitment to the spleen during *S. aureus* bacteremia.

4 Discussion

The IL-1, IL-17, and TNF-α cytokines contribute to host defense against *S. aureus* skin and orthopedic infections (5–8). Although IL-1, IL-17, and TNF-α cytokine levels in circulation have been associated with predictive outcomes in patients with *S. aureus* bacteremia (4, 9–12), whether these cytokines mechanistically promote host survival and the cell types involved in these responses is under-investigated. Thus, we tested mice deficient in IL-1, IL-17, and TNF-α cytokines in a

10.3389/fimmu.2023.1171934

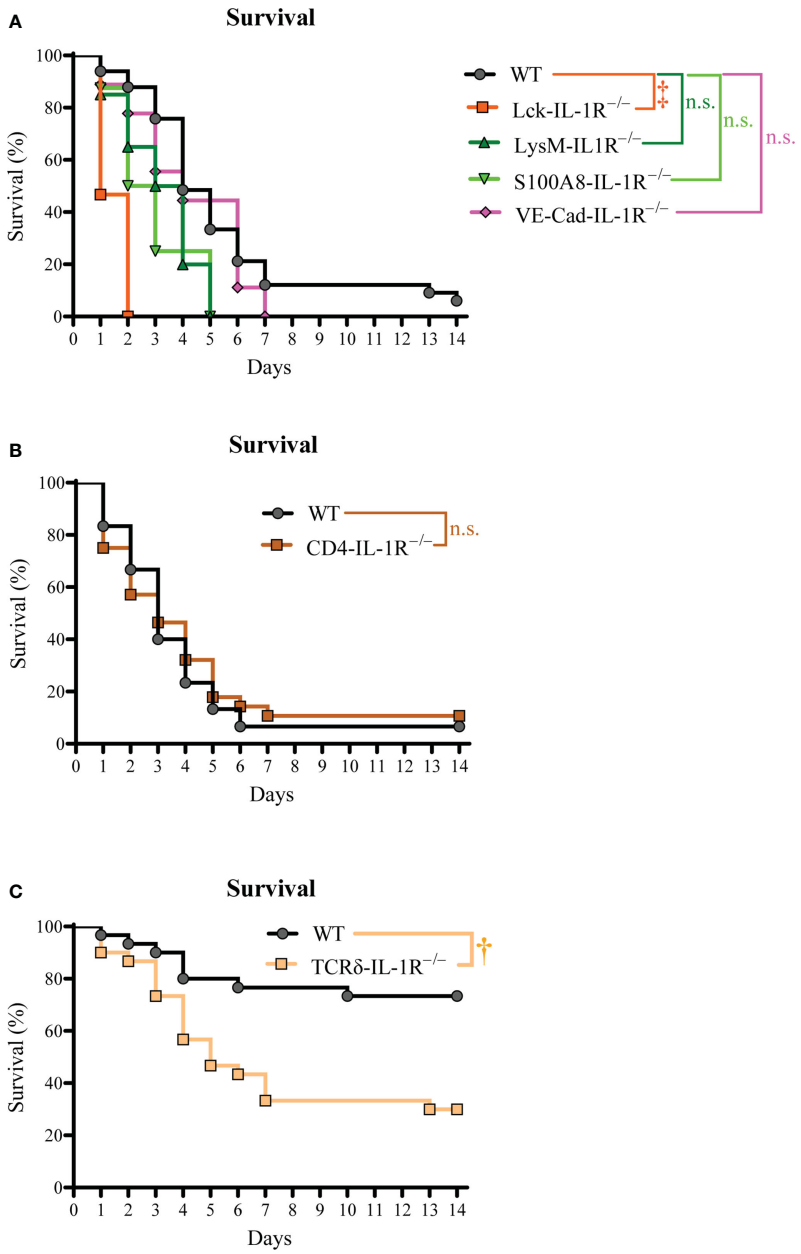

FIGURE 2
γδ T cell-intrinsic IL-1R signaling promotes survival during *S. aureus* bacteremia. The *S. aureus* bacteremia infection was performed on Lck-IL-1R$^{-/-}$, LysM-IL-1R$^{-/-}$, S100A8-IL-1R$^{-/-}$, VE-Cad-IL-1R$^{-/-}$, CD4-IL-1R$^{-/-}$, and TCRδ-IL-1R$^{-/-}$ mice. **(A)** Survival (%) of Lck-IL-1R$^{-/-}$, LysM-IL-1R$^{-/-}$, S100A8-IL-1R$^{-/-}$, VE-Cad-IL-1R$^{-/-}$ mice (n=8-35 per group, average inoculum = 5.4 × 10^7 CFUs). **(B)** Survival (%) of WT and CD4-IL-1R$^{-/-}$ mice (n=28-30 per group, average inoculum = 5.4 × 10^7 CFUs). **(C)** Survival (%) of WT and TCRδ-IL-1R$^{-/-}$ mice (n=29 per group, average inoculum = 5.4 × 10^7 CFUs). †P < 0.01, ‡P < 0.001, and n.s. = not significant; WT versus Lck-IL-1R$^{-/-}$, LysM-IL-1R$^{-/-}$, S100A8-IL-1R$^{-/-}$, VE-Cad-IL-1R$^{-/-}$, CD4-IL-1R$^{-/-}$, TCRδ-IL-1R$^{-/-}$ as calculated by log rank (Mantel-Cox) test. Data were combined from at least 2 independent experiments.

preclinical mouse model of *S. aureus* bacteremia and discovered that IL-1R signaling was important for host survival. Furthermore, we identified γδ T cells as the cell type that drives IL-1R-mediated host survival against *S. aureus* bacteremia. These results provide several important insights into the protective host responses during *S. aureus* bacteremia.

First, we found that IL-1R signaling contributed to host survival during *S. aureus* bacteremia, which aligns with previously published reports (26, 27). Similarly, IL-1R signaling promotes host defense against *S. aureus* skin, orthopedic, and pneumonia infections (5, 8, 28). Interestingly, we found that both IL-1α and IL-1β were important in our model, suggesting they have non-redundant roles in host survival. This may be explained by the differences in expression profiles between the cytokines. For instance, IL-1α is constitutively expressed in non-immune cell types (29), whereas IL-1β is induced (30). Moreover, IL-1α has a nuclear localization sequence that is absent in IL-1β (31), which has important implications in inflammation (32). Understanding the differential mechanisms of protection between IL-1α and IL-1β against *S. aureus* bacteremia will be the focus of future work.

10.3389/fimmu.2023.1171934

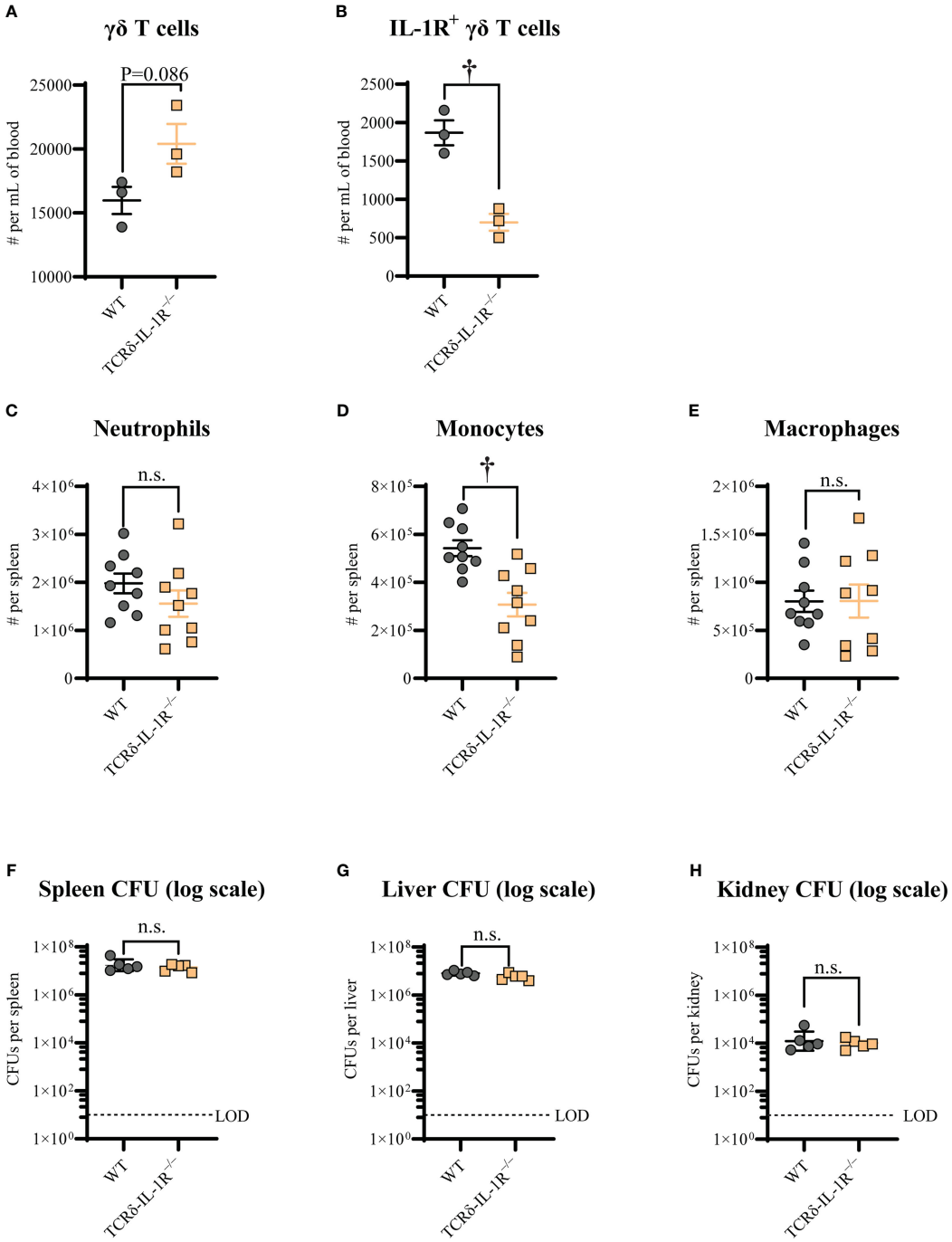

FIGURE 3
γδ T cell-intrinsic IL-1R signaling promotes monocyte recruitment during *S. aureus* bacteremia. WT and TCRδ-IL-1R−/− mice were treated daily with 100 µl of 1 mg/ml tamoxifen in sunflower oil injected intraperitoneally for 5 consecutive days. The bacteremia infections were performed 10 days after the last tamoxifen injection. After 3h post-infection, peripheral blood and spleen were collected for flow cytometry analysis, spleen, liver, and kidney were collected for ex vivo CFU enumeration. Mean cell numbers ± SEM for total γδ T cells **(A)**, IL-1R$^+$ γδ T cells **(B)**, neutrophils **(C)**, monocytes **(D)**, and macrophages **(E)**. Ex vivo CFU (geometric mean ± geometric SD) for spleen **(F)**, liver **(G)**, and kidney **(H)**. n=3 per group for A and B, n=9 per group for C, D, and **(E)** n=5 per group for F, G, and **(H)** †P < 0.01 and n.s. = not significant; WT versus TCRδ-IL-1R−/− as calculated by Student's t test. Data are combined or representative from 2 independent experiments.

We also discovered that TNF-α and IL-17A/F did not influence host survival during *S. aureus* bacteremia at the dose tested. This was unexpected, as both TNF-α and IL-17A/F drive host defense against *S. aureus* at other infection sites (*e.g.*, skin and orthopedic implants) (5–7, 33, 34). However, in a baboon model of group A streptococcal bacteremia infection, anti-TNF-α monoclonal antibody therapy improved survival outcomes (35). Similarly, heightened TNF-α production correlated with persistent rather than resolving bacteremia in patients (12). Another possibility for the lack of phenotype in TNF-α deficient mice is that lymphotoxin-

α signals through the TNF-α receptors (36, 37), which may have compensated for TNF-α deficiency in our *S. aureus* bacteremia model. Although IL-17A did not improve survival outcomes during bacteremia in our model, IL-17A limits the systemic dissemination of *S. aureus* from skin infection to kidneys (38). Thus, IL-17A may be more important in the control of *S. aureus* infections in the tissue rather than protection once bacteremia has occurred. Although not analyzed in this study, there may be a role for IL-10 in the infectious process during *S. aureus* bacteremia, as this cytokine correlates with mortality in humans (11, 12). Collectively, our findings do not support a role for TNF-α and IL-17A/F in survival outcomes during *S. aureus* bacteremia in our preclinical mouse model.

We uncovered that γδ T cell-intrinsic IL-1R signaling was crucial for host survival during *S. aureus* bacteremia. Our findings may relate to prior studies on the protective role of γδ T cells and other T cells against *S. aureus* skin infections and nasal colonization (7, 8, 39–41). In contrast, IL-1R signaling on non-hematopoietic cells was critical for protection against *S. aureus* skin infections (8). Thus, these findings indicate that the protective cell type that provides the IL-1R signal against *S. aureus* infections is context-dependent. Given that IL-1R deficient mice succumbed to *S. aureus* bacteremia within 2 days, our findings suggested that γδ T cell-mediated IL-1R signaling occurs soon after infection. In fact, γδ T cells are an innate source of pro-inflammatory responses driven by IL-1 cytokines independent of T cell receptor engagement (42, 43), perhaps explaining the importance of IL-1R signaling on this T cell subset for rapid protection against *S. aureus* bacteremia infections. However, since IL-17A/F cytokines were not important for host survival herein, and γδ T cells produce IL-17 cytokines in response to IL-1R signaling (42), it begs the question of how γδ T cell-intrinsic IL-1R signaling is mediating protection against *S. aureus* bacteremia? Our findings suggested that γδ T cell-intrinsic IL-1R signaling promotes monocyte recruitment to the spleen during *S. aureus* bacteremia as a mechanism of protection. This may relate to the known role of IL-1β to induce the monocyte-recruiting chemokine, CCL2 (44, 45). Other potential explanations include γδ T cell production of antimicrobial peptides, IL-22, and neutrophil recruiting chemokines to promote host survival (46, 47), which have been associated with protection against *S. aureus* at other infection sites (13, 48). Understanding the localization and mechanism of protection of the γδ T cell-specific IL-1R response during *S. aureus* bacteremia will be part of our future interrogations.

There were limitations. For instance, our study was conducted with a single *S. aureus* strain, limiting the broader conclusions of our findings. However, other studies have tested additional *S. aureus* strains in IL-1R deficient mice or mice treated with IL-1Ra with similar results (26, 27, 49), suggesting that IL-1R-mediated survival is not specific to a single *S. aureus* strain. Moreover, we used a high inoculum of *S. aureus* in the bacteremia model (*i.e.*, LD90), which may have missed phenotypes present in a lower inoculum (*e.g.*, LD50). Another limitation to the study is the possibility that the phenotypes in our cell-specific IL-1R deficient mice are due to changes in cytokine production in IL-1α and IL-1β rather than IL-1R-specific mechanisms. The use of tamoxifen to delete IL-1R in the TCRδ-IL-1R$^{-/-}$ mice may have influenced the immune responses upon the *S. aureus* bacteremia infection (*e.g.*, neutrophil function) (50), which was observed in Figure 2C. To control for these effects, we similarly treated the control WT comparison group with tamoxifen. Importantly, deletion efficiency in γδ T cells in Lck^{cre} and TCRδ^{creER} mice is ~20% and ~60%, respectively (18, 51), leaving the possibility that IL-1R signaling on other T cell subsets not specifically tested in this study (*e.g.*, NK T cells and MAIT cells) contributed to host survival during *S. aureus* bacteremia infections. Addressing these limitations will be performed in our future work.

Taken together, the results of this study indicate that γδ T cell-intrinsic IL-1R signaling promotes host survival during *S. aureus* bacteremia infections. Thus, IL-1R on γδ T cells may serve as a host-directed therapeutic target for the treatment of *S. aureus* bacteremia infections and potentially other antibiotic-resistant infections. Potential therapeutic strategies could include IL-1R agonism or neutralizing the IL-1R antagonist (IL-1Ra) to promote survival during *S. aureus* bacteremia. However, further studies are warranted to understand the protective mechanisms of γδ T cell-intrinsic IL-1R signaling against *S. aureus* bacteremia.

Data availability statement

The raw data supporting the conclusions of this article will be made available by the authors, without undue reservation.

Ethics statement

The animal study was reviewed and approved by the Johns Hopkins Animal Care and Use Committee (Protocol #: MO21M378).

Author contributions

YW and NA conceived and designed the study. YW conducted the experiments. YW, MA, DD, and CY collected the data. YW analyzed the data. YW and NA wrote the manuscript. All authors reviewed the final version of the manuscript.

Funding

This study was funded in part by grants R01AR073665 (NA), R01AI111205 (NA), and R01AI146177 (NA) and from the United States National Institute of Arthritis and Musculoskeletal and Skin Diseases (NIAMS) and National Institute of Allergy and Infectious Diseases (NIAID).

Acknowledgments

The IL-1α$^{-/-}$, IL-1β$^{-/-}$, and IL-17A/F$^{-/-}$ mice were kindly provided by Dr. Yoichiro Iwakura (University of Tokyo). The VE-Cad-IL-1R$^{-/-}$ mice were a gift from Dr. Michael O'Connell (NIH/NIAID). The *S. aureus* USA300 strain, SF8300, was a kind gift from Dr. Binh Diep (UCSF).

Conflict of interest

NA has received previous grant support from Pfizer and Boehringer Ingelheim and has been a paid consultant for Janssen Pharmaceuticals.

The remaining authors declare that the research was conducted in the absence of any commercial or financial relationships that could be constructed as a potential conflict of interest.

Publisher's note

Supplementary material

The Supplementary Material for this article can be found online at: https://www.frontiersin.org/articles/10.3389/fimmu.2023.1171934/full#supplementary-material

SUPPLEMENTARY FIGURE 1
Gating strategy. **(A)** The gating strategy of myeloid cells in spleen **(B)** the gating strategy of T cells in peripheral blood.

References

1. Weiner-Lastinger LM, Abner S, Edwards JR, Kallen AJ, Karlsson M, Magill SS, et al. Antimicrobial-resistant pathogens associated with adult healthcare-associated infections: summary of data reported to the national healthcare safety network, 2015-2017. *Infect Control Hosp Epidemiol* (2020) 41:1–18. doi: 10.1017/ice.2019.296

2. Lam JC, Stokes W. The golden grapes of wrath - staphylococcus aureus bacteremia: a clinical review. *Am J Med* (2023) 136:19–26. doi: 10.1016/j.amjmed.2022.09.017

3. Proctor RA. Immunity to staphylococcus aureus: implications for vaccine development. *Immun to. Microbiol Spectr* (2019) 7. doi: 10.1128/microbiolspec.GPP3-0069-2019

4. Fowler VG, Allen KB, Moreira ED, Moustafa M, Isgro F, Boucher HW, et al. Effect of an investigational vaccine for preventing staphylococcus aureus infections after cardiothoracic surgery: a randomized trial. *JAMA* (2013) 309:1368–78. doi: 10.1001/jama.2013.3010

5. Wang Y, Ashbaugh AG, Dikeman DA, Zhang J, Ackerman NE, Kim SE, et al. IL-1β and TNF are essential in controlling an experimental orthopaedic implant associated infection. *J Orthop Res* (2020) 38:1800–9. doi: 10.1002/jor.24608

6. Cho JS, Pietras EM, Garcia NC, Ramos RI, Farzam DM, Monroe HR, et al. IL-17 is essential for host defense against cutaneous staphylococcus aureus infection in mice. *J Clin Invest* (2010) 120:1762–73. doi: 10.1172/JCI40891

7. Marchitto MC, Dillen CA, Liu H, Miller RJ, Archer NK, Ortines RV, et al. Clonal Vgamma6+Vdelta4+ T cells promote IL-17-mediated immunity against staphylococcus aureus skin infection. *Proc Natl Acad Sci U.S.A.* (2019) 116:10917–26. doi: 10.1073/pnas.1818256116

8. Miller LS, O'Connell RM, Gutierrez MA, Pietras EM, Shahangian A, Gross CE, et al. MyD88 mediates neutrophil recruitment initiated by IL-1R but not TLR2 activation in immunity against staphylococcus aureus. *Immunity* (2006) 24:79–91. doi: 10.1016/j.immuni.2005.11.011

9. Miller LS, Fowler VG, Shukla SK, Rose WE, Proctor RA. Development of a vaccine against staphylococcus aureus invasive infections: evidence based on human immunity, genetics and bacterial evasion mechanisms. *FEMS Microbiol Rev* (2020) 44:123–53. doi: 10.1093/femsre/fuz030

10. McNeely TB, Shah NA, Fridman A, Joshi A, Hartzel JS, Keshari RS, et al. Mortality among recipients of the Merck V710 staphylococcus aureus vaccine after postoperative s. aureus infections: an analysis of possible contributing host factors. *Hum Vaccin Immunother* (2014) 10:3513–6. doi: 10.4161/hv.34407

11. Rose WE, Eickhoff JC, Shukla SK, Pantrangi M, Rooijakkers S, Cosgrove SE, et al. Elevated serum interleukin-10 at time of hospital admission is predictive of mortality in patients with staphylococcus aureus bacteremia. *J Infect Dis* (2012) 206:1604–11. doi: 10.1093/infdis/jis552

12. Minejima E, Bensman J, She RC, Mack WJ, Tuan Tran M, Ny P, et al. A dysregulated balance of proinflammatory and anti-inflammatory host cytokine response early during therapy predicts persistence and mortality in staphylococcus aureus bacteremia. *Crit Care Med* (2016) 44:671–9. doi: 10.1097/CCM.0000000000001465

13. Malhotra N, Yoon J, Leyva-Castillo JM, Galand C, Archer N, Miller LS, et al. IL-22 derived from γδ T cells restricts staphylococcus aureus infection of mechanically injured skin. *J Allergy Clin Immunol* (2016) 138:1098–107.e3. doi: 10.1016/j.jaci.2016.07.001

14. Randad PR, Dillen CA, Ortines RV, Mohr D, Aziz M, Price LB, et al. Comparison of livestock-associated and community-associated staphylococcus aureus pathogenicity in a mouse model of skin and soft tissue infection. *Sci Rep* (2019) 9:6774. doi: 10.1038/s41598-019-42919-y

15. Miller RJ, Crosby HA, Schilcher K, Wang Y, Ortines RV, Mazhar M, et al. Development of a staphylococcus aureus reporter strain with click beetle red luciferase for enhanced *in vivo* imaging of experimental bacteremia and mixed infections. *Sci Rep* (2019) 9:16663. doi: 10.1038/s41598-019-52982-0

16. Gordon O, Dikeman DA, Ortines RV, Wang Y, Youn C, Mumtaz M, et al. The novel oxazolidinone TBI-223 is effective in three preclinical mouse models of methicillin-resistant staphylococcus aureus infection. *Microbiol Spectr* (2022) 10: e0245121. doi: 10.1128/spectrum.02451-21

17. Ravipati A, Nolan S, Alphonse M, Dikeman D, Youn C, Wang Y, et al. IL-6R/STAT3-signaling in keratinocytes rather than T cells induces psoriasis-like dermatitis in mice. *J Invest Dermatol* (2021) 142:1126–35. doi: 10.1016/j.jid.2021.09.012

18. Zhang B, Wu J, Jiao Y, Bock C, Dai M, Chen B, et al. Differential requirements of TCR signaling in homeostatic maintenance and function of dendritic epidermal T cells. *J Immunol* (2015) 195:4282–91. doi: 10.4049/jimmunol.1501220

19. Wang Y, Dikeman D, Zhang J, Ackerman N, Kim S, Alphonse MP, et al. CCR2 contributes to host defense against staphylococcus aureus orthopedic implant-associated infections in mice. *J Orthop Res* (2021) 19:409–19. doi: 10.1002/jor.25027

20. Mantovani A, Dinarello CA, Molgora M, Garlanda C. Interleukin-1 and related cytokines in the regulation of inflammation and immunity. *Immunity* (2019) 50:778–95. doi: 10.1016/j.immuni.2019.03.012

21. Dmitrieva-Posocco O, Dzutsev A, Posocco DF, Hou V, Yuan W, Thovarai V, et al. Cell-Type-Specific responses to interleukin-1 control microbial invasion and tumor-elicited inflammation in colorectal cancer. *Immunity* (2019) 50:166–80.e7. doi: 10.1016/j.immuni.2018.11.015

22. Kwiecinski JM, Crosby HA, Valotteau C, Hippensteel JA, Nayak MK, Chauhan AK, et al. Staphylococcus aureus adhesion in endovascular infections is controlled by the ArlRS-MgrA signaling cascade. *PloS Pathog* (2019) 15:e1007800. doi: 10.1371/journal.ppat.1007800

23. Dillen CA, Pinsker BL, Marusina AI, Merleev AA, Farber ON, Liu H, et al. Clonally expanded γδ T cells protect against staphylococcus aureus skin reinfection. *J Clin Invest* (2018) 128:1026–42. doi: 10.1172/JCI96481

24. Ishigame H, Kakuta S, Nagai T, Kadoki M, Nambu A, Komiyama Y, et al. Differential roles of interleukin-17A and -17F in host defense against mucoepithelial bacterial infection and allergic responses. *Immunity* (2009) 30:108–19. doi: 10.1016/j.immuni.2008.11.009

25. Brown AF, Murphy AG, Lalor SJ, Leech JM, O'Keeffe KM, Mac Aogáin M, et al. Memory Th1 cells are protective in invasive staphylococcus aureus infection. *PloS Pathog* (2015) 11:e1005226. doi: 10.1371/journal.ppat.1005226

26. Hultgren OH, Svensson L, Tarkowski A. Critical role of signaling through IL-1 receptor for development of arthritis and sepsis during staphylococcus aureus infection. *J Immunol* (2002) 168:5207–12. doi: 10.4049/jimmunol.168.10.5207

27. Verdrengh M, Thomas JA, Hultgren OH. IL-1 receptor-associated kinase 1 mediates protection against staphylococcus aureus infection. *Microbes Infect* (2004) 6:1268–72. doi: 10.1016/j.micinf.2004.08.009

28. Robinson KM, Choi SM, McHugh KJ, Mandalapu S, Enelow RI, Kolls JK, et al. Influenza a exacerbates staphylococcus aureus pneumonia by attenuating IL-1β production in mice. *J Immunol* (2013) 191:5153–9. doi: 10.4049/jimmunol.1301237

29. Rider P, Voronov E, Dinarello CA, Apte RN, Cohen I. Alarmins: feel the stress. *J Immunol* (2017) 198:1395–402. doi: 10.4049/jimmunol.1601342

30. Dinarello CA. Overview of the IL-1 family in innate inflammation and acquired immunity. *Immunol Rev* (2018) 281:8–27. doi: 10.1111/imr.12621

31. Gabay C, Lamacchia C, Palmer G. IL-1 pathways in inflammation and human diseases. *Nat Rev Rheumatol* (2010) 6:232–41. doi: 10.1038/nrrheum.2010.4

32. Cohen I, Idan C, Rider P, Peleg R, Vornov E, Elena V, et al. IL-1α is a DNA damage sensor linking genotoxic stress signaling to sterile inflammation and innate immunity. *Sci Rep* (2015) 5:14756. doi: 10.1038/srep14756

33. Archer NK, Adappa ND, Palmer JN, Cohen NA, Harro JM, Lee SK, et al. Interleukin-17A (IL-17A) and IL-17F are critical for antimicrobial peptide production and clearance of staphylococcus aureus nasal colonization. *Infect Immun* (2016) 84:3575–83. doi: 10.1128/IAI.00596-16

34. Kudva A, Scheller EV, Robinson KM, Crowe CR, Choi SM, Slight SR, et al. Influenza a inhibits Th17-mediated host defense against bacterial pneumonia in mice. *J Immunol* (2011) 186:1666–74. doi: 10.4049/jimmunol.1002194

35. Stevens DL, Bryant AE, Hackett SP, Chang A, Peer G, Kosanke S, et al. Group a streptococcal bacteremia: the role of tumor necrosis factor in shock and organ failure. *J Infect Dis* (1996) 173:619–26. doi: 10.1093/infdis/173.3.619

36. Wajant H, Pfizenmaier K, Scheurich P. Tumor necrosis factor signaling. *Cell Death Differ* (2003) 10:45–65. doi: 10.1038/sj.cdd.4401189

37. Croft M, Benedict CA, Ware CF. Clinical targeting of the TNF and TNFR superfamilies. *Nat Rev Drug Discovery* (2013) 12:147–68. doi: 10.1038/nrd3930

38. Chan LC, Chaili S, Filler SG, Barr K, Wang H, Kupferwasser D, et al. Nonredundant roles of interleukin-17A (IL-17A) and IL-22 in murine host defense against cutaneous and hematogenous infection due to methicillin-resistant staphylococcus aureus. *Infect Immun* (2015) 83:4427–37. doi: 10.1128/IAI.01061-15

39. Cho JS, Guo Y, Ramos RI, Hebroni F, Plaisier SB, Xuan C, et al. Neutrophil-derived IL-1β is sufficient for abscess formation in immunity against staphylococcus aureus in mice. *PloS Pathog* (2012) 8:e1003047. doi: 10.1371/journal.ppat.1003047

40. Archer NK, Harro JM, Shirtliff ME. Clearance of staphylococcus aureus nasal carriage is T cell dependent and mediated through interleukin-17A expression and neutrophil influx. *Infect Immun* (2013) 81:2070–5. doi: 10.1128/IAI.00084-13

41. Mulcahy ME, Leech JM, Renauld JC, Mills KH, McLoughlin RM. Interleukin-22 regulates antimicrobial peptide expression and keratinocyte differentiation to control staphylococcus aureus colonization of the nasal mucosa. *Mucosal Immunol* (2016) 9:1429–41. doi: 10.1038/mi.2016.24

42. Sutton CE, Lalor SJ, Sweeney CM, Brereton CF, Lavelle EC, Mills KH. Interleukin-1 and IL-23 induce innate IL-17 production from gammadelta T cells, amplifying Th17 responses and autoimmunity. *Immunity* (2009) 31:331–41. doi: 10.1016/j.immuni.2009.08.001

43. Duan J, Chung H, Troy E, Kasper DL. Microbial colonization drives expansion of IL-1 receptor 1-expressing and IL-17-producing gamma/delta T cells. *Cell Host Microbe* (2010) 7:140–50. doi: 10.1016/j.chom.2010.01.005

44. Kaplanov I, Carmi Y, Kornetsky R, Shemesh A, Shurin GV, Shurin MR, et al. Blocking IL-1β reverses the immunosuppression in mouse breast cancer and synergizes with anti-PD-1 for tumor abrogation. *Proc Natl Acad Sci U.S.A.* (2019) 116:1361–9. doi: 10.1073/pnas.1812266115

45. Da Ros F, Carnevale R, Cifelli G, Bizzotto D, Casaburo M, Perrotta M, et al. Targeting interleukin-1β protects from aortic aneurysms induced by disrupted transforming growth factor β signaling. *Immunity* (2017) 47:959–73.e9. doi: 10.1016/j.immuni.2017.10.016

46. Ismail AS, Severson KM, Vaishnava S, Behrendt CL, Yu X, Benjamin JL, et al. Gammadelta intraepithelial lymphocytes are essential mediators of host-microbial homeostasis at the intestinal mucosal surface. *Proc Natl Acad Sci U.S.A.* (2011) 108:8743–8. doi: 10.1073/pnas.1019574108

47. Ribot JC, Lopes N, Silva-Santos B. γδ T cells in tissue physiology and surveillance. *Nat Rev Immunol* (2021) 21:221–32. doi: 10.1038/s41577-020-00452-4

48. Dong X, Limjunyawong N, Sypek EI, Wang G, Ortines RV, Youn C, et al. Keratinocyte-derived defensins activate neutrophil-specific receptors Mrgpra2a/b to prevent skin dysbiosis and bacterial infection. *Immunity* (2022) 55:1645–62.e7. doi: 10.1016/j.immuni.2022.06.021

49. Ali A, Na M, Svensson MN, Magnusson M, Welin A, Schwarze JC, et al. IL-1 receptor antagonist treatment aggravates staphylococcal septic arthritis and sepsis in mice. *PloS One* (2015) 10:e0131645. doi: 10.1371/journal.pone.0131645

50. Corriden R, Hollands A, Olson J, Derieux J, Lopez J, Chang JT, et al. Tamoxifen augments the innate immune function of neutrophils through modulation of intracellular ceramide. *Nat Commun* (2015) 6:8369. doi: 10.1038/ncomms9369

51. Fiala GJ, Schaffer AM, Merches K, Morath A, Swann J, Herr LA, et al. Proximal. *J Immunol* (2019) 203:569–79. doi: 10.4049/jimmunol.1701521

frontiers | Frontiers in Immunology

TYPE Original Research
PUBLISHED 08 August 2023
DOI 10.3389/fimmu.2023.1172892

OPEN ACCESS

EDITED BY
Daolin Tang,
University of Texas Southwestern Medical Center, United States

REVIEWED BY
Robert Patrick Richter,
University of Alabama at Birmingham, United States
Zhengyu He,
Shanghai Jiao Tong University, China

*CORRESPONDENCE
Guoping Lu
13788904150@163.com
Yufeng Zhou
yfzhou1@fudan.edu.cn
Weiming Chen
13817556013@163.com

†These authors have contributed equally to this work

RECEIVED 23 February 2023
ACCEPTED 21 July 2023
PUBLISHED 08 August 2023

CITATION
Ying J, Zhang C, Wang Y, Liu T, Yu Z, Wang K, Chen W, Zhou Y and Lu G (2023) Sulodexide improves vascular permeability via glycocalyx remodelling in endothelial cells during sepsis.
Front. Immunol. 14:1172892.
doi: 10.3389/fimmu.2023.1172892

Sulodexide improves vascular permeability via glycocalyx remodelling in endothelial cells during sepsis

Jiayun Ying[1†], Caiyan Zhang[1†], Yaodong Wang[1], Tingyan Liu[1], Zhenhao Yu[1], Kexin Wang[2], Weiming Chen[1*], Yufeng Zhou[2,3,4*] and Guoping Lu[1*]

[1]Department of Critical Care Medicine, Children's Hospital of Fudan University, Shanghai, China, [2]Institute of Pediatrics, Children's Hospital of Fudan University, National Children's Medical Center, and the Shanghai Key Laboratory of Medical Epigenetics, International Co-laboratory of Medical Epigenetics and Metabolism, Ministry of Science and Technology, Institutes of Biomedical Sciences, Fudan University, Shanghai, China, [3]National Health Commission (NHC) Key Laboratory of Neonatal Diseases, Fudan University, Shanghai, China, [4]State-level Reginal Children's Medical Center, Children's Hospital Of Fudan University at Xiamen (Xiamen Children's Hospital), Fujian Provincial Key Laboratory of Neonatal Diseases, Fujian, China

Background: Degradation of the endothelial glycocalyx is critical for sepsis-associated lung injury and pulmonary vascular permeability. We investigated whether sulodexide, a precursor for the synthesis of glycosaminoglycans, plays a biological role in glycocalyx remodeling and improves endothelial barrier dysfunction in sepsis.

Methods: The number of children with septic shock that were admitted to the PICU at Children's Hospital of Fudan University who enrolled in the study was 28. On days one and three after enrollment, venous blood samples were collected, and heparan sulfate, and syndecan-1 (SDC1) were assayed in the plasma. We established a cell model of glycocalyx shedding by heparinase III and induced sepsis in a mouse model via lipopolysaccharide (LPS) injection and cecal ligation and puncture (CLP). Sulodexide was administrated to prevent endothelial glycocalyx damage. Endothelial barrier function and expression of endothelial-related proteins were determined using permeability, western blot and immunofluorescent staining. The survival rate, histopathology evaluation of lungs and wet-to-dry lung weight ratio were also evaluated.

Results: We found that circulating SDC1 levels were persistently upregulated in the non-alive group on days 1 and 3 and were positively correlated with IL-6 levels. Receiver operating characteristic curve analysis showed that SDC1 could distinguish patients with mortality. We showed that SDC1-shedding caused endothelial permeability in the presence of heparinase III and sepsis conditions. Mechanistically, sulodexide (30 LSU/mL) administration markedly inhibited SDC1 shedding and prevented endothelial permeability with zonula occludens-1 (ZO-1) upregulation via NF-κB/ZO-1 pathway. In mice with LPS and CLP-induced sepsis, sulodexide (40 mg/kg) administration decreased the plasma levels of SDC1 and increased survival rate. Additionally, sulodexide alleviated lung injury and restored endothelial glycocalyx damage.

Conlusions: In conclusion, our data suggest that SDC1 predicts prognosis in children with septic shock and sulodexide may have therapeutic potential for the treatment of sepsis-associated endothelial dysfunction.

KEYWORDS

sepsis, sulodexide, glycocalyx remodeling, endothelium barrier function, Syndecan-1

Introduction

Sepsis is an immune dysregulation caused by an infection that results in organ dysfunction (1). It is one of the main causes of death in critically ill children. A recent study showed that sepsis-related deaths account for 19.7% of global deaths (2).

Vascular endothelial cells have an important role in regulating vascular smooth muscle tone, vessel barrier formation, systemic and local inflammation, and coagulation and thus play a central role in sepsis pathogenesis (3). The glycocalyx is a matrix coating of the luminal surface of vascular endothelial cells and is largely comprised of proteoglycans with attached or intercalated glycosaminoglycans (4, 5). Damage to the glycocalyx leads to endothelial dysfunction in sepsis, thereby increasing vascular permeability (6). Enzymatic damage to the glycocalyx reduces the expression of two endothelial cell proteins integral in maintaining vascular barrier function: zonula occludens-1 (ZO-1), present in tight junctions, and VE-cadherin integral to adherens junctions integrity (7). Syndecan-1 (SDC1), a heparan sulfate proteoglycan of the endothelial glycocalyx, affects the interaction of extracellular matrix components and soluble ligands with the cell surface. Prior work has demonstrated that SDC1 levels are elevated in adults with sepsis with higher SDC1 levels corresponding with greater mortality risk (8). Together, these data may suggest that in the setting of sepsis, shedding of SDC1 from the endothelial glycocalyx may increase endothelial permeability through a reduction in ZO-1/VE-cadherin expression.

Sulodexide is a composite of fast-mobility heparin and dermatan sulfate (9) with anti-inflammatory and glycocalyx-protective properties (10, 11). Its anti-inflammatory properties appear to lie in its ability to attenuate NF-kB activation as observed in human retinal endothelial cells (12). Moreover, its contribution to glycocalyx remodeling appears to attenuate endothelial monolayer permeability as observed in mouse models of sepsis (13). Though the precise mechanisms by which sulodexide contributes to glycocalyx restoration and endothelial cell signaling have not been fully characterized, this molecule serves as an attractive therapy to ameliorate sepsis-induced endotheliopathy.

Here, we report a previously unidentified role of SDC1 in mediating endothelial permeability during sepsis and its prognosis. This study revealed higher levels of plasma SDC1 in non-surviving septic shock children, compared with surviving children, and the levels were positively associated with IL-6. Notably, the administration of sulodexide promoted SDC1-remodeling and blockaded NF-κB pathway, resulting in improvement of endothelial permeability, along with ZO-1 upregulation. In addition, sulodexide administration attenuated SDC1 shedding and improved survival outcomes in murine sepsis. Our study suggests that sulodexide administration raises the prospect of preventing vascular leakage by remodeling the endothelial glycocalyx during sepsis.

Methods

Patient enrollment and sample collection

This prospective cohort study was registered with ClinicalTrials.gov (NCT03996720) and approved by the Children's Hospital of Fudan University (Protocol No. 2018219). Pediatric patients (age 29 days to 18 years) were enrolled within 48 hours of admission to the pediatric intensive care unit (PICU) at Children's Hospital of Fudan University for septic shock. The study period ran from January 2019 to December 2020. The diagnosis of septic shock was informed by the 2005 International Consensus Conference on Sepsis in Children Guidelines (14). The exclusion criteria were death within 24 h after entering the PICU, immunosuppressant use, or immunodeficiency. We collected and analyzed medical records, including demographic data and prognoses. Blood samples were collected in ethylenediaminetetraacetic acid (EDTA) tubes on the first and third day after inclusion and centrifuged at 400 × *g* for 10 min to separate plasma. The plasma was then frozen at -80°C for future analysis.

Enzyme-linked immunosorbent assay

SDC1, heparan sulfate, and IL-6 were detected in human or mouse plasma using commercially available enzyme-linked immunosorbent assay (ELISA) kits (SDC1 human CD138, Abcam, UK; mouse SDC1, Jianglai, China; human heparan sulfate, Yaji, China; mouse heparan sulfate, Yaji, China; mouse IL-6, Kelu, China; human IL-6, Kelu, China). Plasma levels of SDC1, heparan sulfate, and IL-6 detected by ELISA were then calculated using four-parameter logistic curves generated by standards according to the manufacturer's instructions.

Animals

Specific pathogen-free (SPF) male C57BL/6J mice (3-4 weeks, 12-15 g) were obtained from JieSiJie Laboratory Animals (Shanghai, China). Appropriate temperature and humidity were controlled during a day-night cycle in the laboratory where the mice were housed. Food and water were easily obtained, and all animal experiments were conducted with ethical approval from the Animal Studies Committee of the Children's Hospital of Fudan University (approval number: 2018219).

Endotoxemia model

The mice were randomly allocated to four groups (n = 5/experiment): LPS+SDX, LPS, SDX, and control. Within the groups, mice were injected intraperitoneally (*ip.*) with LPS (30 mg/kg body weight/mouse, Sigma, #L2630) and/or treated intragastrically (*ig.*) with sulodexide (40 mg/kg/mouse; Alfa Wassermann S.P.A.). Equal amounts of saline or sulodexide were injected into the control mice or mice in the SDX group. In the survival experiment, we recorded the mortality in each group three times a day for 120 h after LPS injection. For general anesthesia, 1% tribromoethanol was administered, and the mice were sacrificed 12 h later. Blood and lung samples were collected from the surviving mice.

CLP-induced polymicrobial sepsis model

We randomly grouped the mice into four (n = 5/experiment): control, CLP, SDX, and CLP+SDX. The CLP-induced sepsis model was developed based on previous literature (15). Briefly, after anesthesia with 1% tribromoethanol, laparotomy was performed. Cecum was ligated with 4-0 silk to 1 cm and punctured with a 22-gauge needle. Subsequently, a small mound of feces was squeezed from the hole after removing the needle. The peritoneum was sutured with a 6-0 silk suture, and the skin was intermittently sutured with a 4-0 silk suture. The same operation was performed on the control mice without ligation and perforation. The CLP mice were and/or intragastric (*ig.*) sulodexide (40 mg/kg). An equivalent volume of normal saline (NS) was injected into the control mice. After surgery, all the mice were subcutaneously resuscitated in 40 mL/kg saline. All the mice were sacrificed 24 h later. Retro-orbital blood and lung samples were collected from the surviving mice.

Wet-to-dry lung weight ratio

The wet-to-dry (W/D) lung weight ratio indicated the degree of pulmonary edema. The left lungs were obtained and weighed. After the lungs were heated in oven at 60°C for 48 h, they were weighed again. The dry-to-wet weight ratio was then determined.

Cell culture

Mouse microvascular endothelial cells (MLMECs) were obtained from the Core Technology Facility of Center for Excellence in Molecular Cell Science. Human umbilical vein endothelial cells (HUVECs) were provided by the Cell Bank of the Chinese Academy of Sciences Shanghai Branch (Shanghai, China). The passage number was from passage 3 (P3) to 8 (P8). The MLMECs/HUVECs were cultured in Dulbecco's modified Eagle medium (DMEM) containing 10% fetal bovine serum (Gibco, MD, USA) and 1% streptomycin and penicillin (Hyclone). Cells were placed in an incubator at 37°C, 5% CO_2, and 95% humidity.

Cell treatment conditions

The MLMECs were allocated into four groups: (i) control group; cells were treated with serum-free medium for 2 h; (ii) heparinase III group; cells were treated with 15 mU/mL heparinase III (H8891, Sigam-Aldrich) for 2 h, 4 h, or 8 h, (iii) SDX group; cells were treated with 30 LSU/mL SDX for 2 h, and (iv) heparinase III +SDX group; cells were pretreated with 30 LSU/mL SDX for 2 h, then with 15 mU/mL heparinase III for 2 h, 4 h, or 8 h.

Pulmonary histopathology evaluation

The left lungs of mice were removed and fixed in 4% paraformaldehyde. Subsequently, embedding, dewaxing, and hydration were performed, after which the sections were cut into slides, stained with hematoxylin and eosin, and observed under a microscope. The degree of lung injury was evaluated based on the degree of inflammatory cell infiltration and congestion of the lung tissue.

Immunofluorescent staining of lung tissues, MLMECs, and HUVECs

Lung tissue sections were deparaffinized with xylene and dehydrated with ethanol. The antigen was retrieved before immunofluorescence, and MLMECs were grown on a Confocal Dish (Dianrui, Shanghai, China) with proper treatment. Cells were fixed with 4% paraformaldehyde and ruptured using 0.1% Triton X-100. After blocking with 5% donkey serum, cells were prepared for immunofluorescence. Both were incubated with goat anti-mouse primary antibody to SDC1 (1:100; af3190, R&D Systems). They were then incubated with secondary antibodies conjugated to Alexa Fluor-488 (1:100; A12398, Thermo Scientific). For immunocytochemistry, HUVECs were incubated with rabbit anti-human primary antibody to SDC1 (1:100; ab128936, Abcam). They were then incubated with secondary antibodies conjugated to Alexa Fluor-488 (1:100; ab150077, Abcam). For the detection of heparan sulfate, MLMECs/HUVECs were incubated with primary mouse IgM to F58-10E4 (1:100; 370255-S, Amsbio) and then with secondary antibodies conjugated to Alexa Fluor-488 (1:1000; A10680, Thermo Scientific). Cell nuclei were counterstained with 4,6′-diamidino-2-phenylindole (DAPI). After staining, the cells were observed under a confocal laser scanning microscope SP8 (Leica Microsystems, Wetzlar, Germany), and images were recorded with LAS AF Lite 2.6.0 (Leica Microsystems, Wetzlar, Germany).

Western blot

MLMECs were lysed using RIPA buffer (Beyotime Biotechnology, Shanghai, China) containing protease and phosphatase inhibitors (Thermo Fisher Scientific, Carlsbad, CA, USA). Equal amount of protein (20 g per well) was added to a sodium dodecyl sulfate-polyacrylamide gel and separated by electrophoresis. The protein was transferred onto PVDF membranes (Millipore). Membranes were blocked with 5% skim milk in 0.1% Tween 20. Next, the membrane was incubated with primary antibody at 4°C. The membrane was then incubated with a horseradish peroxidase-conjugated secondary antibody. ECL system (Invitrogen) was used to detect signals. The following primary antibodies were used: ZO-1 (1:1000; 339100l, Invitrogen), VE-cadherin (1:1000; ab33168, Abcam), NF-κB/p65 (1:1000; 8242S, Cell Signaling Technology), NF-KB/p-p65 (1:1000; 3033S, Cell Signaling Technology), and β-actin (1:5000; 3700S, Cell Signaling Technology).

RNA extraction and quantitative real-time PCR analysis

TRIzol reagent was used to extract total RNA from MLMECs. Reverse transcription was performed using a reverse transcription kit (Takara, Tokyo, Japan) according to the manufacturer's instructions. RT-qPCR was performed using the SYBR Premix Ex Taq (Takara, Tokyo, Japan) on a LightCycler 480 II (Roche, Sweden). The evaluation of relative expression of mRNA was through the $2^{-\Delta\Delta Ct}$ method which normalized the expression of GAPDH. The primers used for RT-qPCR are listed in Supplemental Table 1.

Evaluation of endothelium barrier permeability

MLMECs were cultured using the Transwell system (0.4 μm pore size polyester membrane inserts, Corning, Union City, CA, USA). Measurement of FD40 across the endothelium was used to evaluate endothelial barrier permeability (16). The MLMECs were treated with or without heparinase III (15 mU/mL) or SDX (30 LSU/mL). We added 0.1 mg/mL of FD40 to the upper inserts and an equal amount of serum-free medium was added to the lower compartments of the Transwell system for 60 min. Fluorescence across the upper inserts was measured at excitation and emission wavelengths of 490 and 520 nm, respectively.

Statistical analyses

All experiments were carried out at least 3 times independently. After conducting a normality test, data was analyzed by the Student's t-test or one-way ANOVA followed by Tukey's analysis (for normally distributed data); and showed as the means ± SEM through SPSS v21.0 (SPSS Inc., Chicago, IL, USA). The Receiver Operating Characteristic (ROC) curve was used to determine the area under the curve (AUC) for SDC1 expression. GraphPad Prism 7.00 (GraphPad Software, La Jolla, CA, USA) and Adobe Photoshop CC 14.0 (Adobe, San Jose, CA, USA) were used for processing. p values less than 0.05 were considered significant.

Results

SDC1 is a predictor of prognosis in children with septic shock

We studied 28 children with septic shock who were admitted to the PICU of Children's Hospital of Fudan University. Of these patients, nine died and 19 survived 28 days after admission (Supplemental Table 2). We found that SDC1 levels in the non-survival group were significantly upregulated compared to those in the survival group with septic shock on the first (day 1) and third day (day 3). On day 1, the median SDC1 levels in patients in the survival and non-survival groups were 375 (IQR 258-769) ng/mL and 983 (IQR 843-1398) ng/mL, respectively ($p = 0.002$). IL-6 levels were also significantly upregulated in the non-survival groups (Figure 1A). However, there was no difference in the levels of heparan sulfate between the survival and non-survival groups on day 1 (Figure S1A). Higher SDC1 levels were associated with higher IL-6 levels (Figure 1B). However, on day 3, the levels of SDC1, unlike heparan sulfate, were still higher in patients in the non-survival group (median 573 (IQR 257-914) ng/mL) than those in the survival group (median 210 (IQR 124-499) ng/mL) ($p = 0.05$) (Figure S1B). The SDC1 levels decreased over time in the two groups compared to heparan sulfate levels (Figure 1C). The ROC curve showed that the accuracy of plasma SDC1 on day 1 for predicting mortality was 0.856 (Figure 1D). Taken together, these data suggest that SDC1 expression is a prognostic predictor in children with septic shock.

Sulodexide decreased heparinase III-induced shedding of SDC1 in MLMECs

SDC1 is a member of a small family of transmembrane proteoglycans that are mainly expressed on the cell surface, and the main marker of endothelial glycocalyx degradation (17). To reduce the effect of endothelial cell inflammation on the glycocalyx stimulated by LPS, we used heparinase III as a specific hydrolytic agent of the glycocalyx to explore the effect of glycocalyx shedding on endothelial cells. Although heparinase III is not predicted to cause SDC1 shedding based upon its expected site of activity at heparan sulfate molecules, reducing the amount of heparan sulfate by addition of bacterial heparinase III can elevate SDC1 shedding dramatically (18–20). Sulodexide is a glycosaminoglycan consist of heparan sulfate and dermatan sulfate with anti-inflammatory property, which reduces the release of LPS-stimulated inflammatory mediators from macrophages (21). Heparin and

10.3389/fimmu.2023.1172892

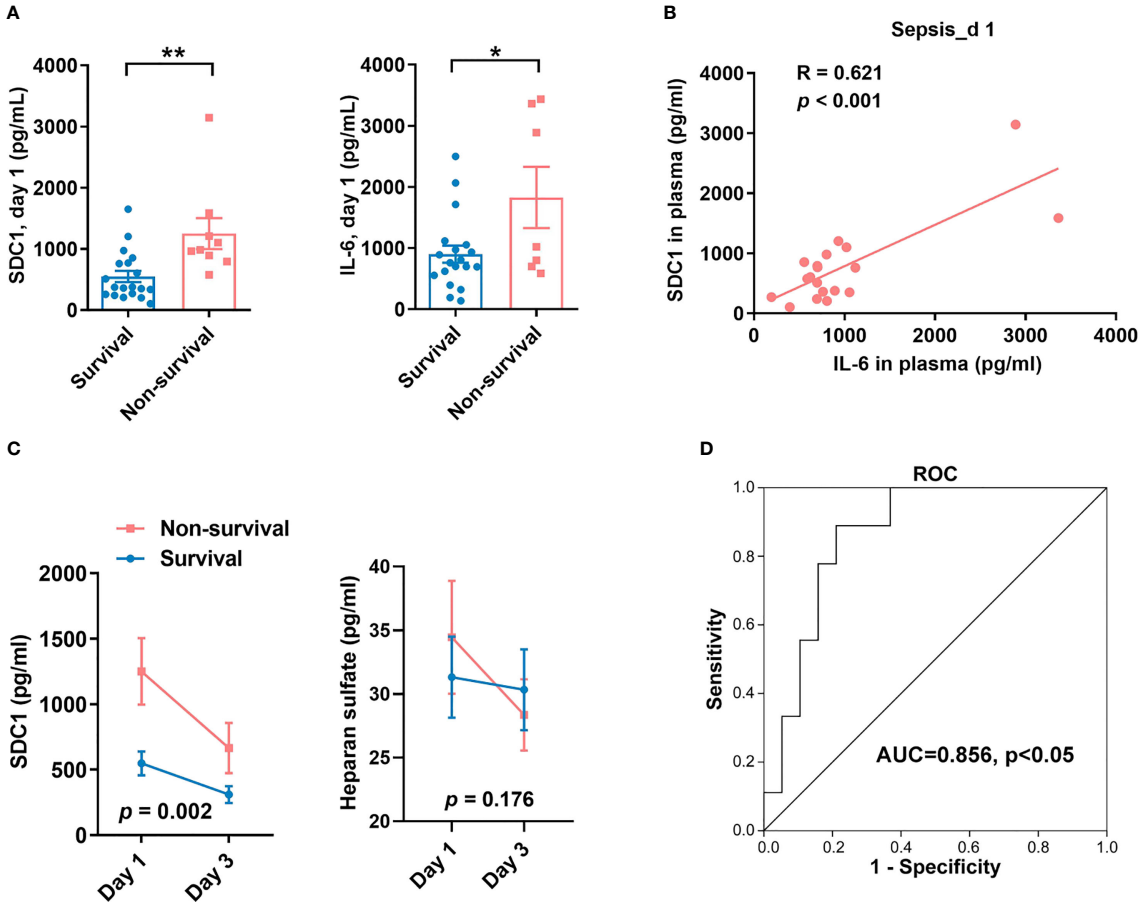

FIGURE 1
Syndecan-1 (SDC1) is a prognosis biomarker of children with septic shock. **(A)** ELISA to detect the levels of SDC1and IL-6 in plasma from 28 children with sepsis within 24 hours of PICU admission (day 1). **(B)** Correlation between levels of IL-6 and SDC1. **(C)** Changes of levels of SDC1 and heparan sulfate in plasma from day 1 to day 3. **(D)** ROC curve analysis of SDC1 expression on day 1 between survival group and non-survival group. Bars and error bars represent the mean ± SEM; *$p < 0.05$, **$p < 0.01$.

heparin derivatives, as the main components of sulodexide, are believed to bind acute-phase and complement proteins, cytokines, and growth factors (22). In addition, sulodexide has numerous antiproteolytic effects via modulation of serine and metalloprotease enzymes, and matrix metalloproteinases, which are also involved in shedding of the glycocalyx (23).

To test the effect of sulodexide on the endothelial glycocalyx layer, we performed MLMECs and HUVECs culture conditions in presence of heparinase III. As expected, heparan sulfate was removed from the endothelium by heparinase III (Figures S2A, B). Notably, the administration of heparinase III also induced the shedding of SDC1 from the membrane of MLMECs, and the administration of supplemental sulodexide significantly presented a rescue at different times (Figures 2A–C). The same result was found in HUVECs (Figures S2C, D). Next, we assessed whether sulodexide increased SDC1 levels in MLMECs by upregulating the expression of the *SDC1* gene. Therefore, we measured *SDC1* mRNA expression under these conditions. However, we found no difference in the different treatment groups on *SDC1* mRNA expression (Figure S2E). Thus, these data showed that sulodexide could improve heparinase III-induced SDC1 expression, but not by increasing *SDC1* gene expression.

Sulodexide prevented endothelial permeability through enhancing ZO-1 expression

The effect of sulodexide on EC barrier function was assessed using a Transwell system (Figure 3A). We found that SDX decreased heparinase-III-induced endothelial permeability (Figure 3B). Sulodexide also prevented heparinase-induced endothelial cell permeability in HUVECs (Figure S3A). Interestingly, permeability improved in the SDX group compared to the control group. VE-cadherin and ZO-1 were important components that play crucial roles in the maintenance of EC barrier (24, 25). We aimed to determine whether endothelial barrier dysfunction due to SDC1 shedding is associated with ZO-1 and VE-cadherin. Notably, 2 h or 4 h after treatment with heparinase III, the levels of VE-cadherin and ZO-1 markedly decreased, as determined by western blot analysis (Figures 3C, D). Interestingly, the administration of supplemental sulodexide upregulated heparinase III-induced ZO-1 levels rather than VE-cadherin levels (Figures 3C, D; S3B, C). Altogether, these data suggest that sulodexide can prevent glycocalyx shedding-induced endothelial permeability by increasing ZO-1 expression.

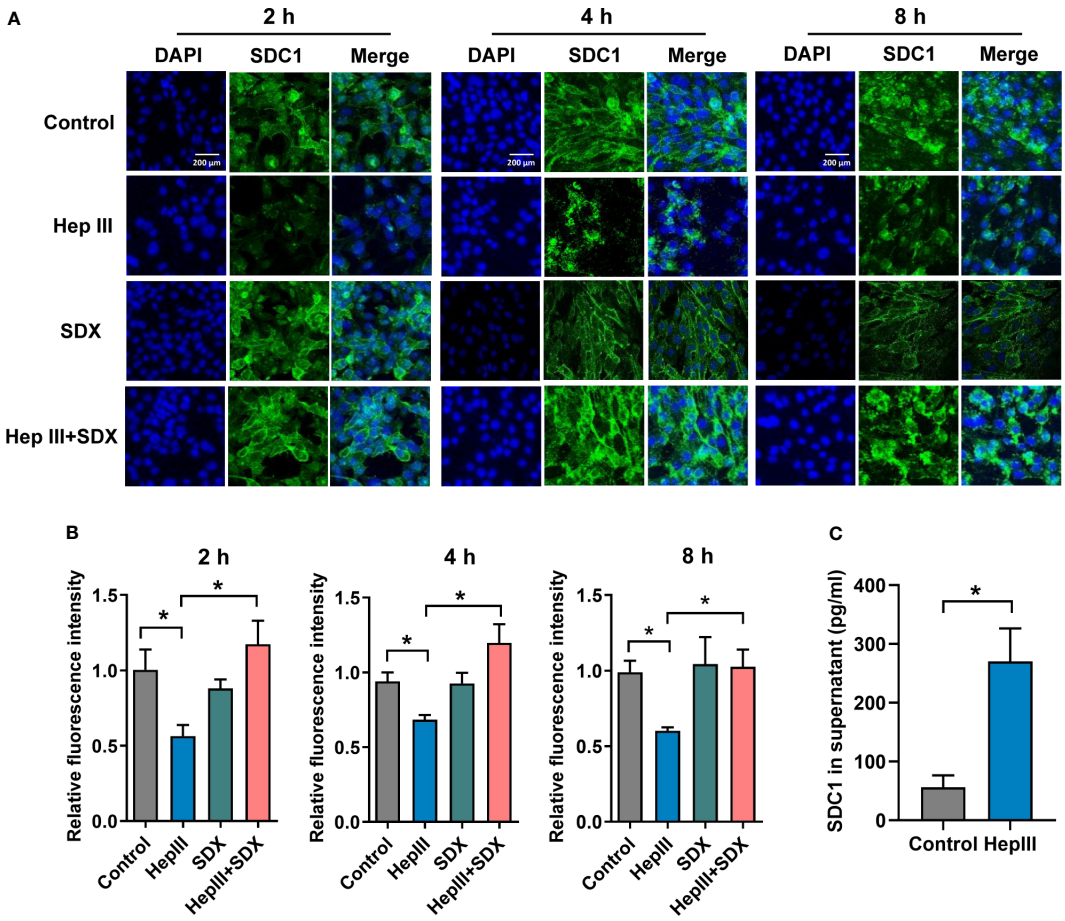

FIGURE 2
Sulodexide decreased heparinase III-induced shedding of SDC1 in MLMECs. **(A)** MLMECs were treated with 15 mU/mL Hep III for 2 h, 4 h, or 8 h. Cells in Hep III+SDX group were treated with 30 LSU/mL sulodexide for 2 h before. Cells in the SDX group were treated with sulodexide for 2 h, and then with PBS in the same volume. Representative image of immunofluorescence of SDC1 on MLMECs, scale bar = 200 μm. **(B)** Densitometry of immunofluorescence of SDC1 on MLMECs. **(C)** ELISA to detect the levels of SDC1 in MLMECs supernatant with treatment of Hep III for 2 h. Data were expressed as the means ± SEM; $*p < 0.05$.

Sulodexide improved permeability via abolishing activation of NF-κB signaling

Under various pathophysiological conditions, NF-κB plays an important role in inflammatory phenotypic changes as a transcription factor in endothelial cells (26). After glycocalyx disruption, shear stress leads to the upregulation of ICAM-1 protein expression and increased NF-κB activation (27). However, it is unclear whether the expression of ZO-1 is mediated by the NF-κB pathway when heparinase III degrades the glycocalyx. To address this, we evaluated the levels of NF-κB/p-p65 and NF-κB/p65 in total. Phosphorylated p65 levels markedly increased within 15/30 min of heparinase treatment and decreased with the addition of sulodexide in MLMECs/HUVECs (Figures S4A, B). With the administration of sulodexide, phosphorylated p65 decreased after heparinase treatment in MLMECs/HUVECs (Figures 4A, B). Similarly, the administration of Bay 11-7082, an inhibitor of NF-κB, markedly attenuated heparinase III-induced increases in phosphorylated p65 and increased the expression of ZO-1 (Figures 4C-F). Collectively, our results revealed that the activation of NF-κB signaling contributes to the expression of ZO-1 when heparinase III degrades the glycocalyx in MLMECs/HUVECs. Notably, sulodexide can promote the remodeling of glycocalyx and improve permeability by preventing NF-κB/ZO-1 signaling overactivation (Figure 4G).

Inhibition of SDC1 shedding by sulodexide improved lung injury and prevented death in septic mice

We established a sepsis model using CLP and LPS (Figure 5A). First, we measured SDC1 levels in the plasma of mice with sepsis. We found that SDC1 was upregulated in mice with sepsis. With the administration of sulodexide, the SDC1 level was downregulated, and the survival rate of mice with sepsis improved (Figures 5B-E). However, sulodexide treatment did not reduce IL-6 levels during sepsis (Figures 5B, D). Taken together, these data suggested that sulodexide restored the survival rate and decreased SDC1 expression in the plasma of mice with sepsis.

10.3389/fimmu.2023.1172892

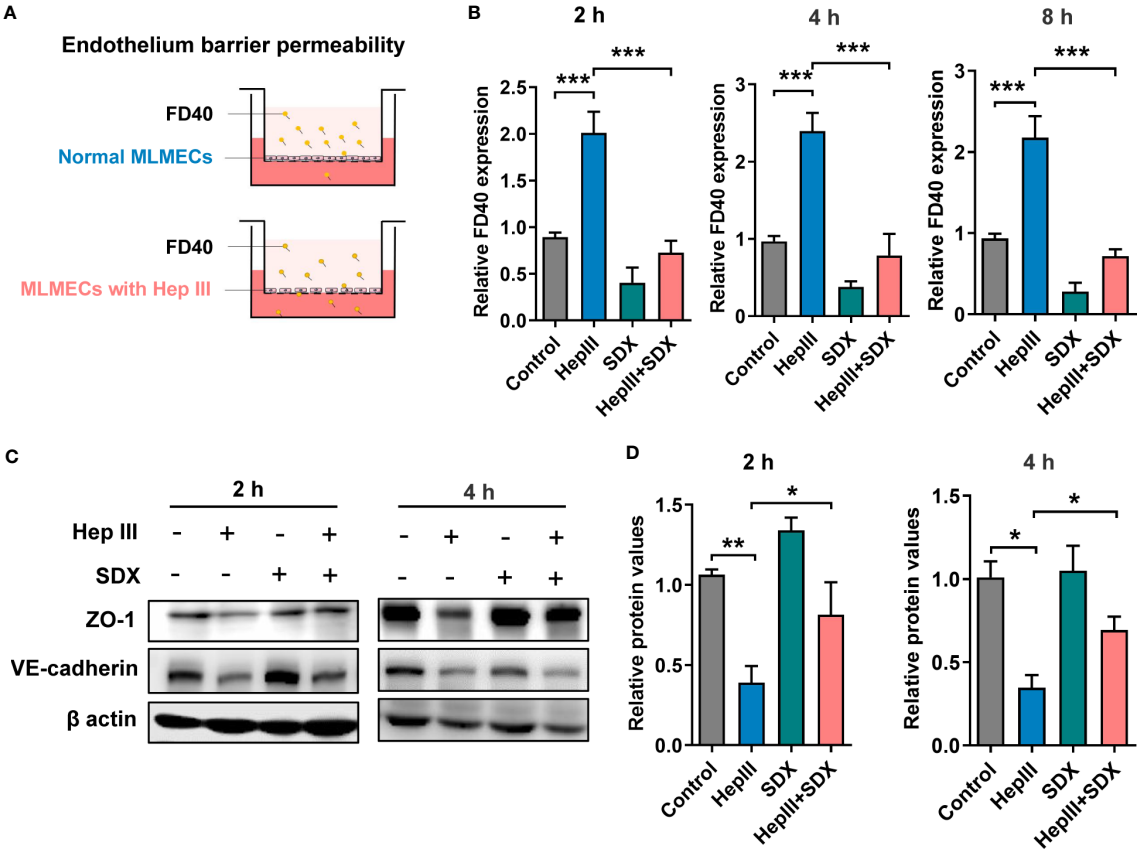

FIGURE 3
Sulodexide improved endothelial permeability resulting from glycocalyx shedding-induced ZO-1 disruption. **(A)** Pattern diagram for transwell model. MLMECs were treated with 15 mU/mL Hep III for 2 h, 4 h or 8 h, and/or 30 LSU/mL SDX for 2 h, respectively. **(B)** Relative fluorescence value of FD40 that passed through the inserts was assayed for 2 h, 4 h, or 8 h. **(C)** Levels of ZO-1 and VE-cadherin were quantified by western blot for 2 h or 4 h. **(D)** Statistical analysis of the levels of ZO-1. Data were expressed as means ± SEM; $*p < 0.05$, $**p < 0.01$, $***p < 0.001$.

We evaluated the histology of the lungs in mice. Notably, in the LPS/CLP group, lung tissues were remarkably damaged, unlike those in the control group. Compared with the LPS/CLP group, there was a marked improvement in morphological features in the LPS+SDX/CLP+SDX group (Figures 5F, S5A). To determine pulmonary vascular permeability in mice, we measured the wet/dry (W/D) ratio of lung tissues. As expected, the LPS/CLP increase in W/D in the lung tissues were significantly inhibited by sulodexide (Figures 5G, S5B). Finally, we assessed glycocalyx damage by measuring SDC1 expression lung tissues fluorescent labeling of the lung tissue. In the sepsis model, SDC1 expression was lower than in the control group. Sulodexide helped preserve SDC1 expression in the lung tissues of the sepsis model (Figures 5H, I, S5C). Altogether, these data show that sulodexide prevented lung injury and sepsis-induced the shedding of endothelial glycocalyx in mice.

Discussion

This study provides evidence of the protective effects of sulodexide on the glycocalyx induced by sepsis and heparinase III. First, we found that SDC1 levels in the plasma of children with septic shock were related to prognosis. *In vitro*, we observed that sulodexide inhibited the shedding of SDC1 and heparinase III-provoked hyperpermeability in MLMECs, and significantly restored the heparinase III-induced suppression of ZO-1, but not VE-cadherin. Furthermore, we found that the permeability improves via the NF-κB/ZO-1 pathway when heparinase III degrades glycocalyx. Third, sulodexide downregulated SDC1 levels *in vivo* and restored the survival rate of mice with sepsis. Additionally, sulodexide alleviated lung injury and restored endothelial glycocalyx damage.

Sepsis is a dysregulated response to an infection that affects all organs. The endothelium is an important component involved in the process of sepsis (28). Endothelial function can affect sepsis prognosis. The glycocalyx on the surface of the endothelium forms a part of the endothelial function. During sepsis, the glycocalyx may be shed by various mechanisms, such as metalloproteinases, heparanase, and hyaluronidases (29). SDC1 and heparan sulfate are the main components of glycocalyx (30). Previous studies have shown that SDC1 is a prognostic marker in patients with sepsis (31, 32). Our findings confirm that SDC1 is associated with mortality. However, in our study, the other two components were not related to the prognosis in children with septic shock. Thus, SDC1 may serve as a biomarker for the prognosis of children with sepsis.

10.3389/fimmu.2023.1172892

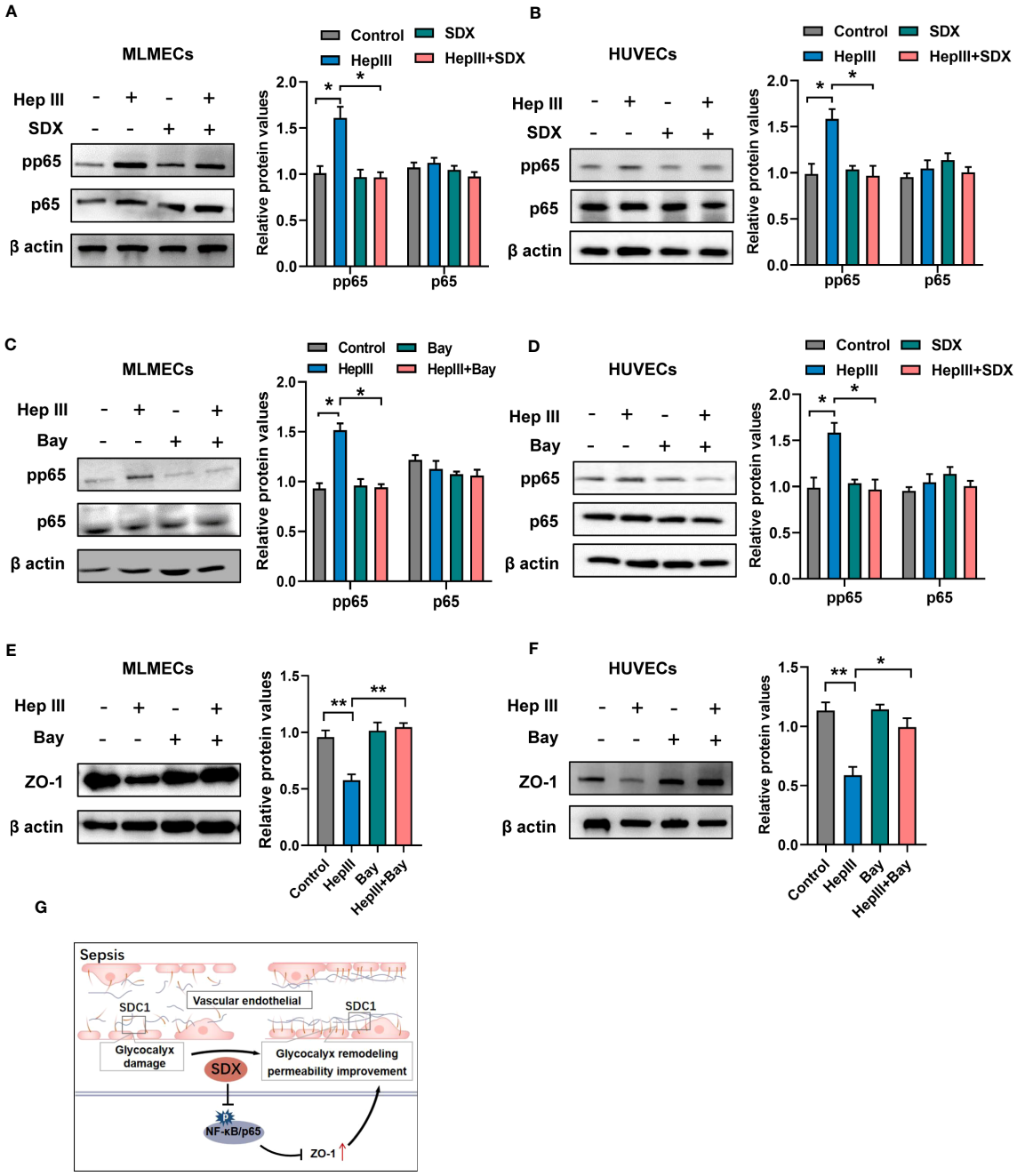

FIGURE 4
Sulodexide promoted permeability via abolishing activation of NF-κB signaling **(A, B)** MLMECs **(A)**/HUVECs **(B)** were treated with 15 mU/mL Hep III for 15/30 min. Cells in the Hep III+SDX group were pre-treated with 30 LSU/mL sulodexide for 2 h. Cells in the SDX group were treated with sulodexide for 2 h without Hep III. **(C, D)** MLMECs **(C)**/HUVECs **(D)** were treated with 40 μM/mL Bay 11- 7082 for 12 h. Cells were then treated with or without 15 mU/mL Hep III for 15/30 min. The levels of NF-κB/p-p65 and NF-κB/p65 were quantified by western blot. **(E, F)** MLMECs €/HUVECs **(F)** were treated with 40 μM/mL Bay 11- 7082 for 12 h. Cells were then treated with or without 15 mU/mL Hep III for 15/30 min. The levels of ZO-1 were quantified by western blot. **(G)** A schematic pattern. SDX protects vascular permeability via glycocalyx remodeling against sepsis *in vivo* and *in vitro*. Data were expressed as the means ± SEM; $*p < 0.05$, $**p < 0.01$.

In vascular homeostasis, during sepsis, heparanase causes the glycocalyx to shed (33). Heparanase can degrade heparan sulfate chains of the glycocalyx. Heparanase inhibition may have beneficial effects on endothelial function by blocking glycocalyx shedding and disruption (34). Doxycycline and heparin were used to inhibit glycocalyx degradation in previous studies (35, 36). Sulodexide is similar in composition to glycocalyx and has an anti-heparanase effect (37). In this study, treatment of MLMECs exposed to heparinase III with sulodexide was effective in preventing glycocalyx degradation, especially with SDC1. *In vivo*, sulodexide restored the survival rate and decreased plasma expression of SDC1 in septic mice. In addition, sulodexide alleviated lung injury and restored endothelial glycocalyx damage in mice with sepsis. Consistent with our data, sulodexide accelerated EG regeneration *in vitro* (13).

10.3389/fimmu.2023.1172892

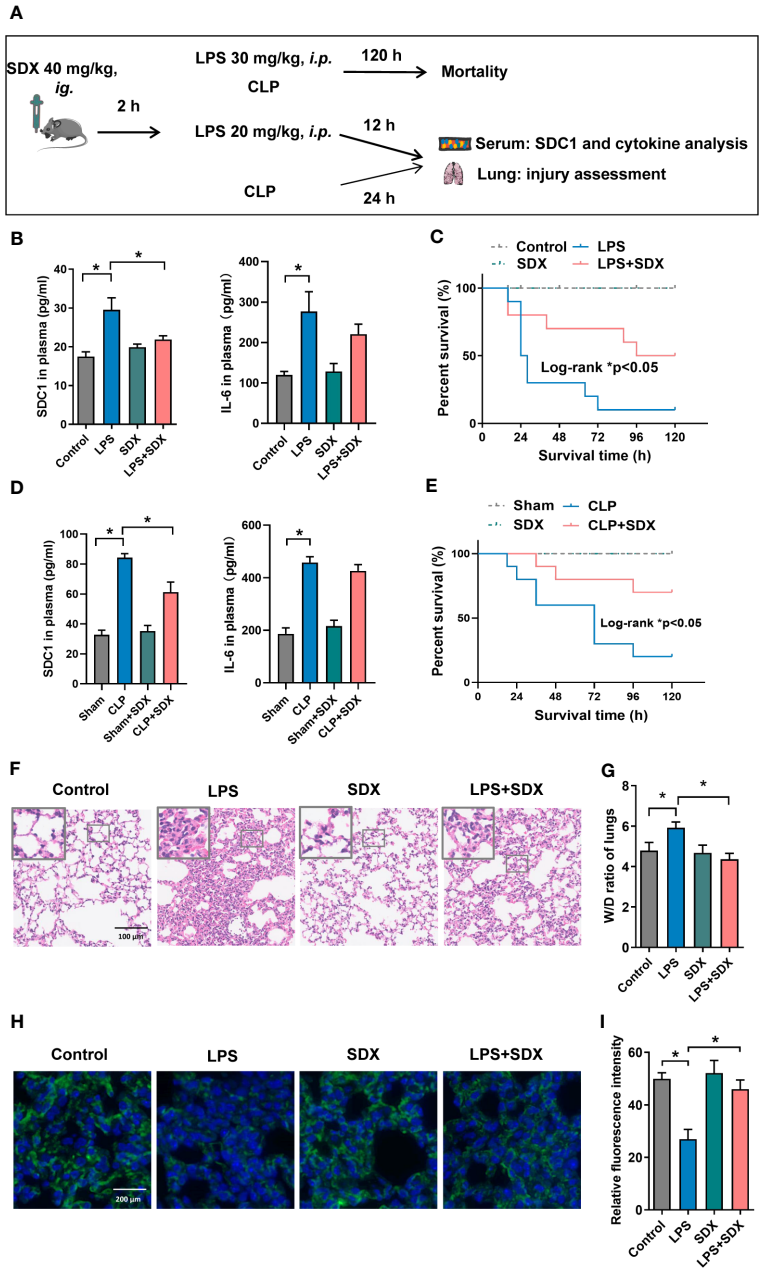

FIGURE 5
Inhibition of SDC1 shedding by Sulodexide improved lung injury and survival in septic mice. **(A)** Pattern diagram of the septic mouse model. Mice were pretreated with sulodexide (40 mg/kg) for 2 h before LPS injection or CLP procedure and those mice were observed for 12 h following LPS and 24 h following CLP before euthanasia. **(B, D)** ELISA to detect the plasma levels of SDC1 and IL-6 in the LPS (20 mg/kg)-challenged **(B)** and CLP-induced **(D)** septic model. **(C, E)** Survival curves after sulodexide administration to LPS (30 mg/kg)-challenged **(C)** and CLP-induced **(E)** mice, n=10/group/experiment. **(F)** Representative lung tissue sections stained with HE at ×100 **(D)** in LPS-induced sepsis model. **(G)** Lung tissue W/D weight ratio in LPS- induced sepsis model. **(H)** Representative immunofluorescence images of SDC1 in lungs, scale bar = 200 μm. **(I)** Densitometry of SDC1 immunofluorescence in lungs. Data are expressed as means ± SEM; $*p < 0.05$.

The traditional Starling's principle is thought to regulate vascular permeability. Hydrostatic and oncotic forces inside and outside the vascular lumen determine filtration across the microvasculature. However, the glycocalyx, as the structural determinant of the oncotic gradient, is a part of the revised Starling equation (38, 39). Sulodexide can restore the shredded endothelial glycocalyx and prevent further degradation. A previous study showed that glycocalyx perturbations and increased vascular permeability were partially reversed following sulodexide administration in patients with type 2 diabetes (40). In our preliminary experiments, the significant increase in heparinase III-induced endothelial permeability was curtailed by sulodexide treatment. Correction of endothelial permeability is likely related to the structural and functional restoration of the glycocalyx. In addition, the restoration of cell-to-cell junctions can decrease endothelial permeability. In a previous study, upregulation of

SDC1 significantly restored occludin and ZO-1 expression in sepsis (41). In this study, we found that sulodexide upregulated ZO-1 expression following heparinase III administration. However, VE-cadherin expression was not restored by the sulodexide treatment. Thus, sulodexide may contribute to the synthesis of the endothelial glycocalyx via an unclear mechanism.

It has been demonstrated that NF-κB is a transcription factor of inflammation in sepsis. Previous studies reported that when the glycocalyx was removed, the activity of NF-κB changed (27). Consistently, sulodexide protects human retinal endothelial cells from high-glucose damage via downstream NF-κB activity (12). However, MCTR1 and PCTR1 stabilized the glycocalyx via NF-κB pathway, thereby improving the endothelial barrier in sepsis (42, 43). In this study, we found that sulodexide also restored endothelial glycocalyx and improved permeability via the NF-κB/ZO-1 pathway. A previous study showed that SDC1-high-Exos or overexpression of SDC1 overexpression were significantly associated with endothelial function restoration (44).

There were several important limitations to this study. Heparinase III, which specifically hydrolyzes heparan sulfate and can directly lead to glycocalyx shedding, was preferred as a stimulus for *in vitro* glycocalyx investigation in our study. However, in the presence of heparinase III, SDC1 and heparan sulfate were both degraded. A method to specifically shed heparan sulfate or SDC1 *in vitro* is lacking. Moreover, SDC1 and heparan sulfate affect NF-κB activation in previous studies (44–46). In this study, we attempted to link heparinase III-induced SDC1 shedding to downstream upregulation of p65 activity and resultant loss of ZO-1 expression. However, avoiding the influence of heparan sulfate remains difficult. The investigation on SDC1 and heparan sulfate in NF-κB/ZO-1 signaling remains to be comprehensively established. Moreover, heparan sulfate fragments may promote NF-κB signaling in endothelial cells (47). Therefore, we cannot completely rule-out an increase in NF-κB signaling by shed heparan sulfate fragments released from the endothelial glycocalyx following heparinase III treatment. Finally, our *in vitro* experiments were performed under static conditions. Conditioning endothelial cells with shear stress impacts glycocalyx composition (48) and more closely recapitulates the *in vivo* environment. Therefore, further work is required to validate our findings in flow conditioned endothelial cells.

In summary, this study demonstrated a previously unknown role of SDC1 in prognosis for children with septic shock and promoting vascular permeability by inducing ZO-1 disruption mediated by NF-κB dependent signaling in ECs. Sulodexide administration may thus serve as a helpful treatment in sepsis by attenuating glycocalyx shedding and downstream EC signaling that promotes vascular leakage.

Data availability statement

The raw data supporting the conclusions of this article will be made available by the authors, without undue reservation.

Ethics statement

The studies involving humans were approved by the Ethics Board in the Children's Hospital of Fudan University. The studies were conducted in accordance with the local legislation and institutional requirements. Written informed consent for participation in this study was provided by the participants' legal guardians/next of kin. The animal study was approved by the Ethics Board in the Children's Hospital of Fudan University. The study was conducted in accordance with the local legislation and institutional requirements.

Author contributions

YZ and GL designed, supervised, and coordinated the overall research. JY and CZ developed the experimental protocol and analyzed the experiments. YW carried out additional work in response to comments from reviewers. TL, KW, and YW contributed to the development of the experimental protocols. JY and TL collected clinical samples. JY, CZ, WC, YZ. and GL wrote the manuscript. All authors contributed to the article and agreed to submit the manuscript.

Funding

This work was supported by grants from the National Key R&D Program of China (2021YFC2701800 and 2021YFC2701805 to GL; 2021YFC2701802 to YZ), the National Natural Science Foundation of China (82241038, 81974248 to YZ, 82202374 to CZ), and the Shanghai Committee of Science and Technology (23ZR1407600, 21140902400, 21ZR1410000, 19ZR1406400 to YZ, and 22ZR1408500 to CZ).

Conflict of interest

The authors declare that the research was conducted in the absence of any commercial or financial relationships that could be construed as a potential conflict of interest.

Publisher's note

Supplementary material

The Supplementary Material for this article can be found online at: https://www.frontiersin.org/articles/10.3389/fimmu.2023.1172892/full#supplementary-material

SUPPLEMENTARY FIGURE 1
Glycocalyx as biomarkers to predict the prognosis of children with septic shock. **(A)** ELISA to detect the levels of heparan sulfate in plasma from children with sepsis on day 1. **(B)** Levels of SDC1 and heparan sulfate in plasma from septic children on day 3. Bars and error bars represent the mean ± SEM; *$p < 0.05$; ns, no significance.

SUPPLEMENTARY FIGURE 2
Sulodexide decreased heparinase III-induced shedding of SDC1 in MLMECs/HUVECs. **(A)** MLMECs or HUVECs were treated with 15 mU/mL Hep III for 2 h. Representative images of immunofluorescence of heparan sulfate, scale bar = 200 μm. **(B)** ELISA to detect the levels of heparan sulfate in supernatant of MLMECs or HUVECs-treated with Hep III for 2 h. **(C)** HUVECs were treated with 15 mU/mL Hep III for 2 h. Cells in the Hep III +SDX group were treated with 30 LSU/mL sulodexide for 2 h before Hep III treatment. Cells in the SDX group were treated with sulodexide for 2 h, and then with PBS in the same volume. Representative images of immunofluorescence of SDC1 on HUVECs, scale bar = 200 μm. **(D)** ELISA to detect the levels of SDC1 in supernatant of HUVECs-treated with Hep III for 2 h. **(E)** MLMECs were treated with 15 mU/mL Hep III for 2 h, 4 h, or 8 h. Cells in Hep III+SDX group were treated with 30 LSU/mL sulodexide for 2 h before. Cells in the SDX group were treated with sulodexide for 2 h, and then with PBS in the same volume. *SDC1* mRNA expression was measured by RT-qPCR. Data are presented as the mean ± SEM. *$p < 0.05$; **$p < 0.01$.

SUPPLEMENTARY FIGURE 3
Sulodexide improved endothelial permeability resulting from glycocalyx shedding-induced ZO-1 disruption. **(A)** HUVECs were treated with 15 mU/mL Hep III for 2 h, and/or 30 LSU/mL SDX for 2 h, respectively. Relative fluorescence value of FD40 that passed through the inserts was assayed. **(B)** The levels of Zonula occludens-1 (ZO-1) and VE-cadherin were quantified by western blot for 8 h. **(C)** Statistical analysis of the levels of VE-cadherin for 2 h, 4 h, or 8 h. Data are presented as the mean ± SEM; **$p < 0.01$, ***$p < 0.001$.

SUPPLEMENTARY FIGURE 4
Heparinase III induced the activation of NF-κB signaling. **(A, B)** MLMECs **(A)**/HUVECs **(B)** were treated with 15 mU/mL Hep III for 0 min, 15 min, 30 min, 60 min, 120 min. The levels of NF-κB/p-p65 and NF-κB/p65 were quantified by western blot. Data are presented as the mean ± SEM; *$p < 0.05$.

SUPPLEMENTARY FIGURE 5
Inhibition of SDC1 shedding by Sulodexide improved lung injury and in CLP-induced sepsis mice. Sulodexide (40 mg/kg) was administered to mice for 2 h and then CLP was administrated for 24 h. **(A)** Representative lung tissue sections stained with HE at ×100 **(D)** in CLP-induced sepsis model. **(B)** Lung tissue W/D weight ratio in CLP-induced sepsis model. **(C)** Representative immunofluorescence images of SDC1 in lungs, scale bar = 200 μm. Data are expressed as means ± SEM; *$p < 0.05$.

References

1. Seymour CW, Liu VX, Iwashyna TJ, Brunkhorst FM, Rea TD, Scherag A, et al. Assessment of clinical criteria for sepsis: for the third international consensus definitions for sepsis and septic shock (Sepsis-3). *JAMA* (2016) 315(8):762–74. doi: 10.1001/jama.2016.0288

2. Rudd KE, Johnson SC, Agesa KM, Shackelford KA, Tsoi D, Kievlan DR, et al. Global, regional, and national sepsis incidence and mortality, 1990-2017: analysis for the global burden of disease study. *Lancet* (2020) 395(10219):200–11. doi: 10.1016/S0140-6736(19)32989-7

3. Ince C, Mayeux PR, Nguyen T, Gomez H, Kellum JA, Ospina-Tascón GA, et al. The endothelium in sepsis. *Shock* (2016) 45(3):259–70. doi: 10.1097/SHK.0000000000000473

4. Reitsma S, Slaaf DW, Vink H, van Zandvoort MA, oude Egbrink MG. The endothelial glycocalyx: composition, functions, and visualization. *Pflugers Arch* (2007) 454(3):345–59. doi: 10.1007/s00424-007-0212-8

5. Kolsen-Petersen JA. The endothelial glycocalyx: the great luminal barrier. *Acta Anaesthesiol Scand* (2015) 59(2):137–9. doi: 10.1111/aas.12440

6. Van Teeffelen JW, Brands J, Stroes ES, Vink H. Endothelial glycocalyx: sweet shield of blood vessels. *Trends Cardiovasc Med* (2007) 17(3):101–5. doi: 10.1016/j.tcm.2007.02.002

7. Nikmanesh M, Shi ZD, Tarbell JM. Heparan sulfate proteoglycan mediates shear stress-induced endothelial gene expression in mouse embryonic stem cell-derived endothelial cells. *Biotechnol Bioeng* (2012) 109(2):583–94. doi: 10.1002/bit.23302

8. Anand D, Ray S, Srivastava LM, Bhargava S. Evolution of serum hyaluronan and syndecan levels in prognosis of sepsis patients. *Clin Biochem* (2016) 49(10-11):768–76. doi: 10.1016/j.clinbiochem.2016.02.014

9. Callas DD, Hoppensteadt DA, Jeske W, Iqbal O, Bacher P, Ahsan A, et al. Comparative pharmacologic profile of a glycosaminoglycan mixture, sulodexide, and a chemically modified heparin derivative, Suleparoide. *Semin Thromb Hemost* (1993) 19 (Suppl 1):49–57.

10. Carroll BJ, Piazza G, Goldhaber SZ. Sulodexide in venous disease. *J Thromb Haemost* (2019) 17(1):31–8. doi: 10.1111/jth.14324

11. Mannello F, Ligi D, Raffetto JD. Glycosaminoglycan sulodexide modulates inflammatory pathways in chronic venous disease. *Int Angiol* (2014) 33(3):236–42.

12. Giurdanella G, Lazzara F, Caporarello N, Lupo G, Anfuso CD, Eandi CM, et al. Sulodexide prevents activation of the PLA2/COX-2/VEGF inflammatory pathway in human retinal endothelial cells by blocking the effect of AGE/RAGE. *Biochem Pharmacol* (2017) 142:145–54. doi: 10.1016/j.bcp.2017.06.130

13. Song JW, Zullo JA, Liveris D, Dragovich M, Zhang XF, Goligorsky MS. Therapeutic restoration of endothelial glycocalyx in sepsis. *J Pharmacol Exp Ther* (2017) 361(1):115–21. doi: 10.1124/jpet.116.239509

14. Goldstein B, Giroir B, Randolph AInternational Consensus Conference on Pediatric Sepsis. International pediatric sepsis consensus conference: definitions for sepsis and organ dysfunction in pediatrics. *Pediatr Crit Care Med* (2005) 6(1):2–8. doi: 10.1097/01.PCC.0000149131.72248.E6

15. Rittirsch D, Huber-Lang MS, Flierl MA, Ward PA. Immunodesign of experimental sepsis by cecal ligation and puncture. *Nat Protoc* (2009) 4(1):31–6. doi: 10.1038/nprot.2008.214

16. Deng HF, Wang S, Wang XL, Li L, Xie F, Zeng ZW, et al. Puerarin protects against LPS-induced vascular endothelial cell hyperpermeability via preventing downregulation of endothelial cadherin. *Inflammation* (2019) 42(4):1504–10. doi: 10.1007/s10753-019-01014-0

17. Johansson PI, Stensballe J, Rasmussen LS, Ostrowski SR. A high admission syndecan-1 level, a marker of endothelial glycocalyx degradation, is associated with inflammation, protein C depletion, fibrinolysis, and increased mortality in trauma patients. *Ann Surg* (2011) 254(2):194–200. doi: 10.1097/SLA.0b013e318226113d

18. Yang Y, Macleod V, Miao HQ, Theus A, Zhan F, Shaughnessy JD Jr, et al. Heparanase enhances syndecan-1 shedding: a novel mechanism for stimulation of tumor growth and metastasis. *J Biol Chem* (2007) 282(18):13326–33. doi: 10.1074/jbc.M611259200

19. Hadigal S, Koganti R, Yadavalli T, Agelidis A, Suryawanshi R, Shukla D. Heparanase-regulated Syndecan-1 shedding facilitates herpes simplex virus 1 egress. *J Virol* (2020) 94(6):e01672–19. doi: 10.1128/JVI.01672-19

20. Ramani VC, Pruett PS, Thompson CA, DeLucas LD, Sanderson RD. Heparan sulfate chains of syndecan-1 regulate ectodomain shedding. *J Biol Chem* (2012) 287 (13):9952–61. doi: 10.1074/jbc.M111.330803

21. Mannello F, Ligi D, Canale M, Raffetto JD. Sulodexide down-regulates the release of cytokines, chemokines, and leukocyte Colony Stimulating Factors from human macrophages: role of glycosaminoglycans in inflammatory pathways of chronic venous disease. *Curr Vasc Pharmacol* (2014) 12(1):173–85. doi: 10.2174/15701611116613126144025

22. Young E. The anti-inflammatory effects of heparin and related compounds. *Thromb Res* (2008) 122(6):743–52. doi: 10.1016/j.thromres.2006.10.026

23. Mannello F, Medda V, Ligi D, Raffetto JD. Glycosaminoglycan sulodexide inhibition of MMP-9 gelatinase secretion and activity: possible pharmacological role against collagen degradation in vascular chronic diseases. *Curr Vasc Pharmacol* (2013) 11(3):354–65. doi: 10.2174/1570161111311030010

24. Nusrat A, Parkos CA, Verkade P, Foley CS, Liang TW, Innis-Whitehouse W, et al. Tight junctions are membrane microdomains. *J Cell Sci* (2000) 113(10):1771–81. doi: 10.1242/jcs.113.10.1771

25. Vestweber D, Winderlich M, Cagna G, Nottebaum AF. Cell adhesion dynamics at endothelial junctions: VE-cadherin as a major player. *Trends Cell Biol* (2009) 19 (1):8–15. doi: 10.1016/j.tcb.2008.10.001

26. Csiszar A, Wang M, Lakatta EG, Ungvari Z. Inflammation and endothelial dysfunction during aging: role of NF-kappaB. *J Appl Physiol (1985)* (2008) 105 (4):1333–41. doi: 10.1152/japplphysiol.90470.2008

27. McDonald KK, Cooper S, Danielzak L, Leask RL. Glycocalyx degradation induces a proinflammatory phenotype and increased leukocyte adhesion in cultured endothelial cells under flow. *PloS One* (2016) 11(12):e0167576. doi: 10.1371/journal.pone.0167576

28. Dolmatova EV, Wang K, Mandavilli R, Griendling KK. The effects of sepsis on endothelium and clinical implications. *Cardiovasc Res* (2021) 117(1):60–73. doi: 10.1093/cvr/cvaa070

29. Uchimido R, Schmidt EP, Shapiro NI. The glycocalyx: a novel diagnostic and therapeutic target in sepsis. *Crit Care* (2019) 23(1):16. doi: 10.1186/s13054-018-2292-6

30. Schmidt EP, Yang Y, Janssen WJ, Gandjeva A, Perez MJ, Barthel L, et al. The pulmonary endothelial glycocalyx regulates neutrophil adhesion and lung injury during experimental sepsis. *Nat Med* (2012) 18(8):1217–23. doi: 10.1038/nm.2843

31. Piotti A, Novelli D, Meessen JMTA, Ferlicca D, Coppolecchia S, Marino A, et al. Endothelial damage in septic shock patients as evidenced by circulating syndecan-1, sphingosine-1-phosphate and soluble VE-cadherin: a substudy of ALBIOS. *Crit Care* (2021) 25(1):113. doi: 10.1186/s13054-021-03545-1

32. Saoraya J, Wongsamita L, Srisawat N, Musikatavorn K. Plasma syndecan-1 is associated with fluid requirements and clinical outcomes in emergency department patients with sepsis. *Am J Emerg Med* (2021) 42:83–9. doi: 10.1016/j.ajem.2021.01.019

33. Lerner I, Hermano E, Zcharia E, Rodkin D, Bulvik R, Doviner V, et al. Heparanase powers a chronic inflammatory circuit that promotes colitis-associated tumorigenesis in mice. *J Clin Invest* (2011) 121(5):1709–21. doi: 10.1172/JCI43792

34. Shu J, Santulli G. Heparanase in health and disease: the neglected housekeeper of the cell? *Atherosclerosis* (2019) 283:124–6. doi: 10.1016/j.atherosclerosis.2019.01.017

35. Potje SR, Costa TJ, Fraga-Silva TFC, Martins RB, Benatti MN, Almado CEL, et al. Heparin prevents in *vitro* glycocalyx shedding induced by plasma from COVID-19 patients. *Life Sci* (2021) 276:119376. doi: 10.1016/j.lfs.2021.119376

36. Lipowsky HH, Sah R, Lescanic A. Relative roles of doxycycline and cation chelation in endothelial glycan shedding and adhesion of leukocytes. *Am J Physiol Heart Circ Physiol* (2011) 300(2):H415–22. doi: 10.1152/ajpheart.00923.2010

37. Hoppensteadt DA, Fareed J. Pharmacological profile of sulodexide. *Int Angiol* (2014) 33(3):229–35.

38. Levick JR, Michel CC. Microvascular fluid exchange and the revised Starling principle. *Cardiovasc Res* (2010) 87(2):198–210. doi: 10.1093/cvr/cvq062

39. Iba T, Levy JH. Derangement of the endothelial glycocalyx in sepsis. *J Thromb Haemost* (2019) 17(2):283–94. doi: 10.1111/jth.14371

40. Broekhuizen LN, Lemkes BA, Mooij HL, Meuwese MC, Verberne H, Holleman F, et al. Effect of sulodexide on endothelial glycocalyx and vascular permeability in patients with type 2 diabetes mellitus. *Diabetologia* (2010) 53(12):2646–55. doi: 10.1007/s00125-010-1910-x

41. Zhang D, Zhang JT, Pan Y, Liu XF, Xu JW, Cui WJ, et al. Syndecan-1 shedding by matrix metalloproteinase-9 signaling regulates alveolar epithelial tight junction in lipopolysaccharide-induced early acute lung injury. *J Inflammation Res* (2021) 14:5801–16. doi: 10.2147/JIR.S331020

42. Li H, Hao Y, Yang LL, Wang XY, Li XY, Bhandari S, et al. MCTR1 alleviates lipopolysaccharide-induced acute lung injury by protecting lung endothelial glycocalyx. *J Cell Physiol* (2020) 235(10):7283–94. doi: 10.1002/jcp.29628

43. Wang XY, Li XY, Wu CH, Hao Y, Fu PH, Mei HX, et al. Protection conjugates in tissue regeneration 1 restores lipopolysaccharide-induced pulmonary endothelial glycocalyx loss via ALX/SIRT1/NF-kappa B axis. *Respir Res* (2021) 22(1):193. doi: 10.1186/s12931-021-01793-x

44. Zhang C, Guo F, Chang M, Zhou Z, Yi L, Gao C, et al. Exosome-delivered syndecan-1 rescues acute lung injury via a FAK/p190RhoGAP/RhoA/ROCK/NF-κB signaling axis and glycocalyx enhancement. *Exp Cell Res* (2019) 384(1):111596. doi: 10.1016/j.yexcr.2019.111596

45. Zhang Y, Wang Z, Liu J, Zhang Z, Chen Y. Suppressing Syndecan-1 shedding ameliorates intestinal epithelial inflammation through inhibiting NF-κB pathway and TNF-α. *Gastroenterol Res Pract* (2016) 2016:6421351. doi: 10.1155/2016/6421351

46. Ren JD, Fan L, Tian FZ, Fan KH, Yu BT, Jin WH, et al. Involvement of a membrane potassium channel in heparan sulphate-induced activation of macrophages. *Immunology* (2014) 141(3):345–52. doi: 10.1111/imm.12193

47. Goodall KJ, Poon IK, Phipps S, Hulett MD. Soluble heparan sulfate fragments generated by heparanase trigger the release of pro-inflammatory cytokines through TLR-4. *PloS One* (2014) 9(10):e109596. doi: 10.1371/journal.pone.0109596

48. Giantsos-Adams KM, Koo AJ, Song S, Sakai J, Sankaran J, Shin JH, et al. Heparan sulfate regrowth profiles under laminar shear flow following enzymatic degradation. *Cell Mol Bioeng* (2013) 6(2):160–74. doi: 10.1007/s12195-013-0273-z

Frontiers in Immunology

Explores novel approaches and diagnoses to treat immune disorders.

The official journal of the International Union of Immunological Societies (IUIS) and the most cited in its field, leading the way for research across basic, translational and clinical immunology.

Discover the latest Research Topics

See more →

Frontiers

Avenue du Tribunal-Fédéral 34
1005 Lausanne, Switzerland
frontiersin.org

Contact us

+41 (0)21 510 17 00
frontiersin.org/about/contact